TRANSIENT NUMERICAL SIMULATION OF HEAT TRANSFER PROCESSES DURING DRILLING OF GEOTHERMAL WELLS

by

Edgar Rolando Santoyo-Gutiérrez

Telford Institute of Environmental Systems

Water Resources Research Group

University of Salford, Salford, UK

Submitted in Partial Fulfilment of the Requirements

of the Degree of Doctor of Philosophy, September 1997

To:

my wife (Guille) and children (Anahí, Edgar and Sócrates),

my mother (Mrs. Leobarda Gutiérrez Pineda)

my father (Mr. Ramón Santoyo Tapia†)

my brother (Sócrates Santoyo Gutiérrez),

my mother in law (Mrs. Guillermina Alquisira),

my nieces,

my family in laws and

my friends

to whom this work is dedicated, for their invaluable support and comprehension along all my life.

TABLE OF CONTENTS

CHAPTER 3 LITERATURE REVIEW

CHAPTER 4 STATIC_TEMP COMPUTER CODE

CHAPTER 5 TRANSPORT AND THERMOPHYSICAL PROPERTIES OF DRILLING MATERIALS

CHAPTER 7 ESTIMATION OF CONVECTIVE HEAT TRANSFER COEFFICIENTS OF DRILLING FLUIDS

CHAPTER 8 THEORY AND DEVELOPMENT OF THE WELLBORE THERMAL SIMULATOR

CHAPTER 11 SUMMARY AND CONCLUSIONS

LIST OF FIGURES

LIST OF TABLES

ACKNOWLEDGEMENTS

The author wishes to thank the Instituto de Investigaciones Eléctricas (IIE) Cuernavaca, México and the Consejo Nacional de Ciencia y Tecnología (CONACyT) for their financial support in the development of this research project.

The author would also like to express his appreciation to Dr. Alfonso García for his excellent assistance and supervision throughout the course of this investigation.

A debt of gratitude is owed to Professor F. A. Holland from the University of Salford, for the supervision of this thesis and for his continuing valuable advice.

The author would also like to extend his thanks to Dr. Julián Sánchez (Executive Director of the IIE), Dr. David Nieva (Director of the Energy Resources Division of IIE) and M.I. Víctor M. Arellano (Head of the Geothermal Department of IIE) for supporting the participation in the IIE/University of Salford cooperative programme.

Thanks are also due to Dr. Gilberto Espinosa for his valuable assistance in the development of this investigation.

The author would also like to express his sincere thanks to Dr. Pablo Mulás del Pozo, Director of the Energy Programme of the Universidad Nacional Autónoma de México (UNAM), who strongly supported the IIE/University of Salford cooperative programme.

Additional thanks are due to the Telford Research Institute of the University of Salford for their support received during the final stage of this research and especially to Professor Ian D. Cluckie and his Water Resources Research Group.

A debt of gratitude is also owed to Dr. Ernest Wilde, Director of the Overseas Educational Development Office of the University of Salford for his valuable support.

Thanks are also due to the Comisión Federal de Electricidad (CFE) for providing useful information about current drilling practices in the area of research.

The author wishes to thank all the staff of the Geothermal Department, in particular to M.Sc. Sócrates Santoyo-Gutiérrez and Dr. Christopher Heard for their valuable advice.

The author greatly appreciates the tireless work of Mrs. M.E. Calderon and the late Fís. Andrés Estebaranz† to facilitate the successful operation of the IIE/University of Salford in-house postgraduate degree programme.

TRANSIENT NUMERICAL SIMULATION OF HEAT TRANSFER PROCESSES DURING DRILLING OF GEOTHERMAL WELLS

Ph.D. candidate: Edgar Rolando SANTOYO GUTIERREZ

Abstract

The transient thermal history of a well drilling system has been identified as one of the main problems that the geothermal well drilling industry needs to solve. In particular, the estimation of temperatures, in and around a geothermal well during drilling (circulation) and shut-in (thermal recovery) conditions, is required.

To overcome this problem, a computer simulator (WELLTHER) has been developed which uses a direct solution method to solve the finite difference equations describing the transient heat transfer processes in a wellbore during drilling and shut-in operations in the presence of the lost circulation to the formation. The new computer simulator uses a numerical model to account for the transient convective heat transfer in the formation surrounding a well, due to lost circulation. This feature of the present simulator is important, since previous wellbore simulators consider the heat transfer process in the formation (rock) as a merely conductive problem. The WELLTHER simulator is capable of accounting for these losses at any point in the well and it has been applied to the study of several Mexican geothermal wells. The results show that the effect of lost circulation on the shut-in temperature profiles can be reproduced satisfactorily. Likewise, a parametric analysis, carried out using the simulator, indicates that a number of assumptions made in previous numerical models are invalid and that certain factors ignored in previous models have a significant effect on the dynamic wellbore temperature distribution.

Finally, a coupling of the new simulator with another computer code (STATIC_TEMP) can be used as a tool to infer more reliably the static formation temperatures in geothermal systems.

Chapter 1

INTRODUCTION

1.1 Introduction

This chapter includes a description of the main problem that motivated the present research work. A justification of the thesis work in terms of its impact and application in the geothermal well drilling industry is outlined. The main objectives of this work and the manner that the thesis was structured in order to attain the proposed objectives are also described.

1.2 Problem Description

In the last decade, considerable interest has been generated in the study of heat transfer processes associated with the drilling and completion operations of geothermal wells.

The transient thermal history of a well drilling system has been identified as one of the main problems that the geothermal well drilling industry needs to solve. This information is very useful and vital for a correct drilling job design and execution as well as for deciding whether drilling should be stopped or continued.

Particularly, a better understanding of the dynamic temperature distribution of: (i) the circulating drilling fluids, (ii) the wellbore system and (iii) the surrounding formation (including the static formation temperatures, SFT), is required to predict the transient thermal behaviour of the well during and after drilling and completion operations.

Accurate knowledge of these temperatures has the potential to benefit a wide variety of applications. In geothermal well drilling and completion operations, these temperatures can be used in the following activities:

- To improve drilling fluid formulation by providing information on the actual circulating temperatures so as to enable modifications to be designed and implemented to the drilling fluid programme as higher temperature zones are drilled.
- To improve cementing programme design, particularly with regard to the amount of retarder required and the setting time.
- To improve casing selection to prevent thermal stress problems.
- To identify the location of fluid inflow regions or lost circulation zones.
- To improve other aspects of well design related to packer fluids and drill bits selection, downhole valves and equipment design.

Additionally, during the development and exploitation stages of geothermal reservoirs, improvement in the determination of the SFT is needed for the following activities:

- estimation of the heat content in the geothermal reservoir,

- evaluation of geothermal gradients,
- interpretation of electric logs,
- evaluation of in-situ formation thermal conductivities,

and

- evaluation of volumetric formation factors (fluid-reservoir).

Normally, SFTs are obtained from information generated during geothermal well drilling and completion activities.

Determination of the transient temperature distribution in and around a geothermal wellbore under drilling and shut-in conditions is a very complex task. Many variables influence these temperatures, which are continuously changing as a result of the continuous circulation of drilling fluid. Basically, the magnitude of the thermal disturbance produced by the drilling fluid circulation process depends upon:

(a) the duration of the drilling process,

(b) the time elapsed after drilling stoppages,

(c) the well geometry,

(d) the thermophysical and transport properties of drilling materials (mud, cement, and casing) and formation (rock),

(e) the nature of heat exchange between the well and the surrounding formation,

and

(f) the presence of fluid flow to the formation, when it occurs during well drilling (lost circulation processes).

Therefore, a reliable and accurate estimation of such temperature distributions requires a complete dynamic thermal study related to the drilling fluid flow in and around the wellbore including the heat transfer processes associated with it.

1.3 Justification

Usually, downhole circulating and formation temperatures in a geothermal well under construction are obtained by means of: (i) temperature logging; (ii) empirical correlations or (iii) analysis of fluid inclusions. However, these measurements only provide a partial knowledge of such temperatures.

In the first case, such temperatures are obtained by direct measurement using downhole temperature recording devices. Although temperature logging is being used as a routine to measure downhole temperatures in the geothermal well drilling activities, it has been limited by problems related to high temperature, hostile borehole conditions and unusual geological environments (fractured or igneous). It has been demonstrated that temperature logs provide only isolated data points for this transient quantity. These tools cannot provide sufficient information to establish the importance of the variables influencing downhole circulating temperatures or SFTs.

Typically, an approximation to SFTs is obtained from in-situ logging operations conducted during the well drilling stage. Return to equilibrium temperatures is usually obtained from temperature logs and classical analytical methods are then used to infer SFT [Dowdle and Cobb (1975); Hasan and Kabir (1994); Ascencio et al (1994)]. However, the SFT values obtained by this way are always less than the initial temperatures of the formation [Nielsen et al (1990)]. More accurate SFT estimates should be obtained in this way when the temperature logs are carried out at longer drilling stoppages. However, this process can take from several hours up to several months to reach the original equilibrium state. Clearly, by this time well logging tests are not economically feasible because they can increase the cost of well drilling. In fact, temperature logs can represent up to 10% of the total cost of a geothermal well which normally ranges from 1 to 2 millions of US dollars [Capuano (1992].

In the second case, the use of empirical correlations developed by the American Petroleum Institute (API) have had limited success in predicting downhole circulating temperatures in geothermal wells [Kutasov and Targhi (1987)]. These correlations usually overestimate such temperatures since they were originally developed for the oil drilling industry which differs notably from the geothermal drilling technology.

Finally, in the third case, analysis of fluid inclusions found in drilling cuttings or core samples can be performed to infer the initial formation temperature but they are impractical for the drilling industry because they are time consuming and therefore, costly [Fujino and Yamasaki (1985)].

After analysing these cases, an accurate, reliable and economic alternative means for predicting the transient temperature distribution in and around geothermal wells under drilling and completion conditions is required. Perhaps the only way to obtain the best approximation of these temperatures is by use of computer simulators. Numerical simulators represent an important alternative for the determination of such temperatures, with the additional advantages of fast temperature calculation, low cost or at least a reduction of the total drilling cost, in-situ applicability and transportability, among others. Experience has demonstrated that numerical simulators can be used to account for most of the complexities of the heat transfer mechanisms that occur in a geothermal well drilling system.

In the past, a number of computer simulators have been developed to provide an approach to the solution of the heat transfer problem relating drilling fluid circulation, wellbore geometry and the surrounding formation. Unfortunately, the majority of them have been developed to apply in the oil well industry. This problem has created a serious limitation when such simulators need to be applied to study heat transfer processes in the geothermal well drilling systems.

Some of these simulators have assumed the coupling of a pseudo-steady heat flow model in the wellbore with a fully transient heat conductive model for the formation [Raymond (1969); Holmes and Swift (1970); Arnold (1990); Hernandez et al (1993)]. Thus, the application of such simulators in the geothermal well drilling systems have only provided approaches to the calculation of downhole temperatures in and around the well because they do not correctly simulate the unsteady nature of the heat transfer problem.

Many other simulators have been developed to improve such temperature predictions by coupling a fully transient heat flow model in the wellbore with a fully transient heat conductive model for the formation [Raymond (1969); Keller et al (1973); Wooley (1980); Marshall and Bentsen (1983); Corre et al (1984); Bittleston (1990); Beirute (1991)]. Although these simulators have improved the thermal analysis of the heat transfer problem, they have been applied with limited success because they have not fully reproduced the temperature measurements recorded during the well drilling and completion. This phenomenon has been observed mainly in geothermal wells where there have been reported significant problems of lost circulation (drilling fluid losses to the formation). Furthermore, none of the previous simulators considers the temperature dependance of the transport and thermophysical properties of the drilling fluids and cement slurries.

After a detailed review of the main assumptions considered by all previous simulators, two important limitations can be identified as responsible for the unsuccessful prediction of downhole temperature logs. The first one is related to the thermophysical and transport properties of the drilling fluid, cement slurries and formation (rocks). These have been considered as constants, which are independent of temperature. A careful analysis of this assumption reveals that its application is invalid because it is well known that these properties vary with temperature, especially in the case of the drilling fluids.

Regarding this, the composition of these drilling materials has been recognised as one of the main parameters that affects the calculation of: the fluids' thermal and transport properties and the convective heat transfer coefficients. These in turn influence the estimation of the downhole circulating drilling fluid and formation temperatures. Unfortunately, at present in the well drilling literature, information on reliable correlations for the calculation of thermophysical and transport properties of drilling fluids and cement slurries is unavailable or seldom available.

However, in the case of drilling fluids, some attempts have been made in some simulators to consider the variation of their properties with temperature by making use of the thermodynamic properties of water. Moreover, water is a Newtonian fluid and drilling fluids tend to exhibit a temperature dependent non-Newtonian behaviour. Therefore, it is also expected that this assumption will lead to significant errors in the calculation of the real convective heat transfer coefficients of drilling fluids and the corresponding downhole circulating fluid and formation temperatures.

The second limitation, and maybe the most important one, is that the heat transfer models adopted by all previous simulators only represent the drilling fluid circulation process under ideal conditions, i.e. the presence of drilling fluid losses to the formation is neglected. This ideal assumption has suggested that only purely conductive heat transfer models are considered within the rock formation as the dominant heat transfer mechanism. However, it is well known that the lost circulation problem is not unusual during drilling operations. In fact, the presence of lost circulation problems is being used in the geothermal well drilling industry as a tool to identify highly permeable zones and to decide when the drilling process must be stopped. Drilling fluid can get lost to the formation at rates of up to about 4 $m^3\ hr^{-1}$ (25 $bbl\ hr^{-1}$) [Luhesi (1983)].

Evidently, the effect of drilling fluid losses to the formation can be extremely important in the determination of the downhole circulating fluid and formation temperatures. If a circulation loss occurred at a depth where temperature logs were measured, then it would be necessary to assess its effect on these temperature measurements. This suggests that a convective heat transfer process must be included in the conductive formation model. This correction implies a series of difficulties because realistic solutions of heat transport equations have to consider the effects of: (i) tridimensional fluid flow (which normally is unknown); (ii) disturbances in the flow field caused by drilling; (iii) the contrast between the thermal properties of the rock and the drilling fluid; i.e. effective rock properties and (iv) vertical and lateral variations in the thermal properties of the formation. Although a rigorous quantitative analysis of the influence of such factors is a very complex task, several assumptions can be made in order to take into account these thermal effects.

From this critical analysis, it is clear that an improved transient wellbore thermal simulator that overcomes some of the limitations described above is required in order to determine more accurately downhole temperatures in and around geothermal wells under drilling and shut-in conditions. Therefore, the development of a new wellbore thermal simulator with these purposes in mind is clearly justified. It represents a challenge to be overcome in heat transfer studies. The direct benefit will be an extensive application in the geothermal well drilling industry with the potential for substantial savings in drilling costs.

1.4 Objectives of the Research Work

The main objective of the thesis is to study the actual unsteady state of the heat transfer processes associated with geothermal well drilling and the temperature distributions of the circulating drilling fluids and the surrounding formation. The specific objectives of the present research work are as follows:

(i) To develop an experimental programme to evaluate the rheological (non-Newtonian) behaviour of drilling fluids.

(ii) To perform an analysis to evaluate the convective heat transfer coefficients of drilling fluids considering the non-Newtonian nature of drilling fluids.

(iii) To develop a new transient wellbore thermal simulator (WELLTHER) for computing downhole circulating drilling fluid and formation temperatures in geothermal wells under actual drilling and shut-in conditions.

(iv) To validate the wellbore simulator with analytical solutions and data reported in the technical literature.

(v) To test the computer model with field data obtained from geothermal wells drilled in the Mexican geothermal fields.

(vi) To carry out a complete sensitivity analysis based on the effects of thermophysical and transport properties of drilling materials on the temperature distributions of the circulating drilling fluids and the formation.

(vii) To analyse the thermal behaviour of geothermal well drilling systems in the presence of lost circulation problems.

1.5 Thesis Structure

In order to achieve the proposed overall and specific objectives, this thesis has been divided into eleven chapters and six appendices.

Chapter 1 presents the introduction of the thesis together with a complete description and justification of the research work. Chapter 2 discusses general aspects related to geotermal energy and the geothermal well drilling technology.

Chapter 3 summarises a literature review of the state of the art on analytical and numerical simulation methods for determining circulating drilling fluid and formation temperatures in geothermal and oil well drilling operations. Chapter 4 presents the development of the computer program (STATIC_TEMP) for estimating static formation temperatures from geothermal well drilling temperature data. Chapter 5 describes the importance of the transport and thermophysical properties of drilling materials on the temperature distributions in geothermal well drilling systems. The non-Newtonian behaviour of drilling fluids and their temperature dependance in particular is analysed. Chapter 6 describes an experimental investigation based on the measurement of the viscosity of drilling fluids at different temperatures. Chapter 7 covers an extensive literature review for the selection and evaluation of the most suitable correlations for estimating convective heat transfer coefficients of non-Newtonian drilling fluids.

Chapters 8, 9 and 10 describe the development of the new transient thermal wellbore simulator (WELLTHER) in terms of: the overall physical model, the numerical solution algorithm and the programming architecture. Validation and application tests with data reported in the literature and acquired field data during the drilling process of Mexican geothermal wells are also included.

Finally, a complete discussion of the results and conclusions of this research work are included in Chapters 11 and 12, respectively. Appendices I-V include the listings of the computer codes as well as a brief description of the numerical methods employed by WELLTHER and publications generated during the present study.

1.6 References

F.C. Arnold, Temperature variation in a circulating wellbore fluid, Journal of Energy Resources Technology, 112 79-83 (1990).

F. Ascencio, A. García, J. Rivera and V. Arellano, Estimation of undisturbed formation temperatures under spherical-radial heat flow conditions, Geothermics **23** 317-326 (1994).

R.M. Beirute, A circulating and shut-in well temperature profile simulator, Journal of Petroleum Technology, **September** 1140-1146 (1991).

S.H. Bittleston, A two-dimensional simulator to predict circulating temperatures during cementing operations, Proceedings of The 65th Annual Technical Conference and Exhibition, Society of Petroleum Engineers of AIME, New Orleans, LA, USA, **September 23-26**, 443-454 (1990).

L.E. Capuano, Geothermal versus oil and gas: A comparison of drilling practices, Geothermal Resources Council Bulletin, **April** 113-116 (1992).

B. Corre, R. Eymard and A. Guenot, Numerical computation of temperature distribution in a wellbore while drilling, Proceedings of The 59th Annual Technical Conference and Exhibition, Society of Petroleum Engineers of AIME, Houston, Texas, USA, **September 16-19**, 12 p. (1984).

W.L. Dowdle and W.M. Cobb, Static formation temperature from well logs - an empirical method, Journal of Petroleum Technology, **November** 1326-1330 (1975).

T. Fujino and T. Yamasaki, The use of fluid inclusion geothermometry as an indicator of reservoir temperature and thermal history in the Hatchobaru geothermal field, Japan, Geothermal Resources Council, Transactions, **9** 429-433 (1985).

A.R. Hasan and C.S. Kabir, Static reservoir temperature determination from transient data after mud circulation, SPE Drilling & Completion, **March** 17-24 (1994).

I. Hernandez, A. Garcia, y M. Morales, Estimacion de temperaturas de los fluidos de perforacion durante la circulacion: Geotermia, Revista Mex. de Geoenergia, **9** 305-319 (1993).

C.S. Holmes and S.C. Swift, Calculation of circulating mud temperatures, Journal of Petroleum Technology, **June** 670-674 (1970).

H.H. Keller, E.J. Couch and P.M. Berry, Temperature distribution in circulating mud columns, Society of Petroleum Engineers Journal, **February** 23-30 (1973).

I.M. Kutasov and A.K. Targhi, Better deep-hole BHTC estimations possible, Oil & Gas Journal, **May** 71-73 (1987).

M.N. Luhesi, Estimation of formation temperature from borehole measurements, Geophys. J. R. Astr. Soc. **74** 747-776 (1983).

D.W. Marshall and R.G. Bentsen, A computer model to determine the temperature distributions in a wellbore, The Journal of Canadian Petroleum, **January-February** 63-75 (1982).

S.B. Nielsen, N. Balling and H.S. Christiansen, Formation temperatures determined from stochastic inversion of borehole observations, Geophys. J. Int., **101** 581-590 (1990).

L.R. Raymond, Temperature distribution in a circulating drilling fluid, Journal of Petroleum Technology, **21** 333-341 (1969).

G.R. Wooley, Computing downhole temperatures in circulation, injection, and production wells, Journal of Petroleum Technology, **September** 1509-1522 (1980).

Chapter 2

GEOTHERMAL ENERGY

2.1 Introduction

This chapter presents some general aspects related to geothermal energy, including the use of this renewable resource in electric power generation. Then the present status of geothermal energy in the world together with Mexican experience in geothermal power generation is discussed briefly. A general description of the drilling technology used in geothermal wells along with the most common associated problems are also included. The thermal behaviour of the drilling fluid circulation system is analyzed as a heat exchange device. Then the physical model of it and the main heat transfer processes involved are outlined. Finally, the problem of determining static formation temperatures and the importance of its potential application to the geothermal industry are also described.

2.2 Basic Concepts of Geothermal Energy

Geothermal energy, in the comprehensive sense, is defined as the natural energy of the earth. This renewable energy has its origins in the deeper zone of the earth. Enormous amounts of thermal energy are generated and stored in the Earth's core, mantle and crust. The heat is transferred from the interior towards the surface mostly by thermal conduction, and this conductive heat flow makes temperatures rise with increasing depth in the crust on average by 25 to 30 °C/km; commonly called the *«geothermal gradient»* [Dickson and Fanelli (1995)].

The recoverable thermal energy theoretically suitable for direct applications has been estimated as 2.9×10^{24} Joules, which is approximately 10,000 times the present annual world consumption of primary energy without regard to grade [Armstead (1983)].

A geothermal resource can exist when the conditions of a heat source, a heat holding medium (the formation) and a carrying medium (water) are identified [Capuano (1992)]. These three conditions exist in various combinations around the world. Geothermal resources may be developed in the following environments:

(a) liquid-dominated reservoirs,

(b) vapour-dominated reservoirs,

(c) hot-dry rock systems,

and

(d) geopressured geothermal reservoirs.

A typical dynamic vapour-dominated geothermal reservoir is shown in Fig. 2.1.

The depths of geothermal reservoirs vary from quite shallow, as shown by hot springs and fumaroles, to depths below 5 km. The deeper reservoirs (1 to 5 km) are usually hotter. These resources are also known as ***«high enthalpy geothermal resources»*** and are suitable for commercial electric power generation; see Fig. 2.2 [Santoyo (1991); Arellano (1996)]. In this case, hot water at temperatures ranging from about 200 °C to more than 300 °C, is brought from the underground reservoir to the surface through drilled wells, and is flashed to steam in special vessels by reducing the pressure. The steam is separated from the liquid and fed to a turbine engine, which drives a generator. Spent geothermal fluid (brine) is reinjected into peripheral parts of the reservoir to help maintain the reservoir pressure and to dispose of the residual fluid to avoid pollution problems [Mulás et al (1987)].

In contrast to these hotter and deeper reservoirs, there is another kind of hydrothermal system known as ***«low enthalpy geothermal resources»***. These systems are characterized by shallow reservoirs which have fluid temperatures less than 200 °C. These resources are suitable primarily for direct utilisation in space heating, horticulture, fish farming, bathing or process heat applications [Freeston (1996)].

2.3 World Distribution of Geothermal Utilisation

Geothermal energy is found in most parts of the world and is being exploited by conventional technology; see Fig. 2.3. Geothermal energy represents a large potential energy source, not only for electric power production, but also for process heat conversion and refrigeration. Commercial production on the basis of hundreds of MWe has been used for over three decades both for electricity generation and direct utilisation. At present, 50 countries have quantifiable geothermal utilisation and about 80 countries have identified geothermal resources.

Electricity from geothermal origin has been produced in 21 countries (38 TWh/a) and a direct application is recorded in 35 countries (34 TWh/a) [Stefansson (1995)]. Annually, about 38 TWh are generated in geothermal power plants, whereas the annual use of direct heat amounts to about 34 TWh [Huttrer (1995); Freeston (1996)].

Table 1.1 summarizes data related to electricity generation from geothermal energy in the world. The electrical power generation cost with these geothermal resources is around US$ 0.04/kWh. Even though electricity production from these resources is equally common in industrialized and developing countries, it plays a more important role in the latter.

The world distribution of direct utilisation is different (Table 1.2). With the exception of China, direct utilisation is an important business mainly in the industrialized and Central and Eastern European Countries [Bresee (1992)]. This is to some extent evident, as most of these countries have cold winters where a significant share of the overall energy budget is related to heating problems. Therefore, space heating is the dominant type of direct use (34 %) of geothermal energy, however, other common direct uses are bathing (14 %), greenhouses (14 %), heat pumps (13 %) for air cooling and heating, fish farming (9 %), and industry (9 %). The production cost/kWh for direct utilisation is highly variable, but commonly under US$ 0.02 /kWh [Freeston (1996)].

2.4 Status of Geothermal Energy in Mexico

The total installed electricity capacity in Mexico is approximately 32,166 MWe. At present in Mexico, geothermal energy makes a contribution of 2.3 % to the electrical power generation; Table 1.3 [Comision Federal de Electricidad (1997)].

Mexico is the third country in the world to have geothermal power plants in commercial operation [Quijano (1993); Hiriart-LeBert and Gutierrez-Negrin (1994)]. The Comision Federal de Electricidad (Federal Electricity Commission, CFE) of Mexico has an installed capacity of 753 MWe in geothermal power plants (620 MWe in Cerro Prieto, Baja California Norte; 98 MWe in Los Azufres, Michoacan and 35 MWe in Los Humeros, Puebla).

The locations of these geothermal fields and the new geothermal zones under exploration (Tres Virgenes, B.C.S.; El Ceboruco, Nayarit; Laguna Salada, B.C.N.; Pathe, Hidalgo; Araro, Michoacan, Las Derrumbadas and Acoculco in Puebla and La Primavera, Jalisco) are shown in Fig. 2.4. Proven geothermal reserves indicate a feasible total of 1144 MWe to be installed by the end of the present century [Quijano and Gutierrez-Negrin (1995)]. CFE plans to reach this installed capacity by means of the exploration and exploitation of new geothermal zones.

2.5 Geothermal Well Drilling Technology

The exploitation of geothermal resources, either for electric power generation or for any direct heat use, involves a series of activities to solve problems related to its efficient utilisation. These activities are summarised in the following list.

(a) Appropriate sites for the drilling and completion of geothermal wells must be selected.

(b) The geothermal reservoir has to be characterised in order to accurately estimate the available energy.

(c) The rates of exploitation should be decided to optimise the recovery of this energy.

(d) Geothermal fluids must be controlled and disposed of.

(e) Appropriate heat transfer and energy conversion equipment must be designed.

Drilling and completion activities account for a major part of the overall cost of a geothermal project. These activities also have a significant effect on the useful life of the geothermal wells, specifically on the future production regime of the geothermal field.

The major methods and equipment used for drilling deep geothermal wells are extensions of those that have been developed for oil and gas drilling. Unfortunately, basic oil and gas drilling and completion technology have been employed, modified and sometimes abandoned in an effort to adapt them to geothermal drilling and completion technologies. As a result, new technologies have been developed for the geothermal drilling industry. Details of these technologies have been presented in numerous papers reported in the literature [Botai and Cigni (1985); Santoyo et al (1991) and others].

2.5.1 Drilling process

Kelsey and Carson (1987) have listed the following activities which are involved in the drilling and completion of geothermal wells:

(i) Well planning. Long before there is any activity at the prospective well site, specialists (engineers, geologists, and managers) will have obtained the necessary rights and permits, designed the well, and selected its location. Their decisions rely on exploration techniques, such as geochemical, geological, geophysical and hydrological methods. The exploration results are important at this stage for they determine the needs for site preparation and road access as well as for well depth, wellbore size, and special surface equipment.

(ii) Site preparation. Many geothermal reservoirs are found in mountainous terrain which complicates drill site selection and drilling. Topography often limits the number of possible locations for drilling sites. This reduces the per-well site preparation cost but requires drilling programmes that include directional drilling, i.e. purposely deviating the wellbore from the vertical in order to reach the desired target in the reservoir. Typically, site preparation accounts for approximately 5 % of the total cost of a well.

(iii) Drilling operations. Figure 2.5 shows a sketch of a drilling system that would support operations at a deep geothermal well.

(iv) Well completion. Once a geothermal well has been drilled to the depth required to maintain sufficient production, the well is completed. This practice involves preparing the well for a long duration production cycle (~20 years) [Morales et al (1990)]. This means providing for the stability of the wellbore by installing the final protective steel casing and preparing for production by reversing any damage that may have been done to the formation by the drilling fluids. This involves lowering steel pipe into the well, hanging it from the surface with the rig hoisting equipment, and then cementing the casing to the formation. The cementing operation involves mixing a slurry of water and cement, pumping it down the casing, and displacing the slurry with another fluid or a solid plug thus forcing the cement up the annular space and the formation.

(v) Stimulation techniques for production. Occasionally, the production rate from a well is below the level deemed adequate for economic recovery and consideration is given to methods to increase production. Several options are available for increasing well productivity but none is generally applicable or widely used in geothermal drilling. Low production rates are due to poor hydraulic coupling between the well and the resource. The coupling can be a

function of both distance between the well and a producing feature such as a high pressure fracture system and permeability or resistance to fluid flow. Regularly it is assumed that the well was drilled within a reasonable distance of the resource, and so the stimulation options involve methods of increasing the permeability. If this is not true, drilling a new well is the only viable option. Low permeability may be an inherent reservoir characteristic or it may be due to action taken in the drilling of the well. Lost circulation material (material added to the mud to plug zones of major fluids loss) used while drilling can plug pore spaces or fractures in the producing formation and lower the natural, near-wellbore permeability. In these cases, an acid wash is usually sufficient to eliminate the near-wellbore damage.

2.5.2 Drilling equipment

The major components of a drilling system and their primary functions are discussed below.

(a) Drilling rig. Its purpose is to support the drill string and casing and its size is determined by how much weight it is designed to lift.

(b) Bit. The bit is the system component that actually penetrates the rock formation that is being drilled.

(c) Drill pipe. In the simplest drilling configuration, the bit is attached to the drill pipe which runs from the surface to the bit. The pipe transmits torque, tensile forces (tension in the upper elements and compression in the lower elements) and fluids.

(d) Drill collars. These components are thick-walled, heavy tubulars similar to a drill pipe. They are often put in the drill string just above the bit to provide additional weight-on-bit.

(e) Rotary. The rotary or rotary table converts mechanical or electrical energy from the rig´s power plant to the drill string torque. Located on the rig floor, it is the drive mechanism for rotary drilling from the surface. The rotary table transmits torque to the drill string through a special length of pipe called the kelly.

(f) Mud. Drilling fluid can take any of several forms. The most common is a water-based solution of clay minerals from which the term "mud" is drawn, but drilling muds can also be oil-based. Air is sometimes used in conjunction with or in place of mud, and other fluids can also be used. The type of drilling fluid that is used depends on the formation being drilled. The top parts of most hydrothermal reservoirs are drilled with water-based muds. The mud serves several functions in the drilling of a well. Some of the most important are to:

- lubricate, clean and cool the bit and drill string to reduce friction losses,
- maximise the rate of penetration,
- lift the drill cuttings from the formation face to the surface,
- balance any downhole pressures to prevent uncontrolled influx of formation fluids into the well,
- lubricate contact between the borehole wall and the drill string and casing,
- minimise borehole instability,
- avoid the borehole collapsing or fracturing and lost circulation,

- protect fragile formations from chemical or physical damage,
- minimise (toxic) drilling waste,

and

- maximise kick detection sensitivity.

(g) Downhole motors. In some situations the drilling torque is applied not at the surface by the rotary table, but downhole by a downhold mud motor. When this occurs, the power is carried down the drill string in the form of hydraulic energy in the mud. It is imparted by the mud pumps on the surface and extracted by either a positive displacement pump or a turbine.

(h) Casing. Once a portion of a hole is drilled, it often must be stabilised against collapse and other possible problems. This is done by lining the hole with steel pipe called the casing. Since the formations penetrated by a single borehole can be quite different, it is necessary to case major proportions of a well as they are drilled. As a result, the normal well reduces in diameter as it gets deeper since sequentially smaller diameter casings must be used. Often the bottom part of a geothermal well is left open in the production interval in order to maximise production or a liner is used.

(i) Cement. The casing strings that line the hole are set in place and grouted into the formations with cement. This protects and stabilises the casing and also protects formations and aquifers via a sealing process.

(j) Logging. Several times during and after the drilling of a well it may be logged by measuring equipment that is lowered into it. The logging tools are used to measure the characteristics of the hole and the formations it penetrates. These tools are typically lowered into the well with a cable or wireline.

(k) Measurement-while-drilling (MWD). An MWD system is built around sensors at the bottom of the drill string that measure various parameters such as the physical orientation of the hole and the nature of the formation. The measurements are telemetered to the surface by a mud-pressure pulsing system and displayed to the driller. Because of high operating costs and their limitations at high temperatures, MWD systems are commonly used only on the directional portions of expensive wells, and they are not often used in geothermal drilling.

2.5.3 Geothermal well drilling costs

Geothermal wells typically cost from two to four times the of an oil or gas well drilled to the same depth; see Fig. 2.6 [Kelsey and Carson (1987)]. The main areas where geothermal well drilling differs from oil and gas well drilling are the following:

(i) Temperature: Oil and gas wells rarely exceed 100°C while deep geothermal wells are profitable only when the temperature exceeds 250°C. High temperatures detrimentally affect elastometric components, drilling fluids, tubular goods (drill pipe and casing), and completion cements.

(ii) Formations: Geothermal resources are generally found in areas of igneous and/or metamorphic geology, which are normally very hard rock and abrasive formations.

(iii) Fluids: The highly saline nature of geothermal fluids and reservoirs tends to increase the corrosion rates on downhole components, and the dissolved solids contained in the production fluid can cause excessive scaling problems during the production phase.

(iv) Pressure: Geothermal reservoirs are typically underpressured meaning that formation in-situ pressure is less than the hydrostatic pressure. This leads to problems of lost circulation (drilling fluid not returning to the surface) and poor cementing of the casing during the completion phase. Both problems arise because fluids in the wellbore will preferentially flow into the formation rather than returning up the annulus to the surface. This is not exclusively a geothermal problem, but it is more frequent and severe than in oil and gas drilling because of the nature of hydrothermal reservoirs.

In the majority of geothermal wells drilled, all the above conditions occur to some degree. A combination of these conditions with common drilling problems (such as cementing, lost circulation, stuck pipe, fishing, high temperature and others) can increase significantly the overall cost of the drilling and completion process [Carson and Lin (1982)]. Due to the range of drilling conditions, the overall drilling cost of geothermal wells ranges between US$ 410 and US$ 820 per meter of holes drilled [Capuano (1992)]. Considering these costs and an average well depth of 2000 m, the overall cost of a geothermal well ranges between 0.8 and 1.6 millions of US dollars. However, there are some cases reported in the Mexican geothermal well drilling industry that indicate the drilling cost can be increased up to US$ 1000 per meter. Accurate data of the Mexican geothermal well costs are confidential and are consequently unavailable.

At present around 400 wells have been drilled in the Mexican geothermal industry for exploitation and exploration purposes. The drilling experience indicates that the well depth and the drilling time have a strong dependence on the total drilling cost of a completed geothermal well; see Figs. 2.7 and 2.8 [Edwards et al (1982); Garcia (1996)]. Major contributing factors to the total well drilling cost are related to: drilling, cementing, casing, logging, completion and miscellaneous activities.

Approximately 47 % of this cost is attributed to the drilling factor which includes all the costs related to: the drilling contract, the equipment rent, drilling fluids, chemical additives, site location, construction and restoration; see Fig. 2.9.

2.5.4 Drilling problems

Problems that arise in geothermal drilling and completion account for a significant portion of geothermal well costs. Drilling and completion problems play a larger part in geothermal drilling than they do in drilling for oil and gas wells. To a certain extent this can be attributed to the nature of the resource and the fact that most geothermal drilling and completion methods have been directly adapted from petroleum drilling technology.

The most common severe problems encountered in drilling and completing geothermal wells are lost circulation, stuck pipe, inadequate cementing, the presence of high temperature, corrosion, environmental problems, fishing, side tracking, casing and rig problems. Even though the occurrence of all of these problems have an impact on the overall drilling cost, the lost circulation and the estimation or prediction of the bottomhole temperatures are the major problems that the geothermal well drilling industry needs to solve because they affect the other common problems. For example, lost circulation can cause or aggravate stuck pipe and cementing problems, or it can affect significantly the temperature distribution in the wellbore. On the other hand, the presence of high temperature can affect the stability of the drilling fluids (muds) and cement slurries as well as the lifetime of the wellhead control equipment (drill bits, logging tools, seals, etc).

Lost circulation. Lost circulation of mud is the most troublesome and costly problem in drilling in oil and geothermal wells. Lost circulation is the partial or total loss to the formation voids of the drilling fluid used during drilling operations [Fig. 2.10A; Messenger (1981)].

Mud losses vary in type, severity and location in the hole. This problem can occur in several types of formations, including highly permeable formations (unconsolidated), fractured formations and cavernous zones containing large voids or channels; see Fig. 2.11 [Chilingarian and Vorabutr (1981)]. When this problem takes place, the fluid column loses at least some of its ability to control wellbore pressures and perform its other functions. A key factor in preventing lost circulation is to keep control of the mud density in order to keep the mud hydrostatic pressure as low as possible yet high enough to control formation pressures in other well zones.

Another important consideration is the depth to which the casing string is installed. If the casing is set too shallow, the formation below the bottom of the casing may not be strong enough to support the mud hydrostatic pressure needed to control formation pressures lower in the hole. When this drilling problem occurs, it is corrected by means of a sealing process where plugging materials are added to the mud. Under these conditions, a precise volume of plugging materials is circulated to the lost circulation zone to seal it off; see Fig. 2.10B.

Temperature logging. Geothermal reservoirs may contain fluids with temperatures that sometimes can reach 500 °C, compared with 100 to 200 °C in deep oil and gas wells. So, it is expected that high temperature can produce problems with drilling fluids, drill bits, logging tools, cement slurries, cementing procedures and wellhead control equipment. For example, excessive temperature can adversely affect the performance of conventional tricone rotary drill bits. Drill bit failure is a major problem in drilling high temperature geothermal wells because bearing seals cannot resist these hot environments.

Moreover, if a combination of high temperature with lost circulation problems takes place in under pressured fractures, this combination can produce poor cement bonding.

Thus, poor cement bonding in turn can result in severe casing problems due to high temperature. In order to prevent the occurrence of these problems, accurate temperature measurements of the geothermal formation are required. These measurements can be used to select the most appropiate materials for the geothermal well drilling operations reducing in this way the overall geothermal well drilling cost.

In relation to this, downhole logging tools are being used in the geothermal well drilling industry. However, there is a limitation with logging tools capable of operating at these high temperatures. Commonly, temperature logging devices can be classified as: (i) downhole recording systems (maximum recording mercury thermometers), (ii) mechanical recording thermometers and (iii) surface recording systems [temperature sensors usually communicated by cable linking or optical fiber sensors; Hurtig et al (1994)]. During the early days of well logging, temperature logging was a major part of the total logging capability. Particularly, borehole temperature data derived from these kinds of measurements can be used in the following geothermal well drilling applications:

(a) determination of geothermal gradient,

(b) determination of lithology,

(c) location of structural anomalies,

(d) location of fluid inflow zones,

(e) location of fluid injection (or lost circulation) zones,

(f) location of artificially fractured zones,

(g) location of casing leaks and channels,

(h) location of primary cement top,

(i) location of squeeze cement zones,

and

(j) determination of hole size changes (caves).

Typically, logging activies have represented up to 7 % of the overall well drilling cost; see Fig. 2.9.

2.5.5 Thermal behaviour of the drilling fluid circulation

In the process of drilling, the drilling fluid (mud) is circulated through the drill pipes and hole, and so can change the temperature of the formation (rock) through which the hole is being drilled [Raymond (1969); Thompson and Burgess (1985); Arnold (1990); Beirute (1991)].

The circulation of the mud during the drilling operations is shown schematically in Fig. 2.12. Basically, the process of circulation can be described in three main regions.

(i) Mud enters the drill pipe at the surface and flows down the drill pipe.

(ii) Mud exits the drill pipe through the bit and enters the annulus at the bottom.

(iii) Mud passes up the annulus and returns to the surface.

The mud temperature in each region is dependent upon a number of different thermal processes. In region 1, the mud enters the drill pipe at a specified temperature, T_0. As the fluid passes down the pipe in the z direction, its temperature is determined by the rate of heat convection down the drill pipe and heat exchange with the annulus fluid, and time, $T_1(z,t)$. Region 2 of the circulation process merely requires that the mud temperature at the exit of the drill pipe be the same as the mud temperature at the entrance of the annulus, $T_2(z,t)$.

Thus in region 3, where the mud flows up the annulus, its temperature is determined by the rate of heat convection up the annulus, the rate of heat exchange between the annulus and the drill pipe, the rate of heat exchange between the formation adjacent to the annulus and the mud in the annulus, and time. Finally, if there is no lost circulation of mud, it returns to the surface with a temperature $T_2(0,t)$. Thus the mud temperature is a function of the circulation rate, circulation time, fluid properties, and, most importantly, the heat transfer characteristics of the conduit and its associated film heat transfer coefficients.

The thermal analysis of this physical model shows that this circulation process can be defined as a heat exchange system. In such a process, mud moves downward inside the drill pipe and upward through the annulus between the rods and the drill hole. The system thus acts as a counterflow heat exchanger from which there is an additional heat exchange to the rock outside the drill hole [Jaeger (1961)].

Temperature distributions in presence of lost circulation problems. As was mentioned, the physical model of the overall well drilling system given in the previous section shows the thermal behaviour under ideal drilling conditions i.e., no fluid losses. This ideal behaviour is often modified due to the occurrence of drilling problems. Several types of problems can take place. Lost circulation of mud is a very common problem that normally occurs during drilling activities. This problem leads to a more complex heat transfer model because mud lost to the formation considerably affects the surrounding formation temperatures due to the heat convection processes involved. Under these conditions, the total mud mass flowrate present in a wellbore is given by the following equation:

$$W_1 = W_2 + W_3 \tag{1}$$

where W_1 and W_2 are the inlet and oulet mud mass flowrates, respectively and W_3 represents the amount of mud lost during circulation (see Fig. 2.10A).

Normally, during well drilling operations some service companies frequently perform temperature surveys to locate these lost circulation zones [Chilingarian and Vorabutr (1981)].

2.6 Static Formation Temperatures

Temperature is one of the most important parameters of the geothermal reservoirs that need to be accurately estimated. This is necessary in order to define the feasibility of exploiting these resources efficiently for electric power generation or process heat applications. The static formation temperature (undisturbed downhole temperature) is one of the most critical parameters used as an indicator of the available energy confined in a geothermal reservoir [Dowdle and Cobb (1975)].

The static formation temperature should be determined as accurately as possible for a number of reasons. In-situ saturation distributions computed from resistivity logs require accurate formation water resistivities that depend on temperature. Reliable estimates of downhole temperatures are important in designing the deep-well drilling and cementing programme and in evaluating the reservoir/fluid formation volume factors. Also, the static temperature is necessary for establishing geothermal gradients that can be used to estimate the temperatures of deeper zones [Beirute (1991)]. More recently, new exploration techniques have used temperature as a mappable proximity parameter. In general form, an accurate estimation of the undisturbed temperature is required for the:

(i) estimation of the heat content in geothermal reservoirs,

(ii) interpretation of electrical logs,

(iii) design of the drilling and completion programmes for geothermal wells,

(iv) establishment of the thermal gradients,

and

(v) evaluation of the volumetric formation factors (fluid-reservoir).

2.6.1 Importance of determining static formation temperatures in geothermal wells.

One of the consequences of the well drilling process is that the formation (rock) is cooled because of the continuous mud circulation. Thus a slow recovery back to the geothermal temperature only occurs when drilling and circulation cease. Complete temperature recovery in a new well may take anywhere from a few hours to a few months, depending on the formation, well characteristics, and the mud circulation time.

Figure 2.13 shows the temperature distribution found in a typical geothermal well during drilling [Raymond (1969)]. From Fig. 2.13, several thermal processes can be observed. During the mud circulation, a cooling process occurs at the bottomhole, while the upper parts of the well are heated. At the mid well depth no heating or cooling occurs. Once mud circulation is stopped, the bottom-hole temperature tends to attain the thermal equilibrium or the static formation temperature (SFT). This trend is shown as an asymptotic dashed line. An inverse thermal process can be observed near the surface, while the mid-well temperature profile remains nearly constant.

This thermal behaviour indicates that an accurate estimate of SFT requires long shut-in periods. However, a long wait for complete temperature recovery could cause a sizeable increase in drilling costs. Hence a less time consuming method is needed to calculate SFT using early shut-in data.

When lost circulation problems occur during the well drilling process, the thermal behaviour of the system is more complex due to the different number of heat transfer processes involved. Consequently, the methods used to estimate SFT would be more complicated. Normally, temperatures are recorded during logging operations in the mud circulation process or during the warm-up period of the well. These measured temperatures are usually lower than the static temperature due to the cooling effect of the mud circulation process and because they are logged at early times during shut-in (typically 6-24 hours after ceasing mud circulation).

The accurate prediction of the undisturbed formation temperature and the temperature distribution in the whole geothermal system (wellbore and surroundings) throughout drilling operations have long been a clear objective that will be attained during this research work.

2.7 References

V.M. Arellano, Introduccion a la energia geotermica, Curso de divulgacion sobre geotermia (Cap. 1), Eds. V.M. Arellano y R. Ayala, IV Congreso Nacional Asociacion Geotermica Mexicana (AGM), Guadalajara, Jalisco, Mexico, p. 1-25 (1996).

H.C.H. Armstead, Geothermal energy: its past, present and future contributions to energy, 2nd. Edition, London, U.K. (1983).

F.C. Arnold, Temperature variation in a circulating wellbore fluid, Journal of Energy Resources Technology, **112** 79-83 (1990).

R.M. Beirute, A circulating and shut-in well-temperature-profile simulator, Journal of Petroleum Technology, **September** 1140-1146 (1991).

A. Bottai and U. Cigni, Completion techniques in deep geothermal drilling, Geothermics, **14** 309-314 (1985).

J.C. Bresee, Geothermal energy in Europe: The Soultz hot dry rock project, Gordon & Breach, U.K. (1992).

L.E. Capuano, Geothermal versus oil and gas: A comparison of drilling practices, Geothermal Resources Council Bulletin, **April** 113-116 (1992).

C.C. Carson and Y.T. Lin, The impact of common problems in geothermal drilling and completion, Geothermal Resources Council Bulletin, Transactions **6** 195-198 (1982).

G.V. Chilingarian and P. Vorabutr, Drilling and drilling fluids, lost circulation (chapter 14), Developments in Petroleum Science 11, Elsevier Amsterdam, Oxford, New York, USA **11** 537-557 (1981).

Comision Federal de Electricidad, Home page: Installed capacity of electricity in Mexico, Internet **www.cfe.gob.mex/international** (1997).

M.H. Dickson and M. Fanelli, Geothermal energy, UNESCO Energy Engineering Learning Package, John Wiley Ltd, U.K. (1995).

W.L. Dowdle and W.M. Cobb, Static formation temperature from well logs - An empirical method, Journal of Petroleum Technology, **November** 1326-1330 (1975).

L.M. Edwards, G.V. Chilingar, H.H. Rieke and W.H. Fertl, Handook of geothermal energy, Gulf Publishing Company, Book Division, Houston, Tx., USA (1982).

D. Freeston, Direct uses of geothermal energy 1995, Geothermics, **25** (2) 189-214 (1996).

A. Garcia, Simulacion de los fenomenos de flujo en pozos geotermicos: desarrollos y aplicaciones, Boletin IIE, **Julio/Agosto** 172-181 (1996).

G. Hiriart-LeBert and L.C.A. Gutierrez-Negrin, Geothermal development in Mexico, Geothermal Resources Council, Transactions, **18** 269-274 (1994).

E. Hurtig, S. Groβwig, M. Jobmann, K. Kühn and P. Marshall, Fibre-optic temperature measurements in shallow boreholes: experimental application, for fluid logging, Geothermics, 23 355-364 (1994).

G.W. Huttrer, The status of world geothermal power production 1990-1994, Proc. World Geothermal Congress 1995, Florence, Italy, **1** 3-14 (1995).

J.C. Jaeger, The effect of the drilling fluid on temperatures measured in bore holes, Journal of Geophysical Research, **66** (2) 563-569 (1961).

J. Kelsey and C.C. Carson, Geothermal drilling - drilling for geothermal energy, Geothermal Science & Technology, **1** (1) 39-61 (1987).

J.U. Messenger, Lost circulation, Penn Well Books, PennWell Publishing Company, Tulsa Oklahoma, U.S.A., ISBN 0-87814-175-8 p. 108 (1981).

J.M. Morales, A. Garcia and S. Santoyo-Gutierrez, Developments in geothermal energy in Mexico - part thirty-one: predictions of geothermal cement durability from field tests, J. Heat Recovery Systems and CHP, **10** (5/6) 491-498 (1990).

P. Mulás, D. Nieva and F.A. Holland, Developments in geothermal energy in Mexico-part one: general considerations, J. Heat Recovery Systems and CHP, **5** (4) 277-283 (1985).

B.W.. Pipkin, Geology and the environment, West Publishing Company, New York, USA, pp. 116 (1994).

J.L. Quijano, Present development of the Los Azufres geothermal field in Mexico, Geothermal Resources Council, Bulletin August, pp. 168-173, (1993).

J.L. Quijano and L.C.A. Gutierrez-Negrin, Present situation of geothermics in Mexico, Proc. World Geothermal Congress 1995, Florence, Italy **1** 245-250 (1995).

L.R. Raymond, Temperature distribution in a circulating drilling fluid, Journal of Petroleum Technology, **March** 333-341 (1969).

E. Santoyo, Modelacion matematica de yacimientos geotermicos bifasicos en estado estacionario para la determinacion de perfiles de composicion y temperatura, Tesis de Maestria, UAEM-Morelos, Mexico, 81 p. (1991).

S. Santoyo-Gutierrez, A. Garcia, M. Morales, J. Perezyera and A. Rosas, Applied technology in the solution of geothermal drilling problems of deep wells in La Primavera caldera (Mexico), Journal of Volcanology and Geothermal Research, **47** 195-208 (1991).

V. Stefansson, WEC Survey of energy resources, World Energy Council, London, U.K., p. 294 (1995).

M. Thompson and T.M. Burgess, The prediction and interpretation of downhole mud temperature while drilling, Proc. of the 60th Annual Technical Conference and Exhibition of the Society of Petroleum Engineers, Las Vegas NV, USA, **September** 22-25, SPE 14180, p. 12. (1985).

D.E. White, L.J.P. Muffler and A.H. Truesdell, Vapor-dominated hydrothermal system compared with hot-water system. Economic Geology, **66** 75-97 (1971).

Country	Installed Capacity MWe	Annual Output GWh
United States (USA)	2,817	16,491
Philippines	1,051	5,470
Mexico	753	5,877
Italy	626	3,417
Indonesia	309	1,048
Japan	299	1,722
New Zealand	286	2,193
El Salvador	105	419
Nicaragua	70	290
Costa Rica	60	447
Iceland	50	265
Kenya	45	348
China	28	98
Turkey	20	68
Russian Fed.	11	25
France	4	24
Portugal	3	na
Romania	2	na
Greece	2	na
Argentine	0.6	na
Thailand	0.3	na
Zambia	0.2	na
Others	7	40
Total	6,549	38,242

Table 2.1

1994 World geothermal installed and generation power; na: not available [data taken from: Hiriart-LeBert and Gutierrez Negrin (1994); Stefansson (1995)].

Country	Installed Capacity MWt	Annual Output GWh
China	2,143	5,527
United States (USA)	1,874	3,859
Iceland	1,443	5,878
Hungary	638	2,795
France	456	2,006
Japan	319	1,928
Italy	308	1,008
New Zealand	264	1,837
Georgia	245	2,136
Russian Fed.	210	673
Turkey	140	552
Romania	137	765
Switzerland	110	243
Slovakia	100	502
Tunisia	90	788
Serbia	80	660
Macedonia	70	142
Poland	63	206
Mexico	28	74
Others	329	1935
Total	9,047	33,514

Table 2.2

1994 World direct use of geothermal energy [data taken from: Hiriart-LeBert and Gutierrez-Negrin (1994); Stefansson (1995)].

Type	Number of Plants	Capacity (MWe)
Steam	28	13,370
Combined cycled	5	1,890
Geothermal	5	753
Turbo gas	29	1,178
Dual	1	2,100
Internal combustion	11	86
Mobile internal combustion	---	42
Mobile turbo gas	---	130
Hydroelectric	62	9,056
Nuclear	1	1,309
Coal	2	2,250
Aeolian	1	2
Total	145	32,166

Table 2.3

Total installed capacity of electricity in Mexico [CFE (1997)].

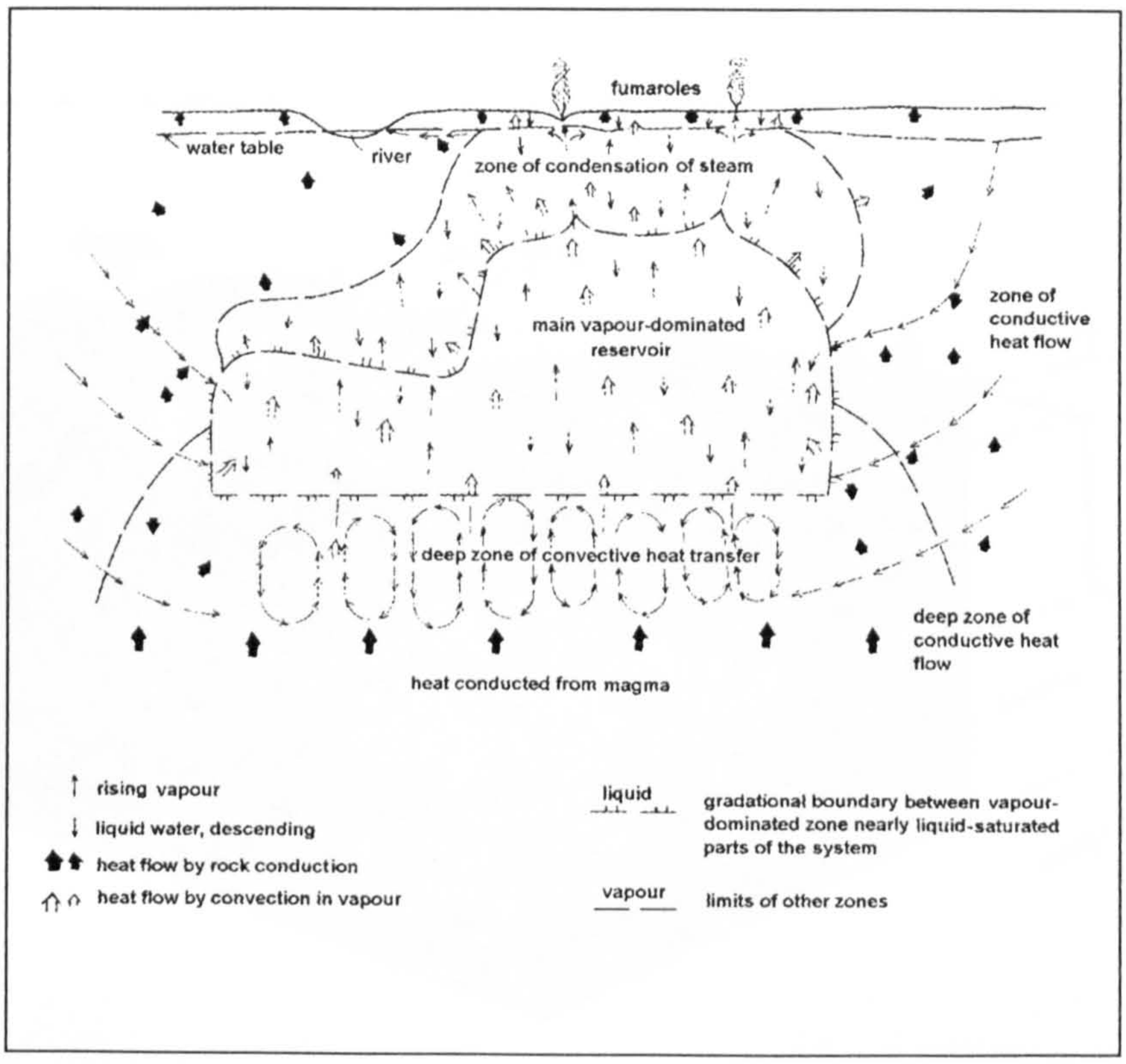

Fig. 2.1 Model of dynamic vapour-dominated geothermal reservoir surrounded by water saturated ground [modified after White et al (1971)].

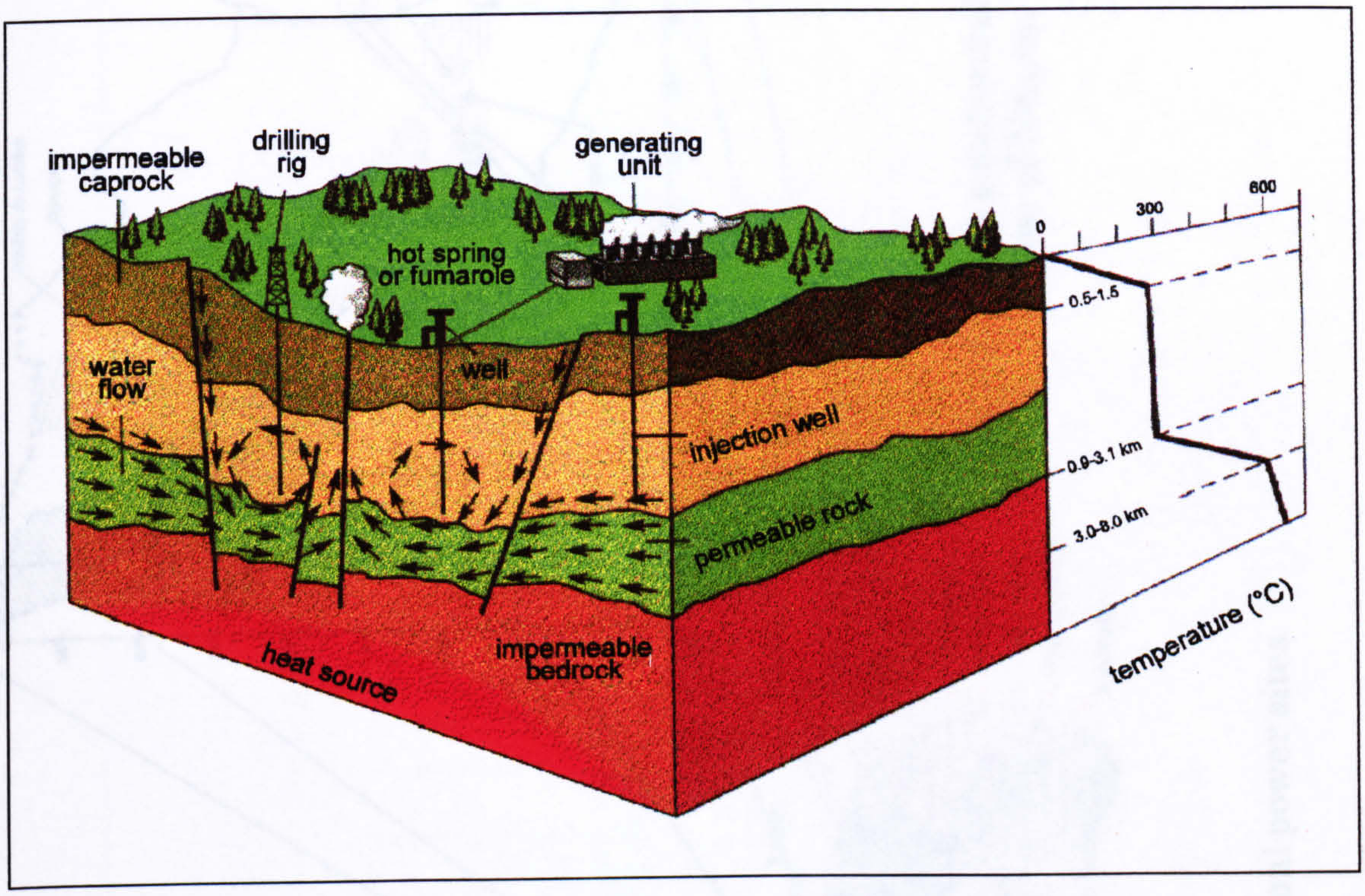

Fig. 2.2 Simplified diagram of the exploitation of a geothermal reservoir for electricity generating purposes [modified after Pipkin (1994)].

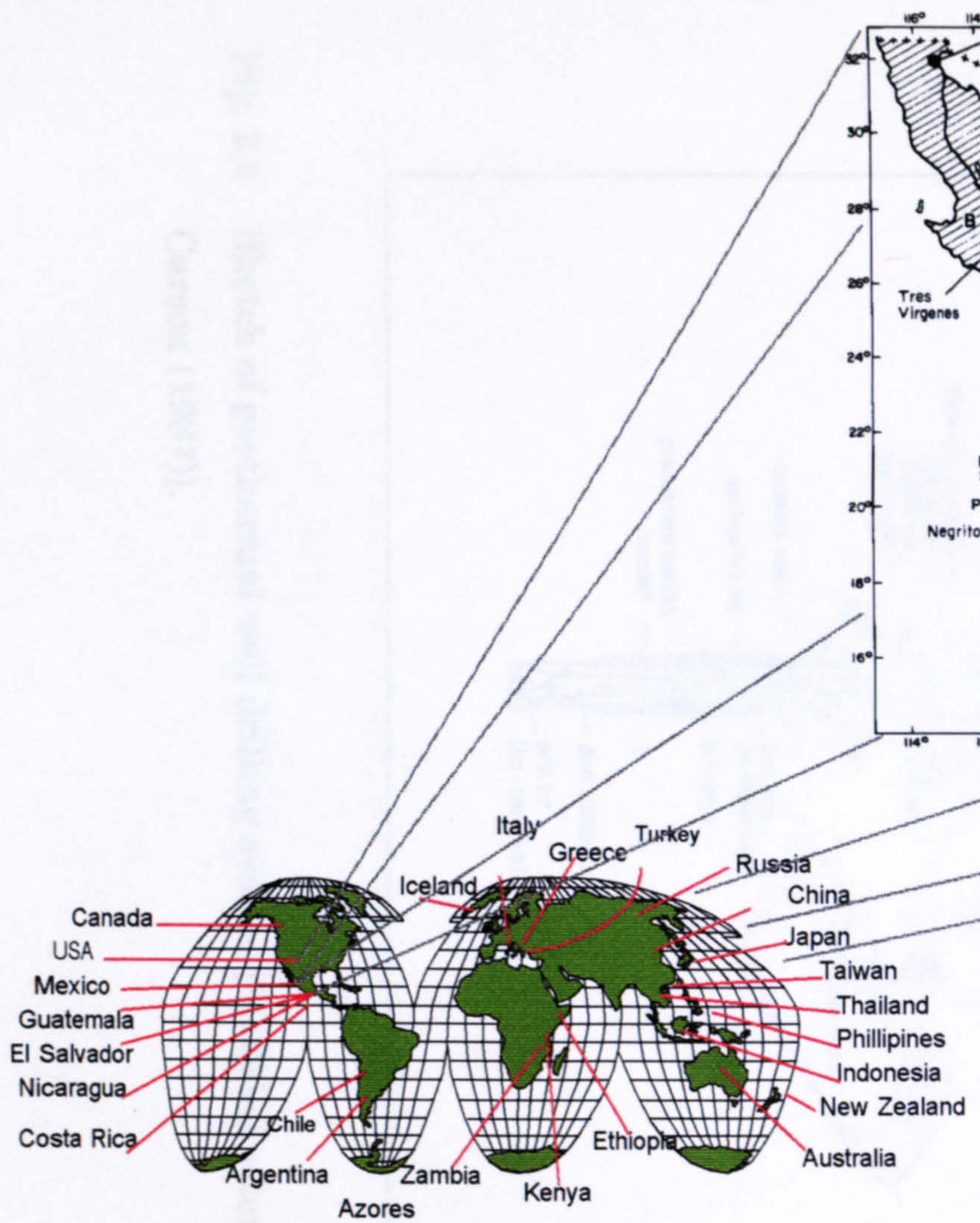

Fig. 2.3 Location of geothermal power sites.

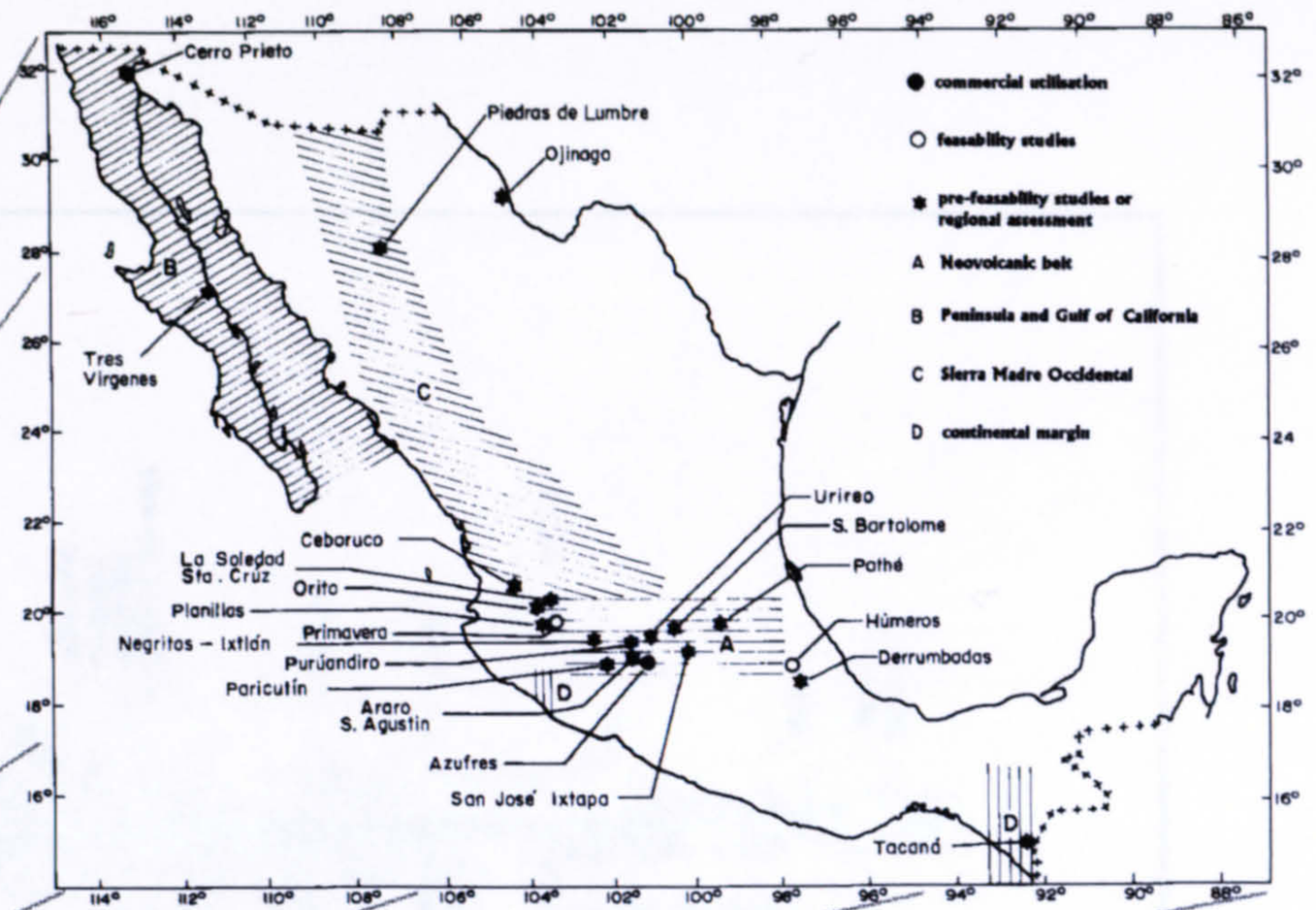

Fig. 2.4 Main geothermal fields and hydrothermal zones of Mexico.

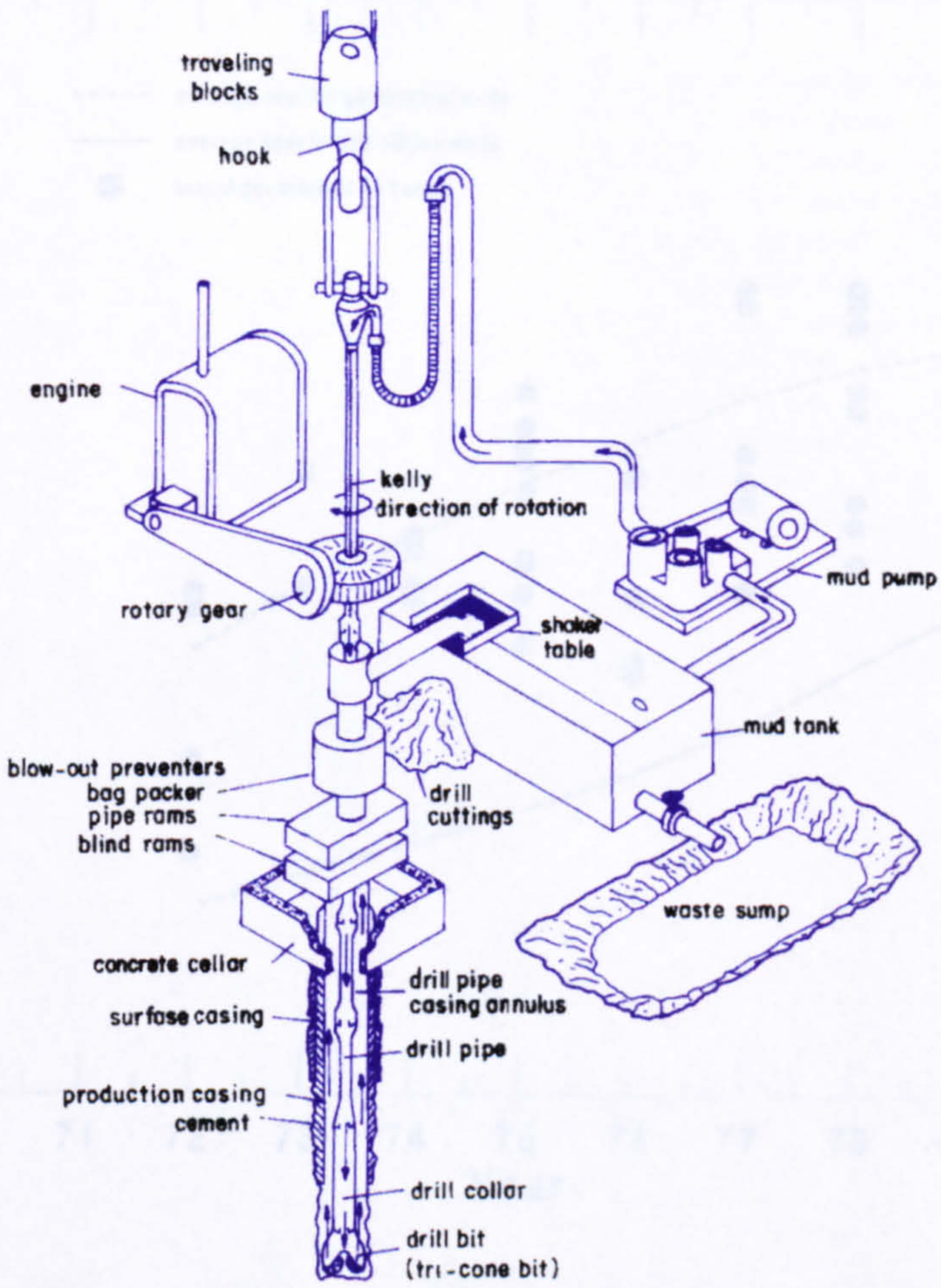

Fig. 2.5 Sketch of geothermal well drilling system [Modified after Kelsey and Carson (1987)].

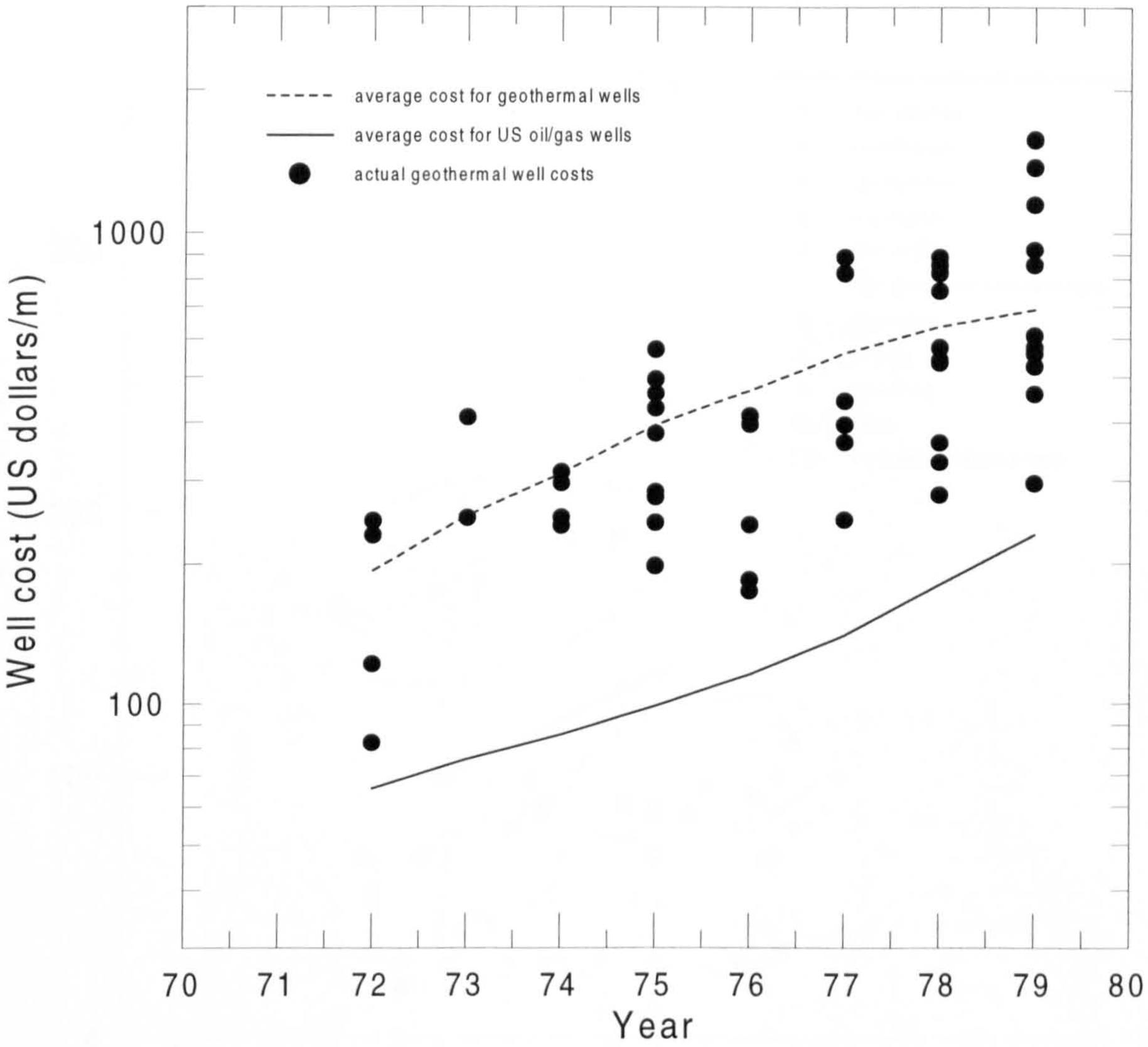

Fig. 2.6 Time cost escalation of completed geothermal wells [Modified after Carson and Yin (1982)].

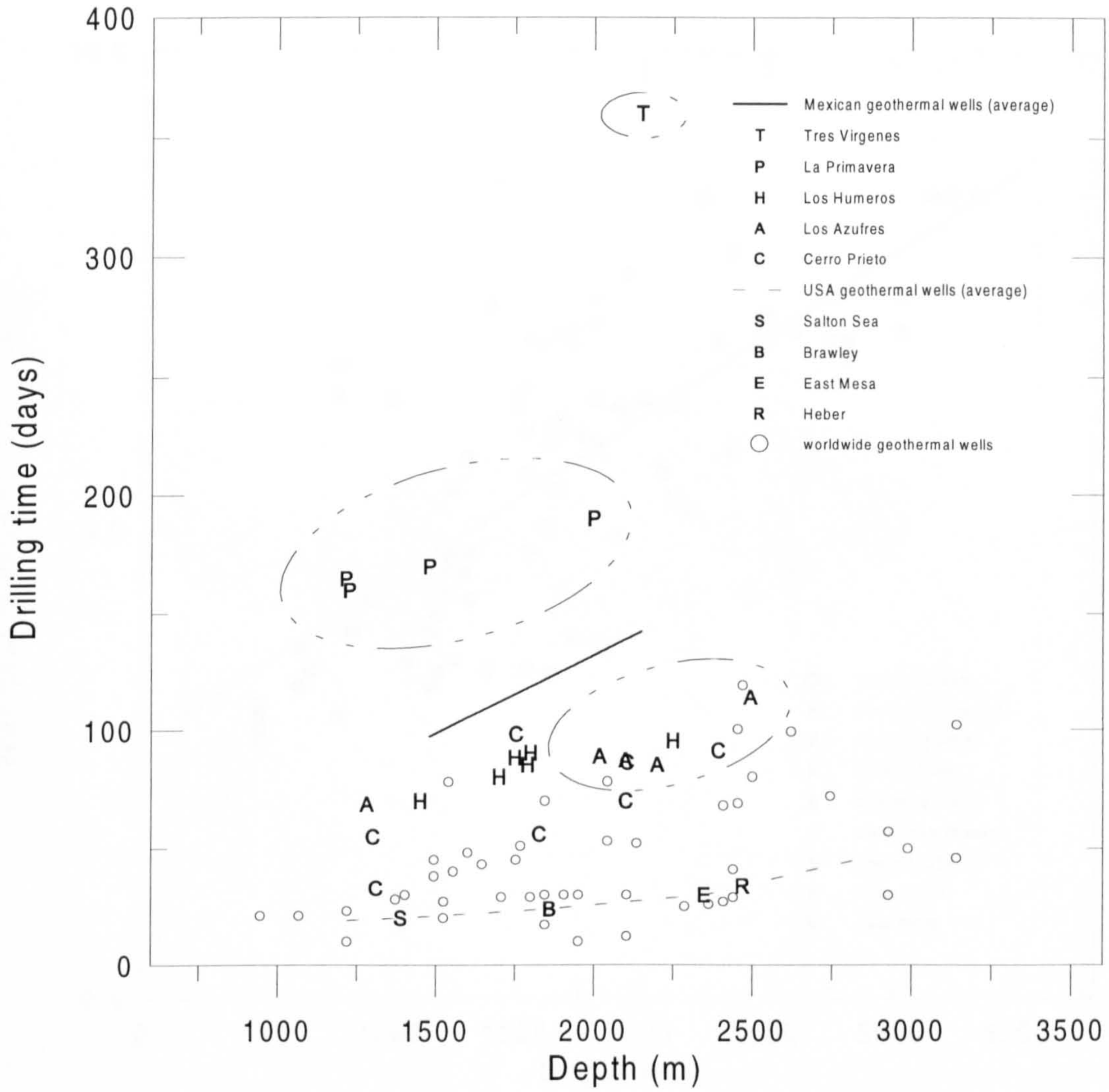

Fig. 2.7 Historic average drilling time data for wells in Mexican and American geothermal fields.

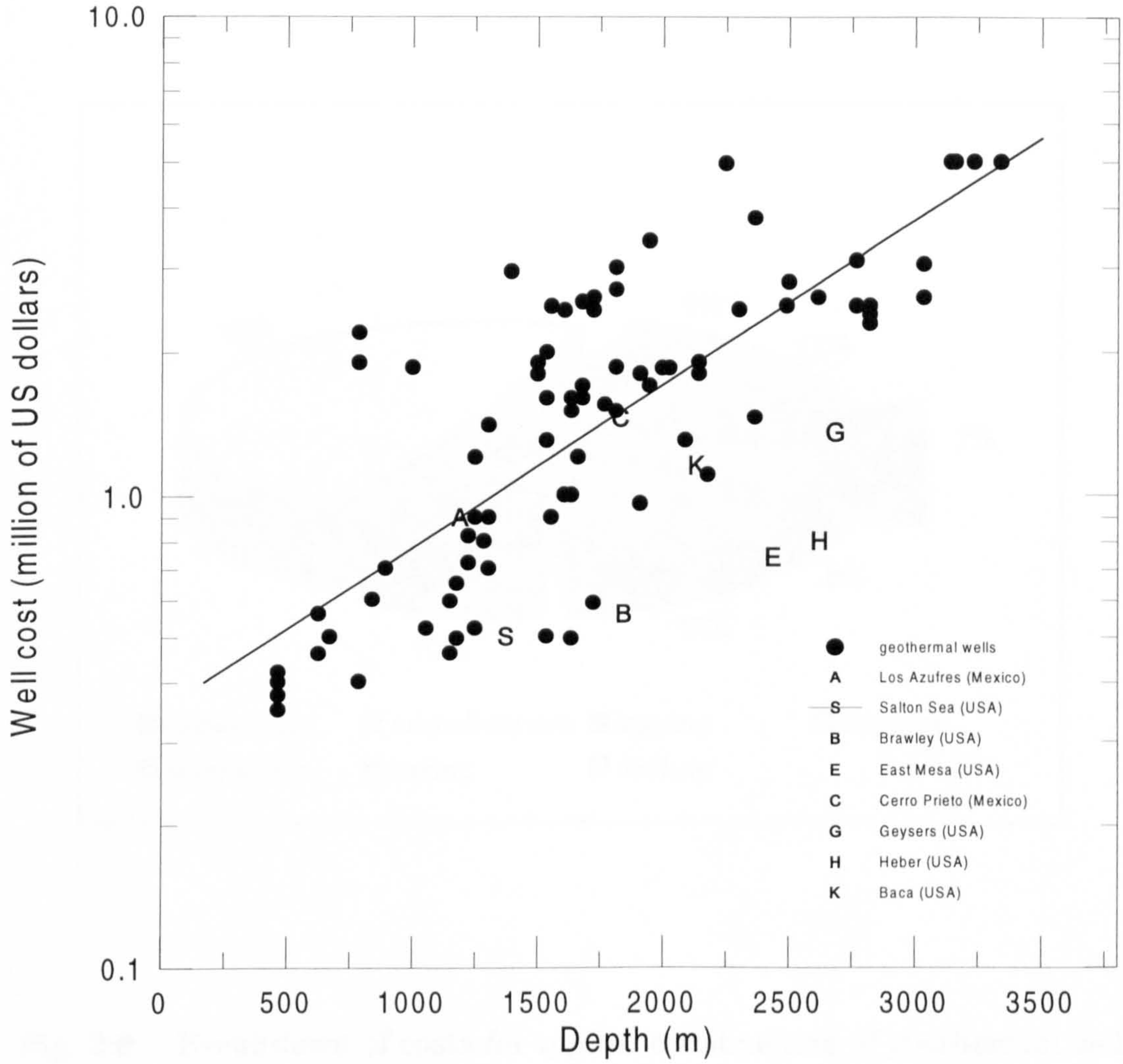

Fig. 2.8 Completed well cost pattern for Mexican and American geothermal wells.

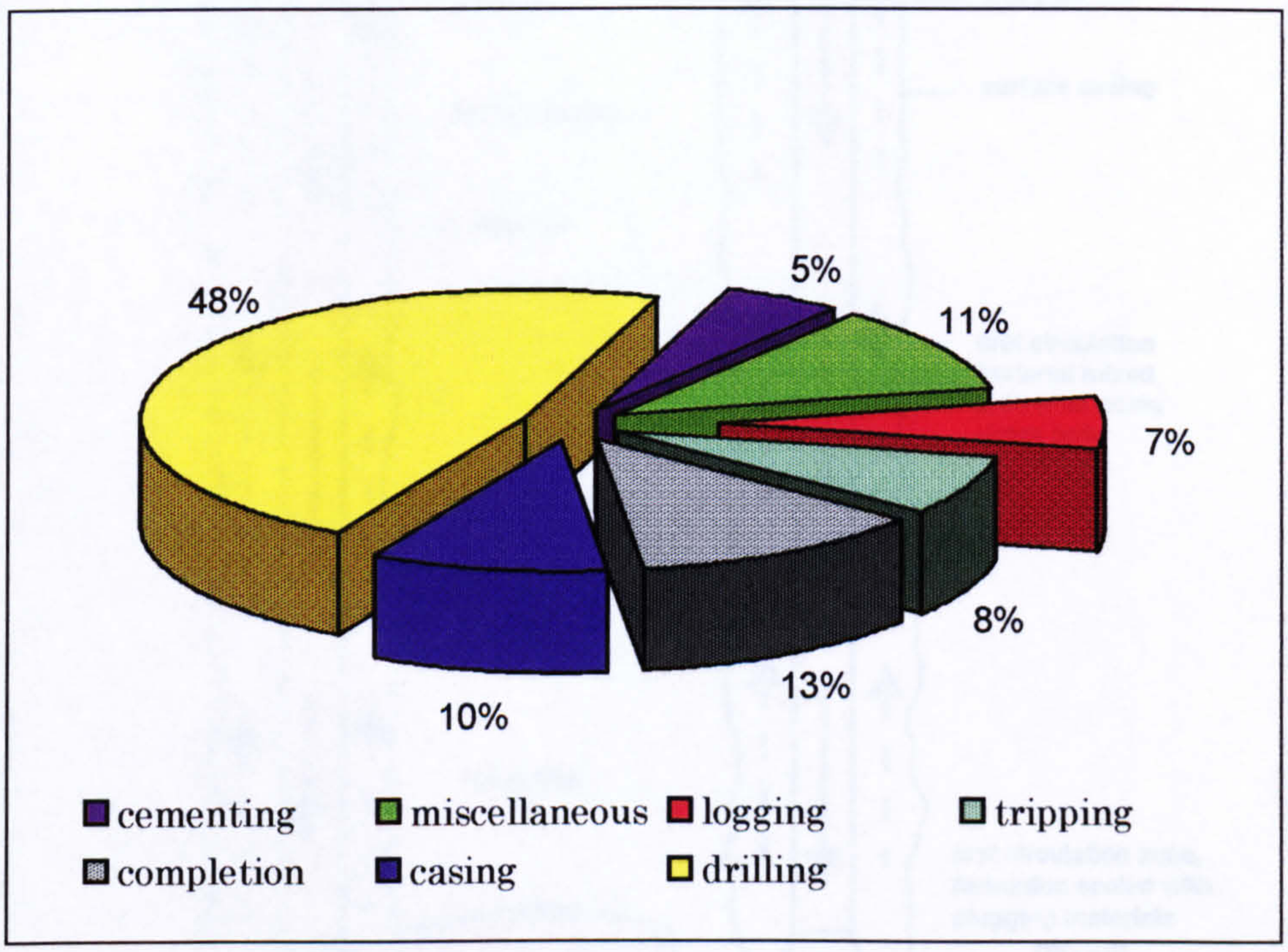

Fig. 2.9 Breakdown of costs for typical construction of geothermal wells. Percentages represent the total well cost by operation.

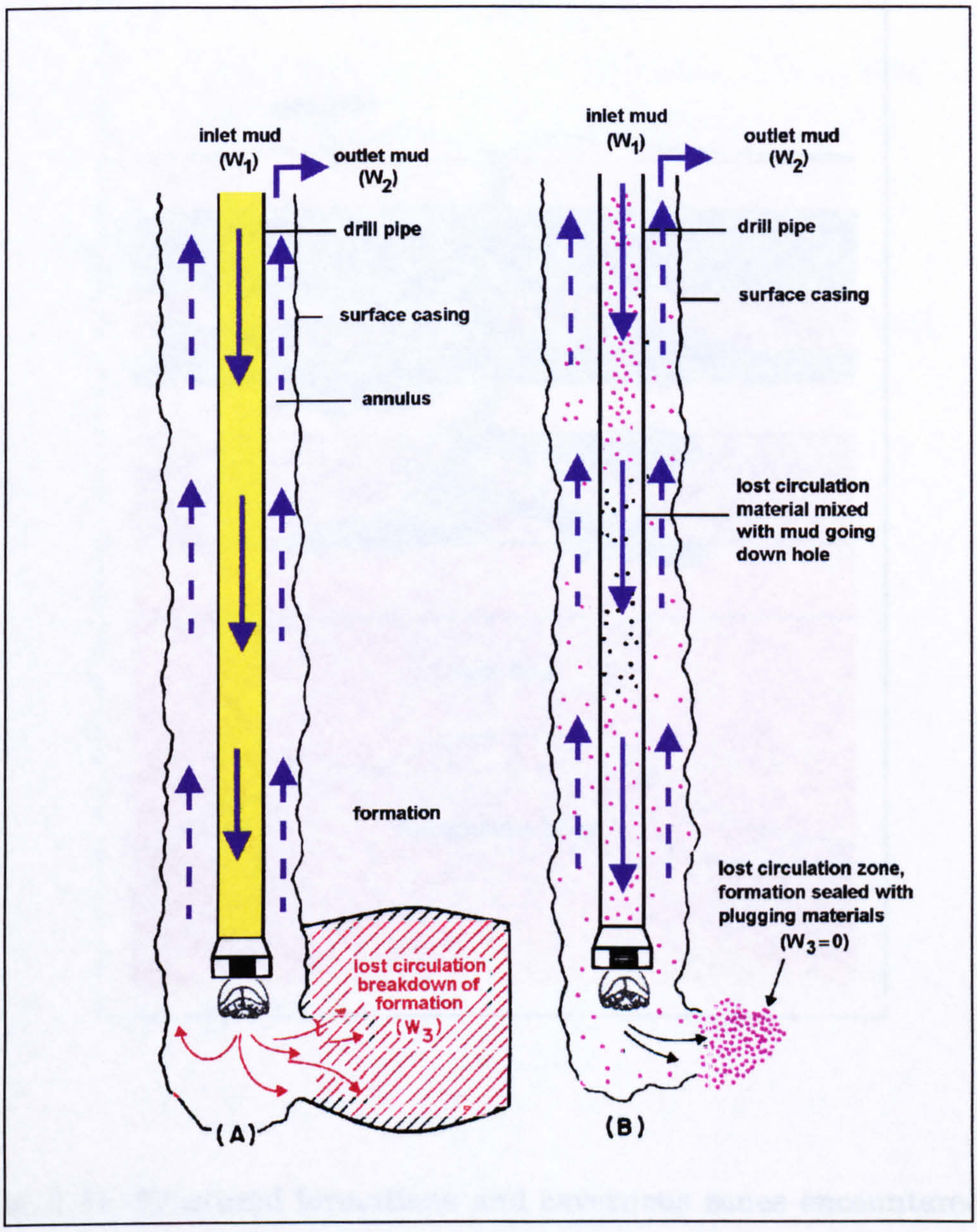

Fig. 2.10 Schematics of a lost circulation problem in a geothermal wellbore.

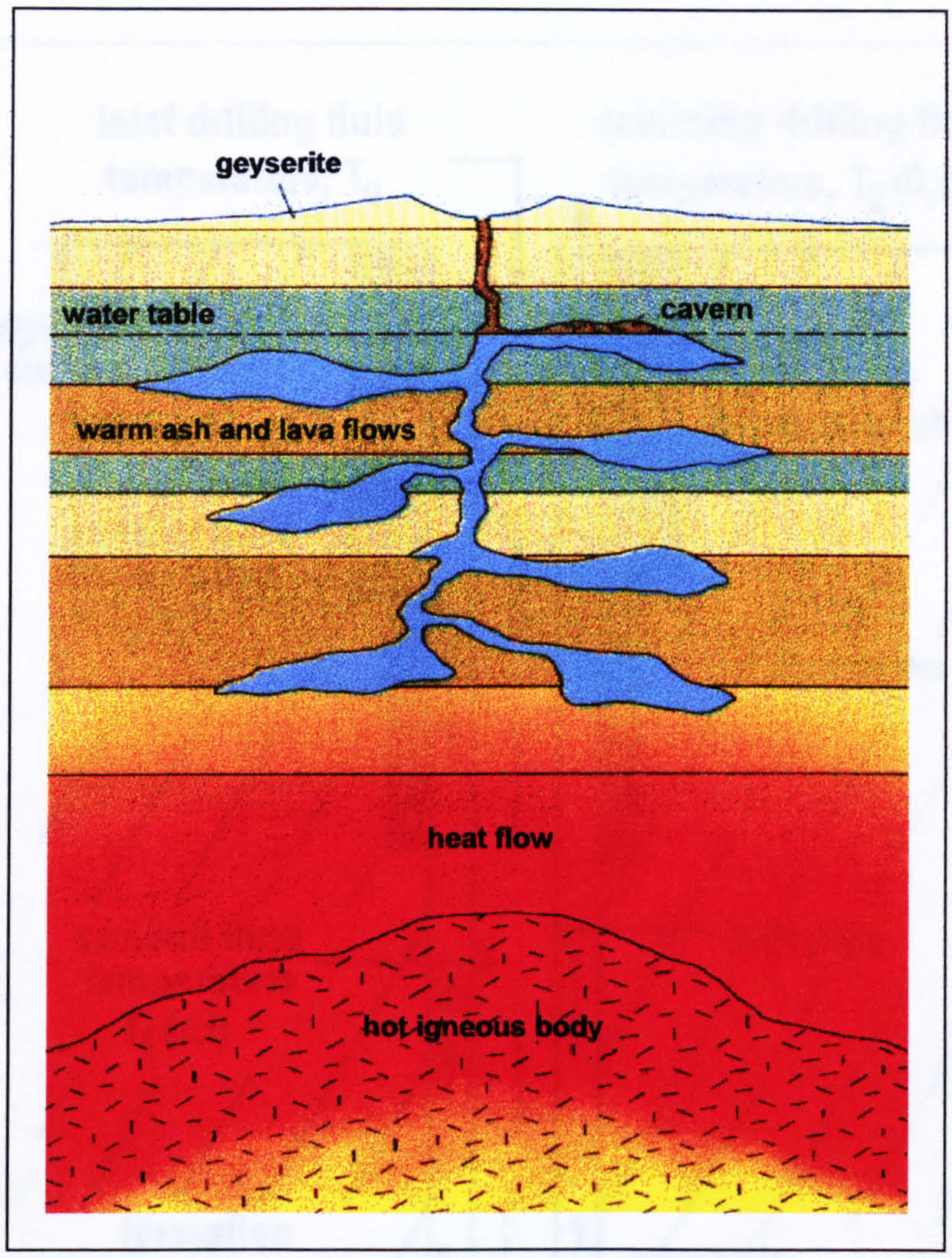

Fig. 2.11 Fractured formations and cavernous zones encountered in geothermal reservoirs located in volcanic areas [modified after Pipkin (1994)].

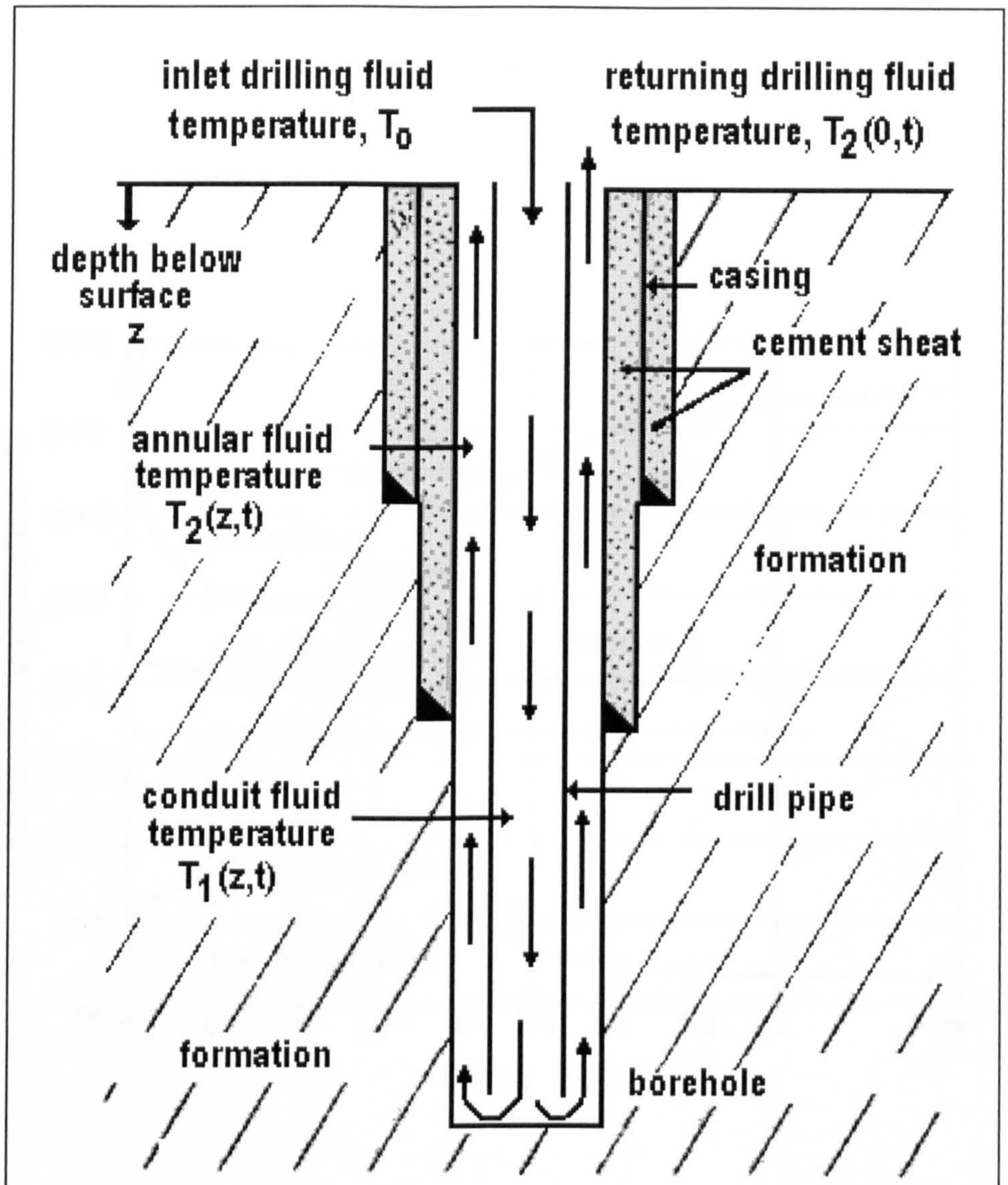

Fig. 2.12 Circulating drilling fluid system [Modified after Arnold (1990)].

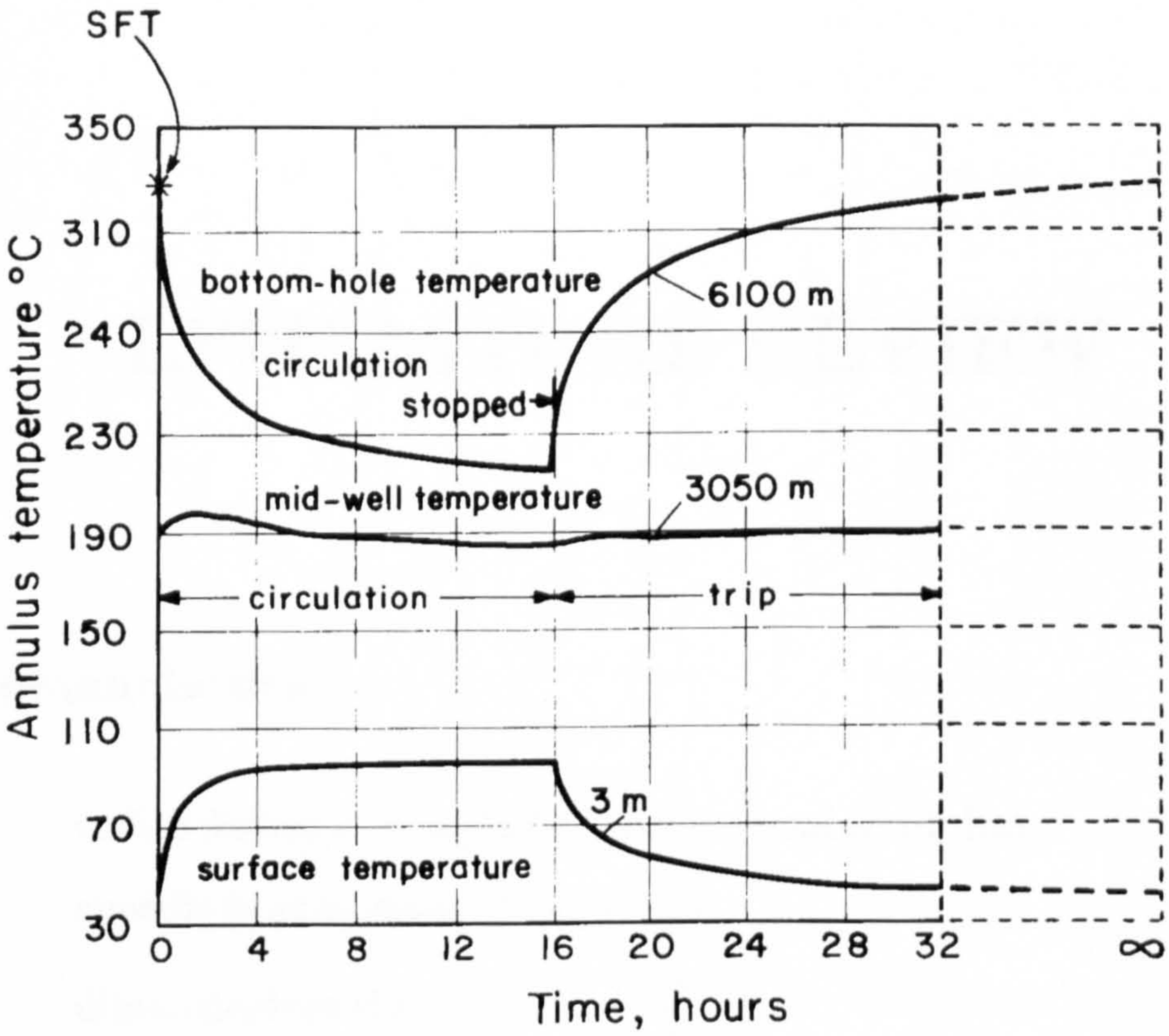

Fig. 2.13 Temperature distribution for various depths in a typical geothermal well during drilling operations [Modified after Raymond (1969)].

Chapter 3

LITERATURE REVIEW

3.1 Nomenclature

a	radial distance from well axis of thermal front [m]
Cp	specific heat capacity [J kg^{-1} $°C^{-1}$]
DHT	dimensionless Horner time, $\left(\frac{t'+\Delta t}{\Delta t}\right)$
k	thermal conductivity [W m^{-1} $°C^{-1}$]
Q	strength of line heat source [W m^{-1}]
Q'	$Q/4\pi k$ [°C]
r	radius [m]
r_D	dimensionless radius, $\left(\frac{r}{a}\right)$
r_w	wellbore radius [m]
t	time [s]
t'	duration of line heat source [s]

t_D	dimensionless time, $\left(\frac{t\,\alpha}{a^2}\right)$
T	temperature [°C]
T_i	static formation temperature, SFT [°C]
Δt	time elapsed since end of duration of heat source (shut-in time) [s]
ΔT	temperature transient [°C]

Greek symbols

α	formation thermal diffusivity, $k/\rho\, C_p$ [$m^2\ s^{-1}$]
γ	Euler's constant (0.5772...)
ρ	density [$kg\ m^{-3}$]

Special functions

E_i (-x)	exponential integral, $\int_x^{\infty} \frac{e^{-u}}{u} du$

3.2 Introduction

This chapter presents a literature review of the state of the art on the application of heat transfer studies to predict the thermal behaviour of a geothermal well under drilling and shut-in (thermal recovery) conditions. The review is divided into two sections. The first one is related to the main analytical methods available in the drilling literature for determining static formation temperatures. The second one is related to the analysis of the principal numerical simulators available for estimating the temperature distribution in and around geothermal wells under and after circulating conditions. The literature was analysed in order to gain more insight into the physical processes involved with the thermal behaviour of a drilling fluid circulation system which was described in previous chapters.

In order to estimate the true formation temperature from the bottomhole temperature (BHT) measurements, two classes of methods have been developed to represent the thermal disturbance associated with the drilling and the subsequent thermal recovery during the shut-in period. One class concentrates on the bottom region of the wellbore where BHTs are actually measured. These tools are normally referred to in the drilling industry as analytical methods. The other class (numerical simulators) attempts to simulate the evolution of the temperature of the complete drilling fluid column, and requires a detailed knowledge of the drilling history such as the drilling fluid composition, the inlet and outlet temperatures, the fluid circulation rate, the geothermal gradient, and the rock petrophysical properties.

3.3 Analytical Methods for Estimation of Static Formation Temperatures (SFT)

In the past, several analytical techniques have been proposed and used to infer undisturbed temperatures or SFTs. The first attempts were made by Bullard in 1947, who represented the effect of the circulation of drilling fluids as a constant line-source of heat on the wellbore axis. The drilling process was conventionally considered to introduce a constant temperature anomaly or heat supply to the circulating mud, starting at the time the drill bit cuts through the depth and ending at the time the well is shut-in.

Bullard (1947) modelled the return to the equilibrium process as a line-source of heat in an infinite and homogeneous medium under radial heat conduction conditions. Bullard's calculations demonstrated that for accurate geothermal measurements, the thermal recovery time of a well is very long (≈ 10 to 20 times the total time spent in drilling).

Lanchenbruch and Brewer (1959) extended Bullard's approach to include the effects of (i) the variation of the source strength with time, and (ii) the finite diameter of the well. The mathematical basis of this heat transfer model was expressed by means of the solution of the constant linear heat source equation for a duration t', which was described previously by Carslaw and Jaeger (1959) as :

$$T = Q' \int_0^{t'} \exp\left[\frac{-r_w^2}{4\,\alpha\,(\Delta t - t')}\right] \frac{dt'}{(\Delta t - t')} \qquad (3.1)$$

The exact solution of equation (3.1) for time Δt after the end of the application of the line source is given by:

$$\Delta T = Q'\left\{ E_i\left(\frac{-r_w^2}{4\,\alpha\,\Delta t}\right) - E_i\left[\frac{-r_w^2}{4\,\alpha\,(\Delta t + t')}\right]\right\} \qquad (3.2)$$

in which $E_i(-x)$ is the exponential integral. For small values of x ($x \ll 1$), this integral was approximated by the following simplified equation.

$$E_i\,(-x) = \gamma + (\ln x) - x + \frac{1}{4}\,x^2 + O\,(x^3) \qquad (3.3)$$

where γ is the Euler constant. However, since $x \ll 1$, this equation was again reduced to:

$$E_i = \gamma + \ln x \qquad (3.4)$$

Considering this approximation and after several mathematical steps, equation (3.2) was replaced by a simple equation that represents the behaviour of SFT against the drilling time parameters Δt and t'.

$$\Delta T = Q' \ln\left(\frac{t' + \Delta t}{\Delta t}\right) \qquad (3.5)$$

This simplification is valid when $\Delta t >> r_w^2 / 4\alpha$. Under these conditions a plot of T against $\ln\left(\frac{t'+\Delta t}{\Delta t}\right)$ produces a straight line, whose intercept yields the approximated value of the static formation temperature (T_i).

$$T = T_i + Q' \ln\left(\frac{t'+\Delta t}{\Delta t}\right) \qquad (3.6)$$

Even though this approach has some limitations, it has been widely used as the basis of the majority of the improved models which have been developed for determining the equilibrium formation temperatures in oil and geothermal wells. This method is known as the Horner method or Horner plot.

Timko and Fertl (1972) suggested that the temperatures recorded during the drilling operations could be extrapolated to estimate SFTs. They assumed that the maximum recorded temperatures correspond to the BHT but these values cannot represent absolute temperatures unless the wellbore and the surrounding formation had reached the thermal equilibrium. Timko and Fertl (1972) recommended the use of the Horner temperature plot for estimating SFTs. This method is similar to the conventional reservoir pressure recovery method for determining the initial reservoir pressure [Horner (1951)]. During this study the apparent applicability of this technique for predicting SFTs was partially demonstrated. Essentially, the mathematical basis of this method was an extension of the approximation to the full line-source solution given previously by Bullard (1947), which was reduced to the following equation:

$$BHT = T_i - A \cdot \log\left(\frac{t'+\Delta t}{\Delta t}\right) \qquad (3.7)$$

In this case, the t' and Δt variables in equation (3.6) were interpreted as the duration of the drilling fluid circulation and the shut-in time (time elapsed between the end of the drilling fluid circulation and the BHT measurement), respectively.

The method involves plotting the dimensionless Horner time (DHT) against the BHT for a number of successive measurements. This results in a straight line whose intercept (T_i) with the temperature axis (extrapolated to an infinite shut-in time) gives an estimate of the SFT. The slope of this Horner line (A) is an unknown constant which depends on the Q' value. Even though the application of this method provided a good approximation of the SFTs, Timko and Fertl (1972) concluded their study by establishing that differences between the BHT and the actual formation temperatures should be expected (up to 30 °C).

An explanation for these differences was later studied and justified by Dowdle and Cobb (1975); Luhesi (1983); Drury (1984); Shen and Beck (1986) and Deming (1989) who evaluated the validity and the possible error sources of the Horner method. Dowdle and Cobb (1975) found that the pressure and the temperature build-up methods are not completely analogous because the Horner type analysis of temperature was not mathematically correct. However, they established that under the assumption of short circulating times, the technique may be used for reliable estimates of SFT, mainly in regions where high geothermal gradients exist which indicates that logged temperatures are significantly less than the SFTs. On the other hand, Luhesi (1983) and Shen and Beck (1986) pointed out that the accuracy of the Horner model increases as the ratio of shut-in time to circulation time increases. In particular, Shen and Beck (1986) demonstrated that the Horner method does not begin to accurately approximate the actual rise of temperature in the wellbore until it has been shut-in at least as long as the duration of the drilling fluid circulation.

Deming (1989) identified two main drawbacks related to the application of the Horner technique: (i) it cannot be applied to single BHTs, and (ii) although shut-in time is usually found on log headers, accurate information on the duration of circulation times is often not found. Deming (1989) established that perhaps the more serious of these problems is that the temperature-time data sets are frequently not available for most drilled wells. When multiple temperature-time

data are available, the primary practical difficulty in applying the Horner method is that information on the duration of the circulation is almost always unavailable or rarely reliable.

Manetti (1973) developed a fitting function for the time-temperature curve of deep geothermal wells. The function proposed by Manetti (1973) also provided an approximation to the equilibrium temperature values. This numerical methodology was based on the study of thermal transients resulting from disturbances induced by drilling operations without circulation losses. The method was proved and validated in shallow geothermal holes. Essentially, the method considers the thermal exchange with formations (deriving from drilling, mud circulation, etc.) as a thermal emission produced through a cylindrical surface source, whose radius is equal to that of the hole. Thus, the thermal processes derived from this source were simulated by means of the solution of Fourier's equation for heat conduction:

$$\nabla^2 T = \frac{1}{\alpha} \frac{\partial T}{\partial t} \qquad (3.8)$$

where α represents the thermal diffusivity. Equation (3.8) was solved by means of the so-called source solutions [Bullard (1947); Lachenbruch and Brewer (1959)]. Manetti (1973) concluded the study establishing that the temperature measured at various depths after drilling tends asymptotically to return by conduction to the initial undisturbed values.

Albright (1975) treated the thermal recovery process of a drilled well as a problem of temperature relaxation. Assuming the relaxation time constant to be invariant only within individual time intervals but allowing it to vary from interval to interval, Albright (1975) tried to determine the SFT from a linear regression of the calculated relaxation constants and the extrapolated formation temperatures for individual time intervals. The major innovative aspect

considered by this technique was to analyse BHTs in order to estimate SFTs from measurements made in a substantially shorter time than other previous methods. Even though his results showed that estimation by extrapolation is valid when the transient temperature has reached a few degrees (< 10 °C) from the SFT, the use of the earlier BHT invariably led to an underestimation of SFTs.

Middleton (1979) suggested a similar graphical technique to the Manetti method. His technique was based on a set of master curves where the SFT is inferred from an analytical solution of the temperature behaviour at the centre of a circular borehole as a function of time and under bottomhole conditions. This approximation was expressed as:

$$BHT = T_i + \Delta T\left[\exp\left(\frac{-r_w^2}{4\alpha t} - 1\right)\right] \qquad (3.9)$$

In this case, the parameters that require to be varied are ΔT (the difference between the SFT and the drilling fluid temperature) and the thermal diffusivity (α) of the region around the point of measurement. Hence, by matching one of the curves to the successive temperatures from the BHT, a SFT value can be estimated. A comparison between Middleton's method and the classical Horner plot was performed by Leblanc et al. (1982). In this study, it was established that even both methods require three or more successive BHTs. The Horner plot requires an accurate knowledge of the circulation time, whereas the Middleton approximation requires an accurate estimate of the thermal diffusivity of the contents of the wellbore.

Roux et al. (1980) demonstrated that the conventional Horner method usually underestimates the SFT unless the shut-in time is large compared with the circulation time. Roux et al. (1980) developed a new method to calculate the SFT from early shut-in data recorded in geothermal wells which is an improved version of the classical Horner plot. The proposed method was based on the line-

source solution to the diffusivity equation (3.8). This solution enables the radial conductive heat flow in an infinite system with a vertical line sink withdrawing heat at a constant rate, to be estimated. Thus, this improved method introduces an empirical correction factor in the slope of the Horner straight line based on the dimensionless circulation time and the time since the cessation of mud circulation. Theoretically, this characteristic enables the SFT to be determined either for short or long circulation times.

Barelli and Palama (1981) proposed a curve matching method for evaluating the SFT during drilling stoppages. This method is based on simple graphics suitable for field use and for deciding the duration of the break to minimise drilling costs. These graphics were generated by consideration of a hypothesis related to the temperature distribution around a wellbore after drilling stops, which was expressed by the following equation:

$$T(t,r) = T_i - \Delta T \cdot \upsilon(t,r) \qquad (3.10)$$

where $\upsilon(t,r)$ represents the solution of the heat conduction problem in cylindrical symmetry which was solved by the Laplace transform method. As a result of this solution, two families of curves were obtained and represented by the following equation:

$$T(t,r) = T + (T_i - T) \cdot \psi(t_D, r_D) \qquad (3.11)$$

This new equation was simplified by means of a trial and error procedure to finally derive two graphical methods to predict SFT using the following equation:

$$T(t) = T + (T_i - T) \cdot \exp\left(-\frac{a^2}{4kt}\right) \qquad (3.12)$$

Kritikos and Kutasov (1988) developed the so called two-point method to determine SFTs. Their analytical method was developed for use with

temperature measurements taken a short time after the cessation of well drilling. These temperature logs are extrapolated to obtain undisturbed temperature gradients. In order to determine the shut-in wellbore temperature, Kritikos and Kutasov (1988) assumed that the temperature of the drilling mud at a given depth is constant during the drilling process. To determine the temperature along the well axis, after the circulation of the drilling fluid has ceased, Kritikos and Kutasov (1988) used the solution of the thermal diffusivity equation (3.8) under radial coordinates. This equation allows the description of cooling along the axis of a cylindrical body with a known initial distribution placed in an infinite medium at a constant temperature. The difference in thermal properties of drilling fluids and formations was neglected. The main characteristic of the method is that it requires only two temperature measurements in a well under steady-state thermal conditions to predict the SFT. Its application is limited by the accuracy of BHT measurements and by the knowledge of the dimensionless circulation times which are not normally taken or available during the course of drilling operations.

Cao et al. (1988) developed a numerical method to accurately model the thermal estabilisation of a wellbore using inverse techniques. The method is based on mathematical and physical principles underlying BHT stabilisation. From this method five unknown geophysical factors can be simultaneously determined: (1) the SFT; (2) the drilling fluid circulation temperature; (3) the thermal invasion distance of the drilling fluid to the formation; (4) the formation thermal conductivity; and (5) an efficiency factor for heating the drilling fluid in the wellbore after the end of circulation. Cao et al. (1988) indicated that the major feature of their method is that it is a true inverse procedure that uses only three BHTs to infer the previous five unknown factors because these parameters are involved in a non-linear manner. However, they demonstrated that temperature logged data with an uncertainty of 1 °C may yield significant errors up to 50 °C in the estimation of SFT values. Finally, Cao et al. (1988) found a good agreement with SFT values predicted by means of the Horner method.

Hasan and Kabir (1994) developed one of the most recent methods to simulate the transient heat transfer processes that occur during the drilling operations of geothermal and oil wells. The method provides a general solution of the thermal diffusivity equation with appropriate boundary conditions. This solution allows the use of the transient drilling fluid temperature data taken at early times in the estimation of SFTs. Hasan and Kabir (1994) showed that the temperature analog of the Horner method (log/linear approximation) is valid only for large circulation times and is not applicable to cases where the drilling fluid circulation time is less than 30 hours. Regarding this time constraint, Hasan and Kabir (1994) developed an analytical solution to evaluate the transient heat transfer from the drilling fluid to the formation using a cylindrical source well. This was done by means of the study of both conductive and convective heat transfer mechanisms which are involved directly in the overall well drilling process. The main advantage of the Hasan and Kabir model is that the SFT can be reliably estimated from very early time data, which allows rig time to be saved because waiting periods can be minimized to a large extent.

Ascencio et al. (1994) developed a novel and quick method to calculate the SFT in geothermal wells. The method involves considerations related to the heat flow process. It assumes spherical and radial heat flow in the surrounding formation instead of the cylindrical radial heat flow, which is normally assumed by other methods. Ascencio et al. (1994) established that at the total well depth, the process heat flow lines are not formally radial and heat enters the wellbore from all directions, probably more in a spherical and radial configuration than in a horizontal cylindrical radial form. The analytical solution of this method indicates that, at sufficiently longer times, the transient temperature during the return to equilibrium conditions varies linearly with $1/\sqrt{t}$. The main characteristic of this method is that the circulation time is not explicitly required. This is an advantage since, in practice, its estimation is uncertain and difficult to evaluate with sufficient accuracy using conventional methods [Deming (1989)].

As illustrated in this literature review, the real thermal disturbance associated with a drilling process can be considered as the temperature distribution caused by heat sources moving through an inhomogeneous medium. The physics of this process is too complicated. Therefore, it should be recognized that in the light of the actual physical process, the assumptions taken by most of the methods are somewhat unrealistic. Hence the SFT values estimated by those methods are too low and only provide approaches to the true undisturbed temperatures. It has been demonstrated that the departure from the actual undisturbed temperature regime depends upon several factors such as the:

(a) heat flow mechanisms (conductive and convective),
(b) original temperature distribution,
(c) thermophysical properties of rocks and drilling fluids,
(d) rates of drilling fluid circulation,
(e) casing and cementation of the well,
and
(f) presence of drilling fluid losses to the formation.

Unfortunately, there is no unique analytical solution available to estimate accurately the net effect of these factors. Most of the analytical methods described in this section consider that the thermal recovery process of a geothermal or an oil well drilling system follows the physical law of logarithmic decay in the presence of purely conductive heat transfer processes. However, there are some more realistic approximations to this wellbore equilibration problem which are reported in the drilling literature. These approximations have been obtained by means of sophisticated models that explicitly include a finite well radius, finite circulation time and different thermal properties for drilling fluids and rocks [Lee (1982); Luhesi (1983) and Shen and Beck (1986)]. Such models provide a better understanding of the temperature build-up in a wellbore during shut-in operations. In these models, the sensitivity of the temperature build-up in the wellbore to (i) the thermal properties of the drilling fluid and the

surrounding rock (formation), (ii) the duration of the circulation, (iii) the well diameter and (iv) the fluid flow into and out of the well is considered. Nevertheless, the practical application of these models for estimating SFT is usually hampered by lack of data. The lack of simplifying assumptions in simpler models results in a large number of unknown variables. In particular, information regarding the thermophysical and transport properties of the formation and drilling fluids is seldom available. Parameters such as the thermal diffusivity of rock do not vary much for most earth materials. Moreover, in the case of the thermophysical properties, there is no information reported in the technical literature that shows its behaviour as a consequence of changes in temperature and pressure of the geothermal well drilling systems.

3.4 Wellbore Numerical Simulators.

As was mentioned in the introduction to this chapter, this second section will be oriented to the analysis of heat transfer studies related to the development and application of numerical simulators for determining the temperature distribution in and around geothermal wells under and after circulating conditions. Some differences exist among the analytical methods and the heat transfer models of the numerical simulators. The most important of them is related to the capabilities that a simulator offers to provide a full description of the temperature distributions or the thermal history exsiting in a wellbore under steady-state or transient conditions, when it is being drilled or after this process has finished. The evaluation of the temperature distribution in and around a wellbore is a very complex task that depends on a large number of unknown variables. For this reason, any heat transfer model must contain simplifying assumptions to enable a solution to be obtained. *«The more complicated the model, the more data are required»*. At present, there are several numerical models reported in the literature for estimating BHTs and wellbore temperature distributions. Some of these have been designed for practical application, and

each includes a variety of simplifying assumptions. The earlier, hand solved methods tend to be the most simplified and inaccurate.

The first attempts were conducted by Farris (1941) who carried out a study of static and stabilised circulating temperatures in five oil wells of the Gulf coast. Farris (1941) developed charts to correlate BHTs with depth for five shallow wells, which ranged from 1600 m to 3400 m deep. Notwithstanding the obvious inaccuracy and oversimplification involved in the use of Farris charts, and their restrictive application, the American Petroleum Institute (API) recommended their use for determining setting schedules for cement slurries [API (1974)]. The severe deficiencies of these charts prompted research into more accurate mathematical models for determining circulating temperatures.

Edwardson et al. (1962) developed a heat transfer model for computing changes in the formation temperature caused by the circulation of the drilling fluid before and after drilling operations. The basis of this model is the mathematical solution of the differential equation of heat conduction under radial coordinates. Thus, the temperature distribution around a wellbore was defined by means of the following equation.

$$\frac{\partial^2 T}{\partial r^2} + \frac{1}{r}\frac{\partial T}{\partial r} = \frac{1}{\alpha}\frac{\partial T}{\partial t} \qquad (3.13)$$

The solution of this equation was presented in graphical form to determine the formation temperature disturbance at various radii for arbitrary drilling fluid circulation histories. The temperature distribution inside the wellbore was not considered. Edwardson et al. (1962), concluded their studies by establishing that the formation temperature disturbances caused by the circulating drilling fluid are quite significant near the wellbore.

Tragesser et al. (1967) expanded Edwardson's model to develop a new method to estimate temperatures as a function of well depth, hole size, pump rate and time, fluid and formation thermophysical properties and thermal status of the well. In this way the calculation technique provides a transient of temperatures at varying depths in both the casing and annulus of the well. These studies concluded by establishing that the maximum temperatures occur in the well annulus and that they mainly depend on the pumping rate.

Raymond (1969) made one of the best attempts at predicting the fluid temperature during drilling fluid or cement circulation. During these studies, generalised models to predict these temperatures at both transient and pseudo-steady state conditions were developed. Raymond (1969) supported the use of the principle of superposition and the van Everdingen and Hurst functions to provide a numerical solution for unsteady conditions [van Everdingen and Hurst (1949)]. However, he contended that the pseudo-steady state condition provides sufficient accuracy for all practical purposes. Such models allow the estimation of the drilling fluid temperature as a function of position and time. These calculations showed that the circulation lowers considerably the temperatures of both the bottomhole fluid and the rock and that the maximum circulating fluid temperature occurs one-fourth to one-third of the way up the annulus.

Raymond (1969) found that all the temperatures in the circulating fluid system are changing with time and that a true steady state is never attained. However, he observed that after one or two drilling fluid circulations the temperatures do not change appreciably. During these trips, the drilling fluid system tends quite rapidly towards the geothermal gradient and its temperature distribution as a function of depth is within 10 % of the geothermal gradient after 16 hours of trip time (shut-in time). Raymond (1969) concluded that the temperature of the formation 3.0 m from the wellbore is essentially undisturbed during the drilling process.

Even though the Raymond procedures provided acceptable approaches to the heat transfer problem involved in a well drilling system, they were limited by insufficient data on downhole drilling fluid properties and uncertainties in values for the heat transfer coefficients. A detailed evaluation of this model was carried out by Sump and Williams (1973) and Kutasov et al. (1988) who compared the predicted and measured values of circulating BHTs. They indicated that none of the Raymond methods adequately predicts the drilling fluid circulation temperatures. Average differences up to 12 % were found. These differences were explained by the fact that several of the main characteristics of the drilling process were not taken into consideration by this model. These are as follows:

(i) The amount of time that a formation is exposed to the drilling fluid circulation depends on the depth (the maximum periods of exposure correspond with shallowest depth).
(ii) The temperature of the drilling fluid at a given depth depends on the current total depth.
(iii) The discontinuity of the drilling fluid circulation affects the process during drilling.
(iv) The presence of the casing strings cemented at various depths has an adverse effect.
(v) The impact of the energy sources caused by drilling also affects the process.

Despite these limitations, it is very important to note that in terms of the theoretical development of the heat transfer relationships for a wellbore, the work proposed by Raymond (1969) is one of the most comprehensive methods available in the literature. It is this work that has served as a basis for all the recent research on the subject.

Holmes and Swift (1970) developed a simple numerical model to predict logged bottomhole drilling fluid temperatures. This method also was used to provide initial temperatures in predicting drilling fluid column temperature buildup after

circulation has stopped. The model assumes that the heat transfer between the annular fluid and the formation can be approximated by steady state linear heat transfer. Temperatures were calculated as a function of well depth, drilling fluid circulation rate, circulating fluid characteristics, reservoir properties and drill-pipe size. This model has the advantage of being simple and more accurate than previous methods, but the assumption of steady state heat flow is a critical one which is only satisfied after impractically long circulation times.

Keller et al. (1973) extended Raymond's general method to develop a model for describing the two-dimensional transient heat transfer in and around a wellbore. This model included the presence of multiple casing strings as well as the effects of energy sources in the drilling system which were neglected by the Raymond method. The model developed considers a drilling fluid flowing down a drill pipe and returning up the annulus. The results derived from this model showed that the use of steady-state solutions gives good estimates of circulating drilling fluid temperatures. The transient solution presented by these authors is better suited to matching temperature logs. Keller et al. (1973) concluded that the viscous flow energy, rotational energy and drill bit energy have a significant effect on the overall energy balance of the drilling system. Their energy contribution to the drill pipe, the annulus and the drill bit were approximately estimated as: 37.3 kW, 72 kW and 168 kW, respectively.

Sump and Williams (1973) developed an improved model to predict and to account for the thermal evolution in well cementing operations. This model is based on the original version of the Raymond model. Essentially, the improvement of this model considers a different procedure to calculate the film heat transfer coefficients and the formation thermal conductivities. These thermal parameters were determined from a regression analysis of field data on seven wells. Sump and Williams (1973) concluded their studies by establishing that the API techniques for predicting drilling fluid circulation and cementing temperatures are not accurate. They found that the API procedures produce

significant differences between the predicted BHTs and the logging temperatures. These differences normally range from 16.4 % to 27.8 % whereas the approximations of their method showed smaller differences that range from 4.7 % to 16.1 %.

Wooley (1980) developed the first transient computer model (GEOTEMP) to predict BHTs with application to either the geothermal or the oil well drilling industry. The model was formulated to determine the transient BHTs in: (i) the wellbore (under flowing or shut-in conditions), (ii) the casing and cement regions and (iii) the surrounding formation. GEOTEMP considers some features of the drilling process which were neglected by the previous Raymond model. These features include the effects related to: (i) well depth change with time, (ii) discontinuity in the drilling fluid circulation, (iii) variation of drilling fluid properties with depth, and (iv) the complexity of the completion wellbore design. The physical and mathematical assumptions considered by this model were validated with some exact solutions reported by Carslaw and Jaeger (1959). With the applicaction of this model, Wooley (1980) evaluated the effect of inlet temperatures and the flow rate of drilling fluid on the BHTs. He pointed out that at lower flow rates of drilling fluid, the BHTs are strongly affected. Wooley (1980) demonstrated that the transient response in the flowing stream is very important for short time periods, such as drilling and cementing operations or production and injection start-up.

Marshall and Bentsen (1982) developed a computer model to determine the temperature distributions in a wellbore when it is being drilled or cemented. This objective was attained by means of the physical and mathematical formulation of a coupled system of four partial differential equations. These equations describe the energy balances for the drill pipe, the drill pipe wall, the annulus and the formation. Marshall and Bentsen (1982) used an optimised solution based on a finite differences scheme using a band algorithm which is not subject to the limitations of convergence or stability. During the applications of this model,

Marshall and Bentsen (1982) identified that the wellbore temperature distribution is affected by the following parameters: (i) the thermophysical properties of the drilling fluid (specific heat capacity and density) and the formation (thermal conductivity); (ii) the drilling fluid flow rate; (iii) the drilling fluid inlet temperature; (iv) the geothermal gradient; (v) the circulation time; (vi) the wellbore depth; and (vii) the heat generation produced within the drilling system. They used the predicted annulus temperature profiles to evaluate the influences of each of the above parameters on the thermal behaviour of the well drilling system. In the general form, the majority of their results showed a similar behaviour to those previously reported by Keller et al. (1973) and Wooley (1980). Apparently, the main difference existing between the Marshall and Bentsen model and the other models was a reduction of the simulation time [Corre et al. (1984)]. The earlier models normally take much computer time to solve the differential equations matrix because they use iterative methods whereas this model uses an optimised numerical technique (a band algorithm). Marshall and Bentsen (1982) concluded their studies by establishing that the assumption of steady state in the wellbore heat transfer process should not be adopted because this state is almost never attained.

Mitchell (1982) developed a model for calculating BHTs, pressures, fluid densities and velocities in geothermal and oil well drilling operations and with a special application to drilling systems that uses compressible fluids as the drilling fluid. Mitchell extended the wellbore heat transfer theory used previously by Wooley (1980) to develop a new wellbore simulator (GEOTEMP2). This simulator is an extensively modified version of a previous version called GEOTEMP. The major technical features involved in this simulator are the modelling of: (i) the drilling processes using air and mist, and (ii) the two-phase flow of water and steam either for injection or production processes. GEOTEMP2 uses a fully transient thermal analysis of the wellbore and the formation to determine the circulating and shut-in temperatures and it considers the possibility of using compressible drilling fluids such as air or nitrogen. The first few applications of this simulator

were conducted by Duda (1985). He carried out a computer simulation to study the cooling effects produced in a wellbore during the circulation and injection processes. The potential cooling effects were investigated by means of the computer code GEOTEMP2. This computer program was applied to simulate heat transfer from the wellbore to the surrounding rock formation. Duda (1985) indentified the heat conduction process as the main mechanism responsible for warming the wellbore. Following steady-rate circulation, the wellbore temperatures were found to rise quickly after shut-in, approaching the undisturbed temperature within one day. The results of the simulation showed that higher flow rates produce lower wellbore temperatures. In these cases, the mud tends to give lower wellbore temperatures as the mud weight is increased and the shut-in fluid temperature rises rapidly when the only cooling mechanism is circulation.

Arnold (1990) indicated that when a fluid is circulated in a wellbore, the temperature profile can be determined by the transfer of heat from surrounding formations to the fluid. He developed an analytical solution of the differential equations describing this heat transfer process. His solution assumes a steady flow of heat in the wellbore and a transient conduction of heat in the formation. Such a solution was validated by comparison with BHT measurements from the literature. Arnold (1990) carried out a parametric study of the sensitivity to evaluate the effect of operating conditions on bottomhole circulating temperatures. During these studies, the factors evaluated were the formation properties, the rate of circulation and the surface temperature of the fluid entering the drill pipe. Arnold (1990) concluded his studies by demonstrating that apparently a steady state in the wellbore heat flow can be assumed. He observed that BHTs and annular surface temperatures under circulating conditions change very rapidly during the first hours of circulation. At later times, the circulating temperatures continue to change at a decreasing rate. During circulation, the maximum temperature in the circulation fluid was observed in the annulus at a point above the bottom of the wellbore.

A more extensive application of this model was reported by Garcia et al. (1997) who applied the theory of the Arnold solution to develop a new thermal simulator (TEMLOPI) for the estimation of the drilling fluid and formation temperatures during the drilling of geothermal wells. They validated and applied this simulator with data published in the literature and with data derived from some wells drilled in the Los Azufres Mexican geothermal field.

Beirute (1991) developed a comprehensive circulation and shut-in well temperature profile simulator capable of accounting for free fall during cementing operations. The simulator predicts temperatures during the circulation of drilling fluid in a well or during cementing activities. It can also simulate shut-in periods at any point during a given run.

Essentially, this simulator uses a set of rigorous governing differential equations to describe the heat transfer processes in the wellbore system (casing, drill pipe and annulus) and the formations. The governing differential equations are solved by means of a finite differences method. One of the main features of this simulator is that it involves an approximation to represent the variation of the drilling fluid thermal properties and the heat transfer film coefficients in the mathematical formulation of the problem. This was made using the available literature correlations. However, this improvement was only an approach to describe the actual variation because appropriate correlations are not used for non-Newtonian drilling fluids. The simulator was validated using exact analytical solutions reported in the literature. Comparison of simulator runs with field measured well temperature data indicated that the simulator provides a good approximation of these temperatures. Nevertheless, Beirute (1991) identified that the drilling fluid composition and the static temperature profile can significantly affect the reliability of the predictions. Regarding this, he suggested that the compositions of drilling fluids such as muds, spacers and cement slurries are needed to calculate their thermal properties and to estimate the actual convective heat transfer coefficients. In the case of the SFT profile, he

recommended that an effort must be made to obtain the true static temperatures for the drilled area before applying the simulator. This could be made by direct application of the Horner method to extrapolate the BHTs measured during the temperature logging stages.

Summary. As can be seen, a number of simulators have been developed to date in order to tackle the heat transfer problem related to the drilling fluid circulation, wellbore geometry and formation. Some of these simulators have assumed the coupling of a steady state or pseudo-steady heat flow model in the wellbore with a fully transient heat conductive model for the formation. Many others assume the coupling of a fully transient heat flow model in the wellbore with a fully transient heat conductive model for the formation.

Even though these two classes of simulators have attempted to solve the problem associated with the drilling fluid circulation process, most of them are far from reproducing the actual BHT values. Regarding this, two important limitations have been recognised as the responsible sources of the unsuccessful prediction of BHT logs. As was discussed in chapter one, the first one is related to the assumption whereby the thermophysical and transport properties of the drilling fluid, cement slurries and formation are independent parameters of the temperature variation. The second one, and maybe the most important, is that the heat transfer models adopted by all previous simulators only represent the drilling fluid circulation process under ideal conditions, i.e. none of the existing simulators considers the presence of drilling fluid losses to the formation. This ideal assumption considerably simplifies the actual heat transfer problem in the formation model. Many researchers have recognised that the effect of drilling fluid losses to the formation can be extremely important in the accurate determination of the bottomhole circulating fluid and formation temperatures. However, it is a very complex task because it suggests that a convective heat transfer model must be included along with the conductive formation model adopted by the majority of the simulators.

After this critical analysis, a new improved transient wellbore thermal simulator that overcomes the limitations described above is clearly required to determine more accurately downhole temperatures in and around geothermal wells under drilling and shut-in conditions.

3.5 References

J.N. Albright, A new and more accurate method for the direct measurement of Earth temperature gradients in deep boreholes, Proc. 2nd. UN Symp. on the Development of Geothermal Resources, **2** 847-851 (1975).

American Petroleum Institute (API), Recommended practice for testing oil-well cements and cement additives, API RP 10B, Nineteenth Edition, API, Dallas, Tx, USA (1974).

F.C. Arnold, Temperature variation in a circulating wellbore fluid, Journal of Energy Resources Technology, **112** 79-83 (1990).

F. Ascencio, A. García, J. Rivera and V. Arellano, Estimation of undisturbed formation temperatures under spherical radial heat flow conditions, Geothermics, **23** 317-326 (1994).

A. Barelli and A. Palama, A new method for evaluating formation equilibrium temperature in holes during drilling, Geothermics, **10** 95-102 (1981).

R.M. Beirute, A circulating and shut-in well-temperature-profile simulator, Journal of Petroleum Technology, **September** 1140-1146 (1991).

E.C. Bullard, The time necessary for a borehole to attain temperature equilibrium, Astronom. Soc., Monthly Notices, Geophys. Suppl., **5** 125-130 (1947).

S. Cao, I. Lerche and C. Hermanrud, Formation temperature estimation by inversion of borehole measurements, Geophysics, **53** 979-988 (1988).

H.S. Carslaw and J.C. Jaeger, Conduction of heat in solids, 2nd. Edition, Clarendon Press, Oxford, UK (1959).

B. Corre, R. Eymard and A. Guenot, Numerical computation of temperature distribution in a wellbore while drilling, Proceedings of The 59th Annual Technical Conference and Exhibition, Society of Petroleum Engineers of AIME, Houston, Texas, USA, September 16-19, 12 p. (1984).

D. Deming, Application of bottom-hole temperature corrections in geothermal studies, Geothermics, **18** 775-786 (1989).

W.L. Dowdle and W.M. Cobb, Static formation temperature from well logs - an empirical method, Journal of Petroleum Technology, **November** 1326-1330 (1975).

M.J. Drury, On possible source of error in extracting equilibrium formation temperatures from borehole BHT data, Geothermics, **13** 175-180 (1984).

L.E. Duda, Computer simulation of wellbore cooling by circulation and injection, Proc. Tenth Workshop on Geotherm. Res. Eng., Stanford University, USA, January 22-24, pp. 195-200 (1985).

M.J. Edwardson, H.M. Girner, H.R. Parkinson, C.D. Williamson and C.S. Matthews, Calculation of formation temperatures disturbances caused by mud circulation, Journal of Petroleum Technology, **April** 416-426 (1962).

R.F. Farris, A practical evaluation of cements for oil wells, Drilling Production Practice, American Petroleum Institute, pp. 283-292 (1941).

A. Garcia, I. Hernandez, G. Espinoza and E. Santoyo, TEMLOPI, A thermal simulator for estimation of drilling mud and formation temperatures during drilling of geothermal wells, Submitted to Computers & Geosciences (1997).

A.R. Hasan and C.S. Kabir, Static reservoir temperature determination from transient data after mud circulation, SPE Drilling & Completion, **March** 17-24 (1994).

D.R. Horner, Pressure buildup in wells, Proc. Third World Petroleum Congress, The Hague, The Netherlands, Vol. II, p. 503, (1951).

C.S. Holmes and S.C. Swift, Calculation of circulating mud temperatures, Journal of Petroleum Technology, **June** 670-674 (1970).

H.H. Keller, E.J. Couch and P.M. Berry, Temperature distribution in circulating mud columns, Society of Petroleum Engineers Journal, **February** 23-30 (1973).

W.R. Kritikos and I.M. Kutasov, Two-point method for determination of undisturbed reservoir temperature, SPE Formation Evaluation Journal, **March** 222-226 (1988)

I.M. Kutasov, R.M. Caruthers, A.K. Targhi and H.M. Chaaban, Prediction of downhole circulating and shut-in temperatures, Geothermics, **17** 607-618 (1988).

A.H. Lachenbruch and M.C. Brewer, Dissipation of the temperature effect of drilling a well in Arctic Alaska, U.S. Geol. Survey Bulletin 1083-C, pp. 73-105 (1959).

Y. Leblanc, H.L. Lam, L.J. Pascoe and F.W. Jones, A comparison of two methods of estimating static formation temperature from well logs, Geophysical Prospecting, **30** 348-357 (1982).

T.C. Lee, Estimation of formation temperature and thermal property from dissipation of heat generated by drilling, Geophysics, **47** 1577-1584 (1982).

M.N. Luhesi, Estimation of formation temperature from borehole measurements, Geophys. J. R. Astr. Soc., **74** 747-776 (1983).

G. Manetti, Attainment of temperature equilibrium in holes during drilling, Geothermics, **2** 94-100 (1973).

D.W. Marshall and R.G. Bentsen, A computer model to determine the temperature distributions in a wellbore, The Journal of Canadian Petroleum, **January-February** 63-75 (1982).

M.F. Middleton, A model for bottom-hole temperature stabilisation, Geophysics, **44** 1458-1462 (1979).

R.F. Mitchell, Advanced wellbore thermal simulator GEOTEMP2, Research Report, Sandia Laboratories, SAND82-7003/1, Department of Energy, Geotherm. Tech. Develop., Houston, Texas, USA, 79 p. (1982).

L.R. Raymond, Temperature distribution in a circulating drilling fluid, Journal of Petroleum Technology, **March** 333-341 (1969).

B. Roux, S.K. Sanyal and S.L. Brown, An improved approach to estimating true reservoir temperature from transient temperature data, Proc. 50th Annual California Regional Meeting of the Society of Petroleum Engineers, Los Angeles, CA, USA, April 9-11, 9p. (1980).

P.Y. Shen and A.E. Beck, Stabilization of bottom hole temperature with finite circulation time and fluid flow, Geophys. J. R. Astr. Soc., **86** 63-90 (1986).

G.D. Sump and B.B. Williams, Prediction of wellbore temperatures during mud circulation and cementing operations, Journal of Engineering for Industry, Transactions of ASME, **November** 1083-1092 (1973).

D.J. Timko and W.H. Fertl, How downhole temperatures, pressures affect drilling. Part VII: The shale resistivity ratio - A valuable tool for making economic drilling decisions, World Oil, **July** 59-63 (1972).

A.T. Tragesser, P.B. Crawford and H.R. Crawford, A method for calculating circulating temperatures, Journal of Petroleum Technology, **November** 1507-1512 (1967).

A.F. van Everdingen and W. Hurst, The application of the Laplace transformation to flow problems in reservoirs, Transaction, AIME, **186** 305-324 (1949).

G.R. Wooley, Computing downhole temperatures in circulation, injection, and production wells, Journal of Petroleum Technology, **September** 1509-1522 (1980).

Chapter 4

STATIC_TEMP COMPUTER CODE

4.1 Nomenclature

$b(t_{pD})$	slope of semi-log straight line portion of the T_{Dws} curves
B_o	parameter defined in equation (4.53)
c	fluid compressibility [Pa^{-1}]
C	constant defined in equation (4.10)
C_o"	parameter defined in equation (4.48)
Cp	specific heat capacity [J kg^{-1} $°C^{-1}$]
DHT	dimensionless Horner time, $\left(\frac{t'+\Delta t}{\Delta t}\right)$ or $\left(\frac{t_p+\Delta t}{\Delta t}\right)$
D_o	constant (=2.184)
D_1	constant $\left(D_o^2 / 4\right)$
D_2	constant $(\gamma + \ln D_1)$

F_t	shut-in time and circulation time ratio [dimensionless]
g	parameter defined in equation (4.19c)
H	formation thickness [m]
h_{cm}	convective heat transfer coefficient for mud [W m^{-2} °C^{-1}]
k	thermal conductivity [W m^{-1} °C^{-1}]
k_h	formation permeability [m^2]
M	mass of drilling fluid (mud) [kg]
p	pressure of reservoir [Pa]
p_o	initial reservoir pressure [Pa]
p_{wf}	flowing wellbore pressure [Pa]
p_{ws}	wellbore pressure buildup [Pa]
q	constant production rate of the well [m^3 s^{-1}]
$\tilde{q}$	average heat flow [W]
Q_w	heat flow rate [W]
r	radius [m]
r_D	dimensionless radius, $\left(\frac{r}{r_w}\right)$ or $\left(\frac{r_t}{r_w}\right)$
r_t	radius of thermal disturbance [m]
r_{tD}	dimensionless radius of thermal disturbance, $\left(1 + D_o\sqrt{t_{pD}}\right)$
R	radius of thermally perturbed sphere [m]
S	parameter defined in equation (4.33)
t	time [s]
t'	duration of line heat source [s]
t_D	dimensionless time, $\left(\frac{t\,\alpha}{r_w^2}\right)$
t_p	circulation time [s]
t_{pD}	dimensionless circulation time, $\left(\frac{t_p\,\alpha}{r_w^2}\right)$

T	temperature [°C]
T_C	temperature distribution around wellbore under circulation [°C]
T_D	dimensionless temperature, $\frac{(T_i - T_{r,t})}{(T_i - T_m)}$
T_{DB}	dimensionless correction factor for temperature buildup
T_i	static formation temperature, SFT [°C]
T_{SD}	dimensionless wellbore temperature after shut-in
T_{we}	wellbore/formation interface temperature [°C]
T_{ws}	BHT shut-in temperature measured at Δt [°C]
T^*_{ws}	false initial temperature extrapolated to on the Horner plot [°C]
T_{Dws}	dimensionless temperature buildup
T^*_{Dws}	extrapolated dimensionless temperature buildup
U	overall heat transfer coefficient [W m^{-2} $°C^{-1}$]
W	total mass flow rate [kg s^{-1}]
z	wellbore length [m]
Δt	time elapsed since end of duration of heat source (shut-in time) [s]

Greek symbols

α	formation thermal diffusivity, $k/\rho C_p$ [m^2 s^{-1}]
ϕ	formation porosity [dimensionless]
γ	Euler´s constant (0.5772...)
ρ	density [kg m^{-3}]
μ	fluid dynamic viscosity [Pa s]

Special functions

$E_i(-x)$	exponential integral, $\int_x^\infty \frac{e^{-u}}{u} du$

erf (x) error function, $\frac{2}{\sqrt{\pi}}\int_0^x e^{-u^2}du$

ξ dimensionless function defined in equation (4.48)

Subscripts

e formation

m drilling fluid (mud)

w wellbore

4.2 Introduction

This chapter presents the description of the computer code STATIC_TEMP which was developed for estimating static formation temperatures (SFT) from bottomhole temperature (BHT) data. The computer code is based on five analytical methods which are the most commonly used in the geothermal industry. This computer program provides a useful tool that can be used in-situ to determine SFTs during geothermal well drilling operations. Details of the analytical methods employed as well as the computer code (including the numerical algorithm, flow diagrams and the source programs) are outlined. A validation process of this computer code with synthetic and field bottomhole temperature data is also presented.

4.3 Methods for Estimation of Static Formation Temperatures

During the development of this research work, numerous analytical methods for predicting SFTs were compiled, studied and evaluated. From this compilation, five analytical methods have been selected in order to develop a software package that includes the methods most commonly used to predict SFTs in the geothermal industry. All of these methods are summarized in the following list:

(i) the Horner method [Dowdle and Cobb (1975)],

(ii) the improved Horner method [Roux et al (1980)],

(iii) the two-point method [Kritikos and Kutasov (1988)],

(iv) the spherical and radial heat flow method [Ascencio et al (1994)], and

(v) the cylindrical source heat flow models [Hasan and Kabir (1994)].

4.3.1 Line-source solution (Horner method)

One of the methods that is commonly used for estimating undisturbed formation temperature in geothermal well drilling is that proposed by Horner [Manetti (1973)]. The Horner-type method consists of a plot of temperature buildup against the log of the dimensionless Horner time. This method was originally developed for pressure buildup analysis [Horner (1951)]. It considers a well drilled into a reservoir and radial flow to the well, as the main assumptions. Essentially, the method describes pressure behaviour in the well by means of the following flow equation:

$$\frac{\partial^2 p}{\partial r^2} + \frac{1}{r}\frac{\partial p}{\partial r} = \frac{\phi \mu c}{k_h}\frac{\partial p}{\partial t} \qquad (4.1)$$

Equation (4.1) is frequently referred to as the "diffusivity" equation because of its similarity with the diffusivity equation in the heat transfer literature. Horner (1951) proposed the use of the so-called "line-source" solution, whose generalised equation is given by:

$$p = p_o + \frac{q\,\mu}{4\pi\, k_h\, H} E_i\left(-\frac{r^2 \phi \mu c}{4\, k_h\, t}\right) \qquad (4.2)$$

where the E_i-function (exponential integral) is defined by the equation:

$$E_i(-x) = \int_x^{\infty} \frac{e^{-u}}{u}\, du \qquad (4.3)$$

For sufficiently small values of its argument the E_i-function can be approximated by its logarithmic expression, then:

$$E_i(-x) \approx \ln x + \gamma \qquad (4.4)$$

Details related to the complete solution of this equation are reported in the oil reservoir literature [Horner (1951); Matthews and Russell (1967)]. Considering the case of a well producing at a constant rate, located in an infinitely large reservoir and assuming that the initial reservoir pressure is constant, the following set of initial and boundary conditions were taken to modify equations (4.1) and (4.2):

$$p = p_o \quad \text{at} \quad t = 0 \quad \text{for all } r \qquad (4.5)$$

$$\left(r\frac{\partial p}{\partial r}\right)_{r_w} = A' \left(\frac{q\ B\ \mu}{k_h\ H}\right) \qquad (4.6)$$

$$p \rightarrow p_o \text{ as } r \rightarrow \infty \text{ for all } t$$

Combining these conditions with equation (4.1), it was shown that:

$$p_{wf} = p_o - \frac{A'\ q\ B\ \mu}{k_h\ H} \cdot \log\left(\frac{k_h\ t}{\phi\ \mu\ c\ r_w^{\,2}}\right) \qquad (4.7)$$

where A' is a constant, whose value depends on the well and reservoir characteristics; B is the formation volume factor and p_{wf} is the flowing wellbore pressure after any production time, t. It is significant to note that the condition of a constant production rate requires that the pressure gradient, $(\partial p / \partial r)_{rw}$, in the wellbore be constant. Horner (1951) showed that equation (4.7) can be used along with the concept of superposition to develop the equation that describes the wellbore pressure buildup, p_{ws}, for the case of a constant production rate well located in an infinitely large reservoir. The result is given by the following equation:

$$p_{ws} = p_o - \frac{A' q B \mu}{k_h H} \log\left(\frac{t' + \Delta t}{\Delta t}\right) \qquad (4.8)$$

Thus, a graph of p_{ws} against log $[(t'+\Delta t)/\Delta t]$ should form a straight line. Moreover, an extrapolation of the line to unit dimensionless Horner time will yield the initial reservoir pressure, p_o.

Temperature Buildup (Horner-Type Method). The apparent similitude between the Horner temperature plot and the pressure buildup method has indicated that the BHT rise after circulation stops should be analyzed in the same way as the pressure buildup [Manetti (1973)]. Such analysis suggests that the temperature rise can be described by the diffusivity equation of heat which is quite similar to equation (4.1).

$$\frac{\partial^2 T}{\partial r^2} + \frac{1}{r}\frac{\partial T}{\partial r} = \frac{C_p \rho}{k}\frac{\partial T}{\partial t} \qquad (4.9)$$

Thus final solution would be given by:

$$T_{ws} = T_i - C \log\left(\frac{t' + \Delta t}{\Delta t}\right) \qquad (4.10)$$

where $[(t'+\Delta t)/\Delta t]$ is the DHT; whereas t' and Δt are interpreted as the circulation time before shut-in and the time elapsed since circulation stops, respectively. Therefore, a semilog plot of T_{ws} against DHT should be a linear relationship and when extrapolated to infinite shut-in time should produce the static formation temperature, T_i (Fig. 4.1).

4.3.2 Improved Horner method

Roux et al. (1980) developed an improved version of the classical Horner plot to calculate the SFT from early shut-in data in geothermal wells. Roux et al. (1980) considered that the transient temperature in the formation around a well can be

estimated in terms of the dimensionless variables (radial distance and time) using the following modified version of equation (4.9):

$$\frac{\partial^2 T}{\partial r_D^2} + \frac{1}{r_D}\frac{\partial T}{\partial r_D} = \frac{\partial T}{\partial t_D} \qquad (4.11)$$

with initial condition: $T_D\,(r_D,0) = 0$

inner boundary condition: $T_D\,(1,t_D) = 1$

and outer boundary condition: $\lim T_D\,(r_D,t_D) = 1$

$r_D \rightarrow \infty$

Equation (4.11) is a partial differential equation whose solution was originally solved by Ehlig-Economedes (1979). Even though this solution was related to the pressure buildup analysis, Roux et al. (1980) used this approximation for the temperature buildup case in order to form a family of dimensionless Horner-type temperature buildup curves. From these curves, the thermal behaviour between the dimensionless temperature (T_{Dws}) at the wellbore as a function of the dimensionless producing time (t_{pD}), and the DHT was evaluated. As a result of this evaluation, the following equation for the dimensionless temperature buildup (T_{Dws}) was derived.

$$T_{Dws} = \frac{2\pi\, k\, h\,(T_i - T_{ws})}{\tilde{q}} \qquad (4.12)$$

Roux et al. (1980) established that the T_{Dws} and DHT $[(t_p+\Delta t)/\Delta t]$ follow a linear behaviour in a semi-log plot (for constant t_{pD} values). The resultant semi-log equation of the straight line is given by:

$$T_{Dws} = T^*_{Dws}\,(t_{pD}) + b\,(t_{pD}) \cdot \log\left(\frac{t_p + \Delta t}{\Delta t}\right) \qquad (4.13)$$

where $T^*_{Dws}\,(t_{pD})$ is the intercept at unit Horner time and it is defined as:

$$T^*_{Dws} = \frac{2\pi\, k\, h\, (T_i - T^*_{ws})}{\tilde{q}} \qquad (4.14)$$

while, b (t_{pD}) is the slope of the line. Here T^*_{Dws} corresponds to a dimensionless temperature drop between the true static formation temperature (T_i) and a false initial temperature (T^*_{ws}), which is obtained as a first approximation by extrapolation of a conventional Horner plot (Fig. 4.2). Combining and rearranging equations (4.13), (4.14) and (4.15), the final improved equation of the Horner method is obtained:

$$T_i = T^*_{ws} + \beta \cdot T_{DB}\,(t_{pD}) \qquad (4.15)$$

where:

$$T_{DB}(t_{pD}) = \frac{T^*_{Dws}}{b\,(t_{pD})} \qquad (4.16)$$

and δ is the slope of the conventional Horner straight line. T_{DB} (t_{pD}) values are determined from equations obtained by means of a least squares fitting procedure which was proposed by Roux (1979). These equations are functions of DHT ranges and can be summarized in the following list.

For $5 \le DHT \le 10$:

$$T_{DB} = 2.350 + 0.002\,X - 0.061\,X^{1/2} + 4.783\,X^{1/3} - 5.905\,X^{1/4} + 0.036\,X^{1/5} \qquad (4.17a)$$

For $2 \le DHT \le 5$:

$$T_{DB} = 0.25 - 0.007\,X + 0.36\,X^{1/2} - 0.00007\,X^{1/3} - 3.50\,X^{1/4} + 3.15\,X^{1/5} \qquad (4.17b)$$

For $1.25 \le DHT \le 2$:

$$T_{DB} = 0.487 + 0.003\,X - 0.286\,X^{1/2} + 1.407\,X^{1/3} - 0.783\,X^{1/4} - 0.773\,X^{1/5} \qquad (4.17c)$$

where the variable (X) represents t_{pD}.

4.3.3 Two-point method

Kritikos and Kutasov (1988) developed the so-called two-point method to determine the undisturbed formation temperatures. The analytical method was developed for use with temperature measurements taken a short time after the cessation of well drilling. In this method, temperature logs are extrapolated to obtain undisturbed temperature gradients. Kritikos and Kutasov (1988) assumed that the temperature of the drilling fluid (T_m) at a given depth is constant during the drilling process. The variations in the reservoir temperature near the well were determined by means of the solution of the thermal conductivity equation. Kritikos and Kutasov (1988) found that for moderate and large values of the dimensionless circulation time ($t_{pD} > 5$), the temperature distribution function, $T_C(r,t_p)$, in the vicinity of the well can be described by the following relationship:

$$T_C(r,t_p) = \left(1 - \frac{\ln r_D}{\ln r_{tD}}\right)\cdot(T_m - T_i) + T_i \qquad (4.18)$$

To determine the temperature along the well axis, $T_{ws}(0,\Delta t)$, after the circulation of drilling fluid has ceased, Kritikos and Kutasov (1988) used the solution of the thermal diffusivity equation (4.11). This equation describes cooling along the axis of a cylindrical body with a known initial distribution placed in an infinite medium at a constant temperature. Therefore, the dimensionless wellbore temperature (T_{SD}) after shut-in can be estimated by:

$$T_{SD}(t_{pD}, F_t) = 1 - \frac{E_i(-g\cdot r_{tD}^2) - E_i(-g)}{2\ln r_{tD}} \qquad (4.19)$$

for $t_{pD} > 5$:

$$T_{SD} = \frac{T_{ws}(0,\Delta t) - T_i}{T_m - T_i} \qquad (4.19a)$$

$$F_t = \frac{\Delta t}{t_p} \qquad (4.19b)$$

$$g = \frac{1}{4 \cdot F_t \cdot t_{pD}} \tag{4.19c}$$

Equation (4.19) shows that as F_t increases, the function $T_{SD}(t_{pD},F_t)$ decreases with increasing values of t_{pD}. For deep wells and large t_{pD}, Kritikos and Kutasov (1988) assumed that:

$$r_{tD} \approx D_o \sqrt{t_{pD}} \tag{4.20}$$

$$E_i(-g) \approx -\ln t_{pD} - \ln F_t - \ln 4 + 0.5772 \tag{4.21}$$

Substitution into equation (4.19) and after various steps, this equation can be written as follows:

$$\frac{T_{ws}(0,\Delta t) - T_i}{T_m - T_i} = -\frac{E_i(-D_1 / F_t) + \ln F_t - D_2}{\ln t_{pD} + 2 \ln D_o} \tag{4.22}$$

Thus, if two measured temperatures (T_{ws1}, T_{ws2}) are available for a given depth, with $\Delta t=\Delta t_1$ and $\Delta t=\Delta t_2$, a new version of equation (4.22) is obtained:

$$\frac{T_{ws1} - T_i}{T_{ws2} - T_i} = \frac{E_i(-D_1 / F_{t1}) + \ln F_{t1} - D_2}{E_i(-D_1 / F_{t2}) + \ln F_{t2} - D_2} \tag{4.23}$$

Therefore:

$$T_i = T_{ws2} + F(T_{ws1} - T_{ws2}) \tag{4.24}$$

where

$$F = \frac{E_i(-D_1 / F_{t1}) + \ln F_{t2} - D_2}{E_i(-D_1 / F_{t2}) - E_i(-D_1 / F_{t1}) + \ln(F_{t2} / F_{t1})} \tag{4.25}$$

To use this method, two temperature measurements must be performed in a well under transitory thermal conditions. The values Δt_1 and Δt_2 can easily be determined from drilling records and downhole measurements.

4.3.4 Spherical and radial heat flow model

Ascencio et al. (1994) developed a different analytical method to calculate SFT in geothermal wells. Fundamentally, the method involves the considerations related to the heat flow process. It assumes spherical and radial heat flow in the surrounding formation instead of the cylindrical radial heat flow, which is normally assumed by previous methods. In order to represent this heat transfer process, several simplifying assumptions were considered. Basically, the main assumptions are summarized in the following list.

(a) Heat flow is due to conduction only.
(b) Spherical and radial heat flows are considered.
(c) The formation can be treated as a spherical region of radius R, infinite, homogeneous and isotropic with constant thermophysical properties.

Ascencio et al. (1994) proposed that the heat conduction processes under spherical and radial coordinates can be represented as:

$$\frac{\partial^2 T}{\partial r^2}+\frac{2}{r}\frac{\partial T}{\partial r}=\frac{1}{\alpha}\frac{\partial T}{\partial t};\quad 0 < r < \infty, \tag{4.26}$$

with the following initial conditions:

$$T = \begin{cases} T_m, & \text{for } 0 \le r \le R \\ T_i, & \text{for } R < r < \infty \end{cases} \quad \text{at} \quad t = 0 \tag{4.27}$$

Equation (4.26) was written in a dimensionless form as:

$$\frac{\partial^2 T_D}{\partial r_D^2}+\frac{2}{r_D}\frac{\partial T_D}{\partial r_D}=\frac{\partial T_D}{\partial t_D};\quad 0 < r_D < \infty, \tag{4.28}$$

whose initial conditions were given by:

$$T_D = \begin{cases} 1, & \text{for } 0 \le r_D \le 1 \\ 0, & \text{for } 1 < r_D < \infty \end{cases} \text{ at } \quad t = 0 \tag{4.29}$$

A solution of equation (4.28) was originally proposed by Jost (1960) who established that it is given by:

$$T_D = \frac{1}{2}\left\{\operatorname{erf}\left[\frac{r_D + 1}{2\sqrt{t_D}}\right] - \operatorname{erf}\left[\frac{r_D - 1}{2\sqrt{t_D}}\right]\right\}$$

$$+ \frac{1}{r_D}\sqrt{\frac{t_D}{\pi}}\left\{\exp\left[-\frac{(r_D + 1)^2}{4t_D}\right] - \exp\left[-\frac{(r_D - 1)^2}{4t_D}\right]\right\} \tag{4.30}$$

Ascencio et al. (1994) carried out some simplifications of this equation on the basis of the following criteria:

(i) At the centre of the sphere, when the $r_D \rightarrow 0$, equation (4.30) reduces to

$$T_D = \operatorname{erf}\left[\frac{1}{2\sqrt{t_D}}\right] \tag{4.31}$$

(ii) For sufficiently long times, equation (4.31) can be approximated by

$$T_D = \left[\frac{1}{2\sqrt{\pi t_D}}\right] \tag{4.32}$$

which in terms of real variables becomes

$$T = T_i - m \cdot \frac{1}{\sqrt{t}} \tag{4.33}$$

where

$$m = \frac{R(T_i - T_m)}{\sqrt{\pi\alpha}} \tag{4.34}$$

Equation (4.33) represents a straight line when T and $1/\sqrt{t}$ are plotted. From this equation, the SFT value, T_i, can be obtained as the intercept with the ordinate axis ($t \rightarrow \infty$) that is, when equilibrium temperatures are attained (Fig. 4.3). It is very important to note that this method should only be applied to estimate bottomhole equilibrium temperatures. At other depths, the typical cylindrical and radial coordinate should be preferred.

4.3.5 Cylindrical source heat flow models

Hasan and Kabir (1994) developed a theory to evaluate the transient heat transfer from the drilling fluid to the formation under cylindrical source well conditions. This was done by means of the study of both conductive and convective heat transfer mechanisms in the well drilling process. Hasan and Kabir (1994) described the formation temperature distribution as a function of radial distance, depth and time. Thus, an energy balance on the wellbore fluid enabled the fluid temperature to be related to the wellbore/earth interface temperature and the heat flow, given an overall heat transfer coefficient in terms of a particular well configuration. Then the thermal diffusivity equation (4.9) was used to calculate the variation of the formation temperature with the radial distance from the well and the time. Initially, the formation temperature at any given depth is constant, leading to the following condition,

$$\lim_{t \to 0} T = T_i \tag{4.35}$$

At the infinite or outer boundary, the formation temperature does not change with the radial distance, i.e.,

$$\lim_{r \to \infty} \frac{\partial T}{\partial r} = 0 \tag{4.36}$$

The other boundary condition related to the heat flow rate at the interface of the wellbore and the formation is governed by Fourier's law of heat conduction,

$$\frac{dQ_w}{dz} = -\left[\frac{2\pi k_e}{W} \frac{r\,\partial T}{\partial r}\right]_{r=r_w} \tag{4.37}$$

To facilitate the solution and in order to get a more general applicability of the solution, the thermal diffusivity equation (4.9) was changed into dimensionless variables in a similar manner to equation (4.11). As a result of this heat transfer

analysis, three reduced equations were considered by Hasan and Kabir (1994) to describe the transient heat transfer in the wellbore/formation system.

(i) The complete transient heat transfer between wellbore and formation is analyzed as the heat loss per unit time per unit length by means of the following equation.

$$\frac{dQ_w}{dz} = M\, C_{pm} \frac{dT_{ws}}{dt} \qquad (4.38)$$

(ii) The heat transfer between the well centre and the wall is described by means of Fourier's law of heat conduction:

$$\frac{dQ_w}{dz} = -\, 2\pi\, r\, U\, (T_{ws} - T_{we}) \qquad (4.39)$$

In this case, mud is the only element of resistance to heat transfer in the well. Hence, U is interpreted as the free convection in the wellbore $U = h_{cm}$.

(iii) Finally, the heat transfer related to the temperature difference between the well wall (at the well/earth interface) and the SFT (T_i), is calculated by:

$$\frac{dQ_w}{dz} = -\, 2\pi\, k_e\, \frac{(T_{we} - T_i)}{T_D} \qquad (4.40)$$

where T_D represents the solution of the thermal diffusivity equation obtained by use of the cylindrical source well [Hasan and Kabir (1991)].

By combination of the heat transfer equations (4.38), (4.39) and (4.40), a simple differential equation was obtained to describe the variation of mud temperature with time:

$$\frac{dT_{ws}}{dz} = \frac{\left(\frac{dQ_w}{dz}\right)}{M\, c_{pm}} = -\left(\frac{2\pi}{M\, c_{pm}}\right)\left(\frac{r U k_e}{k_e + r U T_D}\right)(T_{ws} - T_i) \qquad (4.41)$$

or

$$\frac{dT_{ws}}{dt} = -\frac{(T_{ws} - T_i)}{A''} \tag{4.41a}$$

where A" is defined as a relaxation time parameter and is given by:

$$A'' = -\left(\frac{M\, c_{pm}}{2\pi}\right)\left(\frac{k_e + rUT_D}{rUk_e}\right) \tag{4.42}$$

Equation (4.41a) was rearranged to separate the variables and integrated in the following manner:

$$\frac{dT_{ws}}{(T_{ws} - T_i)} = -\frac{dt}{A''} \tag{4.43}$$

$$-\ln (T_i - T_{ws}) = C_o + \left(\frac{2\pi}{M\, c_{pm}}\right)(rUk_e)\int \frac{dt}{k_e + rUT_D} \tag{4.44}$$

where the constant of integration, C_o, indicates the initial temperature difference between the mud and earth. T_D may be approximated by means of a series of correlations which were reported by Hasan and Kabir (1991) as a function of t_D :

For $t_D < 1.5$

$$T_D = 1.1282\sqrt{t_D}\left(1 - 0.3\sqrt{t_D}\right) \tag{4.45}$$

For $t_D > 1.5$

$$T_D = (0.4063 + 0.5 \ln t_D)\left(1 + \frac{0.6}{t_D}\right) \tag{4.46}$$

Therefore, when equation (4.45) for t_D is chosen (for short times), a new version of equation (4.44) was obtained to represent the mud circulation in the well drilling:

$$\ln(T_i - T_{ws}) = -C_o - \left(\frac{2\pi}{M\, c_{pm}}\right)(rUk_e)\left(\frac{r^2}{\alpha}\right)\cdot\int \frac{dt_D}{k_e + rU\left[1.13\sqrt{t_D}\left(1 - 0.3\sqrt{t_D}\right)\right]} \tag{4.47}$$

After several mathematical reducing steps, Hasan and Kabir (1994) proposed a solution of the mud temperature, T_{ws}, in terms of the SFT (T_i) which is given by:

$$T_{ws} = T_i - C_o" \ \xi(t_D) \tag{4.48}$$

This equation represents a general solution to evaluate the transient heat transfer between the wellbore mud and the formation. Consequently, the effect of mud circulation on the formation temperature distribution was evaluated by application of the superposition principle. Therefore, equation (4.48) was modified in terms of dimensionless variables to give:

$$T_{ws} = T_i - C_o" \ [\xi(t_{pD}+\Delta t_D) - \xi(\Delta t_D)] \tag{4.49}$$

This analytical expression suggests that a plot of T_{ws} against $[\xi(t_{pD}+\Delta t_D)- \xi(\Delta t_D)]$ should result in a straight line. The intercept yields the static formation temperature (SFT) with slope, $C_o"$ (Fig. 4.4). The calculation necessary to apply the strict solution presented in equation (4.49) is to some extent complex because it requires a considerable amount of well drilling data. In this context, Hasan and Kabir (1994) demonstrated that the estimation of the free convective heat transfer coefficient, h_{cm}, for the mud constitutes a serious problem because there are no reliable correlations available that allow it to be calculated. Furthermore, the thermophysical and transport properties of muds as a function of p, T, and composition are not available. Therefore, it is not always possible to use directly the rigorous solution proposed by equation (4.49), except if all these data are available. Hence, Hasan and Kabir (1994) simplified the calculation procedure in order to derive three approximate solutions which allow the evaluation of SFT values as a reasonable alternative.

Exponential approach. This approximation results from the assumption that the relaxation parameter A" given by equation (4.42), is a constant. This would be true for a combination of small values of t_D and a low heat transfer coefficient for the mud. Consequently the integration of equation (4.43) from t=0 (T_i) to t=t (T_{ws}) yields:

$$T_{ws} = T_i - C_o" e^{-t/A"} \tag{4.50}$$

Thus, a plot of transient temperature data against $e^{-t/A"}$ should result in a straight line, with the SFT as an intercept (Fig. 4.5). The use of the superposition principle to account for mud circulation before shut-in does not change the form of equation (4.50) because of its exponential nature. Therefore,

$$T_{ws} = T_i - C_o" \left(e^{-t_p/A"} - 1\right) e^{-\Delta t/A"} \tag{4.51}$$

Log/linear approach. This approximation is based on similar assumptions used in the classical Horner method [Dowdle and Cobb (1975)]. The assumptions considered are the following.

(i) The mud has been circulating for a long time. This means that the formation temperature distribution can be estimated by logarithmic aproximation using equation (4.46), which was developed according to the studies previously reported by Ramey (1962) and Hasan and Kabir (1991).

(ii) The mud temperature at the wellbore centre, T_{ws}, may be assumed to be equal to the temperature at the interface of the wellbore and the earth because a very high heat transfer coefficient for the mud is assumed.

Considering these assumptions, an equation for the dimensionless temperature, T_D, may then be written as a function of T_{ws}:

$$T_{ws} = T_i - B_o T_D \tag{4.52}$$

where

$$B_o = \frac{dQ_w}{dz} \frac{1}{(2\pi k)} \tag{4.53}$$

Thus, for a total dimensionless mud circulation time, t_{pD}, and after combining equations (4.53) and (4.46), a general equation is obtained:

$$T_{ws} = T_i - B_o\,(0.406 + 0.5 \ln t_D) \qquad (4.54)$$

Considering the superposition principle for the evaluation of the mud temperature for a period of Δt_D after the cessation of circulation, equation (4.54) is modified to:

$$T_{ws} = T_i - 0.5\,B_o \ln\left(\frac{t_p + \Delta t}{\Delta t}\right) \qquad (4.55)$$

Therefore, a plot of the mud temperature against the logarithm of the DHT, should be linear. The intercept at DHT = 1.0 (i.e. a very long Δt), should give the SFT value (see Fig. 4.1). Note that this approximation presupposes that the heat exchange between the formation and the wellbore is zero after the mud circulation has stopped. It is important to note that this assumption is reasonable at very long times, but it may be invalid at intermediate times when significant heat transfer may occur.

Time root approximation. This approach is based on the superposition principle applied to equation (4.52), using the proposed correlation for short times, i.e. $t_D < 1.5$ (equation 4.45), instead of the log/linear approximation for $t_D > 1.5$ (equation 4.46) for long times. Hence, equation (4.52) can be modified to:

$$T_i - T_{ws} = B_o\,[T_D\,(t_{pD} + \Delta t_D) - T_D(\Delta t_D)] \qquad (4.56)$$

or

$$T_{ws} = T_i - 1.1282\,B_o\,F'\,(t_D) \qquad (4.57)$$

where

$$F'(t_D) = \left(\sqrt{t_{pD} + \Delta t_D}\right)\left(1 - 0.3\sqrt{t_{pD} + \Delta t_D}\right) - \sqrt{t_{pD}}\left(1 - 0.3\sqrt{t_{pD}}\right) \qquad (4.59)$$

Thus, a plot of T_{ws} against $F'(t_D)$ should yield a straight line with SFT (T_i) as the intercept (Fig. 4.6).

In general terms, the description of all the main equations related to the cylindrical heat source model were given in this section. Details of the complete mathematical procedure are presented by Hasan and Kabir (1994).

4.4 Description of the Computer Code (STATIC_TEMP)

A software package for estimating SFTs from well drilling temperature data was developed (STATIC_TEMP). It provides a useful tool that can be used in-situ to determine the SFT during geothermal well drilling operations. In this section, a complete description of STATIC_TEMP is presented. Computer architecture and the numerical algorithms used in the software development are described.

4.4.1 Software development

STATIC_TEMP is a computer program developed for estimating the static formation temperatures. This computer code is based on the equations of five analytical methods which were referred to in the previous section. STATIC_TEMP was originally written in the Fortran 77 language for a Vax/Vms V5.3 Digital computer system. However, another version for personal computers was also developed. Figure 4.7 shows the flow diagram of the main program. In its general form, the architecture of the computer program developed is:

(i) a main program (STATIC_TEMP),

(ii) two input data files (WELL_DRILL and KRITIKOS),

(iii) five output data files (HORNER, ROUX, KRITIKOS, ASCENCIO and HASAN),

and

(iv) ten subroutines, one for each calculation method (HORNER, ROUX, ROUX_CORRECTION, KRITIKOS, KRIT, INTGEXP, ASCENCIO, HASAN, METHODS and THERMAL_PROP).

STATIC_TEMP is the main program that selects the analytical method to be used and calls the appropriate subroutine to predict the final SFT. Also, STATIC_TEMP enables the number of temperature log analyses to be considered.

HORNER is a subroutine that facilitates the estimation of the SFT by means of the line-source solution described by Manetti (1973) and Dowdle and Cobb (1975). Furthermore, the HORNER subroutine loads the main results of all the calculations into the output data file (HORNER.OUT). The flow diagram of the HORNER subroutine is shown in Fig. 4.8.

ROUX is a subroutine that provides the means to estimate the SFT using the equations proposed by the improved Horner method [Roux et al (1980)]. The ROUX subroutine calls the ROUX_CORRECTION subroutine for correcting the SFT calculated by the Horner approximation. Finally, ROUX stores the results obtained from the complete calculation in the output data file (ROUX.OUT). Figures 4.9 and 4.9a show the flow diagrams of the ROUX and ROUX_CORRECTION subroutines, respectively.

KRITIKOS is a subroutine that calculates the SFT by means of the equations of the two-point analytical method proposed by Kritikos and Kutasov (1988). The KRITIKOS subroutine enables the temperature measurement data to be read from the input data file (KRITIKOS.DAT). It also performs the main logical and sequential calculations that the two-point method requires. KRITIKOS calls the KRIT and INTGEXP subroutines for estimating the argument of the E_i function and the value of its integral form, respectively. Finally, KRITIKOS dumps the results obtained from the complete calculation in the output data file (KRITIKOS.OUT). The flow diagram of the KRITIKOS subroutine is shown in Fig. 4.10.

ASCENCIO is a subroutine that allows the estimation of the SFT by the spherical and radial heat flow solution proposed by Ascencio et al (1994).

Additionally, the ASCENCIO subroutine dumps the results obtained in the SFT calculation into the output data file (ASCENCIO.OUT). The flow diagram of the ASCENCIO subroutine is shown in Fig. 4.11.

HASAN is a subroutine that determines SFT values by means of the cylindrical-source solution suggested by Hasan and Kabir (1994). The HASAN subroutine calls the METHODS subroutine for selecting the approximation method to calculate the SFT. Four analytical solutions are available. The METHODS subroutine calls the THERMAL_PROP subroutine to read the petrophysical and transport properties of both the drilling fluid and formation. Finally, the HASAN subroutine stores the results obtained in the SFT calculation into the output data file (HASAN.OUT). Figures 12 and 12a show the flow diagrams of the HASAN and METHODS subroutines, respectively. A final listing of the computer source program is included in Appendix I.

4.4.2 Numerical algorithm

All the analytical methods that were incorporated into the STATIC_TEMP use the linear regression method to yield the final SFT, when shut-in temperature data against time parameters are plotted. Typically, under these graphical conditions, the intercept of the straight line always yields the final static formation temperature, while the slope will produce some heat flow or time parameters [Dowdle and Cobb (1975); Hasan and Kabir (1994)]. Therefore, a numerical algorithm based on the least squares fit to a straight line method was incorporated in each of the analytical methods according to the numerical methodology proposed by Drury (1984).

4.5 Validation Tests of STATIC_TEMP

STATIC_TEMP was validated by use of synthetic well temperature data reported by Shen and Beck (1986). Petrophysical and transport properties of both drilling fluid and formation were available in the same research work. Table 4.1 presents

a complete compilation of these data. A heat transfer analysis made by these authors indicated that the true formation temperature related to these well drilling values is equal to 80°C. Shen and Beck (1986) predicted this SFT value by means of a constant temperature wellbore model with no convective heat transfer (i.e. assuming only conductive heat transfer in the drilling system). Even though Shen and Beck's model is different to some of the analytical methods included in the STATIC_TEMP program, the SFT value (80 °C) can be used as a good indicator to validate the computer code and the analytical methods considered.

All the temperature data employed in the numerical calculation were included in the general input data file (WELL_DRILL.DAT). Essentially these data are related to:

(a) the number of temperature logs (NDAT),
(b) the mud circulation time (t_p),
(c) the name of the well drilled,
(d) the depth,
(e) the shut-in time after the cessation of drilling (Δt),
and
(f) the shut-in temperatures (T_{ws}).

Additional data related to the petrophysical and transport properties for both the formation and drilling fluid must be given to the computer code by an interactive process. With respect to this information, STATIC_TEMP requires the following data:

1. specific heat capacity of formation (C_{pe}),
2. specific heat capacity of wellbore fluid (C_{pm}),
3. convective heat transfer coefficient for mud (h_{cm}),
4. thermal conductivity of formation (k_e),
5. thermal conductivity of mud (k_m),

6. mass of mud (M),
7. radial distance from the wellbore (r),
8. wellbore radius (r_w)

and

9. mud density (ρ_m).

4.5.1 Results of the validation tests

A listing of the validation results obtained by means of the computer program are presented numerically in Table 4.2 and graphically in Fig. 4.13. The results presented in them reflect the static formation temperatures obtained after application of the analytical methods incorporated in the STATIC_TEMP. Because the true formation temperature for the synthetic well drilling data is known [Shen and Beck (1986)], the absolute accuracy of these methods can be evaluated. The computer validation suggests in all the cases simulated that the SFT was underestimated (Fig. 4.14). Also, the STATIC_TEMP predicts that the rigorous approximation [proposed by Hasan and Kabir (1994)] yields results very close to the true values [difference = 0.6% (79.5°C)], while, the farthest value from the true temperature was derived from the application of the time-root approximation [difference = 23.2% (61.4 °C)]. This high deviation was previously reported and justified by Hasan and Kabir (1994).

4.5.2 Estimation errors

A numerical criterion developed by Drury (1984) was adopted to evaluate the errors involved in the calculation of SFT values by the line heat source methods. The method helps to visualize how the use of the approximation (equation 4.4) can lead to significant errors in the SFT calculation. The method considers the effect produced by thermophysical rock properties, well radius and drilling time parameters on the calculation of the SFT. In order to carry out this evaluation, the dimensionless parameters θ and β were introduced.

The value of θ is given by the Fourier number (r_w^2/α t') while β is defined as the ratio of the solutions of equations 3.2 and 3.5 (given in chapter 3) for a particular set of r_w, α, Δt and t' values. Thus, Drury's criterion is directly related to the value that the β parameter will take. When β adopts values greater than unity (β>1), this parameter can be understood as an amount by which the approximate solution (equation 3.5) for the thermal effect of a line source exceeds the exact solution (equation 3.2). This indicates that the approximate solution for the exponential integral (equations 3.4 or 4.4) must be used carefully in the final calculation of SFT. On the other hand, when β=1, the approximate solution proposed by equations (3.4 or 4.4) can be used reliably.

In order to apply Drury's criterion, a numerical algorithm was developed and codified in a spreadsheet. The procedure estimates the β parameter as a function of the ratio Δt/t' for different values of θ. Table 4.3 shows a summary of the results obtained by means of this numerical procedure. A plot of β against Δt/t' is shown in Fig. 4.15. From this figure, it can be observed that when θ is small the ratio β is also small for Δt/t' values between 0.01 and 10. Under these conditions, any error introduced by using the approximation of equation (4.4) to obtain the SFT would be negligible. If θ is large for Δt/t' values between 0.1 and 10, the ratio β will be large too. Therefore, the temperature anomaly predicted from equation (3.5) may be quite different than that predicted from the exact solution (equation 3.2). This deviation could produce serious errors in the final estimation of the SFT. When such conditions occur, it is recommended that the data should be corrected by means of the exact solution given by the equation (3.2).

A similar behaviour is observed when the parameter β is plotted against the dimensionless Horner time; DHT(Fig. 4.16). In this case, when large values of θ and DHT<10 are considered, the ratio β takes a value which indicates that the simplified solution differs greatly from the exact solution.

From these studies it can be observed that θ becomes a critical parameter in the estimation of the SFT so that, in practical conditions, it is important to determine as accurately as possible the magnitude of this parameter. This estimation could be made from a knowledge of the main thermophysical formation properties (k, ρ, Cp or α), wellbore radius and time parameters.

Thus, an accurate knowledge of θ and β is needed in order to decide if equation (4.4) provides a valid and reliable approximation for the exponential integral contained in the linear heat source equation (3.1) from which the majority of the analytical methods are derived.

Examples of application. In order to apply the numerical criterion described above, a set of shut-in temperature data were considered and discussed. The borehole temperature measurements (BHT) were taken from the CH-A well drilling activities carried out in the Chipilapa geothermal field [Iglesias et al (1995)]. A summary of these measurements is presented in Table 4.4. The BHT were used to estimate the SFT by means of the STATIC_TEMP computer code. The numerical processing of the CH-A well data was carried out using the following methods:

(a) the Horner method [Dowdle and Cobb (1975)],

(b) the improved Horner method [Roux et al (1980)],

(c) the two-point method [Kritikos and Kutasov (1988)],

and

(d) the spherical method [Ascencio et al (1994)].

A summary of the results obtained during these calculations is presented in Table 4.5. The estimated static formation temperature from the shut-in temperature data indicates values close to 244 °C. The thermal behaviour of the CH-A well data can be evaluated if the temperature profiles derived from these numerical runs are plotted (Fig. 4.17). In Fig. 4.17, a profile related to the

homogenisation temperature of the geothermal reservoir and the water boiling curve temperatures are included. Apparently, the homogenisation temperatures reflect the equilibrium state attained by the fluid under unperturbed reservoir conditions. Therefore, a comparison among the SFTs from several numerical methods and the homogenisation temperatures provides an excellent reference of the true reservoir temperature. The homogenisation temperatures for the CH-A well were previously determined by Gonzalez et al (1995) using the fluid inclusions technique. In the case of the boiling curve temperatures, these show the highest values of all temperature data sets because they are related to pure water.

From Fig. 4.17, the shut-in temperature profile of the CH-A well shows a severe distortion at two different depth ranges (i.e. 500 to 1000m and 1500 to 2500m). This anomalous profile is due to the presence of drilling fluid lost in circulation, which occurred at these depths during well drilling activities [Iglesias et al (1993)]. Under these conditions, convective heat transfer predominates at these depths. Therefore, it is expected that the SFT calculated by means of the proposed numerical methods (**a-d**) will underestimate these temperatures. This assertion can be supported since all the estimative methods employed consider only the conductive effects as the predominant heat transfer process in the well during shut-in. Even though both heat transfer mechanisms (conduction and convection) should be considered in the SFT estimation, all sets of results obtained in the CH-A thermal estimation provide similar SFT estimates for this geothermal well.

Finally, the SFT values calculated for the CH-A well were evaluated by means of Drury's criterion. This evaluation was carried out because all the methods considered [except method (d)] use the simplified solution (equation 3.5) in the final calculation of SFT. In order to evaluate the β parameter, real values of the θ and the ratio $\Delta t/t'$ were required for the CH-A well. Therefore, a compilation of the thermophysical formation properties was performed. Average thermophysical

rock properties were obtained from the database reported by Contreras et al (1994). The compiled average data are as follows:

(i) thermal conductivity (k=1.63 W m^{-1} $°C^{-1}$),

(ii) total density (ρ=2680 kg m^{-3}),

and

(iii) specific heat capacity (Cp=962.96 J kg^{-1} $°C^{-1}$)

From these data, calculations of the thermal diffusivity were carried out. The results indicated an average value of $\alpha=6.1\times10^{-7}$ m^2 s^{-1}. The wellbore radius is 0.2159 m and the determined ratio is $\Delta t/t'=0.88$ (for $\Delta t=190$ and $t'=215$ hours). These data were obtained from the CH-A well completion database which was reported by Iglesias et al (1993). From these data, the corresponding θ value is 0.1, so θ enables β to be obtained from Fig. 4.15. This procedure gives a final value of $\beta=1.02$, which demonstrates that in this particular case the proposed simplified solution (equation 3.5) provides a good approximation for the calculation of the true reservoir temperature.

Summary. A new software package for estimating static formation temperatures (SFT) was developed. STATIC_TEMP is the computer program that can provide an accurate in-situ estimation of the formation temperatures which is typically required for a variety of well drilling applications. This computer capability allows the determination of SFT during and after mud circulation. Consequently, the STATIC_TEMP constitutes a useful tool that can be used realiably during geothermal well drilling operations.

A numerical criterion to evaluate possible sources of error associated with the calculation of static formation temperatures through the line heat source methods was studied and discussed. The method was applied to evaluate the SFT values calculated for the CH-A well from the Chipilapa geothermal field (El Salvador).

4.6 References

F. Ascencio, A. Garcia, J. Rivera and V. Arellano, Estimation of undisturbed formation temperatures under spherical-radial heat flow conditions, Geothermics **23** 317-326 (1994).

E. Contreras, D. Renteria y M. Guevara, Estudio y evaluacion de metodologias para estimar propiedades termofisicas de rocas a partir de analisis quimicos y estudios petrograficos, Informe Final IIE/11/5568/I 01/F, 177 p. (1994).

W.L. Dowdle and W.M. Cobb, Static formation temperature from well logs - an empirical method, Journal of Petroleum Technology, **November** 1326-1330 (1975).

M.J. Drury, On a possible source of error in extracting equilibrium formation temperatures from borehole BHT data, Geothermics **13** (3) 175-180 (1984).

C. Ehlig-Economedes, Transient rate decline and pressure buildup for wells produced at constant pressure, Ph.D Dissertation, Petroleum Engineering Department, Stanford University, CA, USA (1979).

E. Gonzalez-Partida, A. Garcia-Gutierrez and V. Torres-Rodriguez, Thermal and petrologic study of the CH-A well from the Chipilapa-Ahuachapan geothermal area, Accepted for publication in Geothermics (in press), 6 p. (1997).

A.R. Hasan and C.S. Kabir, Heat transfer during two-phase flow in wellbores: Part I - Formation temperature, Paper SPE 22866 presented at the 1991 SPE Annual Technical Conference and Exhibition, Dallas, Texas (USA), Oct. 6-9, 469-478 (1991).

A.R. Hasan and C.S. Kabir, Static reservoir temperature determination from transient data after mud circulation, SPE Drilling & Completion, **March** 17-24 (1994).

D.R. Horner, Pressure buildup in wells, Proc. Third World Petroleum Congress, The Hague, The Netherlands, Vol. II, p. 503, (1951).

E. Iglesias, R.J. Torres, E. Contreras, E. Gonzalez, G. Izquierdo, M. Guevara y D. Renteria, Estudios geocientificos y de ingenieria de reservorios del campo geotermico de Chipilapa, Inf. Tec. del Pozo CH-A, IIE/IRV-IF-002, 74 p. (1993).

E. Iglesias, A. Campos-Romero and J. Torres, A reservoir engineering assessment of the Chipilapa, El Salvador, geothermal field, Proc. of the International Geothermal Congress, Italy, 6 p. (1995).

W.R. Kritikos and I.M. Kutasov, Two-point method for determination of undisturbed reservoir temperature, SPE Formation Evaluation Journal, **March** 222-226 (1988).

G. Manetti, Attainment of temperature equilibrium in holes during drilling, Geothermics, **2** 94-100 (1973).

C.S. Matthews and D.G. Russell, Pressure buildup and flow tests in wells, Society of Petroleum Engineers of AIME, SPE Monographs, 168 p. (1967).

H.J. Ramey Jr., Wellbore heat transmission, Journal of Petroleum Technology (JPT), **April** 427-435 (1962).

B. Roux, An improved approach to estimating true reservoir temperature from transient temperature, M.S. Thesis, Stanford University, CA, USA (1979).

B. Roux, S.K. Sanyal and S.L. Brown, An improved approach to estimating true reservoir temperature from transient temperature data, 50th Annual California Regional Meeting of the Society of Petroleum Engineers, Los Angeles, CA, USA, April 9-11, 9 p. (1980).

P.Y. Shen and A.E. Beck, Stabilization of bottom hole temperature with finite circulation time and fluid flow, Geophys. J. R. Astr. Soc. **86** 63-90 (1986).

Time [hr]	Drilling fluid temperature [°C]	Thermophysical properties	Units
2.5	56.6	$k_e = 2.510$	[W m^{-1} °C^{-1}]
5.0	61.3	$\rho_e.Cp_e = 2.09x10^6$	[J m^{-3} °C^{-1}]
7.5	64.3		
10.0	66.6	$k_m = 0.610$	[W m^{-1} °C^{-1}]
15.0	69.6	$\rho_m.Cp_m = 4.19x10^6$	[J m^{-3} °C^{-1}]
20.0	71.7		
		$r_w = 0.108$	[m]
		$r = 0.108$	[m]
		$t_n = 5.0$	[hr]
		$M = 140.0$	[kg]
SFT =	80.0 °C		

Table 4.1

Synthetic well drilling data [taken from Shen and Beck (1986)].

	Temperature predictions [°C]						
	[1]	[2]	[3]	[4]	[5]	[6]	[7]
	55.54	57.16	55.59	57.56	55.54	60.82	57.37
	62.38	63.99	62.34	60.86	62.38	61.27	60.96
	65.45	67.06	65.33	63.65	62.45	62.39	63.77
	67.22	68.83	67.12	66.01	67.22	63.99	66.07
	69.21	70.82	69.23	69.69	69.21	68.22	69.65
	70.30	71.90	70.49	72.33	70.30	73.41	72.28
SFT	74.06	75.67	78.64	78.99	74.06	61.44	79.52

[1] Horner method,
[2] improved Horner method,
[3] spherical and radial method,
[4] exponential approximation of the cylindrical source solution,
[5] log-linear approximation of the cylindrical source solution,
[6] time-root approximation of the cylindrical source solution,
and
[7] rigorous approximation of the cylindrical source solution.

Table 4.2

Numerical results obtained from the application of STATIC_TEMP to the synthetic well drilling data.

$\Delta t/t'$	ln DHT (eq. 3.5)	θ	$(-x_1)$	$(-x_2)$	$E_i(-x_1)$	$E_i(-x_2)$	$E_{i\text{-}tot}$ (eq. 3.2)	β
1.0	0.6931	10.00	2.500	1.2500	0.0249	0.1464	-0.1215	5.7
3.0	0.2877		0.833	0.6250	0.2926	0.4323	-0.1397	2.1
5.0	0.1823		0.500	0.4167	0.5598	0.6752	-0.1155	1.6
7.0	0.1335		0.357	0.3125	0.7800	0.8756	-0.0956	1.4
8.5	0.1112		0.294	0.2632	0.9204	1.0046	-0.0842	1.3
10.0	0.0953		0.250	0.2273	1.0443	1.1194	-0.0751	1.3
0.1	2.3979	3.00	7.500	0.6818	0.0001	0.3870	-0.3869	6.2
0.5	1.0986		1.500	0.5000	0.1000	0.5598	-0.4598	2.4
1.0	0.6931		0.750	0.3750	0.3403	0.7462	-0.4059	1.7
5.0	0.1823		0.150	0.1250	1.4645	1.6234	-0.1590	1.1
7.0	0.1335		0.107	0.0938	1.7607	1.8815	-0.1208	1.1
10.0	0.0935		0.075	0.0682	2.0867	2.1754	-0.0887	1.1
0.0	4.6151	1.00	25.000	0.2475	0.0000	1.0520	-1.0520	4.4
0.1	2.3979		2.500	0.2273	0.0249	1.1194	-1.0945	2.2
0.5	1.0986		0.500	0.1667	0.5598	1.3745	-0.8147	1.3
1.0	0.6931		0.250	0.1250	1.0443	1.6234	-0.5791	1.2
5.0	0.1823		0.050	0.0417	2.4679	2.6421	-0.1742	1.0
10.0	0.0953		0.025	0.227	3.1365	3.2296	-0.0931	1.0
0.0	4.6151	0.30	7.500	0.0743	0.0001	2.0959	-2.0958	2.2
0.1	2.3979		0.750	0.0682	0.3403	2.1754	-1.8351	1.3
0.5	1.0986		0.150	0.0500	1.4645	2.4679	-1.0034	1.1
1.0	0.6931		0.075	0.0375	2.0867	2.7433	-0.6567	1.1
5.0	0.1823		0.015	0.0125	3.6374	3.8173	-0.1798	1.0
10.0	0.0953		0.008	0.0068	4.3231	4.4178	-0.0946	1.0
0.0	4.6151	0.10	2.500	0.0248	0.0249	3.1462	-3.1213	1.5
0.1	2.3979		0.250	0.0227	1.0443	3.2296	-2.1853	1.1
0.5	1.0986		0.050	0.0167	2.4679	3.5337	-1.0658	1.0
1.0	0.6931		0.025	0.0125	3.1365	3.8173	-0.6808	1.0
5.0	0.1823		0.005	0.0042	4.7261	4.9076	-0.1815	1.0
10.0	0.0953		0.003	0.0023	5.4167	5.5118	-0.0951	1.0
0.0	4.6151	0.03	0.750	0.0074	0.3403	4.3330	-3.9927	1.2
0.1	2.3979		0.075	0.0068	2.0867	4.4178	-2.3311	1.0
0.5	1.0986		0.015	0.0050	3.6374	4.7261	-1.0887	1.0
0.9	0.7591		0.009	0.0040	4.1963	4.9509	-0.7546	1.0
1.0	0.6931		0.008	0.0038	4.3231	5.0125	-0.6894	1.0
5.0	0.1823		0.002	0.0013	5.9266	6.1086	-0.1821	1.0
10.0	0.0953		0.001	0.0007	6.6190	6.7142	-0.0952	1.0
0.0	4.6151	0.01	0.250	0.0025	1.0443	5.4267	-4.3824	1.1
0.1	2.3979		0.025	0.0023	3.1365	5.5118	-2.3753	1.0
0.5	1.0986		0.005	0.0017	4.7261	5.8214	-1.0953	1.0
1.0	0.6931		0.003	0.0013	5.4167	6.1086	-0.6919	1.0
5.0	0.1823		0.001	0.0004	7.0242	7.2064	-0.1822	1.0
10.0	0.0953		0.000	0.0002	7.7171	7.8124	-0.0953	1.0

Table 4.3

Estimated errors for the linear heat source equation applying Drury's criterion.

Depth (m)	T/275 (6 hr)	T/276 (12 hr)	T/277 (26.57 hr)	T/278 (47.10 hr)	T/280 (95.27 hr)	T/282 (190.5 hr)
		Temp. Logs shut-in temperature data (°C)				
248	52	52	65	68	100	105
448	62	65	90	95	105	106
748	78	92	110	122	132	148
948	85	94	122	139	152	169
1248	102	118	132	145	155	166
1548	90	102	116	130	145	160
1748	86	97	108	122	132	145
1998	86	95	99	114	124	136
2048	86	95	99	114	124	136
2098	86	95	99	114	124	136
2148	95	95	99	114	124	136
2198	95	102	111	120	130	138
2248	100	103	112	122	132	140
2298	102	104	114	124	136	145
2348	111	111	116	126	138	156
2690	231	231	235	237	239	240

Table 4.4

Shut-in temperature data taken from the drilling activities of CH-A geothermal well [data taken from Iglesias et al (1995)].

Well	[1]	[2]	[3]	[4]	[5]
	Temperature °C				
CH-A	243.7	243.3	242.1	244.1	244.0

(1) Horner method,
(2) improved Horner method,
(3) two-point method,
(4) spherical method,
and
(5) homogeneization temperatures taken from Gonzalez et al (1995).

Table 4.5

Estimated static formation temperatures for CH-A well from Chipilapa geothermal field.

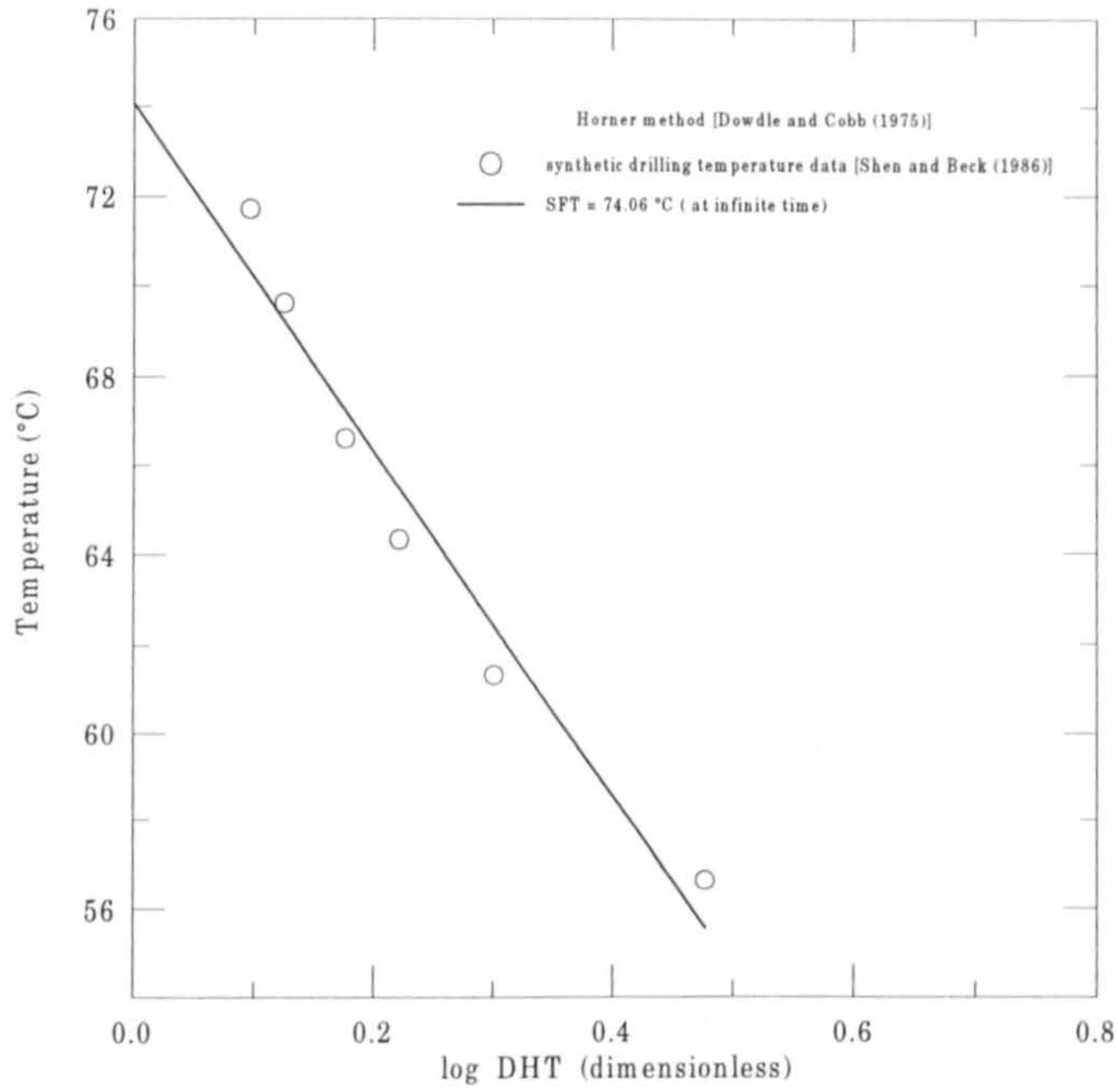

Fig. 4.1 Evaluation of the static formation temperature by means of the classical Horner method.

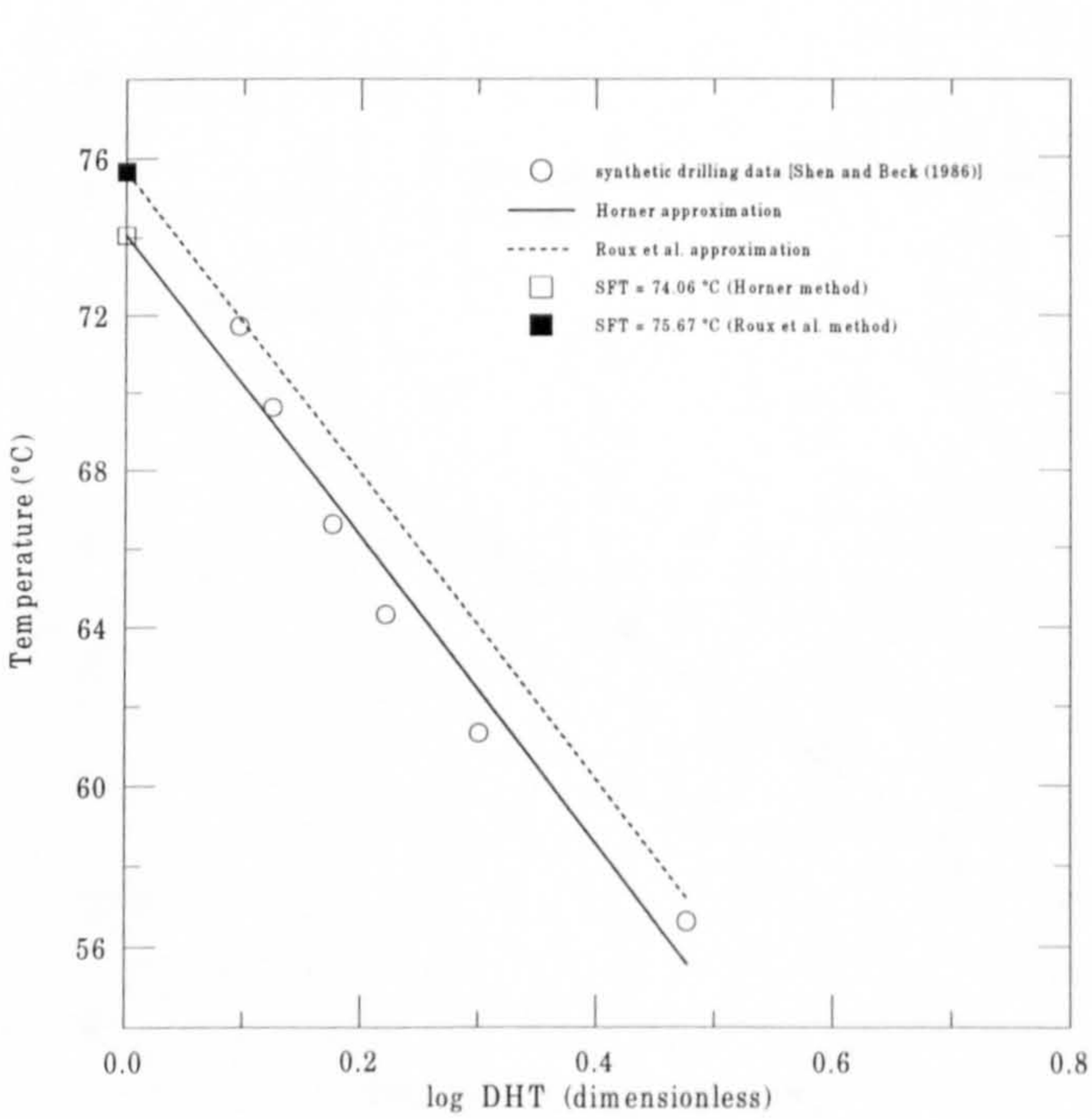

Fig. 4.2 Evaluation of the static formation temperature by means of the classical and improved version of the Horner method.

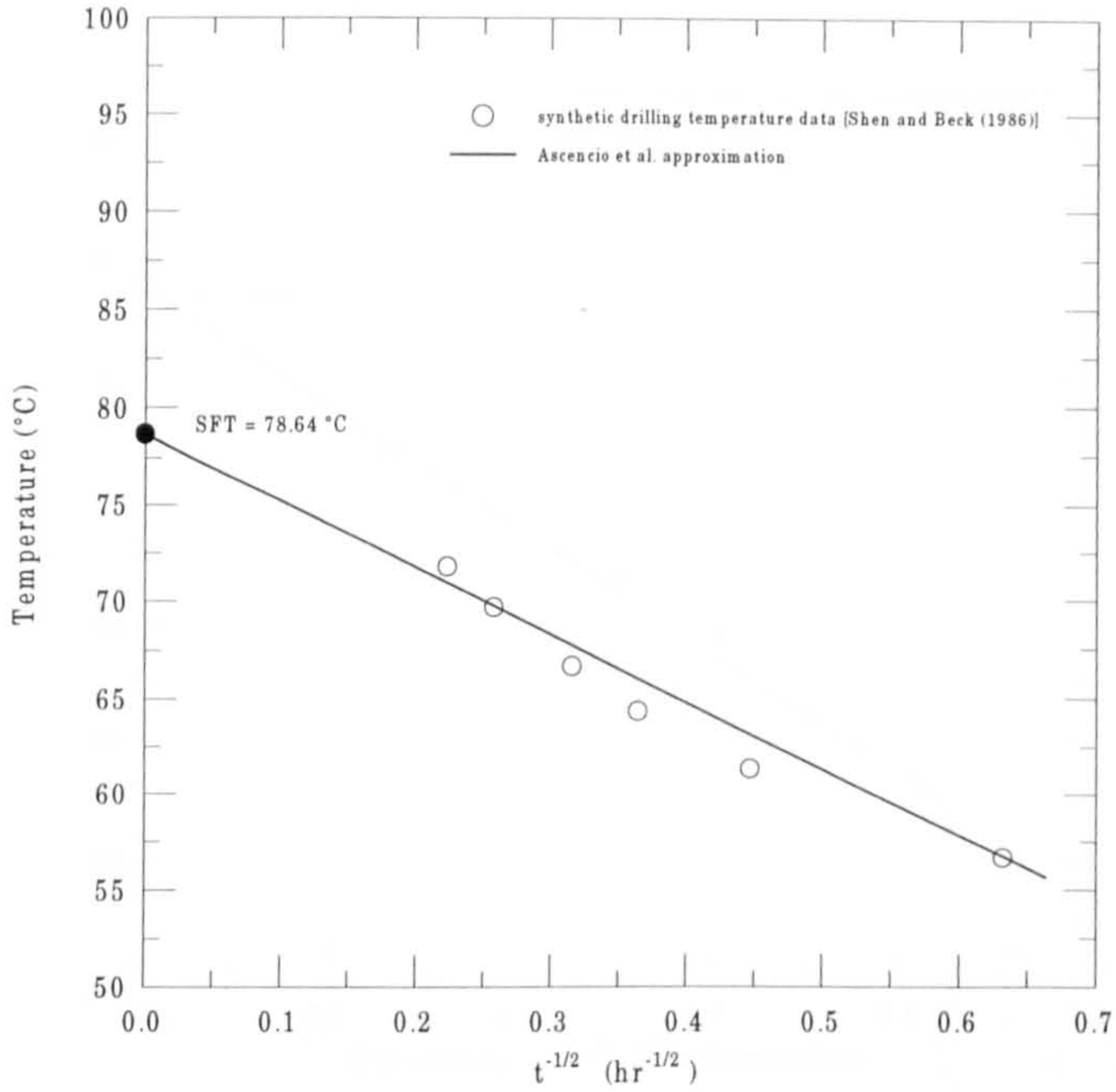

Fig. 4.3 Evaluation of the static formation temperature by means of the Ascencio et al. (1994) method.

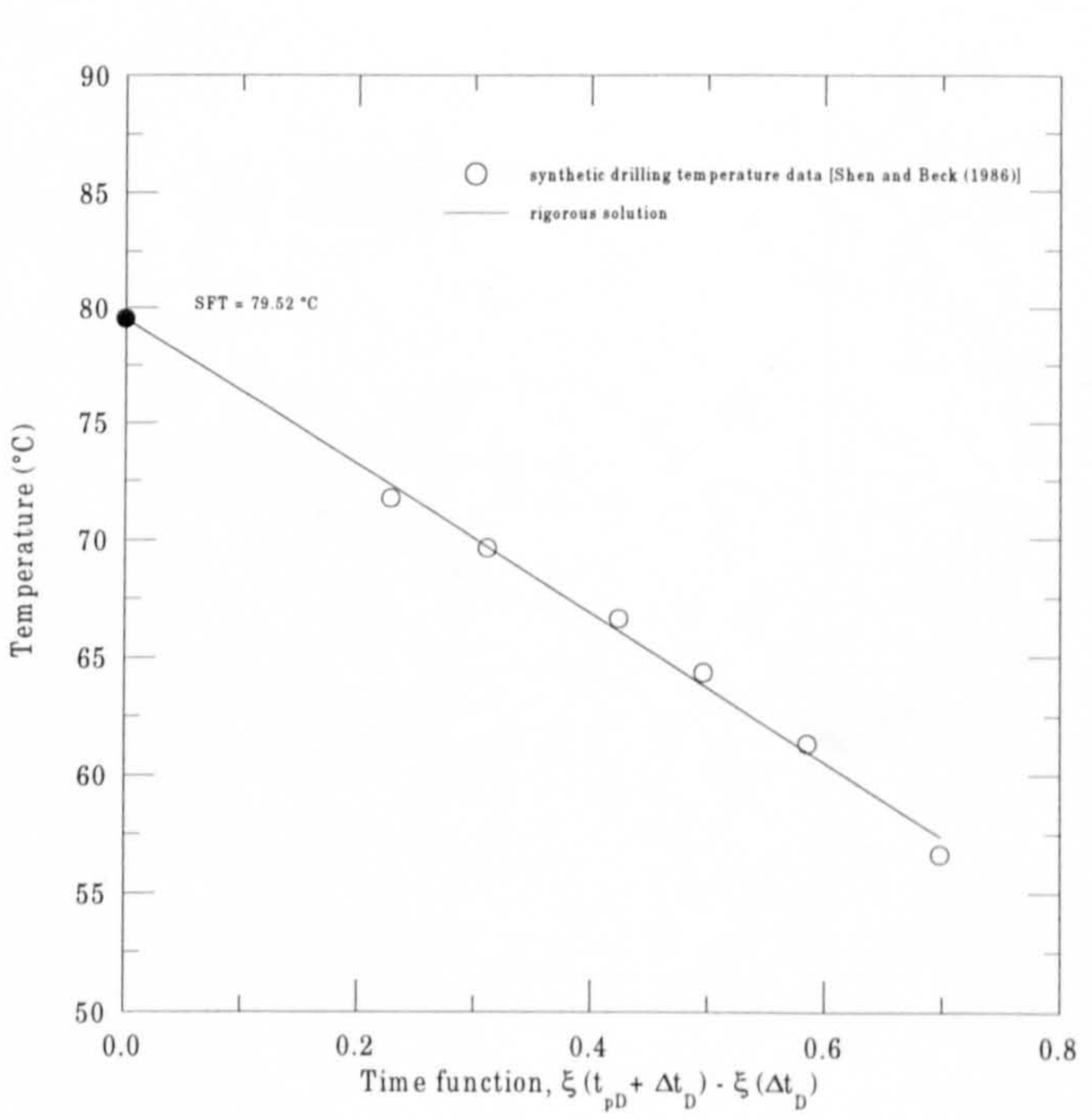

Fig. 4.4 Evaluation of the static formation temperature by means of the rigorous solution of the Hasan and Kabir (1994) method.

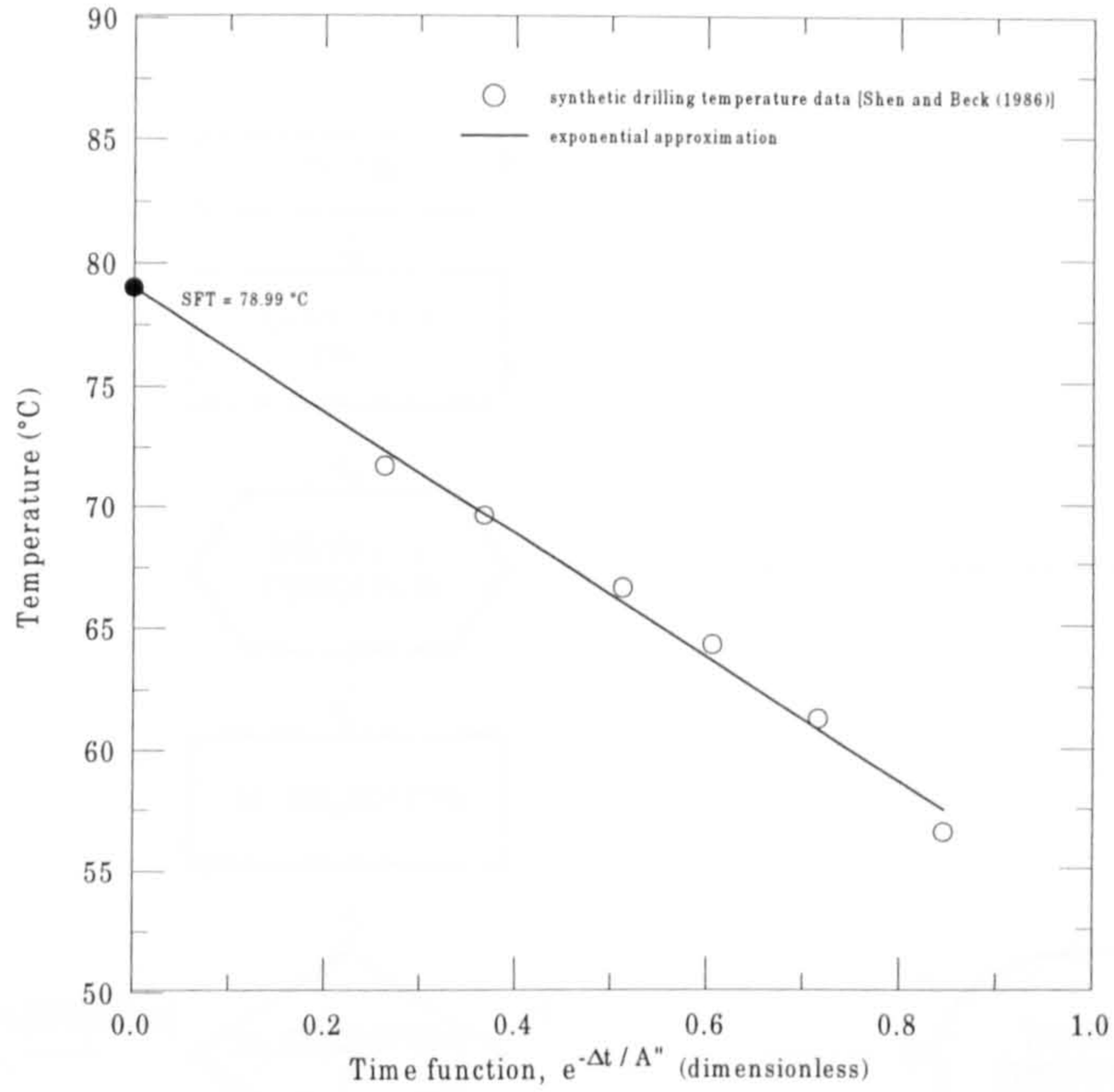

Fig. 4.5 Evaluation of the static formation temperature by means of the exponential approximation of the Hasan and Kabir (1994) method.

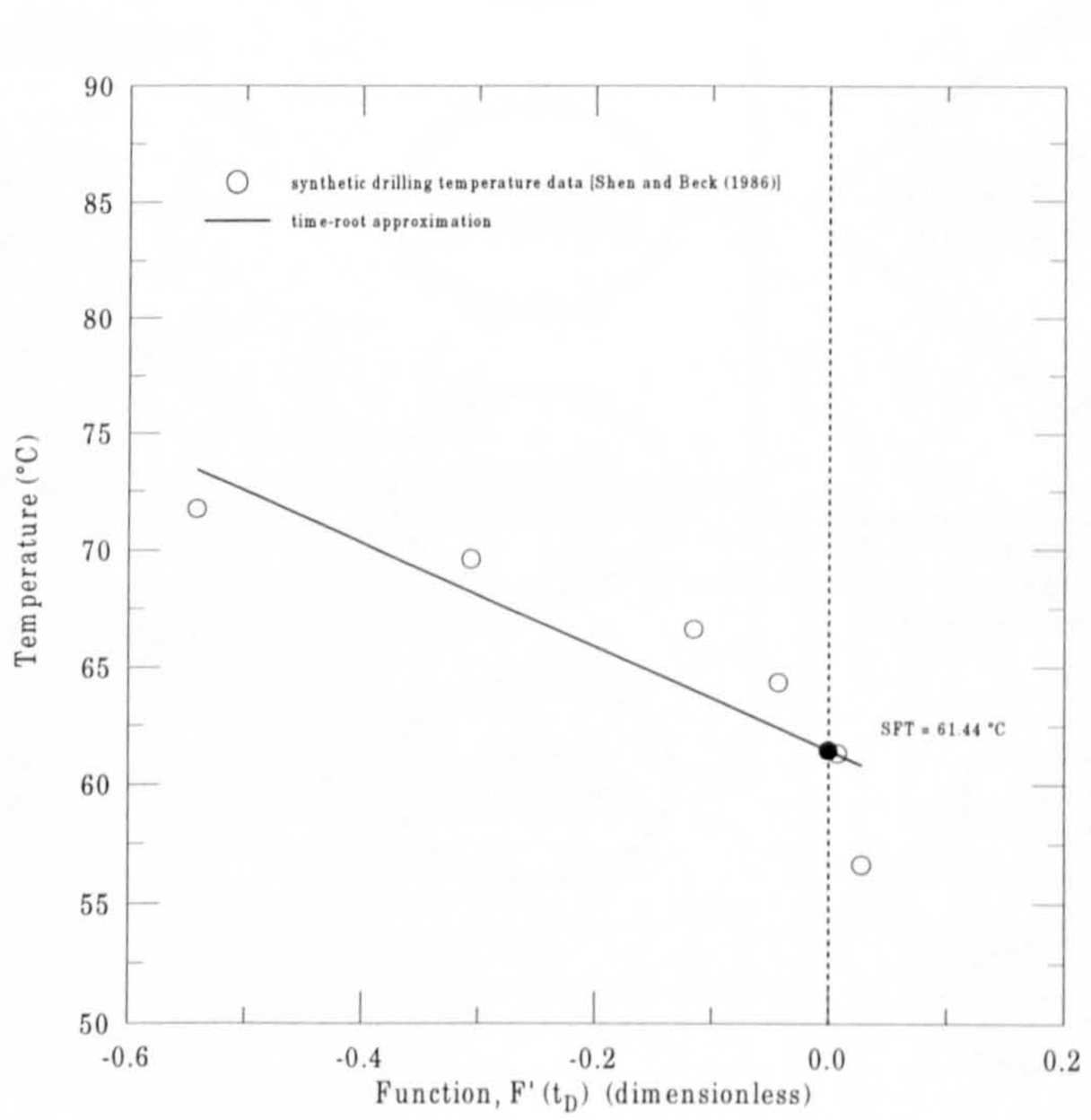

Fig. 4.6 Evaluation of the static formation temperature by means of the time-root approximation of the Hasan and Kabir (1994) method.

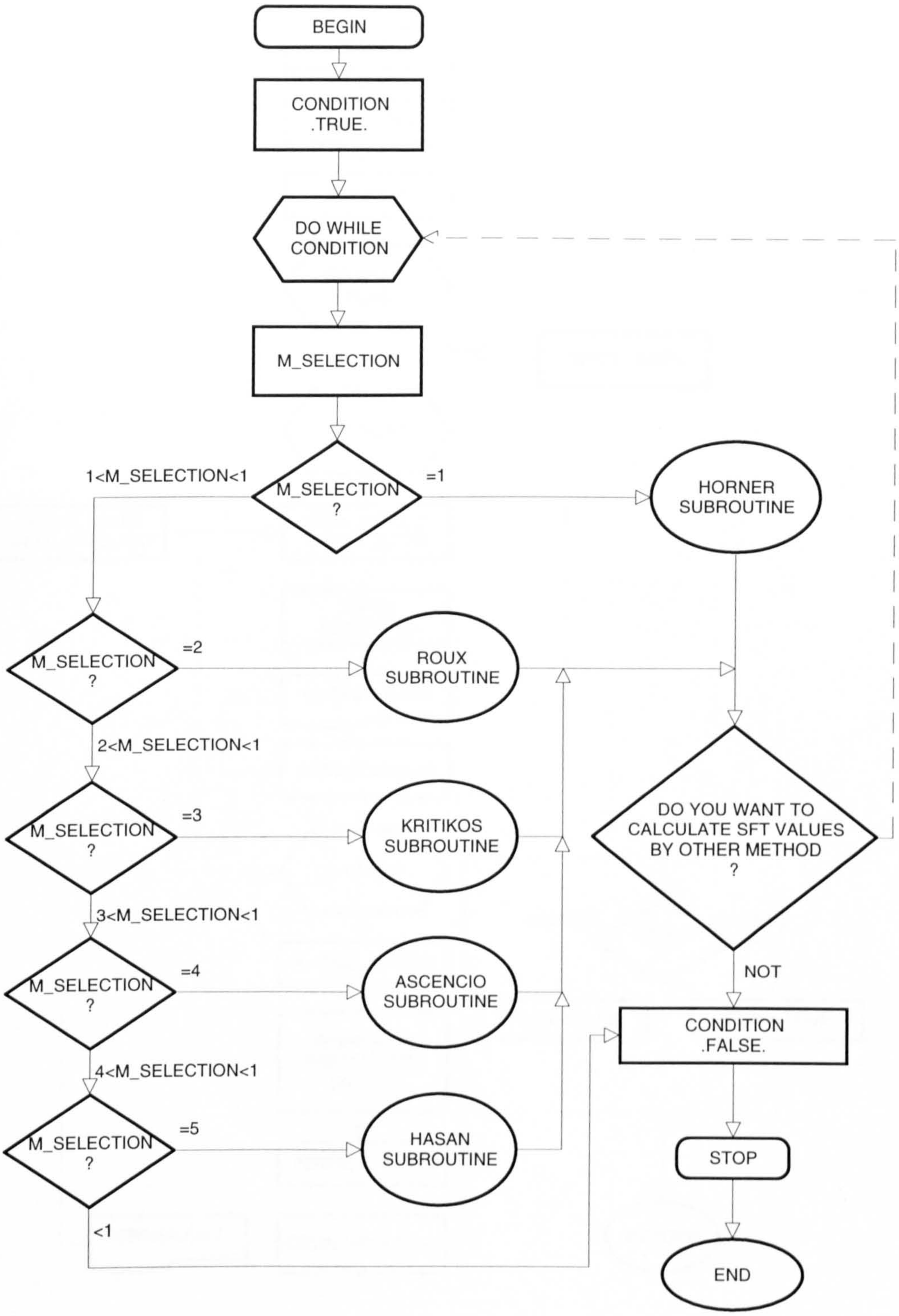

Fig. 4.7 Flow diagram of the main computer code (STATIC_TEMP).

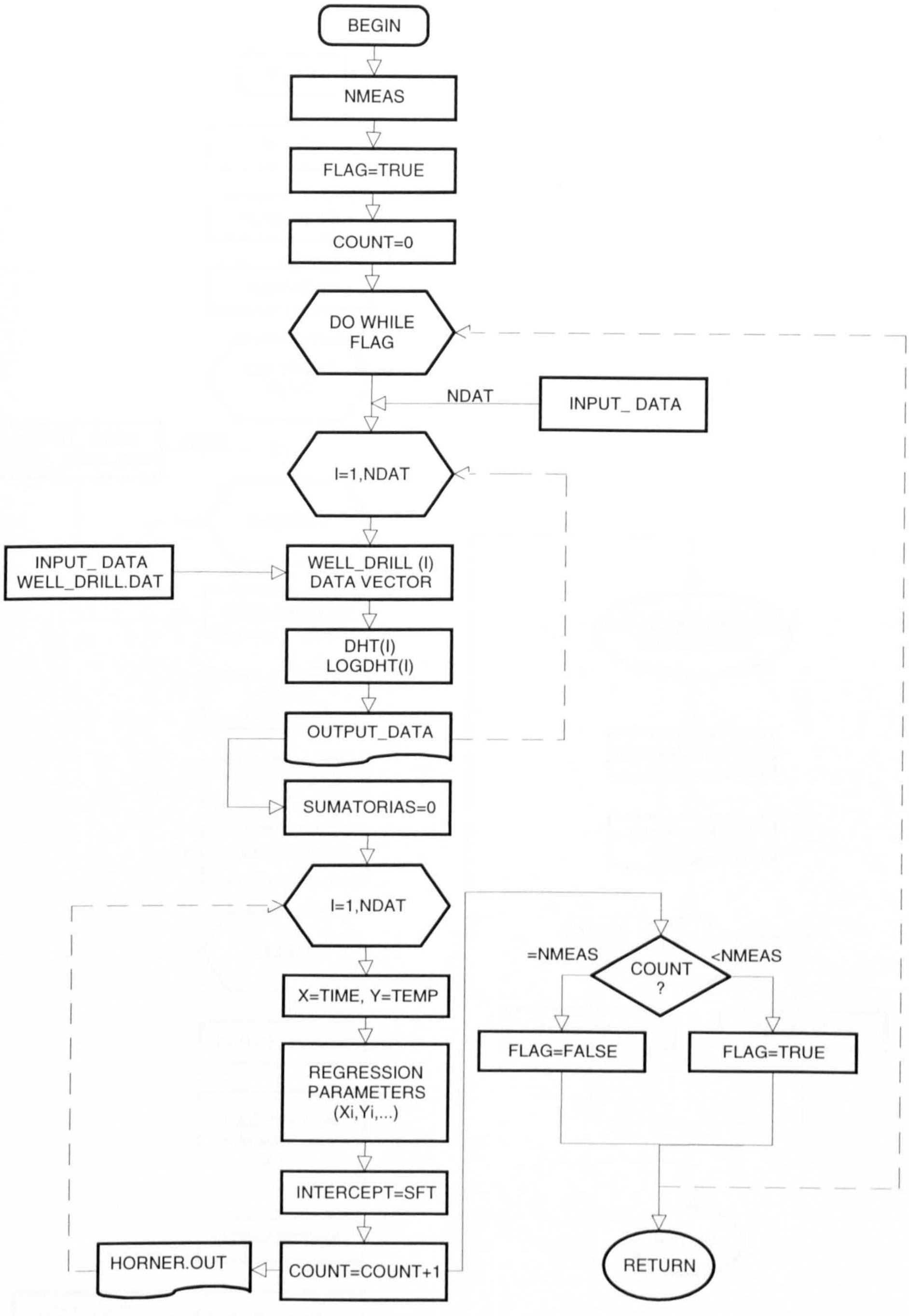

Fig. 4.8 Flow diagram of the HORNER subroutine.

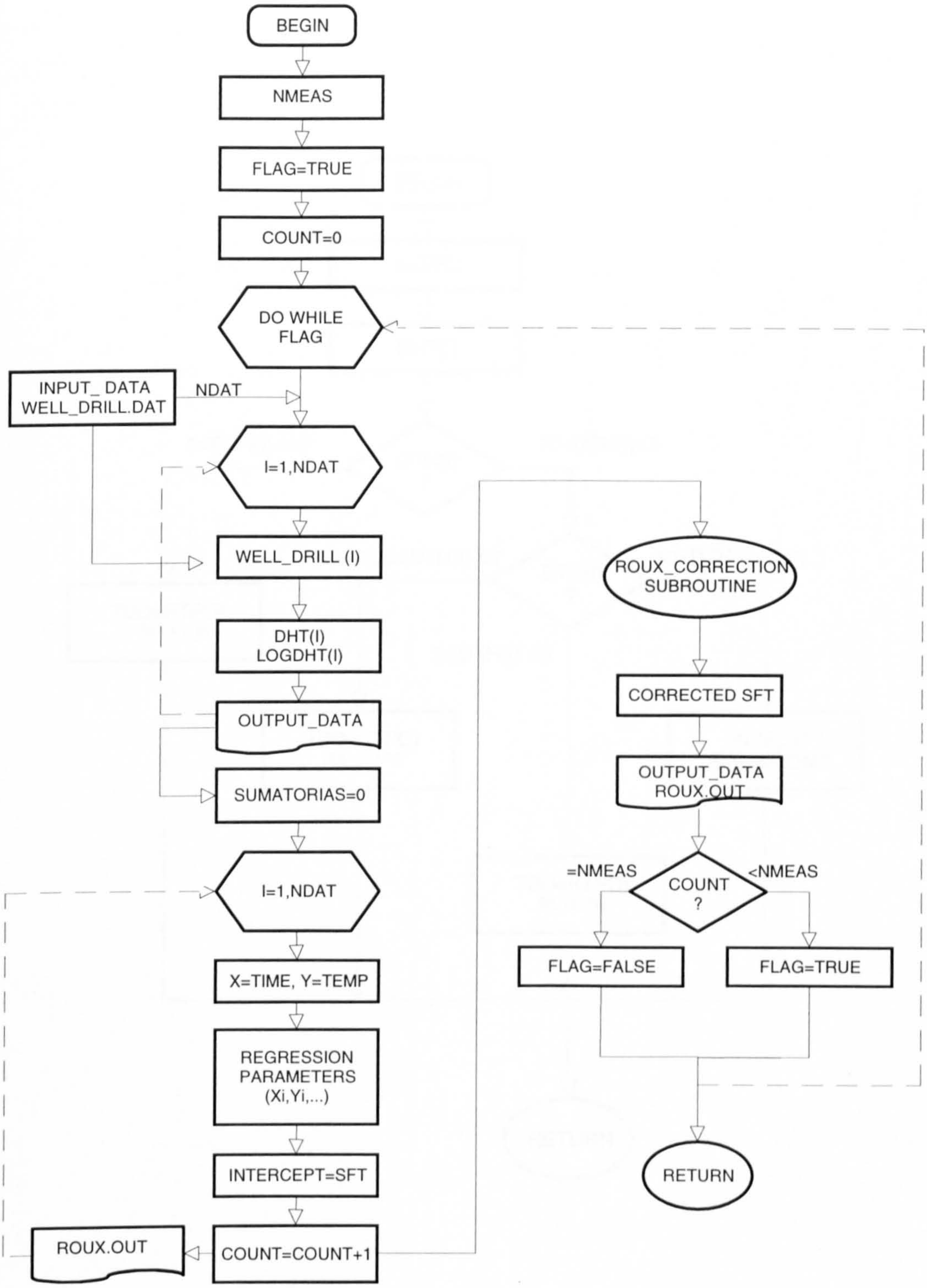

Fig. 9 Flow diagram of the ROUX subroutine.

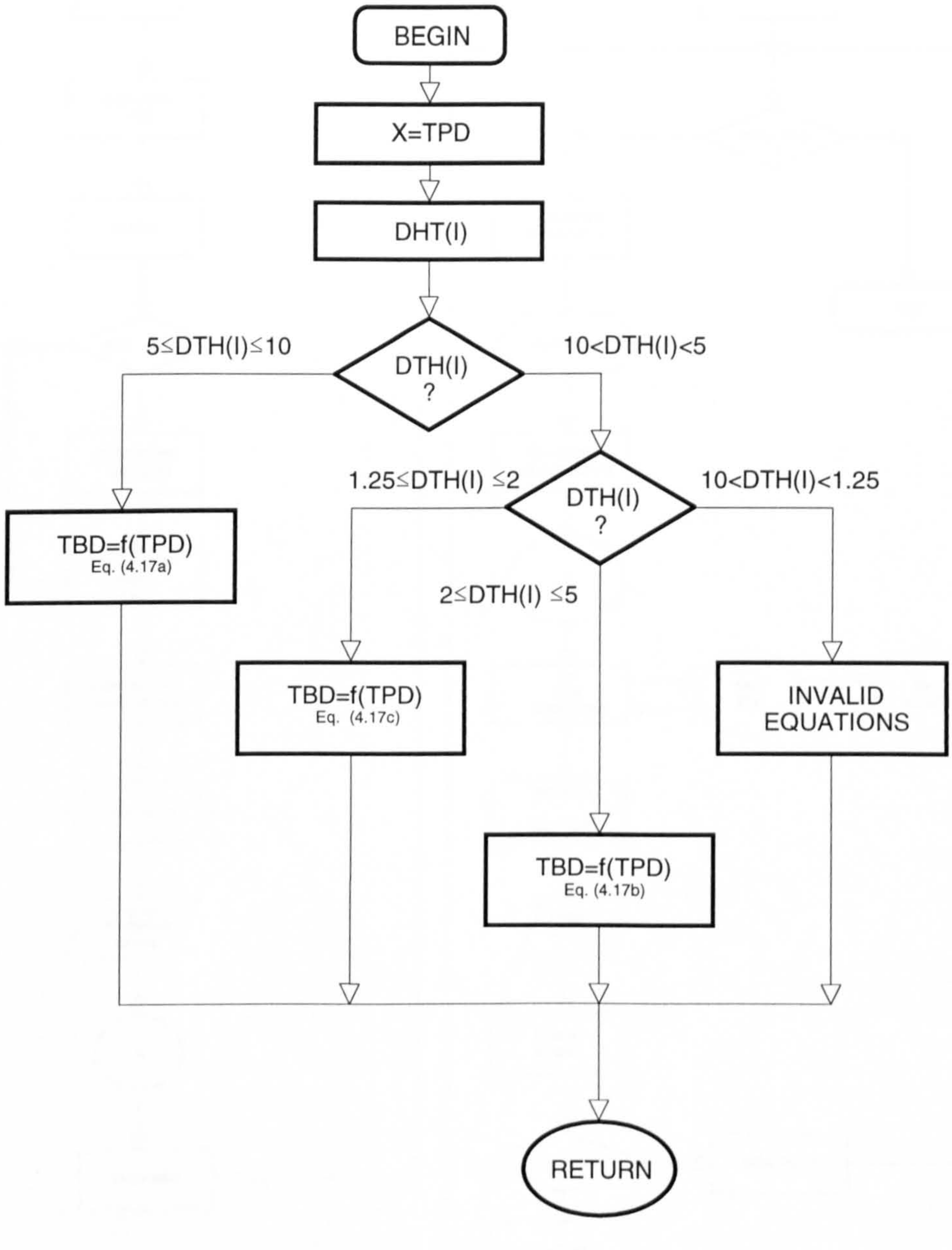

Fig. 9a Flow diagram of the ROUX_CORRECTION subroutine.

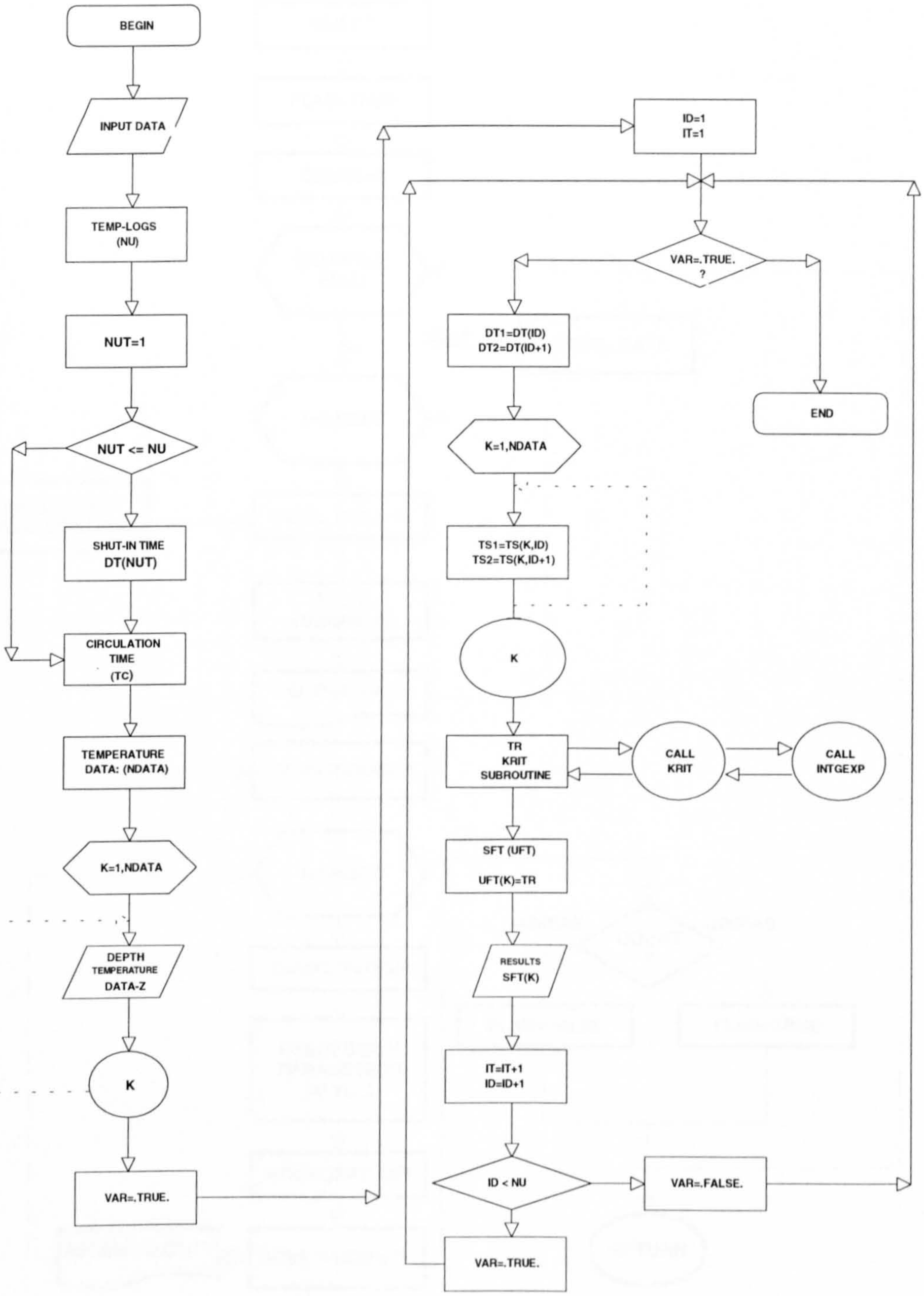

Fig. 4.10 Flow diagram of the KRITIKOS subroutine.

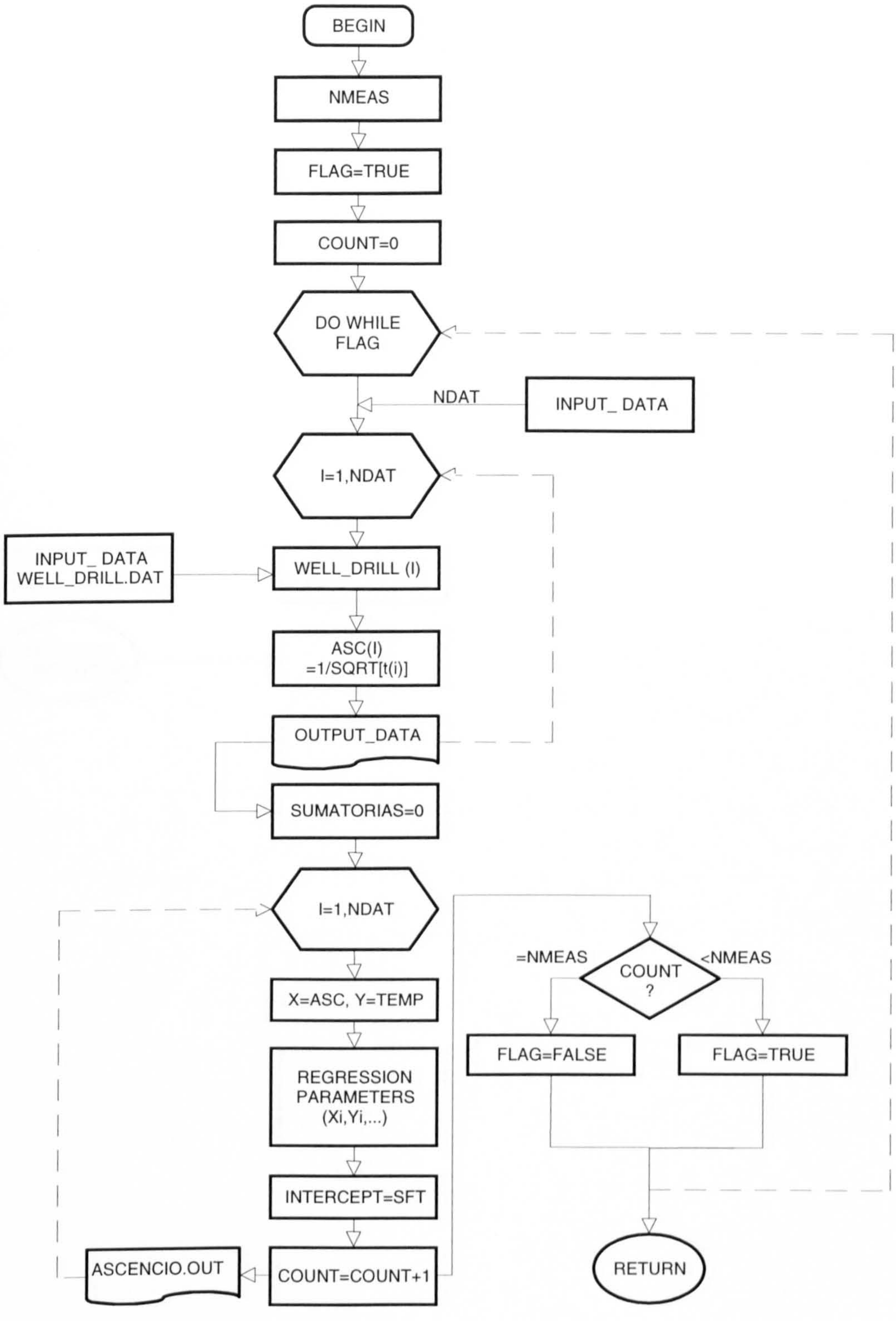

Fig. 4.11 Flow diagram of the ASCENCIO subroutine.

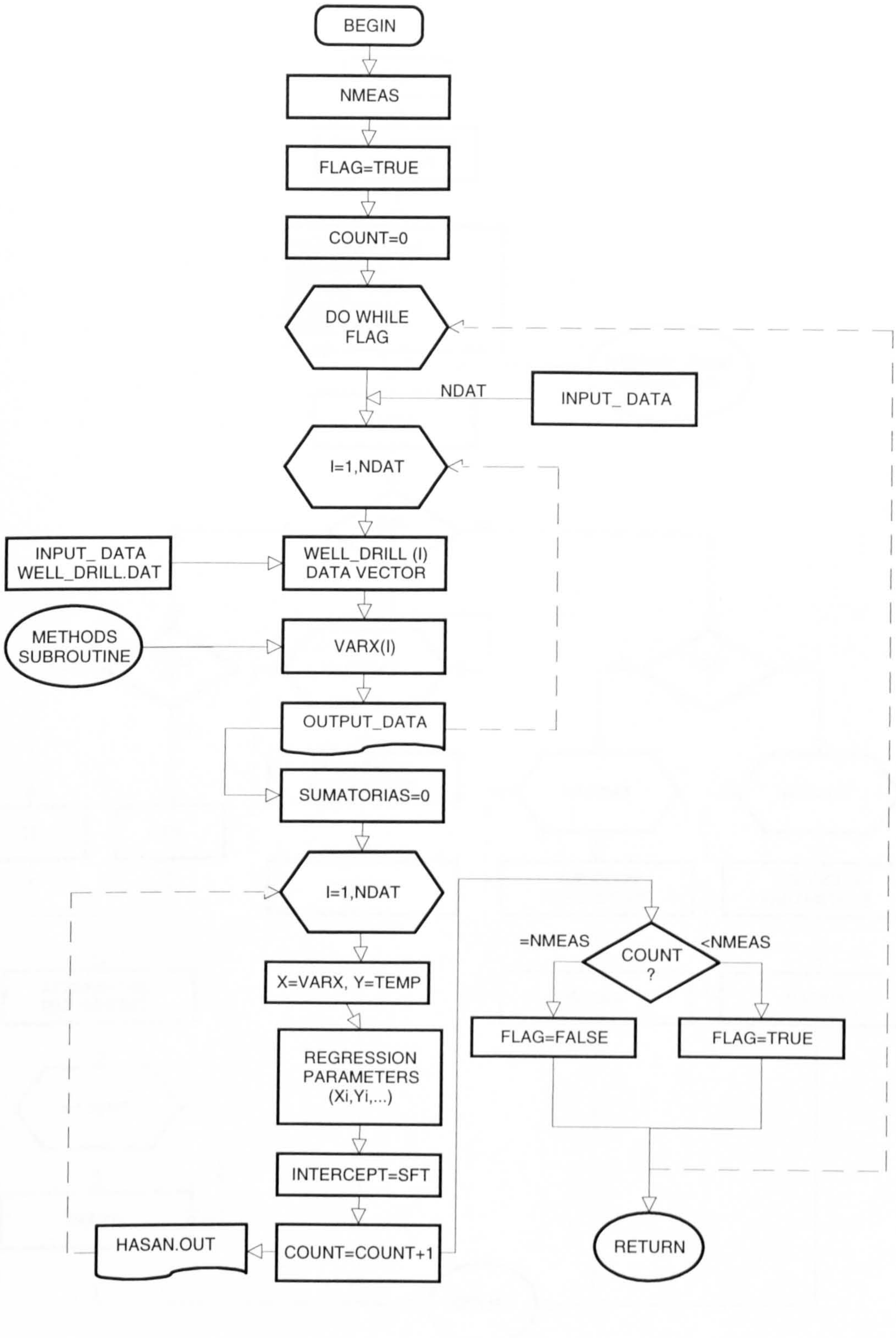

Fig. 4.12 Flow diagram of the HASAN subroutine.

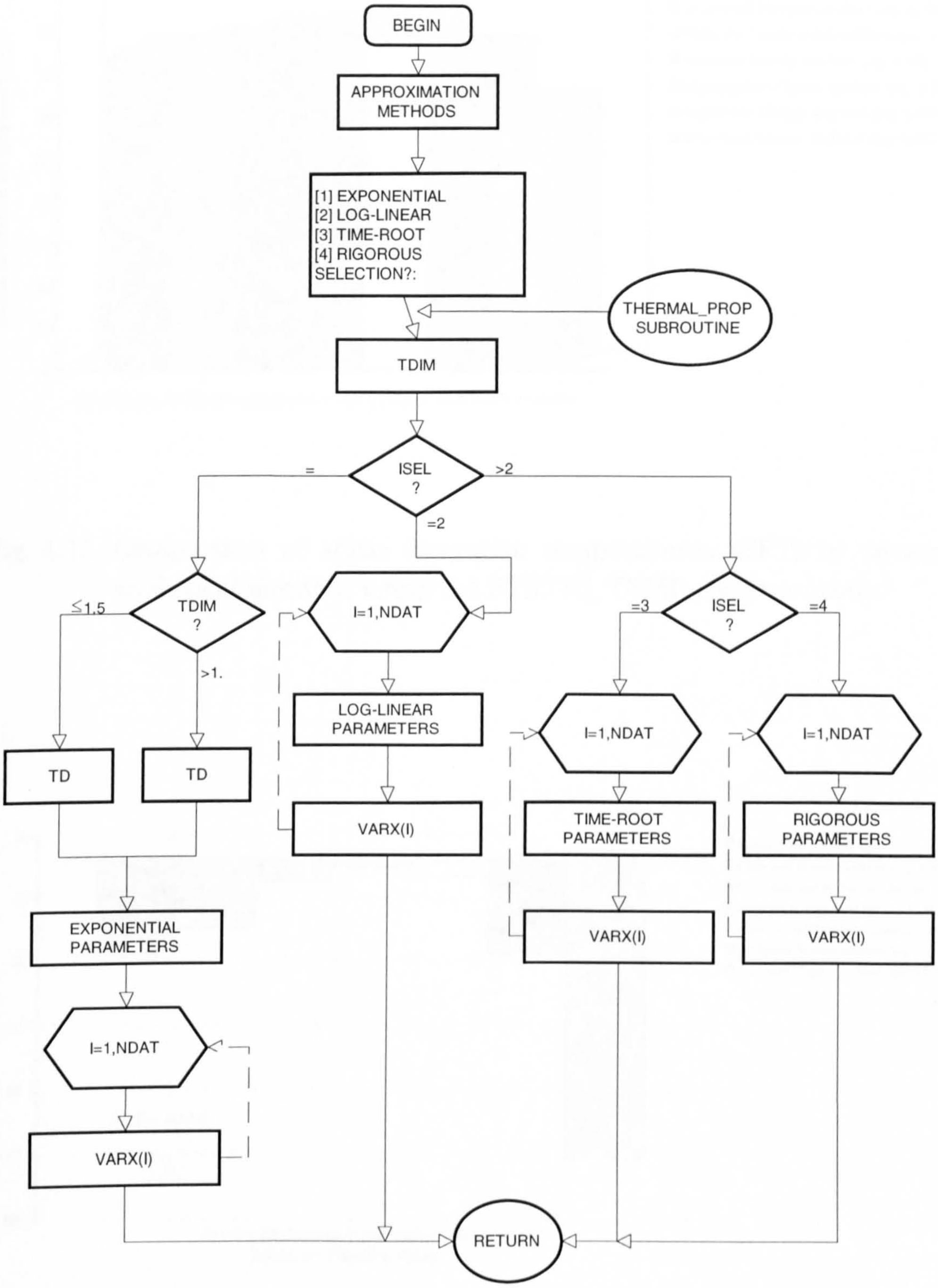

Fig. 4.12a Flow diagram of the METHODS subroutine.

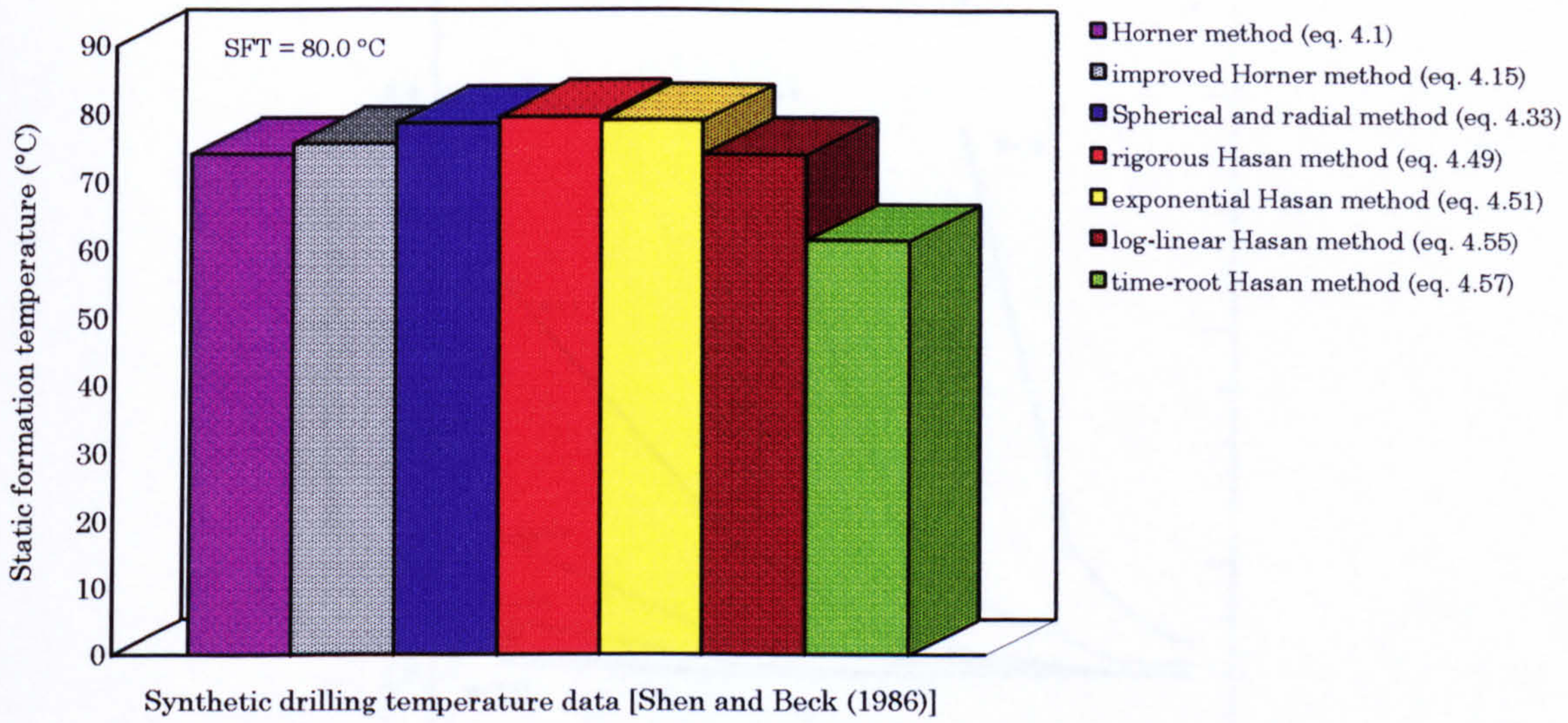

Fig. 4.13 Comparison of static formation temperatures (SFT) by several analytical methods using the STATIC_TEMP computer code.

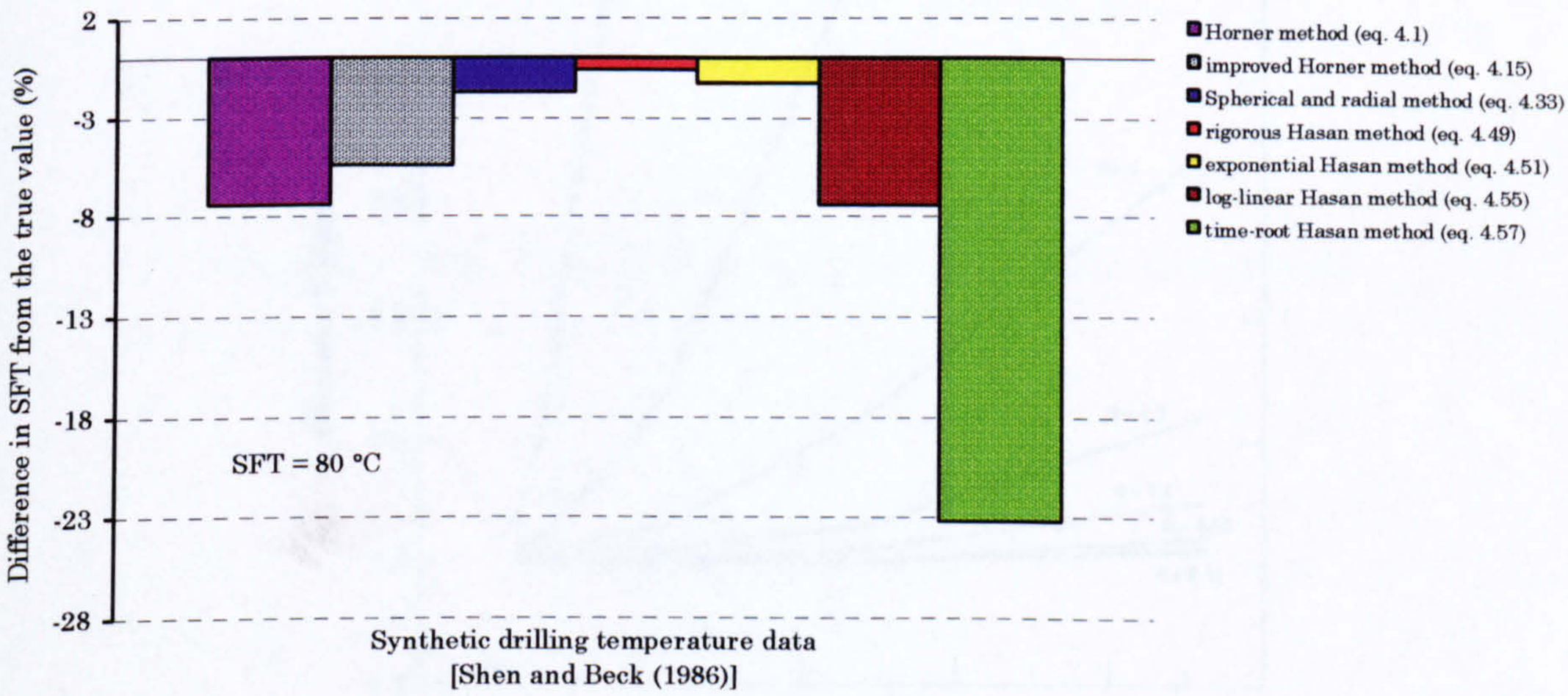

Fig. 4.14 Behaviour of the accuracy in the SFT values calculated by several analytical methods using the STATIC_TEMP computer code.

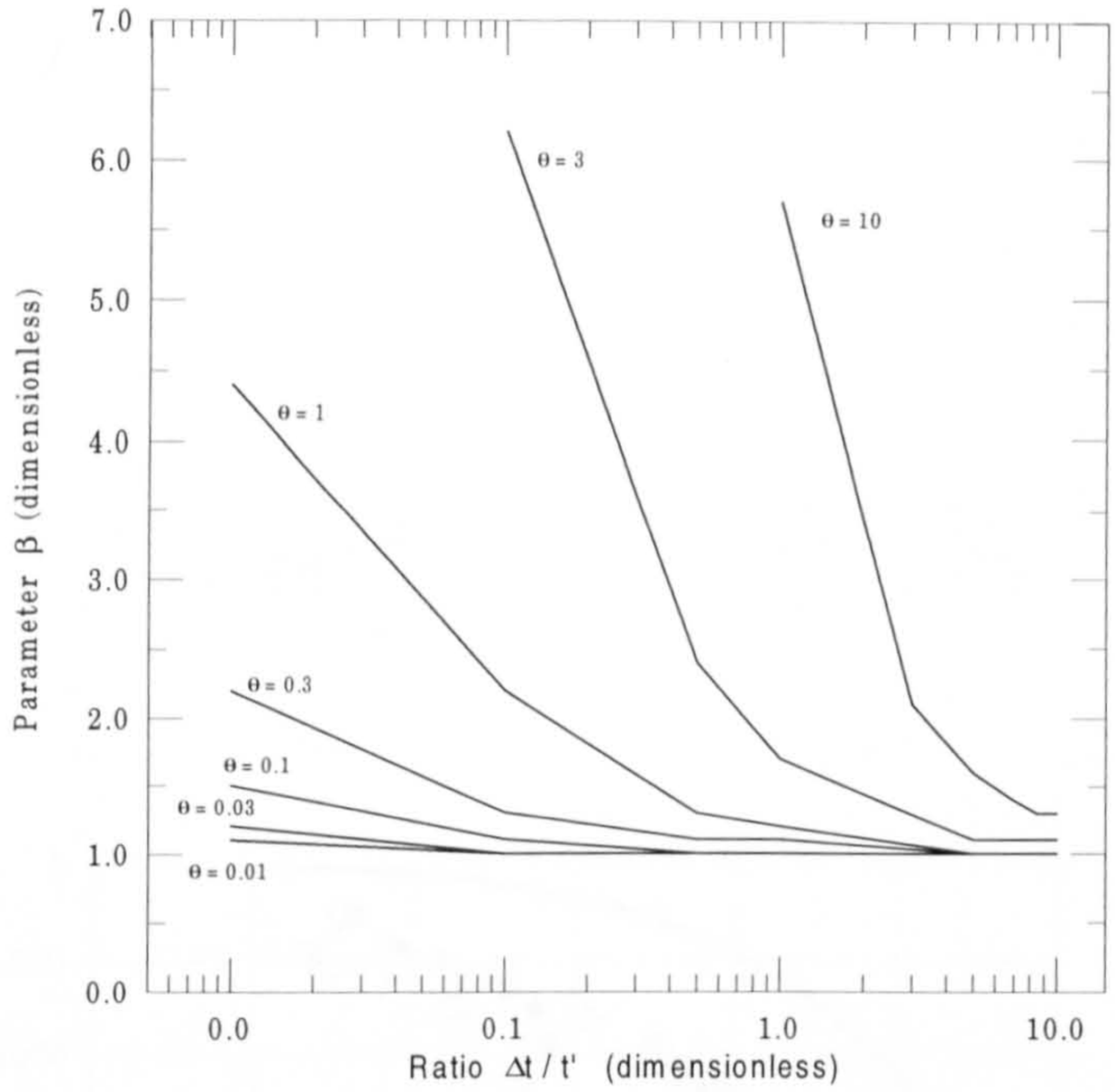

Fig. 4.15 Plots of parameter β as function of the ratio Δt/t' for different values of the parameter θ.

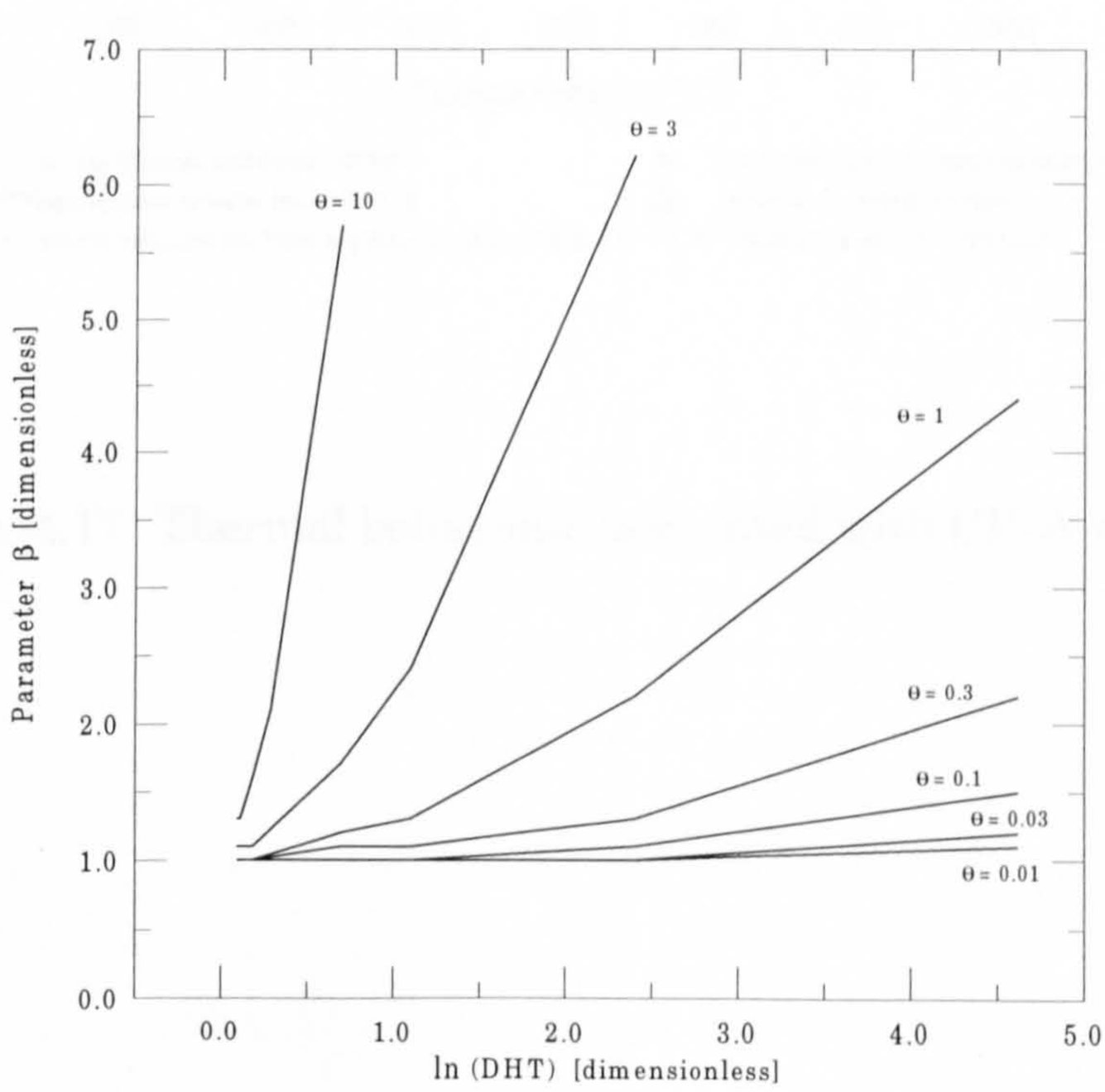

Fig. 4.16 Plots of parameter β as function of the dimensionless Horner time for different values of the parameter θ.

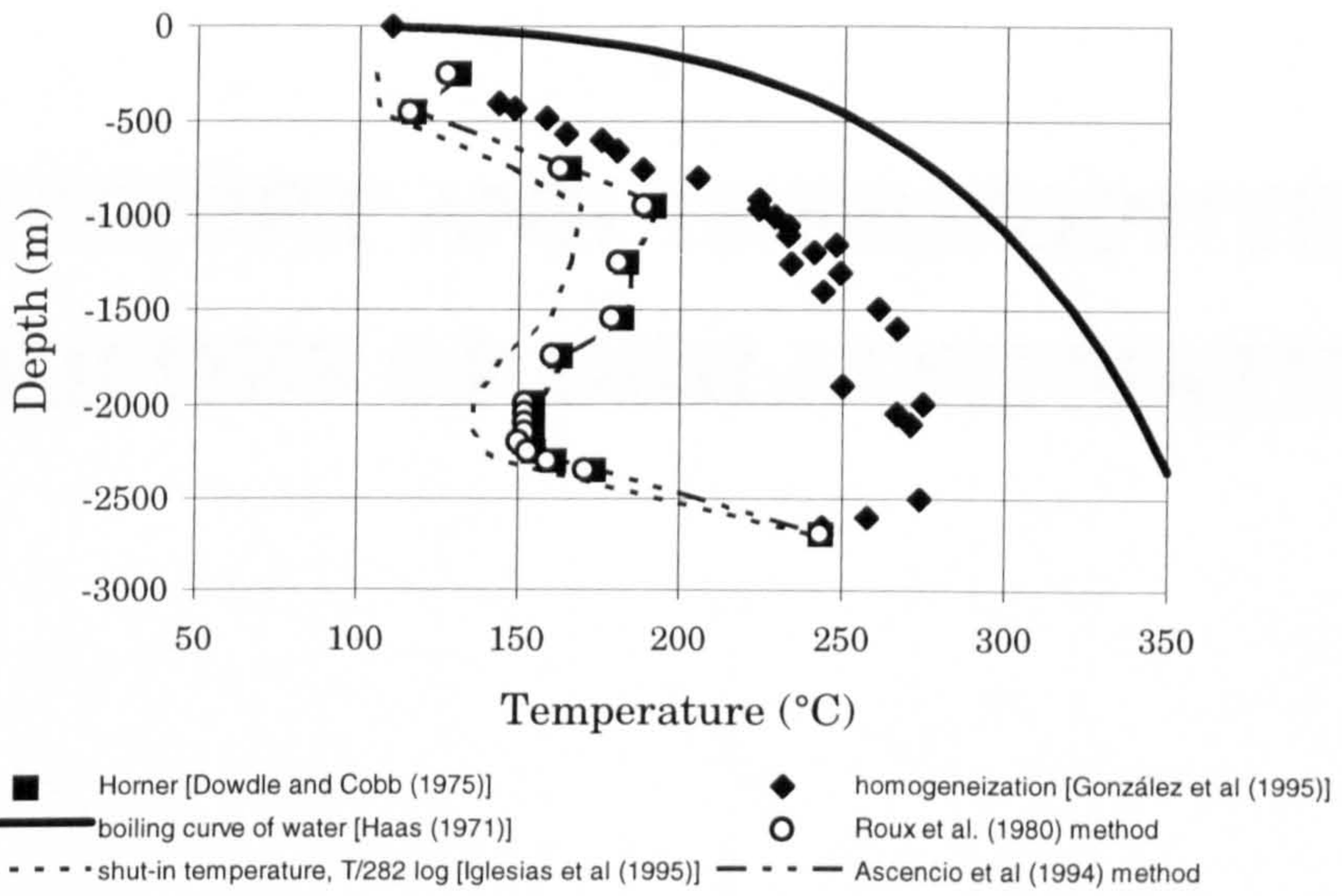

Fig. 4.17 Thermal behaviour associated with CH-A well

Chapter 5

TRANSPORT AND THERMOPHYSICAL PROPERTIES OF DRILLING MATERIALS

5.1 Nomenclature

C_i	consistency index [Pa s]
Cp	specific heat capacity [J kg^{-1} $°C^{-1}$]
D	inner diameter of drill pipe [m]
D_i	inner diameter of annulus [m]
D_o	outer diameter of annulus [m]
k	thermal conductivity [W m^{-1} $°C^{-1}$]
n	flow behaviour index [dimensionless]
n'	flow behaviour index [dimensionless]
r	radius [m]
T	temperature [°C]

v	linear velocity [m s^{-1}]
z	depth [m]

Greek symbols

$\dot{\gamma}$	shear rate [s^{-1}]
$\dot{\gamma}_R$	shear rate at the drill pipe or annulus [s^{-1}]
$\bar{\dot{\gamma}}$	shear rate giving $\bar{\tau}$ [s^{-1}]
τ	shear stress [Pa]
$\bar{\tau}$	geometric mean shear stress [Pa]
τ_o	yield point [Pa]
τ_y	yield stress [Pa]
μ	dynamic viscosity [Pa s]
μ_e	effective viscosity [Pa s]
η	plastic viscosity [Pa s]
ρ	density [kg m^{-3}]

5.2 Introduction

The study of the heat transfer processes in geothermal wells during drilling and shut-in conditions requires a knowledge of the corresponding transport and thermophysical properties of the drilling fluids and the main components of the wellbore system (drill pipes, casings, set cements and surrounding formation). This chapter presents a theoretical study to define the behaviour of these properties with temperature. In particular, a comprehensive description of the non-Newtonian behaviour of drilling fluids is presented in order to select the most appropiate rheological model for these fluids and to define an experimental programme to obtain empirical correlations of viscosity with temperature. These numerical correlations will be subsequently used in the estimation of the convective heat transfer coefficients of drilling fluids.

5.3 Transport and Thermophysical Properties of Drilling Fluids

The transport and thermophysical properties of the drilling fluids in a wellbore, which is being drilled, strongly influence the heat transfer between the wellbore and the formation. There are two important contributions of the drilling fluid to the heat transfer. First, the transport of energy up and down inside the wellbore is accomplished by the fluid flow process, which is dependent on the fluid properties. Second, the radial heat conduction from the wellbore must pass through the annular fluids between casings. In this case, the fluid properties control the heat conduction process, and determine the existence of natural convection, for which the properties again govern the heat flow. Normally, the fluid properties that are involved in the heat transfer mechanisms of a drilling process are: (i) the dynamic viscosity, (ii) the density, (iii) the specific heat capacity, (iv) the thermal conductivity and (v) the volume coefficient of thermal expansion. The dynamic viscosity affects the convection heat transfer; the density and the specific heat capacity affect the accumulation of energy; and the thermal conductivity controls the transfer of heat through the drilling fluid. The thermal expansion coefficient has only a minimum effect and it is always neglected [Wooley (1980); Garcia et al (1997)].

The transport and thermophysical properties of drilling fluids are temperature dependent, at least for water-based fluids. The geothermal industry literature includes little or no data on the actual drilling fluid transport and thermophysical properties. In fact, to date, the thermophysical properties have been ignored by the American Petroleum Institute (API) because these fluids are mainly composed of water. Consequently, it has been generally assumed that the water thermophysical properties can be used to represent the drilling fluid properties, especially if only small temperature differences are experienced by the drilling fluid during the circulation process. This has been the general practice, in spite of the fact that a number of authors have pointed out the importance of measuring these properties in order to evaluate their effect on the

estimation of downhole temperatures during drilling and shut-in operations [Wooley (1980); Marshall and Bentsen (1982); Corre et al (1984); Beirute (1991)]. However, a few laboratory experiments have been performed on several field drilling fluids. For example, Corre et al (1984) suggested a useful set of general empirical equations to correlate the variation of the heat capacity and thermal conductivity properties of water-based drilling fluids with temperature.

For water-based drilling fluids: potassium chloride (KCl) - polymer mixtures (density of 1100 kg m^{-3}):

$$Cp = 3440 + 2.72\ T \tag{5.1}$$

$$k = 0.585 + 2.3x10^{-3}\ T \tag{5.2}$$

Unfortunately, the temperature range of validity of these equations was not reported and, therefore, this problem limits its generalised application. Wooley (1980) proposed different correlations for estimating the specific heat capacity and the thermal conductivity of drilling fluids as a function of the density and the solids fraction parameter. Unfortunately, these empirical correlations were given in the english unit system. The solids fraction parameter (SF) was defined by means of the following equation:

$$SF = 0.0798\ (\rho - 8.33) \tag{5.3}$$

for $8.33 < \rho < 10.3$, and

$$SF = 0.0318\ (\rho - 10.3) + 0.162 \tag{5.4}$$

for $\rho > 10.3$, where the fluid density (ρ) is given in lb U.S. gal^{-1}. Having determined this parameter, the specific heat capacity can be computed from the equation:

$$Cp = 1.0 - 0.777\ SF \tag{5.5}$$

where the specific heat capacity (Cp) is given in BTU lb^{-1} $°F^{-1}$.

Like the specific heat capacity, the thermal conductivity can be computed from the solids fraction parameter by the following equation:

$$k_i = 0.399 + 9.60\ SF \tag{5.8}$$

where the thermal conductivity (k_i) is given in BTU hr^{-1} ft^{-1} $°F^{-1}$.

Other researchers have been using constant values to represent the thermophysical properties of the drilling fluid in several heat transfer studies to determine the temperature distribution under circulation and shut-in conditions. For reference, some of these values are included in Table 5.1.

5.4 Non-Newtonian Behaviour of Drilling Fluids

One of the main objectives related to this investigation, is to obtain an accurate knowledge of the transport properties (viscosity and density) of the geothermal drilling fluids. Wooley (1980) and Marshall and Bentsen (1982) indicated that the transport properties of these drilling fluids, in a well, strongly control the heat exchange between the wellbore and the formation. Consequently, an experimental study based on the variability of these fluid properties with temperature, needs to be made. At present, in the technical literature, information related to this behaviour is not fully available. Such information was only briefly reported by Wooley (1980) and Marshall and Bentsen (1982). Even though the estimation of the thermodynamic properties of drilling fluids forms part of the research project which is being carried out by Morales (1997), an experimental investigation related to the rheological study of drilling fluids must also be carried out. This experimental methodology will provide a better knowledge of these transport properties and thus a more accurate understanding of the heat transfer processes that occur during geothermal well drilling.

The basis of any model of the drilling process is the drilling fluid or mud. The drilling fluid serves a variety of purposes such as cooling the bit, transporting

formation cuttings to the surface and controlling subsurface pressures. Drilling fluids have progressed, over the years, from clay suspensions to highly complex substances both rheologically and chemically. This is further compounded by the fact that the rheology and chemistry can vary significantly, even during the course of drilling a single geothermal well, depending on the dominant conditions. Obviously some form of consistency must be used, at the cost of accuracy, since it is not feasible to design a drilling fluid programme incorporating all the requirements of the rheology and chemistry of the mud. The only valid generalization about drilling fluids is that they are non-Newtonian. Even so, several early researchers on this matter assumed that these fluids can be considered as Newtonian fluids [Van Olphen (1950)]. This assumption was incorrectly made due to the fact that very little was known about their non-Newtonian fluid behaviour. The constitutive equation that describes the rheological behaviour of Newtonian fluids is given by the viscosity law equation [Bird et al (1975); Holland and Bragg (1995)]:

$$\tau_{rz} = \mu \frac{dv_z}{dr} \tag{5.9}$$

In the case of all non-Newtonian fluids, there is no single constitutive equation to describe exactly their relationship between the shear stress (τ_{rz}) and the shear rate ($\dot{\gamma}=dv_z/dr$) over all ranges of shear rates. Even if such an equation could be developed, its intricacy would defy engineering application. Slawomirski (1975) derived a constitutive equation for time independent drilling fluids which illustrates this. Although three major categories of non-Newtonian systems are recognized, namely, time independent, time dependent and viscoelastic, only the time independent system has received a substantial degree of study. Fortunately the large majority of industrial non-Newtonian fluids, including drilling fluids, fall into this category. The time independent fluids can be further subdivided as:

(i) Bingham plastic fluids,

(ii) pseudoplastic fluids,

and

(iii) dilatant fluids.

Numerous simplified empirical models have been developed to relate the shear stress to the shear rate for these fluids, especially the pseudoplastics which constitute the largest and probably the most important class of non-Newtonian fluids. Skelland (1967) summarized the most important of these equations. Slawomirski (1975) contended that the majority of drilling fluids are time dependent and thixotropic, but the equations to describe such behaviour are so complicated as to be inapplicable to engineering problems. Hence it is generally accepted that drilling fluids can be typified either by the Bingham plastic model:

$$\tau_{rz} = \tau_y + \eta \left(-\frac{dv_z}{dr} \right) \tag{5.10}$$

or the Ostwald-deWaele power law model:

$$\tau_{rz} = C_i \left(-\frac{dv_z}{dr} \right)^{n'} \tag{5.11}$$

This power law model is easily applied and hence the large majority of the research on non-Newtonian flow uses this model as the best for typifying pseudoplastics. Bingham plastic fluids, on the other hand, are found only rarely, although high solids drilling fluids are well described by this model. When the required functions of a drilling fluid are considered, it is obvious that a pseudoplastic would be the most appropiate type of fluid. It is shear thinning so that, at the high shearing rates present at the bit, the pressure drop is minimized, whereas at the low shear rates in the annulus the viscosity is increased, thus enabling the large volume of cuttings to be efficiently removed. However, using the power law model is more a matter of convenience than of

theoretical validity, as it has certain disadvantages. Drilling fluids typically possess a yield value which cannot be accounted for by this model. Furthermore the power law model predicts infinite viscosities and zero viscosities in the limits of very low and very high shear rates, respectively. Real fluids, however, exhibit a finite and constant viscosity at zero shear rate. The use of this model also requires that the two defining parameters C_i and n' remain constant over the entire range of shear stress. Unfortunately these limitations appear to be important for drilling applications, when the drilling fluid properties are assumed to be dependent on temperature [Fisk and Jamison (1988)]. Nevertheless, some have considered these constraints as a justification for the use of the Bingham plastic model rather than the power law model. Surprisingly, it is still used today despite its limitations being much more significant than those of the power law model. The Bingham model accounts for the yield values typical of most drilling fluids, but it assumes a linear relationship between shear stress and shear rate after an initial yield [Monicard (1982)]. This is not true for drilling fluids. Another negative feature is that no explicit relationship can be derived between the shear stress and the volumetric flow rate.

As can be observed, little work has been done on the equations necessary to describe fully the behaviour of drilling fluids in geothermal wells.

5.4.1 Bingham model

Some materials are quite fluid at higher shear rates but flow little or not at all if the shear is reduced below a certain level, called the yield point (τ_o). At rates above the yield point, the shear stress may become proportional to the shear rate and the fluid then behaves like a Newtonian fluid. Thus, the Bingham model can describe the change in stress (τ) as a function of shear rate ($\dot{\gamma}$) through the following general equation:

$$\tau = \tau_0 + \eta\,\dot{\gamma} \qquad (5.12)$$

Very few fluids actually follow this model. However, the empirical significance of the constants has become so firmly entrenched in drilling technology since the yield point (τ_o) and the plastic viscosity (η) are probably two of the best known properties of drilling fluids. They can be calculated either from Fann V-G viscometer readings (R) at 1021 and 510 sec^{-1} (600 and 300 rpm) by means of the following equations:

$$\eta = R_{600} - R_{300} \tag{5.13}$$

and

$$\tau_o = R_{300} - \eta \tag{5.14}$$

or, by means of a more accurate method, using a linear regression of a complete rheological database at a given temperature. Thus, the intercept and the slope of this straight line will represent the yield point (τ_o) and the plastic viscosity (η), respectively. Finally, the effective viscosity (μ_e) of the mud at a given temperature can be estimated in the drill pipe or in the annulus section of the wellbore, depending on the governing flow regime in each section. Therefore, if the flow regime is laminar, the effective viscosity (μ_e) of the mud in the drill pipe can be estimated by the equation:

$$\mu_e = \eta + \frac{\tau_o}{8(v/D)} \tag{5.15}$$

while, in the annulus section it can be calculated by the equation

$$\mu_e = \eta + \frac{\tau_o}{12v/(D_o - D_i)} \tag{5.16}$$

In the case of turbulent flow, the yield point of the mud (τ_o) can be neglected for both the drill pipe and annulus sections, and then the effective viscosity (μ_e) may be assumed equal to the plastic viscosity (η). Summarizing, the Bingham model

has gained widespread acceptance in the drilling industry and is simple to visualize. However, it does not accurately represent the behaviour of a drilling fluid at very low shear rates (in the annulus) or at very high shear rates (at the bit).

5.4.2 Power law (Ostwald-de Waele) model

Pseudoplastic fluids, like Newtonian fluids, will flow under any applied stress, however small. Moreover, in contrast to Newtonian fluids, the shear stress is not proportional to the shear rate, but to its n^{th} power; hence the name power law fluids. The equation of the power flow model is given by the equation

$$\tau = C_i \cdot \dot{\gamma}^n \tag{5.17}$$

where C_i is the consistency index and n is the dimensionless flow behaviour index, which is either unity or smaller than unity for pseudoplastic fluids. If n is equal to unity, the equation (5.17) becomes identical with the equation of flow of a Newtonian fluid having the viscosity C_i. A plot of shear stress against shear rate on linear coordinates results in a curve. It is apparent from the logarithmic form, however, that a plot of τ against $\dot{\gamma}$ gives a straight line on log-log coordinates where C_i represent the intercept and n the slope.

$$\log \tau = \log C_i + n \log \dot{\gamma} \tag{5.18}$$

Accordingly, a linear regression of the logarithm of rheological data (log τ against log $\dot{\gamma}$) will enable the value of the power law parameters to be determined. Finally, in a similar form to the Bingham model, the effective viscosity can be subsequently estimated in the drill pipe or in the annulus section of the wellbore independently of the type of flow regime that predominates at any time [Monicard (1982)]. Hence, if the flow regime is laminar or turbulent, then the effective viscosity (μ_e) of the mud in the drill pipe can be approximated by the equation:

$$\mu_e = C_i\left(\frac{8v}{D}\ \frac{3n+1}{4n}\right)^{n-1} \tag{5.19}$$

while, in the annulus section it can be computed by the equation

$$\mu_e = C_i\left(\frac{12v}{D_o - D_i}\frac{2n+1}{3n}\right)^{n-1} \tag{5.20}$$

In recent years, the Ostwald-de Waele or "power law" model has gained popularity in the drilling technology industry because it provides a better rheological description of muds than the Bingham model. Nevertheless, several disadvantages have been detected. One of them is that it provides more information in the low shear rate condition than for high shear rates.

5.4.3 Robertson and Stiff (yield pseudoplastic) model

Actual shear stress/shear rate data for many fluids place them in the category of yield pseudoplastics. These fluids exhibit a yield stress as well as a nonlinear relationship between shear stress and shear rate once the flow is initiated (Fig. 5.1). Robertson and Stiff (1976) presented a different model for describing the rheological behaviour of this type of drilling fluid, which can also be reliably extended to cement slurries. The principal advantages claimed for this model are the following.

(a) It provides better fits for the rheological data than other viscous models.

(b) It gives explicit relations for the velocity fields, wall shear rates, and flow rate/pressure drop relations for flow in drill pipes and annulus sections.

The Robertson-Stiff model is represented by the following equation:

$$\tau = A\,(\dot{\gamma} + C)^B \tag{5.21}$$

It adequately describes the relationship between shear rate and shear stress for most drilling fluids and cement slurries. Thus, it can be seen that when B is equal to unity and C is equal to zero, equation (5.21) becomes a model that describes the flow properties of a Newtonian fluid. When B is equal to unity and C is non-zero, the mud is a Bingham plastic fluid. When B differs from unity and C is zero, the mud follows the power law model. Parameters A and B can be considered in a similar way to the constants of the power law model. However, the third parameter C, has a somewhat different implication than the yield stress of the Bingham model. In this model, it appears as a correction to the shear rate rather than the shear stress, and the term ($\dot{\gamma}$+C) can be considered as the "effective shear rate". i.e. the shear rate that would be required for a power law fluid to produce the same shear stress.

To evaluate the parameters, the shear stress corresponding to several shear rates is plotted or correlated by means of an interpolation numerical process [Bevington (1969)]. The geometric mean of the shear stress is then calculated from the equation

$$\bar{\tau} = (\tau_{min} \cdot \tau_{max})^{1/2} \tag{5.22}$$

and the corresponding value of $\dot{\gamma}$ is obtained by interpolation and used to obtain the value of the parameter C from the following equation:

$$C = \frac{\dot{\gamma}_{min} \cdot \dot{\gamma}_{max} - \bar{\dot{\gamma}}^2}{2\bar{\dot{\gamma}} - \dot{\gamma}_{min} - \dot{\gamma}_{max}} \tag{5.23}$$

It is evident that the logarithmic form of equation (5.21) plots as a straight line on log-log coordinates:

$$\log \tau = \log A + B \log(\dot{\gamma} + C) \tag{5.24}$$

Thus, if log τ and log($\dot{\gamma}$+C) data are fitted by linear regression, the intercept and slope of this line will represent the value of the parameters A and B, respectively. Likewise, Robertson and Stiff (1976) proposed simple explicit equations to relate the volumetric flow rate and the shear rate at the drill pipe wall and in the annulus section. For the drill pipe wall, the explicit expression is given by the equation

$$\dot{\gamma}_R = \frac{3B+1}{4B} \cdot \frac{8v}{D} + \frac{C}{3B} \tag{5.25}$$

while, in the annulus section of the wellbore, the explicit equation is

$$\dot{\gamma}_R = \frac{2B+1}{3B} \cdot \frac{12v}{(D_o - D_i)} + \frac{C}{2B} \tag{5.26}$$

Hence, the effective viscosity of the mud in the drill pipe or in the annulus can be subsequently determined combining either explicit equations (5.25) or (5.26) with the following equation:

$$\mu_e = \frac{A(\dot{\gamma}_R + C)^B}{\dot{\gamma}_R} \tag{5.21}$$

The accuracy of this model was evaluated by Beirute and Flumerfelt (1977) who found a good match with the experimental data derived from rheological tests of cement slurries.

5.5 Numerical Methodology to Generate Viscosity Correlations

The generation of the viscosity equations for drilling fluids as a function of temperature or pressure is one of the main challenges of fluids rheology [Ravi and Sutton (1990)]. These correlations are required for the development and the application of wellbore thermal simulators to study and determine a thermal history of a geothermal well during and after drilling activities.

Typically, the viscosity of these fluids in these thermal simulators is computed assuming that the mud behaves as pure water (Newtonian fluid). Hence, the viscosity can be estimated using numerical correlations for this component, such as the equations reported by Zyvoloski and O´Sullivan (1980). However, considering that the drilling fluid behaves as a non-Newtonian fluid, this assumption is erroneously adopted. Therefore, representative numerical correlations of viscosity as a function of temperature need to be developed.

Experimental data available in the literature on the high temperature and high pressure rheology of drilling fluids is quite limited [American Petroleum Institute (1985); Kellingray et al (1990)]. The maximum temperature and pressure in these studies were 118°C and 82 MPa, respectively. Preliminary results derived from these studies show, that compared to the effect of temperature on rheology, the effect of pressure can be neglected. As a general rule, the temperature effect is high for oil based muds and low for water based muds. This latter type of mud is the most common drilling fluid used in the geothermal well drilling industry. In general, the effective viscosity of these fluids decreases when the temperature is increased which suggests that the temperature effect can be described by a mathematical correlation. However, any approximation will predict viscosities only up to the thermal degradation point of any component of the fluid. Above this temperature, the fluid flow properties do not follow any mathematical model [American Petroleum Institute (1985)]. Although there is a risk of mud thermal degradation, the importance of developing viscosity equations is justified since this degradation process normally occurs at temperatures close to 200 °C. Furthermore, at the present time, there are several chemical additives based on polymeric components which extend the mud thermal stability up to 250 °C. Thus, useful numerical correlations could be obtained and applied below this temperature range. For this reason, in this research project, a numerical methodology to generate viscosity correlations was developed (VISCOSITY algorithm).

This general methodology is to enable the rheological data of drilling fluids to be used in the calculation of plastic and effective viscosities by means of several mathematical flow models at different temperatures. The numerical algorithm is based on the following three considerations.

(i) The first is the rheological data that were obtained from the experimental tests carried out during this research project.

(ii) The second is the rheological database available in the drilling industry literature.

(iii) The third is the proprietary information belonging to the Instituto de Investigaciones Electricas (I.I.E.)

When a rheological database (viscosity and temperature) has been generated, a polynomial regression process can be carried out. This will be used to derive viscosity functions for several drilling fluid systems which will subsequently be coupled to the wellbore thermal simulator (WELLTHER).

The flow diagram of the VISCOSITY numerical algorithm is presented in Fig. 5.2. Several numerical procedures were implemented both to perform the analysis of rheological data and to obtain mud viscosity/temperature equations. Specifically, four options are considered by the VISCOSITY algorithm to produce a viscosity equation. These options are presented in the following list.

(1) The first is the application of a viscosity correlation for pure water which was proposed by Zyvoloski and O'Sullivan (1980).

(2) The second is to use empirical correlations derived from the rheological analysis of viscosity and temperature data reported in the drilling fluid literature.

(3) The third is to use empirical equations derived from the rheological analysis of viscosity and temperature in some drilling fluid samples.

(4) The fourth is to use empirical equations generated from the rheological analysis of the shear stress and shear rate data logged in situ during the well drilling operations.

In the fourth option, VISCOSITY selects the best mathematical flow model (Bingham, Ostwald-de Waele or Robertson-Stiff model) to describe the rheological behaviour of the mud used during well drilling activities and to predict its effective viscosity.

5.5.1 Software development. As a result of the numerical methodology implemented in the VISCOSITY algorithm, two computer programs were written to perform the numerical calculations (MODEL and POLYREG). Both computer codes were written in the Fortran 77 language for a Vax/Vms V5.3 Digital computer system.

MODEL computer code. In general form, the architecture of this computer code is organized by:

(1) a main program (MODEL),

(2) an input data file (POWER),

and

(3) six subroutines (BINGHAM, POWER_LAW, IMPOWER_LAW, LINEFIT C_PARAMETER and SORT).

MODEL is the main program that selects the mathematical flow model to be used in the rheological data analysis and calls the appropiate subroutine to predict the final value of viscosity at a given temperature.

BINGHAM is a subroutine that allows the estimation of the mud effective viscosity and its respective error by means of the rheological data analysis using the Bingham plastic flow model.

POWER_LAW is a subroutine that enables the estimation of the mud effective viscosity and its respective error to be determined by the rheological data analysis using the power law model.

IMPOWER_LAW is a subroutine that provides an estimation of the effective mud viscosity and its respective error using a rheological data analysis by the Robertson-Stiff flow model. The IMPOWER_LAW subroutine calls the C_PARAMETER subroutine for the calculation of the constants involved with the yield pseudoplastic flow model. The C_PARAMETER subroutine calls the SORT subroutine for sorting of the shear rate data vector and then, performs an interpolation numerical process of all the rheological data input.

The BINGHAM, POWER_LAW and IMPOWER_LAW subroutines call the LINEFIT subroutine to apply a linear regression algorithm to the rheological data. The LINEFIT subroutine uses a numerical method based on a straight line fit which is described by Bevington (1969).

POLYREG computer code. Rheological studies conducted by Ravi and Sutton (1990) indicate that the mud viscosity and temperature data typically follow a polynomial function of the second degree. Therefore, the numerical algorithm for these types of equations needs to be implemented. POLYREG is a computer code that enables the data regression process of two variables (y and x) to be performed. POLYREG uses a Gaussian numerical method for polynomial functions of n-degree which is fully described by Bevington (1969). A complete listing of the computer source codes (MODEL and POLYREG) are included in Appendix II.

5.6 Thermophysical Properties of Geothermal Formations

The formation that surrounds the well is formed by several types of rocks which vary with depth and the rock-fluid interaction present. Each type has different characteristics and thermophysical properties. The environmental conditions

prevailing in geothermal reservoirs are unique for each field. In addition, the lithology of most of the geothermal formations is normally heterogeneous and complex. The reliable knowledge of the thermophysical properties of the formation can be only obtained by the characterisation of actual drilling cuttings or core samples [Brigaud et al (1990); Contreras et al (1990); Middleton (1993) and (1994)]. Because of the complexity of laboratory measurements, it is very difficult to obtain accurate thermophysical property values, and in many circumstances laboratory methods for measuring these properties are unsatisfactory. For this reason, there are only a few data reported in the geothermal drilling literature. Middleton (1994) measured matrix thermal conductivities from dry drill cuttings. Drury (1988) determined that the thermal diffusivity data of crystalline rocks generally ranges from 0.6 to 1.9 $mm^2\ s^{-1}$. However, for water saturated sediments this parameter is usually limited to the range of 0.4 to 1.0 $mm^2\ s^{-1}$.

A general list of the thermal conductivity values of formation materials usually found in subsurface reservoirs is presented in Tables 5.1, 5.2 and 5.3.

5.6.1 Previous work for Mexican geothermal formations

Thermal conductivity and other physical parameters of core samples from the Cerro Prieto geothermal field were determined by Martinez (1978). Brine saturated and dry test specimens were evaluated at different temperatures using a thermal conductivity standard method developed by Somerton (1973).

Several research projects dealing with the measurements of rock properties have been carried out at the Instituto de Investigaciones Electricas (IIE) under the sponsorship of the Mexican Comision Federal de Electricidad (CFE). These experimental works are part of a general programme for the development and exploitation of geothermal energy in Mexico. From 1984 to 1990, the thermophysical properties measurements were made on rock samples extracted from outcrops and drill cores or using drill cuttings.

Contreras et al (1986) and Garcia et al (1988a) performed the thermophysical characterisation of rocks from the Los Azufres geothermal field. These studies included measurements of five different andesite outcrops. Contreras et al (1986) characterised andesite samples from eight outcrops and four drill cores of the Los Azufres geothermal field. The thermophysical properties measured were: (i) thermal conductivity, (ii) thermal diffusivity, and (iii) thermal expansion. Iglesias et al (1987) characterised samples from twenty drill cores from fifteen wells of the Los Azufres geothermal field. The samples covered a wide range of depths (400-3000 m) over the field. A considerable number of specimens extracted from the cores were characterised.

The thermophysical properties of rocks from the La Primavera geothermal field and the Los Humeros geothermal field have been characterised by Garcia et al (1988b), respectively. All of these research projects were developed at the Petrophysical and Mechanical Rock Laboratory (PMRL) of the IIE. These projects have enabled an extensive database on the formation thermophysical properties to be created. These data are considered as confidential information, i.e. the property of IIE. This limitation does not allow all the information derived from these studies to be published. However, some values can be carefully selected in order to be used during the numerical simulations of the heat transfer processes.

5.7 Thermophysical Properties of Cement and Casing Materials

5.7.1 Cements

The API specifications do not cover all the properties required for cements to be used over broad geothermal application ranges. However, they provide a method to classify the Portland cement for wells. These specifications guarantee that the product meets certain minimum requirements by specifying the required properties. These properties describe cements for specification purposes. However, well cements should have other properties and characteristics to provide the necessary down hole functions.

The physicochemical properties of API cement classes are normally defined by API in the specification 10 [API (1990)] but, unfortunately, it does not include measurements of the thermal properties for cements. For this reason, to date all the work carried out for the estimation of the temperature distribution in geothermal formations does not include the effect of the annular cement section of the wells. Some papers deal with the temperature profile determined throughout the well during the circulation of fluids. The thermophysical properties of drilling fluids have been determined only at room temperature and atmospheric pressure and thermophysical properties data for cement slurries and set cements do not exist [Beirute (1991), Garcia et al (1993)]. Therefore, information on properties such as the thermal conductivity and the thermal diffusivity of cement slurries and set cement are required.

Laboratory investigations related to the heat transfer in steam injection wells were carried out by Cain et al (1966). For these purposes, a casing pipe of 20.32 cm (8.5 in) in diameter was cemented in a 31.75 cm (12 in) diameter hole and was used to measure the thermal conductivity of various cementing compositions. They concluded that when steaming a 20.32 cm diameter casing, it takes around eight hours for the cement sheath to reach the casing temperature. Thermal conductivity measurements with this method will vary for a given cementing composition due to chemical reactions, moisture or saturation changes in the cement due to increases in temperature. A summary of thermal conductivity data for cement, concrete and well cement systems reported in different publications is shown in Tables 5.1 and 5.4.

5.7.2 Casing and drilling pipes

The drill pipe and the casing pipe used in geothermal wells are manufactured according to API standards. The API classification for casing, tubing and drill pipes is based on the pipe minimum tension strength. The pipes are described using the following characteristics: (i) nominal diameter (outside diameter, in inches); (ii) weight per foot length; (iii) pipe grade; (iv) thickness; and (v) thread and coupling.

The dimensions and strengths of API pipes are also given in tables such as the cementing tables of Halliburton (1978). Pipe data include inside diameter, outside diameter and thickness. Strengths include collapse resistance, internal yield pressure, body yield strength and joint strength. The typical geothermal well construction includes the H-40, J-55, K-55, C-75, L-80 and N-80 types of pipes with the following diameters:

(i) drill pipe diameter of 11.4 cm,

(ii) casing pipe diameters of 76, 51, 34 and 24 cm,

and

(iii) liner diameter of 18 cm.

Usually the thermal conductivity of pipes is high. A typical value is 45 W m^{-1} $°C^{-1}$. This is high compared with other materials in the well (0.6 to 2.25 W m^{-1} $°C^{-1}$ for drilling fluids, 0.29 to 1.73 for cements and 0.45 to 5.8 W m^{-1} $°C^{-1}$ for rocks). Therefore, similar values of thermal conductivity for carbon steel have been typically used in heat transfer studies during geothermal well drilling operations (Table 5.1).

5.8 References

American Petroleum Institute (API), The rheology of oil-well drilling fluids, American Petroleum Institute, Production Department, API Bulletin 13D, Second Edition, 28 p. (1985).

American Petroleum Institute (API), Specification for materials and testing for well cements (Spec. 10), Fifth Edition, Washington, D.C., USA, July: 9-17 (1990).

F.C. Arnold, Temperature variation in a circulating wellbore fluid, Journal of Energy Resources Technology, **112** 79-83 (1990).

R.M. Beirute, A circulating and shut-in well-temperature-profile simulator, Journal of Petroleum Technology, **September** 1140-1146 (1991).

R.M. Beirute and R.W. Flumerfelt, An evaluation of the Robertson-Stiff model describing rheological properties of drilling fluids and cement slurries, Society of Petroleum Engineers Journal, **April** 97-100 (1977).

P.R. Bevington, Data reduction and error analysis for physical sciences, Chapter six: Least squares fit to a straight line, McGraw-Hill Book Company, First Edition, New York, USA, 92-113 (1969).

R.B. Bird, W.E. Stewart and E.N. Lightfoot, Transport phenomena, Ed. John Wiley & Sons, Inc., New York, USA (1975).

F. Brigaud, D.S. Chapman and S. Le Douaran, Estimating thermal conductivity in sedimentary basins using lithologic data and geophysical well logs: AAPG Bulletin, **74** 1459-1477.

J. E. Cain, S. H. Shryock and G. Carter, Cementing steam injection wells in California, Journal of Petroleum Technology, **18** (4) 431-436 (1966).

S. Cao, I. Lerche and C. Hermanrud, Formation temperature estimation by inversion of borehole measurements, Geophysics, **53** 979-988 (1988).

E. Contreras, E. Iglesias and A. Razo, Initial measurements of petrophysical properties on rocks from the Los Azufres, Mexico, geothermal field, Proc. Eleventh Workshop Geotherm. Res. Eng., Stanford University, Stanford, CA, USA, January 21-23, pp. 51-57 (1986).

E. Contreras, Garcia, A. and B. Dominguez, Developments in geothermal energy in Mexico-Part twenty eight, The role of petrophysical studies in the development of the Mexican geothermal resources, Heat Recovery Systems & CHP, **10** (3) 213-230 (1990).

B. Corre, R. Eymard and A. Guenot, Numerical computation of temperature distribution in a wellbore while drilling, Proceedings of The 59th Annual Technical Conference and Exhibition, Society of Petroleum Engineers of AIME, Houston, Texas, USA, September 16-19, 12 p. (1984).

M. J. Drury, A simple needle probe method for measuring thermal diffusivity of unconsolidated materials, Geothermics, **17** (5/6) 757-763 (1988).

A. Garcia, E. Contreras and B. Dominguez, Predicting thermal conductivity of rocks from easily measurable properties, Proc. Thirteenth Workshop Geothermal Reservoir Engineering, Stanford University, Stanford CA, USA, January 19-21, pp. 323-327 (1988a).

A. Garcia, E. Contreras and E. Iglesias, Developments in geothermal energy in Mexico-Part Seventeen: Thermal conductivity of drill cores from the Los Azufres geothermal field: Experimental results and accurate prediction method, Heat Recovery Systems & CHP, **8** (4) 289-297 (1988b).

A. Garcia, J. M. Morales and I. Hernandez, Estimacion de temperaturas de los fluidos de perforacion durante la circulacion, Geotermia, Rev. Mex. de Geoenergia, Mexico, **9** (3) 305-319 (1993).

A. Garcia, E. Santoyo, G. Espinoza and I. Hernandez, Estimation of temperatures in geothermal wells during circulation and shut-in in the presence of lost circulation. Submitted to Transport and Porous Media (1997).

J.V. Fisk and D.E. Jamison, Physical properties of drilling fluids at high temperatures and pressures, Proceedings of the IADC/SPE 17200 Drilling Conference, Dallas, Texas, U.S.A., 257-265 (1988).

Halliburton, Section 200: Dimensions and strengths, Halliburton Cementing Tables, Halliburton Inc., Duncan, OK, USA, 32 p. (1978).

F.A. Holland and R. Bragg, Fluid flow for chemical engineers, 2nd Edition, Edward Arnold, A Division of Hodder Headline PLC, London, UK (1995).

A.R. Hasan and C.S. Kabir, Static reservoir temperature determination from transient data after mud circulation, SPE Drilling & Completion, **March** 17-24 (1994).

V.T. Hoang, Estimation of in-situ thermal conductivities from temperature gradient measurements, Ph.D Thesis, University of California, Berkeley, USA (1980).

K. Horai and S. Baldridge, Thermal conductivity of nineteen igneous rocks, II: Estimation of the thermal conductivity of rock from the mineral and chemical compositions, Physics Earth Planet. Interior, **5** 157-166 (1972).

E. R. Iglesias, E. Contreras, A. Garcia and B. Dominguez, Petrophysical properties of twenty drill cores from the Los Azufres, Mexico, geothermal field, Proc. Thirteenth Workshop Geothermal Reservoir Engineering, Stanford University, Stanford, CA, USA, January 20-22, pp. 195-201 (1987).

D.S. Kellingray, C. Greaves and R.P. Dallimer, High temperature and high pressure rheology of oil well cement slurries, Proceedings of the 1990 British Society of Rheology International Conference on Rheology of Fresh Cement and Concrete, Liverpool, U.K., March 26-29 (1990).

M.N. Luhesi, Estimation of formation temperature from borehole measurements, Geophys. J. R. Astr. Soc. **74** 747-776 (1983).

D.W. Marshall and R.G. Bentsen, A computer model to determine the temperature distributions in a wellbore, The Journal of Canadian Petroleum, **January-February** 63-75 (1982).

L. F. Martinez, Thermal conductivity of core samples from the Cerro Prieto geothermal field: experimental results and improved prediction method, Proc. First Symposium on the Cerro Prieto Geothermal Field, Baja California, Mexico, San Diego, CA, USA, Sep. 20-22, pp. 342-356 (1978).

M.F. Middleton, A transient method of measuring the thermal properties of rocks: Geophysics, **58** 357-365 (1993).

M.F. Middleton, Determination of matrix thermal conductivity from dry drilling cuttings, AAPG Bulletin, **78** 1790-1799 (1994).

R. Monicard, Drilling mud and cement slurry rheology manual, Ed. Technip 27 Rue Ginoux 75737 Paris, France (1982).

M. Morales, An experimental study of the thermophysical properties of geothermal drilling fluids and cements, Monthly Progress Report, In-house Post Graduate Programme Instituto de Investigaciones Electricas, Mexico with the University of Salford, U.K., January, 10 p. (1997).

S.B. Nielsen, N. Balling and H.S. Christiansen, Formation temperatures determined from stochastic inversion of borehole observations, Geophys. J. Int., **101** 581-590 (1990).

M. Ozisik, Heat transfer: A basic approach, McGraw Hill, Singapore, pp. 101-351 (1985).

R. H. Perry and C. H. Chilton, Chemical engineer's handbook, Fifth edition, McGraw-Hill, USA, **Vol. 1** 3-280 (1973).

K.M. Ravi and D.L. Sutton, New rheological corelation for cement slurries as a function of temperature, Proc. 65th Annual Technical Conference and Exhibition of the Society of Petroleum Engineers, New Orleans, U.S.A., 455-462 (1990).

R.E. Robertson and H.A. Stiff, An improved mathematical model for relating shear stress to shear rate in drilling fluids and cement slurries, Society of Petroleum Engineers Journal, **February** 31-37 (1976).

P.Y. Shen and A.E. Beck, Stabilization of bottom hole temperature with finite circulation time and fluid flow, Geophys. J. R. Astr. Soc., **86** 63-90 (1986).

A.H. Skelland, Non-Newtonian flow and heat transfer, Ed. John Wiley & Sons Inc., New York, U.S.A. (1967).

M.R. Slawomirski, Rheological behaviour of oil well drilling fluids, Int. J. Rock Mech. Min. Sci. Geomech. Abstr., **12** 115-123 (1975).

W. H. Somerton, Thermal properties of hydrocarbon bearing rocks at high temperatures and pressures, University of California, Berkeley, CA, USA, API Res., Project No. 117 (Final Report), 83 p. (1973).

A.T. Tragesser, P.B. Crawford and H.R. Crawford, A method for calculating circulating temperatures, Journal of Petroleum Technology, **November** 1507-1512 (1967).

J. Van Olphen, Pumpability rheological properties and viscometry of drilling fluids, Inst. Pet. J., **36** 223-227 (1950).

G. P. Willhite, Over-all heat transfer coefficients in steam and hot water injection wells, Jornal of Petroleum Technology, **19** (5) 607-615 (1967).

G.R. Wooley, Computing downhole temperatures in circulation, injection, and production wells, Journal of Petroleum Technology, **September** 1509-1522 (1980).

G.A. Zyvoloski and M.J. O'Sullivan, Simulation of gas dominated, two phase geothermal reservoir, Society of Petroleum Engineering Journal, **20** 52-58 (1980).

Source	Drilling fluid			Formation			Casing			Cement		
	ρ	k	Cp	ρ	k	Cp	ρ	k	Cp	ρ	k	Cp
Tragesser et al (1967)	1227.	0.64	3935.	---	2.25	879.	---	---	---	---	---	---
Hoang (1980)	1310.	0.79	---	2700.	2.56	---	---	---	---	---	---	---
Wooley (1980)	1318.	1.05	4115.	2240.	1.73	1256.	7840.	45.3	460.5	1664.	1.038	837.
Luhesi (1983)	1200.	0.70	4166.	2700.	1.90	1222.	---	---	---	---	---	---
Marshall and Bentsen (1983)	1197.	1.74	1675.	2640.	2.25	837.	8048.	43.3	418.7	3136.	0.690	2093.
Corre et al (1984)	1100.	0.60	2600.	2700.	3.00	800.	7800.	40.0	400.0	2700.	0.700	2000.
Shen and Beck (1986)	1200.	0.61	3491.	2700.	2.51	774.	---	---	---	---	---	---
Cao et al (1988)	1200.	2.92	3500.	2200.	2.90	900.	---	---	---	---	---	---
Arnold (1990)	1200.	2.25	3935.	2640.	2.25	880.	---	43.3	---	---	---	---
Nielsen et al (1990)	1200.	20.00	3488.	2400.	2.80	1150.	---	---	---	---	---	---
Hasan and Kabir (1994)	1200.	0.66	3965.	2200.	1.43	---	---	---	---	---	---	---

*** The units of each thermophysical properties are described in the nomenclature section**

Table 5.1

Average thermophysical properties of drilling and formation materials used in some heat transfer studies carried out during the estimation of downhole temperatures in geothermal well drilling operations.

Mineral	Chemical composition	k (W m^{-1} $°C^{-1}$)
Quartz	SiO_2	7.70 7.11*
Plagioclase	$Na\ Al_2\ Si_3\ O_8$ - $Ca\ Al\ Si_3\ O_8$	2.15
Orthoclase	$K\ Al_2\ Si_3\ O_8$	2.30
Muscovite	$(K\ Na)\ Al_2\ (OH)_2\ (Al\ Si_3\ O_{10})$	2.20
Calcite	$CaCO_3$	3.60 3.14 *
Chlorite	$(Mg\ Fe\ Al)_6\ (OH)_8\ ((Al\ Si)_4\ O_{10})$	4.34
Biotite	$K\ (Mg\ Fe)_3\ (OH)_2\ (Al\ Si_3\ O_{10})$	2.34
Hornblende	$Na\ Ca_2\ (Mg\ Fe\ Al)_5\ (OH)_2\ (Si\ Al_8\ O_{22})$	3.10
Magnesite	$MgCO_3$	5.85
Sphene	$Ca\ Si\ Ti\ O_5$	2.34

Table 5.2

Thermal conductivities of some rocks forming minerals at 23 °C [Horai and Baldridge (1972) and Middleton (1994)*].

Rock type	ρ (kg m^{-3})	k (W m^{-1} $°C^{-1}$)
Dolomite	2700.	4.99 4.98*
Limestone	2560.	2.56 2.50*
Shale	-------	1.76
Sandstone	-------	4.12 4.20*
Clay	1470.	0.91 0.80*
Coal	1050.	0.24 0.50*
Chert	2560.	4.53
Slate	2760.	1.99

Table 5.3

Thermal conductivities of some reservoir rocks [Hoang (1980) and Middleton (1994)*]

Source	Cement system	k (W m^{-1} °C^{-1})
Cain et al (1966)	oil well cement at 162 °C	1.44
Cain et al (1966)	oil well cement at 286 °C	0.92
Willhite (1967)	saturated water	0.86 - 1.04
Willhite (1967)	dry	0.34 - 0.69
Somerton (1973)	oil well cement	0.52 - 1.38
Perry and Chilton (1973)	cement at 90 °C	0.29
Perry and Chilton (1973)	concrete	0.76 - 0.93
Ozisik (1985)	cement	0.29 - 1.16

Table 5.4

Thermal conductivity values reported in the technical literature for some cement and concrete samples.

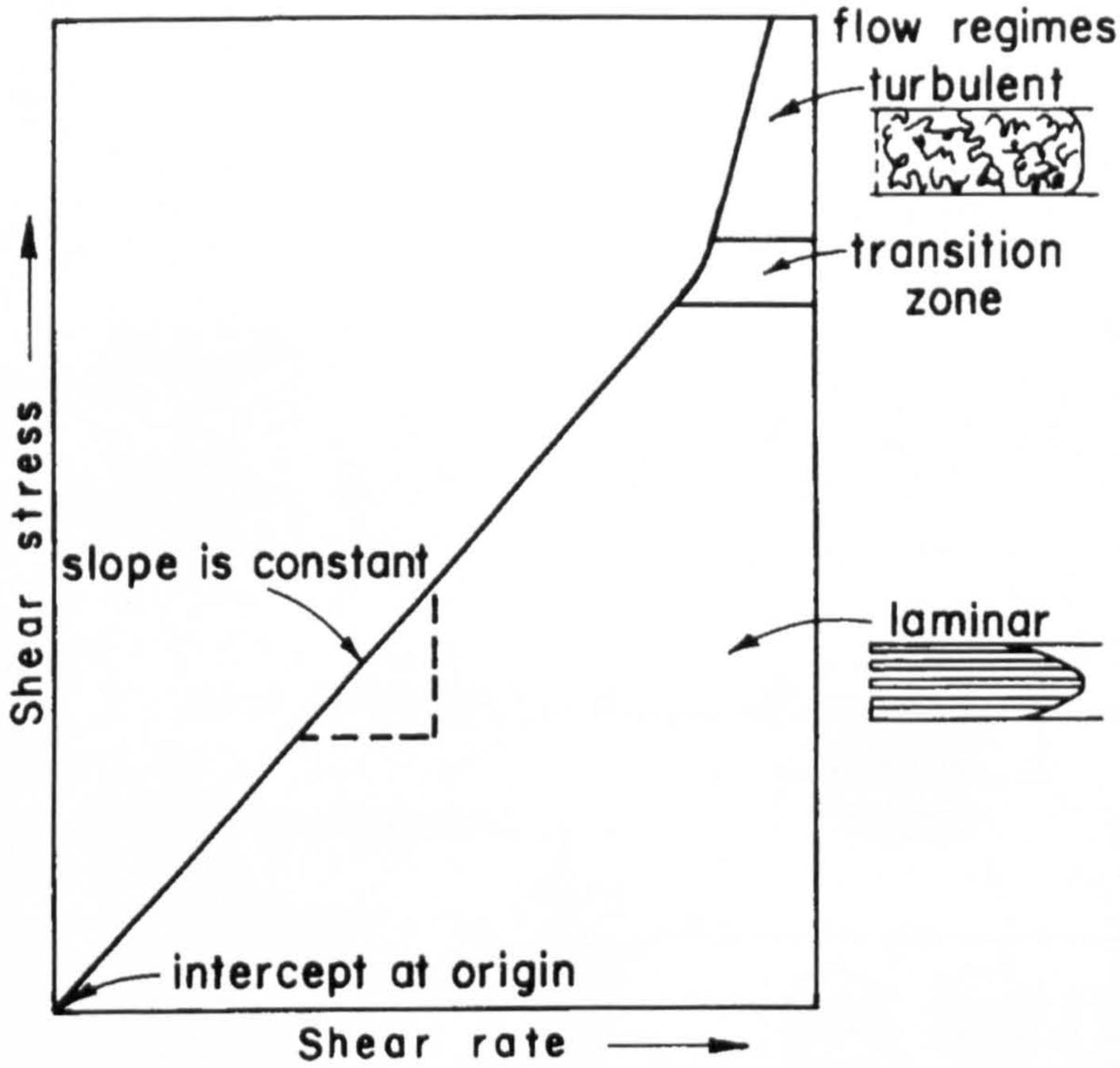

Fig. 5.1a Plot of shear stress against shear rate for a Newtonian fluid (flow regime and velocity profile inside drill pipe are shown in small drawings).

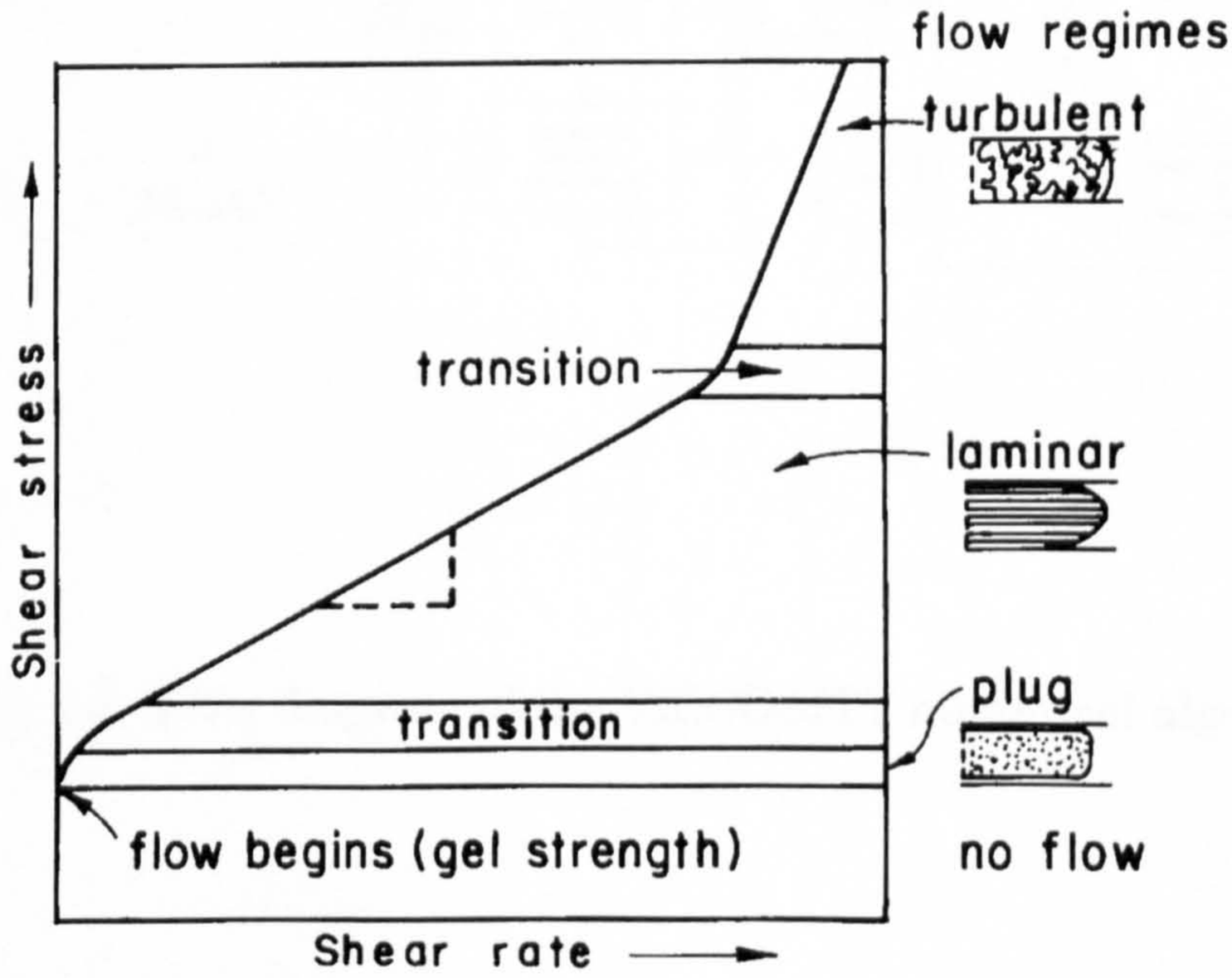

Fig. 5.1b Plot of shear stress against shear rate for a pseudoplastic non-Newtonian fluid (velocity profiles of various types of flow are shown).

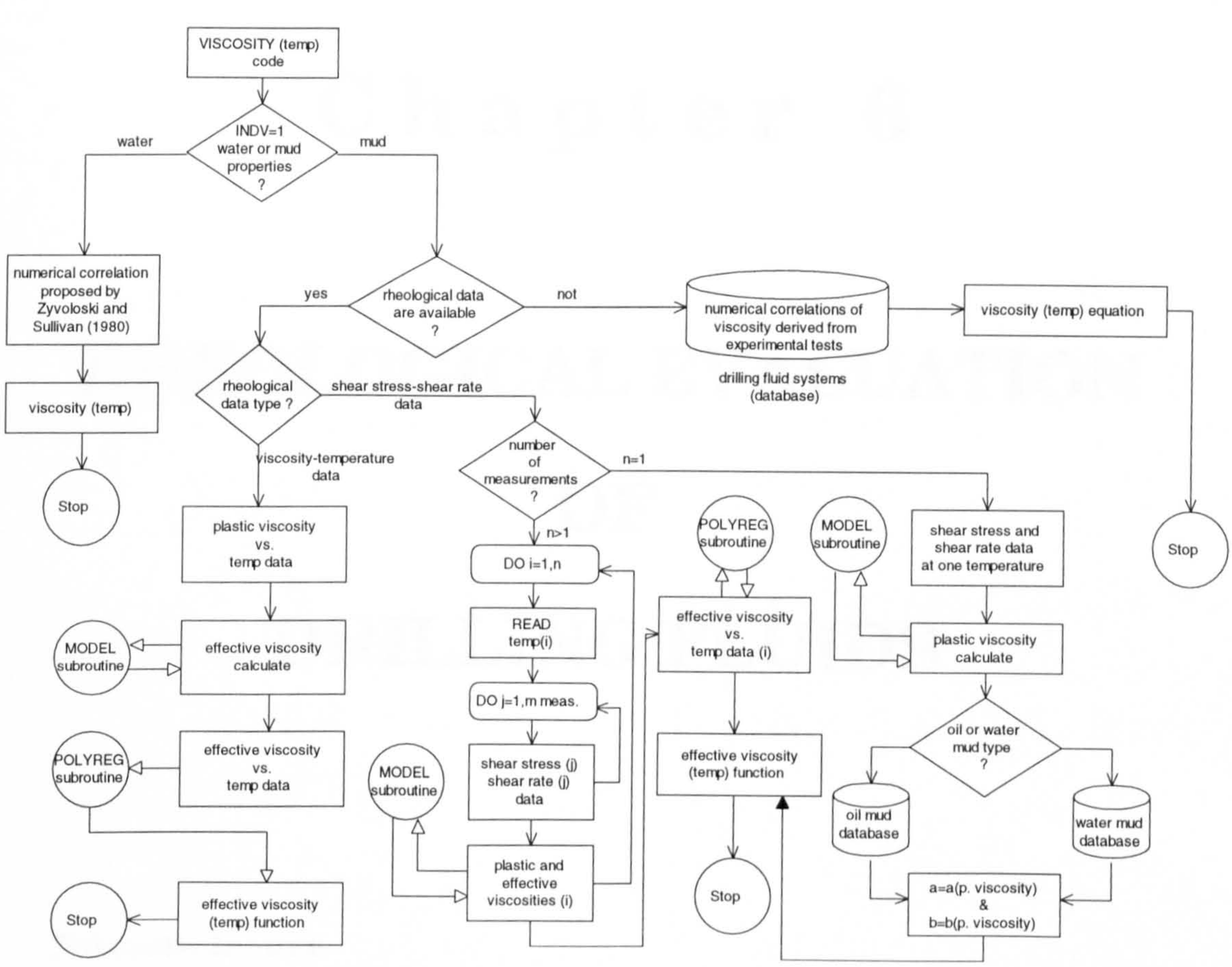

Fig. 5.2 Flow diagram of the VISCOSITY numerical algorithm.

Chapter 6

RHEOLOGICAL EVALUATION OF DRILLING FLUIDS

6.1 Nomenclature

P	reservoir pressure [kPa]
T	temperature [°C]
t	time [s]

Greek symbols

$\dot{\gamma}$	shear rate [s^{-1}]
τ	shear stress [Pa]
μ	dynamic viscosity [mPa·s] or [cp]
ρ	density [kg m^{-3}]

6.2 Introduction

Viscosity and temperature data derived from dynamic experimental tests of drilling fluid systems (DFS) were obtained and analyzed. As a result of these analyses, new correlations of viscosity as a function of temperature were derived. These viscosity correlations were obtained using the numerical algorithm implemented in the VISCOSITY numerical algorithm. Viscosity correlations were subsequently saved in a database called VISTEMPEQ. Additionally, dynamic viscosity and temperature data reported in the geothermal well drilling literature were compiled. After analyzing these data, additional numerical correlations of viscosity with temperature were obtained. These viscosity correlations were also generated by use of the MODEL and POLYREG subroutines and saved in the same VISTEMPEQ database.

This database will be used by the wellbore thermal simulator (WELLTHER) to provide a means for predicting the viscosity of drilling fluids at circulating temperatures. A complete listing of all the DFS used and their respective generated viscosity equations are presented.

6.3 Experimental Work

Experimental and theoretical studies based on viscosity measurements of drilling fluids (muds) were performed at the drilling fluid laboratory (DFLAB) of the Instituto de Investigaciones Electricas (I.I.E.), Cuernavaca, Mexico. These studies were conducted to determine the effects of elevated geothermal temperatures on the drilling fluids' rheological properties (viscosity and density) [Santoyo (1996)].

Numerical correlations of viscosity as a function of temperature were derived from these rheological tests. Thus, a rheological database of viscosity equations for different drilling fluid systems (DFS) was created and called VISTEMPEQ.

This database will be suitable to describe the rheological behaviour of the most common mud systems used in the drilling of geothermal wells. It is expected that the VISTEMPEQ database will increase the capabilities of the wellbore thermal simulator (WELLTHER) to accurately evaluate the overall heat transfer processes and the temperature distributions in the wellbore and the formation under drilling conditions. It is planned to use these viscosity equations in the calculation of the dimensionless flow parameters (Reynolds, Prandtl and Nusselt numbers). These parameters will be used to estimate the convective heat transfer coefficient of the fluid during the well drilling process.

In this section, a listing of the DFS and their respective derived viscosity equations is presented. A complete description of the experimental rheological programme which was carried out at the I.I.E. is outlined and reported in the monthly progress reports of this research project [Santoyo (1996)].

6.3.1 Numerical methodology to generate viscosity correlations

It is well known that the viscosity of any drilling fluid decreases when the temperature is increased. This behaviour suggests that the temperature effect can be described by a numerical correlation, if dynamic data for viscosity and temperature are available.

Experimental data available in the literature on the high temperature rheology of drilling fluids is quite limited [Fisk and Jamison (1988)]. Even though the majority of these studies indicate that the temperature is the main parameter that affects the mud viscosity, they do not report numerical correlations to describe the thermal behaviour of this transport property. Currently, there are no correlations available in the literature or being used in the drilling industry which consider the effects of temperature on mud rheology. Therefore, the generation of viscosity equations as a function of temperature is an important goal that needs to be met in order to study the heat transfer processes that usually dominate in geothermal wells under drilling conditions.

Theoretically, the use of these numerical correlations would be limited to the calculation of mud viscosities at temperatures below the thermal degradation point of the fluid (approx. 200 °C). However, this temperature limit can be extended up to 250 °C with the addition of polymeric components to the drilling mud. Above this extended temperature, the fluid flow properties would not follow any mathematical model [American Petroleum Institute (1985)].

In order to generate viscosity correlations, rheological data derived from DFS were analyzed by the numerical algorithm implemented in the MODEL and POLYREG subroutines. Fundamentally, this numerical analysis was based on the experimental rheological data obtained from the following sources:

(i) the dynamic experimental tests conducted at the DFLAB of the I.I.E.,

(ii) an unpublished rheological database property of the DFLAB of the I.I.E.,

and

(iii) experimental data available in the literature.

6.3.2 Experimental programme of dynamic viscosity measurements

Experimental tests were carried out to generate viscosity correlations for various mud systems. These tests were conducted at the DFLAB of the I.I.E. using a Fann 50C viscometer. This viscometer is a rheometer that enables the determination of rheological properties under dynamic temperature and pressure conditions to be performed. The specific objectives of this experimental work were:

(i) to use a high-pressure and high-temperature viscometer (Fann 50C) to obtain dynamic rheological data for eleven DFS,

(ii) to determine whether the data can be correlated by some mathematical flow model applying the numerical algorithm implemented in the VISCOSITY computer code,

(iii) to derive mud effective viscosity and temperature correlations using the numerical algorithm implemented in the POLYREG subroutine, and

(iv) to save the derived viscosity-temperature correlations in the VISTEMPEQ database and to couple to the numerical wellbore thermal simulator (WELLTHER) in order to predict temperature distributions during and after well drilling operations.

6.3.3 Experimental details

Selection of drilling fluid systems (DFS). Drilling muds are composed of liquids and solids. Typically, the liquid portion used is water. The solid portion is usually a blend of commercial clays, barite, polymers, thinners and other chemical additives along with drilled solids.

Most drilling muds are classified as water-based muds. In some areas very few problems are encountered and the drilling mud consists of only water and native solids. In other areas it is necessary to add clays to the mud to increase the viscosity and gelling character of the mud. The most commonly used clays are montmorillonites, often referred to as bentonites. Commercial bentonite is not a pure material. It has been estimated that the best material available is about 60 % to 70 % sodium montmorinollite [Tschirley (1983)]. The remaining portion might be calcium montmorillonite or other low yield clays such as kaolinite, illinite or chlorite.

Considering the nature of these materials, the best high temperature drilling muds from commercial materials available in the Mexican well drilling industry were selected. Eleven water-based drilling fluids were formulated to carry out the dynamic rheological tests. The composition of the tested drilling fluids is characterised by different formulations of bentonite. These formulations were prepared using four different types of materials along with water and some additives and polymers to avoid thermal degradation of the mud during the tests.

Bentonite formulations were prepared using homogeneous mixing techniques which are proposed by the API specifications [Ravi and Sutton (1990)]. The densities of each sample were measured immediately after mixing. The complete composition of these DFS are given in Table 6.1. The qualitative mineralogical composition of each bentonite was determined by X-Ray diffraction in the X-Ray laboratory of the I.I.E. The quantitative chemical composition of these bentonite samples was found using ion chromatography and standard wet chemical methods. The results obtained in both qualitative and quantitative measurements are summarised in Table 6.2.

Equipment. The Fann viscometer model 50C is a concentric cylinder, rotational type viscometer (Fig. 6.1). This instrument is commonly used to measure the flow properties of drilling fluids at elevated temperatures and pressures. The Fann 50C is designed in the same fashion as the unpressured viscometer. The upper operating limits are 260 °C and 6896 kPa. The viscometer is equipped with a standard rotor cup with a sample capacity of 50 ml. The drilling fluid must be contained in the annular space between two cylinders with the outer sleeve being driven at a controlled rotational velocity. Torque is exerted on the inner cylinder or bob by the rotation of the outer sleeve in the drilling fluid. This torque is then measured to determine the flow properties. Data are recorded either on an X-Y recorder or strip chart recorder. This instrument has infinitely variable rotor speeds from 1 to 625 rpm with a viscosity range of 0.001 to 300 Pa·s. The temperature range of 0 to 260 °C is programmable. The main advantage that this equipment offers over the other viscometers is that the viscosity measurements can be done at transient temperature conditions. This characteristic enables the viscosity measurement of the fluid at geothermal drilling conditions to be simulated.

The viscosity is measured by shearing a thin film of the liquid between concentric cylinders. The outer cylinder can be rotated at a constant rate and the shear stress measured in terms of the deflection of the inner cylinder (or bob), which is suspended by a torsion spring (Fig. 6.2).

The sample can be heated up to 260 °C by an oil bath which is also used for cooling the sample. Pressures in the sample cup can reach up to 6896 kPa and are produced by a nitrogen gas cylinder or by a compressed air line which can be controlled using a pressure regulator.

The temperature and viscosity of the mud are automatically logged by a Houston instrument two pen strip recorder [Houston (1990)]. Thus, the viscosity and temperature variations are given in the form of a rheogram for each fluid analysed (Fig. 6.3). Complete operating specifications of the Fann 50C viscometer is presented in the manufacturer manual [Fann Instrument Co. (1989)].

Calibration of the Fann 50C viscometer (operating conditions for the dynamic rheological tests). Before beginning the dynamic rheological test of the prepared DFS, a standard calibration test of the equipment is performed. This calibration required fixing the operating conditions of the Fann 50C instrument. These operating conditions are summarised in Table 6.3. Viscometer calibration is carried out as a typical shear stress calibration test using a standard fluid of known viscosity and temperature characteristics. Silicone oils with a viscosity range of 50 to 200 mPa.s are recommended by the manufacturer. Details of the calibration and operating procedures are described by the manufacturer's manual [Fann Instrument Co. (1989)].

Once the calibration test is concluded, the viscosity and temperature measurements of the samples can be performed. Thus, an accurate volume of 50 ml of mud must be placed at the sample cup. This sample volume must be a precise measurement, because an excess or insufficient amount of mud can affect the flow viscometer system. An excess of mud could contaminate the bearings and seals of the system, while, an insufficient mud volume could cause mixing of the sample and pressurising oil at the interface.

After introducing the sample, the dynamic test is initiated using the Fann 50C operating conditions shown in Table 6.3.

Fann 50C data are recorded on a rheogram using a two channel potentiometric servo recorder. These channels are used separately to record the temperature and viscosity data. Dynamic rheological data are transferred to a personal computer to be analysed.

6.4 Analysis of Experimental Results

Numerical data analyses were made using the MODEL and POLYREG subroutines, which were developed to generate numerical correlation of viscosity as a function of temperature.

6.4.1 Viscosity and temperature data

Viscosity and temperature data obtained from the dynamic rheological tests for the tested DFS are summarized in Table 6.4. Plots of viscosity and temperature data under dynamic conditions are shown in Figs. 6.4 to 6.14. From these figures several observations can be made. In the majority of the cases presented here, the mud viscosity decreases with an increase in the temperature and time parameters. This decrease does not take place indefinitely and viscosity reaches (or approaches) a constant value at a certain temperature and time. This could be related to the thermal degradation of each tested mud. Above this point, an increase in the mud viscosity is observed probably due to mud gelation processes.

6.4.2 Database of viscosity and temperature correlations (VISTEMPEQ)

Plots of viscosity and temperature data are shown in Figs. 6.15 to 6.25. From these figures it is clearly shown that viscosity and temperature data can be correlated by means of a polynomial equation of the second-degree. Therefore, the MODEL and POLYREG subroutines were applied to the rheological data. Thus, numerical analyses of data led to the derivation of the polynomial equations that describe the dynamic thermal behaviour of mud viscosities. Plots of these viscosity equations are shown simultaneously in Figs. 6.15 to 6.25 for each mud system tested.

Viscosity-temperature correlations from these dynamic rheological tests are summarized in Table 6.5. Values of constants, temperature ranges of application, regression coefficients (R_c) and average errors are presented in the same table.

6.4.3 Conclusions of the experimental work

Eleven drilling fluid systems commonly used in the drilling of geothermal wells were rheologically evaluated. The composition of these fluids was characterized by different formulations of bentonite. Transport properties (viscosity and density) and chemical analyses of these muds were determined. As a result of these dynamic rheological tests, viscosity correlations of eleven drilling fluids systems were developed. Thirteen viscosity-temperature correlations were derived. A statistical evaluation of these equations indicated associated errors in the range of 1.7% to 15.1%. The magnitude of these errors depends on the complex rheological behaviour of each DFS used. These equations were saved in the VISTEMPEQ database for their subsequent use in the wellbore thermal simulator (WELLTHER).

6.5 Analysis of Experimental Data Available in the Literature

Two additional sources of rheological dynamic data were analyzed. The first was a source based on the unpublished rheological property data from the DFLAB and the second was a source derived from experimental data available in the literature. This activity enables new correlations between viscosity and temperature to be derived. These correlations increased the number of viscosity equations in the VISTEMPEQ database. The numerical methodology developed in the MODEL and POLYREG subroutines was newly applied to analyze all the compiled rheological data.

6.5.1 Unpublished rheological data property of the DFLAB

The DFLAB of the I.I.E. has developed several research projects based on the rheological evaluation of DFS for geothermal well drilling applications [Mulás et al. (1985)]. From these projects, extensive experience in the preparation of

drilling mud formulations has been obtained. These formulations have been used for distinct geological strata and thermodynamic conditions that usually predominate in geothermal reservoirs. Since 1982, the DFLAB has evaluated numerous DFS to be applied during geothermal well drilling activities in Mexican geothermal fields, such as Cerro Prieto, Baja California; Los Azufres, Michoacan; Los Humeros, Puebla and La Primavera, Jalisco [Santoyo-Gutierrez et al. (1991)].

Comprehensive rheological evaluations carried out by the DFLAB enabled various drilling problems, such as lost circulation, thermal degradation, and mud gelation, that normally occur during these operations, to be solved. Additionally, collaborative programmes with other Mexican and foreign institutions have allowed the rheological evaluation of drilling materials to be reliably applied in the drilling of geothermal wells [Bottai et al. (1986)].

Selection of drilling fluid systems from the DFLAB database. To date, all the research projects developed at the DFLAB have enabled an extensive database on mud transport and physicochemical properties to be created. These data are considered as confidential information, i.e. the property of I.I.E. *This limitation does not allow all the information derived from these rheological studies to be published*. However, some of the DFS evaluated can be carefully selected in order to publish only the viscosity-temperature correlations that are linked to the DFS, avoiding the presentation of a detailed programme of the experimental tests, or the complete composition of these DFS.

As a result of this procedure, eleven DFS were chosen. Table 6.6 shows a general description of the physical composition of these systems which are classified as water-based muds. All of these systems use a mixture of bentonite and some polymer materials.

Numerical analysis of the viscosity and temperature data for the selected DFS. In the majority of the cases analyzed, mud viscosity decreases with an increase in temperature. These decreases do not occur indefinitely and

viscosities approach a constant value at a certain temperature. After attaining these conditions, an increase in the mud viscosity is observed due to the effects of the mud gelation processes. Even though these dynamic tests produced sufficient rheological data, a limitation in the temperature range of some of them was detected. This is the case for the DFS that contain bentonite 3% and clays 31% (muds 19-22; Table 6.6). In the majority of these DFS, the maximum temperature recorded was 140 °C.

Viscosity and temperature correlations for the selected DFS. Viscosity and temperature data were correlated by data regression using a second-degree polynomial equation whose numerical algorithm was implemented in the MODEL and POLYREG subroutines. Hence, numerical analyses of data lead to the derivation of the numerical correlations that describe the dynamic and rheological behaviour of mud at high temperatures. These numerical correlations are presented in Table 6.7. Constant values, application temperature ranges, regression coefficients (R_c) and average errors are included in the table. A statistical evaluation of these equations indicated associated errors in the range of 2.4% to 12.6%. The magnitude of these errors depends on the complex rheological behaviour of each DFS used.

6.5.2 Experimental data available in the drilling literature

Currently, there are not sufficient dynamic rheological data for DFS in the literature that allow the viscosity correlations with temperature to be derived. However, a literature review based on the evaluation of rheological mud properties is desirable in order to select DFS that can resist elevated temperatures. With respect to these activities, rheological studies carried out by Guven and Carney (1979) and Carney and Guven (1980) were compiled and analyzed. The majority of these studies indicated that drilling fluids based on fibrous clays such as sepiolite and attapulgite can be used in high temperature environments, such as geothermal reservoirs.

Selection of drilling fluid systems. An extensive study of dynamic rheological tests at high temperatures was performed by Guven et al. (1982). These studies involved a systematic and complete evaluation of rheological properties of the fluids based on fibrous clays (sepiolite and attapulgite) in the temperature range from 25°C to 426°C. Unfortunately, Guven et al. (1982) limited their study to correlate the rheological behaviour of these fluids with the chemical changes occuring in the clay due to the effects of high temperature. These results only confirmed that the pure sepiolite and attapulgite muds are stable at high temperature and that they could be used as a primary formulation for geothermal well drilling operations. From these evaluations, Guven et al. (1982) formulated new geothermal drilling fluids by addition of Wyoming bentonite and various polymers to the primary formulations. These fluids also exhibited an extremely stable rheological behaviour and a low fluid loss when they are subjected to elevated temperatures. On the basis of the dynamic and rheological results obtained by Guven et al. (1982), a selection of thirty-one muds to derive numerical correlations of viscosity with temperature was made. These data were taken from the studies of the following DFS:

A. attapulgite based fluids:
   - A.1. the pure attapulgite fluid,
   - A.2. attapulgite/chloride fluids,
   - A.3. attapulgite/hydroxide fluids,

B. sepiolite based fluids:
   - B.1. the pure sepiolite fluid,
   - B.2. sepiolite/chloride fluids,
   - B.3. sepiolite/hydroxide fluids,

C. new fluid formulations:
   - C.1. conventional base fluids,
   - C.2. attapulgite (or sepiolite)/polymer (SPA) fluids,
   - C.3. sepiolite/English mica fluids,

and

C.4. sepiolite/bentonite/SPA fluids.

A complete description of the physical and chemical composition of all the DFS used is presented in Tables 6.8, 6.9 and 6.10. These fluids were classified by a sequential number, according to the initial order established in the section 6.3.3. Thus, a total of fifty three DFS with their respective numerical correlations of viscosity were saved in the VISTEMPEQ database. In order to continue with the derivation of viscosity correlations, an application of the MODEL and POLYREG subroutines to the data reported by Guven et al. (1982) was carried out.

Numerical analysis of the viscosity and temperature data for the selected DFS. After selecting the DFS, viscosity and temperature data were compiled and numerically analyzed. A complete description of the rheological behaviour of these systems under high temperature conditions was depicted in the viscosity and temperature plots which were originally presented by Guven et al. (1982). In the majority of the analyzed cases, mud viscosity decreases with an increase in temperature. Again, these decreases do not occur indefinitely and viscosities attain (or approach) a constant value at a certain temperature and exposure time. After attaining these conditions, an increase in the mud viscosity was observed due to mud gelation problems.

Viscosity and temperature correlations for the selected DFS. Viscosity and temperature data were correlated by means of a polynomial equation of the second-degree using the MODEL and POLYREG subroutines. Thus, numerical analyses of data led to the derivation of the polynomial equations that describe the dynamic and rheological behaviour of mud at high temperatures. These numerical correlations are summarized in Tables 6.11, 6.12 and 6.13. Constant values, application temperature ranges, regression coefficients (R_c) and average errors are presented in the same table. A statistical evaluation of these equations indicated associated errors in the range of 0.2% to 16.5%. Again, the magnitude of these errors depend on the complex rheological behaviour of each DFS used.

6.5.3 Conclusions of the experimental data analysis (literature)

Eleven DFS (based on bentonites) used in the drilling of geothermal wells were initially evaluated. These bentonites were selected from the unpublished data file property of the I.I.E. Subsequently, thirty-one DFS (based on attapulgite and sepiolite systems) reported in the drilling literature for geothermal applications were analyzed. As a result of these numerical and rheological analyses, forty-two viscosity correlations were derived. Therefore, a total of fifty-three viscosity equations are available in the VISTEMPEQ database. These results constitute the first numerical correlations available to apply in heat transfer studies during the drilling of geothermal wells.

6.6 References

American Petroleum Institute (API), The rheology of oil-well drilling fluids, American Petroleum Institute, Production Department, API Bulletin 13D, Second Edition, 28 p. (1985).

A. Bottai, F. Fabbri, R. Ricciardulli y B. Tarquini, G.H. Barroso, M. Morales, S. Santoyo-Gutierrez, B. Dominguez y G. Gallegos, Estudio de fluidos de perforacion y cementos para pozos geotermicos, Marco de Cooperacion Tecnica Mexico-Italia, Informe Final, Proyecto No. 1884, 85 p. (1986).

L.L. Carney and N. Guven, Investigation of changes in the structure of clays during hydrothermal study of drilling fluids, Society of Petroleum Engineers Journal, **October**, pp. 385-390 (1980).

Fann Instrument Co., Operating instructions, model 50C Fann viscometer, Fann Instrument Corporation, Houston, Texas, USA, 30 p. (1989).

J.V. Fisk and D.E. Jamison, Physical properties of drilling fluids at high temperatures and pressures, Proceedings of the IADC/SPE 17200 Drilling Conference, Dallas, Texas, USA, 257-265 (1988).

N. Guven and L.L. Carney, The hydrothermal transformation of sepiolite to stevensite and the effect of added chlorides and hydroxides, Clays and Clay Mineral, 27, pp. 253-260 (1979).

N. Guven, L.L. Carney, L.J. Lee and R.P. Bernhard, Clay-based geothermal drilling fluids, Final Report for Sandia National Laboratories, SAND 82-7037, 177 p. (1982).

Houston Instrument, Omniscribe B-5000 strip chart recorder instruction manual, Houston Instrument, Div. Bausch & Lomb, Austin, Texas, USA, 21 p. (1990).

P. Mulás, D. Nieva and F.A. Holland, Developments in geothermal energy in Mexico-part one: general considerations, Heat Recovery Systems and CHP, 5 (4) 277-283 (1985).

K.M. Ravi and D.L. Sutton, New rheological corelation for cement slurries as a function of temperature, Proceedings of the 65th Annual Technical Conference and Exhibition of the Society of Petroleum Engineers, New Orleans, USA, 455-462 (1990).

N.K. Tschirley, Testing of drilling fluids, Chapter 4: Drilling and drilling fluids, Developments in Petroleum Science 11, Edited by: G.V. Chilingarian and P. Vorabutr, Elsevier Amsterdam-Oxford-New York, USA, 121-167 (1983).

E. Santoyo, Estimation of static formation temperatures in the presence of fluid losses during well drilling, Monthly Progress Reports, In-House Ph. D Programme Instituto de Investigaciones Eléctricas, México with the University of Salford, U.K., February (21 p.) and March (20 p.) (1996).

S. Santoyo-Gutierrez, A. Garcia, M. Morales, J. Perezyera and A. Rosas, Applied technology in the solution of geothermal drilling problems of deep wells in La Primavera caldera (Mexico), Journal of Volcanology and Geothermal Research, 47 195-208 (1991).

Mud No.	Bentonite Type	%	Supercaltex additive (kg/m^3)	Resinex additive (kg/m^3)	Polymer Type	Polymer (kg/m^3)	Density (kg/m^3)
1	Processed clays	6.2	6.0	10.0	-	0.0	1040.
2	Processed clays	6.2	6.0	10.0	Poly Rx	10.0	1040.
3	Processed clays	6.2	6.0	10.0	Lamsperce	10.0	1040.
4	Processed clays	6.2	6.0	10.0	Miltemp	10.0	1040.
5	Baramin (9%)	9.0	6.0	10.0	Poly Rx	10.0	1060.
6	Bentosund AUS	6.2	6.0	10.0	-	0.0	1050.
7	Bentosund AUS	6.2	6.0	10.0	Poly Rx	10.0	1050.
8	Bentosund AUS	6.2	6.0	10.0	Lamsperce	10.0	1050.
9	Bentosund AUS	6.2	6.0	10.0	Miltemp	10.0	1050.
10	Perfobent	7.5	15.0	10.0	Poly Rx	10.0	1050.
11	Bentosund AUS Sepiolite *	1.4 4.3	0.0	10.0	Cypan	5.4	1020.

*Mud system (11) uses XP-20 cromolignite as an additional additive (10.0 kg/m^3)

Table 6.1

Physical composition of the drilling fluid systems (DFS) tested in the experimental rheological work.

Bentonite Type	Qualitative Analysis	Quantitative Analysis (%)							
		Na	K	Ca	Mg	IS*	SiO_2	Al	Fe
Processed clays	Montmorillonite Plagioclasses Quartz Cristobalite	7.0	0.4	2.0	4.2	12.6	70.9	2.2	0.7
Baramin	Montmorillonite Plagioclasses Quartz Calcite	9.2	1.3	2.3	5.3	8.3	70.1	2.6	0.9
Bentusund AUS	Montmorillonite Albite Plagioclasses Quartz Anortite	12.8	3.6	1.5	1.5	13.1	63.2	2.2	2.1
Perfobent	Montmorillonite Plagioclasses Quartz Calcite	11.8	1.4	3.5	5.1	9.6	64.8	2.4	1.4

* IS: insoluble material

Table 6.2

Chemical and mineralogical composition of the DFS (bentonites) tested.

Operating parameter	Setting values
Initial temperature (T_i)	25.5 °C
Final temperature (T_f)	180.0 °C
Reservoir pressure	3448.2 kPa
Time to attain T_f	1.24 hr
Chart speed	0.25 cm/min
Shear rate	170.0 s^{-1}
Viscosity range	50% (50 mPa.s)
Total time of the test	3.0 hr

Table 6.3

Fann 50C operating conditions for the dynamic rheological tests.

Temp [°C]	Viscosity [mPa.s]										
	Mud 1	Mud 2	Mud 3	Mud 4	Mud 5	Mud 6	Mud 7	Mud 8	Mud 9	Mud 10	Mud 11
25.0	14.0	8.0	2.3	6.5	4.0	14.0	9.6	6.4	7.0	-	7.5
37.5	14.0	8.0	1.5	6.3	3.2	14.0	9.7	6.1	7.0	9.5	7.0
50.0	-	7.5	1.0	-	3.0	-	9.0	5.6	6.4	8.0	6.2
62.5	14.0	7.5	0.8	-	2.9	14.0	9.0	5.1	6.0	7.4	6.0
75.0	-	7.3	0.75	5.6	2.6	-	8.5	5.0	5.9	7.2	6.7
87.5	12.0	7.0	0.5	5.7	2.5	17.5	8.7	4.8	5.7	7.4	7.3
100.0	-	7.0	0.5	-	2.3	-	9.1	4.7	5.5	7.4	8.0
106.3	-	7.0	0.4	-	2.2	-	9.5	4.6	5.5	7.4	8.0
112.5	-	7.0	0.25	-	2.0	-	10.0	4.5	5.6	7.4	8.0
125.0	8.5	7.5	0.25	5.4	2.0	22.5	12.0	-	6.7	7.0	8.3
150.0	6.5	8.7	0.4	5.2	1.75	27.0	14.3	5.0	7.4	5.6	10.6
175.0	-	9.3	5.4	5.0	1.75	-	16.0	5.0	8.2	3.8	14.4
180.0	6.5	9.3	7.6	5.1	1.7	32.5	16.1	4.8	8.5	3.0	14.5
200.0	-	9.3	15.0	5.3	1.3	-	-	5.6	12.0	-	-

Table 6.4

Viscosity and temperature data obtained from the dynamic rheological tests for the selected DFS.

DFS No.	Viscosity equation (mPa.s)	Temperature range (°C)	R_c	Average Error (%)
1	$\mu = 15.7494-0.0405554\ T-8.92239x10^{-5}\ T^2$	$25°C \leq T \leq 180°C$	0.9157	9.6
2	$\mu = 9.2833-0.0498734\ T+2.84197x10^{-4}\ T^2$	$25°C \leq T \leq 180°C$	0.9297	3.1
3	$\mu = 3.1367-0.0480416\ T+2.01353x10^{-4}\ T^2$	$25°C \leq T \leq 150°C$	0.9516	15.1
	$\mu = 51.7208-0.8190551\ T+3.17825x10^{-3}\ T^2$	$150°C \leq T \leq 200°C$	0.9980	4.3
4	$\mu = 6.9439-0.0220237\ T+6.71697x10^{-5}\ T^2$	$25°C \leq T \leq 200°C$	0.9038	1.7
5	$\mu = 4.3506-0.0275101\ T+6.69566x10^{-5}\ T^2$	$25°C \leq T \leq 200°C$	0.9603	4.9
6	$\mu = 13.6045-0.0218310\ T+7.23175x10^{-4}\ T^2$	$25°C \leq T \leq 180°C$	0.9887	3.5
7	$\mu = 11.2084-0.0748142\ T+5.86817x10^{-4}\ T^2$	$25°C \leq T \leq 180°C$	0.9602	3.9
8	$\mu = 7.3834-0.0442881\ T+1.74367x10^{-4}\ T^2$	$25°C \leq T \leq 200°C$	0.9182	2.1
9	$\mu = 9.1839-0.0807539\ T+4.51417x10^{-4}\ T^2$	$25°C \leq T \leq 200°C$	0.9327	4.6
10	$\mu = 15.0036-0.1967140\ T+1.22286x10^{-3}\ T^2$	$37°C \leq T \leq 100°C$	0.9540	2.0
	$\mu = 1.2691+0.1262360\ T-6.44358x10^{-4}\ T^2$	$100°C \leq T \leq 180°C$	0.9969	11.6
11	$\mu = 8.7342-0.0713110\ T+5.78238x10^{-4}\ T^2$	$25°C \leq T \leq 180°C$	0.9805	4.1

Table 6.5

Viscosity-temperature correlations obtained by numerical analysis from the dynamic rheological tests of evaluated DFS.

Mud No.	Drilling fluid type	Polymer
12	bentonite (8%)	water, H_2O
13	bentonite (8%)	Spersene (1%)
14	bentonite (8%)	Spersene (10%)
15	bentonite (8%)	Poly Rx (1%)
16	bentonite (8%)	Poly Rx (10%)
17	bentonite (8%)	Lamsperse (0.05%)
18	bentonite (8%)	Lamsperse (0.75%)
19	bentonite (3%) and clays (31%)	Water, H_2O
20	bentonite (3%) and clays (31%)	Spersene (6.45%)
21	bentonite (3%) and clays (31%)	Poly Rx (6.45%)
22	bentonite (3%) and clays (31%)	Lamsperse (5%)

Table 6.6

Drilling fluid systems (DFS) evaluated in the dynamic rheological tests carried out by Bottai et al (1986).

DFS No.	Viscosity equation (mPa.s)	Temperature range (°C)	R_c	Average Error (%)
12	$\mu = 6.03539+0.201270\ T-6.79160x10^{-5}\ T^2$	$50°C \leq T \leq 187°C$	0.9752	5.1
13	$\mu =11.13480-0.140390\ T+1.09665x10^{-3}\ T^2$	$40°C \leq T \leq 175°C$	0.9804	4.7
14	$\mu = 9.27507-0.096988\ T+67.2322x10^{-5}\ T^2$	$48°C \leq T \leq 190°C$	0.9905	2.6
15	$\mu = 7.73861-0.026873\ T+41.0271x10^{-5}\ T^2$	$50°C \leq T \leq 200°C$	0.9739	4.1
16	$\mu = 6.10896-0.097476\ T+4.82641x10^{-4}\ T^2$	$44°C \leq T \leq 150°C$	0.8036	12.6
17	$\mu = 5.61612-0.074190\ T+39.7087x10^{-5}\ T^2$	$45°C \leq T \leq 175°C$	0.9051	6.9
18	$\mu = 3.46506-0.045122\ T+19.5130x10^{-5}\ T^2$	$30°C \leq T \leq 187°C$	0.9347	8.0
19	$\mu =23.25570+0.251347\ T-11.7261x10^{-4}\ T^2$	$25°C \leq T \leq 140°C$	0.8650	2.4
20	$\mu = 8.71280-0.138870\ T+1.18273x10^{-3}\ T^2$	$25°C \leq T \leq 140°C$	0.9827	3.7
21	$\mu =10.20040-0.198399\ T+1.58082x10^{-3}\ T^2$	$25°C \leq T \leq 140°C$	0.9476	8.5
22	$\mu = 4.02607-0.079922\ T+6.26045x10^{-4}\ T^2$	$30°C \leq T \leq 90°C$	0.9185	4.8
	$\mu =36.80750-0.709150\ T+3.56968x10^{-3}\ T^2$	$88°C \leq T \leq 150°C$	0.9862	9.3

Table 6.7

Viscosity-temperature correlations derived by numerical analysis from the dynamic rheological data obtained by Bottai et al. (1986).

Mud No.	Drilling fluid type	Additives
23	attapulgite	water, H_2O
Attapulgite/chloride based fluids:		
24	attapulgite	sodium chloride, NaCl
25	attapulgite	potasium chloride, KCl
26	attalpugite	calcium chloride, $CaCl_2$
27	attalpugite	magnesium chloride, $MgCl_2$
Attapulgite/hydroxide based fluids:		
28	attapulgite	sodium hydroxide, NaOH
29	attapulgite	potasium hydroxide, KOH
30	attapulgite	calcium hydroxide, $Ca(OH)_2$
31	attapulgite	magnesium hydroxide, $Mg(OH)_2$
32	sepiolite	water, H_2O
Sepiolite/chloride based fluids:		
33	sepiolite	sodium chloride, NaCl
34	sepiolite	potasium chloride, KCl
35	sepiolite	calcium chloride, $CaCl_2$
36	sepiolite	magnesium chloride, $MgCl_2$

Table 6.8

Drilling fluid systems (DFS) evaluated in the dynamic rheological tests carried out by Guven et al (1982).

Mud No.	Drilling fluid type	Additives/polymers
Sepiolite/hydroxide based fluids:		
37	sepiolite	sodium hydroxide, NaOH
38	sepiolite	potasium hydroxide, KOH
39	sepiolite	calcium hydroxide, $Ca(OH)_2$
40	sepiolite	magnesium hydroxide, $Mg(OH)_2$
Conventional drilling fluids:		
41	Wyoming (50%) and Texas (50%) bentonites	water, H_2O
42	Wyoming (50%) and Texas (50%) bentonites	quebracho/NaOH
43	Wyoming (50%) and Texas (50%) bentonites	unical/NaOH
44	Wyoming (50%) and Texas (50%) bentonites	spersene/XP-20/NaOH
Attapulgite/sepiolite/polymers fluids:		
45	sepiolite (83%)	sodium polyacrylates (17%)
46	attapulgite (83%)	sodium polyacrylates (17%)
47	sepiolite (50%) and English mica (33%)	sodium polyacrylates (17%)
48	sepiolite (43%) and English mica (57%)	
49	sepiolite (38%) and English mica (51%)	sodium polyacrylates (11%)
50	sepiolite (41%) and English mica (55%)	sodium polyacrylates (4%)
Other special drilling fluids:		
51	HTM-1: sepiolite (34%), Wyoming bentonite (11%) and brown coal (45%)	sodium polyacrylates (5.6%)/ NaOH (4.4%)
52	GDF-1: sepiolite (71%) and Wyoming bentonite (18%)	sodium polyacrylates (19%)
53	GDF-2: sepiolite (42%), Wyoming bentonite (14%) and English mica (28%)	sodium polyacrylates (14%)/ NaOH (2%)

Table 6.9

Drilling fluid systems (DFS) evaluated in the dynamic rheological tests performed by Guven et al (1982).

Drilling fluid type	Quantitative analysis (%)									
	SiO_2	MgO	Al_2O_3	Fe_2O_3	CaO	K_2O	Na_2O	P_2O_5	TiO_2	Li_2O
Attapulgite based fluids	68.0	10.5	12.0	5.0	1.7	1.0	0.7	-	0.7	-
Sepiolite based fluids	67.1	26.5	2.7	0.6	1.5	0.5	0.3	-	-	0.1

Table 6.10

Chemical analysis of the drilling fluid systems used by Guven et al (1982) in the dynamic rheological tests.

DFS No.	Viscosity equation (mPa.s)	Temperature range (°C)	R_c	Average Error (%)
23	$\mu = 10.40430 - 0.127160\ T + 0.457029 \times 10^{-3}\ T^2$	$25°C \leq T \leq 175°C$	0.9965	4.3
	$\mu = -2.54915 + 0.061199\ T - 0.191080 \times 10^{-3}\ T^2$	$175°C \leq T \leq 260°C$	0.9686	11.5
24	$\mu = 7.14647 - 0.044831\ T + 9.053340 \times 10^{-5}\ T^2$	$50°C \leq T \leq 260°C$	0.9992	1.2
25	$\mu = 5.95200 - 0.052614\ T + 0.164560 \times 10^{-3}\ T^2$	$25°C \leq T \leq 200°C$	0.9633	6.7
	$\mu = 11.19170 - 0.069228\ T + 0.112418 \times 10^{-3}\ T^2$	$200°C \leq T \leq 260°C$	0.9979	1.7
26	$\mu = 9.29682 - 0.071169\ T + 0.169307 \times 10^{-3}\ T^2$	$25°C \leq T \leq 260°C$	0.9320	10.9
27	$\mu = 18.01550 - 0.204645\ T + 0.874086 \times 10^{-3}\ T^2$	$25°C \leq T \leq 150°C$	0.9405	6.5
	$\mu = 24.12200 - 0.171777\ T + 0.367096 \times 10^{-3}\ T^2$	$150°C \leq T \leq 260°C$	0.9862	2.1
28	$\mu = 25.22820 - 0.175048\ T + 0.380970 \times 10^{-3}\ T^2$	$25°C \leq T \leq 260°C$	0.9859	5.8
29	$\mu = 3.22151 - 0.027370\ T + 6.303310 \times 10^{-5}\ T^2$	$25°C \leq T \leq 260°C$	0.9949	7.6
30	$\mu = 8.98070 - 0.068857\ T + 0.274829 \times 10^{-3}\ T^2$	$25°C \leq T \leq 150°C$	0.9729	2.8
	$\mu = -3.19960 + 0.097071\ T - 0.297175 \times 10^{-3}\ T^2$	$150°C \leq T \leq 260°C$	0.9984	1.0
31	$\mu = 6.68227 - 0.085265\ T + 0.402524 \times 10^{-3}\ T^2$	$25°C \leq T \leq 200°C$	0.9184	9.2
	$\mu = 61.45680 - 0.438286\ T + 0.822040 \times 10^{-3}\ T^2$	$200°C \leq T \leq 260°C$	0.9129	6.9
32	$\mu = 17.98800 - 0.175354\ T + 0.795942 \times 10^{-3}\ T^2$	$25°C \leq T \leq 150°C$	0.9621	3.2
	$\mu = 38.35960 - 0.261243\ T + 0.453539 \times 10^{-3}\ T^2$	$150°C \leq T \leq 260°C$	0.9996	2.5

Table 6.11

Viscosity-temperature correlations obtained by numerical analysis from the dynamic rheological data obtained by Guven et al. (1982).

DFS No.	Viscosity equation (mPa.s)	Temperature range (°C)	R_c	Average Error (%)
33	μ =16.19680-0.152968 T+0.920589x10^{-3} T^2	25°C ≤ T ≤ 150°C	0.8329	4.7
	μ =64.43840-0.463818 T+0.852838x10^{-3} T^2	150°C ≤ T ≤ 260°C	0.9992	3.5
34	μ =30.49000-0.182814 T+0.957114x10^{-3} T^2	25°C ≤ T ≤ 160°C	0.9655	1.1
	μ =119.3400-0.879444 T+1.655490x10^{-3} T^2	150°C ≤ T ≤ 260°C	0.9990	5.2
35	μ =12.53420-0.085971 T+0.177017x10^{-3} T^2	25°C ≤ T ≤ 260°C	0.9943	4.5
36	μ = 9.31034-0.066779 T+0.133901x10^{-3} T^2	25°C ≤ T ≤ 260°C	0.9545	16.5
37	μ =27.95900-0.028098 T-0.189545x10^{-3} T^2	25°C ≤ T ≤ 260°C	0.9893	3.6
38	μ = 6.23590-0.108384 T+0.599457x10^{-3} T^2	25°C ≤ T ≤ 160°C	0.9791	6.0
	μ =10.76530-0.062808 T+9.930570x10^{-3} T^2	150°C ≤ T ≤ 260°C	0.9105	10.5
39	μ =10.36180-0.074954 T+0.176979x10^{-3} T^2	25°C ≤ T ≤ 260°C	0.9731	7.3
40	μ =37.73500-0.339638 T+1.131710x10^{-3} T^2	25°C ≤ T ≤ 200°C	0.9867	3.4
	μ =87.47330-0.562682 T+1.022600x10^{-3} T^2	200°C ≤ T ≤ 260°C	0.9998	0.25
41	μ =53.79870-0.382211 T+1.752480x10^{-3} T^2	25°C ≤ T ≤ 225°C	0.9463	3.5
42	μ =47.64740-0.413643 T+1.701100x10^{-3} T^2	25°C ≤ T ≤ 250°C	0.9470	6.1
43	μ =36.29280-0.503480 T+1.989220x10^{-3} T^2	25°C ≤ T ≤ 250°C	0.9026	10.3

Table 6.12

Viscosity-temperature correlations obtained by numerical analysis from the dynamic rheological data obtained by Guven et al. (1982).

DFS No.	Viscosity equation (mPa.s)	Temperature range (°C)	R_c	Average Error (%)
44	$\mu = 18.28020 - 0.260958\ T + 1.095710 \times 10^{-3}\ T^2$	$25°C \leq T \leq 160°C$	0.9903	6.1
	$\mu = 92.31050 - 1.129550\ T + 3.597940 \times 10^{-3}\ T^2$	$150°C \leq T \leq 260°C$	0.9987	4.6
45	$\mu = 41.41480 - 0.370241\ T + 0.981620 \times 10^{-3}\ T^2$	$25°C \leq T \leq 260°C$	0.9793	6.2
46	$\mu = 30.81540 - 0.339219\ T + 1.153490 \times 10^{-3}\ T^2$	$25°C \leq T \leq 160°C$	0.9885	4.8
	$\mu = 19.42090 - 0.127329\ T + 2.272840 \times 10^{-4}\ T^2$	$150°C \leq T \leq 260°C$	0.9959	2.4
47	$\mu = 28.04640 - 0.148196\ T + 0.305920 \times 10^{-3}\ T^2$	$25°C \leq T \leq 200°C$	0.9992	0.9
	$\mu = -28.7908 + 0.233707\ T - 0.185430 \times 10^{-3}\ T^2$	$200°C \leq T \leq 260°C$	0.9390	4.5
48	$\mu = 2.33413 - 0.013928\ T + 1.909510 \times 10^{-5}\ T^2$	$25°C \leq T \leq 260°C$	0.9831	8.4
49	$\mu = 31.16690 - 0.333362\ T + 1.051970 \times 10^{-3}\ T^2$	$25°C \leq T \leq 160°C$	0.9999	0.2
	$\mu = 17.63970 - 0.123387\ T + 2.531240 \times 10^{-4}\ T^2$	$150°C \leq T \leq 260°C$	0.9937	2.3
50	$\mu = 0.93171 - 0.007853\ T + 3.329520 \times 10^{-5}\ T^2$	$25°C \leq T \leq 175°C$	0.9065	4.8
	$\mu = 0.606$	$175°C \leq T \leq 260°C$	1.0000	0.0
51	$\mu = 35.93580 - 0.311650\ T + 8.117560 \times 10^{-4}\ T^2$	$25°C \leq T \leq 260°C$	0.9576	11.0
52	$\mu = 37.15100 - 0.300587\ T + 0.825073 \times 10^{-3} T^2$	$25°C \leq T \leq 260°C$	0.9629	7.8
53	$\mu = 41.04740 - 0.468726 T + 1.898400 \times 10^{-3} T^2$	$25°C \leq T \leq 175°C$	0.8953	10.5
	$\mu = 103.3950 - 0.897385\ T + 2.255660 \times 10^{-3}\ T^2$	$175°C \leq T \leq 260°C$	0.9848	2.2

Table 6.13

Viscosity-temperature correlations obtained by numerical analysis from the dynamic rheological data obtained by Guven et al. (1982).

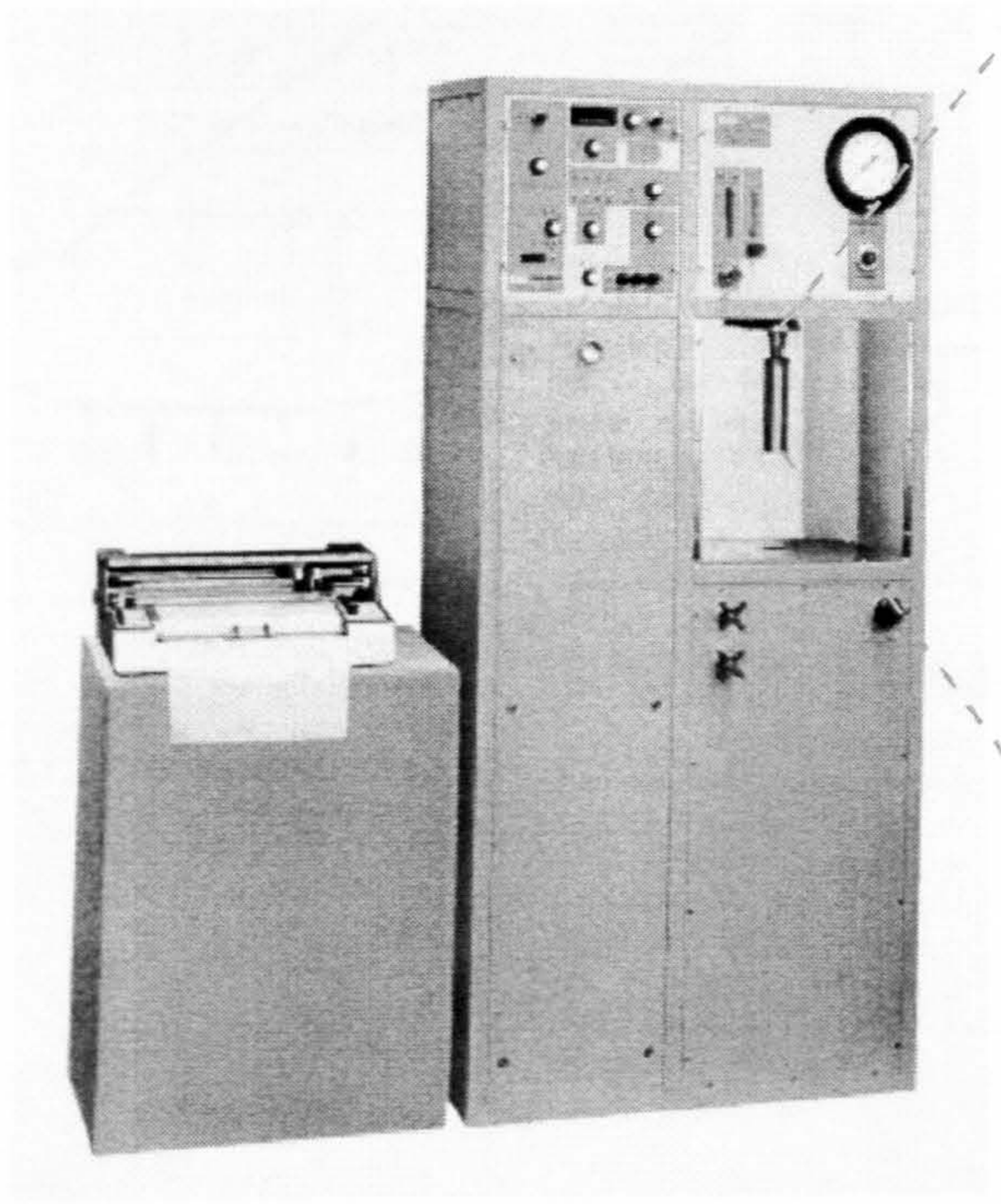

Fig. 6.1 Schematic view of the Fann 50C viscometer.

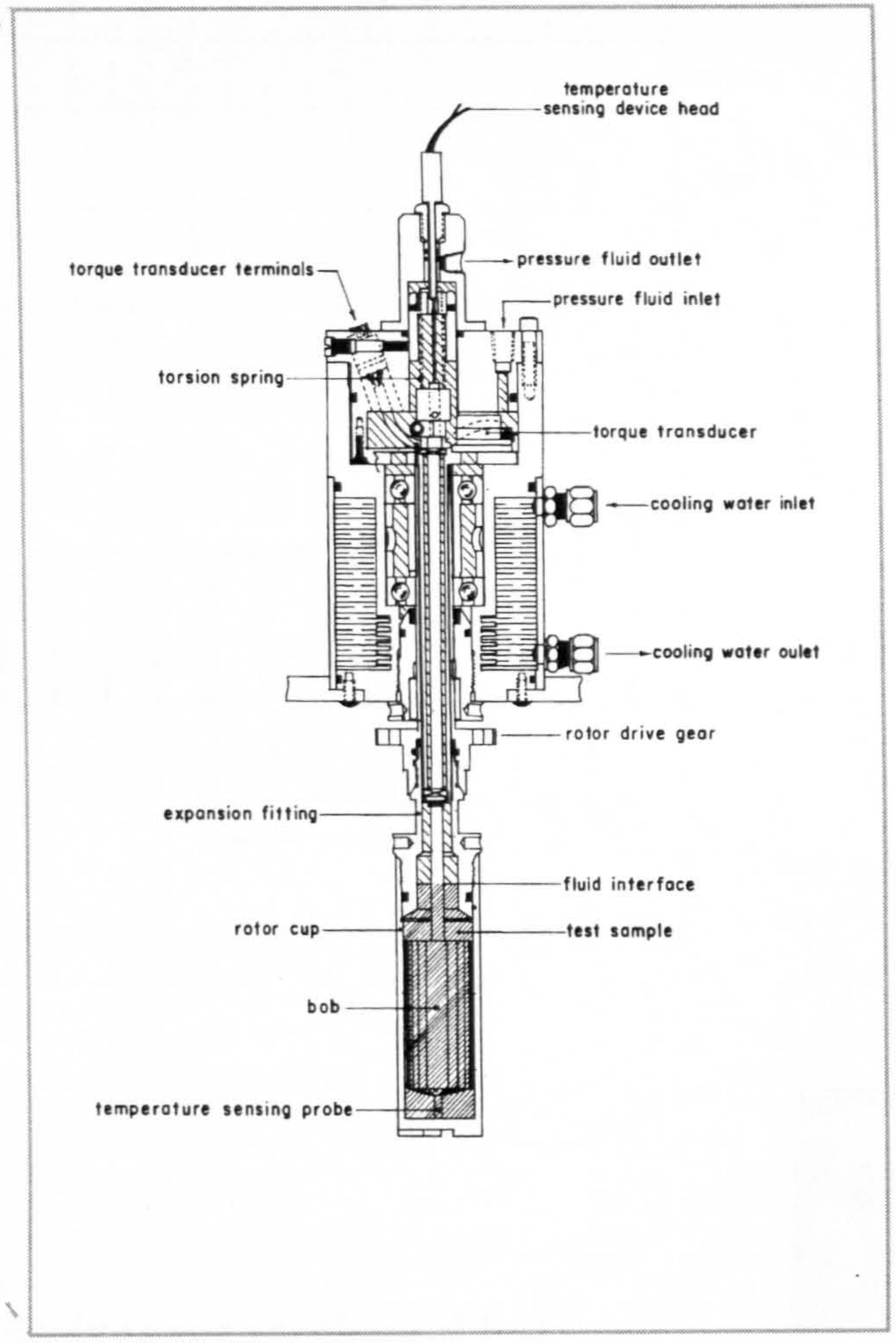

Fig. 6.2 Cross sectional view of the Fann 50C viscometer head.

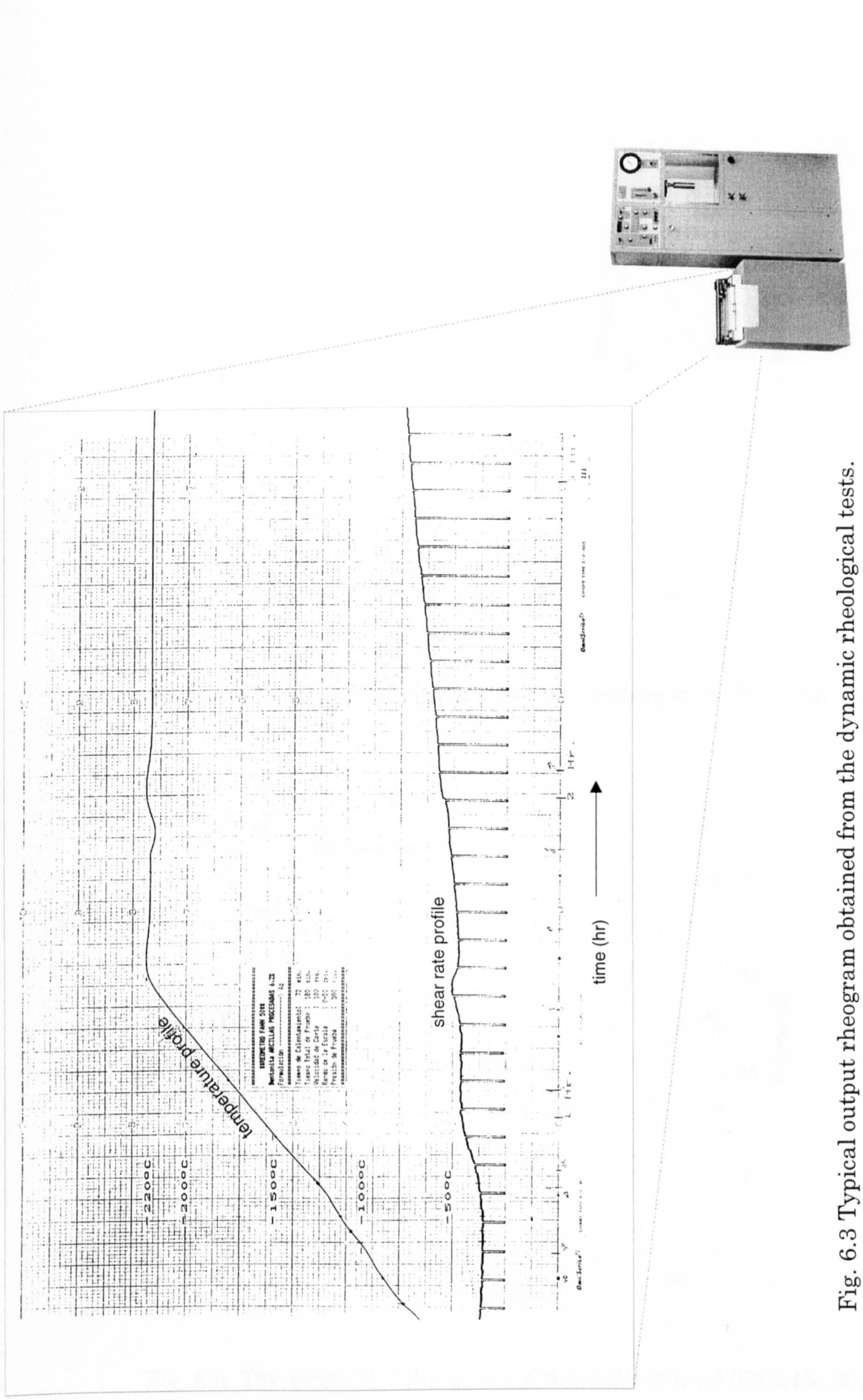

Fig. 6.3 Typical original output rheogram obtained from the dynamic rheological tests.

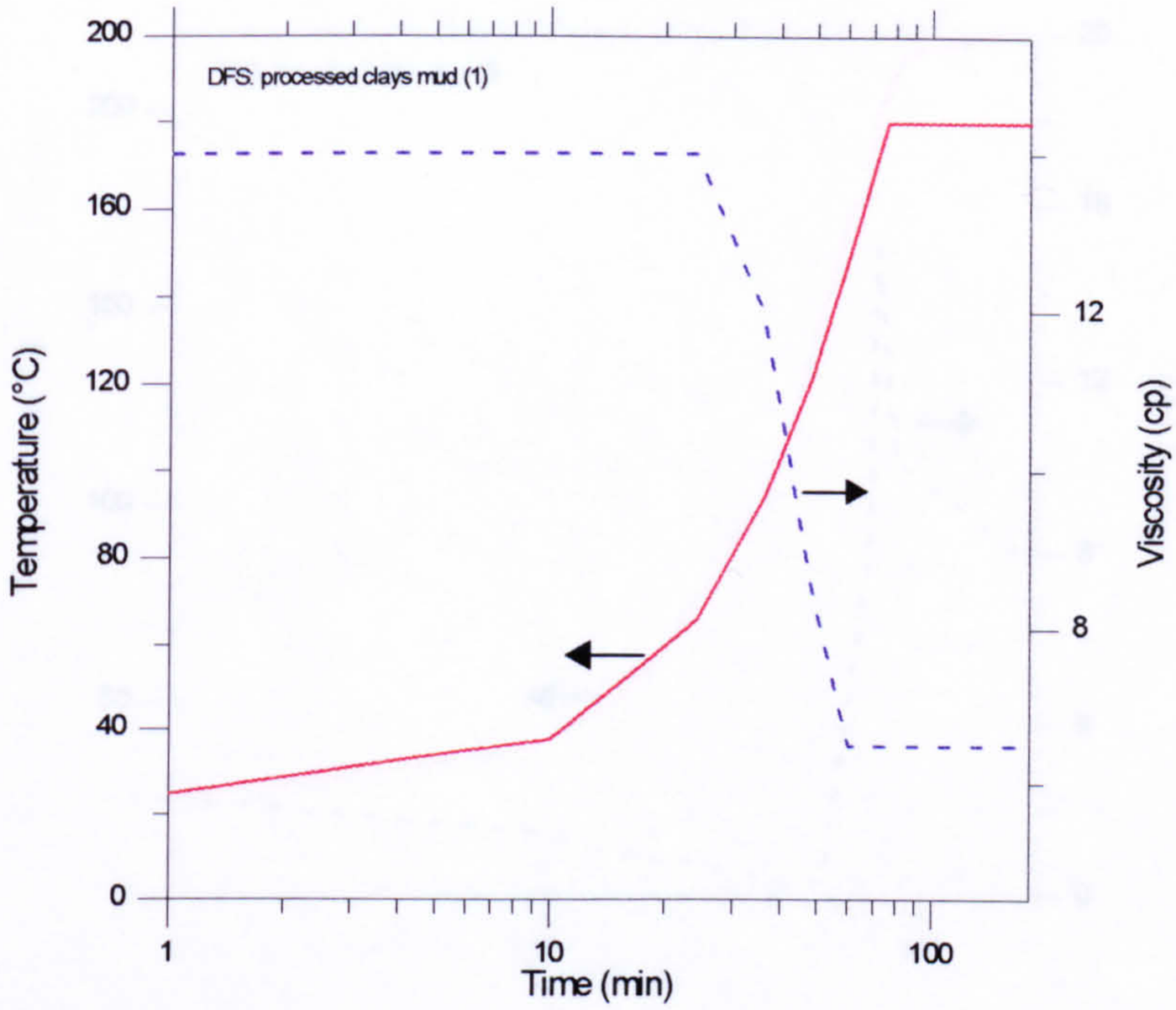

Fig. 6.4 The Fann 50C rheogram of the drilling mud (DFS No. 1).

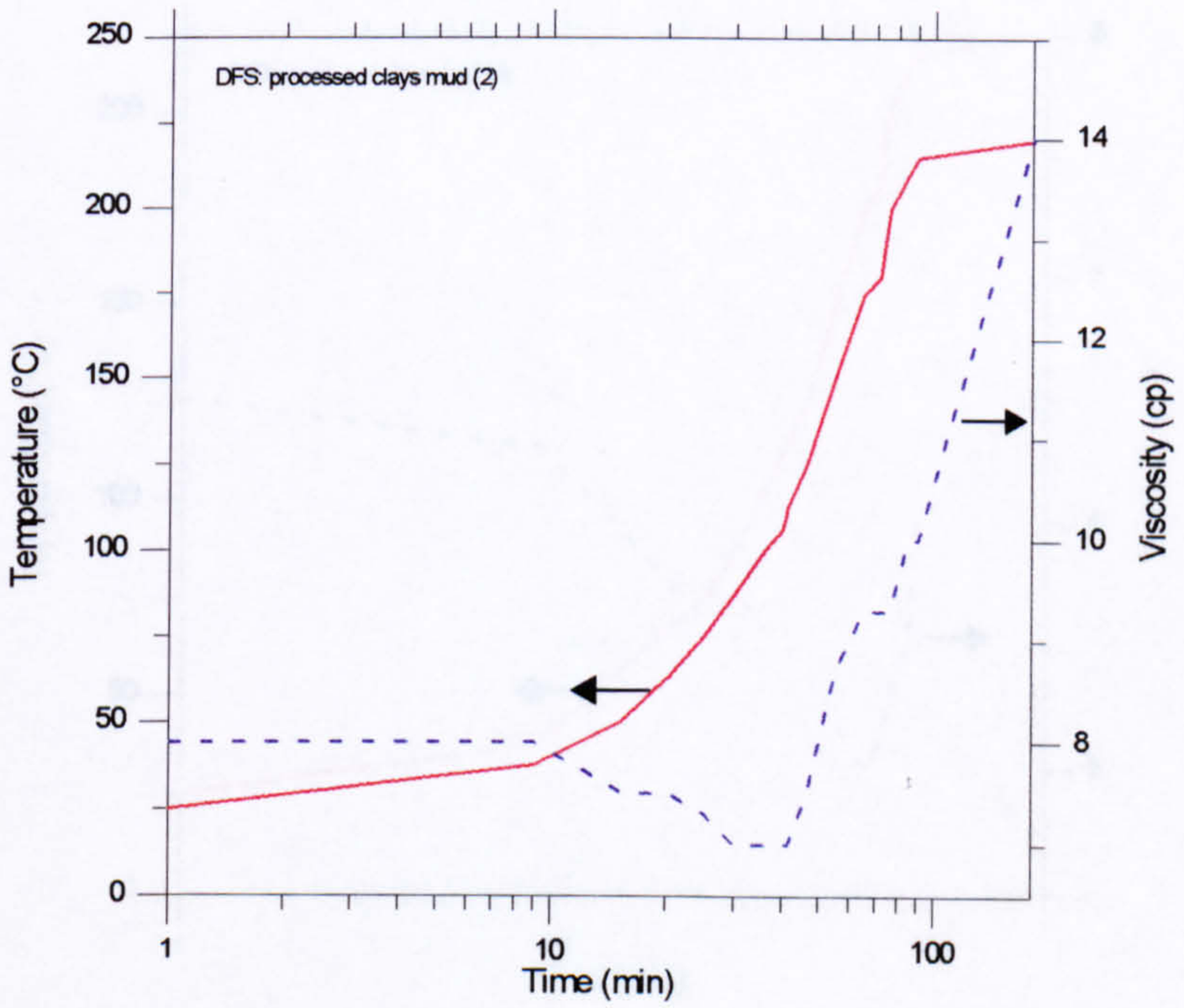

Fig. 6.5 The Fann 50C rheogram of the drilling mud (DFS No. 2).

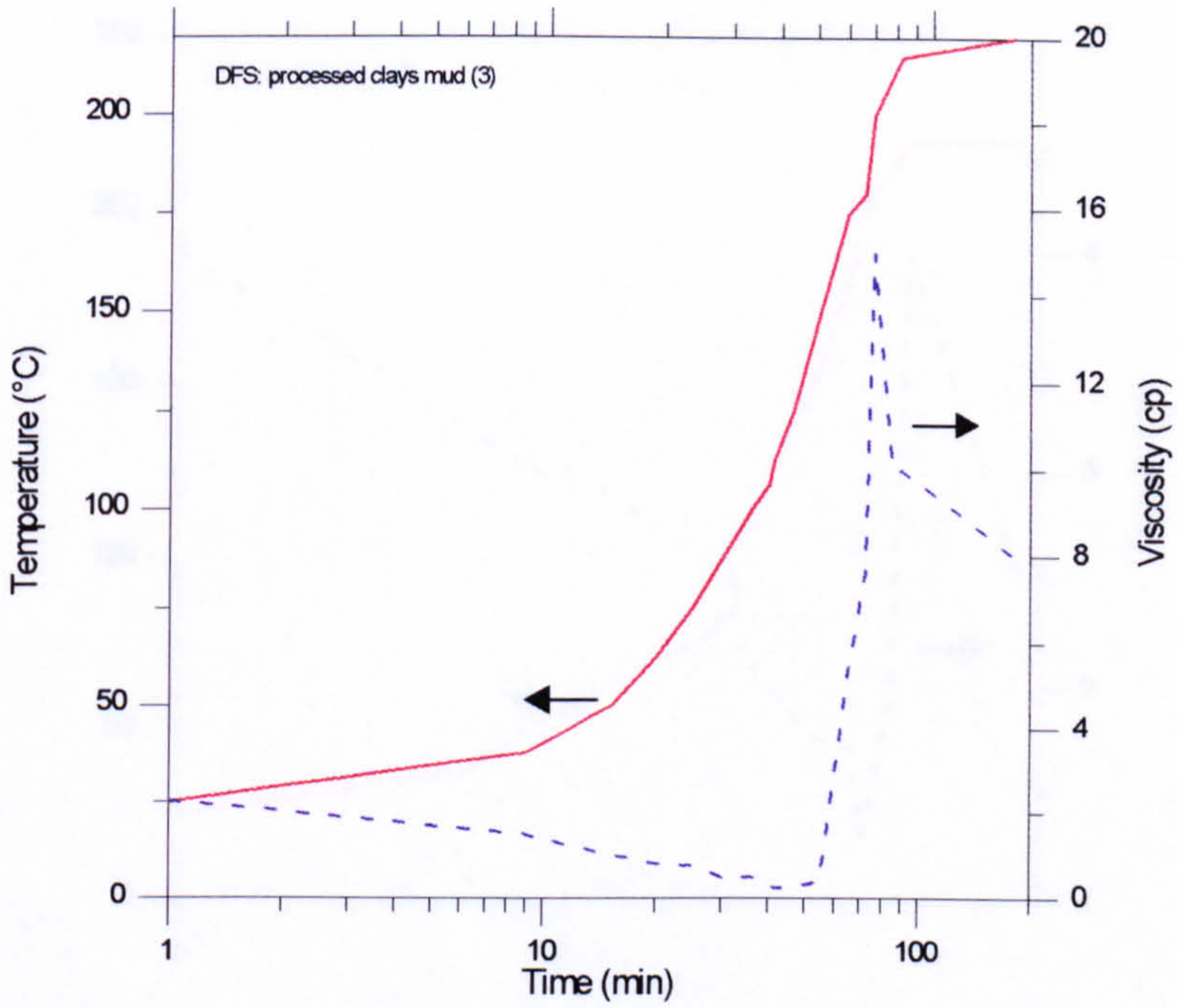

Fig. 6.6 The Fann 50C rheogram of the drilling mud (DFS No. 3).

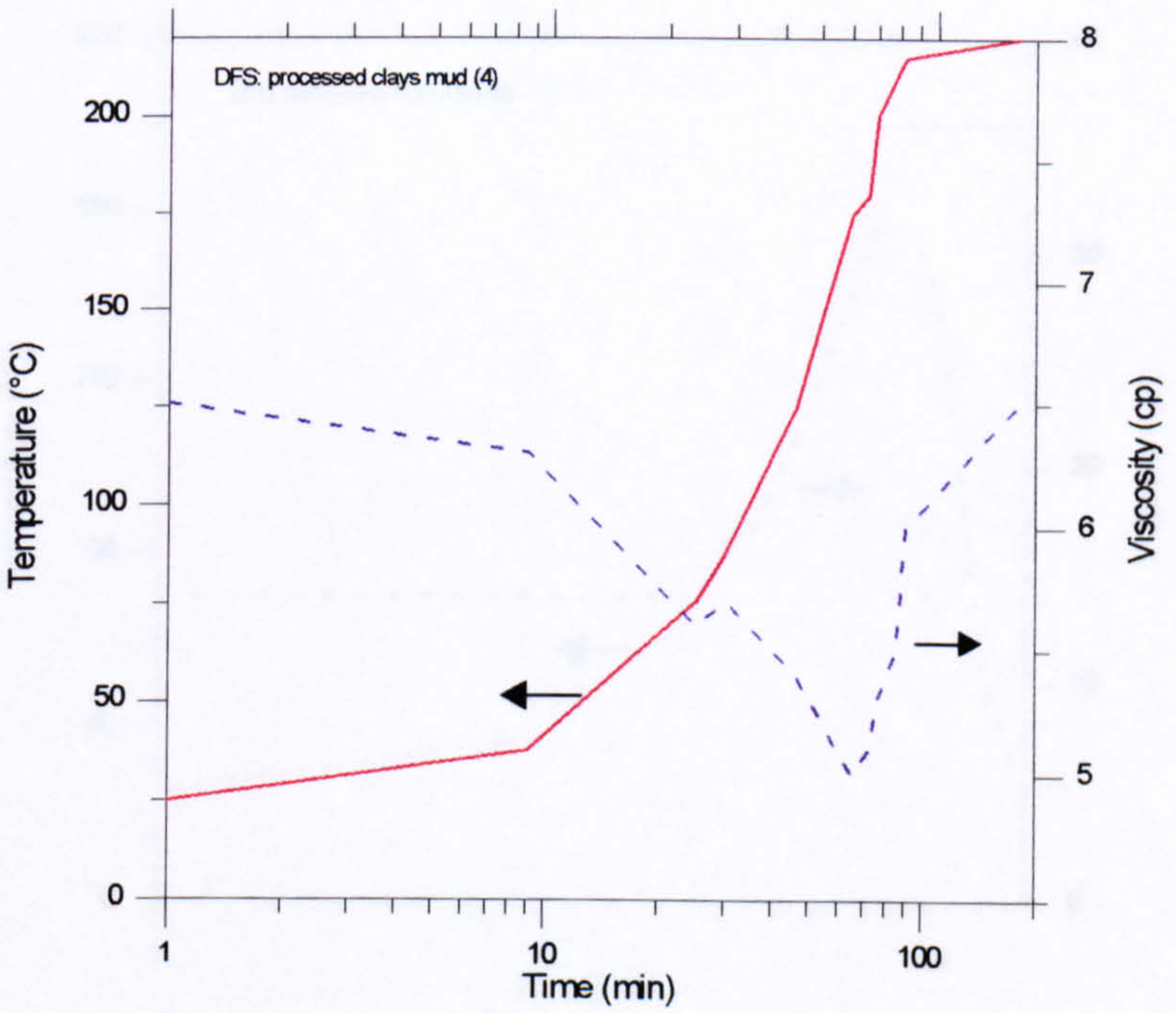

Fig. 6.7 The Fann 50C rheogram of the drilling mud (DFS No. 4).

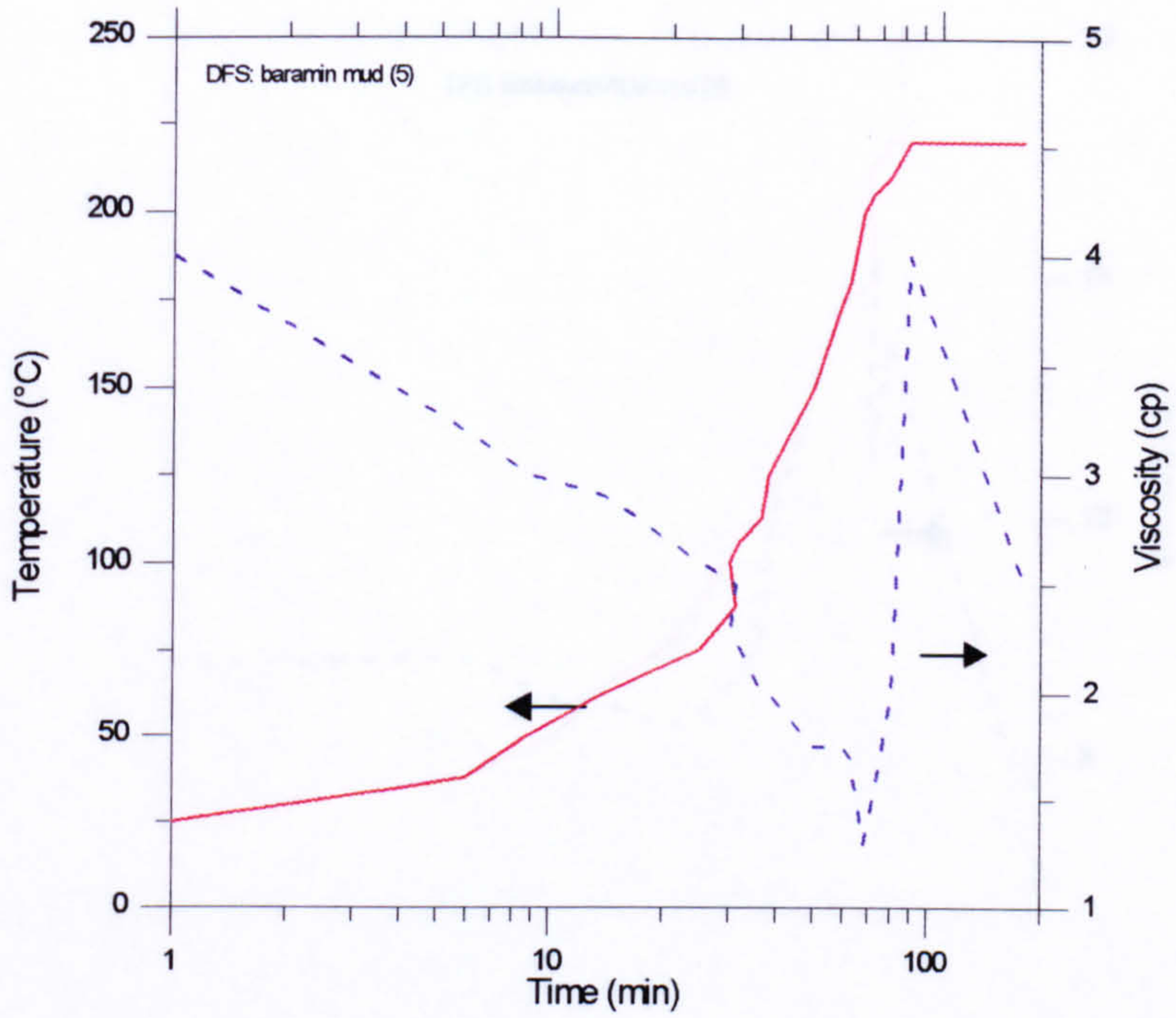

Fig. 6.8 The Fann 50C rheogram of the drilling mud (DFS No. 5).

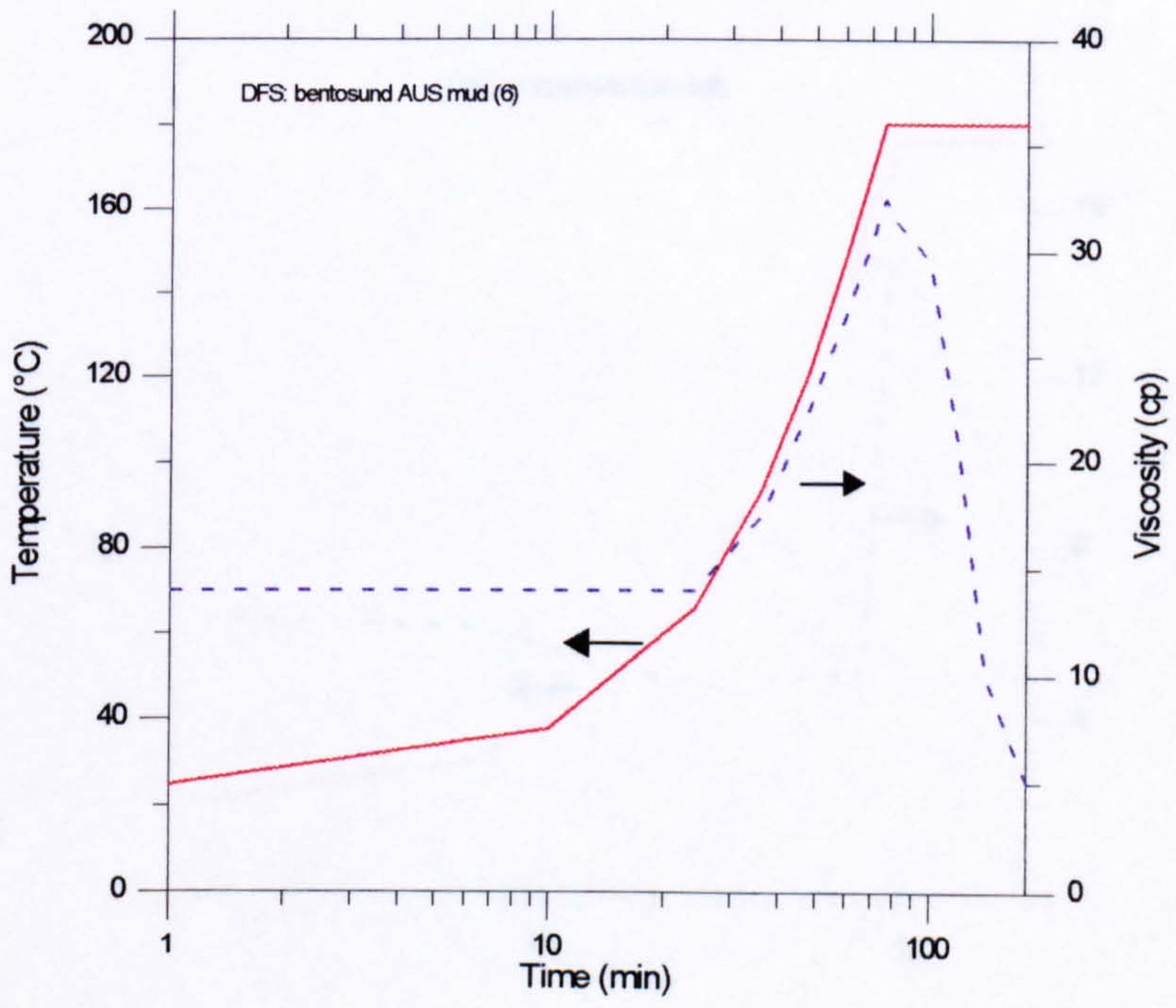

Fig. 6.9 The Fann 50C rheogram of the drilling mud (DFS No. 6).

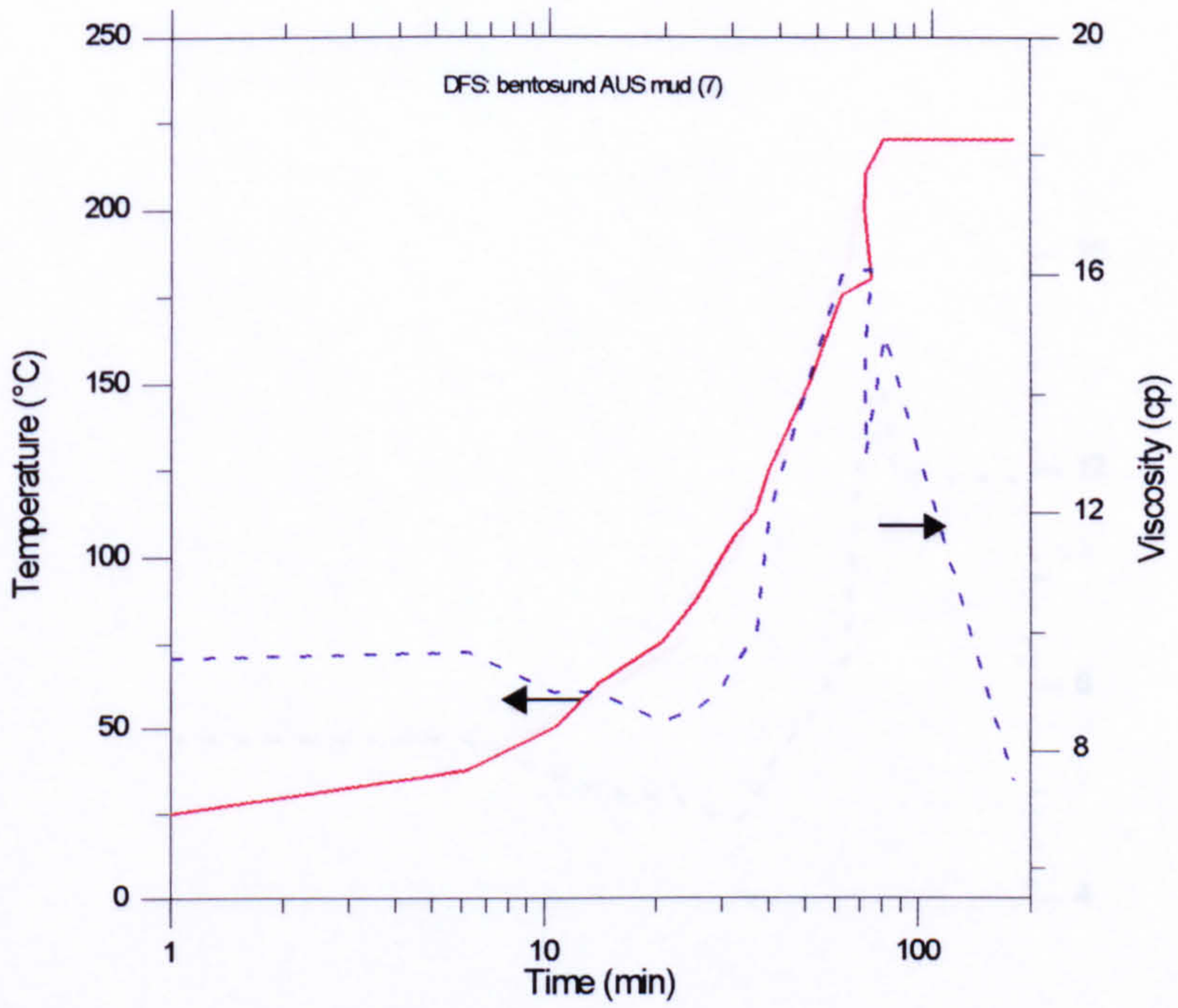

Fig. 6.10 The Fann 50C rheogram of the drilling mud (DFS No. 7).

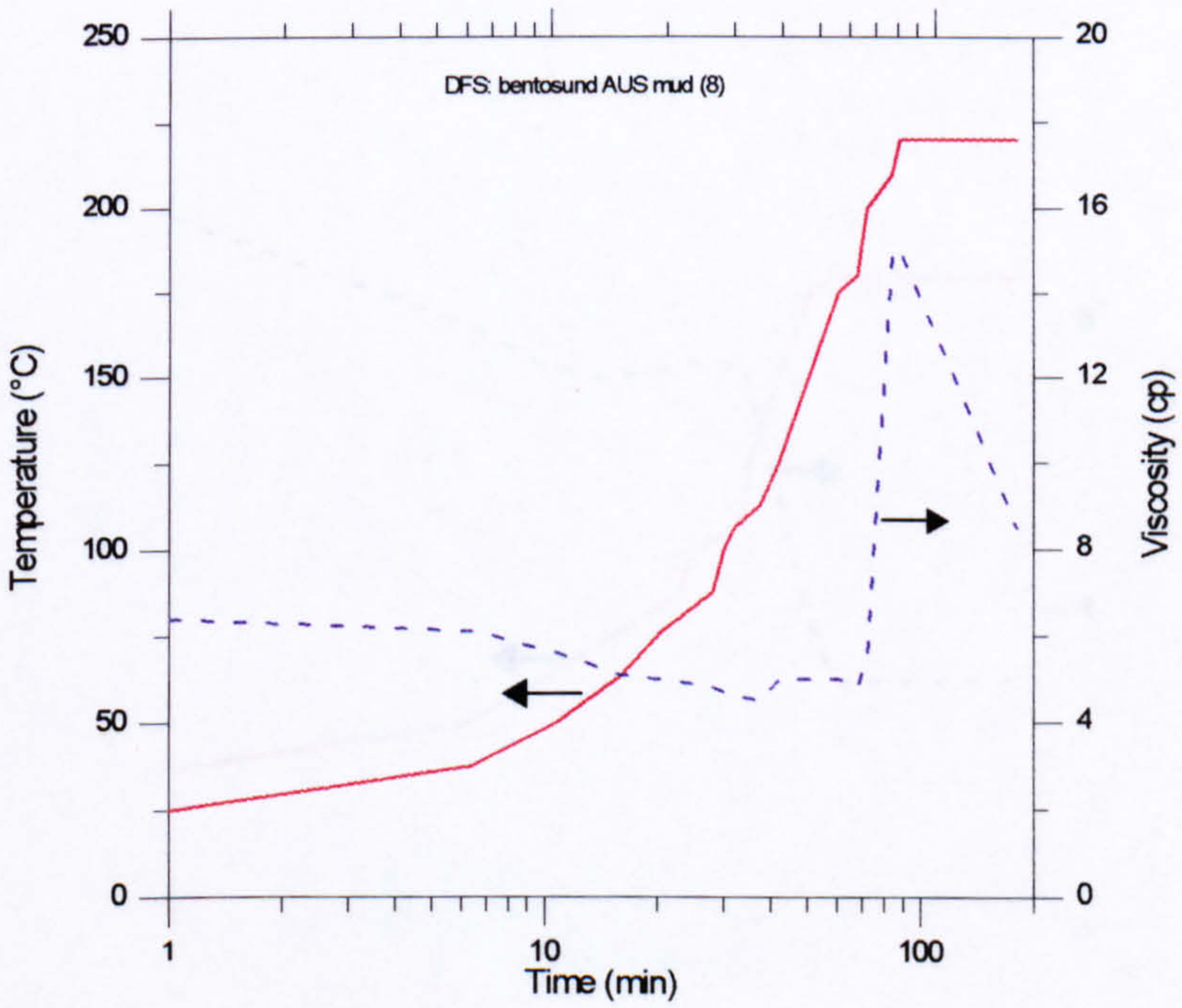

Fig. 6.11 The Fann 50C rheogram of the drilling mud (DFS No. 8).

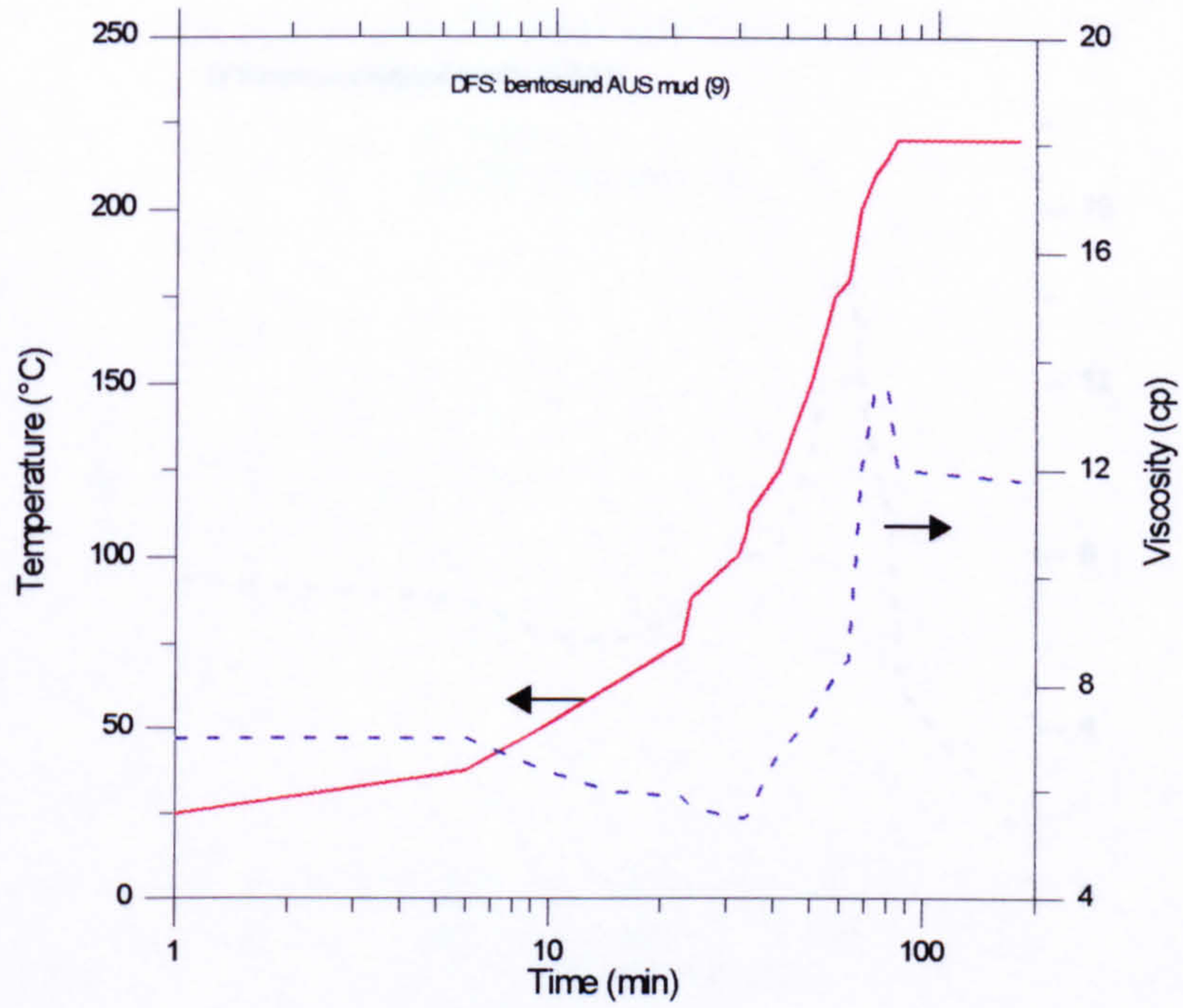

Fig. 6.12 The Fann 50C rheogram of the drilling mud (DFS No. 9).

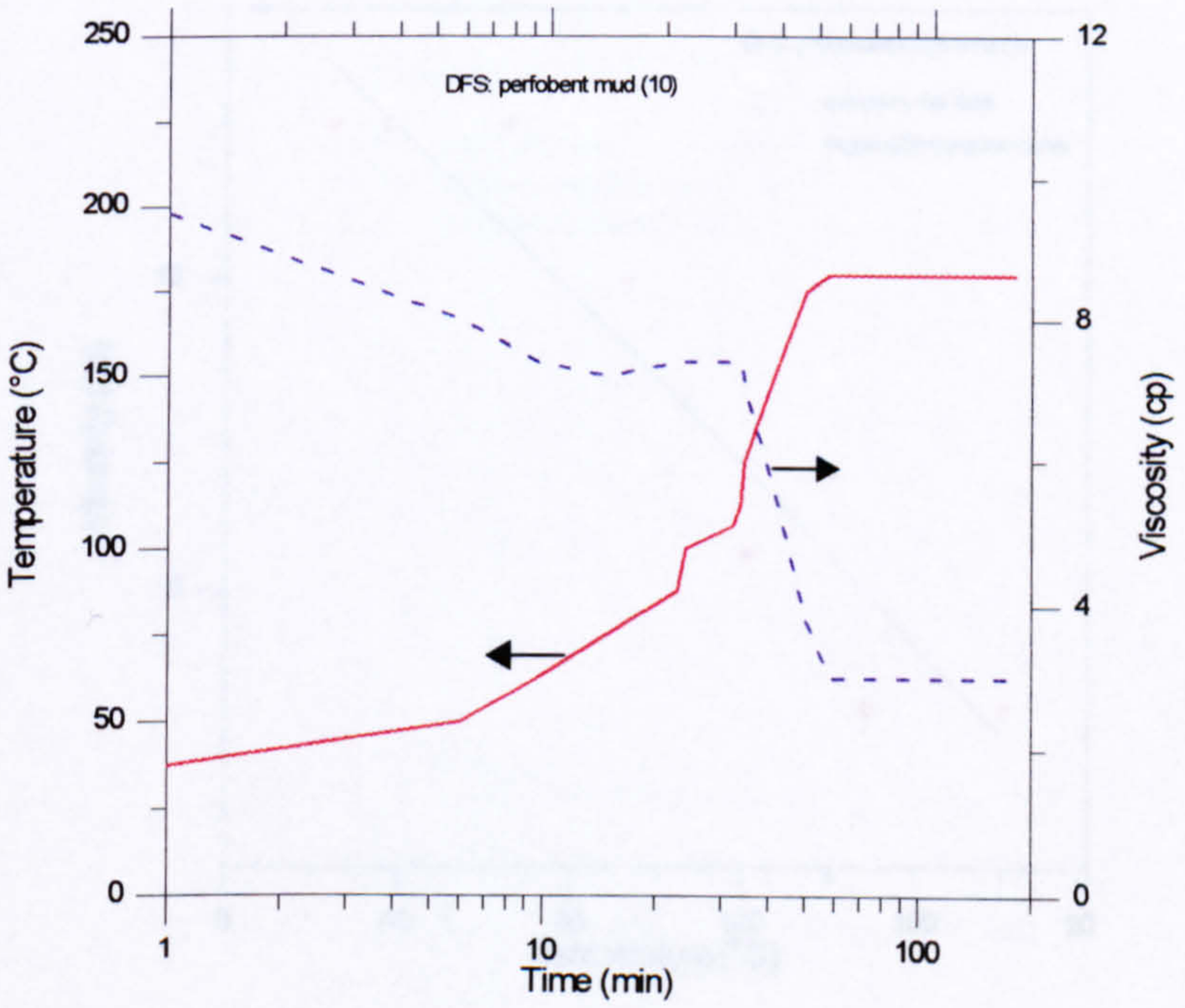

Fig. 6.13 The Fann 50C rheogram of the drilling mud (DFS No. 10).

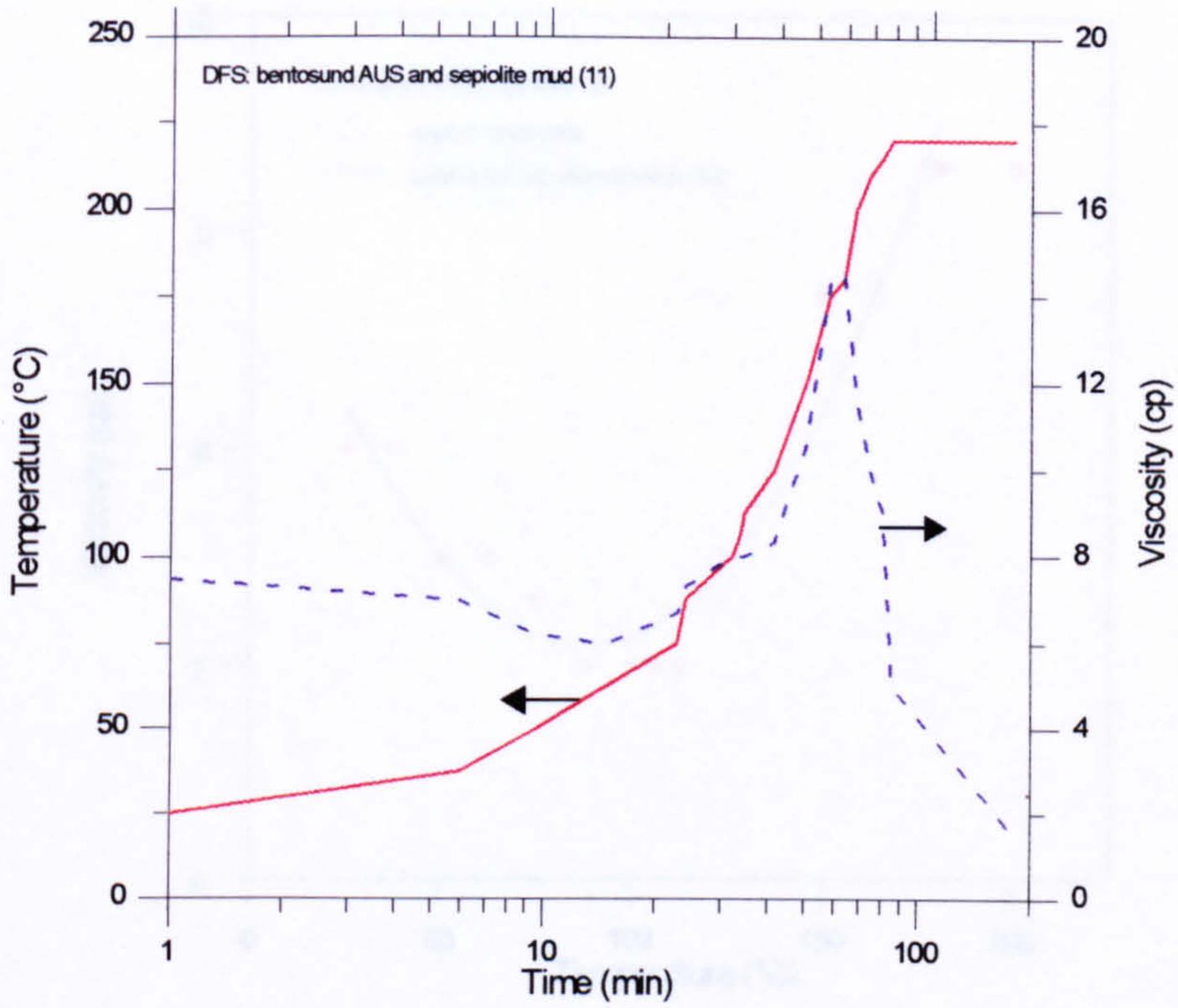

Fig. 6.14 The Fann 50C rheogram of the drilling mud (DFS No. 11).

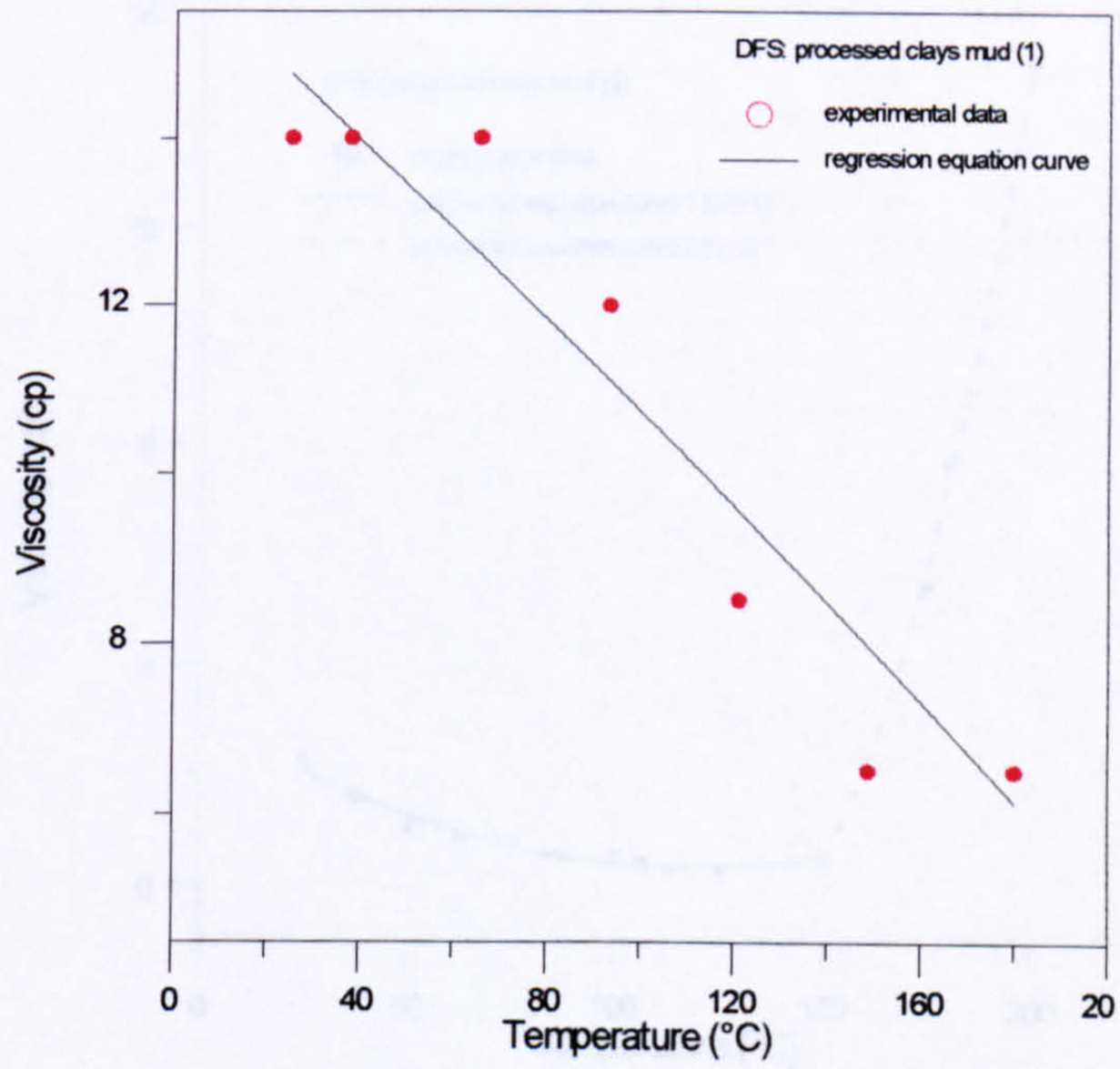

Fig. 6.15 Variation of viscosity with temperature for the drilling mud (DFS 1).

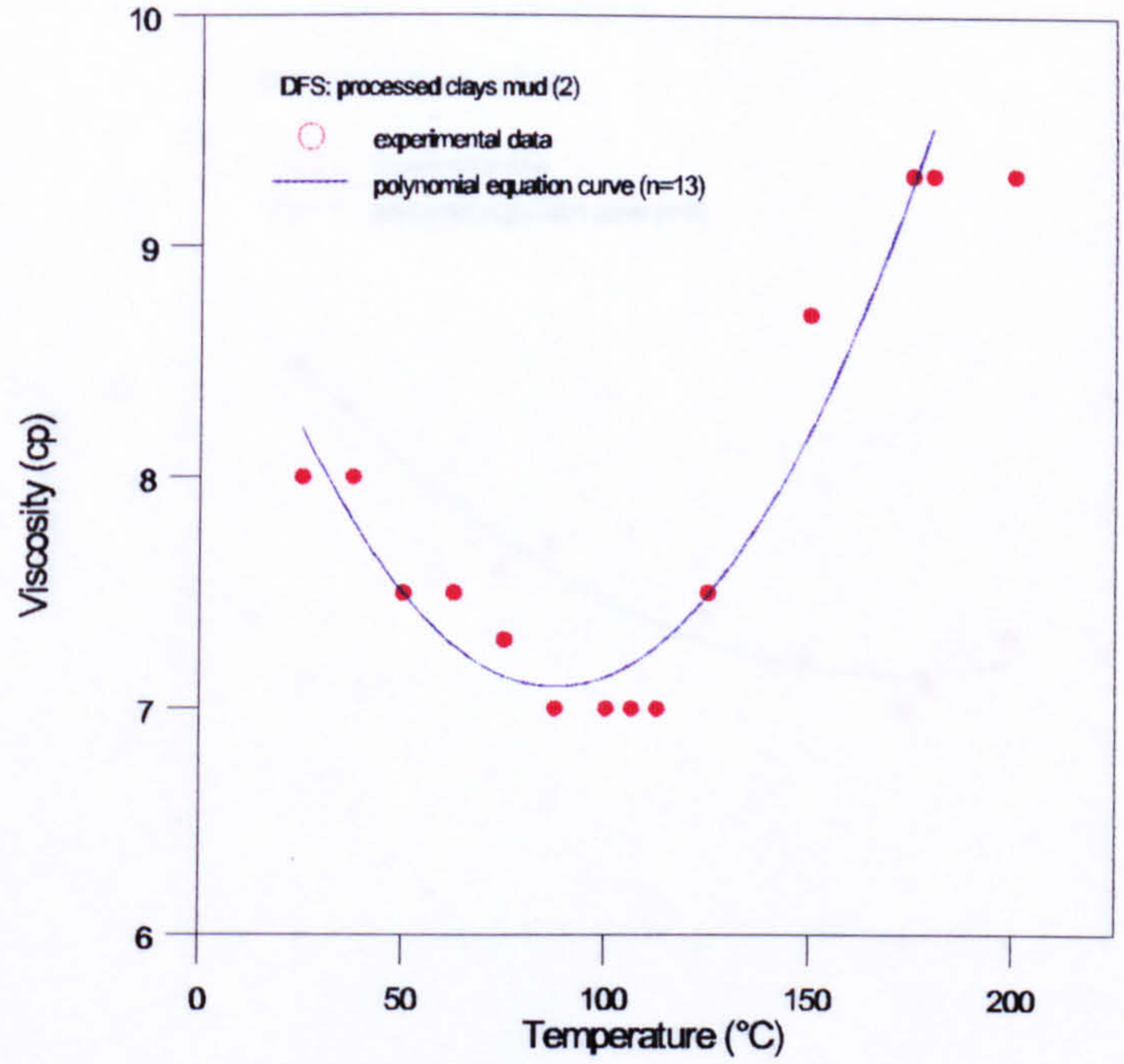

Fig. 6.16 Variation of viscosity with temperature for the drilling mud (DFS 2).

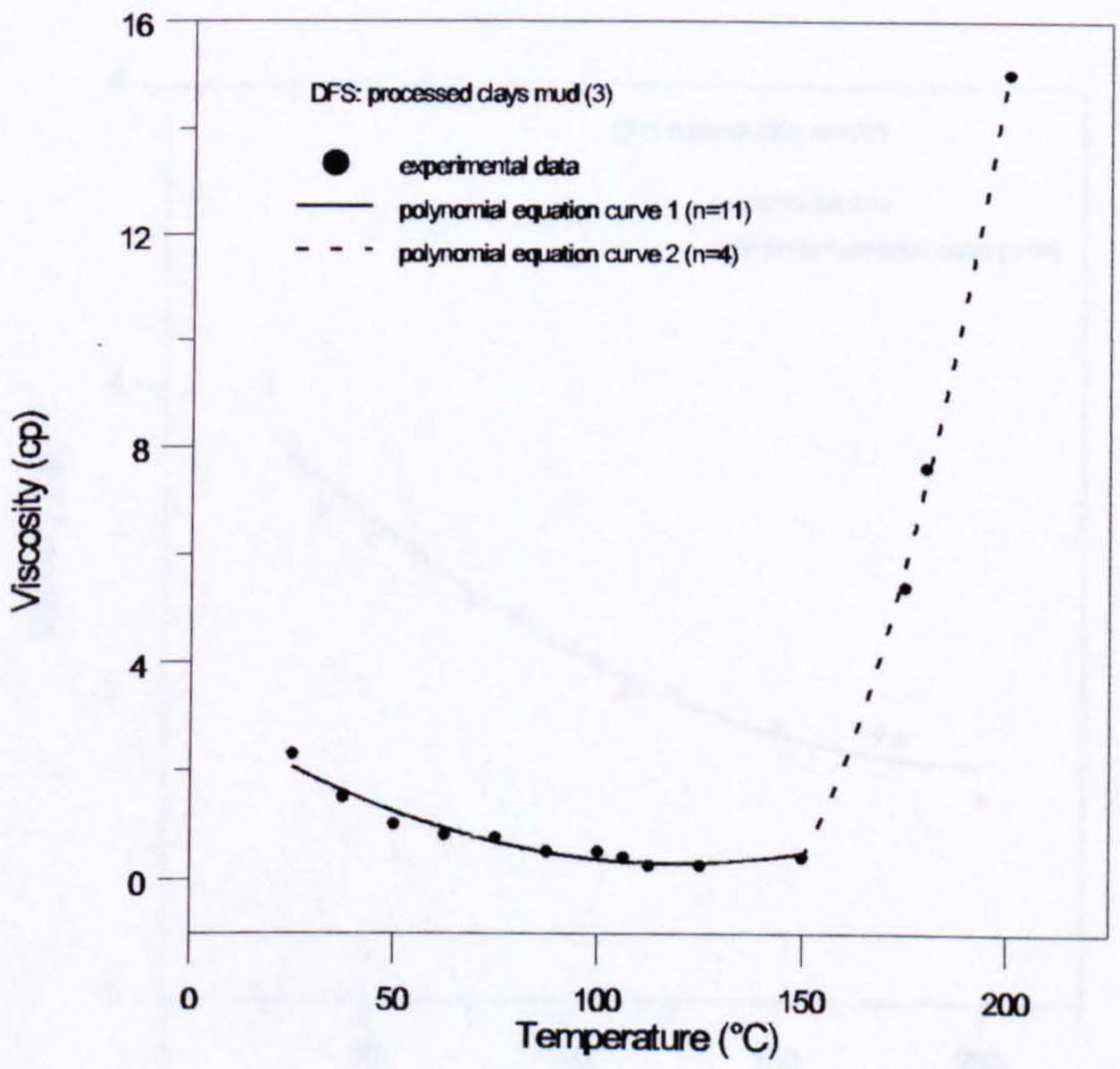

Fig. 6.17 Variation of viscosity with temperature for the drilling mud (DFS 3).

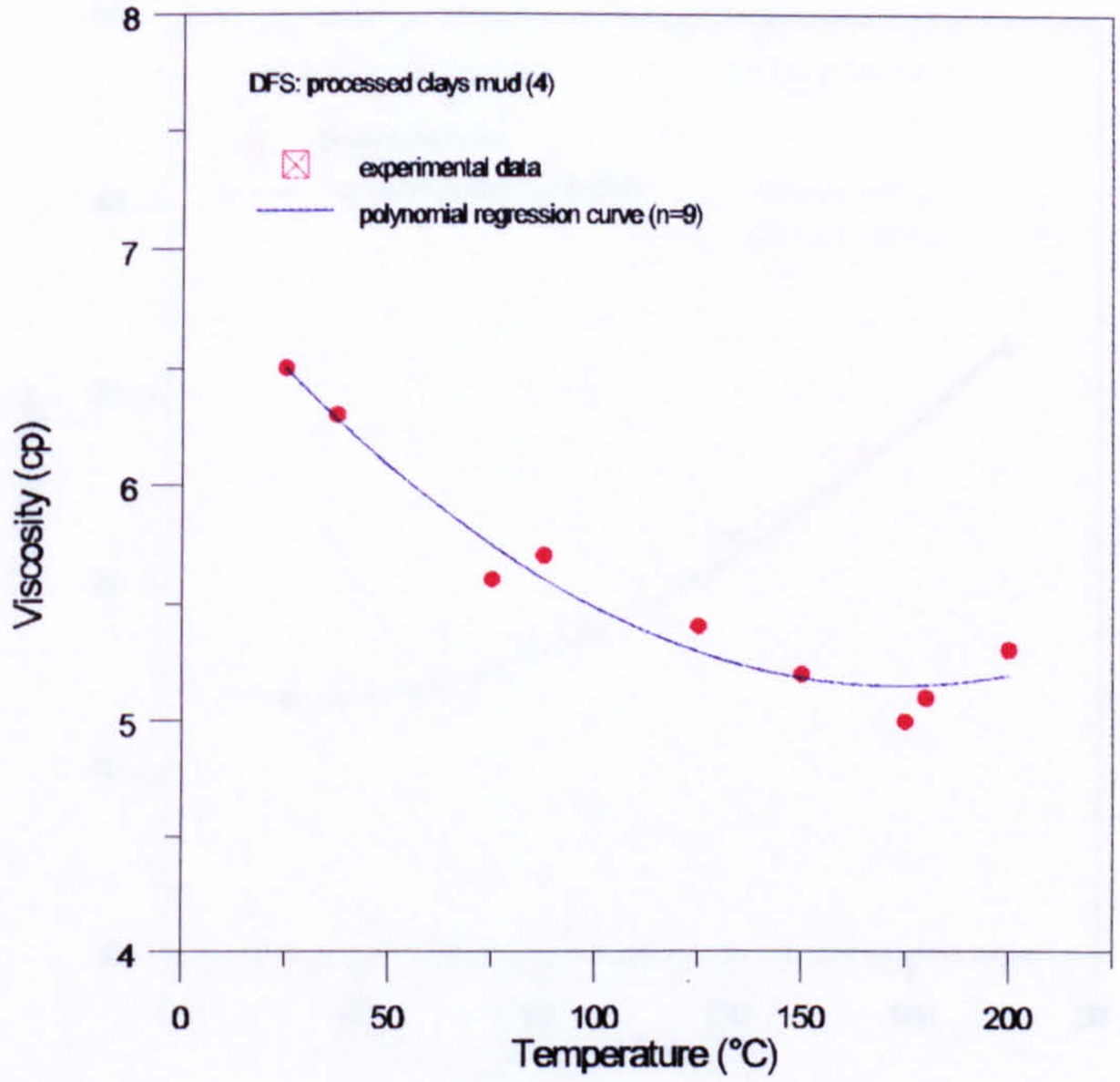

Fig. 6.18 Variation of viscosity with temperature for the drilling mud (DFS 4).

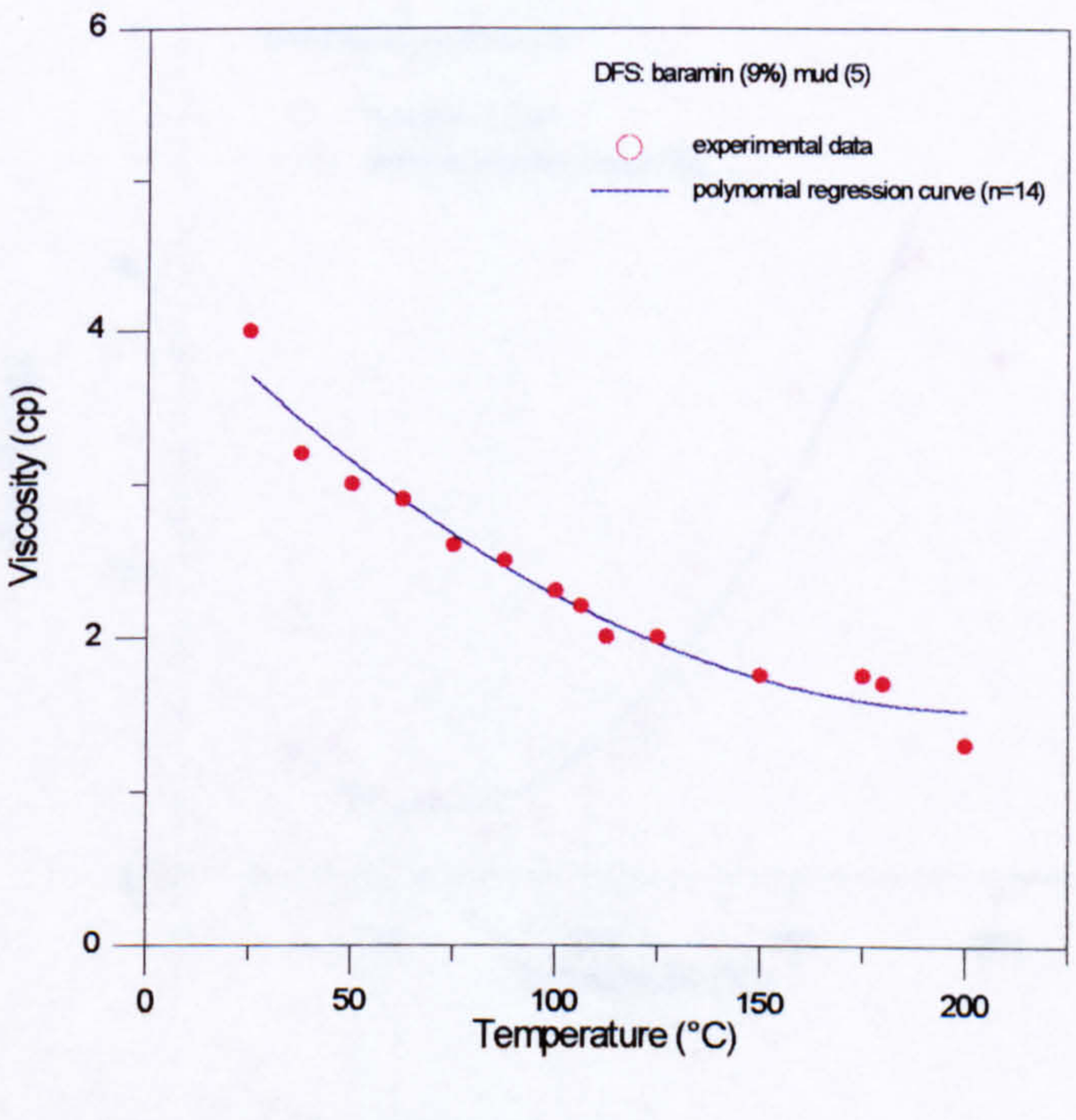

Fig. 6.19 Variation of viscosity with temperature for the drilling mud (DFS 5).

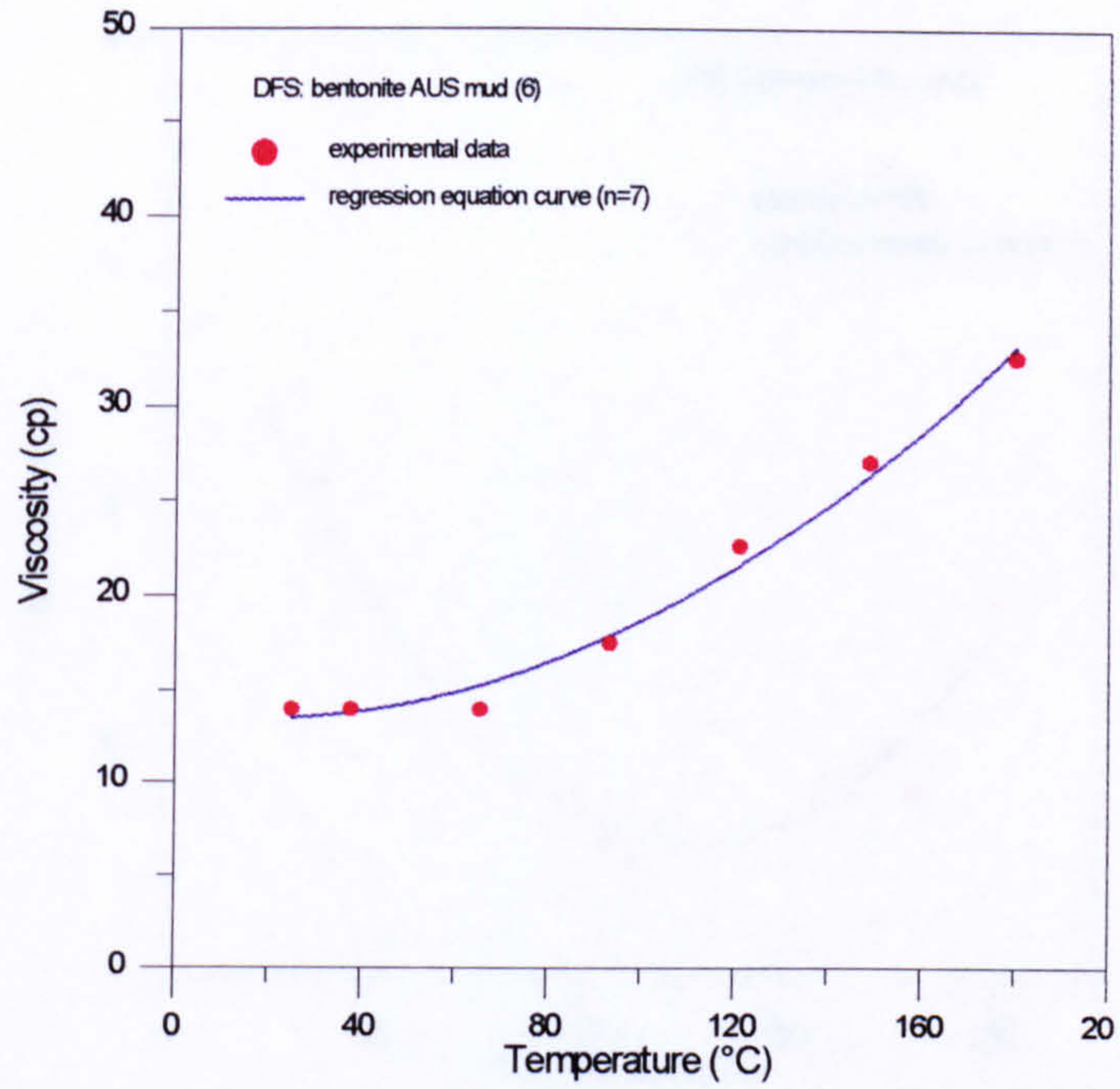

Fig. 6.20 Variation of viscosity with temperature for the drilling mud (DFS 6).

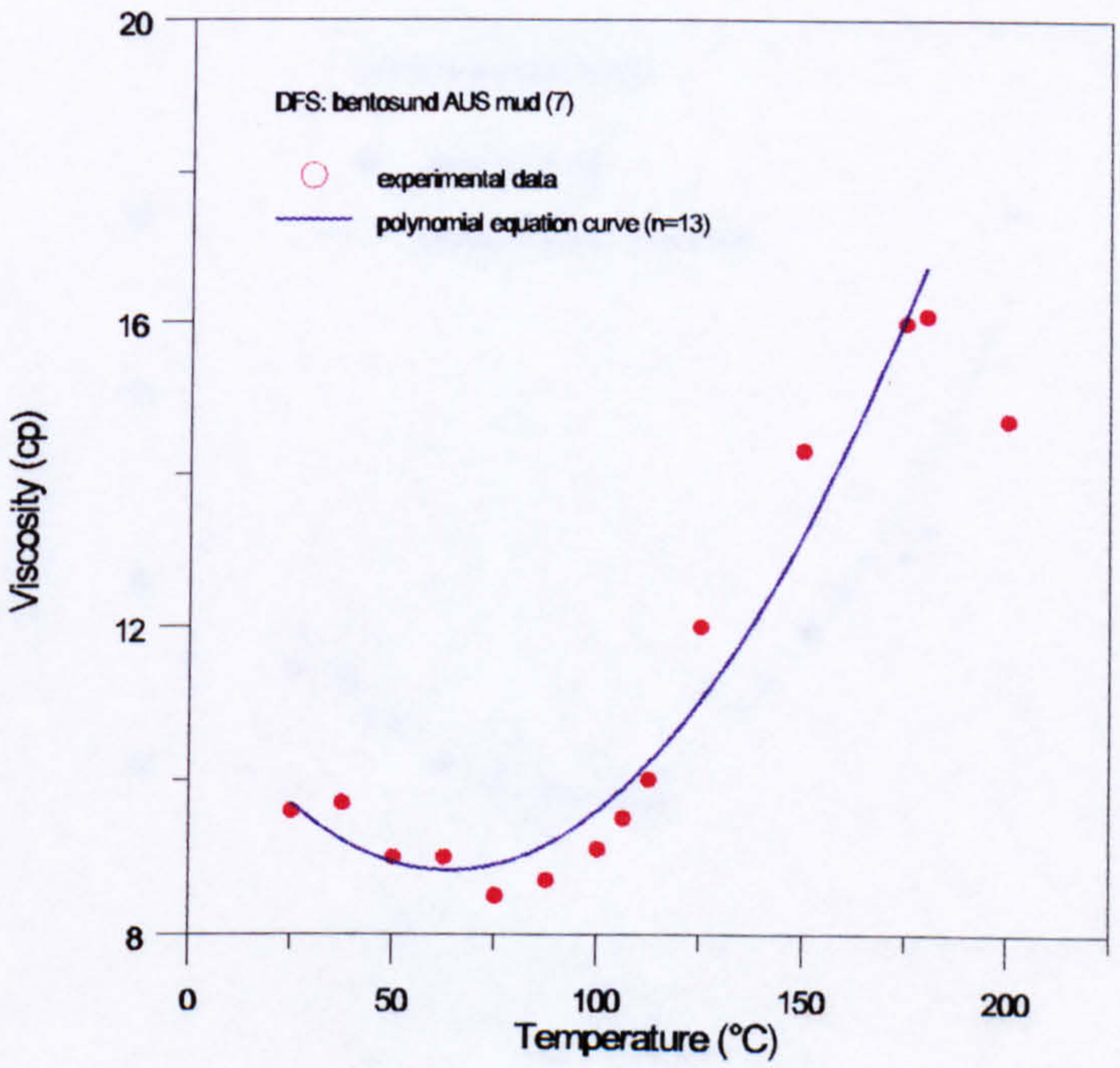

Fig. 6.21 Variation of viscosity with temperature for the drilling mud (DFS 7).

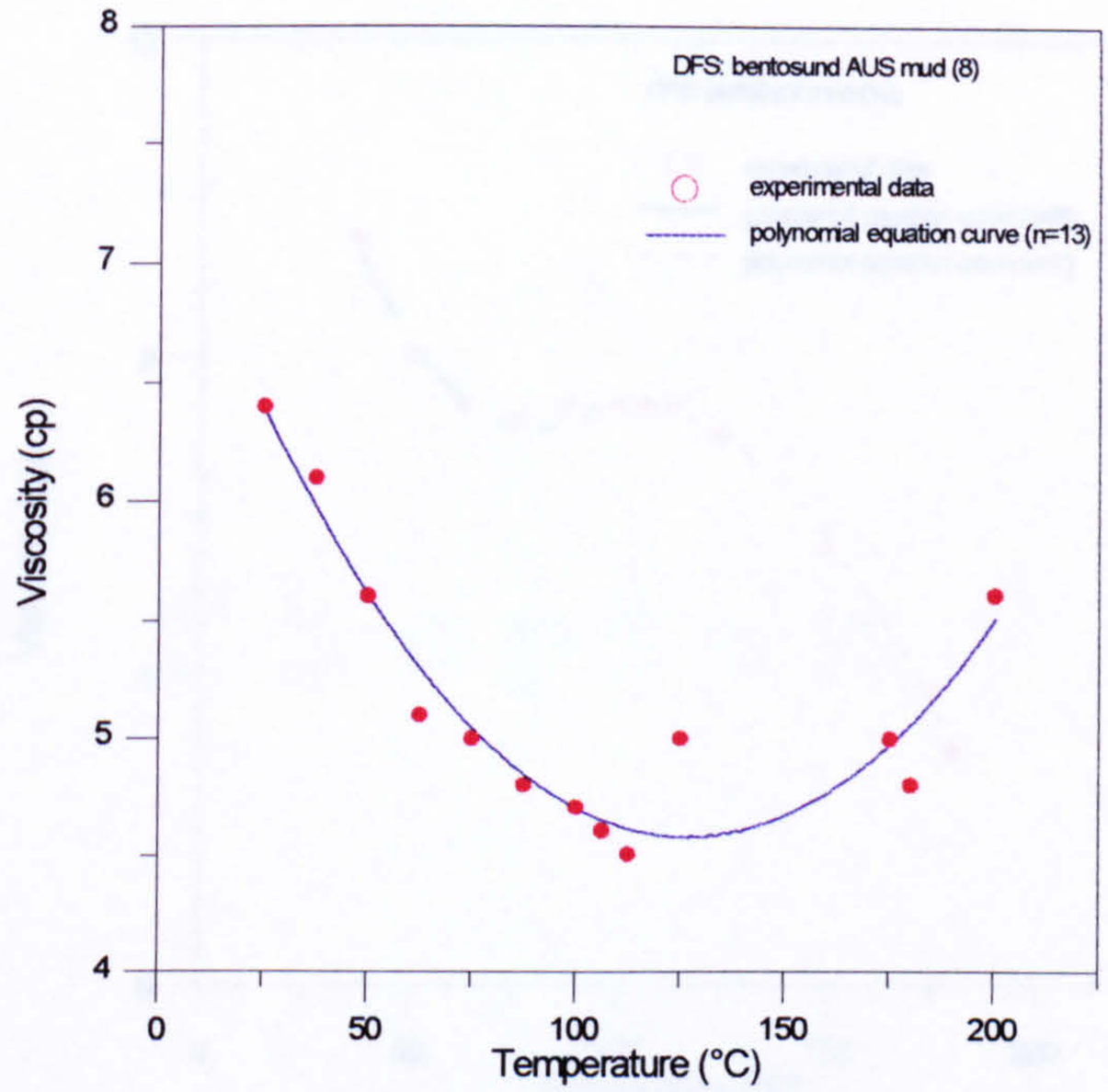

Fig. 6.22 Variation of viscosity with temperature for the drilling mud (DFS 8).

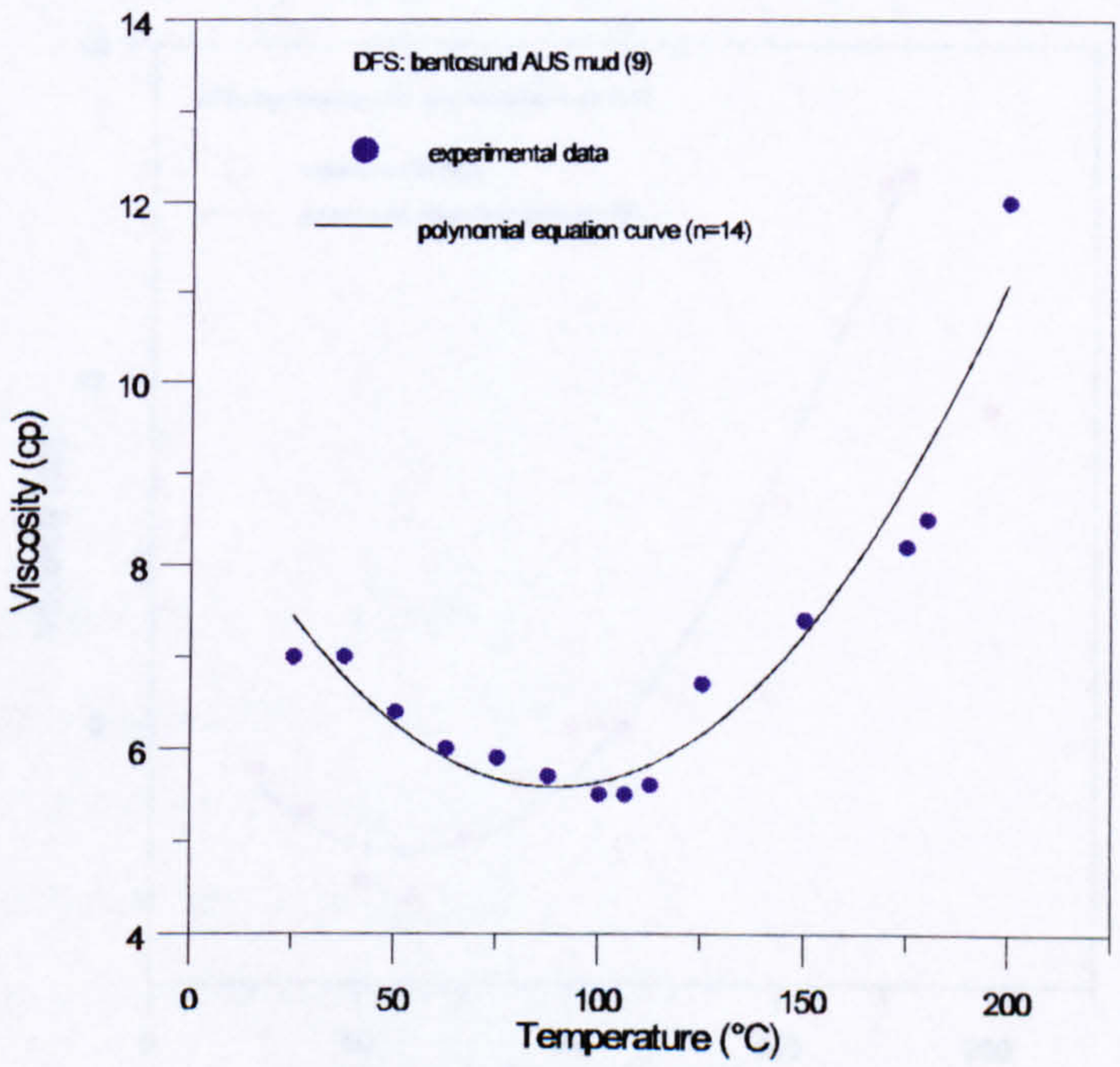

Fig. 6.23 Variation of viscosity with temperature for the drilling mud (DFS 9).

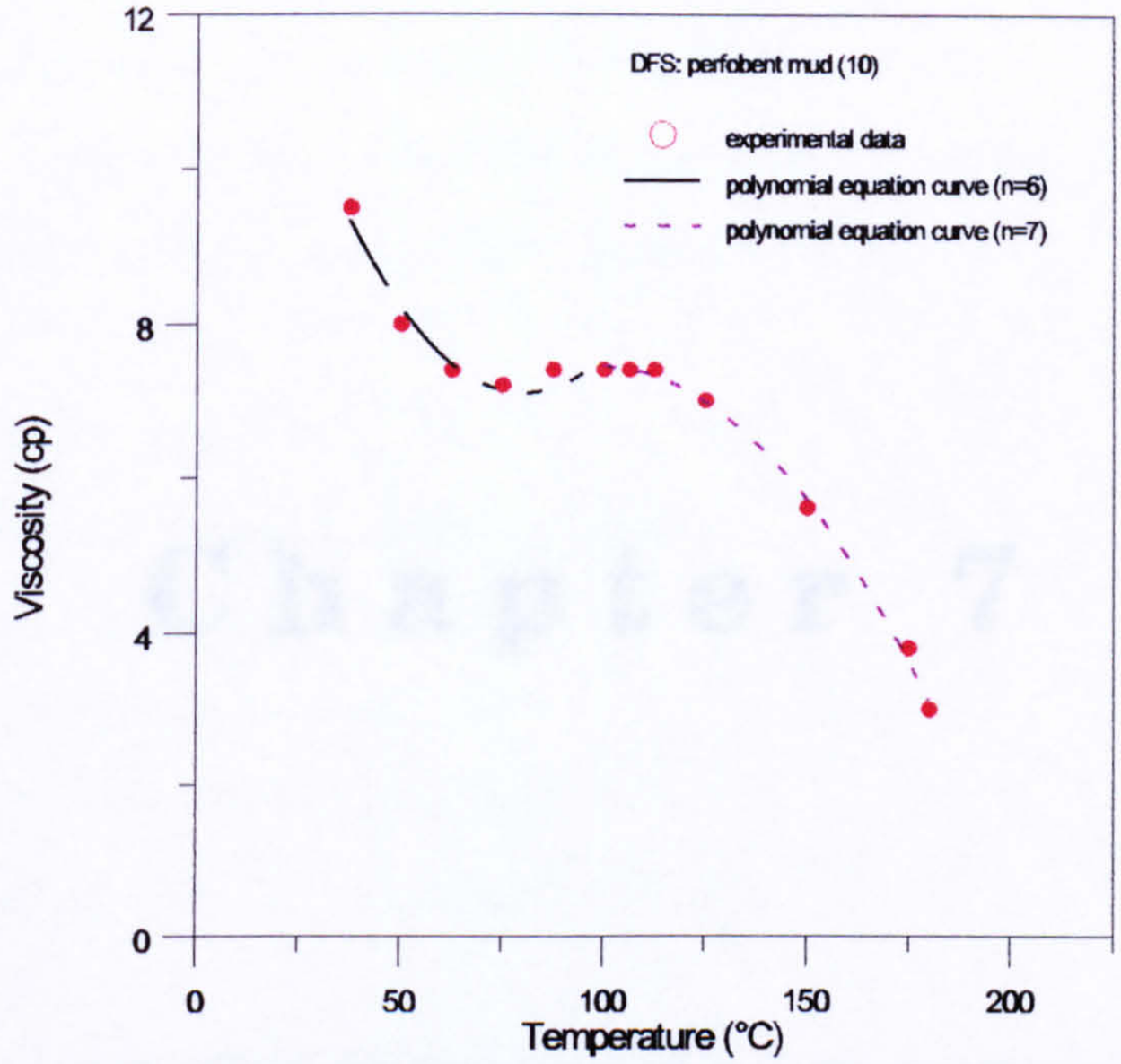

Fig. 6.24 Variation of viscosity with temperature for the drilling mud (DFS 10).

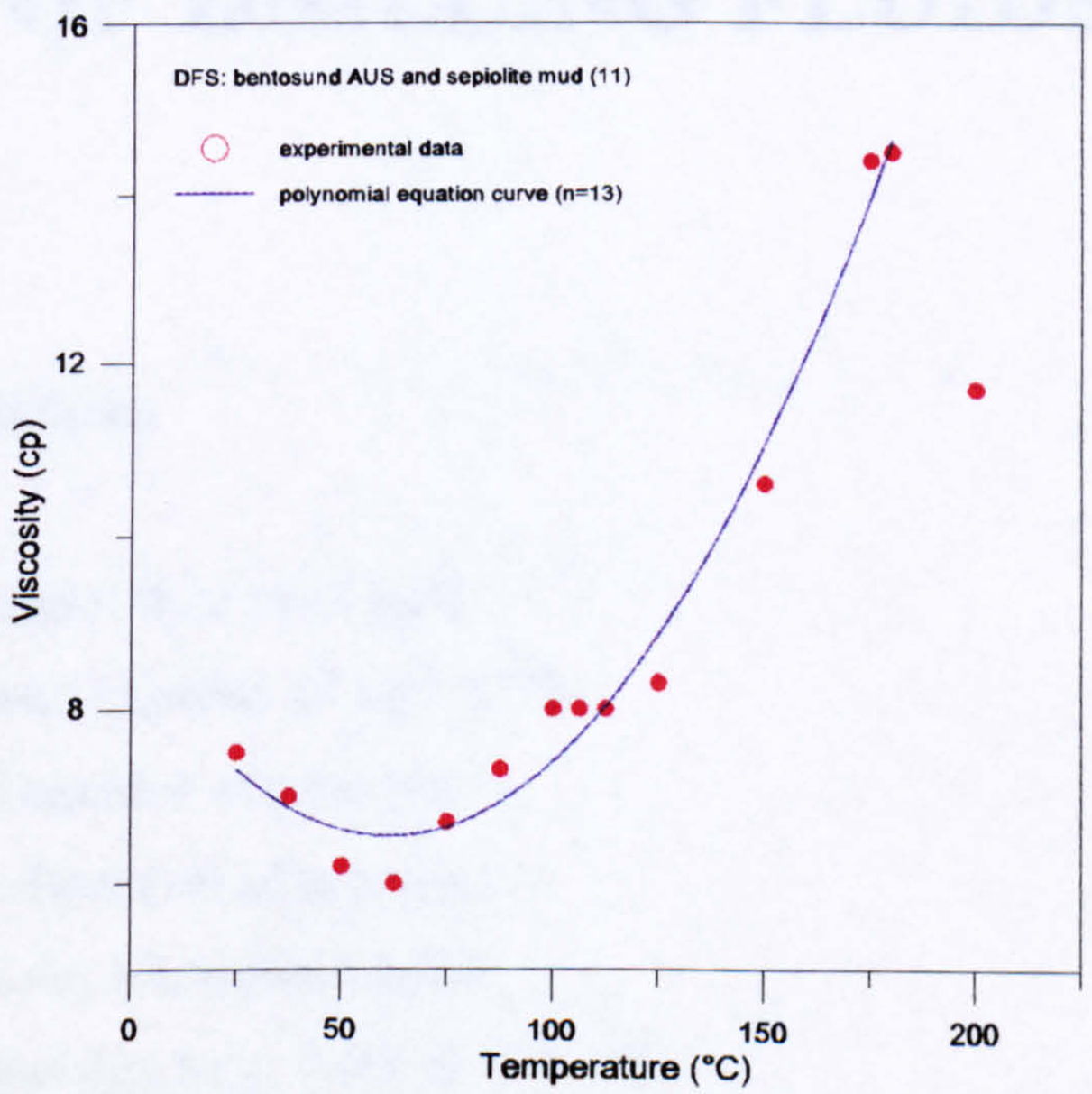

Fig. 6.25 Variation of viscosity with temperature for the drilling mud (DFS 11).

Chapter 7

ESTIMATION OF CONVECTIVE HEAT TRANSFER COEFFICIENTS OF DRILLING FLUIDS

7.1 Nomenclature

A_c cross sectional flow area [m^2]

Cp specific heat capacity [J kg^{-1} $°C^{-1}$]

D internal diameter of pipe [m]

D_h hydraulic diameter of pipe [m]

f friction factor [dimensionless]

g acceleration due to gravity [9.8 m s^{-2}]

Gr Grashof number [dimensionless]

h convective heat transfer coefficient [W m^{-2} $°C^{-1}$]

k	thermal conductivity [W m^{-1} °C^{-1}]
k_{eff}	effective thermal conductivity [W m^{-1} °C^{-1}]
k_{ha}	thermal conductivity of the fluid in the annulus at the average temperature and pressure of the annulus [W m^{-1} °C^{-1}]
L	length [m]
$\dot{m}$	mass flowrate [kg s^{-1}]
Nu	pipe Nusselt number [dimensionless]
P_w	wetted perimeter [m]
Pe	Peclet number [dimensionless]
Pr	Prandtl number [dimensionless]
q	heat transfer rate per unit length [W m^{-1}]
r	radius [m]
Re	Reynolds number [dimensionless]
St	Stanton number [dimensionless]
T	temperature [°C]
T_i	fluid temperature [°C]
T_s	surface temperature [°C]
v	linear velocity [m s^{-1}]

Greek symbols

β	volumetric coefficient of thermal expansion of the fluid in the annulus [°C^{-1}]
μ	dynamic viscosity [Pa·s] or [mPa.s]
ρ	density [kg m^{-3}]
σ	standard deviation error

Subscripts

i	annulus; inner annulus wall
o	outer annulus wall
s	surface

7.2 Introduction

This chapter presents a comprehensive review of the relevant numerical correlations for estimating the convective heat transfer coefficients (CHTC) of drilling fluids (muds). Numerical procedures to estimate the fluid CHTC for both the drill pipe and annulus regions in a geothermal well drilling system are evaluated. Several numerical correlations to calculate CHTC for fully developed laminar and turbulent flow are presented. These correlations enable the CHTC as a function of well dimensions, dimensionless flow parameters and the fluid properties (transport and thermophysical) to be estimated. Newtonian (water) and non-Newtonian drilling fluid properties were used to calculate the dimensionless flow parameters. These were then used to estimate the CHTC. Mud viscosity was identified as the main fluid property that strongly affects the estimation of the mud CHTC. A comparison between Newtonian and non-Newtonian fluid viscosities as a function of temperature was made. Difference errors of up to 99 % were found. These errors were projected into the calculation of the drilling fluid CHTC values using several of the numerical correlations proposed for the Nusselt number. A complete discussion of this numerical evaluation is presented.

7.3 Basic Concepts of the Convective Heat Transfer Coefficients

Convection in wellbore drilling fluids can significantly influence the rate of heat transfer from a well to the surrounding formation during geothermal drilling activities. To accurately model a wellbore that is being drilled, two cases of convection must typically be considered, the rate of heat transfer between the drilling fluid, pipe and annulus and the rate across a naturally convecting annulus [Willhite (1967)]. Moreover, if a lost circulation process occurs during the drilling activities, an additional convective heat transfer phenomenon must also be considered due to the drilling mud invasion to the formation [Garcia et al (1997b)].

In the first case, the heat transfer processes between a fluid and a drill pipe and between a fluid and a wall (annulus) are defined by the surface convection coefficient (h), which is a function of the fluid properties (transport and thermophysical) and the geometry of the well. In the second case, the rate of heat transfer across a naturally convecting fluid is a function of the fluid properties, well dimensions and the temperature difference across the fluid. Finally, in the lost circulation case, the rate of heat transfer between a lost fluid and the formation is defined by the surface convection coefficient, which will be a function of fluid properties and the formation geometry.

The occurrence of these types of heat transfer processes in a wellbore/formation system requires an accurate knowledge of the fluid convective heat transfer coefficients to simulate both natural and forced convection processes. Hence, heat transfer studies to estimate these coefficients as a function of transport (viscosity) and thermophysical properties (density, specific heat capacity, and thermal conductivity) are required. Based on these requirements, several studies to calculate convective heat transfer coefficients (CHTC) have been reported in the geothermal drilling literature [Raymond (1969); Keller et al. (1973); Marshall and Bentsen (1982); Wooley (1980); Arnold (1990); Bittleston (1990); Beirute (1991); and Garcia et al (1997a)]. From these studies some procedures to estimate CHTC by numerical correlations based on dimensionless flow parameters (Reynolds, Prandtl, Peclet and Nusselt) have been proposed. Unfortunately, in the majority of these numerical procedures, the dimensionless correlations have been estimated assuming that the drilling fluid behaves like a Newtonian fluid. This assumption suggested that water properties were used in the calculations of CHTC. However, in Chapter 6, it was demonstrated that this asumption is not valid for drilling fluids because they follow a non-Newtonian behaviour. As a result of these significant differences, an evaluation between Newtonian and non-Newtonian behaviour for estimating dimensionless parameters and CHTC must be carried out. This evaluation will also enable more accurate numerical correlations for determining these parameters to be selected.

7.4 Numerical Correlations to Estimate CHTC

Laboratory measurements have determined the relationship for heat transfer between a fluid and a solid surface [Incropera and DeWitt (1990)]. These CHTC measurements, either for natural or forced convection processes, are correlated in terms of the following dimensionless groups:

(i) The Nusselt number (ratio of total to conductive heat transfer rate) is defined by the equation:

$$Nu = \frac{h\,D}{k} \tag{7.1}$$

where D is the pipe equivalent diameter and k is the thermal conductivity of the fluid.

(ii) The Reynolds number (ratio of inertia to viscous forces) is defined by the equation:

$$Re = \frac{\rho\,v\,D}{\mu} \tag{7.2}$$

where ρ is the density, v is the linear velocity and μ is the dynamic viscosity of the fluid.

(iii) The Prandtl number provides a measure of the relative effectiveness of momentum and energy transport by diffusion in the velocity and thermal boundary layers, respectively. This dimensionless number is given by the equation:

$$Pr = \frac{\mu\,Cp}{k} \tag{7.3}$$

where Cp is the specific heat capacity and k is the thermal conductivity.

(iv) The Peclet number is calculated by the following equation:

$$Pe = Re \cdot Pr \tag{7.4}$$

(v) The Grashof number (Gr) provides a measure of the ratio of the buoyancy forces to the viscous forces in the velocity boundary layer. This dimensionless parameter is normally applied when a natural convection process needs to be modelled and can be calculated by the following equation:

$$Gr = \frac{g \beta \rho^2 L^3 \Delta T}{\mu^2} \tag{7.5}$$

where β is the volumetric coefficient of thermal expansion; g the acceleration of gravity; L the characteristic length and ΔT the temperature difference across the surface.

(vi) The Stanton number (St) is a modified version of the Nusselt number [Lakshminarayanan et al. (1976)] given by the equation:

$$St = \frac{Nu}{Pe} \tag{7.6}$$

(vii) The friction factor (f) is a dimensionless pressure drop for internal flow. The value of this factor depends on the flow regime that predominates in the flow system. For laminar flow (Re<2000) in tubes and pipes, the friction factor may be calculated by the following equation:

$$f = \frac{64}{Re} \tag{7.7}$$

For fully turbulent flow (Re>350,000), the factor is assumed to be constant and equivalent to 0.013. However, in the transition region the definitions are more complex. Two approximations have been used to estimate the transition region:

$$f = \frac{64 + 0.007735(Re - 2000)}{2000} \tag{7.8}$$

for 2000<Re<4000, and

$$f = \frac{0.316}{Re^{0.25}} \tag{7.9}$$

Once the appropiate dimensionless groupings have been specified, accurate numerical correlations to predict the Nusselt numbers in geothermal wells need to be selected. This selection must be done separately for drill pipe and annulus geometry, considering the flow regime and the convection processes that occur in these regions during well drilling activities.

7.4.1 Forced convection correlations for drill circular pipes under laminar flow conditions

The convection heat transfer problem in a circular pipe for laminar flow was treated by Incropera and DeWitt (1990). This theoretical study shows that in a circular pipe characterized by uniform surface heat flux and laminar, fully developed conditions, the Nusselt number is a constant (Nu=4.36), independent of the Re, Pr and axial position. This value can be used to determine the drilling fluid convection coefficients in drill pipes under laminar flow conditions (Re<2000).

7.4.2 Forced convection correlations for drill circular pipes under turbulent flow conditions

A classical numerical correlation for computing the local Nusselt number for fully developed (hydrodynamically and thermally) turbulent flow in a smooth circular pipe is due to Colburn (1933). This correlation was obtained from the Chilton and Colburn analogy by the following equation:

$$\frac{f}{8} = St \cdot Pr^{2/3} = \frac{Nu}{Re \cdot Pr} Pr^{2/3} \tag{7.10}$$

where the friction factor for Re>20,000 is given by the equation:

$$f = 0.184\ Re^{-1/5} \tag{7.11}$$

By substitution of the friction factor value, the Colburn equation changes to:

$$Nu = 0.023\ Re^{4/5}\ Pr^{1/3} \tag{7.12}$$

From this equation, a modified version was obtained by Dittus and Boelter (1930). This numerical correlation is a slightly different and preferred version of the above result and is of the form:

$$Nu = 0.023\ Re^{4/5}\ Pr^{n} \tag{7.13}$$

where n=0.4 for heating ($T_s > T_m$) and 0.3 for cooling ($T_s < T_m$). In this case T_s is the temperature at the surface and T_m is the mean temperature of the bulk fluid. These equations have been confirmed experimentally for the range of the following conditions:

$$\begin{bmatrix} 0.7 \le Pr \le 160 \\ Re \ge 10{,}000 \\ \frac{L}{D} \ge 10 \end{bmatrix} \tag{7.13a}$$

The above equations should be used only for small to moderate temperature differences ($T_s - T_m$) with all the properties evaluated at T_m. For flows characterised by large property variations, the following equation, due to Seider and Tate (1936) is recommended.

$$Nu = 0.027\,Re^{4/5}\ Pr^{1/3}\left(\frac{\mu}{\mu_s}\right)^{0.14} \tag{7.14}$$

for:

$$\begin{bmatrix} 0.7 \le Pr \le 16{,}700 \\ Re \ge 10{,}000 \\ \frac{L}{D} \ge 10 \end{bmatrix} \tag{7.14a}$$

where all the properties except μ_s are evaluated at T_m. For a good approximation, the foregoing correlations may be applied for both a constant surface temperature and heat flux conditions.

Although equations (7.13) and (7.14) are easily applied when they are used in the context of the temperature distributions in geothermal wells during drilling activities, errors as large as 25% may result [Bhatti and Shah (1987)]. Such errors may be reduced to less than 10% through the use of more recent, but generally more complex, correlations [Incropera and DeWitt (1990)].

One correlation, which was used succesfully by Marshall and Bentsen (1982) is attributed to Lakshminarayanan et al. (1976).This equation is given by:

$$St = 0.0710\ Re^{-0.33}\ Pr^{-0.67} \tag{7.15}$$

Another correlation, which is widely used and is attributed to Petukhov, Kirillov and Popov [Petukhov (1970)] is of the form:

$$Nu = \frac{(f/8)\,Re \cdot Pr}{1.07 + 12.7\,(f/8)^{1/2}(Pr^{2/3} - 1)} \tag{7.16}$$

where the friction factor may be obtained from the Moody diagram [(see friction factor charts on pages 349-350 in the book by Holland and Bragg (1995)] or, for smooth tubes, from the following expression:

$$f=(1.82\ \log_{10} Re - 1.64)^{-2} \tag{7.17}$$

The correlation is valid for $0.5<Pr<2000$ and $10^4<Re<5x10^6$.

To obtain agreement with data for smaller Reynolds numbers, Gnielinski in 1976 modified the correlation and proposed an expression of the form [Incropera and DeWitt (1990)]:

$$Nu = \frac{(f/8)\,(Re - 1000)\,Pr}{1 + 12.7\,(f/8)^{1/2}(Pr^{2/3} - 1)} \tag{7.18}$$

where, for smooth tubes, the friction factor is given by the following equation:

$$f=(0.79 \ln Re - 1.64)^{-2} \tag{7.19}$$

This correlation is valid for $0.5<Pr<2000$ and $2300<Re<5x10^6$. When using these correlations, several considerations must be taken into account. Unless specifically developed for the transition region ($2300<Re<10^4$), caution should be considered when applying a turbulent flow correlation for $Re<10^4$. If the correlation was developed for fully turbulent conditions ($Re>10^4$), it may be used as a first approximation at smaller Reynolds numbers, with the understanding that the convection coefficient will be overpredicted. If a high level of accuracy is desired, the Gnielinski correlation, equation (7.18) could be used.

7.4.3 Forced convection correlations for a concentric tube annulus under laminar flow conditions

Many internal flow problems involve heat transfer in a concentric tube annulus. Fluid passes through the annulus formed by the concentric tubes, and convection heat transfer may occur to or from both the inner and outer tube surfaces. In this case, convection coefficients are separately associated with the inner and outer surfaces. Consequently, the corresponding Nusselt numbers would be given by the equations:

$$Nu_i \equiv \frac{h_i D_h}{k} \tag{7.20}$$

$$Nu_o \equiv \frac{h_o D_h}{k} \tag{7.21}$$

where, the hydraulic diameter (D_h) is given by the equation:

$$D_h = \frac{4A_c}{P_w} \tag{7.22}$$

where A_c and P_w are the cross sectional flow area and the wetted perimeter, respectively. A modified version of this equation can be obtained in terms of the inner and outer diameters. This equation is given by the following expression:

$$D_h = \frac{4(\pi/4)(D_o^2 - D_i^2)}{\pi D_o + \pi D_i} = D_o - D_i \qquad (7.23)$$

For the case of fully developed laminar flow with one surface insulated and the other surface at a constant temperature, Nu_i or Nu_o may be obtained from the experimental data published by Kays and Perkins (1972); Table 7.1. If uniform heat flux conditions exist at both surfaces, the Nusselt numbers may be computed from other experimental data published by the same researchers (Table 7.2). In addition to these data tables, the Nusselt numbers for fully developed laminar flow conditions can be estimated by means of a modified version derived from the numerical correlation proposed by Seider and Tate (1936):

$$Nu = 1.86\left(\frac{Re \cdot Pr}{L/D}\right)^{1/3}\left(\frac{\mu}{\mu_s}\right)^{0.14} \qquad (7.24)$$

This equation has been confirmed experimentally for the range of the following conditions:

$$\begin{bmatrix} T_s = \text{constant} \\ 0.48 < Pr < 16{,}700 \\ 0.0044 < \left(\frac{\mu}{\mu_s}\right) < 9.75 \end{bmatrix} \qquad (7.24a)$$

7.4.4 Forced convection correlations for a concentric tube annulus under turbulent flow conditions

For fully developed turbulent flow, the coefficients are a function of the Reynolds and Prandtl numbers. However, to a first approximation the inner and outer convection coefficients may be assumed to be equal, and they may be evaluated by using the hydraulic diameter equation (7.23) with the Dittus and Boelter equation (7.14) [Kays and Perkins (1972)].

7.4.5 Natural or free convection correlations for a concentric tube annulus

Literature concerning natural convection coefficients indicates the difficulty of their evaluation. Although natural convection has been studied between enclosed vertical plates, little work has been done using vertical concentric cylinders. The results of vertical plate studies can be used for estimating CHTC, between vertical concentric cylinders if the effect of curvature is neglected. Natural convection in a fluid filled annulus increases the rate at which heat is transferred across the annular region. The rate of heat flow during natural convection is a function of well dimensions, fluid properties and temperature difference across the annulus. Laboratory measurements have determined the rate of heat flow and expressed the results in terms of an effective thermal conductivity [Willhite (1967)]. If heat is transferred by conduction through the annulus, a material with the same effective thermal conductivity would transfer heat at the same rate as the convecting fluid. A correlation of experimental data for concentric vertical pipes provides an estimate of the effective thermal conductivity [Dropkin and Sommerscales (1965)].

$$k_{eff} = 0.049\, k_{ha} (Gr \cdot Pr)^{0.333} Pr^{0.074} \qquad (7.25)$$

Thus, the use of equations 7.5 and 7.25 enables the problem of the flow of heat through a naturally convecting fluid to be changed and reduced to a problem of heat conduction.

7.5 Effects of the non-Newtonian Fluid Properties on the Calculation of the CHTC

Material properties of the fluids in a geothermal well strongly affect the heat exchange between the well and the formation. Two important contributions of the fluid to heat transfer have been defined. First, the energy transport up and down inside the well is accomplished by the fluid flow. Second, the radial heat conduction from the well must pass through the annular fluids between casings.

7.5.1 Drilling fluid viscosity (μ)

The fluid viscosity is one of the most important variables that affect the convective heat transfer process, when a geothermal well is being drilled. As was previously discussed in the description of the numerical correlations for estimating the fluid CHTC, a strong dependence of the fluid viscosity, and its variation with temperature, on the dimensionless flow parameters and the CHTC was detected. Hence, real viscosity values of drilling fluids (mud) would be desirable for use in the calculation of these parameters. In the geothermal drilling literature, the majority of the studies related to the determination of the drilling fluid CHTC have been performed using viscosities which have been estimated by numerical correlations proposed for water [e.g. Keller et al (1973); Arnold (1990) and Beirute (1991)]. However, as was previously noted in chapter 6, this assumption is not valid since drilling fluids do not behave like Newtonian fluids.

A different numerical approximation to calculate mud viscosities as a function of temperature was proposed by Wooley (1980). This approximation was implemented in the wellbore thermal simulator (GEOTEMP) and it uses data derived from a simple mud rheological evaluation which are corrected by consideration of their non-Newtonian behaviour, based on the assumption that the drilling fluid obeys the power law model. Even though this method has been used as a tool to predict the thermal behaviour of the mud viscosity during drilling applications, it only produces a slight correction. Furthermore, a considerable temperature limitation in this corrected method was detected because it can only be used for temperatures less than 150 °C.

Variation of the drilling fluid viscosity with temperature. In order to evaluate the average errors (or differences) between the viscosity values of the Newtonian and the non-Newtonian fluids at different temperatures (50 °C to 200 °C), a parametric sensitivity analysis was carried out. The non-Newtonian fluid viscosities were represented using the dynamic rheological equation

corresponding to the drilling fluid system (DFS-1: Table 6.1). This equation was selected from the VISTEMPEQ database (see Table 6.5):

$$\mu = 15.7494 - 0.0405554\,T - 8.92239\times10^{-5}\,T^{2} \qquad (7.26)$$

The Newtonian fluid viscosities were calculated by means of the water correlation proposed by Zyvoloski and O'Sullivan (1980):

$$\mu = 0.02414 \cdot 10^{\left[\frac{247.8}{(T+133.15)}\right]} \qquad (7.27)$$

Additionally, a comparison between the actual experimental rheological data (DFS-1) and Wooley's approximation was carried out in the temperature range of 50 °C to 150 °C.

The variation of the calculated viscosities as a function of temperature is presented in Fig. 7.1. As can be observed in this figure, considerable differences between the three considered cases were obtained. It is clearly observed that the mud viscosities estimated by Wooley's algorithm (dotted curve) differ just slightly from those corresponding to the water or Newtonian fluid (solid curve). This behaviour is expected since the Wooley approximation always corrects the mud viscosity (inferred by the power law model) with the corresponding water viscosity value at 21 °C. However, when both viscosity approximations are compared with the actual mud viscosities [derived from dynamic rheological tests carried out on DFS-1 (diamond curve)], significant differences were found (Fig. 7.1). Clearly, from this comparison, underestimated values for the DFS-1 viscosities using Wooley's and water numerical methods were obtained in the range of 50 °C to 150 °C. From this figure, it is evident that the most representative thermal behaviour of the DFS-1 viscosities is related to the dynamic rheological data obtained at the drilling fluid laboratory (diamond curve). Consequently, the DFS-1 viscosities predicted by both the water viscosity and the mud corrected viscosity method (Wooley's algorithm) differ significantly

from real non-Newtonian behaviour. Difference errors up to 99 % were found when the non-Newtonian fluid viscosity values and those corresponding to the viscosity predicted with Wooley's method were quantitatively compared. Therefore, it is expected that these errors are subsequently transferred into the calculation of the drilling fluid CHTC, strongly affecting the estimation of the bottomhole temperature distributions in a geothermal well during drilling.

7.5.2 Density (ρ) and specific heat capacity (Cp)

Even though the density and the specific heat capacity of drilling fluids have less importance than viscosity, they are useful to account for the accumulation of energy in a geothermal well. At present, unfortunately, there is no available information related to reliable numerical correlations to predict these drilling fluid properties. Hence, these properties can be calculated using the numerical correlations for water. A plot of the variation of these water properties with temperature is presented in Fig. 7.2. These curves were calculated using numerical correlations which were proposed by Macedo et al. (1991). Dotted and square curves show the variation of the water density and the water specific heat capacity with temperature, respectively. From this figure small changes in the values of these properties were observed in the temperature range of 50°C to 200°C. The quantification of these changes indicates deviations up to 12.4 % and 8.3 % for the density and the specific heat capacity, respectively. Since these changes are small and the typical values of the mud properties approximately vary in a similar range (see Table 5.1), the estimation of such properties at well drilling temperatures could be approximated by the use of the numerical correlations for water or simply they can be assumed as constants, in the absence of appropriate equations for actual drilling fluids.

7.5.3 Thermal conductivity (k)

Thermal conductivity controls the conduction of heat in the radial direction through the drilling fluid. Although thermal conductivity is dependent on

temperature, some studies have demonstrated that this dependence is weak for geothermal well drilling applications and therefore k could be assume as a constant [Wooley (1980)]. However, if an evaluation of this property is required, the use of water correlations could give an approximation of its variability with temperature. Figure 7.3 shows the variation of the water thermal conductivity with temperature. From this figure, very small changes in the thermal conductivity values are exhibited. Deviations up to 0.73 % in the temperature range of 50 °C to 200 °C were found. Again, it is expected that these variations do not influence the estimation of the mud CHTC and the temperature distribution in and around the wellbore.

7.5.4 Non-Newtonian convective heat transfer coefficients

The non-Newtonian behaviour of drilling fluids is something that all previous publications on the subject of wellbore temperature simulations have essentially ignored. No mention is made of any investigations to find out the effect of the pseudoplasticity of a drilling fluid on the CHTC. All previous work has used the conventional Sieder and Tate correlation, equation (7.14) to estimate the Nusselt number and the drilling fluid CHTC [Raymond (1969); Keller et al. (1973)]. Nevertheless, Sump and Williams (1973), recognized that the use of the Seider and Tate correlation provides anomalously low temperatures. Inherent in the use of the Sieder and Tate correlation is the assumption that flow is turbulent. While this is generally the case within the drill pipe, it is seldom true in the annulus region of the well. Thus, the use of the Seider and Tate correlation, even with the assumption of non-Newtonian flow, is invalid for determining annulus CHTC.

On the other hand, Marshall and Bentsen (1982) suggested the use of the Lakshminarayan equation (7.15) in the drill pipe to estimate more accurately the Nusselt number under fully developed turbulent flow conditions. For the annular region (inner and outer walls, laminar flow), they recommended use of a Nusselt value of 4.12 for both the inner and the outer walls of the annulus under fully developed laminar flow. Wooley (1980) proposed the use of the Dittus and

Boelter equation (7.13) for estimating the drilling fluid CHTC in both the drill pipe and the annulus regions, when forced convection processes occur inside the well. Also, Wooley (1980) proposed the use of the Grashof number to evaluate the drilling fluid CHTC when a natural convection process occurs inside the annulus. This process normally occurs when drilling of the geothermal well has ceased and the fluid temperature returns to the undisturbed formation temperature.

7.5.5 Evaluation of the drilling fluid CHTC correlations

In order to evaluate the accuracy of all of the Nusselt correlations in the calculation of the fluid CHTC for the drill pipe, a documented numerical case in the geothermal well drilling literature was selected. This case corresponds to the drilling activities performed in an oil well which were reported by Raymond (1969). Table 7.3 shows the main data obtained from these operations, which include the well geometry and the drilling fluid mass flowrate. These data enable the associated errors of CHTC values to be estimated. These errors were estimated by application of the statistical propagation error theory which was proposed by Bevington (1969). This methodology evaluates the individual error contribution of each variable (e.g. the dimensionless flow parameters or the fluid properties) to the total error associated in the calculation of the CHTC. Details of the application of this statistical methodology in some earth science studies is fully described by Verma and Santoyo (1995). Table 7.4 presents in a simplified form some of the error equations corresponding to the numerical correlations used in the calculation of the fluid CHTC. Table 7.5 shows the average errors that should be expected for each variable involved in the determination of the CHTC within the temperature range of 10 °C to 210 °C.

After this statistical study, a direct application of all the numerical correlations to estimate the dimensionless Nusselt numbers and the CHTC values of drilling fluids was made. As an important part of this evaluation, two main assumptions related to the use of the drilling fluid properties were considered. The first is the

use of Newtonian fluid (water) properties, while in the second, non-Newtonian fluid properties were considered. When a Newtonian fluid behaviour is assumed, the water viscosity correlation proposed by Zyvoloski and O'Sullivan (1980) was again employed in all the calculations of the fluid CHTC. In the second case, when the drilling fluid behaves like a non-Newtonian fluid, the mud viscosity correlations reported in the VISTEMPEQ database were used to estimate the fluid CHTCs (Table 6.5).

In this context, eleven drilling fluid systems (DFS) were selected from the database to be used in the evaluation procedure. These systems are identified as bentonites and are classified in the database as DFS with sequential numbers from 1 to 11. A temperature range from 50°C to 200°C was used to estimate the viscosity and the thermophysical properties of the drilling fluids. The dimensionless flow parameters were calculated using their respective equations. In the case of the dimensionless Nusselt numbers, they were calculated using the five equations (7.13) to (7.18) previously cited [Dittus and Boelter (1930); Seider and Tate (1936); Lakshminarayan et al (1976); Pethukov et al (1970) and Gnielinski (1976)]. Finally, the drilling fluid CHTC values were determined by use of equation (7.1).

The results derived from the calculation of the Newtonian and the non-Newtonian (DFS-1) CHTC are presented in Tables 7.6 and 7.7, respectively. In each separate case, a good agreement among the results obtained in the calculation of fluid CHTC by four of the Nusselt number correlations was found (deviation errors up to 11 %). Only the Lakshminarayan et al (1976) correlation, equation (7.15), underestimated the CHTC values producing deviation errors up to 56 % with respect to the average tendency shown by the other numerical correlations.

Even though the deviations calculated with the other four equations are low, the Gnielinski equation (7.18) has been recognised as the best numerical correlation that provides the most reliable values for the fluid CHTC on the basis of the fluid

flow regimes. An explanation of this conclusion is that this correlation can be used without errors in the transition flow regime ($2300<Re<10^4$), which constitutes a serious limitation for the other equations. However, it is very important to note that even though the average errors of the Gnielinski equation (Table 7.5) are slightly greater than the other equations, these are only related to the statistical analysis of the mathematically complex nature of its equation.

After analyzing the results obtained in the CHTC calculation, the variation of the drilling fluid CHTC against temperature for all the DFS selected was evaluated, including the ideal case when the water is assumed to be a drilling mud. These variations were separately evaluated by use of the four Nusselt equations cited. Figures 7.4, 7.5, 7.6 and 7.7 show the variation of the fluid CHTC with temperature for the Dittus and Boelter, the Seider and Tate, the Petukhov et al., and the Gnielinski equations, respectively. As can be observed from these figures, very significant differences between the Newtonian and non-Newtonian fluid CHTC values were obtained. Difference errors of up to 400 % were found. When the mud viscosity was calculated using the water numerical correlation, overestimated values of these CHTC values were obtained. Therefore, it is expected that the use of the non-Newtonian numerical correlations for the mud viscosity could more reliably and accurately predict the drilling fluid CTHC values than the corresponding water viscosity.

This evidence was confirmed when the convective coefficients of the DFS-1 system were simultaneously compared with the mud viscosity values estimated by means of the Wooley's correction method and the water viscosity values (Fig. 7.8). Difference error up to 300 % were found in the fluid CHTC when the viscosity values estimated by Wooley's algorithm (circle curve) and the dynamic rheological equation (solid diamond curve) were compared. Difference errors up to 36 % were found when the viscosity values calculated by Wooley's algorithm (circle curve) and the water viscosity equation (solid line) were compared.

All these high differences explain the fact that the temperature profiles predicted by some numerical simulators that use water property values, denote a fast cooling process in the well formation as a consequence of the drilling fluid CHTC overestimation. This cooling process in the wellbore surrounding formation would be significantly less if non-Newtonian viscosity equations were used.

7.6 References

F.C. Arnold, Temperature variation in a circulating wellbore fluid, Journal of Energy Resources Technology, **112** 79-83 (1990).

P.R. Bevington, Data reduction and error analysis for physical sciences, Chapter six: Least squares fit to a straight line, McGraw-Hill Book Company, First Edition, New York, USA, 92-113 (1969).

R.M. Beirute, A circulating and shut-in well temperature profile simulator, Journal of Petroleum Technology, **September** 1140-1146 (1991).

M.S. Bhatti and R.K. Shah, Handbook of single phase convective heat transfer, in S. Kakac, R.K. Shah and W. Aung, Eds., Chapter 4, Wiley-Interscience, New York, USA (1987).

S.H. Bittleston, A two-dimensional simulator to predict circulating temperatures during cementing operations, Paper SPE 20448 presented at the 1990 SPE Annual Technical Conference and Exhibition, New Orleans, LA (USA), Sept. 23-26, 443-454 (1990).

A.P. Colburn, A method of correlating forced convection heat transfer data and comparison with fluid-fluid friction, Trans. AIChE, **29** 174-210 (1933).

F.W. Dittus and L.M.K. Boelter, Publications in engineering, University of California, Berkeley, USA, **2**, p. 443 (1930).

D. Dropkin and E. Sommerscales, Heat transfer by natural convection in liquids confined by two parallel plates inclied at various angles with respect to the horizontal, J. Heat Transfer, Trans., ASME, Series C, **87** 77-84 (1965).

A. Garcia, I. Hernandez, G. Espinoza and E. Santoyo, TEMLOPI, A thermal simulator for estimation of drilling mud and formation temperatures during drilling of geothermal wells, Submitted to Computers & Geosciences (1997a).

A. Garcia, E. Santoyo, G. Espinosa, I. Hernandez and H. Gutierrez, Estimation of temperatures in geothermal wells during circulation and shut-in in the presence of lost circulation, Submitted to Transport in Porous Media (1997b).

F.A. Holland and R. Bragg, Fluid flow for chemical engineers, 2nd Edition, Edward Arnold, A Division of Hodder Headline PLC, London, UK (1995).

F.P. Incropera and D.P. Dewitt, Introduction to heat transfer, John Wiley & Sons, Inc., New York, USA (1990).

W.M. Kays and H.C. Perkins, in Handbook of heat transfer, Chapter 7, W.M. Roshenow and J.P. Harnett, Eds. McGraw-Hill Book Co., New York, USA (1972).

H.H. Keller, E.J. Couch and P.M. Berry, Temperature distribution in circulating mud columns, Society of Petroleum Engineers Journal, **February** 23-30 (1973).

M.S. Lakshminarayanan, R. Lalchandani and M. Raja Rao, Turbulent flow heat transfer in circular tubes, Indian J. Tech., **14** 521-525 (1976).

J. Macedo, J. Zorrila y R. Rosas, Propiedades termofisicas, Documento Final del Simulador de la Central Nucleoelectrica Laguna Verde (CFE), GEVFI1.0/PROY1955/IIE, Cuernavaca, Mor., Mexico (1991).

D.W. Marshall and R.G. Bentsen, A computer model to determine the temperature distributions in a wellbore, The Journal of Canadian Petroleum, **January-February** 63-75 (1982).

B.S. Petukhov, Advances in heat transfer, in T.F. Irvine and J.P. Hartnett, Eds., **Vol. 6**, Academic Press, New York, U.S.A. (1970).

L.R. Raymond, Temperature distribution in a circulating drilling fluid, Journal of Petroleum Technology, **21** 333-341 (1969).

E.N. Seider and G.E. Tate, Heat transfer and pressure drop of liquids in tubes, Ind. Eng. Chem. **28** p. 1429 (1936).

G.D. Sump and B.B. Williams, Prediction of wellbore temperatures during mud circulation and cementing operations, Journal of Engineering for Industry, Transactions of ASME, **November** 1083-1092 (1973).

S.P. Verma and E. Santoyo (1995) New improved equations for Na/K and SiO_2 geothermometers by error propagation. Proc. of the World Geothermal Congress 1995, Florence, Italy, **Vol. 2**, pp. 963-968.

G. P. Willhite, Over-all heat transfer coefficients in steam and hot water injection wells, Journal of Petroleum Technology, **May** 607-615 (1967).

G.R. Wooley, Computing downhole temperatures in circulation, injection, and production wells, Journal of Petroleum Technology, **September** 1509-1522 (1980).

G.A. Zyvoloski and M.J. O'Sullivan, Simulation of gas dominated, two phase geothermal reservoir, Society of Petroleum Engineering Journal, **20** 52-58 (1980).

D_i/D_o	Nu_i	Nu_o
0.00	----	3.66
0.05	17.46	4.06
0.10	11.56	4.11
0.25	7.37	4.23
0.50	5.74	4.43
1.00	4.86	4.86

Table 7.1

Nusselt number for fully developed laminar flow in a circular tube annulus with one surface insulated and the other at constant temperature [Kays and Perkins (1972)].

D_i/D_o	Nu_i	Nu_o
0.00	----	4.364
0.05	17.810	4.792
0.10	11.910	4.834
0.20	8.499	4.833
0.40	6.583	4.979
0.60	5.912	5.099
0.80	5.580	5.240
1.00	5.385	5.385

Table 7.2

Nusselt number for fully developed laminar flow in a circular tube annulus with uniform heat flux maintained at both surfaces [Kays and Perkins(1972)].

Well geometry	Data	Units
Well depth	6100.0	m
Well diameter	0.2191	m
Drill pipe diameter	0.1143	m
Drill pipe thickness	0.0147	m
Well radius	0.1095	m
Drill pipe outer radius	0.0570	m
Drill pipe inner radius	0.0420	m
Drill pipe area	0.0060	m^2
Annulus area	0.1410	m^2
Mass flowrate of mud	15.1	$kg\ s^{-1}$

Table 7.3

Well geometry and flow data of the numerical study reported by Raymond (1969) to predict temperature distributions in a circulating drilling fluid system.

Ref.	Equation	Propagation error equation
(7.2)	$Re = \frac{\rho v D}{\mu}$	$\sigma_{Re}^2 = Re^2\left[\left(\frac{\sigma_D^2}{D^2}\right)+\left(\frac{\sigma_v^2}{v^2}\right)+\left(\frac{\sigma_\rho^2}{\rho^2}\right)+\left(\frac{\sigma_\mu^2}{\mu^2}\right)\right]$
(7.4)	$Pr = \frac{\mu Cp}{k}$	$\sigma_{Pr}^2 = Pr^2\left[\left(\frac{\sigma_\mu^2}{\mu^2}\right)+\left(\frac{\sigma_{Cp}^2}{Cp^2}\right)+\left(\frac{\sigma_k^2}{k^2}\right)\right]$
(7.5)	$Pe = Re \cdot Pr$	$\sigma_{Pe}^2 = Pe^2\left[\left(\frac{\sigma_{Re}^2}{Re^2}\right)+\left(\frac{\sigma_{Pr}^2}{Pr^2}\right)\right]$
(7.7)	$Nu = Pe \cdot St$	$\sigma_{Nu}^2 = Nu^2\left[\left(\frac{\sigma_{Pe}^2}{Pe^2}\right)+\left(\frac{\sigma_{St}^2}{St^2}\right)\right]$
(7.14)	$Nu = 0.023\, Re^{4/5}\, Pr^n$	$\sigma_{Nu}^2 = Nu^2\left[0.64\left(\frac{\sigma_{Re}^2}{Re^2}\right)+ 0.16\left(\frac{\sigma_{Pr}^2}{Pr^2}\right)\right]$
(7.15)	$Nu = 0.027\, Re^{4/5}\, Pr^{0.33}$	$\sigma_{Nu}^2 = Nu^2\left[0.64\left(\frac{\sigma_{Re}^2}{Re^2}\right)+ 0.1089\left(\frac{\sigma_{Pr}^2}{Pr^2}\right)\right]$
(7.16)	$St = 0.0710\, Re^{-0.33}\, Pr^{-0.67}$	$\sigma_{St}^2 = St^2\left[0.111\left(\frac{\sigma_{Re}^2}{Re^2}\right)+ 0.4444\left(\frac{\sigma_{Pr}^2}{Pr^2}\right)\right]$

Table 7.4

Error equations derived from the application of the statistical propagation errors theory to estimate the total error associated with the calculation of the drilling fluid CHTC. σ represents the standard deviation error attributed to each variable in the CHTC calculation procedure.

Variables	Equation No.	Average error (%)
Specific heat capacity (Cp)	See Fig. 7.2	0.7
Density (ρ)	See Fig. 7.2	0.4
Thermal conductivity (k)	See Fig. 7.2	0.5
Viscosity (μ)	(7.28)	0.4
Reynolds number (Re)	(7.2)	3.8
Prandtl number (Pr)	(7.4)	0.6
Peclet number (Pe)	(7.5)	3.8
Stanton number (St)	(7.7)	1.7
Nusselt number (Nu) [1] Dittus and Boelter (1930)	(7.14)	3.1
Nusselt number (Nu) [2] Seider and Tate (1936)	(7.15)	3.1
Nusselt number (Nu) [3] Petukhov et al (1970)	(7.17)	4.3
Nusselt number (Nu) [4] Gnielinski (1976)	(7.19)	4.3
Nusselt number (Nu) [5] Lakshminarayan et al (1976)	(7.16)	4.2
CHTC (h) [1]	(7.1)	3.7
CHTC (h) [2]	(7.1)	3.6
CHTC (h) [3]	(7.1)	4.7
CHTC (h) [4]	(7.1)	4.7
CHTC (h) [5]	(7.1)	4.6

Table 7.5

Average error values obtained during the calculation of fluid CHTC.

T °C	ρ kg/m³	Cp J/kg °C	k W/m °C	μ Pa.s	Pr	v m/s	Re	Nu [1]	Nu [2]	Nu [3]	Nu [4]	Nu [5]	H W/m² °C [1]	H W/m² °C [2]	H W/m² °C [3]	H W/m² °C [4]	H W/m² °C [5]	Error* Diff. %
water properties																		
Newtonian fluid viscosity: water																		
50	987	4174	0.646	0.00054	3.5	2.71	417225	1193	1287	1416	1471	603	9072	9793	10769	11189	4586	9.4
60	983	4174	0.656	0.00046	2.9	2.72	490251	1265	1381	1474	1537	633	9764	10665	11378	11869	4888	8.4
70	978	4178	0.664	0.00040	2.5	2.73	566984	1334	1472	1523	1595	662	10434	11517	11915	12475	5177	7.4
80	973	4185	0.672	0.00035	2.2	2.75	646841	1401	1561	1566	1645	689	11080	12345	12389	13014	5453	6.6
90	967	4196	0.678	0.00031	1.9	2.77	729282	1465	1647	1604	1690	716	11701	13149	12808	13494	5715	6.1
100	961	4209	0.683	0.00028	1.7	2.78	813812	1529	1731	1638	1730	741	12298	13924	13180	13923	5965	5.8
110	953	4226	0.687	0.00025	1.6	2.80	899985	1590	1813	1669	1768	766	12869	14671	13511	14306	6201	5.8
120	946	4246	0.690	0.00023	1.4	2.83	987399	1650	1893	1699	1803	790	13414	15387	13808	14652	6424	6.2
130	938	4269	0.692	0.00021	1.3	2.85	1075699	1710	1972	1728	1836	814	13933	16071	14077	14965	6633	6.7
140	929	4295	0.692	0.00019	1.2	2.88	1164569	1769	2050	1756	1870	837	14426	16722	14321	15250	6829	7.3
150	920	4325	0.692	0.00018	1.1	2.91	1253732	1827	2127	1785	1903	860	14893	17339	14546	15512	7012	8.0
160	910	4357	0.690	0.00017	1.1	2.94	1342945	1886	2204	1814	1937	883	15333	17922	14754	15754	7181	8.7
170	899	4393	0.688	0.00016	1.0	2.97	1431997	1944	2280	1846	1973	906	15746	18468	14949	15980	7337	9.3
180	888	4433	0.684	0.00015	1.0	3.01	1520705	2003	2357	1879	2011	929	16131	18978	15132	16192	7480	10.0
190	877	4475	0.679	0.00014	0.9	3.05	1608913	2063	2433	1915	2050	952	16489	19450	15306	16392	7608	10.5
200	864	4521	0.673	0.00013	0.9	3.09	1696485	2123	2510	1953	2093	975	16819	19884	15473	16581	7723	11.0

[1] Dittus and Boelter (1930); [2] Seider and Tate (1936); [3] Petukhov et al (1970); [4] Gnielinski (1976) and [5] Lakshminarayan et al (1976).

* Average error evaluated with the CHTC values [1] to [4].

Table 7.6

Evaluation of the effect of Newtonian fluid (water) viscosities on the calculations of the drilling fluid CHTC for the drill pipe region of drilled wells under turbulent flow conditions

T °C	ρ kg/m³	Cp J/kg °C	k W/m °C	μ Pa.s	Pr	v m/s	Re	Nu [1]	Nu [2]	Nu [3]	Nu [4]	Nu [5]	H W/m² °C [1]	H W/m² °C [2]	H W/m² °C [3]	H W/m² °C [4]	H W/m² °C [5]	Error* Diff. %
Non-Newtonian fluid viscosity (DFS-1: processed clays, 6.2%)																		
50	987	4174	0.646	0.01350	87.2	2.71	16819	330	288	336	317	207	2511	2188	2553	2413	1572	6.7
60	983	4174	0.656	0.01299	82.7	2.72	17471	333	291	340	323	208	2573	2250	2629	2491	1609	6.7
70	978	4178	0.664	0.01247	78.5	2.73	18202	337	296	346	329	210	2637	2314	2708	2573	1645	6.7
80	973	4185	0.672	0.01193	74.4	2.75	19024	342	301	353	336	213	2704	2381	2792	2659	1683	6.7
90	967	4196	0.678	0.01138	70.4	2.77	19956	347	307	361	345	216	2774	2452	2881	2752	1722	6.8
100	961	4209	0.683	0.01080	66.6	2.78	21019	354	314	370	354	219	2849	2528	2976	2851	1763	6.8
110	953	4226	0.687	0.01021	62.8	2.80	22240	362	322	380	366	223	2929	2609	3079	2958	1806	6.9
120	946	4246	0.690	0.00960	59.1	2.83	23655	371	332	393	378	228	3015	2697	3191	3076	1852	7.1
130	938	4269	0.692	0.00897	55.3	2.85	25313	382	343	407	393	233	3110	2793	3315	3205	1901	7.2
140	929	4295	0.692	0.00832	51.6	2.88	27279	394	356	423	411	240	3214	2900	3452	3349	1954	7.4
150	920	4325	0.692	0.00766	47.9	2.91	29645	409	371	443	431	247	3330	3021	3608	3512	2013	7.7
160	910	4357	0.690	0.00698	44.0	2.94	32544	426	388	466	455	256	3462	3158	3786	3699	2078	8.0
170	899	4393	0.688	0.00628	40.1	2.97	36173	446	410	493	484	266	3615	3318	3994	3917	2153	8.3
180	888	4433	0.684	0.00556	36.0	3.01	40844	471	436	527	519	278	3796	3509	4243	4177	2240	8.7
190	877	4475	0.679	0.00482	31.8	3.05	47075	502	468	569	562	293	4015	3743	4547	4496	2344	9.2
200	864	4521	0.673	0.00407	27.4	3.09	55792	542	510	623	619	312	4291	4041	4934	4900	2474	9.8

[1] Dittus and Boelter (1930); [2] Seider and Tate (1936); [3] Petukhov et al (1970); [4] Gnielinski (1976) and [5] Lakshminarayan et al (1976).

* Average error evaluated with the CHTC values [1] to [4].

Table 7.7

Evaluation of the effect of non-Newtonian fluid (DFS-1) viscosities on the calculations of the drilling fluid CHTC for the drill pipe region of drilled wells under turbulent flow conditions

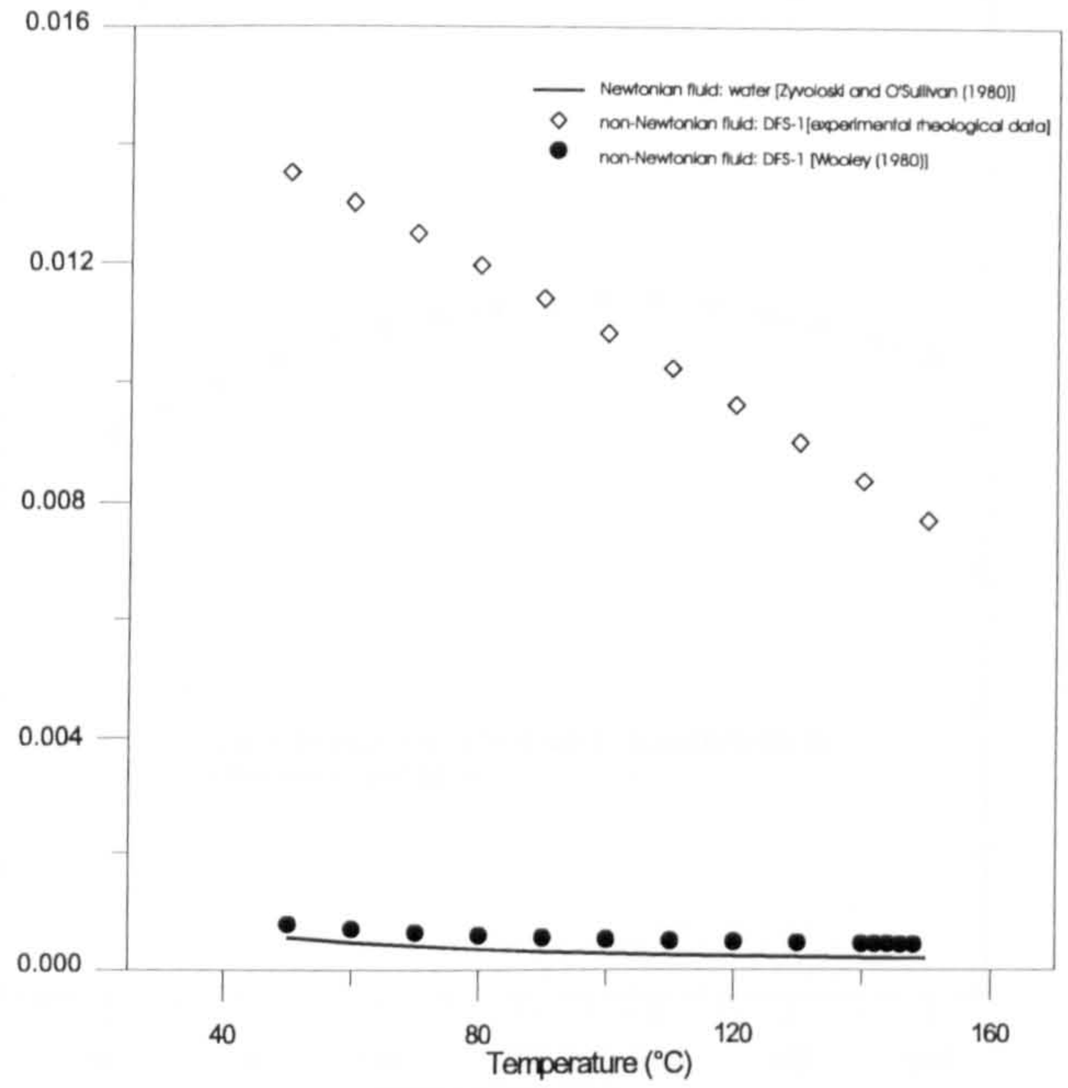

Fig. 7.1 Thermal behaviour of the DFS-1 viscosity assuming that the drilling fluid behaves as a Newtonian fluid (water: solid line), a non-Newtonian fluid (corrected by the Wooley's algorithm: dotted curve) and a non-Newtonian fluid (derived from the dynamic rheological tests: diamond curve).

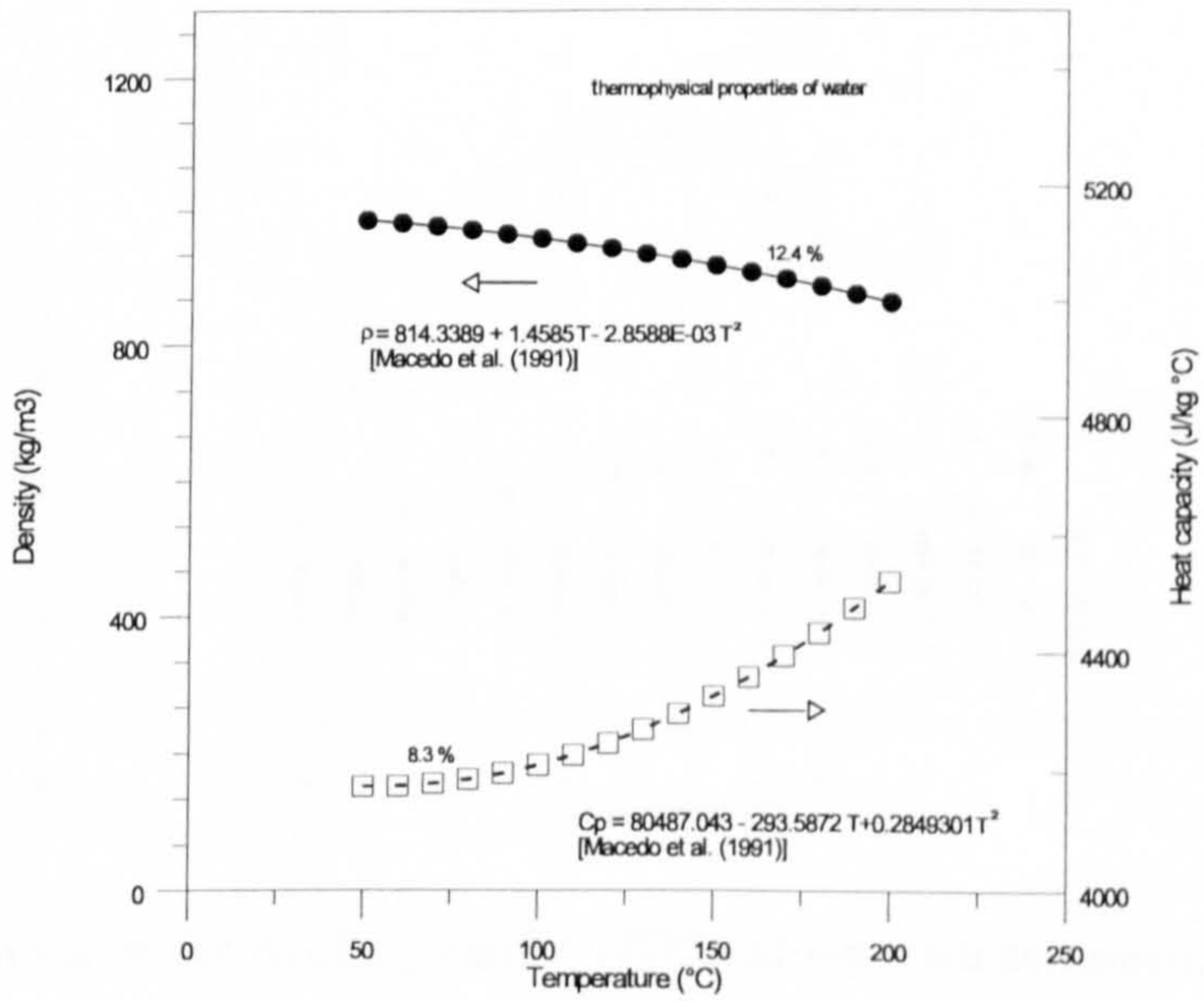

Fig. 7.2 Variation of the density and the specific heat capacity with temperature assuming numerical correlations for water.

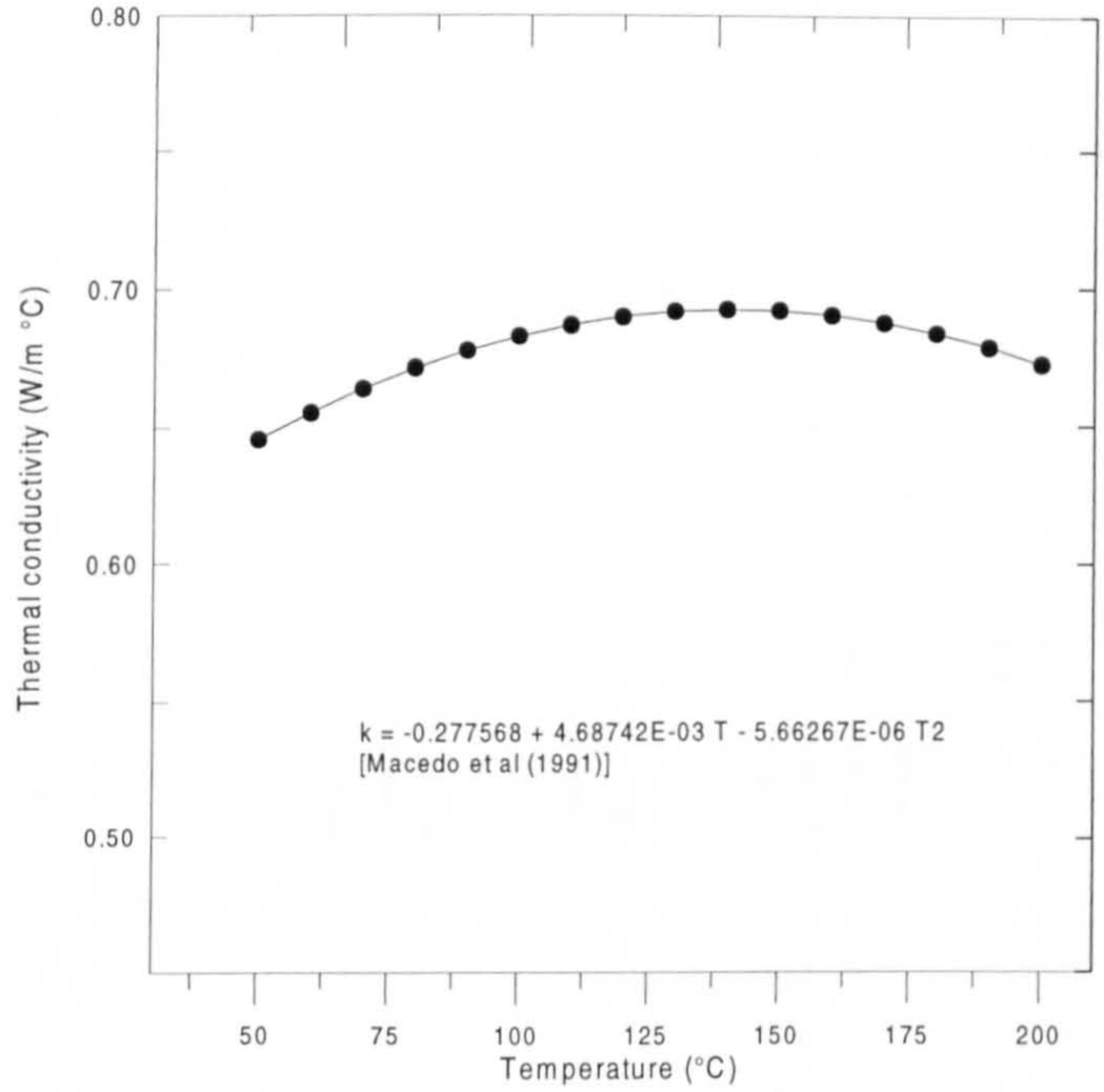

Fig. 7.3 Variation of the thermal conductivity with temperature assuming numerical correlations for water.

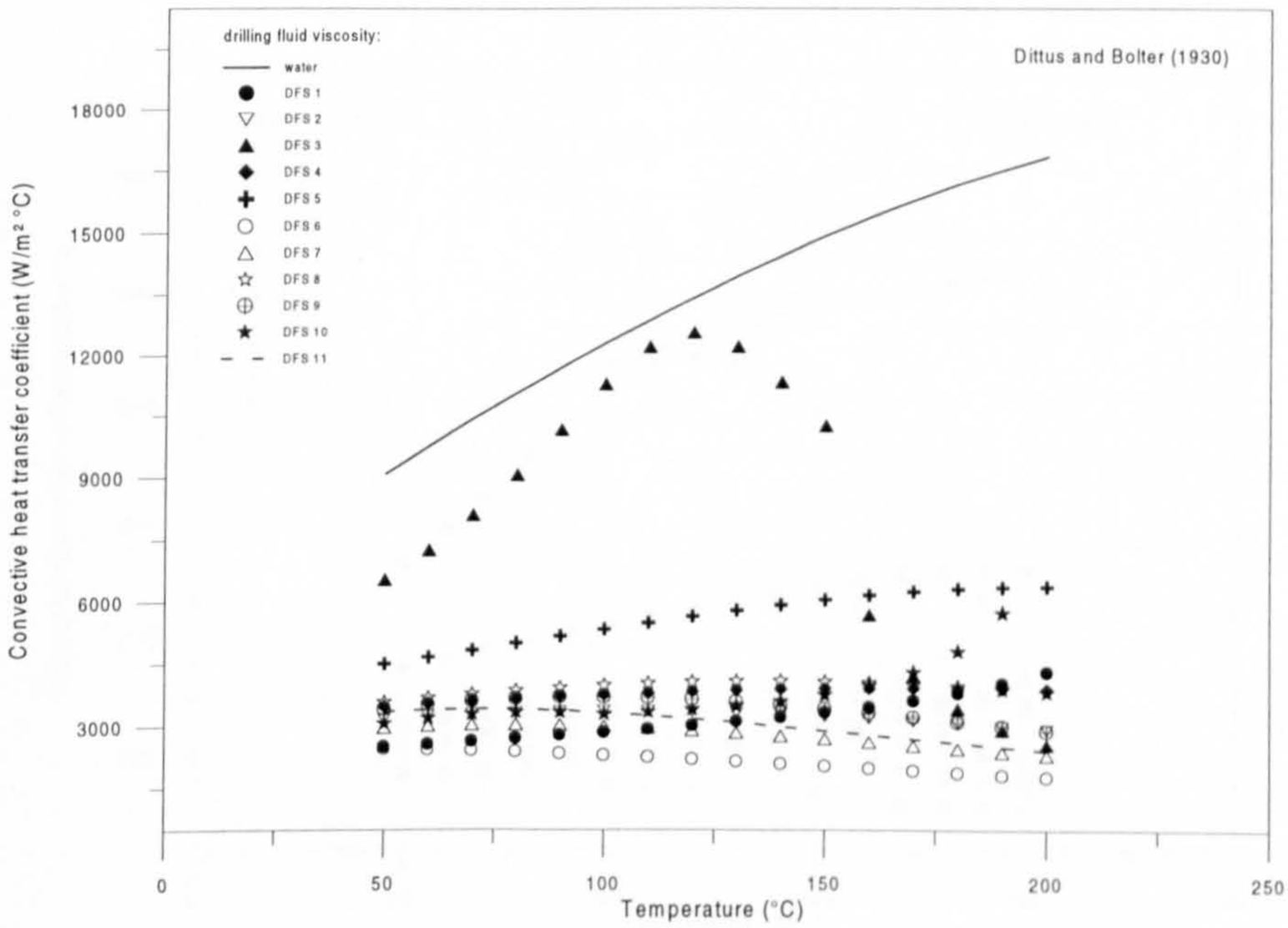

Fig. 7.4 Variation of the drilling fluid CHTC values with temperature assuming different types of drilling fluid systems, including water (solid line). All the fluid CHTC values were calculated by use of the Dittus and Boelter equation.

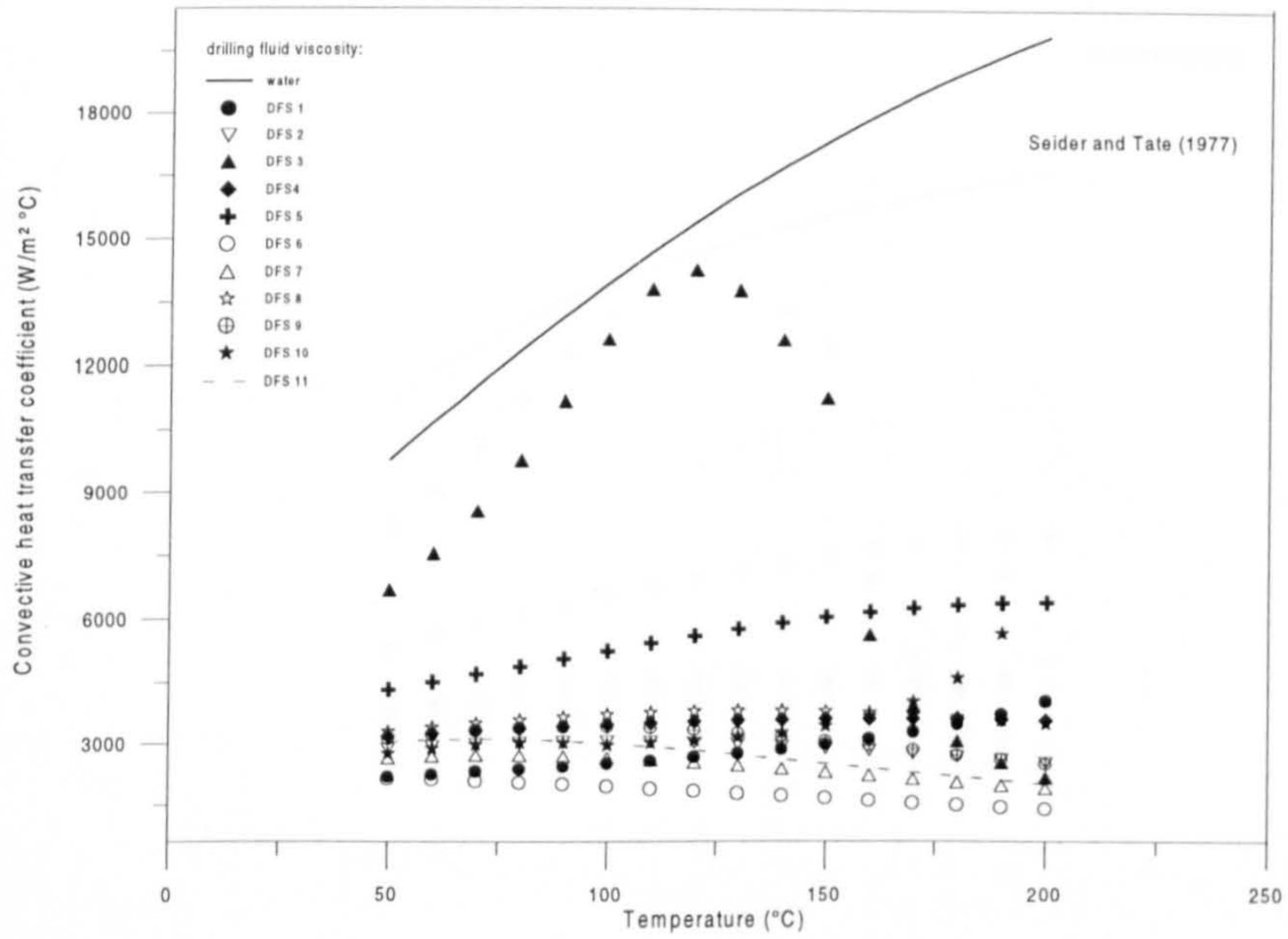

Fig. 7.5 Variation of the drilling fluid CHTC values with temperature assuming different types of drilling fluid systems, including water (solid line). All the fluid CHTC values were calculated by use of the Seider and Tate equation.

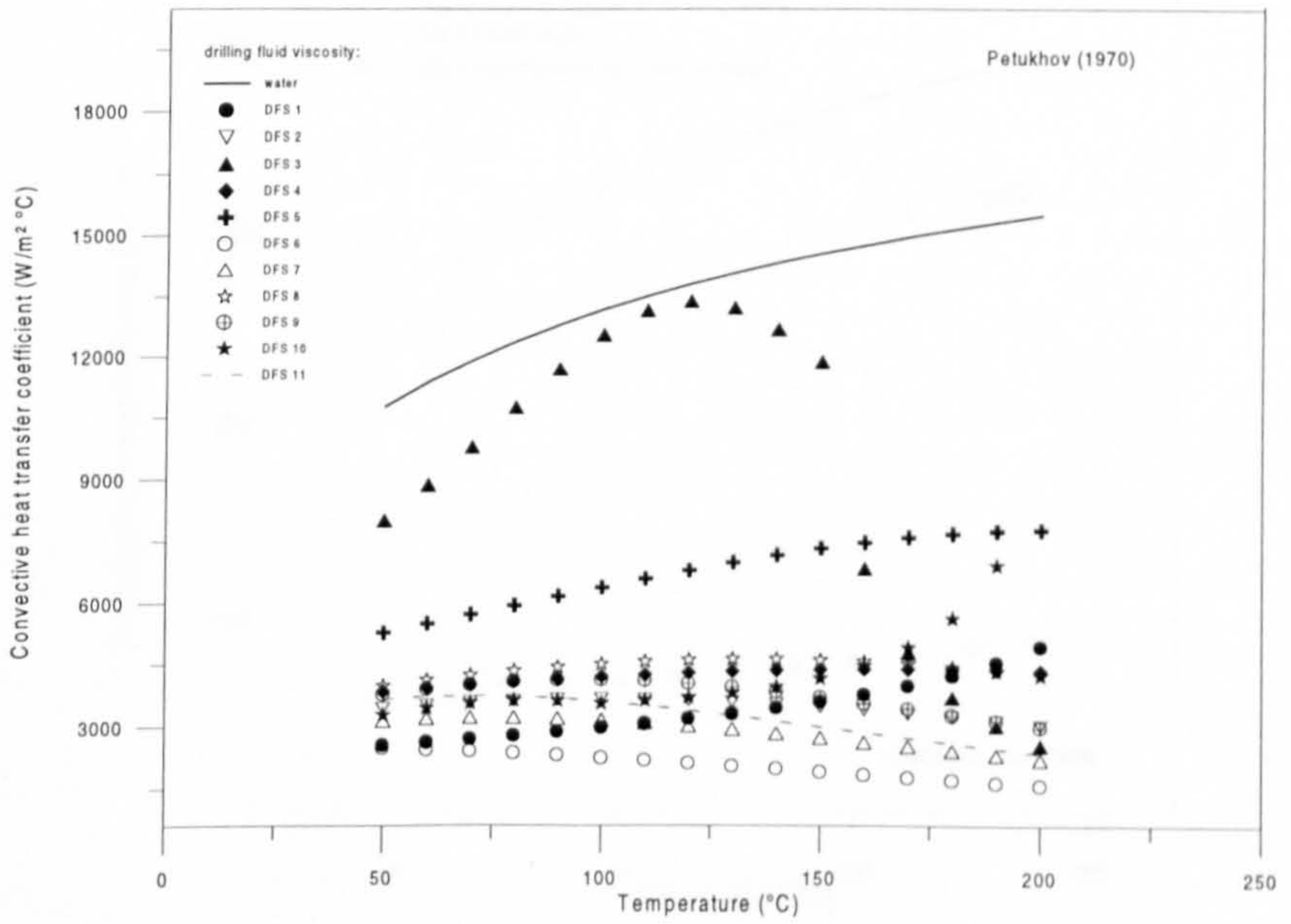

Fig. 7.6 Variation of the drilling fluid CHTC values with temperature assuming different types of drilling fluid systems, including water (solid line). All the fluid CHTC values were calculated by use of the Petukhov et al. equation.

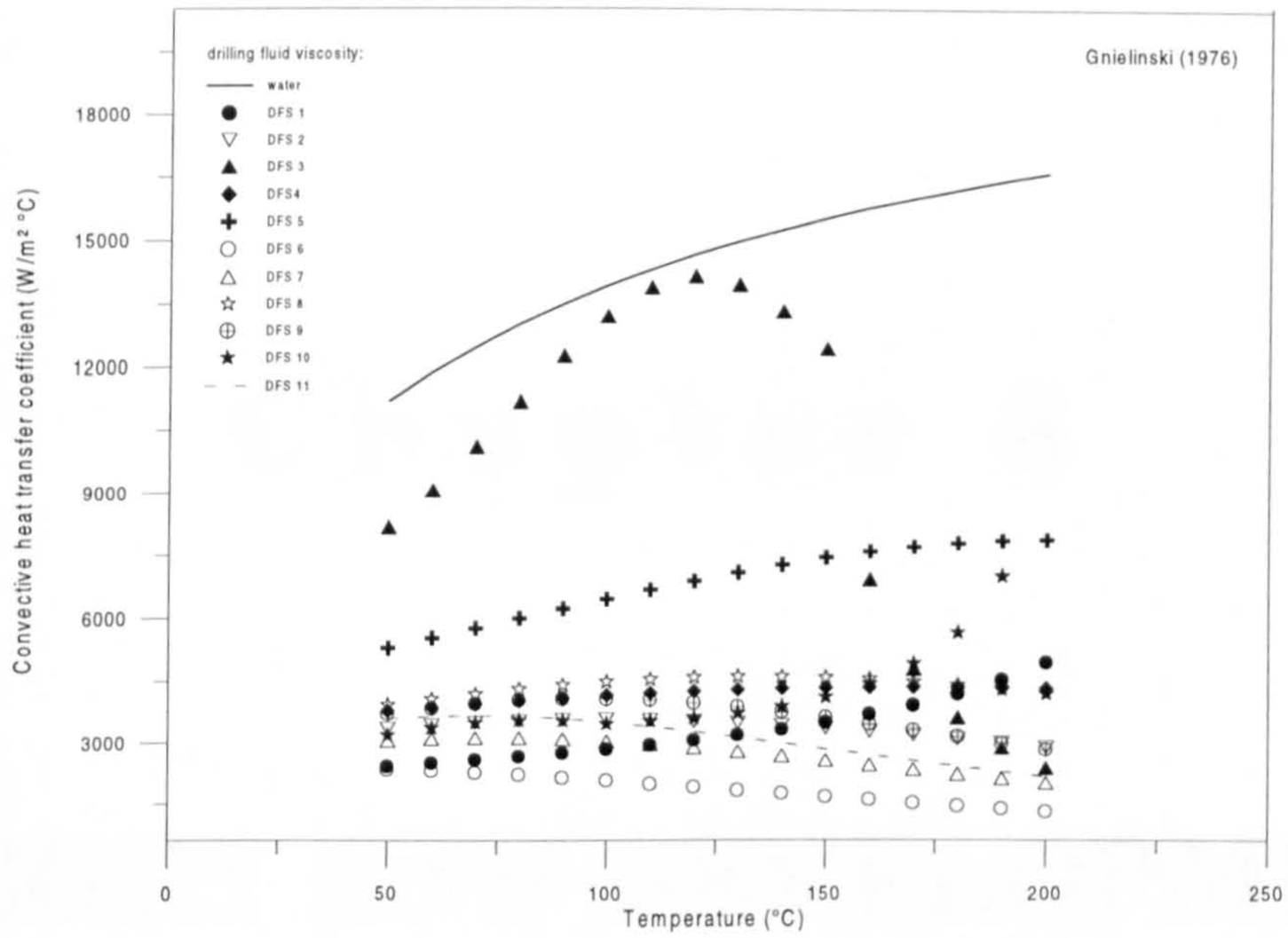

Fig. 7.7 Variation of the drilling fluid CHTC values with temperature assuming different types of drilling fluid systems, including water (solid line). All the fluid CHTC values were calculated by use of the Gnielinski equation.

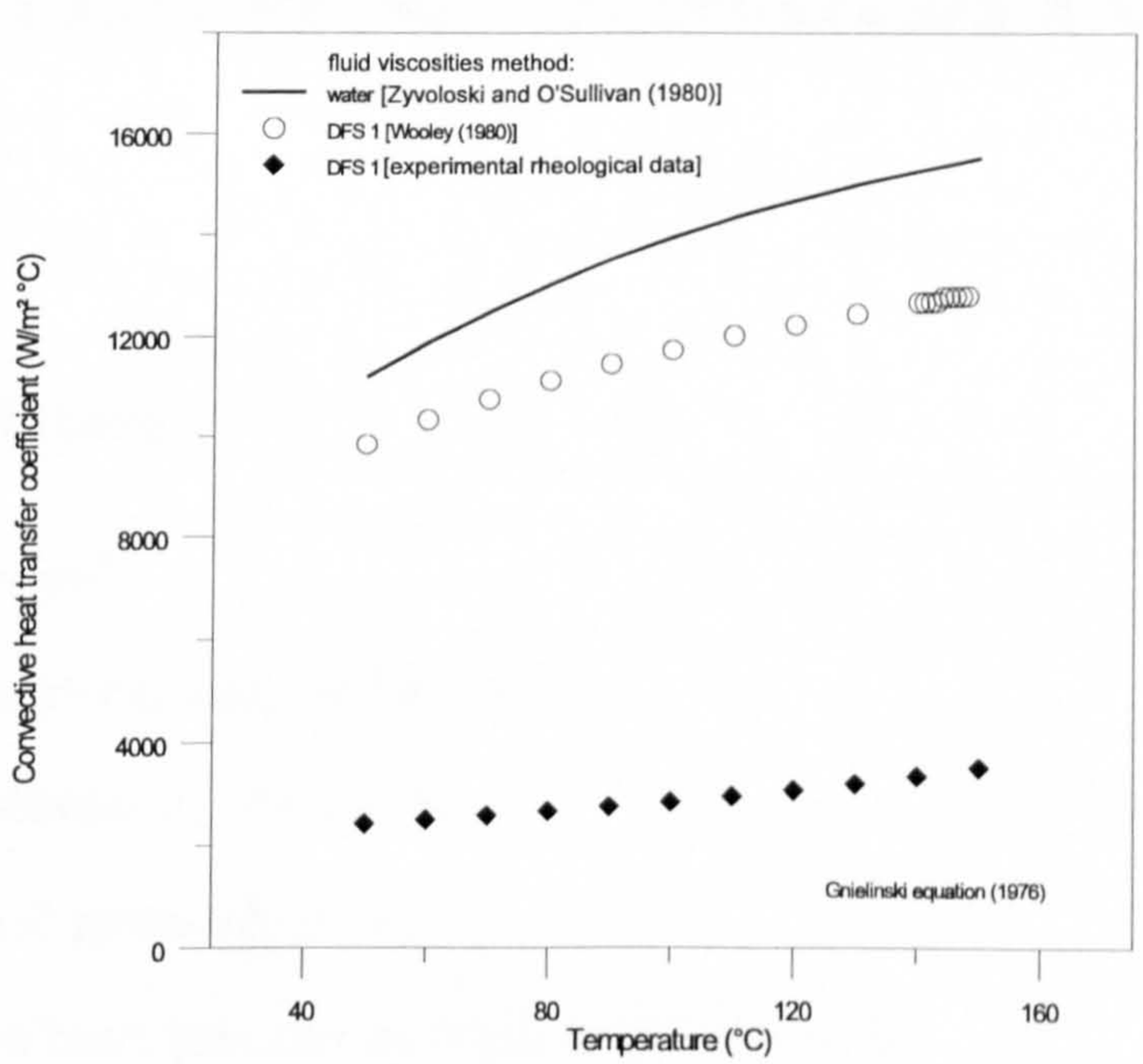

Fig. 7.8 Variation of the drilling fluid CHTC values calculated by use of three different viscosity methods. Wooley's algorithm is indicated by the circle curve; water viscosity method is shown by the solid line and the dynamic viscosity method is denoted by the diamond curve.

Chapter 8

THEORY AND DEVELOPMENT OF THE WELLBORE THERMAL SIMULATOR

8.1 Nomenclature

A	flow area [m^2]
Cp	specific heat capacity [$J\ kg^{-1}\ °C^{-1}$]
D	internal diameter of pipe [m]
G	geothermal gradient [$°C\ m^{-1}$]
h	convective heat transfer coefficient [$W\ m^{-2}\ °C^{-1}$]
k	thermal conductivity [$W\ m^{-1}\ °C^{-1}$]
k_{eff}	thermal conductivity [$W\ m^{-1}\ °C^{-1}$]
L	length [m]

Nu	pipe Nusselt number, hD/k_m [dimensionless]
Pe	Peclet number, Re·Pr [dimensionless]
Pr	Prandtl number, $\mu C_p/k_m$ [dimensionless]
Q	volumetric fluid flow rate [$m^3\ hr^{-1}$]
q	heat flux per unit area [$W\ m^{-2}$]
q_r	radial heat flux per unit area [$W\ m^{-2}$]
q_z	axial heat flux per unit area [$W\ m^{-2}$]
r	radius [m]
Re	Reynolds number, $Dv\rho/\mu$ [dimensionless]
T	temperature [°C]
T_{in}	inlet fluid temperature [°C]
T_{ws}	metal pipe wall temperature at the surface [°C]
t	time [hr]
v	linear velocity [$m\ s^{-1}$]
v_r	radial linear velocity [$m\ s^{-1}$]
v_z	axial linear velocity [$m\ s^{-1}$]
W	drilling fluid mass flowrate [$kg\ hr^{-1}$]
z	depth [m]
Δz	axial increment [m]

Greek symbols

ϕ	formation porosity [dimensionless]
μ	dynamic viscosity [Pa s]
φ	step increment parameter, equation (8.32) [dimensionless]

ρ density [kg m^{-3}]

Subscripts

a annulus; inner annulus wall

ef effective

f formation

m mud or drilling fluid

o outer annulus wall

p drill pipe

s surface

w drill pipe wall

8.2 Introduction

This chapter describes the theory and the mathematical development of the dynamic wellbore thermal simulator (WELLTHER). The numerical simulator was developed for determining transient temperature distributions in and around a geothermal well during circulation and shut-in conditions in the presence of lost circulation. A set of rigorous governing partial differential equations that describe the main heat transfer processes in the geothermal well drilling and shut-in operations was derived. Transient (unsteady-state) heat flow conditions both in the wellbore and the formation were adopted. In the case of the formation, a two-dimensional (vertical and radial) transient conduction and convection model was considered. WELLTHER uses a direct solution method to solve the finite-difference equations describing the transient heat transfer both in the wellbore and the surrounding formation. A complete description of the numerical simulator in terms of the solution algorithm, the computer code architecture, the flow diagrams and the source programs is outlined.

8.3 Description of the Physical Model (WELLTHER)

The physical wellbore drilling model, upon which this numerical simulator is based is shown schematically in Fig. 8.1. This figure shows an actual drilling fluid circulation system, including the circulation losses process to the formation. The thermal behaviour of the overall heat transfer process has been fully described in the section (2.5.5) of Chapter 2. Basically, the circulation process has three phases: (i) the drilling fluid enters the drill pipe at the top (surface), flows down the drill pipe; (ii) the fluid exits the drill pipe through the bit and enters the annulus at the bottom; and (iii) the fluid enters the annulus and flows upwards to the surface. If lost circulation exists then some drilling fluid will flow into the formation and the amount of fluid exiting the well at the surface will depend on the amount of the circulation losses.

Since the temperature in the formation (earth's crust) increases with depth, the drilling fluids come upon increasingly higher temperatures with increased depth. This heated fluid then flows to the surface and tends to heat the wellbore system (casing, annulus, etc.) as it passes through it. Thus, the temperature of the drilling fluid in each phase of the circulation is dependent upon a number of different thermal processes.

In the first phase, the fluid enters the drill pipe at a constant rate and known temperature. The fluid flowing down the drill pipe has a vertical temperature distribution resulting from: (a) the convective heat transfer within the fluid column (and in a minor grade of the heat conduction) and (b) the rate of convective heat transfer radially between the fluid, the drill pipe wall and the annulus. Vertical and radial conduction within the drill pipe wall is also present.

In the second phase, at the bottom of the wellbore, the fluid temperature in the drill pipe and the annulus will be the same due to the mixing process which occurs there.

Finally, in the third phase, when the fluid flows up the annulus, its temperature is dependent upon: (a) the rate of heat convection up the annulus; (b) the rate of radial convection between the annulus fluid, the drill pipe wall and the fluid within the drill pipe; (c) the rate of radial convection between the annulus fluid and the formation or casing; and (d) the radial heat conduction through the surrounding formation.

Additional energy sources should be taken into account for the heat generation within the whole thermal system due to frictional forces and the rotational energy of the drill string and the drill bit.

Since dynamic or transient heat transfer processes occur in both the wellbore and the surrounding formation, the circulation or the shut-in time have an important effect on the temperature distribution in and around the wellbore. With respect to the overall circulation process, five heat transfer regions associated with this circulation process can be identified. Figure 8.2 shows a schematic diagram of the main heat flow regions in a wellbore drilling system.

8.4 Model Assumptions

To develop the energy equations for describing the overall thermal behaviour of the wellbore and the surrounding formation, certain assumptions about the main heat transfer mechanisms and flow behaviour need to be considered. The fundamental assumptions of the WELLTHER model are as follows:

(i) The problem is assumed to be symmetrical around the vertical wellbore axis.

(ii) Heat transfer is in the axial and radial directions and temperature distribution is axisymmetric so that: $\frac{\partial T(z,r,t)}{\partial \theta} = 0$

(iii) Wellbore drilling fluids are assumed to be incompressible and are circulated at a constant rate.

(iv) Fluid flow is turbulent in the drill pipe and laminar in the annulus. These conditions are related to the drilling fluid circulation process.

(v) Fully transient heat flow conditions both in the wellbore and the formation are considered.

(vi) Heat transfer within the drilling fluid is by axial convection. Conduction may be neglected except when the fluid is immobile (specially during the thermal recovery period after the circulation process is stopped).

(vii) The radial temperature gradient within the fluid may be neglected.

(viii) The physical properties of the circulating fluid such as the density, the thermal conductivity and the specific heat capacity are constants. This assumption can be accepted because small changes are expected in these properties during the well drilling process as well as due to the absence of reliable correlations to predict the behaviour of these properties with temperature. In the case of the drilling fluid viscosity, it can be calculated by means of the viscosity-temperature correlations derived from the dynamic rheological tests.

(ix) No fluid phase changes are considered in the drill pipe, the annulus or the formation.

(x) Heat conduction (vertical and radial) is considered in the formation (rock) model. Convection (fluid flow) in the rock is included to describe the lost circulation process. In this case, the rock formation is considered as an isotropic medium with an homogeneous porosity.

(xi) There are no sources or sinks of thermal energy in the formation.

(xii) The thermophysical properties of the formation, cement and pipe metal are constant (ρ, Cp and k).

(xiii) Heat generation by viscous dissipation within the fluid and the thermal expansion effects are neglected.

(xiv) Thermal energy sources or sinks for the fluids in the drill pipe and the annulus are neglected.

(xv) Radiative heat transfer in the wellbore and the formaton is assumed to be negligible.

(xvi) Initial conditions: the fluid temperatures in the wellbore, the annulus and the surrounding formation are initially set at the geothermal gradient temperature values. These temperatures can be given either by the measured static temperature profile or by the local geothermal temperature profile.

(xvii) Drilling fluid velocities in the drill pipe (v_1) and the annulus (v_3) are assumed to be uniform.

8.5 Mathematical formulation of the WELLTHER simulator

The mathematical problem consists of a set of local and instantaneous heat transfer partial differential equations describing the two dimensional transient temperature field T(z,r,t). Mass conservation considers incompressible flow in the axial and radial directions. The solution considers the heat transfer convective effects which appear in the boundary conditions.

The well-formation interface is considered as a porous medium through which fluid may be lost (lost circulation) or gained by the well. The mathematical formulation is generic and versatile since any vertical well can be studied and fluid losses or gains can be simulated at any point in the well. The model also considers the possibility of the drilling fluid can be a mud or simply water. For shut-in conditions, the flow is stagnant and heat transfer is purely conductive.

A general mathematical formulation related to the partial differential equations that need to be applied in the energy balances within the geothermal well drilling system is described in Appendix III. From this generic formulation and

after several reducing steps, an energy equation in cylindrical coordinates that considers the above assumptions reduces to:

$$\rho C_p\left(\frac{\partial T}{\partial t} + v_r\frac{\partial T}{\partial r} + v_z\frac{\partial T}{\partial z}\right) = -\left(\frac{1}{r}\frac{\partial (r\,q_r)}{\partial r} + \frac{\partial q_z}{\partial z}\right) \qquad (8.1)$$

where r and z are the cylindrical coordinates in the radial and the axial directions, T is the temperature, v is the linear velocity, q is the heat flux per unit area, ρ is the density and Cp is the specific heat capacity. Applying the use of the definitions for heat flux:

$$q_r = -k\frac{\partial T}{\partial r} \qquad (8.2)$$

$$q_z = -k\frac{\partial T}{\partial z} \qquad (8.3)$$

leads to:

$$\rho C_p\left(\frac{\partial T}{\partial t} + v_r\frac{\partial T}{\partial r} + v_z\frac{\partial T}{\partial z}\right) = \frac{k}{r}\frac{\partial T}{\partial r} + k\frac{\partial^2 T}{\partial r^2} + k\frac{\partial^2 T}{\partial z^2} \qquad (8.4)$$

where k is the thermal conductivity. The continuity equation in cylindrical coordinates for incompressible flow is given by

$$\frac{1}{r}\frac{\partial (r\,v_r)}{\partial r} + \frac{\partial v_z}{\partial z} = 0 \qquad (8.5)$$

The initial and boundary conditions for equations (8.4) and (8.5) are:

I.C.: $T(r,\ z,\ t=0) = \psi(r,z)$ (8.6)

B.C.1: $q = -k\left(\frac{\partial T}{\partial r}\right)_i = h(T_{solid} - T_{fluid})$ on $A_i\ \forall\ t$ (8.7)

B.C.2: $\left(\frac{\partial T}{\partial r}\right)_{r=0} = 0$ at $r = 0\ \forall\ t$ (8.8)

B.C.3: $$v_z = \frac{W}{\rho A_f} \quad \text{at} \quad z = 0 \quad \forall \ t \tag{8.9}$$

B.C.4: $$v_r = \psi(\phi, W, \rho, A_l) \quad \text{on} \quad A_i \quad \forall \ t \tag{8.10}$$

where T_{solid} is the solid temperature and T_{fluid} is the fluid temperature, A_i is the interfacial area between the rock formation and the fluid, W is the drilling fluid mass flowrate, A_f is the cross sectional area for flow, ϕ is the formation porosity and A_l is the lateral flow area.

Equations (8.4) to (8.10) define in a general form the problem to be solved. However, the following aspects must be defined: (i) the functionality of T at $t = 0$, (ii) the convective heat transfer coefficient, h and (iii) the functionality presented by boundary condition given by equation (8.10). These aspects are addressed later on.

In order to apply all of these equations (8.4 to 8.10), a simplified scheme of the physical well drilling system was considered to define all the regions of it (Fig. 8.2). Figure 8.3 shows schematically an axial section of length Δz, the location and spacing of the radial grid. The radii of this figure correspond to each one of the physical regions in which the well is divided. Basically, five regions or components were identified as indispensable to consider in all the heat transfer analysis: (1) the drill pipe; (2) the drill pipe wall; (3) the annular region; (4) the interface between the well wall (cement or rock formation) and the annular region for fluid return; and (5) the formation (Fig. 8.2).

8.5.1 Mathematical formulation for the drill pipe model (Region 1)

This formulation enables the temperature distribution in the drill pipe to be determined. The model is complemented by the following three considerations:

- The first is the inlet drilling fluid temperature (T_{in}) which is a boundary condition for the model.

- The second is the mass flowrate of the drilling fluid (W). It is needed for calculating the fluid velocity which is a boundary condition for the model.
- The third is the temperature of the drill pipe metal wall (T_2) which is calculated by the drill pipe wall model (region 2).

The convective heat transfer coefficient (h_1) is also needed and is calculated separately in a module of the simulator. Since the flow is in the axial direction, equations (8.4) to (8.10) reduce to:

$$\rho_1 C_{p1}\left(\frac{\partial T_1}{\partial t} + v_{z1}\frac{\partial T_1}{\partial z}\right) = \frac{k_1}{r}\frac{\partial T_1}{\partial r} + k_1\frac{\partial^2 T_1}{\partial r^2} + k_1\frac{\partial^2 T_1}{\partial z^2} \qquad (8.11)$$

$$\frac{\partial v_{z1}}{\partial z} = 0 \qquad (8.12)$$

where the subscript 1 indicates the axial node where the temperature is calculated. The initial and boundary conditions are still valid except boundary condition (B.C. 4) or equation (8.10). For convenience, the boundary condition (1) is rewritten as follows:

$$\text{B.C.1:} \qquad -k_1\left(\frac{\partial T_1}{\partial r}\right)_{r=r_1} = h_1(T_2 - T_1) \quad \text{at } r = r_1 \;\forall\; t \qquad (8.13)$$

As noted, the subscripts were changed to indicate the drill pipe region. It is very important to note that in this section, the radial temperature gradient within the fluid may be neglected $(\partial T/\partial r)_{fluid}=0$.

8.5.2 Mathematical formulation for the drill pipe wall model (Region 2)

This formulation enables the temperature distribution in the drill pipe wall to be estimated. Its conditions are defined by the following five considerations:

- The first is the metal pipe wall temperature at the surface T_{ws} at z=0.
- The second is the drilling fluid temperature (T_1) which is calculated by means of the drill pipe model (region 1).

- The third is the temperature of the return fluid in the annulus (T_a) which is calculated by the annular model (region 3).
- The fourth is the drilling fluid mass flowrate in the drill pipe (W).
- The fifth is the mass flowrate of drilling fluid in the annulus section.

At the boundary, the heat transfer coefficient denoted by h_{11} is needed and is calculated in a module of the simulator for the fluid in the drill pipe and the heat transfer coefficient for the fluid in the annulus h_{22}, which is calculated separately in another module of the simulator. In this case, equations (8.4) to (8.10) reduce to:

$$\rho_2 C_{p2} \frac{\partial T_2}{\partial t} = \frac{k_2}{r}\frac{\partial T_2}{\partial r} + k_2 \frac{\partial^2 T_2}{\partial r^2} + k_2 \frac{\partial^2 T_2}{\partial z^2} \qquad (8.14)$$

where the subscript 2 indicates that the calculations are carried out for the drill pipe metal wall. The initial and boundary conditions I.C.1, B.C.1 and B.C.2 still exist but boundary conditions B.C.3 and B.C.4 no longer apply. During the solution, B.C.1 is applied twice: initially at the interface denoted by $r = r_1$ and then at the interface of the returning fluid by the annular region ($r = r_2$). Explicitly:

$$\text{B.C.1:} \quad - k_1 \left(\frac{\partial T_1}{\partial r}\right)_{r=r_1} = h_{11}(T_2 - T_1) \quad \text{at } r = r_1 \ \forall \ t \qquad (8.15)$$

$$\text{B.C.1.1:} \quad - k_3 \left(\frac{\partial T_3}{\partial r}\right)_{r=r_2} = h_{22}(T_2 - T_3) \quad \text{at } r = r_2 \ \forall \ t \qquad (8.16)$$

where the subscripts denote the particular region under consideration. If lost circulation is present, the velocity in the annulus is affected as well as the heat transfer coefficient h_{22}. These effects are properly considered in the present model.

Modelling of the lost circulation process. Circulation losses are calculated in the drill pipe wall model via the computational strategy. To estimate the

convective heat transfer coefficient in the annulus h_{22} at $r = r_2$, the fluid velocity in the annulus v_{z3} must be known. Of course, this velocity is different if no circulation losses exist. The mass flowrate of the drilling fluid losses (W_{fu}) is accounted for according to:

$$W_{fu} = W \cdot \xi \tag{8.17}$$

where W is the inlet mass flowrate of the drilling fluid and ξ is a multiplier which takes values between 0 and 1. If $\xi = 0$ no losses occur and if $\xi = 1$ all the drilling fluid is lost to the formation. Knowing this value, the axial velocity can be calculated from equation (8.5).

8.5.3 Mathematical formulation for the annular model (Region 3)

This formulation enables the temperature distribution in the annular region to be estimated. Its conditions are defined by the following four considerations:

- The first is the temperature at the bottom of the hole (T_1) which is calculated by means of the drill pipe model (region 1).
- The second is the mass flow rate of drilling fluid (W).
- The third is the temperature of the drill pipe metal wall (T_2) which is calculated by means of the drill pipe wall model (region 2).
- The fourth is the temperature of the annular fluid and the well inside wall (T_4) which is calculated by means of the heat transfer model of the region 4.

The convective heat transfer coefficients at the drill pipe wall, i.e., $r = r_2$ denoted by h_{22} and at $r = r_3$, denoted by h_{33}, are needed. These are calculated in the simulator by means of their corresponding modules. For this case, equations (8.4) to (8.10) are simplified to:

$$\rho_3 C_{p3}\left(\frac{\partial T_3}{\partial t} + v_{z3}\frac{\partial T_3}{\partial z}\right) = \frac{k_3}{r}\frac{\partial T_3}{\partial r} + k_3\frac{\partial^2 T_3}{\partial r^2} + k_3\frac{\partial^2 T_3}{\partial z^2} \tag{8.18}$$

$$\frac{1}{r}\frac{\partial(r\,v_r)}{\partial r} + \frac{\partial v_{z3}}{\partial z} = 0 \qquad (8.19)$$

$$\text{B.C.1.1:} \quad -k_3\left(\frac{\partial T_3}{\partial r}\right)_{r=r_3} = h_{22}(T_2 - T_3) \quad \text{at } r = r_2 \;\forall\; t \qquad (8.20)$$

$$\text{B.C.1.2:} \quad -k_3\left(\frac{\partial T_3}{\partial r}\right)_{r=r_3} = h_{eff}(T_4 - T_3) \quad \text{at } r = r_3 \;\forall\; t \qquad (8.21)$$

where the effective heat transfer coefficient h_{eff} considers the effect of porosity. This effect is quantified according to:

$$h_{eff} = h_{33}(1 - \phi) \qquad (8.22)$$

where h_{33} is the heat transfer coefficient for an impermeable wall and ϕ is the formation porosity.

8.5.4 Mathematical formulation for the interface between the well wall (cement or rock formation) and the annular region for the fluid return model (region 4)

This formulation enables the temperature distribution at the interface between the well wall (cement or rock formation) and the annular region for the fluid return to be calculated. This interface is important since it mathematically couples the surrounding formation with the flow in the annulus and should guarantee continuity of the heat flux during circulation and shut-in conditions. Its boundary conditions are complemented by the following three considerations:

- The first is the annulus fluid temperature (T_3) which is calculated by means of the annular heat transfer model (region 3).
- The second is the rock formation temperature with or without cemented sections (T_5) which is calculated by means of the formation heat transfer model (region 5).

- The third is the mass flowrate of the fluid ascending in the annulus (W).

The convective heat transfer coefficient needed in this case is h_3 which is calculated by its respective module in the simulator. In order to satisfy continuity of heat flow under circulation and shut-in conditions, the energy equation for this case is:

B.C.1.4:

$$k_3 \left(\frac{\partial T_3}{\partial r}\right)_{r=r_3} = h_{eff}(T_4 - T_3) = k_{eff} \left(\frac{\partial T_f}{\partial r}\right)_{r=r_3} \quad \text{at } r = r_3 \; \forall \; t \tag{8.23}$$

where k_{eff} is the effective thermal conductivity which depends on the porosity and the thermal conductivities of the formation and the drilling fluid. This boundary condition guarantees continuity of heat flow under shut-in conditions since for such conditions h_{eff} is zero, otherwise it is given by equation (8.22).

8.5.5 Mathematical formulation for the formation model (Region 5)

This formulation enables the axial and radial temperature distributions in the formation with or without a cemented section to be estimated. The conditions for this region are complemented by the following two considerations:

- The first is the ambient or surface temperature (T_s) at $z = 0$ for all r.
- The second is the temperature at the interface of the well wall (T_4) which is calculated by means of the heat transfer model corresponding to the region 4.

For this case, equations (8.4) to (8.10) simplify to:

$$(\rho C_p)_{eff}\left(\frac{\partial T_f}{\partial t} + v_r \frac{\partial T_f}{\partial r}\right) = \frac{k_{eff}}{r}\frac{\partial T_f}{\partial r} + k_{eff}\frac{\partial^2 T_f}{\partial r^2} + k_{eff}\frac{\partial^2 T_f}{\partial z^2} \tag{8.24}$$

$$\frac{\partial (r\, v_r)}{\partial r} = 0 \tag{8.25}$$

where the physical properties are given by:

$$k_{eff} = k_3^{\phi} k_f^{(1-\phi)} \tag{8.26}$$

$$(\rho C_p)_{eff} = (\rho C_p)_f (1 - \phi) + (\rho C_p)_3 \phi \tag{8.27}$$

where subscripts ϕ and 3 correspond to the formation and the fluid flowing up the annulus, respectively. If $\phi = 0$, the original equations are recovered.

8.5.6 Fluid convective heat transfer coefficients

Heat transfer coefficients are calculated separately for the drill pipe and for the annular region. The heat transfer coefficient for laminar flow in the annulus is calculated from the Seider and Tate (1936) correlation, equation (7.24, Chapter 7):

$$Nu = 1.86(RePr)^{1/3}\left(\frac{D_h}{L}\right)^{1/3}\left(\frac{\mu}{\mu_w}\right)^{0.14} \quad \text{para} \quad Re < 2300 \tag{8.28}$$

where Nu is the Nusselt number, Re is the Reynolds number, Pr is the Prandtl number, D_h is the hydraulic diameter, L is the pipe length and the viscosity ratio is approximately 1. The dimensionless numbers were previously defined and evaluated in Chapter 7, equations (7.1) to (7.4).

For laminar flow inside the drill pipe, the following analytical solution is used:

$$Nu = 4.364 \qquad \text{for} \quad Re < 2300 \tag{8.29}$$

For transitional and turbulent flow, Gnielinsky's correlation [Incropera and Dewitt (1990)] is used:

$$Nu = \frac{(f/8)(Re - 1000)Pr}{1 + 12.7\sqrt{f/8}(Pr^{2/3} - 1)} \quad \text{for} \quad Re > 2300 \tag{8.30}$$

where the friction factor is given by:

$$f = [1.82\log(Re) - 1.64]^{-2} \tag{8.31}$$

The correlation given by equation (8.30) is used for flow both in the drill pipe and the annulus.

8.5.7 Numerical solution scheme

The differential equations described above are transformed into discrete equations using the technique of finite differences in an implicit form. The resulting set of non linear algebraic equations are then solved using an iterative method. The finite difference definitions used in the present case are as follows. The spatial first order discretization is defined as:

$$\frac{\partial T}{\partial \varphi} = \frac{T_m^{t+\Delta t} - T_m^t}{2 \cdot \Delta \varphi} \tag{8.32}$$

where T is the dependent variable, $t+\Delta t$ indicates that the variable is evaluated at the present time, m indicates the node number and $\Delta\varphi$ is the step increment in the space coordinate. In the foregoing equation, the following convention was used:

radial direction: $m = i$ and $\varphi = r$

axial direction: $m = j$ and $\varphi = z$

The second order space derivatives are approximated by:

$$\frac{\partial^2 T}{\partial \varphi^2} = \frac{T_{m+1}^{t+\Delta t} - 2T_m^{t+\Delta t} + T_{m-1}^{t+\Delta t}}{(\Delta\varphi)^2} \tag{8.33}$$

The time discretization at node or cell m is given by:

$$\frac{\partial T}{\partial t} = \frac{T_m^{t+\Delta t} - T_m^t}{\Delta t} \tag{8.34}$$

where t is the time, T_m^t is the value of the calculated variable at the past time, $T_m^{t+\Delta t}$ is the value of the variable at the present time and Δt is the integration time step. Application of the above definitions enables the equation for each region to be written in a single generalized vector form:

$$A\,T_{m-1}^{t+\Delta t} + B\,T_{m}^{t+\Delta t} + C\,T_{m+1}^{t+\Delta t} = D \tag{8.35}$$

where A, B, C and D are the vectors of the coefficients. Equation (8.35) has the form of a tridiagonal matrix which can be solved by Thomas algorithm [(Patankar, 1979)] which is the one of the most efficient algorithms for this type of matrix. Equation (8.35) is directly applied to the following regions 1, 2 and 3.

In the formation, heat transfer is two dimensional and the solution employs the alternating direction algorithm which consists of solving for the temperatures in one direction in an implicit form and solving in an explicit form for the other direction. This process is carried out for half the time step. In the second half of a complete time step, the former explicit direction is changed to an implicit form and the other direction is changed to an explicit form. Mathematically, this can be written as:

- implicit in z (j) and explicit in r (i):

$$A_z T_{i,j-1}^{t+\Delta t/2} + B_z T_{i,j}^{t+\Delta t/2} + C_z T_{i,j+1}^{t+\Delta t/2} = D_z \tag{8.36}$$

- implicit in r (i) and explicit in z (j):

$$A_r T_{i-1,j}^{t+\Delta t/2} + B_r T_{i,j}^{t+\Delta t/2} + C_r T_{i+1,j}^{t+\Delta t/2} = D_r \tag{8.37}$$

Velocity calculation. The velocity in the drill pipe is given by:

$$v_{1,j} = v_{1,j-1} \tag{8.38}$$

where subscript 1 indicates a radial node and subscript j indicates axial nodes. The velocity can also be defined as:

$$v_{1,j-1} = \frac{W}{\rho_1 A_f} \tag{8.39}$$

This velocity is calculated in the drill pipe heat transfer model (region 1) and only changes if the density changes since the mass flowrate is constant. The velocity in

the annulus is affected by the lost circulation and its numerical expression is obtained from equation (8.19):

$$v_{3,j} = v_{3,j-1} - \frac{2 r_3 \Delta z_j}{(r_3^2 - r_2^2)} v_{i+1,j} \quad \text{for } i \geq 2 \ \forall \ j \qquad (8.40)$$

where $v_{i,j} = 0$ due to the drill pipe metal wall. The radial velocity appearing in equation (8.40) may be obtained as a function of the circulation losses:

$$v_{i+1,j} = \frac{W_{fu}}{\rho_3 2\pi r_3 \Delta z_j \phi} \quad \text{for } i \geq 2 \ \forall \ j \qquad (8.41)$$

where W is defined by equation (8.17). Equations (8.40) and (8.41) are calculated in the drill pipe wall heat transfer model (region 2). The velocity in the rock is given by equation (8.25) and after application of the method, can be written as:

$$v_{i,j} = \frac{r_{i-1}}{r_i} v_{i-1,j} \quad \text{for } i \geq 4 \ \forall \ j \qquad (8.42)$$

This velocity is calculated in the formation heat transfer model (region 5).

8.5.8 Evaluation of the coefficient vectors

In this section the coefficient vectors of the finite difference equations system (8.35) corresponding to each region of the well are defined.

- Drill pipe heat transfer model (region 1):

$$A_j = - v_{1j} \left(\frac{\Delta t}{2 \Delta z_j} \right) - \frac{k_1}{\rho_1 Cp_1} \left(\frac{\Delta t}{\Delta z_j^2} \right) \qquad (8.43)$$

$$B_j = 1 + \left(\frac{2 h_{11}}{r_{in}} + \frac{2 k_1}{\Delta z_j^2} + \frac{3 k_1}{r_{in}^2} \right) \left(\frac{\Delta t}{\rho_1 Cp_1} \right) \qquad (8.44)$$

$$C_j = v_{1j}\left(\frac{\Delta t}{2\,\Delta z_j}\right) - \frac{k_1}{\rho_1\, Cp_1}\left(\frac{\Delta t}{\Delta z_j^2}\right) \tag{8.45}$$

$$D_j = T_{1,j}^t + \left(\frac{2\,h_{11}}{r_{in}} + \frac{2\,k_1}{\Delta z_j^2} + \frac{3\,k_1}{r_{in}^2}\right)\left(\frac{\Delta t}{\rho_1\, Cp_1}\right) T_{2,j}^t \tag{8.46}$$

These equations (8.43) to (8.46) apply for j = 2, 3, 4, ..., n; where n represents the total number of elements (or cells) in the axial direction. In order to apply the Thomas algorithm [Patankar (1979)], the following variables need to determined:

$$D_2' = D_2 - A_2\, T_{1,1}^t \tag{8.47}$$

$$D_n' = D_n - C_n\, T_{1,n}^t \tag{8.48}$$

$$T_{1,1}^t = T_{in} \tag{8.49}$$

where T_{in} is the inlet drilling fluid temperature at z=0. In all of these equations, the first subscript of the temperature variables indicate the radial element 1. It is important to note that under the thermal recovery operation (shut-in), the boundary condition is given by:

$$T_{1,1}^t = T_{2,1}^t \tag{8.50}$$

- Drill pipe wall heat transfer model (region 2):

$$A_j = -\frac{k_2}{\rho_2\, Cp_2}\left(\frac{\Delta t}{\Delta z_j^2}\right) \tag{8.51}$$

$$B_j = 1 + \left[\frac{2\,k_2}{\Delta z_j^2} + \frac{3\,k_1}{r_{in}^2 + \frac{1}{2}\left(\frac{r_a - r_{ext}}{2}\right)^2} + \frac{2\,(h_{11}\, r_{in} + h_{12}\, r_{ext})}{\left(r_{ext}^2 - r_{in}^2\right)}\right]\left(\frac{\Delta t}{\rho_2\, Cp_2}\right) \tag{8.52}$$

$$C_j = -\frac{k_2}{\rho_2 Cp_2}\left(\frac{\Delta t}{\Delta z_j^2}\right) \tag{8.53}$$

$$D_j = T_{2,j}^t + \left[\frac{2\left(h_{11}\, r_{in}\, T_{1,j}^t\right) + 2\left(h_{22}\, r_{ext}\, T_{3,j}^t\right)}{\left(r_{ext}^2 - r_{in}^2\right)} + \frac{2\, k_1\left(T_{1,j}^t + T_{3,j}^t\right)}{r_{in}^2 + \left(\frac{r_a - r_{ext}}{2}\right)^2} - \frac{k_1\left(T_{3,j}^t - T_{1,j}^t\right)}{\left(\frac{r_a + r_{ext}}{2}\right)\left(r_{in}^2 + \frac{r_a - r_{ext}}{2}\right)}\right]\left(\frac{\Delta t}{\rho_2\, Cp_2}\right) \tag{8.54}$$

These equations are applied for j=1, 3, 4, ..., n; where n is the total number of elements in the axial direction. In order to apply the Thomas algorithm, the following variables need to be defined:

$$D_1' = D_1 - A_1\, T_{2,1}^t \tag{8.55}$$

$$D_n' = D_n - C_n\, T_{2,n}^t \tag{8.56}$$

- Annular heat transfer model (region 3):

$$A_j = -\, v_{3j}\left(\frac{\Delta t}{2\,\Delta z_j}\right) - \frac{k_3}{\rho_3\, Cp_3}\left(\frac{\Delta t}{\Delta z_j^2}\right) \tag{8.57}$$

$$B_j = 1 + \left[\frac{2\left(h_{22}\, r_{ext} + h_{33}\, r_a\right)}{\left(r_a^2 - r_{ext}^2\right)} + \frac{2\, k_3}{\Delta z_j^2} + \frac{2\, k_3}{\left(\frac{r_a - r_{ext}}{2}\right)^2} + \right]\left(\frac{\Delta t}{\rho_3\, Cp_3}\right) \tag{8.58}$$

$$C_j = -\, v_{3j}\left(\frac{\Delta t}{2\,\Delta z_j}\right) + \frac{k_3}{\rho_3\, Cp_3}\left(\frac{\Delta t}{\Delta z_j^2}\right) \tag{8.59}$$

$$D_j = T^t_{3,j} + \left[\frac{2\,h_{22}\,r_{ext}}{\left(r_a^2 - r_{ext}^2\right)} + \frac{k_3}{\left(\frac{r_a - r_{ext}}{2}\right)^2}\right]\left(\frac{\Delta t}{\rho_3 Cp_3}\right) T^n_{2,j}$$

$$+ \left[\frac{2\,h_{33}\,r_a}{\left(r_a^2 - r_{ext}^2\right)} + \frac{k_3}{\left(\frac{r_a - r_{ext}}{2}\right)^2}\right]\left(\frac{\Delta t}{\rho_3 Cp_3}\right) T^n_{4,j} \qquad (8.60)$$

$$+ \left[\frac{k_3\left(T^n_{4,j} - T^n_{2,j}\right)}{\left(r_a - r_{ext}\right)\left(r_{ext} + \frac{r_a - r_{ext}}{2}\right)}\right]\left(\frac{\Delta t}{\rho_3 Cp_3}\right)$$

These equations are applied for j=1, 3, 4, ..., n-1; where n represents the total number of elements in the axial directions. In order to apply the Thomas algorithm, the following variables need to determined:

$$D'_1 = D_1 - A_1\,T^t_{3,1} \qquad (8.61)$$

$$D'_{n-1} = D_{n-1} - C_{n-1}\,T^t_{3,n} \qquad (8.62)$$

where

$$T^t_{3,n} = T^{t+\Delta t}_{1,n} \qquad (8.63)$$

where $T^{t+\Delta t}_{1,n}$ is the drilling fluid temperature at the bottomhole conditions. In these equations, the first subscript of the temperatures indicates the radial element (e.g. 1, 2, 3, etc..). It is important to note that under shut-in conditions (after the drilling activities are stopped) the boundary conditions are given by:

$$T^t_{3,n} = T^t_{4,n} \qquad (8.64)$$

- Interface between the well wall (cement or rock formation) and the annular region for fluid return model (region 4):

$$T_{4,j}^{t+\Delta t} = \left[\frac{\left(h_{33} + \frac{k_3}{\Delta r_3}\right)}{\left(h_{33} + \frac{k_{ef}}{\Delta r_4} + \frac{k_3}{\Delta r_3}\right)}\right] T_{3,j}^{t+\Delta t} + \left[\frac{\left(\frac{k_{ef}}{\Delta r_4}\right)}{\left(h_{33} + \frac{k_{ef}}{\Delta r_4} + \frac{k_3}{\Delta r_3}\right)}\right] T_{5,j}^{t+\Delta t} \qquad (8.65)$$

This equation is a boundary condition and then it can be directly solved without the use of the Thomas algorithm. The effective thermal conductivity is given by the equation (8.26).

- Formation heat transfer model (region 5):

As was mentioned previously, the solution of this model employs the alternating direction algorithm which consists of solving for the temperatures in one direction in an implicit form and solving in an explicit form for the other direction. Therefore the following applies:

The implicit solution in z(j) and explicit in r(i) [equation (8.36)] enables the coefficient vectors to be estimated by means of the following equations:

$$A_j = -\left[\left(\frac{k_{eff}}{2\,(\rho\,Cp)_{eff}\,\Delta z_j^2}\right)\right]\Delta t \qquad (8.66)$$

$$B_j = 1 + \left[\frac{k_{eff}}{2\,(\rho\,Cp)_{eff}\,\Delta z_j^2}\right]\Delta t \qquad (8.67)$$

$$C_j = \left[\left(\frac{k_{eff}}{2\,(\rho\,Cp)_{eff}\,\Delta z_j^2}\right)\right]\Delta t \qquad (8.68)$$

$$D_j = T^0_{5,j} + \left[\frac{k_{eff}}{(\rho\, Cp)_{eff}\left(\Delta r^2_{i-1} + \Delta r^2_i\right)}\right]\left(T^t_{i+1,j} - 2\,T^0_{5,j} + T^t_{i-1,j}\right)\Delta t$$

$$+\left[\frac{k_{eff}}{(\rho\, Cp)_{eff}\left(\Delta r^2_{i-1} + \Delta r^2_i\right)}\right]\left(T^t_{i+1,j} - T^t_{i-1,j}\right)\Delta t \qquad (8.69)$$

where $T^0_{5,j}$ is the variable on which the iterative process is applied. These equations are applied for: j=1, 3, 4, ..., n; where n is the total number of elements in the axial direction and for i=5, 6, 7, ..., m; where m is the total number of elements in the radial direction. In order to apply the Thomas algorithm, the following variables need to be defined:

$$D'_1 = D_1 - A_1\, T^t_{i,1} \quad \text{for } i \geq 5 \qquad (8.70)$$

$$D'_n = D_n - C_{n-1}\, T^t_{i,n+1} \quad \text{for } i \geq 5 \qquad (8.71)$$

The implicit solution in r(i) and the explicit in z(j) [equation (8.37)] enables the coefficient vectors to be estimated by means of the following equations:

$$A_j = -\left[\left(\frac{k_{eff}}{(\rho\, Cp)_{eff}\left(\Delta r^2_{i-1} + \Delta r^2_i\right)}\right)\right]\Delta t \qquad (8.72)$$

$$B_j = 1 + \left[\frac{2\,k_{eff}}{(\rho\, Cp)_{eff}\left(\Delta r^2_{i-1} + \Delta r^2_i\right)}\right]\Delta t \qquad (8.73)$$

$$C_j = \left[\left(\frac{k_{eff}}{(\rho\, Cp)_{eff}\left(\Delta r^2_{i-1} + \Delta r^2_i\right)}\right)\right]\Delta t \qquad (8.74)$$

$$D_j = T^0_{i,j} + \left[\frac{k_{eff}}{2\,(\rho\,Cp)_{eff}\,\Delta z_j^2}\right]\left(T^t_{i,j+1} - 2\,T^0_{i,j} + T^t_{i,j-1}\right)\Delta t$$

$$+\left[\frac{\left(\frac{k_{eff}}{r_i} - v_{i,j}\,\rho_3\,Cp_3\right)}{2\,(\rho\,Cp)_{eff}\;2\,(\Delta z_j)}\right]\left(T^t_{i,j+1} - T^t_{i,j-1}\right)\Delta t \qquad (8.75)$$

where $T^0_{i,j}$ is the variable on which the iterative process is applied. These equations are applied for: j=1, 3, 4, ..., n; where n is the total number of elements in the axial direction and for i=5, 6, 7, ..., m-1; where m is the total number of elements in the radial direction. In order to apply the Thomas algorithm, the following variables need to be defined:

$$D'_5 = D_5 - A_5\,T^t_{4,j} \qquad (8.76)$$

$$D'_{m-1} = D_{m-1} - C_{m-1}\,T^t_{m,j} \qquad (8.77)$$

8.6 Numerical Grid

A grid system has been defined whereby four temperatures are computed in the wellbore system at each depth. Mathematical cells are designed with the radial boundaries at four locations, the wellbore axis, the wall drill pipe, the annulus and the interface wellbore/formation (Fig. 8.2). The centreline of the fourth cell is located at the wellbore/formation interface.

Temperature nodes are located at the centres of the cells. The first node is for the fluid in the drill pipe, which gives the circulating fluid temperature, or simply a temperature at the wellbore axis during the shut-in process. The second node is located to compute the wall drill pipe temperature. The third node is located to calculate the annular fluid temperature durin the circulation or the shut-in process. The fourth node serves as an interface between the wellbore and the formations calculations by being located at the boundary between the two regions.

Cell dimensions in the wellbore can be defined during the simulation runs on the basis of the wellbore geometry (number of the completion sections). Thus, each cell can be defined to be a hundred meters long and a few centimeters to a few meters in radial width.

Nodal points in the formation are located at the same vertical positions as those in the wellbore. Cell length should be small enough to permit acceptable grid refinement to efficiently model a wellbore, yet sufficiently long to avoid unnecessary computations by using too many grid points. Experience indicates that 30 m to 150 m is a reasonable size. As a reference, one additional row of formation cells are placed below the maximum depth and it serves as a fixed temperature boundary.

In the radial direction temperatures gradients are much greater near the well, so nodal locations are concentrated in this region. A computer subroutine (DATA1) has been written to generate the radial positions of the nodes. Cell width is exponentially increased with radius to produce a grid as illustrated in Fig. 8.3.

8.7 Architecture of the Simulator (WELLTHER)

On the basis of the mathematical development of the models of each of the heat transfer regions involved in the dynamic wellbore thermal simulator, a computer code was developed.

8.7.1 Software development

WELLTHER is a computer code developed for estimating the dynamic temperature distribution in and around a wellbore under drilling and shut-in operations. This computer code is based on the equations of the heat transfer models of a geothermal wellbore drilling system which were referred to in the previous section. WELLTHER was written in the Fortran 77 language using the Microsoft Fortran 77 compiler for personal computers [Microsoft (1990)].

Figure 8.4 shows the flow diagram of the main program. In its general form, the architecture of the computer program developed is:

(i) a main program of the simulator (WELLTHER),

(ii) three input data files (INPUT, DISTEMP, T_DOWN, and PHI),

(iii) eight output data files (REPORT, CIRCULA, RECOVER, ROCK_CIRC, ROCK_REC, TIME, LOST, and PHOTO),

and

(iv) eleven subroutines or modules (DATA, DATA1, INITIAL, TDPIPE, TMET, TANU, TINTER, TROCK, COEFCON, COEFCONA and TRIDAG).

WELLTHER is the main program. It reads the input data and controls the execution of the subroutines or modules for calculating the temperature distributions in each of the heat transfer regions under transient conditions. WELLTHER decides the organisation of the data reading using any of the input data files. WELLTHER also dumps the results of the temperature distribution in and around the wellbore during the transient numerical simulation to the output data files. Figure 8.5 shows a simplified flow diagram of the interaction numerical procedure between the subroutines involved with this program.

DATA is the subroutine that reads and stores all the information related to the characterisation of the geothermal wellbore geometry and the thermophysical and transport properties of the fluid, the drill pipe (casing), the cement materials and the formation. DATA uses the input data file INPUT and dumps all the read information to the output data file REPORT. A simplified flow diagram of this subroutine is presented in Fig. 8.6.

DATA1 is the subroutine that defines the radial and axial grid or mesh of the wellbore and the surrounding formation which will be used during the solution of the finite difference equations system. DATA also assigns all the thermophysical properties to the main components of the system (drill pipe, annulus, formation, casing, cement, etc.). A simplified flow diagram of this subroutine is shown in Fig. 8.7.

INITIAL is the subroutine that enables the initial temperature of the geothermal wellbore system to be estimated by means of a linear approximation (using the surface temperature and the geothermal gradient) or by means of temperature data files obtained either during the wellbore temperature logging or during the itself numerical simulation. Fig. 8.8 shows a simplified flow diagram of this subroutine.

TDPIPE is the subroutine that computes the fluid temperature distribution in the axial direction of the drill pipe during and after the drilling operations (heat transfer region 1). A simplified flow diagram related to the computations performed by this subroutine is presented in Fig. 8.9.

TMET is the subroutine that determines the temperature distribution in the axial direction of the wall drill pipe (heat transfer region 2). This subroutine also computes the mass flowrate distribution due to the fluid losses, the linear velocities of the fluid in the axial direction and the linear velocities of fluid in the radial direction (in the wellbore face). Fig. 8.10 presents a simplified flow diagram of this subroutine.

TANU is the subroutine that computes the fluid temperature distribution inside the annular section of the wellbore during and after the drilling operations (heat transfer region 3). A simplified flow diagram that describes the numerical computations made by this subroutine is shown in Fig. 8.11.

TINTER is the subroutine that estimates the temperature profile in the interface between the annular section and the formation with or without wellbore cementation. Fig. 8.12 shows a simplified flow diagram of this subroutine.

TROCK is the subroutine that computes the linear velocities of the drilling fluid in the axial and radial directions under transient conditions, including the linear velocity of fluid under the lost circulation of it to the formation. TROCK also calculates the temperature distribution both in the axial and the radial directions under dynamic conditions. The capability of the numerical code

(WELLTHER) enables the porosity effects on the rock to be simulated. Figures 8.13a and 8.13b present the simplified flow diagrams of this subroutine.

COEFCONT is the subroutine that enables the convective heat transfer coefficients of the drilling fluid in the drill pipe to be estimated. These calculations can be performed under laminar or turbulent flow conditions. Figure 8.14 shows a simplified flow diagram of this subroutine. COEFCONT also links the VISTEMPEQ database to calculate the drilling fluid viscosities.

COEFCONA is the subroutine that enables the convective heat transfer coefficients of the drilling fluid in the annular section to be estimated. These calculations can be performed under laminar or turbulent flow conditions. Figure 8.15 shows a simplified flow diagram of this subroutine. COEFCONA also links the VISTEMPEQ database to calculate the drilling fluid viscosities.

TRIDAG is the subroutine that solves the tridigonal matrix in order to obtain the solution of the temperatures at the actual time.

8.8 Numerical procedure

The methodology for the solution is briefly described next. The input data file must be prepared with information on the well geometry, the thermophysical properties of the drilling fluid, cement, rock and pipe metal, the fluid viscosity and flowrate and the simulation time. The initial temperature may be calculated by the code from the surface temperature and geothermal gradient if it is linear. However the initial temperature may be calculated from the input in tabular form if it is nonlinear. Data may be input interactively or from an input data file. The distribution of porosity on the inner face of the well and the surrounding formation is fed in tabular form. If an initial temperature is not available, this can be constructed from the temperature logs as a first approximation and refined as the numerical simulation proceeds.

8.9 References

F.P. Incropera and D.P. Dewitt, Introduction to heat transfer, John Wiley & Sons, Inc., New York, USA (1990).

Microsoft, FORTRAN 77 professional development system for MS-DOS, User's Manual, Microsoft Co., 300 p. (1990).

S.V. Patankar, Numerical heat transfer and fluid flow, McGraw-Hill Book Co., New York, USA, pp. 52 (1979).

E.N. Seider and G.E. Tate, Heat transfer and pressure drop of liquids in tubes, Ind. Eng. Chem. **28** p. 1429 (1936).

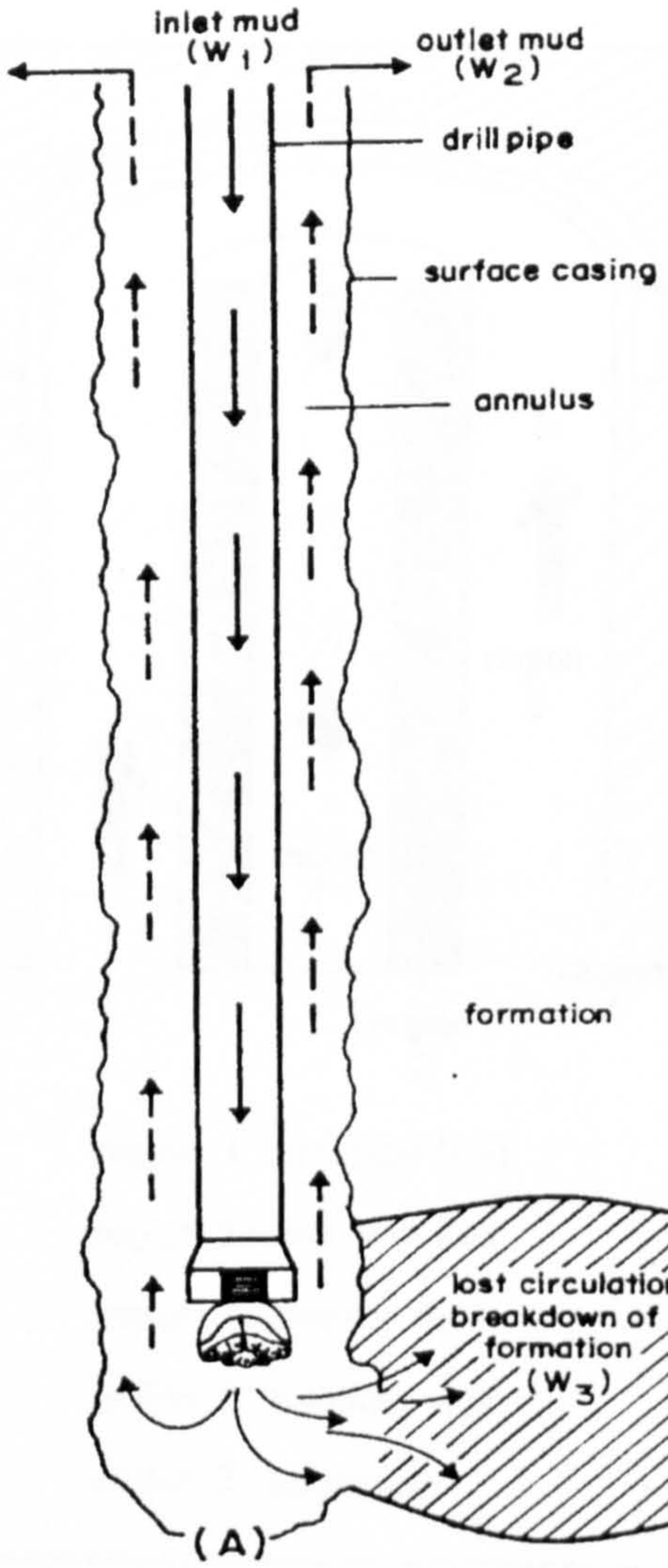

Fig. 8.1 Physical model of the actual drilling fluid circulation and the lost circulation problem during drilling of a geothermal well.

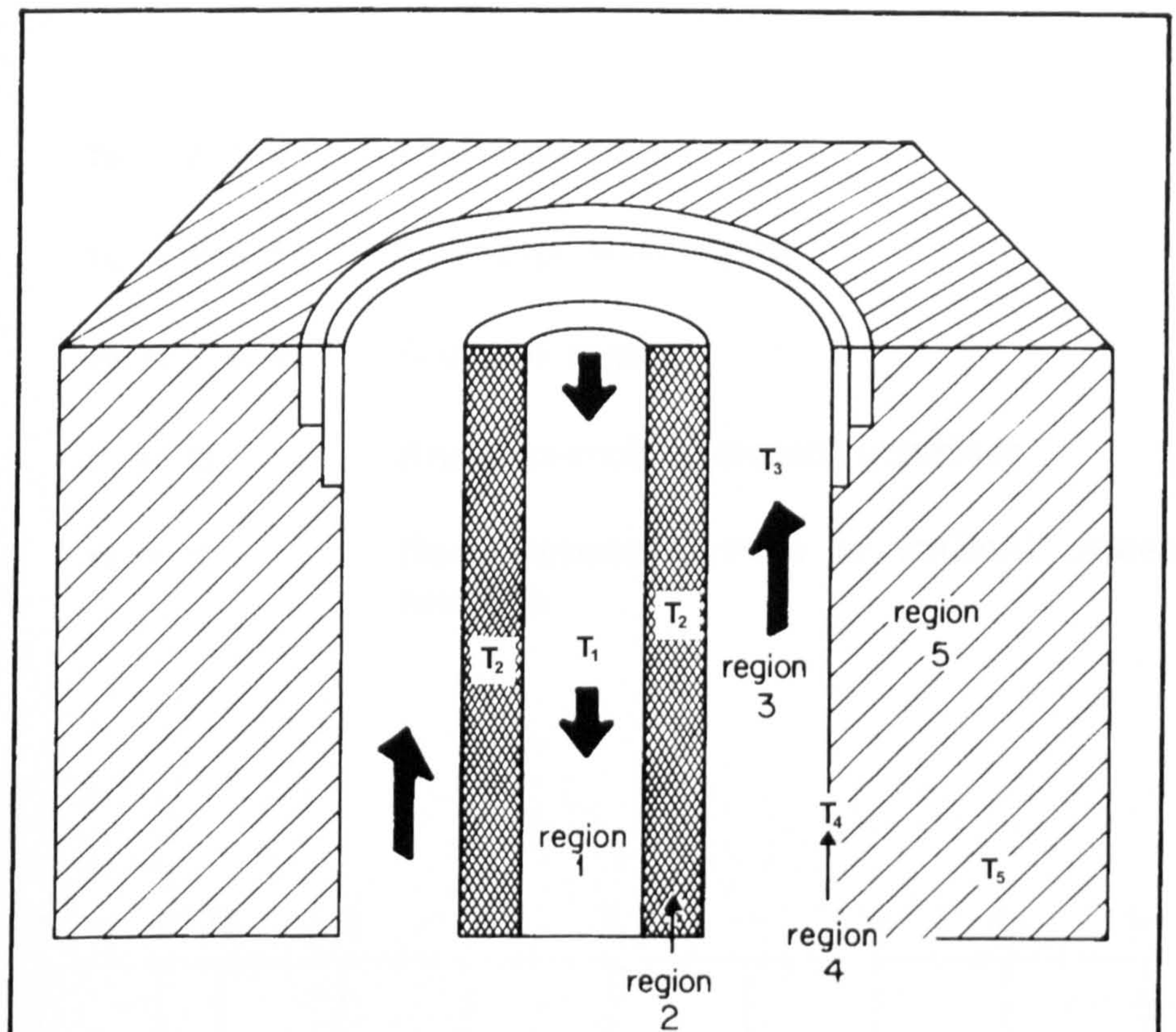

Fig. 8.2 Schematic diagram of the heat flow regions in a wellbore drilling system.

$r_0 \leq r \leq r_1$	Drill pipe region
$r_1 \leq r \leq r_2$	Drill pipe wall region
$r_2 \leq r \leq r_3$	Annular region
$r = r_3$	Annulus-rock or cement interface
$r_3 > r$	Rock formation with or without cement sections

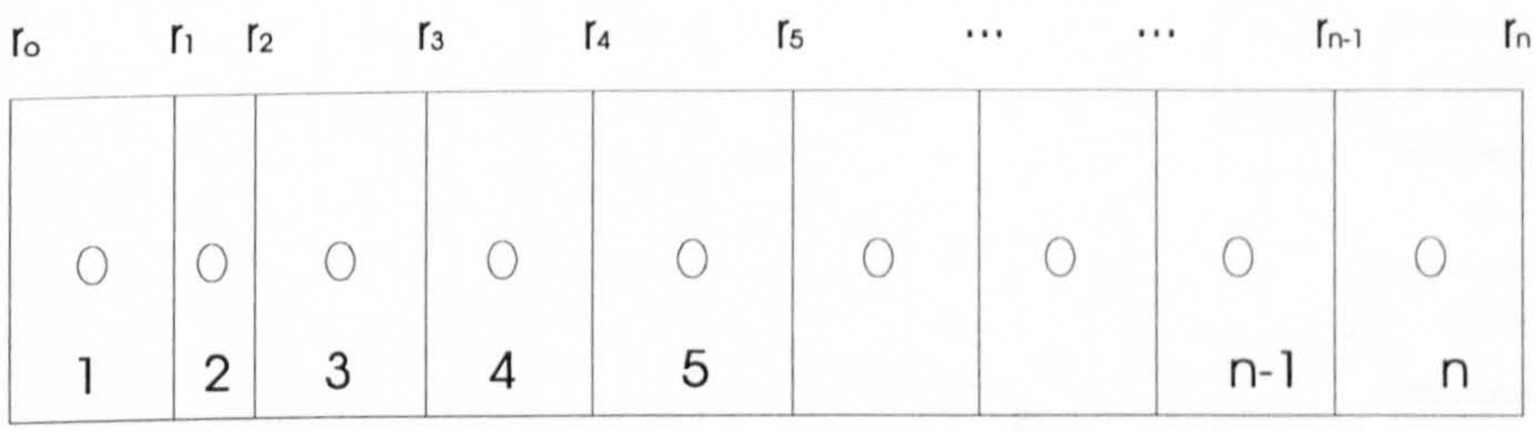

Fig. 8.3 Schematic diagram where r indicates the boundaries of each radial region on an axial segment of the well and "o" indicates the cell where the computations are performed.

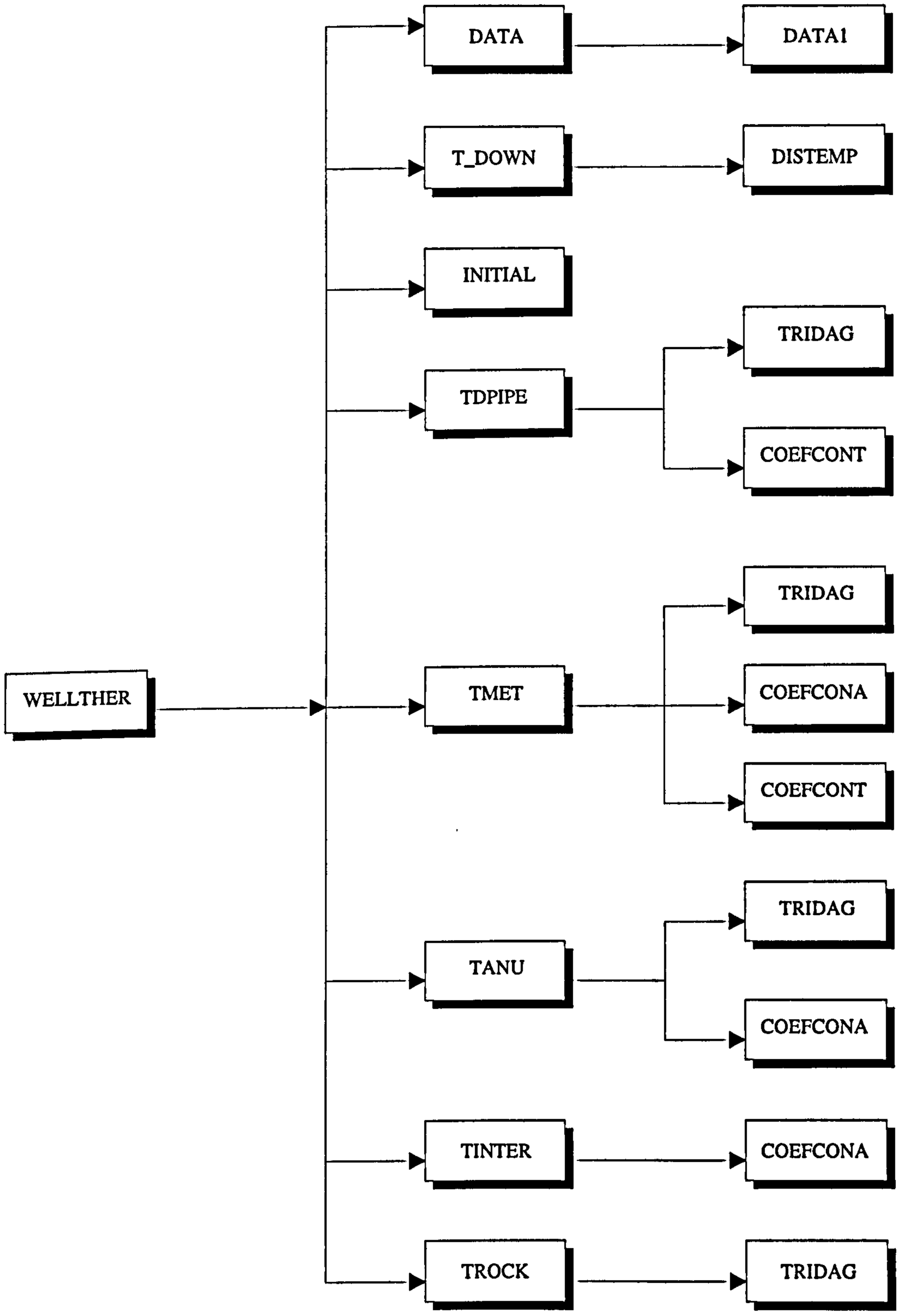

Fig. 8.4 Computer architecture of the dynamic wellbore thermal simulator (WELLTHER).

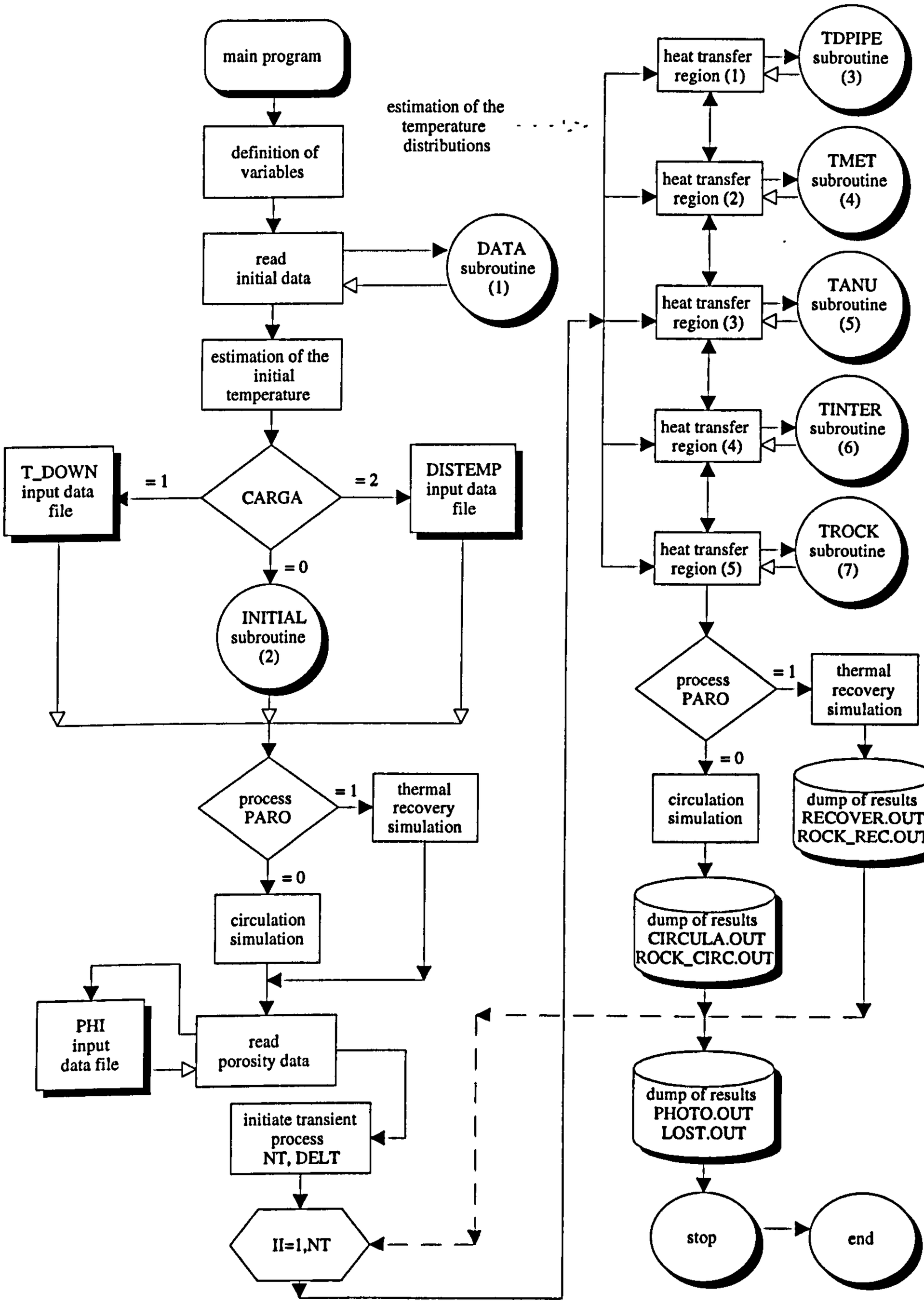

Fig. 8.5 Flow diagram of the main program of the dynamic wellbore thermal simulator (WELLTHER).

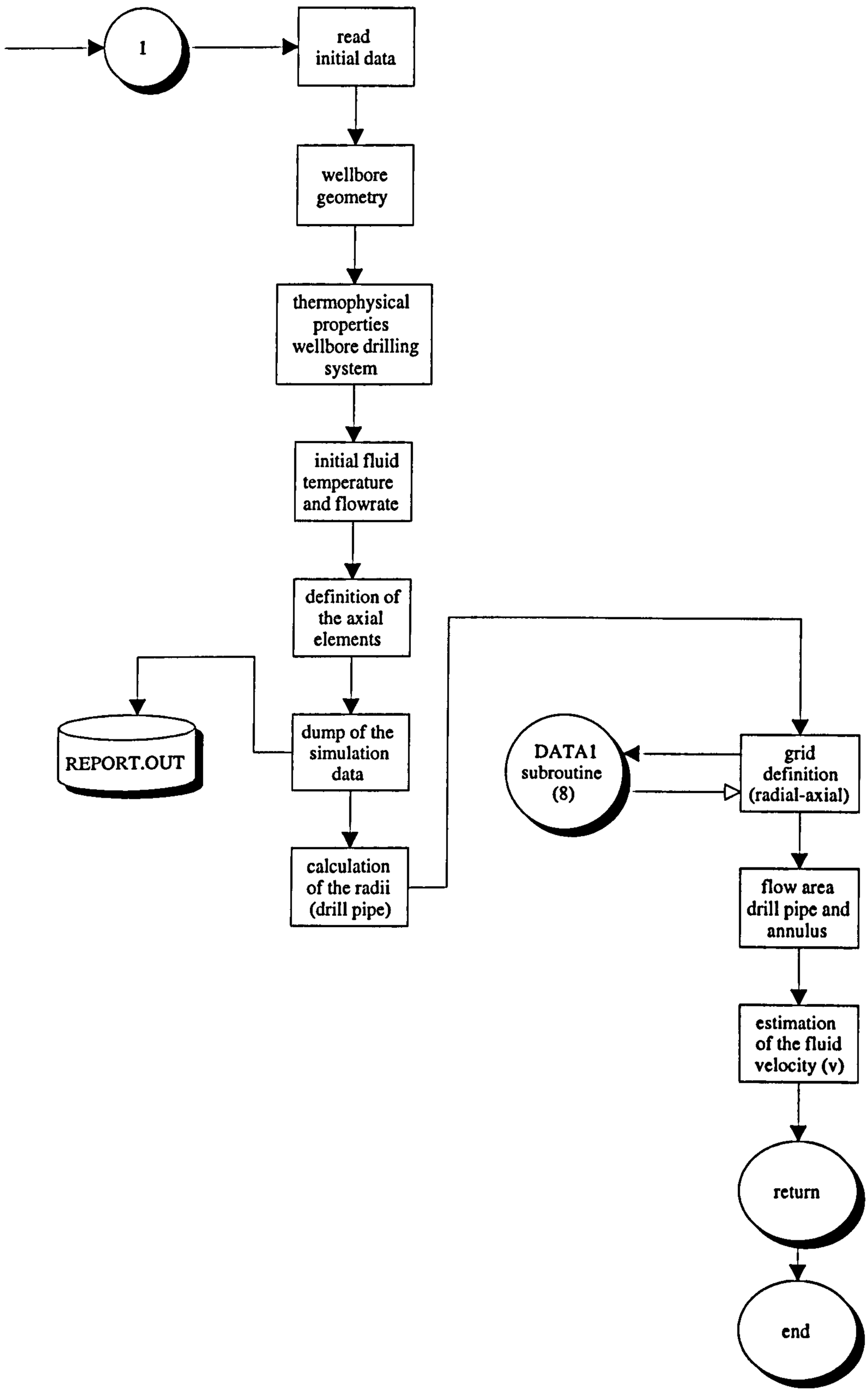

Fig. 8.6 Flow diagram of the DATA subroutine.

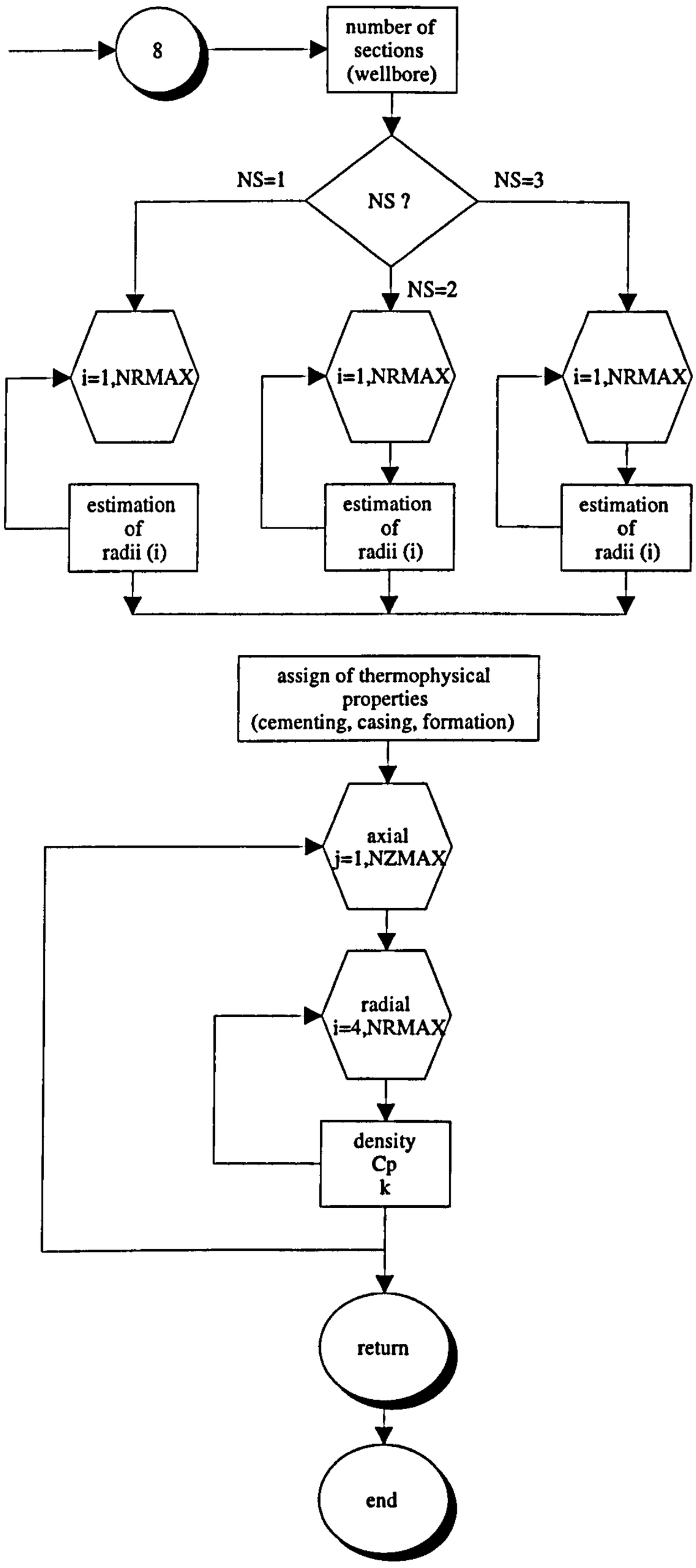

Fig. 8.7 Flow diagram of the DATA1 subroutine.

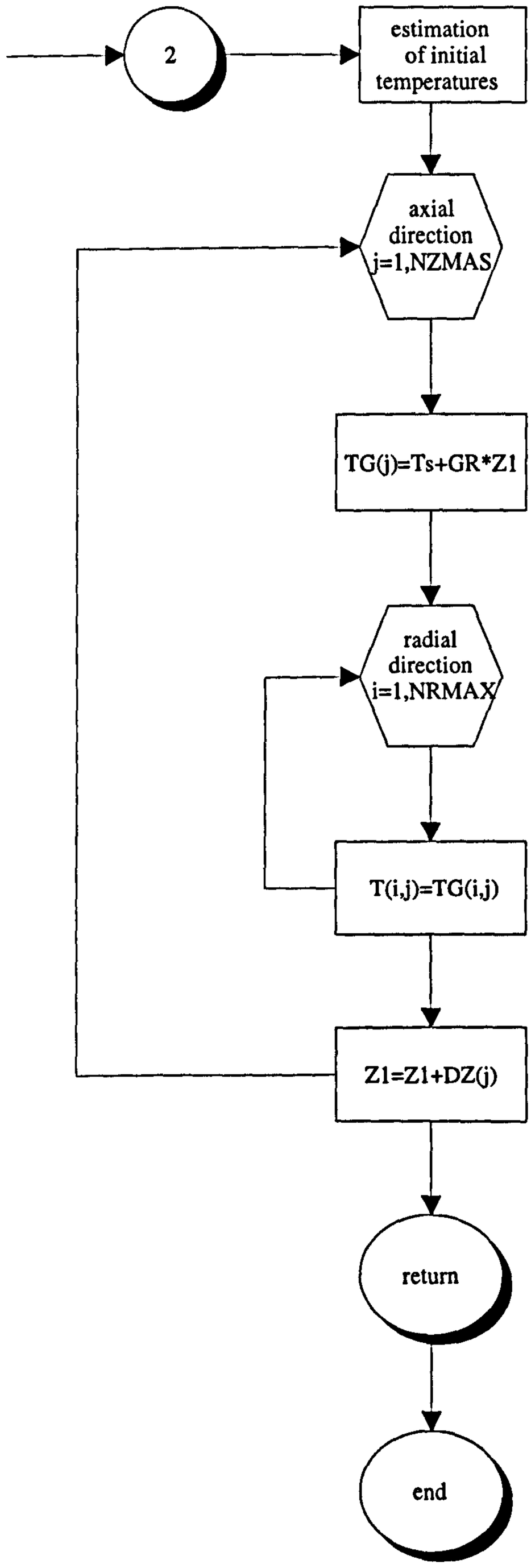

Fig. 8.8 Flow diagram of the INITIAL subroutine.

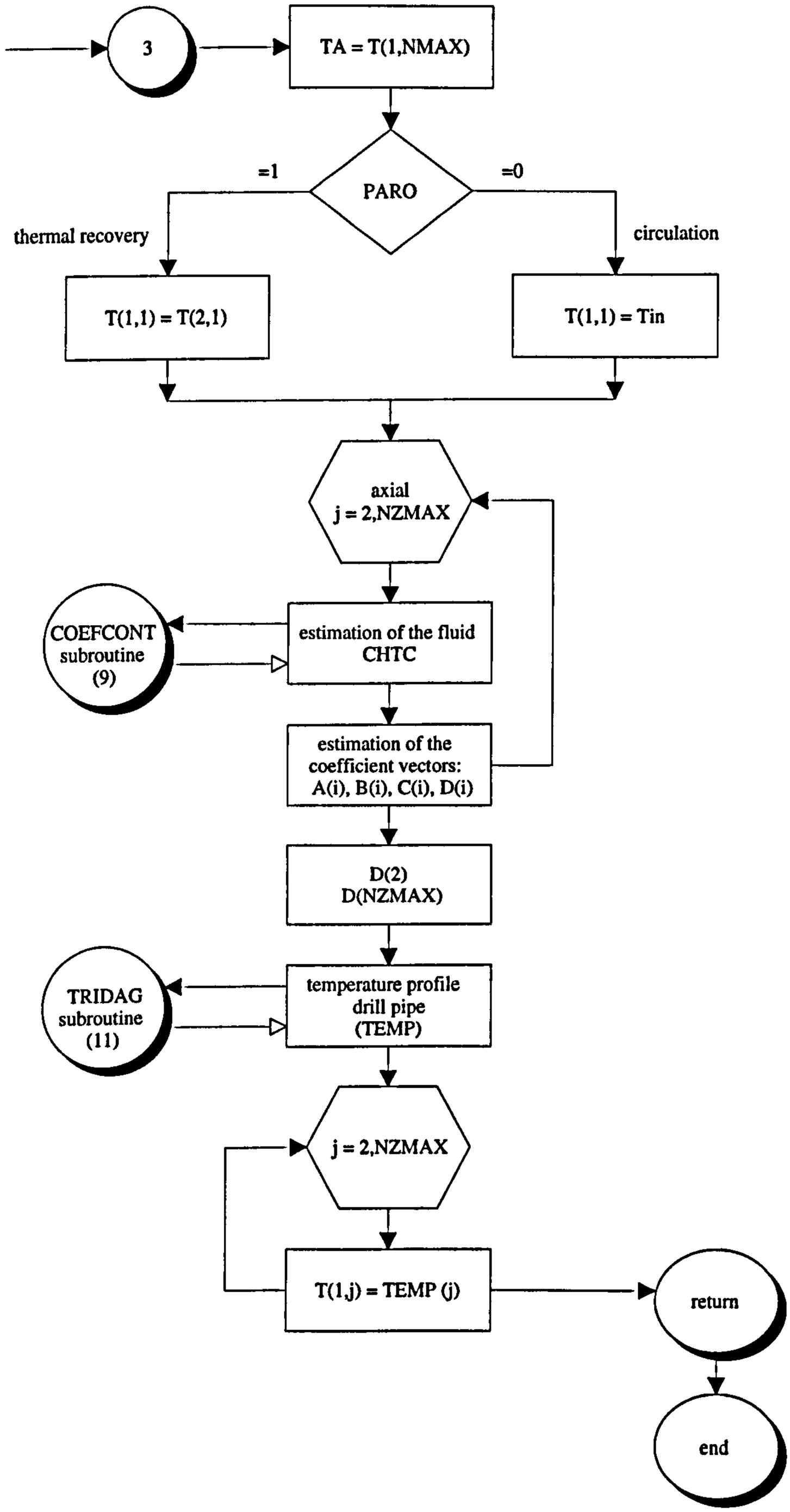

Fig. 8.9 Flow diagram of the TDPIPE subroutine.

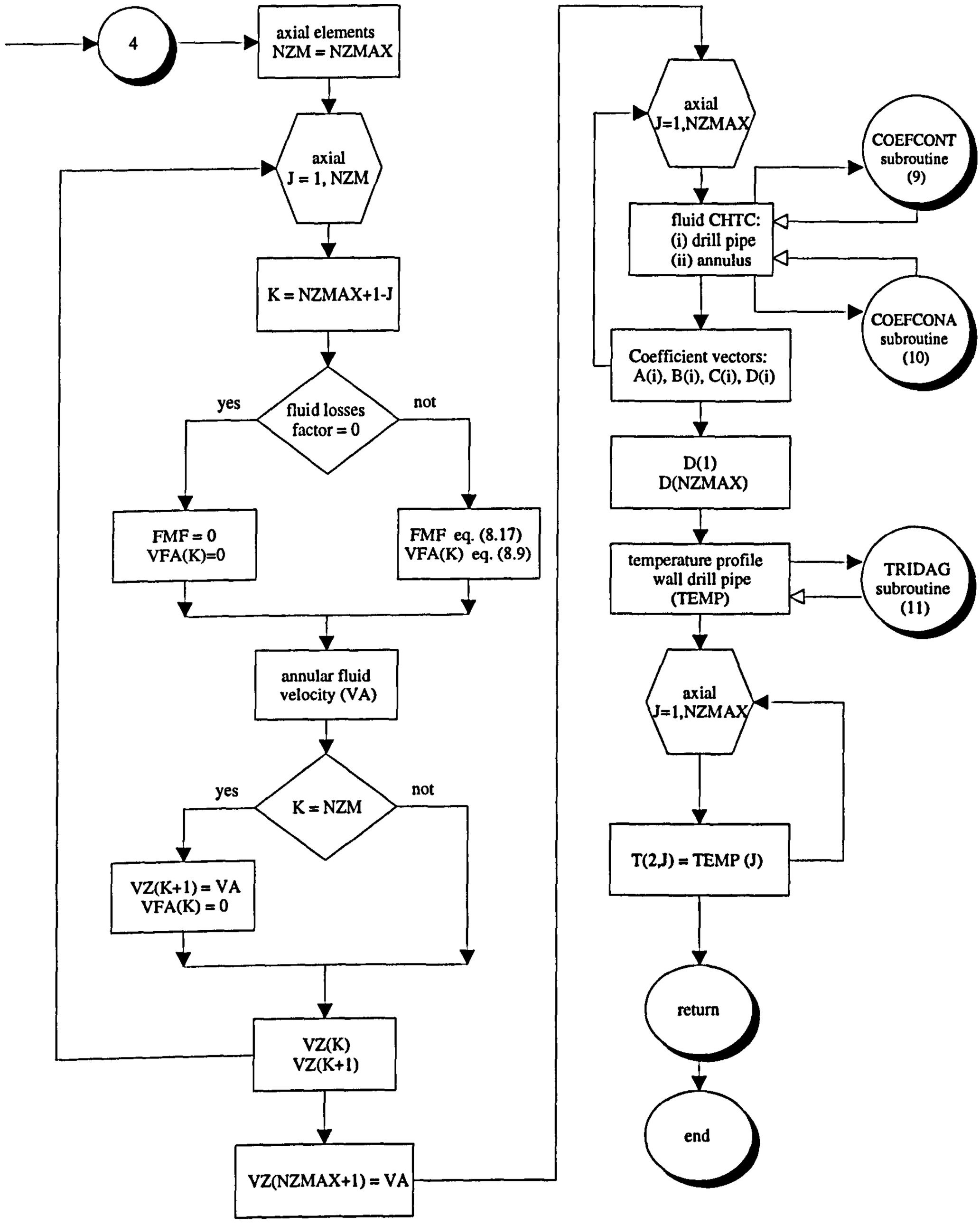

Fig. 8.10 Flow diagram of the TMET subroutine.

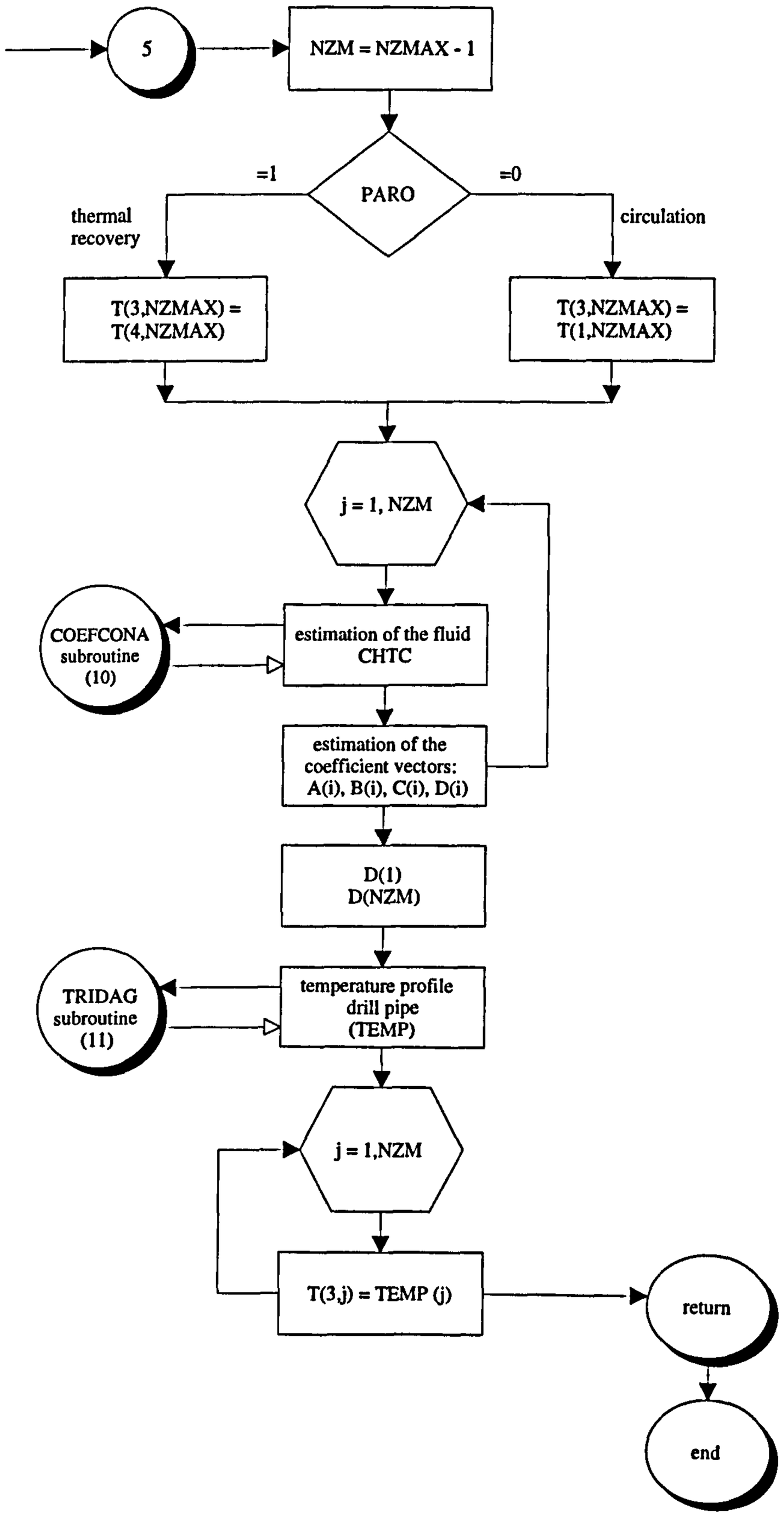

Fig. 8.11 Flow diagram of the TANU subroutine.

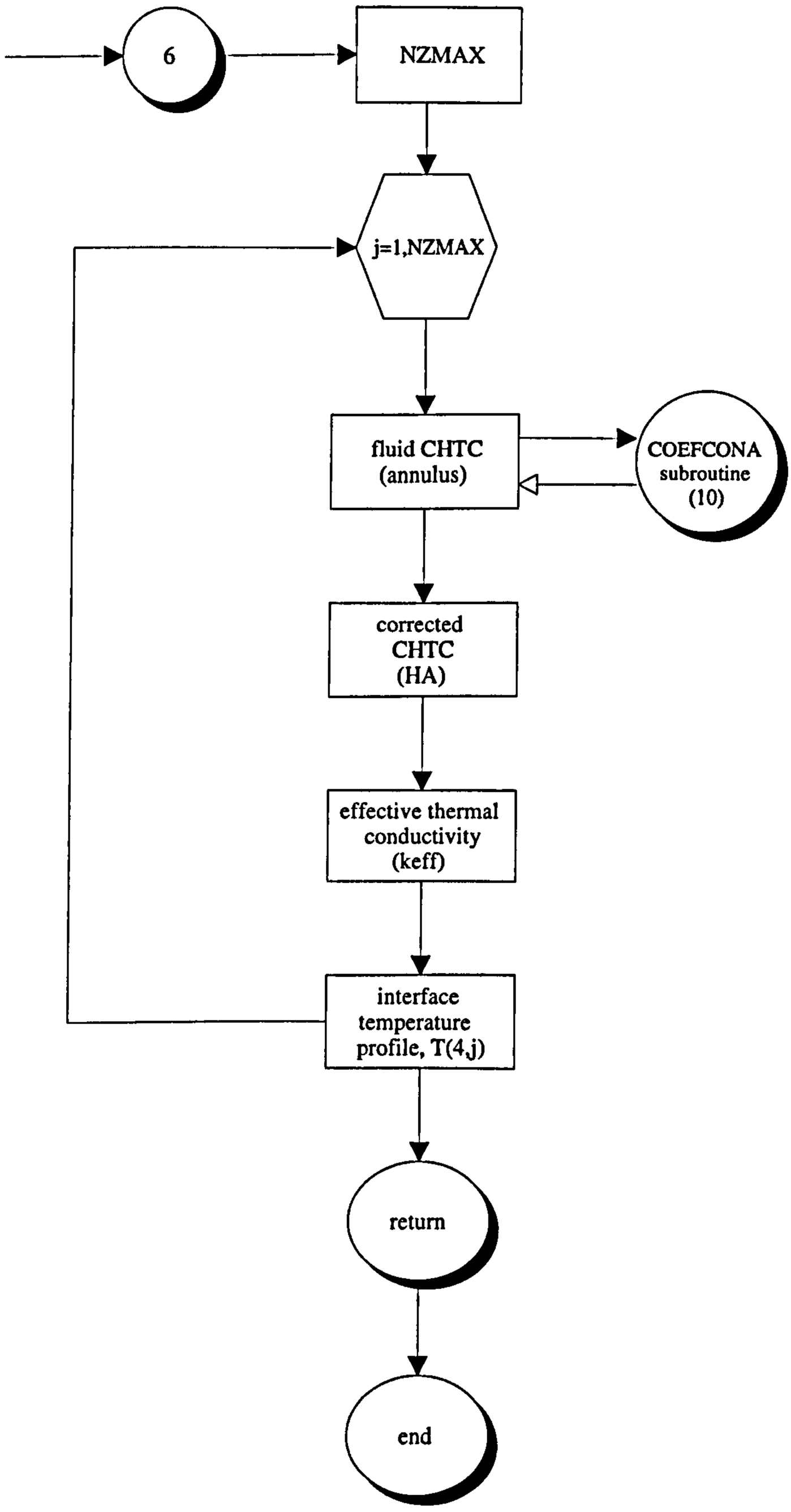

Fig. 8.12 Flow diagram of the TINTER subroutine.

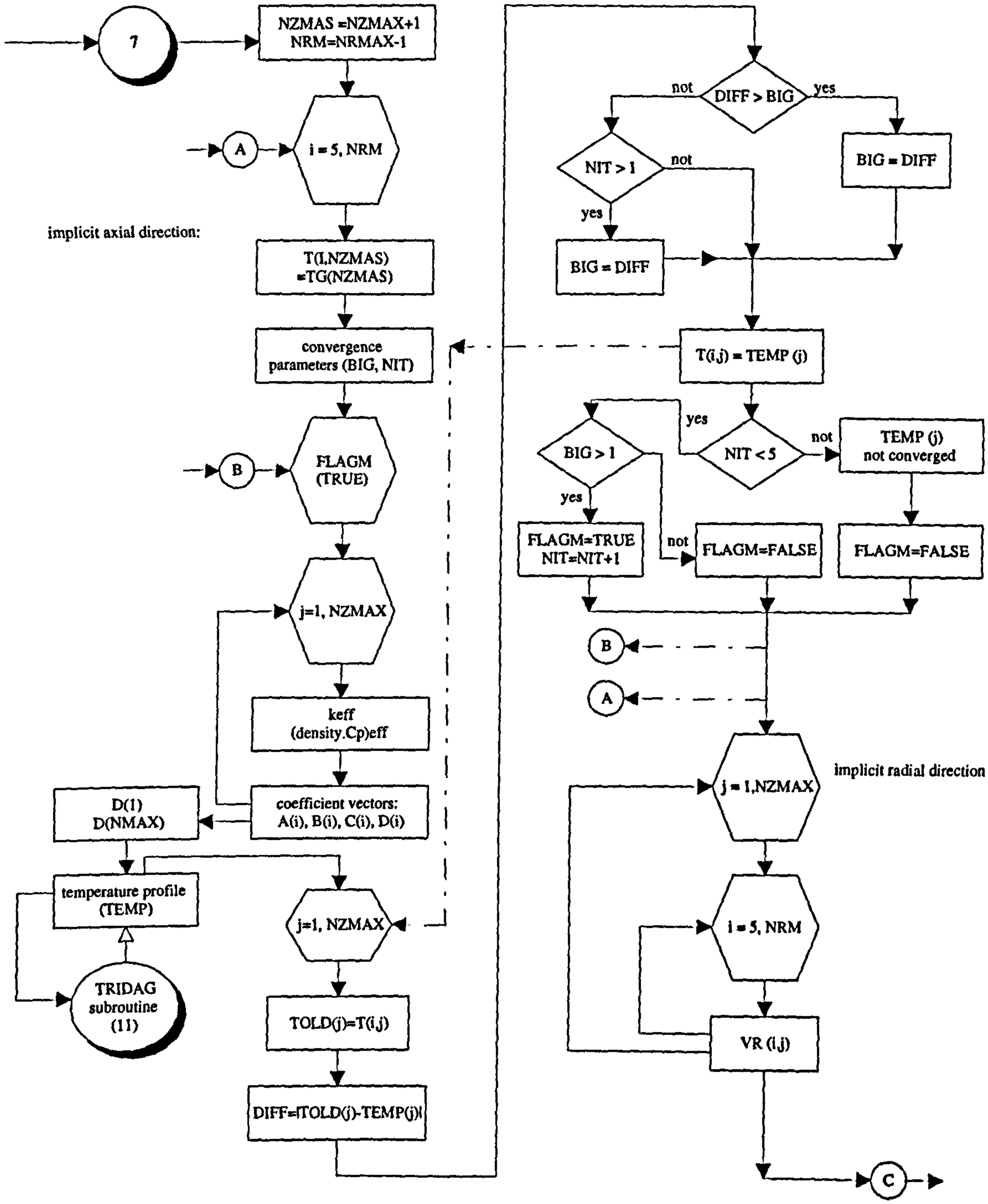

Fig. 8.13a Flow diagram of the TROCK subroutine.

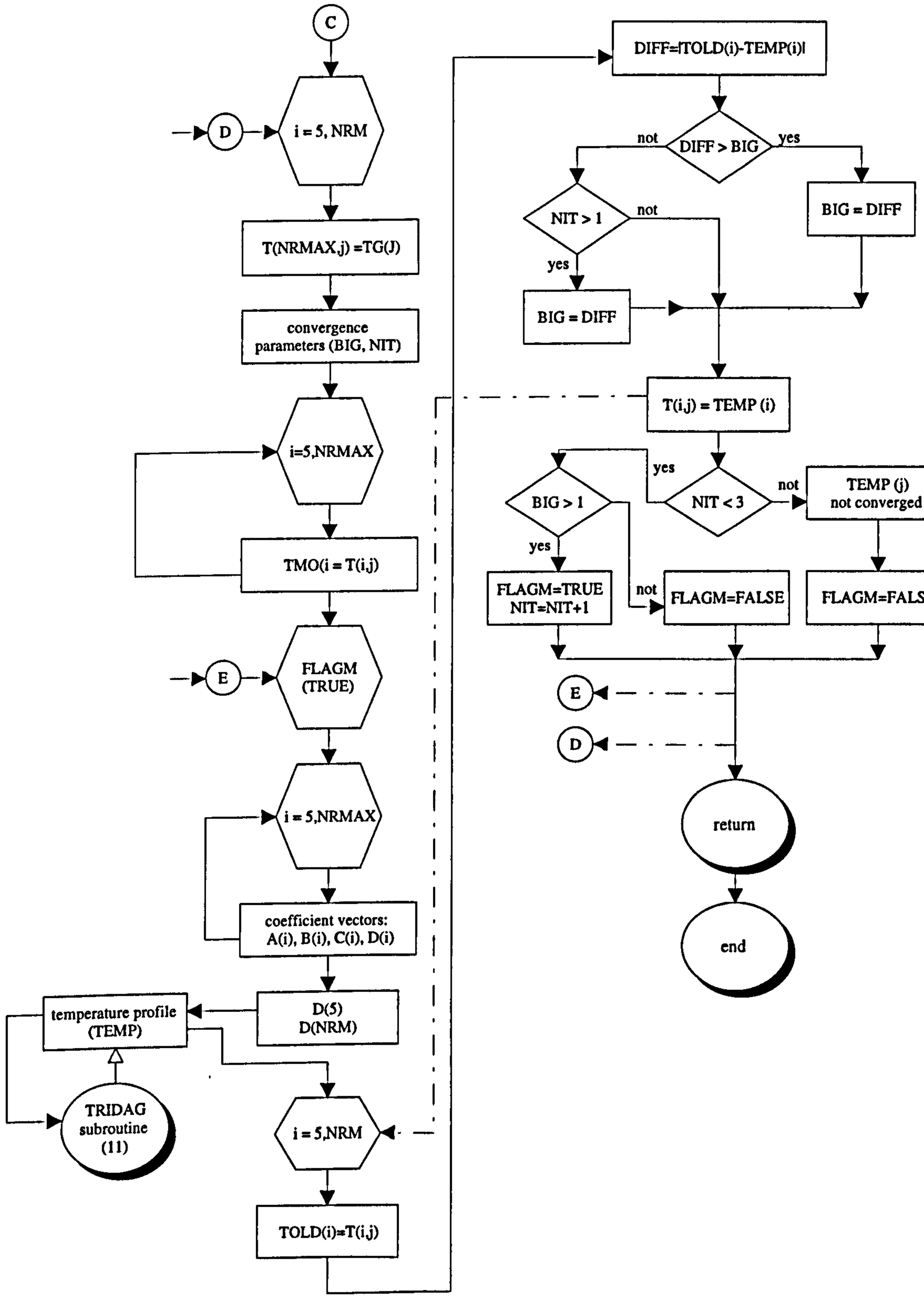

Fig. 8.13b Flow diagram of the TROCK subroutine.

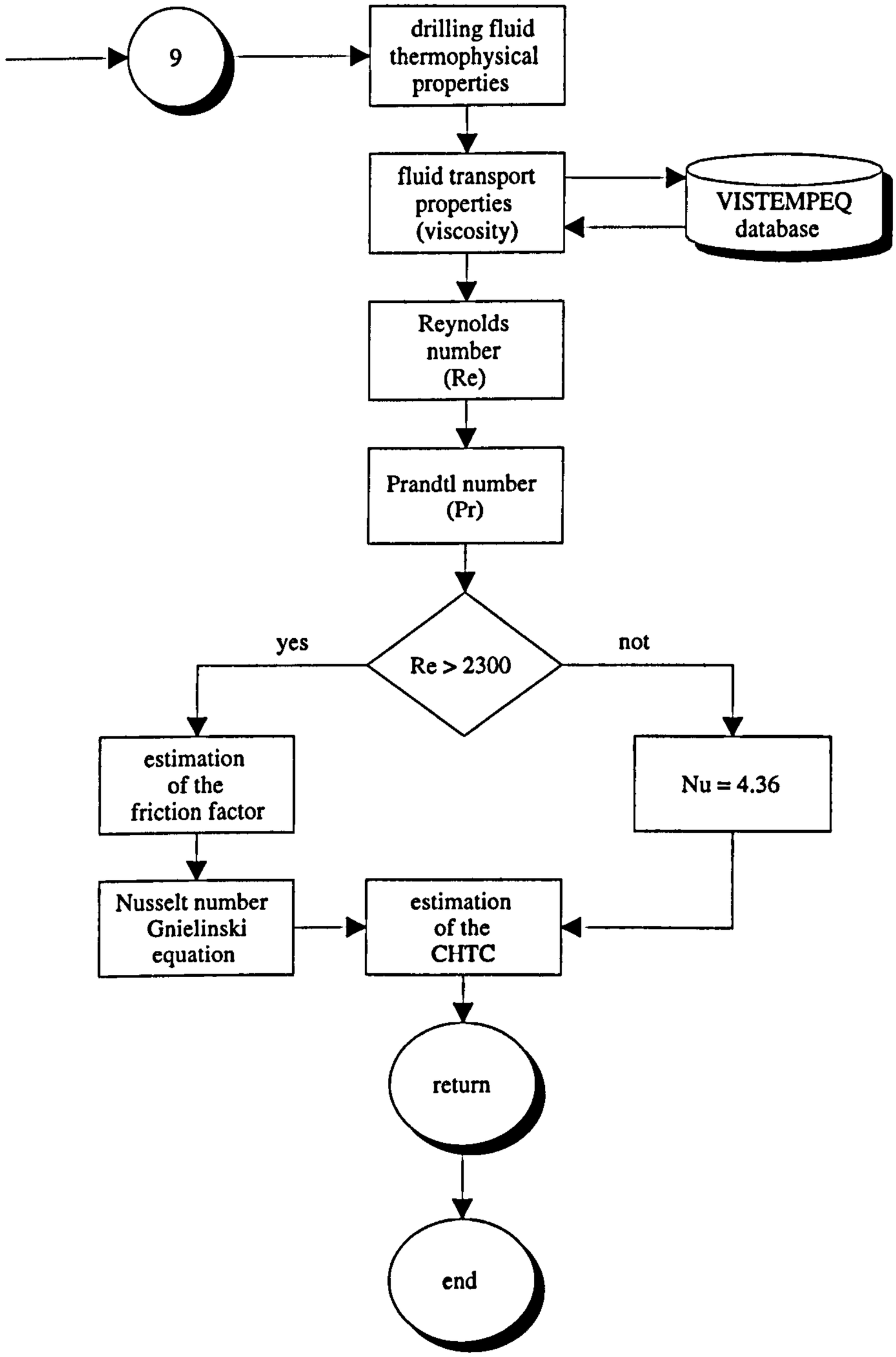

Fig. 8.14 Flow diagram of the COEFCONT subroutine.

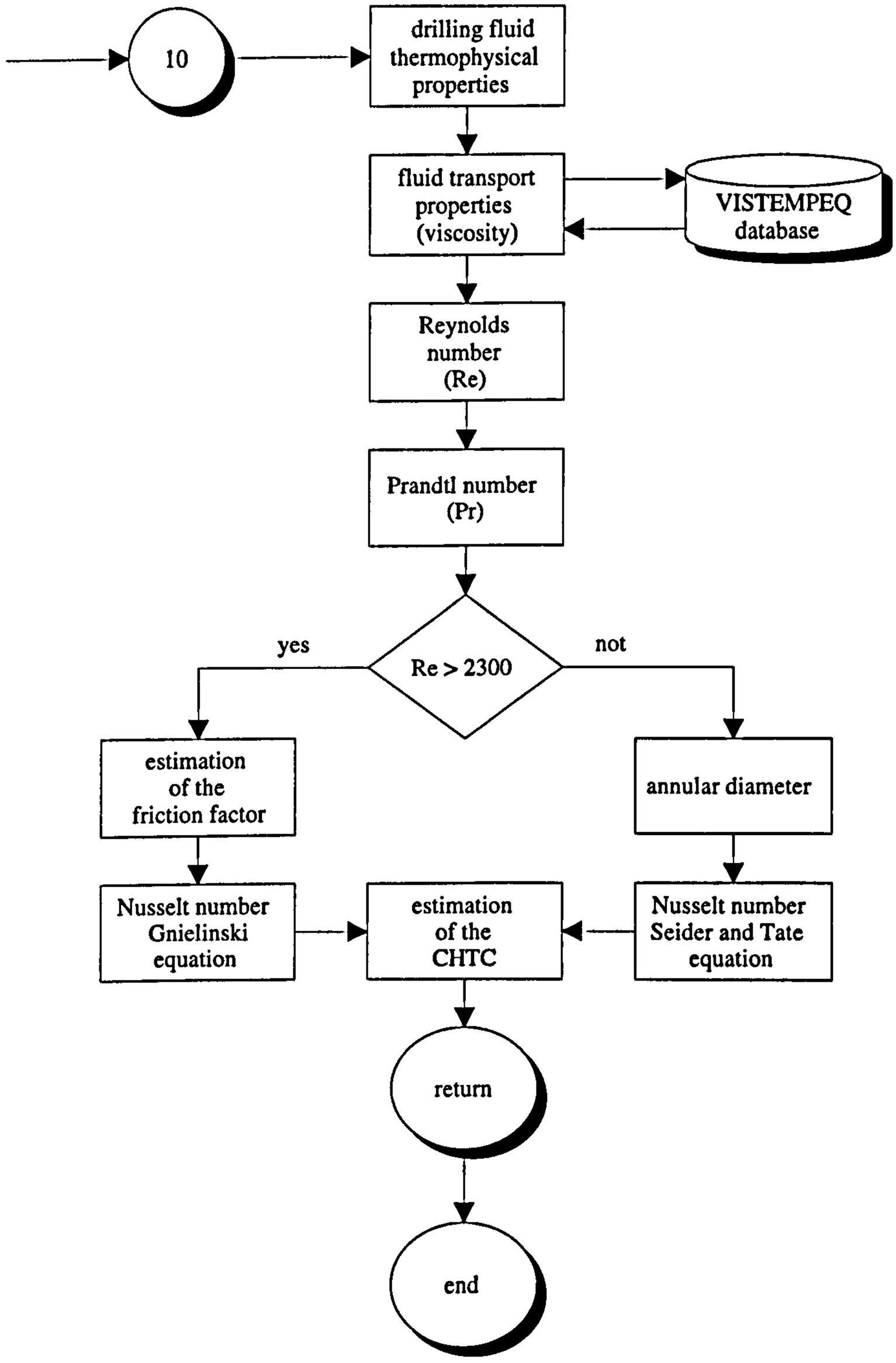

Fig. 8.15 Flow diagram of the COEFCONA subroutine.

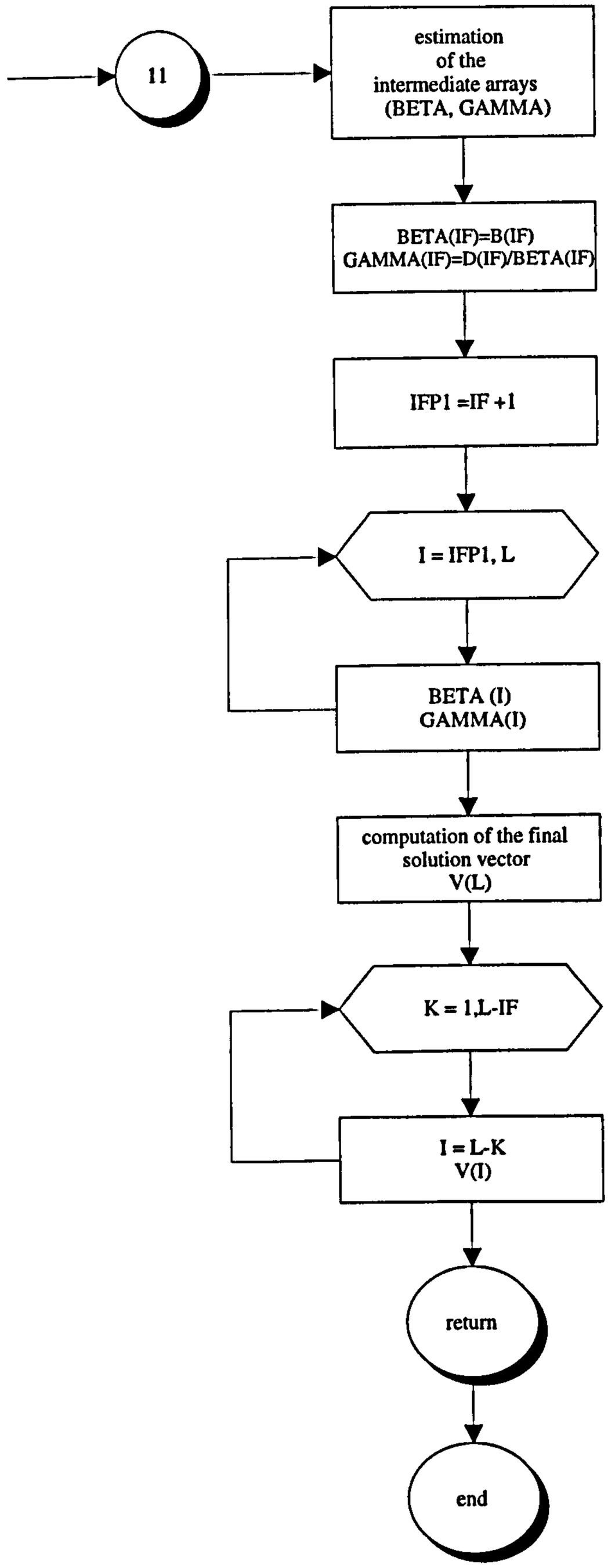

Fig. 8.16 Flow diagram of the TRIDAG subroutine.

Chapter 9

NUMERICAL VALIDATION OF THE WELLBORE THERMAL SIMULATOR

9.1 Nomenclature

Cp	specific heat capacity [J kg^{-1} $°C^{-1}$]
D	internal diameter of pipe [m]
G	geothermal gradient [°C m^{-1}]
h	convective heat transfer coefficient [W m^{-2} $°C^{-1}$]
k	thermal conductivity [W m^{-1} $°C^{-1}$]
L	length [m]
Nu	pipe Nusselt number, hD/k_m [dimensionless]
Pr	Prandtl number, $\mu C_p/k_m$ [dimensionless]

Q	volumetric fluid flow rate [m^3 hr^{-1}]
q	heat flux per unit area [W m^{-2}]
r	radius [m]
Δr	radius step size [m]
Re	Reynolds number, $Dv\rho/\mu$ [dimensionless]
T	temperature [°C]
T_b	bottomhole temperature [°C]
T_o	outlet temperature [°C]
T_{in}	inlet fluid temperature [°C]
t	time [hr]
t_c	circulating time [hr]
Δt	time step size [hr]
v	linear velocity [m s^{-1}]
W	drilling fluid mass flowrate [kg hr^{-1}]
z	depth [m]
Δz	depth step size [m]

Greek symbols

ϕ	formation porosity [dimensionless]
μ	dynamic viscosity [Pa s]
ρ	density [kg m^{-3}]

Subscripts

a	annulus; inner annulus wall
f	formation
m	mud or drilling fluid
p	drill pipe
s	surface
w	drill pipe wall

9.2 Introduction

This chapter presents a numerical validation of the transient wellbore thermal simulator (WELLTHER). Three numerical cases were considered to validate the capabilities of this simulator. The first one is related to the results of testing WELLTHER predictions with an analytical solution. The other two numerical cases consider the comparison of the results provided by the use of the WELLTHER simulator with the actual temperature measured data reported in the technical well drilling literature. Finally, sensitivity studies for evaluating the effect of certain well variables (such as drilling fluid and formation thermophysical properties) on the wellbore and the surrounding formation temperatures are described.

9.3 Numerical validation

Before the simulator could be reliably used to predict temperatures in the complex situation of a geothermal well drilling process or during the thermal recovery stage of the wellbore (after the drilling operations are stopped), it was essential to verify that the mathematical and numerical model had been formulated properly and that the desired partial differential equations will be solved correctly during their numerical solution. For this reason, three numerical cases were selected to validate the main capabilities of the transient wellbore thermal simulator (WELLTHER).

In the first case, a comparison between the temperature values predicted by the simulator and the theoretical temperature results corresponding to the analytical solution of the analogous heat transfer problem postulated by Carslaw and Jaeger (1959) was considered.

In the second case, a comparison between the predicted temperatures (for the fluid and the surrounding formation) and the temperature data reported in the literature for a wellbore of 6,100 m of depth without cementing jobs was used.

Finally, in the third case, a similar comparison between the predicted temperature values by the WELLTHER simulator and the temperature data reported in the literature for a wellbore of 4,575 m of depth with a more complex completion geometry (four casing sections and three cementing sections) was considered.

The last two numerical cases correspond to the numerical simulation of the heat transfer processes associated with the drilling process of geothermal wells which did not present drilling fluid losses to the formation. These validation examples can be grouped as the less complicated heat transfer cases that occur during the well drilling operations. The selection of these cases is justified because there is enough information reported in the literature to enable the validation to be evaluated. The numerical validation of the well drilling operations in the presence of the drilling fluid losses to the formation was not considered here because there is no information reported in the literature to be validated. However, Chapter 10 will include a direct application of the WELLTHER simulator to the interpretation of the logged temperatures in the drilling of some Mexican geothermal wells that have the lost circulation problem. This application constitutes the first documented case in the geothermal well drilling literature that considers the numerical modelling of this kind of heat transfer processes.

9.3.1 Analytical solution (numerical case 1)

A good verification that a numerical unsteady solution has been formulated correctly is that the scheme approaches the analytical steady state solution if the model is allowed to run for a long time. For this purpose, responses from different modules of the simulator were evaluated against a relatively simple analytical solution related to the heat transfer problem. With this objective in mind, the steady state solution to radial temperature distribution in an infinitely long hollow cylinder with fluid flowing inside the cylinder at a constant known temperature was selected.

Carslaw and Jaeger (1959) postulated a solution to the simple heat transfer problem illustrated in Fig. 9.1. Beirute (1991) solved the radial temperature distribution for the problem outlined by means of the following equation:

$$T = T_b - \left(\frac{ha}{k_m}\right)\left[\frac{T_b + \left(\frac{haT_a}{k_m}\right)\ln\left(\frac{b}{a}\right)}{1+\left(\frac{ha}{k_m}\right)\ln\left(\frac{b}{a}\right)} - T_a\right]\ln\left(\frac{b}{r}\right) \qquad (9.1)$$

where T represents the temperature at a radial position r; k_m is the fluid thermal conductivity; a and b are the inner and outer radii of the cylinder. The remaining terms of the equation are described in Fig. 9.2.

During the numerical analysis of this case, the WELLTHER simulator was used to solve this problem assuming a hollow cylinder with a 0.305 m inner diameter and a 15.75 m outer diameter. The constant temperatures at the inner and outer boundaries are 37.7 °C and 148.8 °C, respectively. It is considered that a fluid is circulating inside the cylinder at the constant inner temperature of 37.7 °C while the outer cylinder face is maintained at a constant temperature of 148.8 °C. Table 9.1 summarises the input data that were used during the simulation. From these data, the simulator was allowed to run for a long time (2000 hours) in order to reach the steady state before the data were compared with the temperature results obtained from the analytical solution, equation (9.1). Figure 9.2 shows the temperature values predicted by the WELLTHER simulator under steady state conditions. As can be seen in this figure, a good agreement between the predicted temperatures and the analytical solution was found, Fig. 9.2. Minimum differences (errors) less than 6.5 % were found.

9.3.2 Numerical validation using actual field cases

Before making the numerical validation of these field cases, it is convenient to consider several aspects related to the actual measured temperatures during the well drilling activities. Normally, the drilling data along with field collected

temperature measurements often are incomplete. Very little information is known about the type of formations penetrated by the drill bit. Frequently, insufficient temperature build-up data are available. Log temperatures regularly are reported without the precise depth at which these measurements were taken or without the length of time the well was shut-in before the log data were measured. The lack of these data makes it very difficult to compare the simulator predictions with actual properly measured temperatures because several assumptions need to be made about the unknown well data before the simulations can be performed. For this reason, in the field comparisons that will be considered below, appropiate assumptions and simulator default options will be used for missing data if it is really necessary.

- **Numerical case 2**

On the basis of these considerations, an uncovered wellbore of 6,100 m depth (without cementing jobs) was selected. This field case has been used for a long time by some researchers to validate the development of their numerical simulators [Raymond (1969) and Arnold (1990)]. With respect to this numerical case, there is considerable information related to the thermal behaviour of the circulation process that enables the numerical validation to be reliably evaluated. The geometry of the wellbore is represented schematically in Fig. 9.3. A compilation of the main data related to the well drilling process is summarised in Table 9.2. These data were used as input data for the numerical simulation purposes. Before initiating the simulation runs, a porosity input data file was created. In this input file, the lost circulation option was neglected (ϕ=0) because the information compiled from the well drilling operations did not report the presence of fluid losses to the formation. Likewise, circulating time periods of 24 hours and 48 hours were considered in order to compare subsequently the predicted temperature results with the temperature data reported by Raymond (1969) and Arnold (1990). Figures 9.4 to 9.10 present the results obtained during the numerical simulation of the heat transfer processes asociated with the well drilling operations.

The thermal history of the drilling fluid temperatures in the drill pipe and the annulus regions as well as the initial formation temperatures are shown in Figs. 9.5, 9.6 and 9.7. These curves represent the dynamic response of the system. As was described previously by Raymond (1969), these temperature profiles are functions of time and depth. Raymond (1969) calculated the fluid and formation temperature profiles (including the outlet fluid temperature) and compared such estimations with the actual temperatures measured (Table 9.3). These calculations were made by consideration of the the circulating times of 2 hours and 16 hours. Raymond's calculations show that the outlet fluid temperature (annular region) under circulating conditions rises from 26.7 °C to 60 °C and that it reaches an almost constant level at 63 °C after 16 hours of fluid circulation. A similar thermal behaviour was also observed during the numerical runs performed by the WELLTHER simulator, except that in this case the outlet fluid temperature stabilised at 58.5 °C (Fig. 9.6). In the last 8 hours of circulation, very small changes in the outlet temperature were detected. Normally, in any field situation these changes would be imperceptible.

In the case of the bottomhole temperatures (both the fluid and the formation), they fell very fast from their initial value of 204.4 °C (given by the local geothermal gradient) following the start of the circulation process. An explanation of the thermal behaviour observed is directly associated with the wellbore geometry because it was not fully completed (i.e. it has not presented cementing and casing sections). Therefore, it is expected that the heat transfer processes between the wellbore and the formation are given in a very intense way and very rapidly. Another important point to note with respect to the bottomhole fluid temperature is that it continually changes with time; a steady state condition is never attained at least after 24 hours of the drilling fluid circulation (Fig. 9.7). This fact partially suggests that the numerical simulators that have been developed under steady state assumptions cannot produce reliable temperature profiles of the circulation process associated with the geothermal well drilling.

With respect to the thermal recovery of the drilled wellbore (once the drilling activities were stopped), it was observed after 48 hours of shut-in time that the disturbed formation temperature reaches up to 188 °C (Fig. 9.8). Such a value represents approximately 8 % less than the initial formation temperature of 204.4 °C. This thermal process indicates that the static fluid system approaches the geothermal gradient temperatures quite rapidly (Fig. 9.9). Likewise, it is important to note that the thermal disturbance caused by the fluid circulation only affected the surrounding formation closer to the wellbore axis. The predicted formation temperatures in the radial direction showed that the formation nodes beyond 1.5 m from the wellbore axis were not affected by the thermal disturbances (Fig. 9.10).

The analysis of the thermal recovery process in the drilled wellbore shows that the shut-in response can be governed by the following considerations. Since there is no forced convection during this process, the major way of the heat transfer is either the free convection or the conduction in the fluid as well as the conduction in the formation. However, under shut-in conditions normally the fluid volume in the wellbore is extremelly small compared with the volume of formation whose temperature is affected by the circulation. Hence the heat conduction in the drilling fluid does not participate in the thermal recovery process of the wellbore. An analysis of the thermal system also shows that free convection is not involved because the dimensionless Grashof number (Gr) is too small (from 454 to 927). The ratio Gr/Re^2 indicates values that range from 0.006 to 0.018, which confirms that free convection can be neglected [Incropera and Dewitt (1990). Therefore, under these conditions, the thermal recovery process in the wellbore is only influenced by the conductive heat exchange with the surrounding formation because there are no fluid losses to the formation that could produce convective heat flow that would affect the overall well drilling system.

On the other hand, during the numerical simulations of this field case, it was also observed that the fluid temperature in the drill pipe region rises steadily from the surface to the bottomhole. The returning annular fluid continues to be

heated by the formation and reaches a maximum temperature at the depth range from 5,350 m to 5,600 m (Figs. 9.4 and 9.6). It was demonstrated that the location of this maximum annular fluid temperature is a function of the circulating time and the circulating flowrate. This point will tend to move up as the circulation time or the circulating flowrate increase.

On the basis of the thermal behaviour observed during the drilling operations of this wellbore, the temperature profiles predicted by the use of the WELLTHER simulator show a good agreement with the temperature data reported previously by Raymond (1969) and subsequently by Arnold (1990); Table 9.3. In all instances, the predicted and the actual measured temperatures agreed within 2 °C and 4 °C for the bottomhole and the surface (outlet) conditions, respectively.

- **Numerical case 3**

In this numerical case, a geothermal wellbore of 4,575 m depth with a more complex completion geometry (four casing sections and three cementing sections) was considered. The selection of this field case is justified in order to evaluate the capabilities of the simulator in wells where the completion activities had been carried out. Consequently, it implies that a more complex study of the heat flow processes needed to be performed because they will be restricted by the presence of different well drilling materials (casing or metal, cement, formation and fluids). Figure 9.11 depicts the geometry of the wellbore studied. Details of the well drilling data related to the complete geometry, the thermophysical properties of the wellbore system (formation, casing, cement and fluids) and the flow and the inlet thermal histories are given in Table 9.4. These data were taken from the paper by Marshall and Bensten (1982) and they will be used as input data during the simulation runs to be performed by the WELLTHER simulator. It is convenient to note that this numerical case has been extensively studied [Holmes and Swift (1970) and Keller et al (1973)]. Taking advantage of these studies and for the validation purposes, the temperature values predicted by these authors will be compared with the temperature results obtained in this research work.

Similarly to the previous validation case, before initiating the simulation, a porosity input data file was created. The lost circulation option was also neglected (ϕ=0) because the well drilling information did not report the presence of fluid losses. Circulating time periods of 10 hours, 100 hours and 1000 hours were considered in order to compare directly the temperature predictions with the temperature data estimated by Holmes and Swift (1970); Keller et al (1973) and Marshall and Bentsen (1982).

Since the thermal behaviour of the wells under circulating conditions is very similar to the previously analysed case, the comparison and the discussion of this field case will be concentrated on the analysis of the drilling fluid temperatures in the drill pipe and the annulus regions. Figures 9.12 and 9.13 present the results obtained during the numerical simulation of the heat transfer processes asociated with the well drilling operations at the circulating times previously indicated.

The annulus fluid temperature profiles generated by the WELLTHER simulator at 10 hours, 100 hours and 1000 hours of the drilling fluid circulation are presented in Fig. 9.12. It is observed that the annular fluid temperature deviates from the initial formation temperature (dashed line) very rapidly. This deviation (or the formation cooling process) would appear to be infinite considering the path of the drill pipe and the annulus fluid temperature profiles observed during the simulation. A steady state never would be attained (see the temperature profile corresponding to the 1000 hours, Fig. 9.13). The bottomhole fluid temperature corresponding to 100 hours of the circulation process differs from a theoretical steady state (1000 hours) one by more than 10 °C. These temperature profiles show a good agreement with the temperature values obtained by Marshall and Bentsen (1982); Table 9.5. However, these results contradict the conclusions achieved previously by Swift and Holmes (1970) and Keller et al (1973) because these authors suggested that a steady state solution can provide a good approximation of these temperatures profiles.

With respect to it and after a rigourous analysis of the thermal behaviour in the wellbore, it can be confirmed that the assumption of a steady state condition in the mathematical formulation of models that describe these heat transfer processes is clearly incorrect. Although, if it is considered that an actual fluid circulation process should not exceed circulating times of more than 100 hours (mainly because of the high drilling cost that it represents), then the steady state solution could give at least an approximation for the circulating fluid temperatures.

On the other hand, the thermal behaviour of the returning annular fluid was also studied. It shows a continuous heating process as a consequence of the conductive heat transfer processes with the surrounding formation. In all the circulating times simulated, the returning annular fluid reaches its maximum temperature at the depth range from 4,250 to 4,500 m. (Figs. 9.12 and 9.13).

Finally, after analysing all the temperature profiles predicted in this field case, a quantitative comparison of the bottomhole and the outlet fluid temperature values with the temperature values calculated by the other mentioned models was made. In general form, these comparisons showed a good agreement, specially against the temperature data reported by the Marshall and Bensten model; Table 9.5. For the bottomhole fluid temperatures, average differences of 2.8 % (2.2 °C), 8.8 % (6.9 °C) and 18 % (13.3 °C) were found when the predicted results were compared with the Marshall and Bentsen (1982), the Keller et al (1973) and the Swift and Holmes (1970) predictions, respectively.

For the outlet fluid temperatures, the average differences were bigger. Average differences of 32.7 % (8.8°C), 9 % (2.5 °C) and 5.9 % (1.6 °C) were found for the same order of comparisons. The larger differences observed between the WELLTHER and the Marshall and Bensten predictions can be explained by the fact that the Marshall and Bensten model considers the energy sources derived from the drill pipe rotation and the drill bit friction.

9.4 Parametric sensitivity analysis

Temperature profiles in and around a wellbore under drilling (circulation) and shut-in (thermal recovery) conditions are normally influenced by a lot of variables. Adequately defining these variables for an accurate computation of these temperatures can be difficult and complex, and in some cases impossible. Therefore, it is important to elucidate the effect of each variable on the mentioned temperature profiles. To find out the importance of a variable, a parametric sensitivity analysis must be carried out by computing the circulating and shut-in temperatures in and around a wellbore with several values of those variables, and with all others held constant. These calculations are not intended to provide temperature predictions for any specific wellbore. In principle, the sensitivity calculations should help to evaluate the impact of each variable studied on the computing well drilling and shut-in temperatures. It is important to note that the conclusions based on the sensitivity computations specifically would apply only to the specific conditions used.

From these sensitivity studies, several benefits could result. The first one, is to demonstrate which variables have a stronger effect on the circulating and shut-in temperatures. A second useful result would be related to the determination of how much effort is needed to adequately define each variable. Finally, the third benefit would be to improve the prediction, allowing quick decisions to be made with regard to the importance of certain variables on these temperatures.

9.4.1 Variables tested

Too many variables are involved in the calculation of the wellbore and formation temperatures under drilling and shut-in conditions to permit a complete sensitivity analysis of all of them. Consequently, the following eight variables have been selected for this study:

(i) the inlet drilling fluid temperature,

(ii) the drilling fluid density,

(iii) the drilling fluid flowrate,

(iv) the drilling fluid viscosity,

(v) the drilling fluid specific heat capacity,

(vi) the drilling fluid thermal conductivity,

(vii) the geothermal gradient (initial formation temperatures), and

(viii) the formation thermal conductivity.

The impact of each of these variables on the circulating and the shut-in temperatures will be estimated. Temperatures are computed for two and in some cases for three different values of each variable. Three graphs are presented to illustrate the effects of each variable on these temperature profiles. The first one is related to the plot of the bottomhole temperature against the circulating time. The second one is related to the plot of the drill pipe and the annular temperatures against depth after 24 hours of fluid circulation. Finally, the third plot is related to the drill pipe temperature profiles after 24 hours of the thermal recovery process (shut-in time). The range of values selected for the eight variables are presented in Table 9.6.

As stated above, the results of the sensitivity study can be extended to applications for conditions other than those used in the study, but the conditions of the study are very important. For simplicity, the parametric sensitivity analysis was made using the input data related to the numerical validation case 2 (Table 9.2).

- **Inlet drilling fluid temperature**

The effects of the fluid inlet temperature on the temperature profiles of the annulus and the drill pipe are depicted in Figs. 9.14 and 9.15. Figure 9.14 shows the variation in the returning annular fluid temperature with circulating time for inlet temperatures of 30 °C, 57.7 °C and 70 °C. From this figure, it can be observed that with the lower and the upper inlet temperatures, the annular fluid

returns to the surface with warmer temperatures of 33 °C and 68 °C, respectively (after 24 hours of fluid circulation). These thermal conditions produce small changes (cooling) in the fluid temperature at the deeper zone of the wellbore for the range of inlet temperatures considered (Fig. 9.15). Larger changes are observed from the middle depth of the wellbore to the surface for the same inlet temperature variation. The cool fluid heats as it flows down into the wellbore along a path nearly parallel to the surrounding formation temperatures. As the fluid reaches the deeper zone of the wellbore, the heating rate decreases to near zero, while the temperature reaches 121.3 °C.

The sensitivity of the annulus radial temperatures profiles to fluid inlet temperature is shown in Fig. 9.16. From this figure, it can be observed that the thermal disturbance caused by the circulation process only affects a radial distance of approximately 1 m from the wellbore axis. Beyond this radial distance, the surface temperature remains constant and equivalent to the initial formation temperature. Finally, the variation of the fluid inlet temperatures on the drill pipe temperature profiles under shut-in conditions is plotted in Fig. 9.17. Clearly, it can be observed that the shut-in temperature profiles corresponding to the upper inlet temperature will tend to attain more rapidly the initial formation temperature after a long shut-in time has elapsed.

- **Drilling fluid density**

The fluid density effect on the wellbore temperatures is illustrated in Figs. 9.18 and 9.19. Figure 9.18 shows the variation of the bottomhole temperature of the fluid in the drill pipe with circulating time for fluid densities of 900, 1200 and 2500 kg m^{-3}. The bottomhole temperature decreases more rapidly and to a lower final value with light weight fluid. A fluid with a density of 900 kg m^{-3} reaches 120 °C at bottomhole after 24 hours, a 1200 kg m^{-3} density fluid reaches 121.3 °C, and a 2500 kg m^{-3} density fluid reaches 125 °C. Considering a difference between the lower and the upper values of density (170 %), it causes a final variation of 4.1 % in the bottomhole temperature of the fluid after 24 hours of circulation.

On the other hand, the fluid temperature profiles (i) in the drill pipe and (ii) in the annulus region after 24 hours of circulation for the three densities considered are presented in Fig. 9.19. These curves show an increase in temperature with depth as fluid flows down a wellbore, with little heating at the deeper zone, and a constant cooling as the fluid returns to the surface. As the solids content is increased in a fluid (as a consequence of the drill cuttings lift to the surface), the density increases. Therefore, the ability to carry thermal energy up from the formation causes higher temperatures in heavier circulatings fluids.

- **Drilling fluid flowrate**

Figures 9.20 and 9.21 show the importance of the fluid flowrate for the simulated wellbore case. Transient bottomhole temperature behaviour for flowrates of 15.14 and 75.7 kg s^{-1} is plotted in Fig. 9.20. At a low flowrate, the bottomhole temperature slowly decreases to 121.3 °C after 24 hours of fluid circulation. A rapid cooling process occurs at the high fluid flowrate, of 75.7 °C, reaching 56 °C after 24 hours of circulation.

Figure 9.21 shows the drill pipe and the annulus temperature profiles for the two flowrates evaluated. At a low rate, fluid heats continuously as it flows down the wellbore, following a path just below the geothermal gradient. As it nears the bottomhole, the fluid heats less rapidly reaching a temperature of 121.3 °C at the deeper zone of the wellbore. High circulation rates do not allow sufficient time for the flowing fluid in a wellbore to exchange energy with the formation. Consequently, the surrounding formation temperatures have little effect on fluid temperatures at high drilling fluid flowrates.

Considering the difference between the lower and the upper flowrate values (400 %), it causes a final variation of approximately 53 % in the bottomhole temperature of the drilling fluid after 24 hours of circulation.

- **Drilling fluid viscosity**

The effect of the fluid viscosity on the temperature distribution of a wellbore under circulating and shut in conditions is illustrated from Fig. 9.22 to 9.25. Bottomhole temperature behaviour with circulating time for fluid viscosities of 0.010, 0.045 and 0.050 Pa·s (10, 45 and 50 cp) is plotted in Fig. 9.22. It can be observed that the bottomhole temperature steadily decreases from 204.4 °C to 130 °C for a viscosity of 0.010 Pa·s, 204.4 °C to 121.3 °C for 0.045 Pa·s and 204.4 °C to 110 °C for 0.050 Pa·s. Under the circulation conditions, the higher fluid viscosity (non-Newtonian fluid) tends to insulate the drill pipe region by decreasing the convective heat transfer coefficient. As a result, the cool fluid is not heated as rapidly by the surrounding formation (Fig. 9.23).

It is expected that the drilling fluid tends to be cooler than the water (Newtonian fluid) under similar conditions. The reason for this behaviour is apparent by inspecting the dimensionless Nusselt number correlation which correlates the dimensionless Reynolds and Prandtl numbers for turbulent flow. The convective heat transfer coefficient (which is contained within the dimensionless Nusselt number) depends on the fluid viscosity in a complex way. Careful analysis carried out in the equations associated with the convective coefficient calculation shows that as the fluid viscosity increases, the heat transfer coefficent value decreases. Consequently, higher fluid viscosities are less effective at removing heat from the formation than lower fluid viscosities (e.g. water). This conclusion can be proved by looking at the radial temperature profiles for the fluids with a viscosity of 0.050 Pa·s and 0.010 Pa·s (Fig. 9.24). This thermal behaviour is also reflected in the thermal recovery process of the wellbore. After 24 hours of shut-in time, the fluid with a lower viscosity attains a temperature of 188.8 °C while the fluid with a higher viscosity reaches 183 °C (Fig. 9.25).

Considering the difference between the lower and the upper fluid viscosity values (400 %), it causes a final variation of about 20 % in the bottomhole temperature of the drilling fluid after 24 hours of circulation.

- **Drilling fluid specific heat capacity**

The effect of the fluid specific heat capacity on the temperature distribution of a wellbore under circulating conditions is illustrated in Figs. 9.26 and 9.27. The variation of the bottomhole temperature with circulating time for fluid specific heat capacities of 2500, 3930 and 4500 J kg^{-1} $°C^{-1}$ is represented in Fig. 9.26. It can be observed that the bottomhole temperature steadily decreases from 204.4 °C to 140 °C for 2500 J kg^{-1} $°C^{-1}$, 204.4 °C to 121.3 °C for 3930 J kg^{-1} $°C^{-1}$ and 204.4 °C to 115 °C for 4500 J kg^{-1} $°C^{-1}$. Under these conditions, the higher fluid specific heat capacity tends to insulate the drill pipe region. As a result, the cool fluid is not heated as rapidly by the surrounding formation (Fig. 9.26).

Considering the difference between the lower and the upper fluid specific heat capacity values (80 %), it induces a final variation of almost 18 % in the bottomhole temperature of the drilling fluid after 24 hours of circulation.

- **Drilling fluid thermal conductivity**

The effect of the fluid thermal conductivity on the temperature profiles of the wellbore under circulating conditions is shown in Figs. 9.28 and 9.29. The variation of the bottomhole temperature with circulating time for fluid thermal conductivities of 1.25, 2.25 and 5.0 W m^{-1} $°C^{-1}$ is depicted in Fig. 9.28. It can be seen that the fluid bottomhole temperature uniformly decreases from 204.4 °C to 101.5 °C for 1.25 W m^{-1} $°C^{-1}$, 204.4 °C to 121.3 °C for 2.25 W m^{-1} $°C^{-1}$ and 204.4 °C to 150 °C for 5.0 W m^{-1} $°C^{-1}$ after 24 hours of fluid circulation. Under these conditions, the higher fluid thermal conductivity tends to increase the heat exchange between the drill pipe region and the formation. As a result, the cooler fluid temperature profile will correspond to the lower fluid thermal conductivity value (Fig. 9.29).

Considering the difference between the lower and the upper fluid thermal conductivity values (300 %), it produces a final variation of around 50 % in the bottomhole temperature of the drilling fluid after 24 hours of circulation.

- **Geothermal gradient (initial formation temperature)**

The importance of the undisturbed formation temperature gradient is presented in Figs. 9.30 and 9.31. The transient behaviour of the bottomhole temperatures in the wellbore for geothermal gradients of 0.010, 0.029 and 0.050 °C m^{-1} is plotted in Fig. 9.30. For a 0.010 °C m^{-1} gradient, the bottomhole temperature begins at 87.7 °C and cools to 59.7 °C after 24 hours of fluid circulation. A 0.029 °C m^{-1} gradient produces a cooling process in a bottomhole temperature from 204.4 °C to 121.3 °C. The higher geothermal gradient (0.050 °C m^{-1}) results in a bottomhole temperature of 331.7 °C which cools to 188 °C after 24 hours of fluid circulation. Even though a higher geothermal gradient increases considerably the bottomhole temperature of the wellbore, the difference could be reduced with time due to greater cooling for the high gradient. Figure 9.31 shows the drill pipe and the annulus temperature profiles after 24 hours for two different geothermal gradients. The gradients themselves are also plotted in the same figure. Both curves follow nearly parallel to the formation temperature gradient. Much greater heating is evident for a high temperature gradient wellbore.

Considering the difference between the lower and the upper geothermal gradients (400 %), it causes a final variation of around 215 % in the bottomhole temperature of the drilling fluid after 24 hours of circulation.

As can be seen, the static temperature profile or geothermal gradient is a very important input parameter within the simulation. These input data are required by the simulator to evaluate a representative heat source for the wellbore. True static temperatures are the formation temperatures before the wellbore was drilled. Normally, log temperatures are lower than the true static formation temperatures. If log temperatures are used as input in the simulator, the circulating temperatures predicted would be unrealistically low. Hence, it is very convenient for the simulation to make an attempt to acquire the true static temperatures for the area that will be studied. Several log temperatures taken at increasingly longer periods of time can be extrapolated to a pseudostatic

temperature by means of the analytical methods described in Chapter 4 [Dowdle and Cobb (1975); Roux et al (1980); Kritikos and Kutasov (1988); Ascencio et al (1994) and Hasan and Kabir (1994)]. This approach, however, can lead to conservative static temperature predictions. The longer the wellbore was shut-in after circulation before the log temperatures were taken, the better the approximation to the true static temperatures can be approached when any analytical method is used.

- **Formation thermal conductivity**

The importance of the formation thermal conductivity is presented in Figs. 9.32 and 9.33. This thermophysical variable has only a small effect on flowing fluid temperatures, if the rates are not too low. The variation of the bottomhole temperature with circulating time for formation thermal conductivities of 1.25, 2.25 and 5.0 W m^{-1} $°C^{-1}$ is depicted in Fig. 9.32. It can be seen that the bottomhole temperature regularly decreases from 204.4 °C to 118 °C for 1.25 W m^{-1} $°C^{-1}$, 204.4 °C to 121.3 °C for 2.25 W m^{-1} $°C^{-1}$ and 204.4 °C to 126.2 °C for 5.0 W m^{-1} $°C^{-1}$ after 24 hours of fluid circulation. Under these conditions, the higher fluid thermal conductivity tends to increase slightly the heat exchange between the drill pipe region and the formation. As a result, the cooler fluid temperature profile will correspond to the lower fluid thermal conductivity value (Fig. 9.33).

Considering the difference between the lower and the upper formation thermal conductivity values (300 %), it produces a small variation of about 10 % in the bottomhole temperature of the drilling fluid after 24 hours of circulation.

9.5 Convergence Analysis

The convergence of WELLTHER solutions with the time step size and the grid spacing (axial and radial) was verified. Essentially, there are two main objectives to the time step and grid spacing tests. The first one is to demonstrate that a unique temperature distribution exists in a numerical convergence test. The

second one is related to the selection of the time step size and the grid spacing for an adequate accurate solution with a minimum computing time.

Considering again the comparison of the WELLTHER calculations to the exact solution (numerical case 1), three computer simulations were conducted with three step sizes. From these simulations, two conclusions can be drawn. The first one is related to the apparent dependence of the solution to the size of the time step size. Figure 9.34 shows that the WELLTHER predictions are approaching the exact solution as the time step size is reduced. Convergence of temperature predictions with a reduced time step size is a necessary feature if the solution is unique. The selection of the proper time step size is a complex task that depends on the wellbore geometry, the initial temperatures, the grid spacing (axial and radial) and the temperature gradients. Figure 9.35 shows the behaviour of the elapsed computing time against the time step size in the numerical simulation tests of the case 1. These results were estimated using a personal computer with a Pentium microprocessor (200 mHz). Generally, for large temperature gradients a small time step size is needed. In these numerical studies, a stability criteria proposed by Incropera and Dewitt (1990) was applied. The stability criterion for a radial explicit solution of a partial differential equation system was given by :

$$\Delta t = \frac{F_o \, \Delta r^2}{\alpha} \tag{9.2}$$

$$F_o \, (1 + Bi) \leq \frac{1}{2} \tag{9.3}$$

where Bi is the dimensionless Biot number which is given by:

$$Bi = \frac{h \, \Delta r^2}{k} \tag{9.4}$$

while, the stability criterion for an axial explicit solution of a partial differential equation system was given by :

$$\Delta t = \frac{F_o \, \Delta z^2}{\alpha} \tag{9.5}$$

9.6 References

F.C. Arnold, Temperature variation in a circulating wellbore fluid, Journal of Energy Resources Technology, **112** 79-83 (1990).

F. Ascencio, A. Garcia, J. Rivera and V. Arellano, Estimation of undisturbed formation temperatures under spherical-radial heat flow conditions, Geothermics **23** 317-326 (1994).

R.M. Beirute, A circulating and shut-in well-temperature-profile simulator, Journal of Petroleum Technology, **September** 1140-1146 (1991).

H.S. Carslaw and J.C. Jaeger, Conduction of heat in solids, 2nd. Edition, Clarendon Press, Oxford, UK (1959).

W.L. Dowdle and W.M. Cobb, Static formation temperature from well logs - an empirical method, Journal of Petroleum Technology, **November** 1326-1330 (1975).

A.R. Hasan and C.S. Kabir, Static reservoir temperature determination from transient data after mud circulation, SPE Drilling & Completion, **March** 17-24 (1994).

C.S. Holmes and S.C. Swift, Calculation of circulating mud temperatures, Journal of Petroleum Technology, **June** 670-674 (1970).

F.P. Incropera and D.P. Dewitt, Introduction to heat transfer, John Wiley & Sons, Inc., New York, USA (1990).

H.H. Keller, E.J. Couch and P.M. Berry, Temperature distribution in circulating mud columns, Society of Petroleum Engineers Journal, **February** 23-30 (1973).

W.R. Kritikos and I.M. Kutasov, Two-point method for determination of undisturbed reservoir temperature, SPE Formation Evaluation Journal, **March** 222-226 (1988).

D.W. Marshall and R.G. Bentsen, A computer model to determine the temperature distributions in a wellbore, The Journal of Canadian Petroleum, **January-February** 63-75 (1982).

L.R. Raymond, Temperature distribution in a circulating drilling fluid, Journal of Petroleum Technology, **March** 333-341 (1969).

B. Roux, S.K. Sanyal and S.L. Brown, An improved approach to estimating true reservoir temperature from transient temperature data, 50th Annual California Regional Meeting of the Society of Petroleum Engineers, Los Angeles, CA, USA, April 9-11, 9 p. (1980).

Wellbore geometry				
Wellbore section	1	2	3	4
Wellbore diameter (m)	15.25	0.00	0.00	0.00
Wellbore depth, z (m)	6100.00	0.00	0.00	0.00
Depth step size, Δz (m)	100.00	0.00	0.00	0.00
Drill pipe diameter (m)	0.31			
Thermophysical and transport properties				
Component	k [W m^{-1} $°C^{-1}$]	Cp [J kg^{-1} $°C^{-1}$]	ρ [kg m^{-3}]	μ [Pa.s]
Formation	20.0	880.0	2640.0	------
Cement	0.0	0.0	0.0	------
Casing	43.3	418.7	8048.0	------
Drilling fluid	0.7	3930.0	1200.0	0.5
Flow and temperature data of the well drilling operations				
	Fluid flowrate [kg s^{-1}]	Geothermal gradient [°C m^{-1}]	Surface temperature [°C]	Inlet fluid temperature [°C]
	1000.0	0.007	37.7	37.7

Table 9.1 Input data used by the wellbore thermal simulator (WELLTHER) in the numerical simulation of the analytical solution (numerical case 1).

Wellbore geometry				
Wellbore section	1	2	3	4
Wellbore diameter (m)	0.2191	0.00	0.00	0.00
Wellbore depth, z (m)	6100.00	0.00	0.00	0.00
Depth step size, Δz (m)	100.00	0.00	0.00	0.00
Drill pipe diameter (m)	0.1143			
Thermophysical and transport properties				
Component	k [W m^{-1} $°C^{-1}$]	Cp [J kg^{-1} $°C^{-1}$]	ρ [kg m^{-3}]	μ [Pa.s]
Formation	2.25	880.0	2640.0	------
Cement	0.0	0.0	0.0	------
Casing	43.33	418.7	8048.0	------
Drilling fluid	2.25	3930.0	1200.0	0.045
Flow and temperature data of the well drilling operations				
	Fluid flowrate [kg s^{-1}]	Geothermal gradient [°C m^{-1}]	Surface temperature [°C]	Inlet fluid temperature [°C]
	15.14	0.0292	26.7	57.2

Table 9.2 Input data used by the wellbore thermal simulator (WELLTHER) in the numerical simulation of the field case reported by Raymond (1969) [numerical case 2].

				Logged temperature		Predicted temperature	
Source	z (m)	W (kg s^{-1})	t_c (hr)	T_b (°C)	T_o (°C)	T_b (°C)	T_o (°C)
Raymond (1969)	6100.0	15.14	2.0	143.0	60.0	145.0	60.0
Raymond (1969)	6100.0	15.14	16.0	127.0	63.0	128.0	63.0
Arnold (1990)	6100.0	15.14	2.0	n.d.	n.d.	147.0	59.0
Arnold (1990)	6100.0	15.14	16.0	n.d.	n.d.	147.0	64.0
This work	6100.0	15.14	2.0	n.d.	n.d.	141.6	58.5
This work	6100.0	15.14	16.0	n.d.	n.d.	126.5	58.5
This work	6100.0	15.14	24.0	n.d.	n.d.	121.3	58.5

T_b (bottomhole fluid temperature); T_o (outlet fluid temperature); t_c (circulating time)

Table 9.3 Comparison of the predicted and the actual logged temperatures for the numerical case 2.

Wellbore geometry				
Wellbore section	1	2	3	4
Wellbore diameter (m)	0.6604	0.5080	0.3397	0.2440
Wellbore depth, z (m)	600.0	900.0	1500.0	1500.0
Depth step size, Δz (m)	100.0	100.0	100.0	100.0
Drill pipe diameter (m) Thickness (m)	0.1610 0.0100			
Thermophysical and transport properties				
Component	k [W m^{-1} $°C^{-1}$]	Cp [J kg^{-1} $°C^{-1}$]	ρ [kg m^{-3}]	μ [Pa.s]
Formation	2.25	800.0	2640.0	------
Cement	0.70	2000.0	3140.0	------
Casing	43.75	400.0	8060.0	------
Drilling fluid	1.75	1600.0	1200.0	0.045
Flow and temperature data of the well drilling operations				
	Fluid flowrate [kg s^{-1}]	Geothermal gradient [°C m^{-1}]	Surface temperature [°C]	Inlet fluid temperature [°C]
	15.9	0.0173	15.3	38.0

Table 9.4 Input data used by the wellbore thermal simulator (WELLTHER) in the numerical case 3.

Source	z (m)	t_c (hr)	Predicted temperature	
			T_b (°C)	T_o (°C)
Holmes and Swift (1970)	4600.0	steady-state	85.0	26.3
Keller et al (1973)	4600.0	6.0	95.9	26.6
Keller et al (1973)	4600.0	24.0	89.4	29.3
Keller et al (1973)	4600.0	144.0	81.5	31.8
Marshall and Bentsen (1982)	4600.0	10.0	90.0	33.7
Marshall and Bentsen (1982)	4600.0	100.0	81.8	36.2
Marshall and Bentsen (1982)	4600.0	1000.0	75.0	36.8
This research work	4600.0	10.0	91.7	26.4
This research work	4600.0	100.0	82.5	26.8
This research work	4600.0	1000.0	71.7	27.0

T_b (bottomhole fluid temperature); T_o (outlet fluid temperature); t_c (circulating time)

Table 9.5 Comparison of the predicted bottomhole and outlet temperatures for the numerical case 3.

Variables	Units	Low value	Intermediate value	High value
Fluid inlet temperature (T_{in})	[°C]	30.0	57.7	70.0
Fluid density (ρ)	[kg m^{-3}]	900.0	1200.0	2000.0
Fluid flowrate (W)	[kg s^{-1}]	15.14	--------	75.7
Fluid viscosity (μ)	[Pa.s]	0.010	0.045	0.060
Fluid specific heat capacity (Cp)	[J kg^{-1} $°C^{-1}$]	2500.0	3930.0	4500.0
Fluid thermal conductivity (k_m)	[W m^{-1} $°C^{-1}$]	1.25	2.25	5.00
Geothermal gradient (G)	[°C m^{-1}]	0.010	0.029	0.050
Formation thermal conductivity (k_f)	[W m^{-1} $°C^{-1}$]	1.25	2.25	5.00

Table 9.6 Range of values for the variables used in the parametric sensitivity analysis. The majority of these values were varied considering the original input data of the numerical case 2.

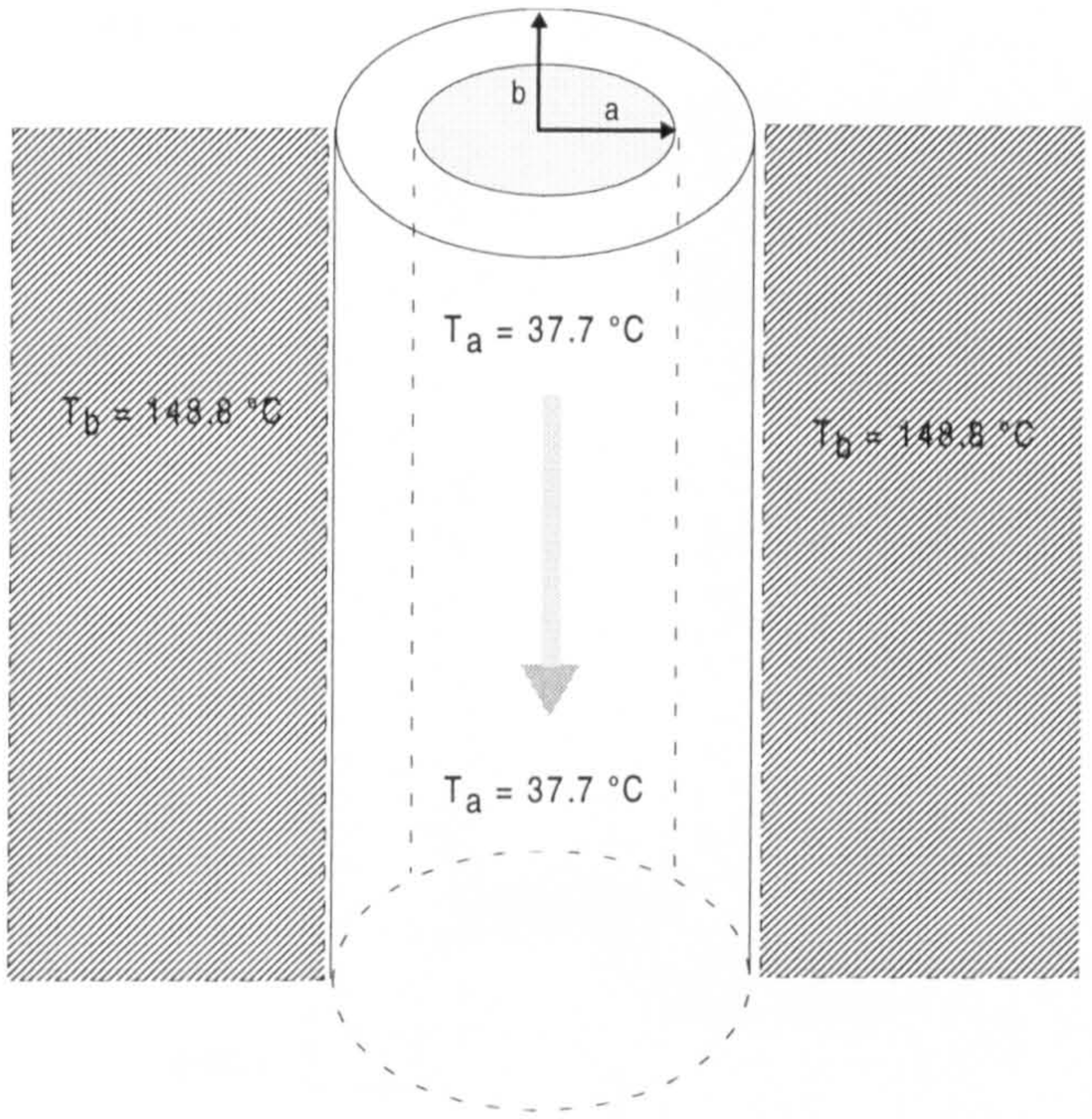

Fig. 9.1 Steady state, infinitely long hollow cylinder [numerical case 1; Carslaw and Jaeger (1959)].

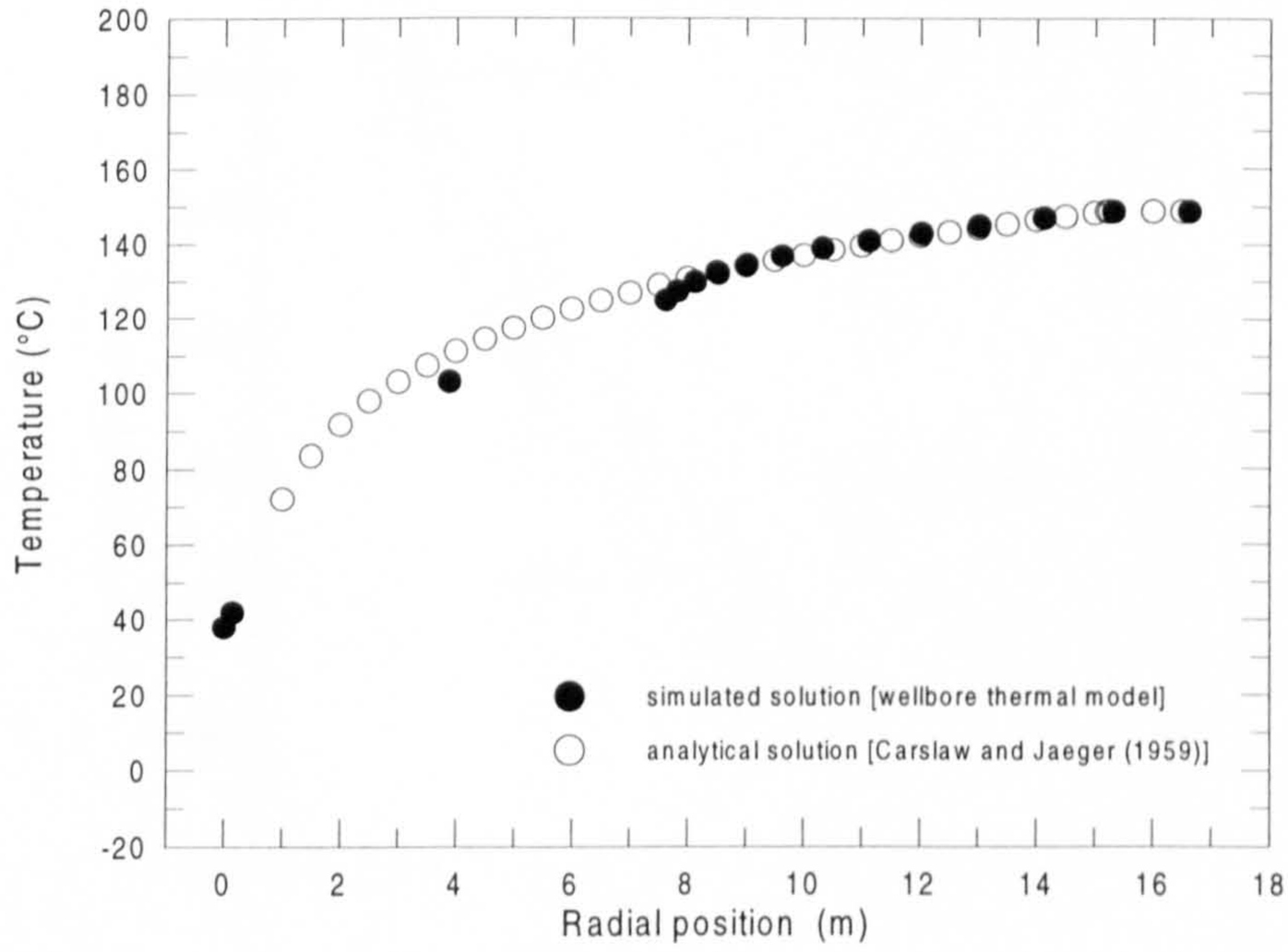

Fig. 9.2 Steady state temperature profile in a hollow cylinder with convection inside (numerical case 1).

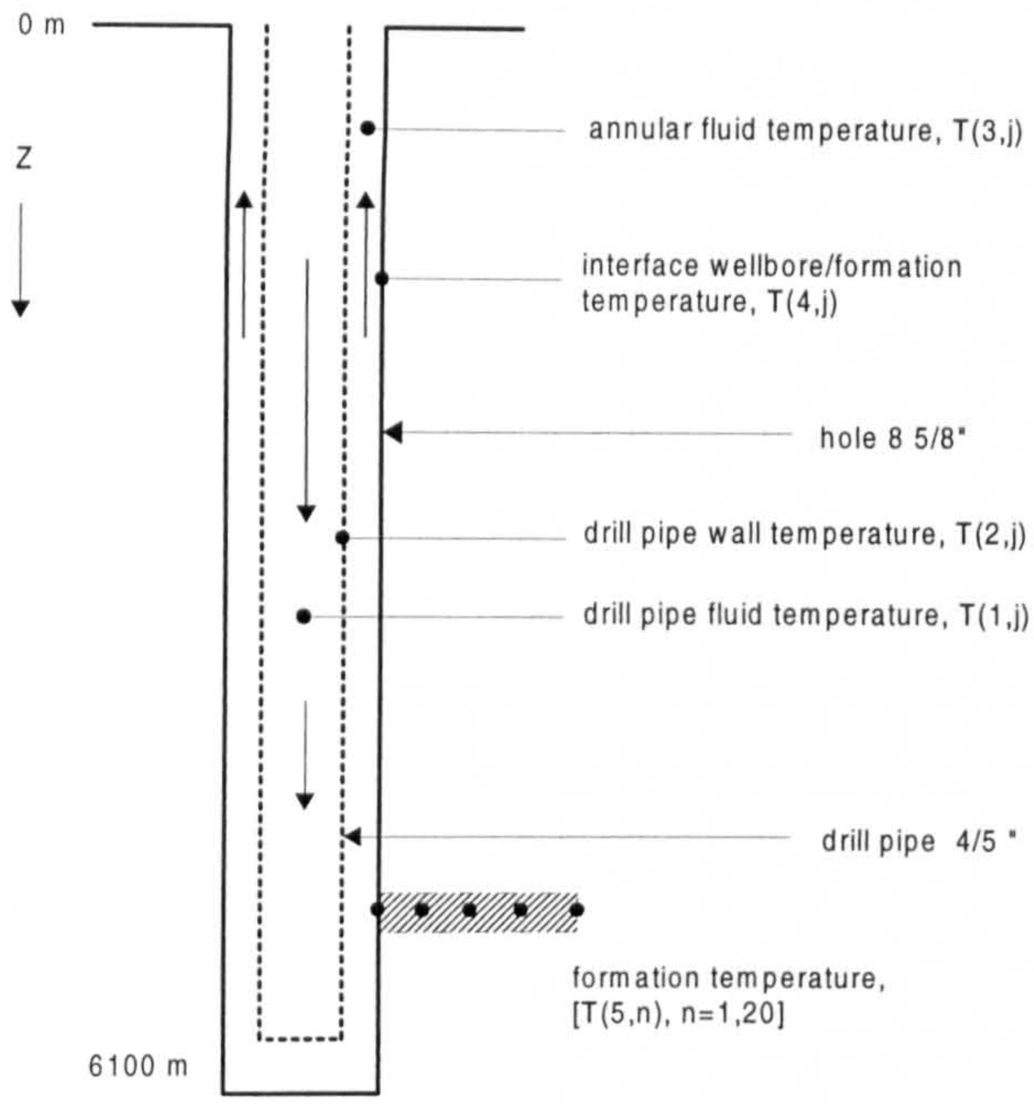

Fig. 9.3 Geometry of the wellbore drilling system (numerical case 2)

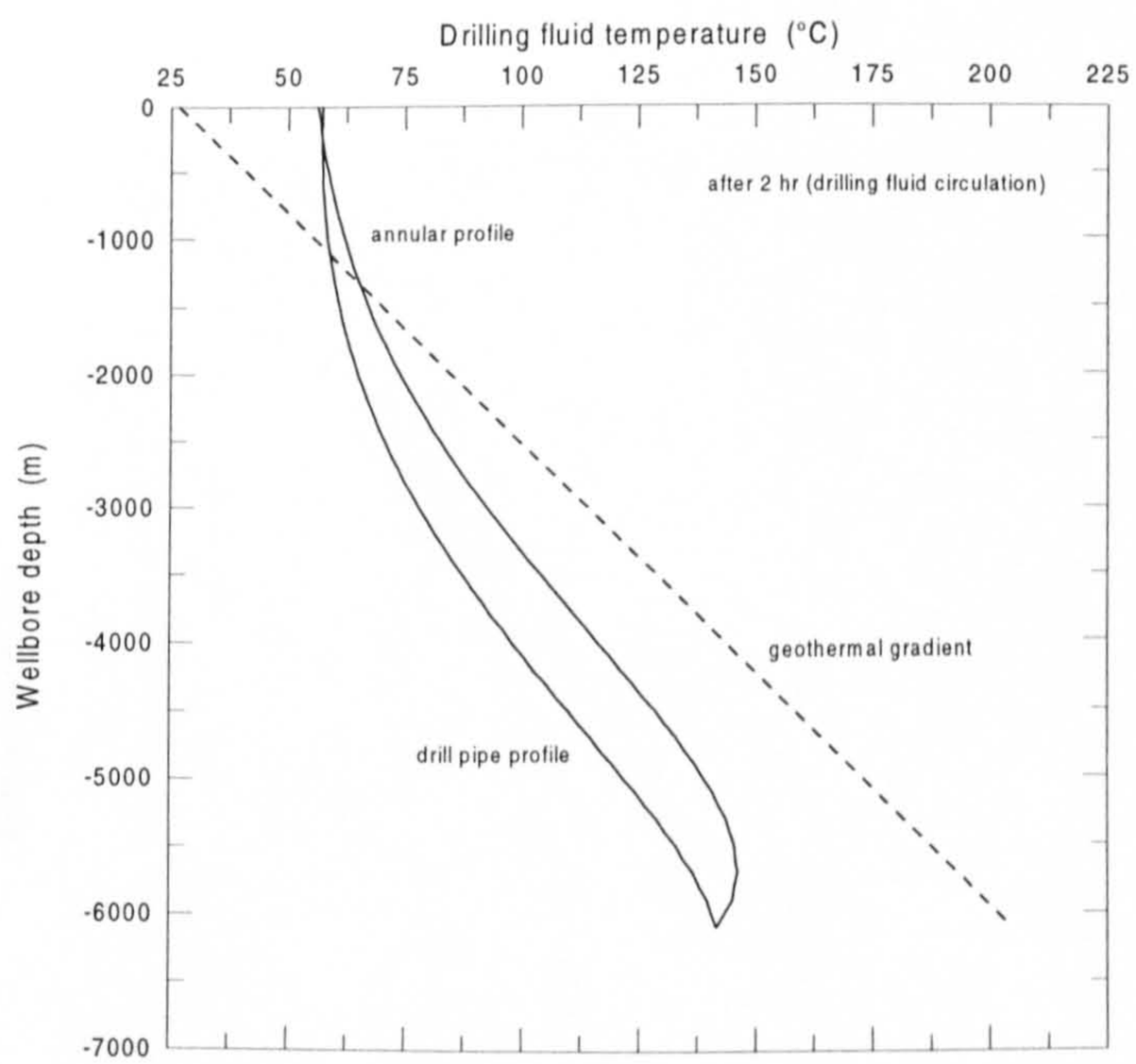

Fig. 9.4 Predicted drill pipe and annular temperature profiles in a 6100 m wellbore after 2 hours of the drilling fluid circulation using the wellbore thermal simulator (WELLTHER).

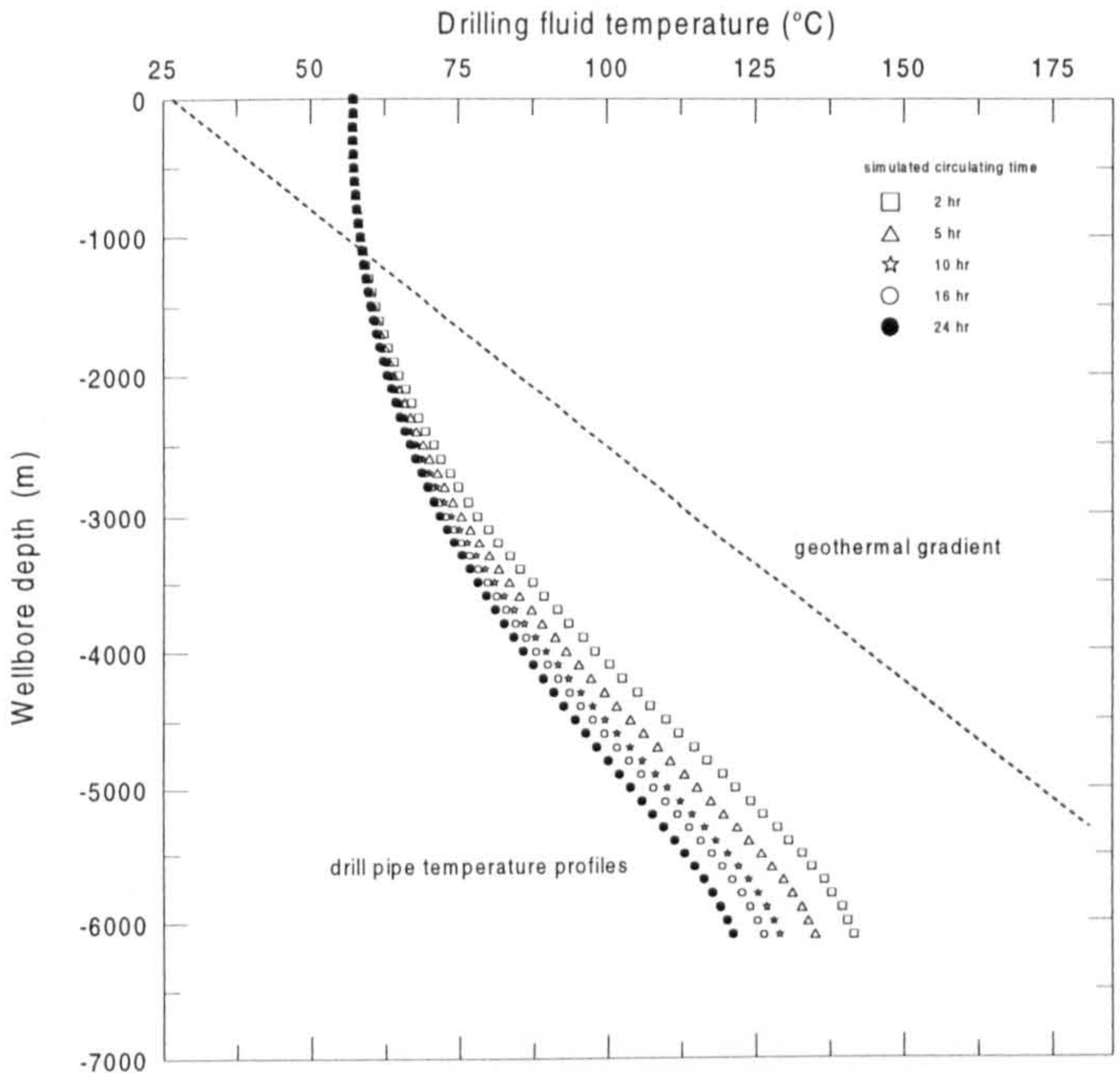

Fig. 9.5 Drill pipe temperature profiles as a function of circulating time for a simulated geothermal wellbore (numerical case 2).

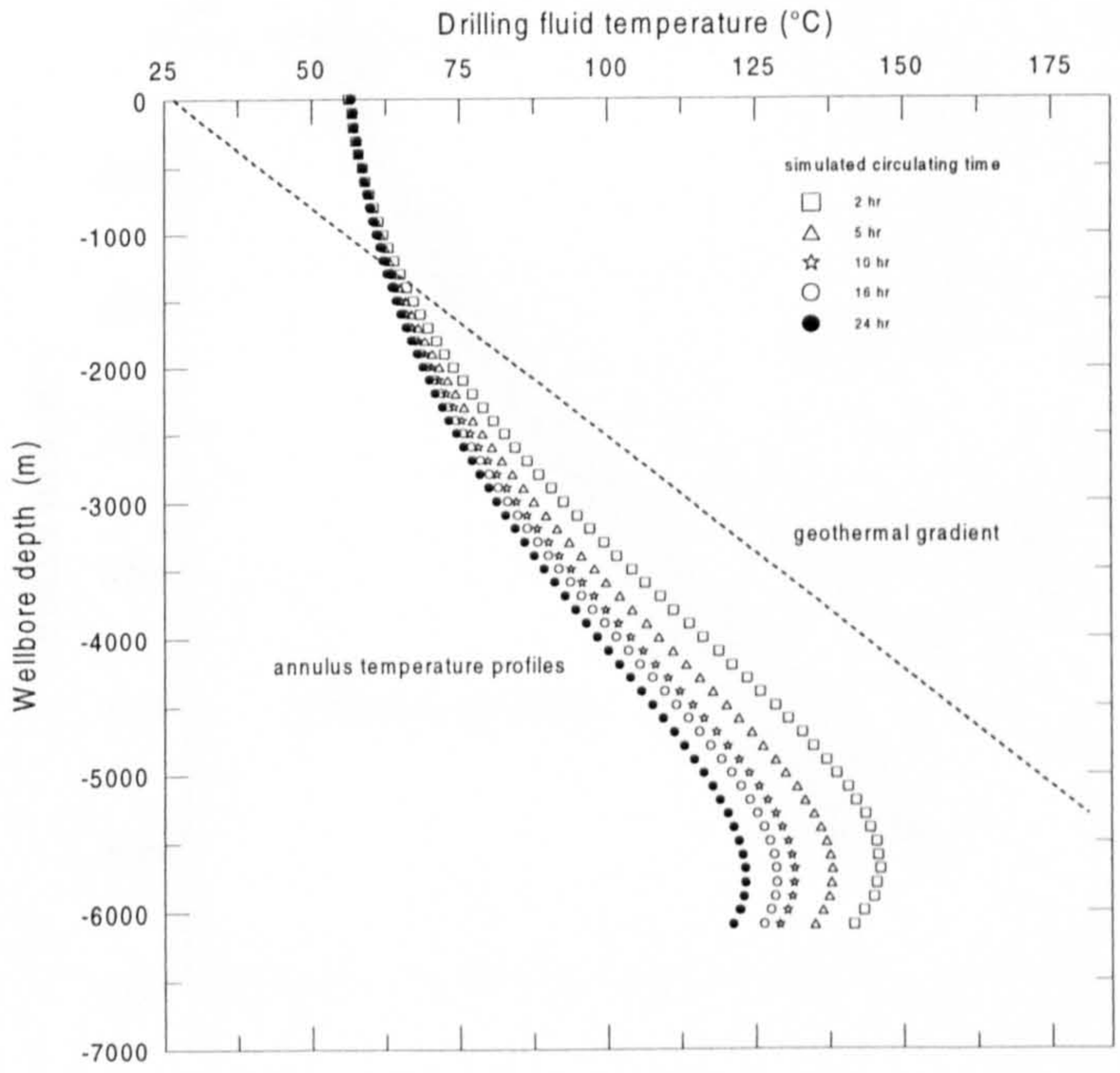

Fig. 9.6 Annulus temperature profiles as a function of circulating time for a simulated geothermal wellbore (numerical case 2).

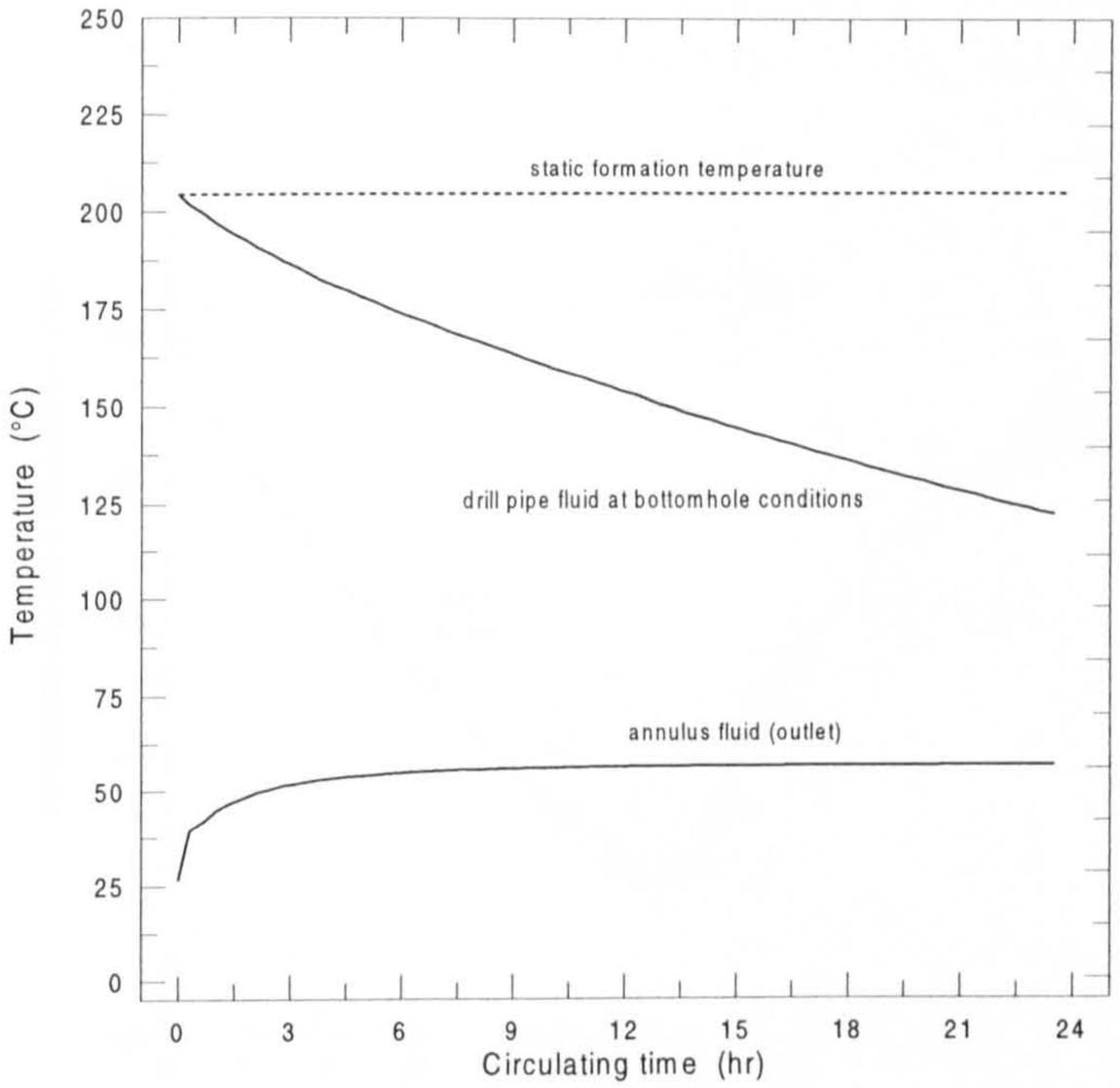

Fig. 9.7 Variation of temperature with circulating time in a 6100 m geothermal wellbore (numerical case 2)

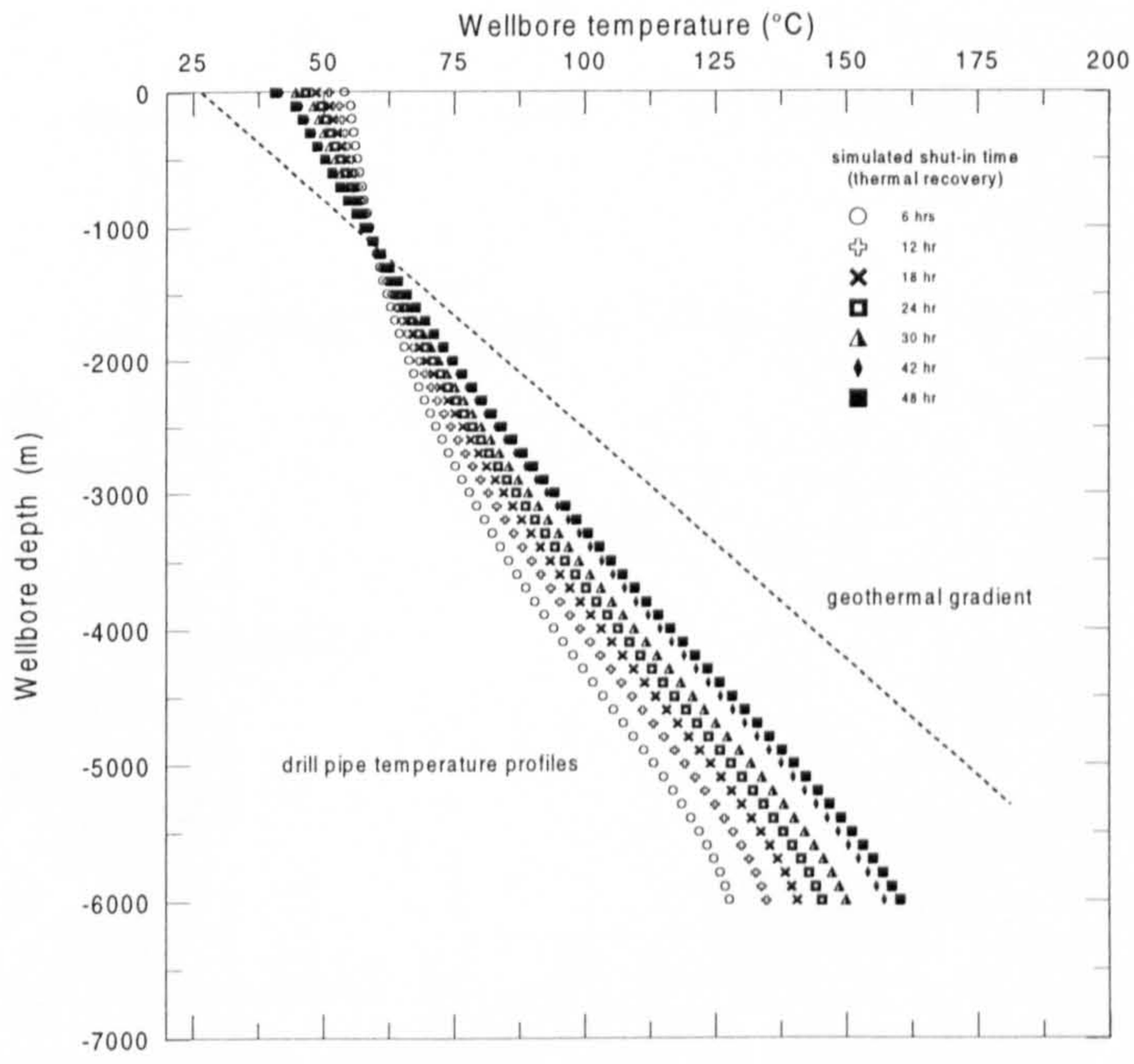

Fig. 9.8 Behaviour of the drill pipe temperature profiles in a 6100 m geothermal wellbore after 48 hours of the thermal recovery (numerical case 2).

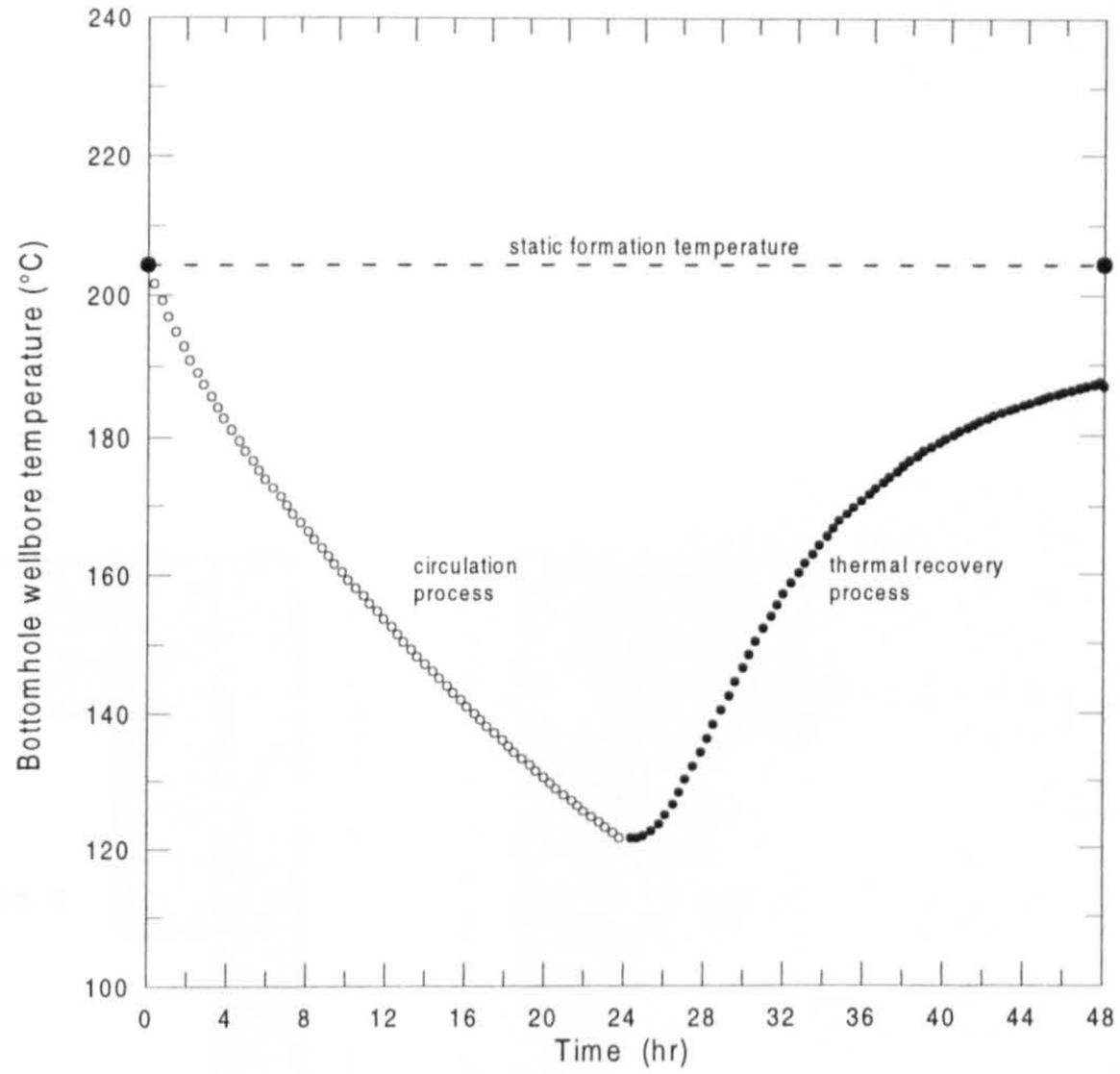

Fig. 9.9 Behaviour of the bottomhole wellbore temperature during the fluid circulation and after thermal recovery processes (numerical case 2).

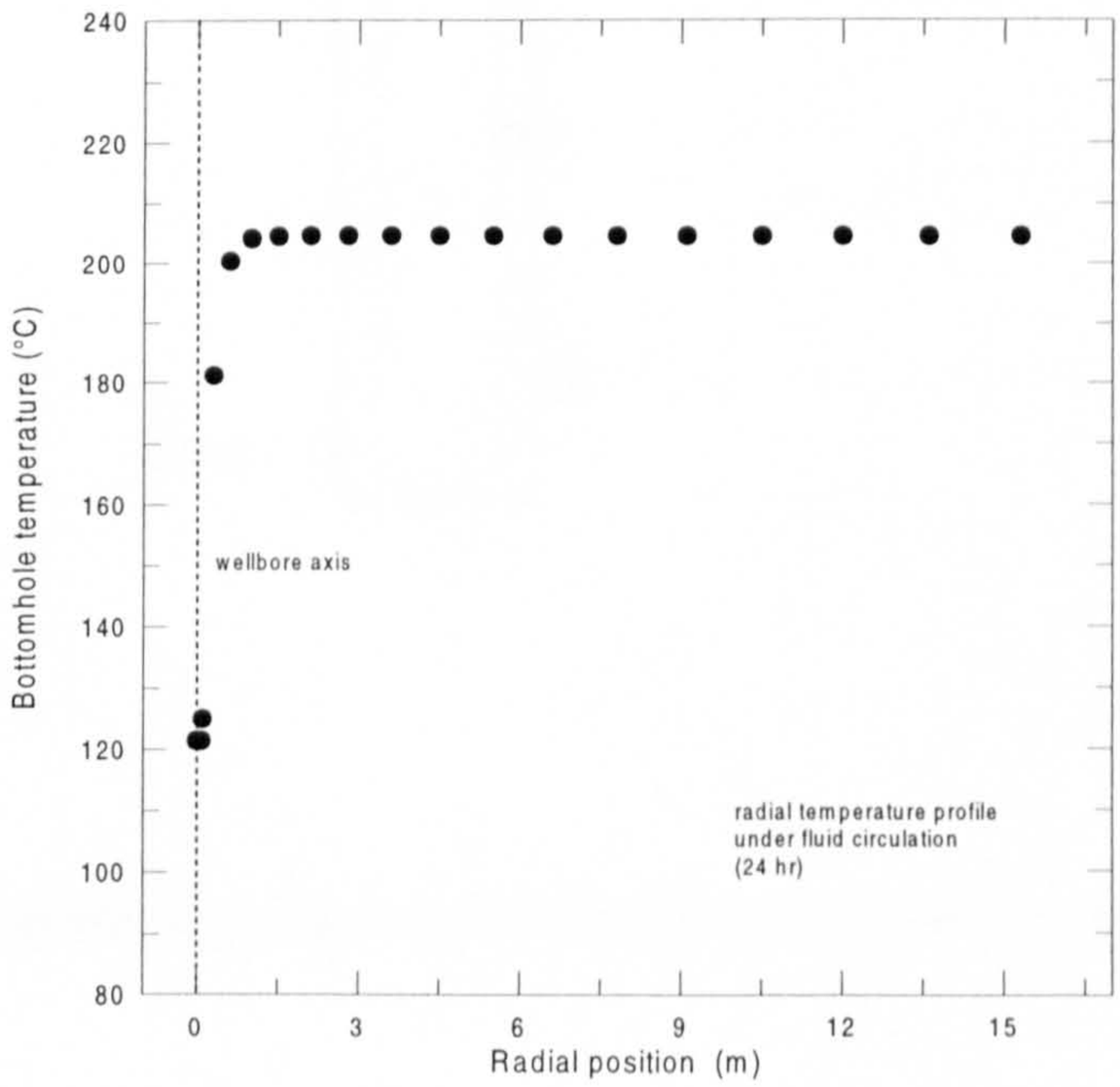

Fig. 9.10 Radial bottomhole temperature profile for a drilling fluid circulation period of 24 hours (numerical case 2).

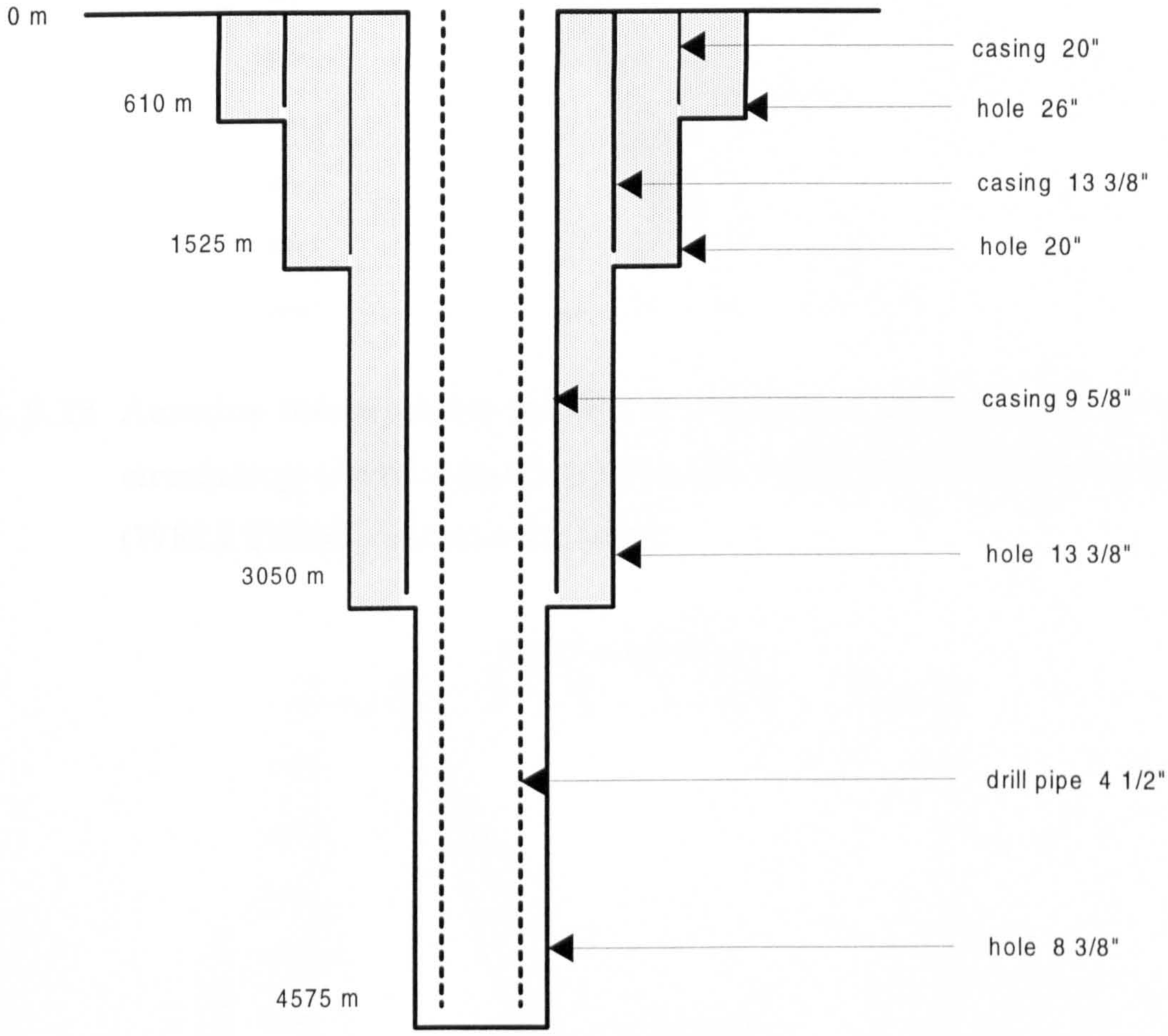

Fig. 9.11 Geometry of the wellbore drilling system (numerical case 3)

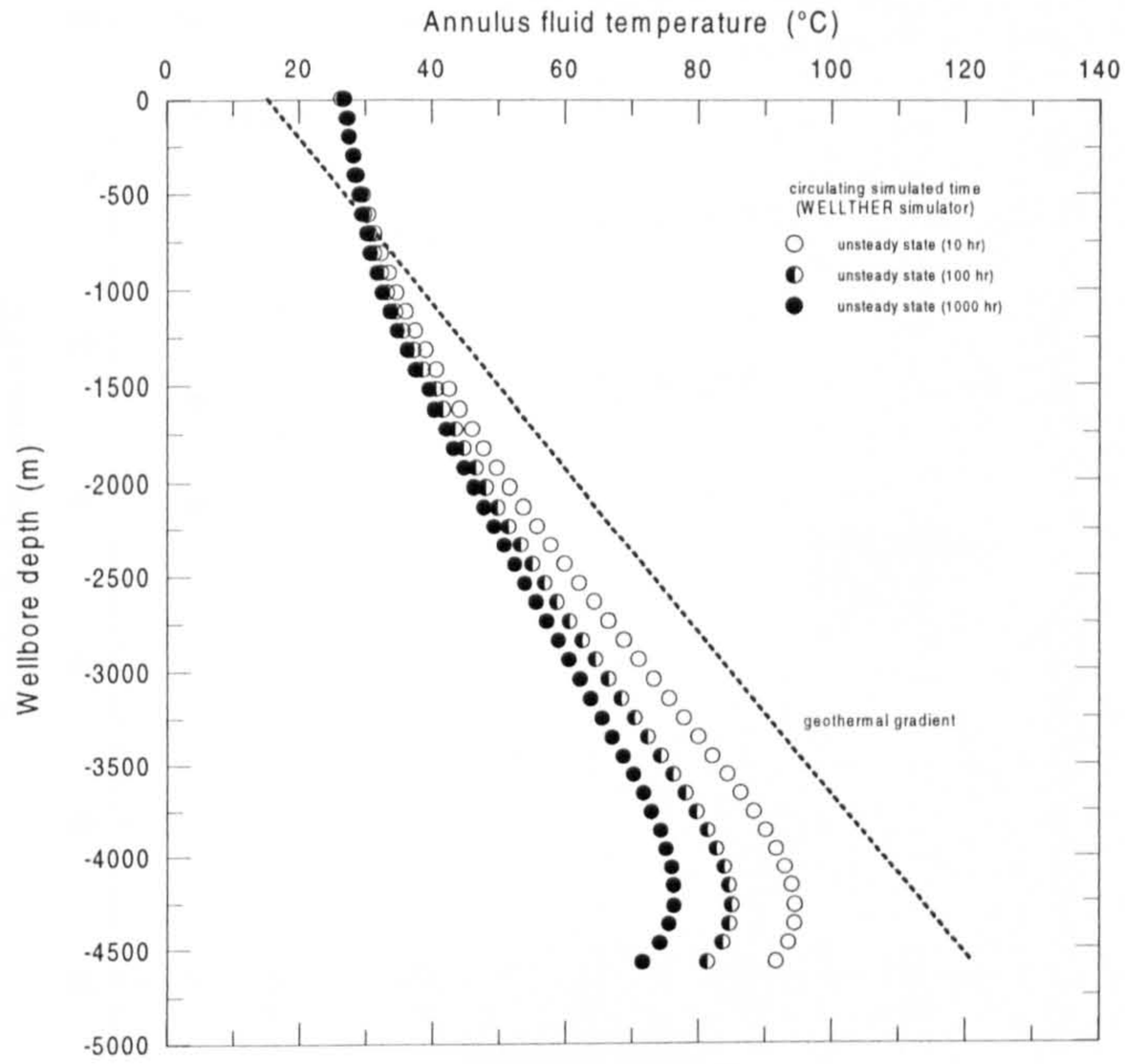

Fig. 9.12 Annulus temperature profiles in a 4,575 m wellbore for several circulating times using the dynamic wellbore thermal simulator (WELLTHER; numerical case 3).

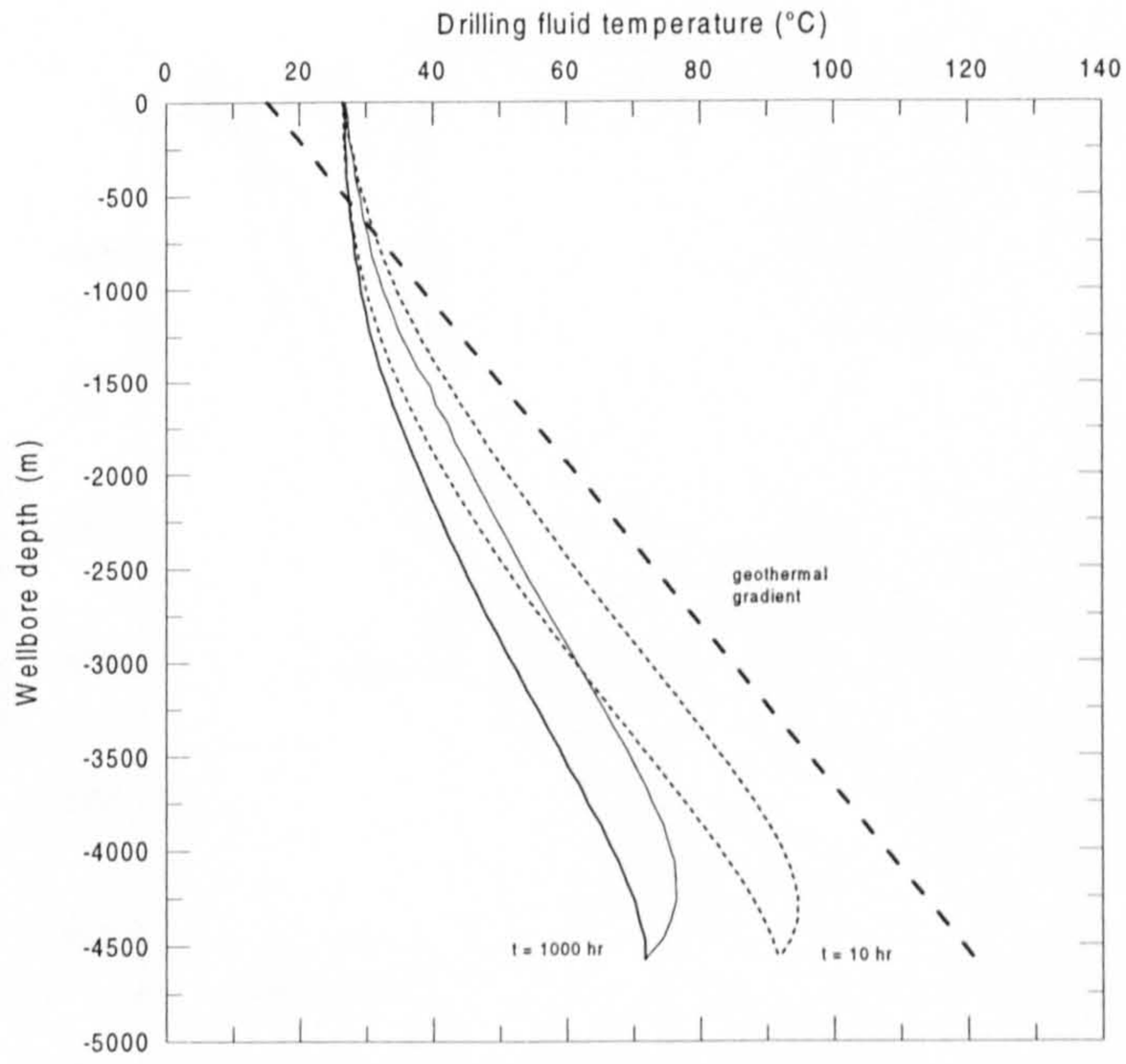

Fig. 9.13 Predicted drill pipe and annular temperature profiles in a 4,575 m wellbore at 10 hours of circulating time and at unsteady state conditions, 1000 hours (numerical case 3).

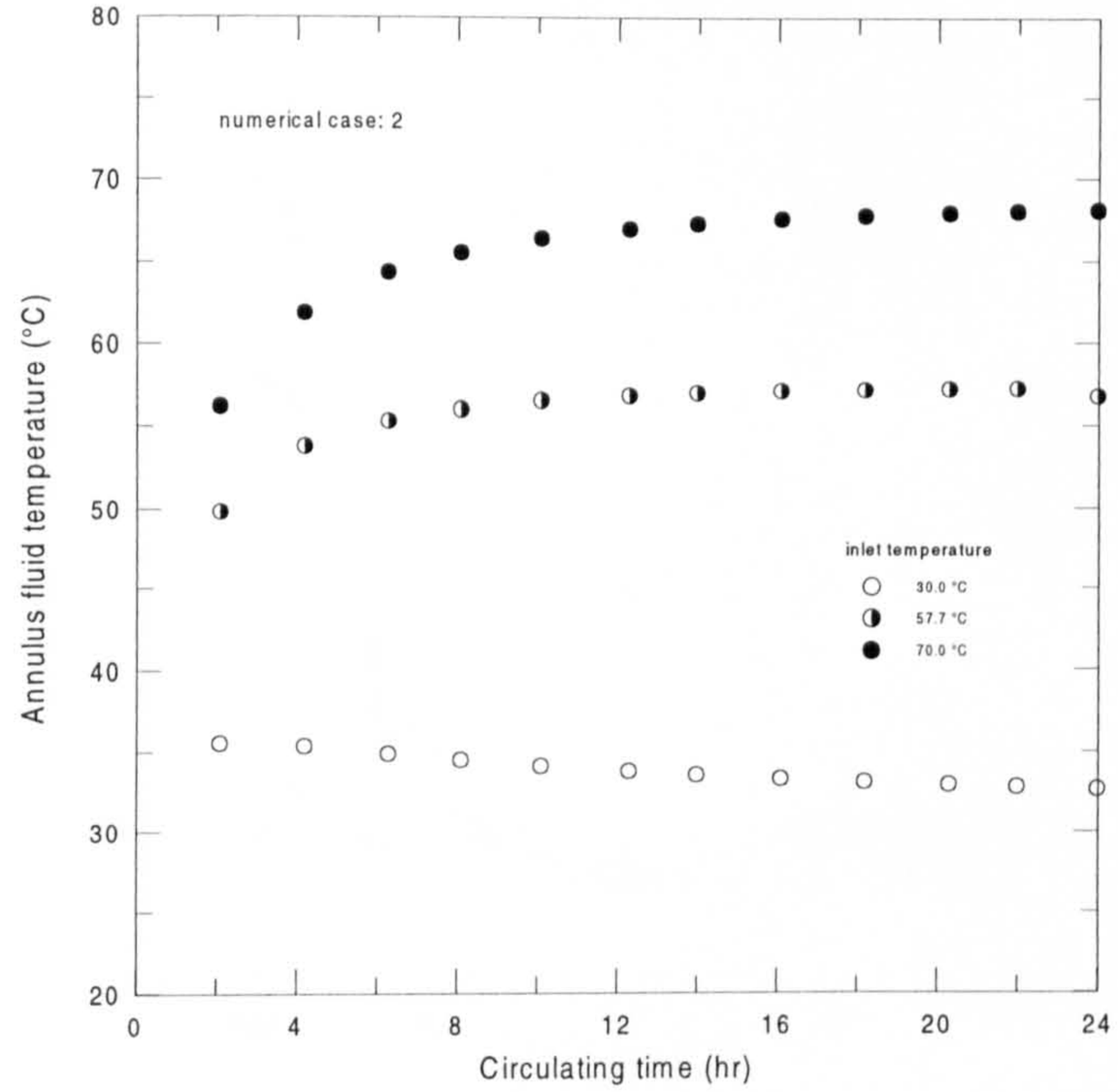

Fig. 9.14 Effect of the inlet drilling fluid temperatures on the annulus fluid temperature under circulating conditions.

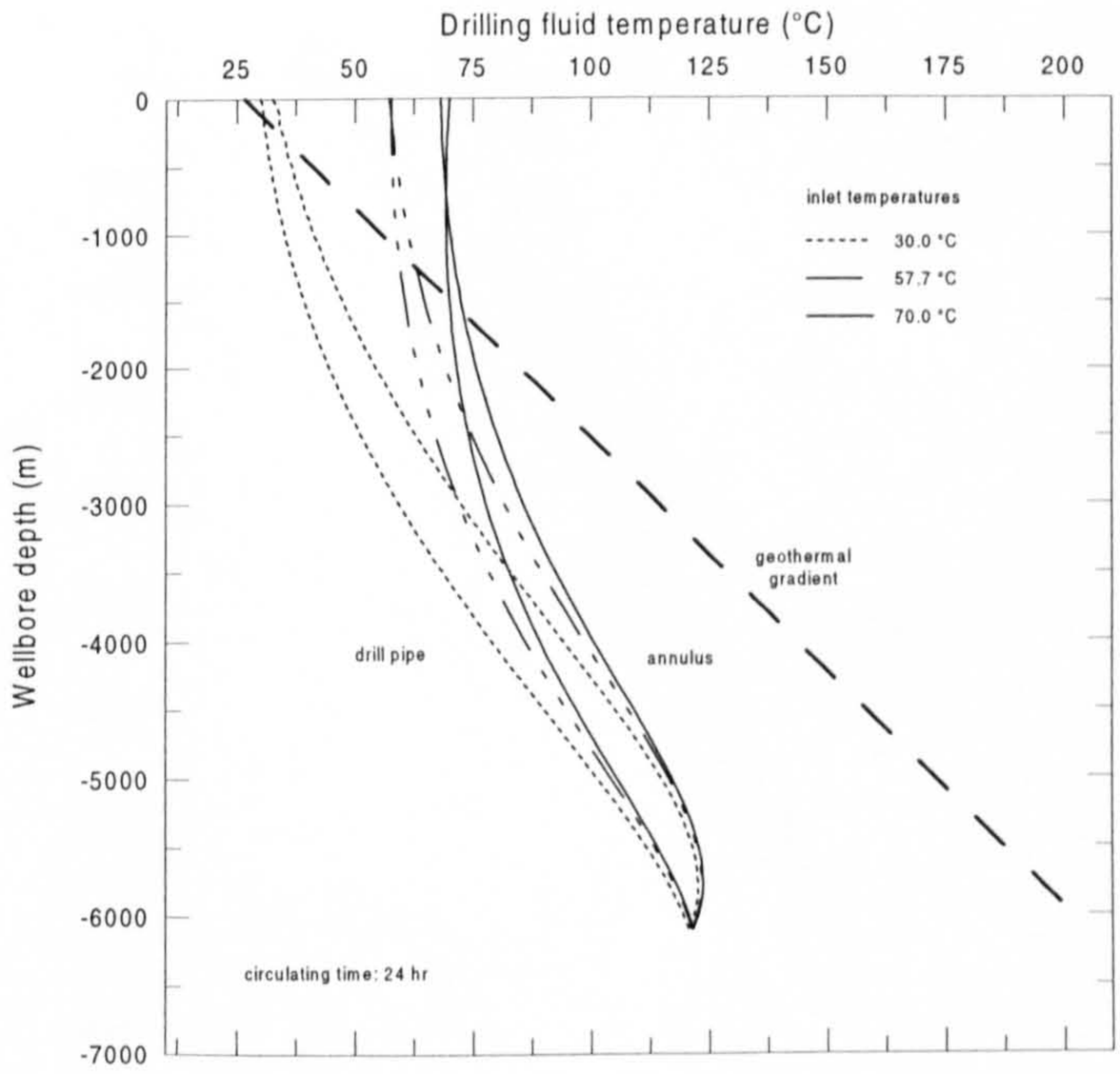

Fig. 9.15 Sensitivity of the circulating fluid temperature profile to the inlet drilling fluid temperature.

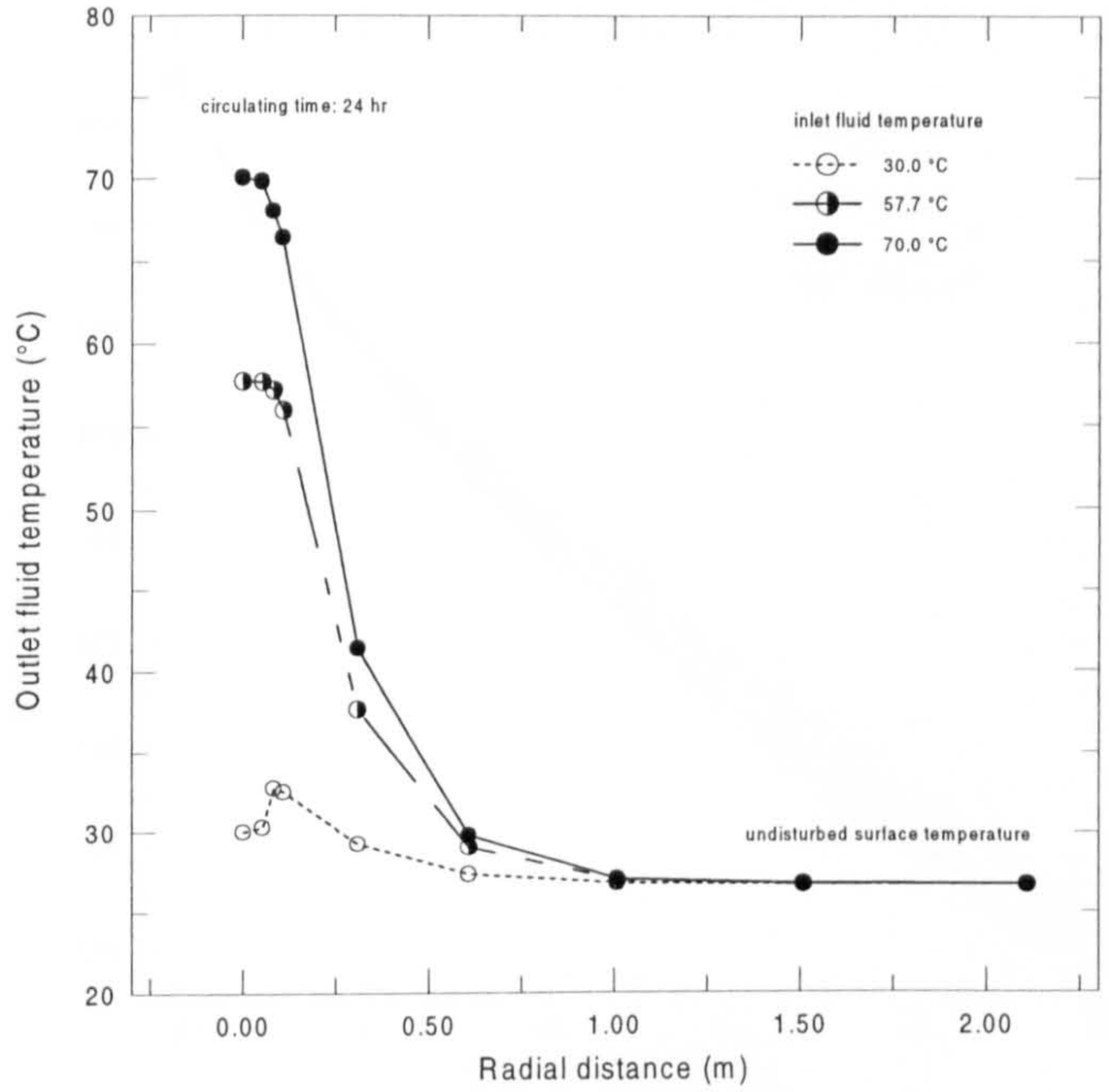

Fig. 9.16 Sensitivity of the radial temperature profiles in the oulet fluid of the annular region to different inlet drilling fluid temperatures.

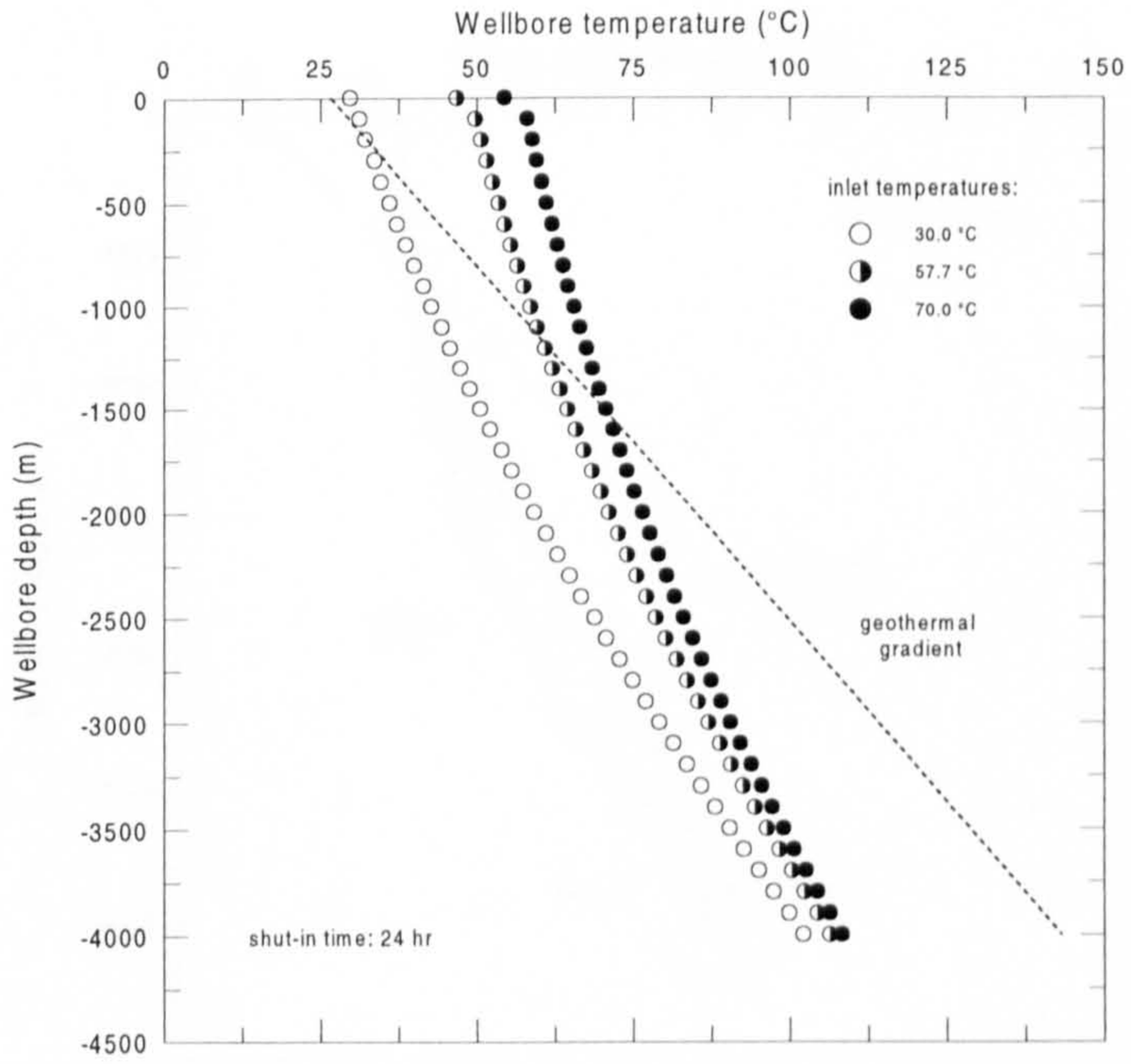

Fig. 9.17 The wellbore temperature profiles inside the drill pipe after 24 hours of the thermal recovery process at three different inlet drilling fluid temperatures.

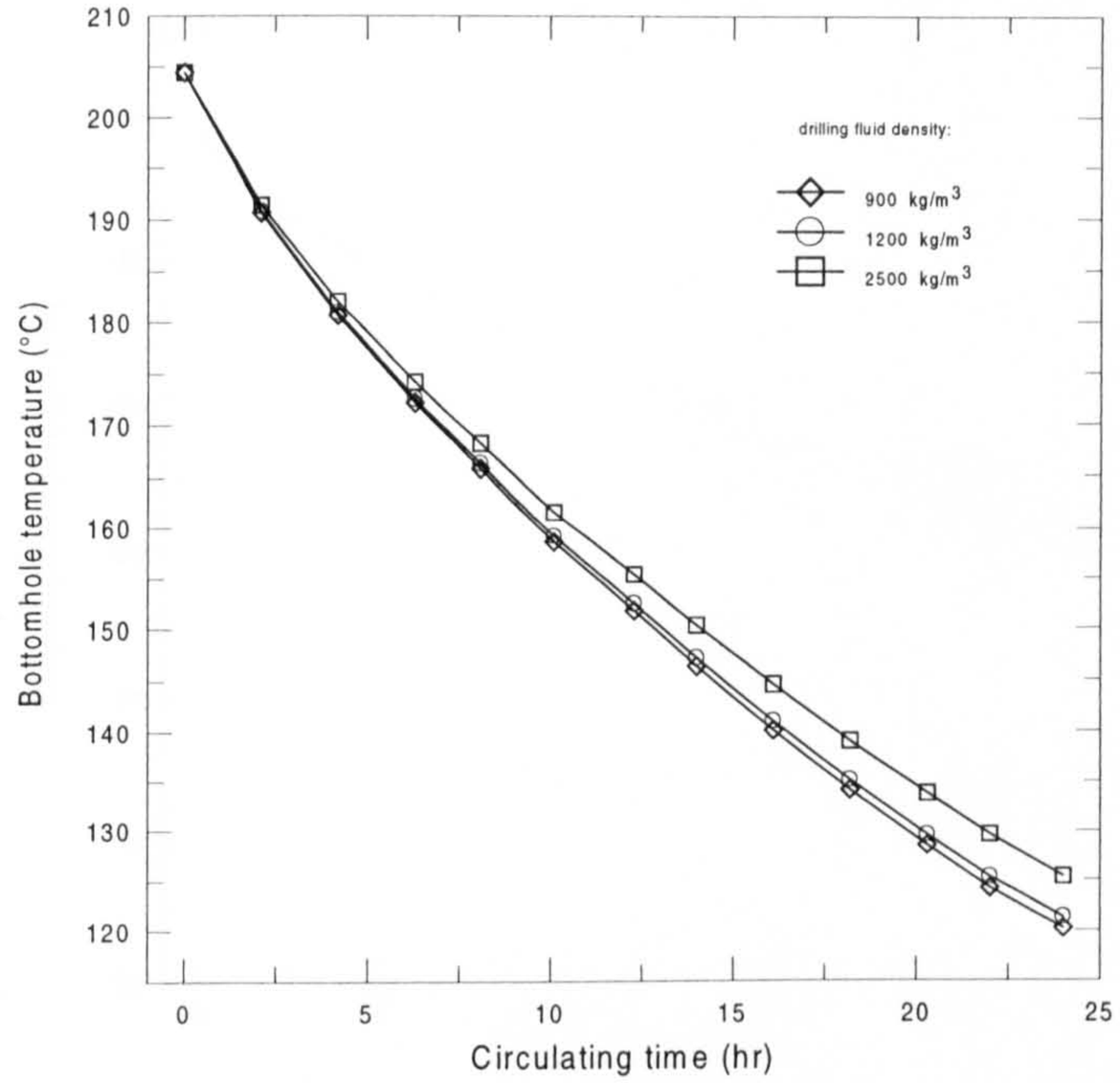

Fig. 9.18 Sensitivity of the bottomhole wellbore temperatures to the drilling fluid density.

Fig. 9.19 Sensitivity of the circulating fluid temperature profile to the drilling fluid density.

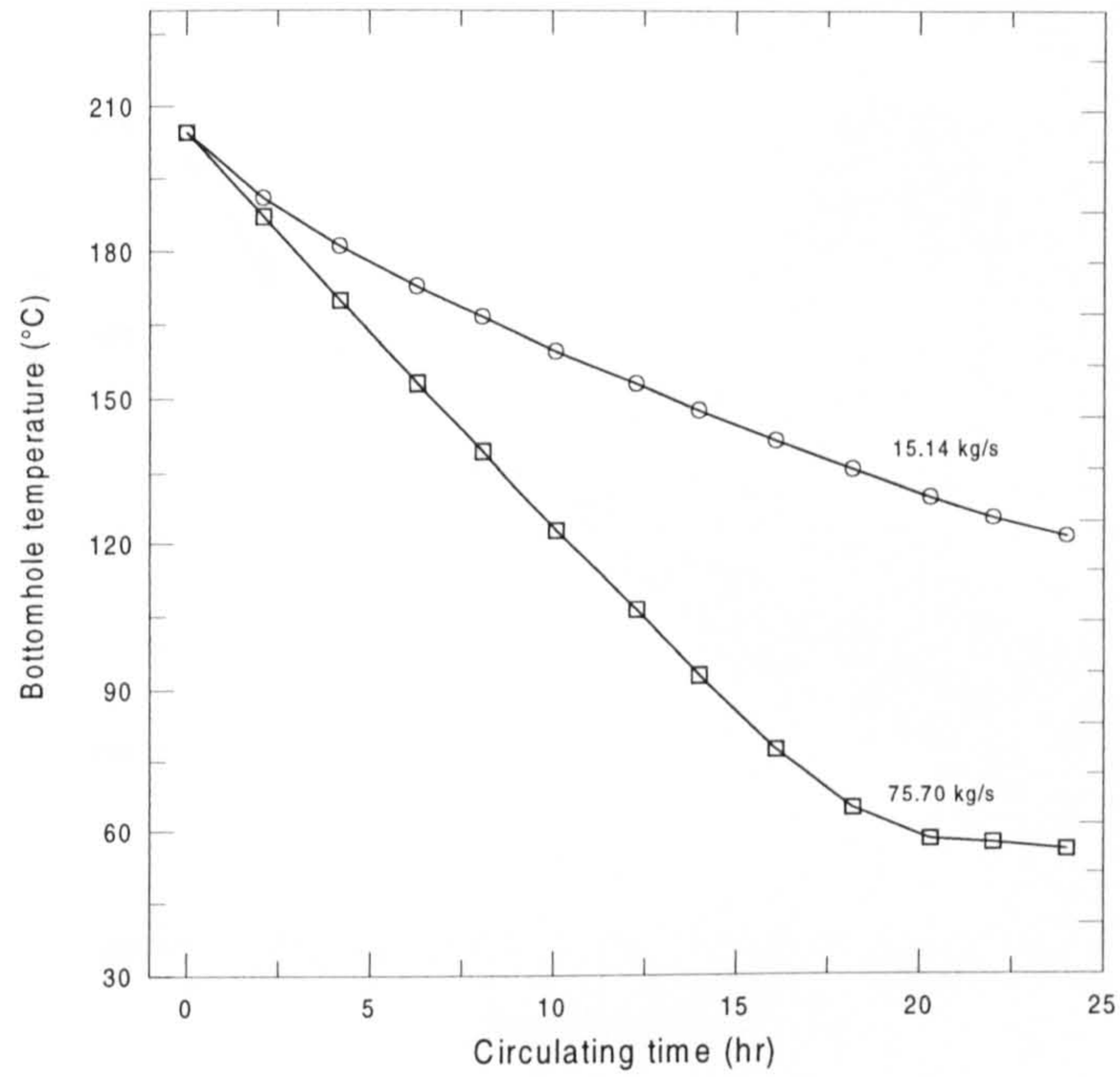

Fig. 9.20 Sensitivity of the bottomhole wellbore temperatures to the drilling fluid flow rate.

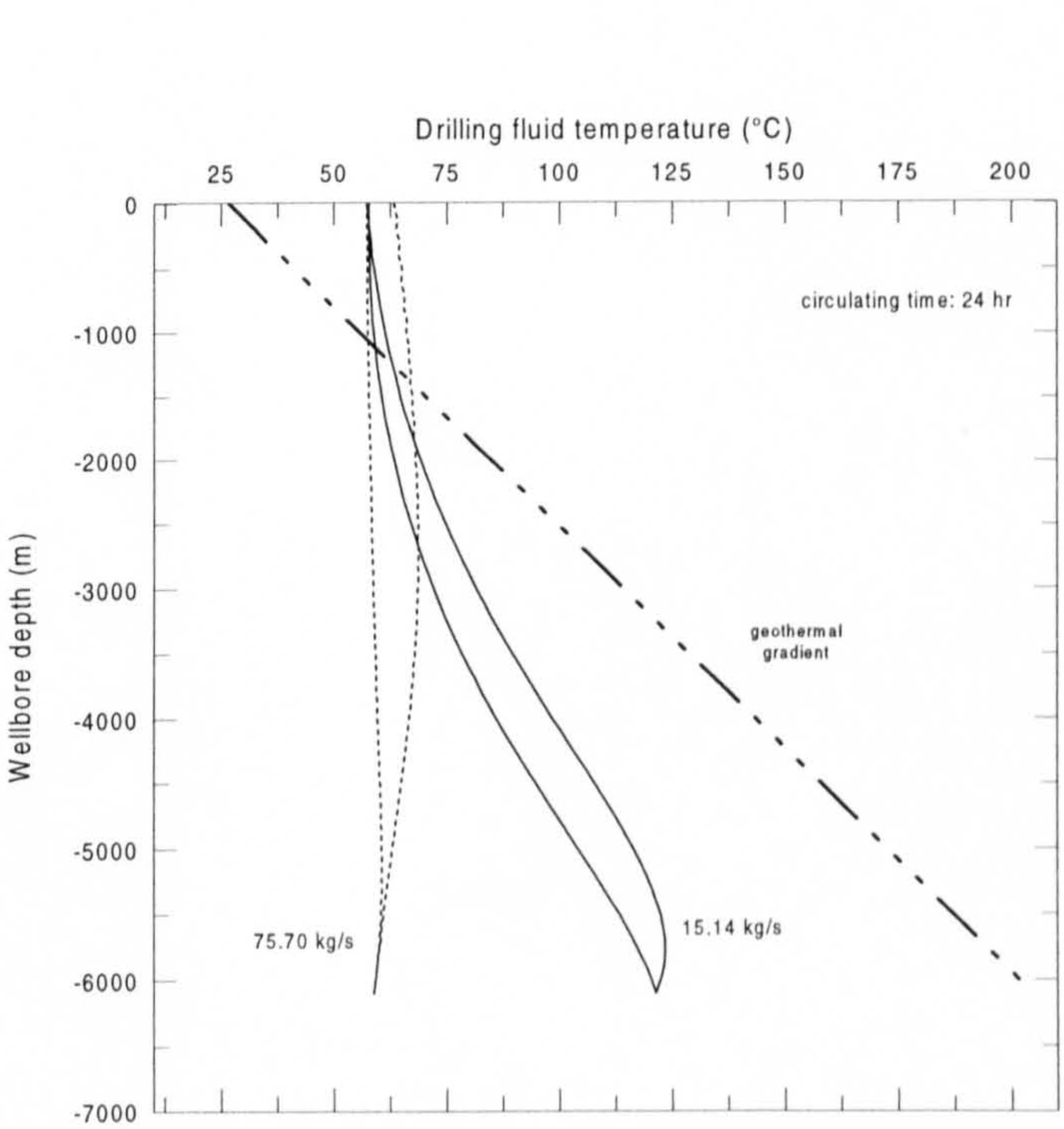

Fig. 9.21 Sensitivity of the circulating fluid temperature profile to the drilling fluid flowrate.

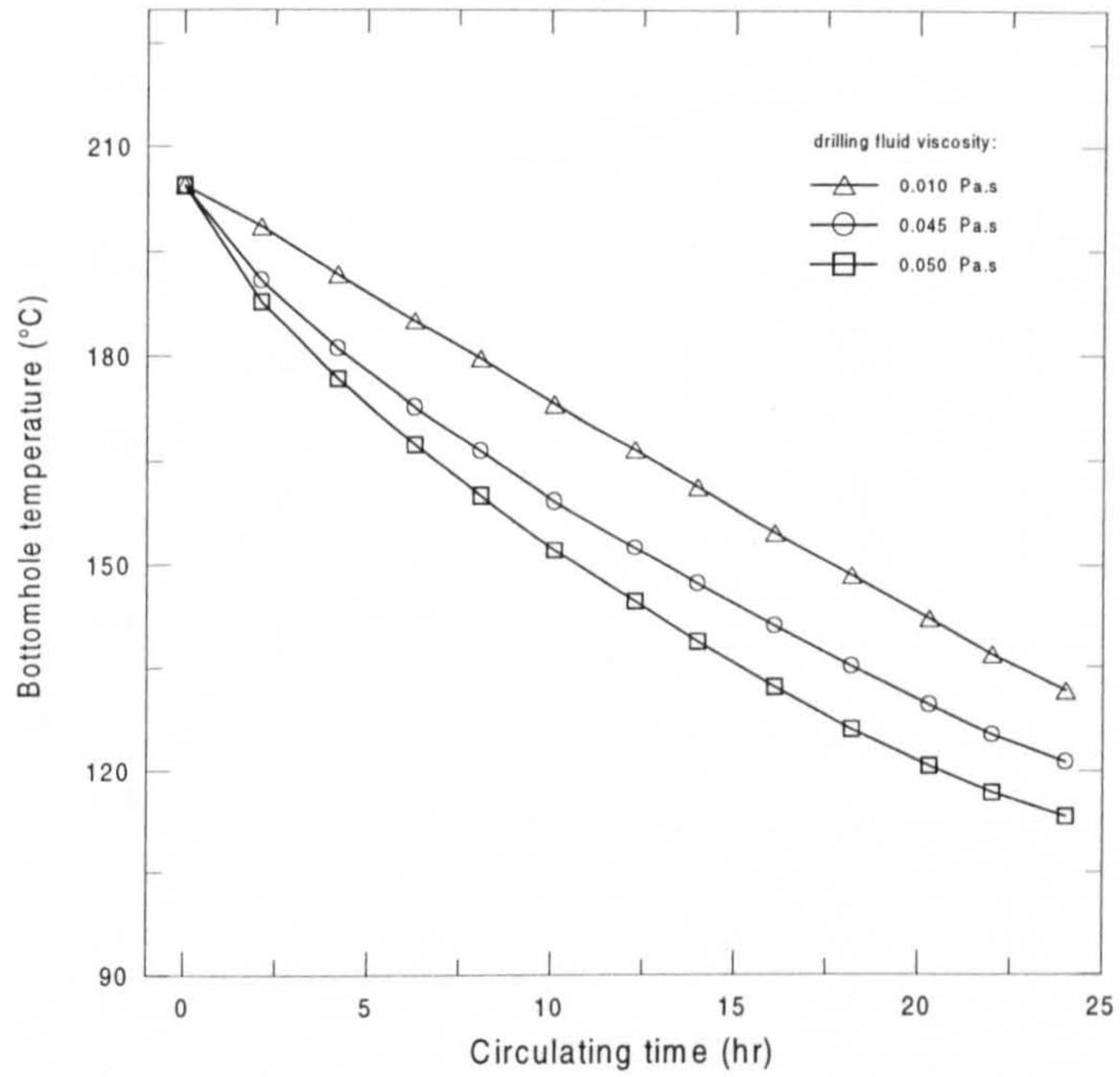

Fig. 9.22 Sensitivity of the bottomhole wellbore temperatures to the drilling fluid viscosity.

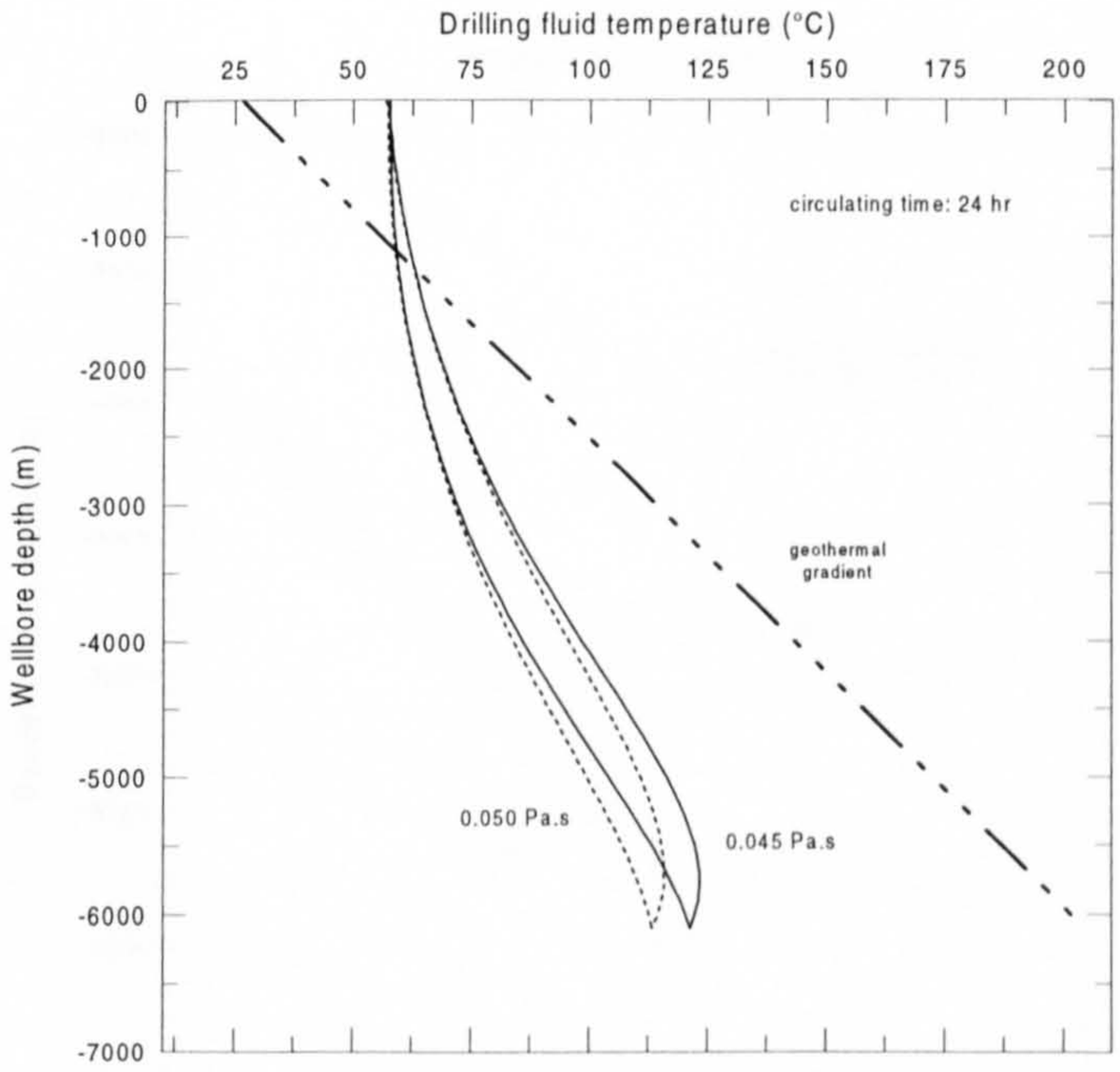

Fig. 9.23 Sensitivity of the circulating fluid temperature profile to the drilling fluid viscosity.

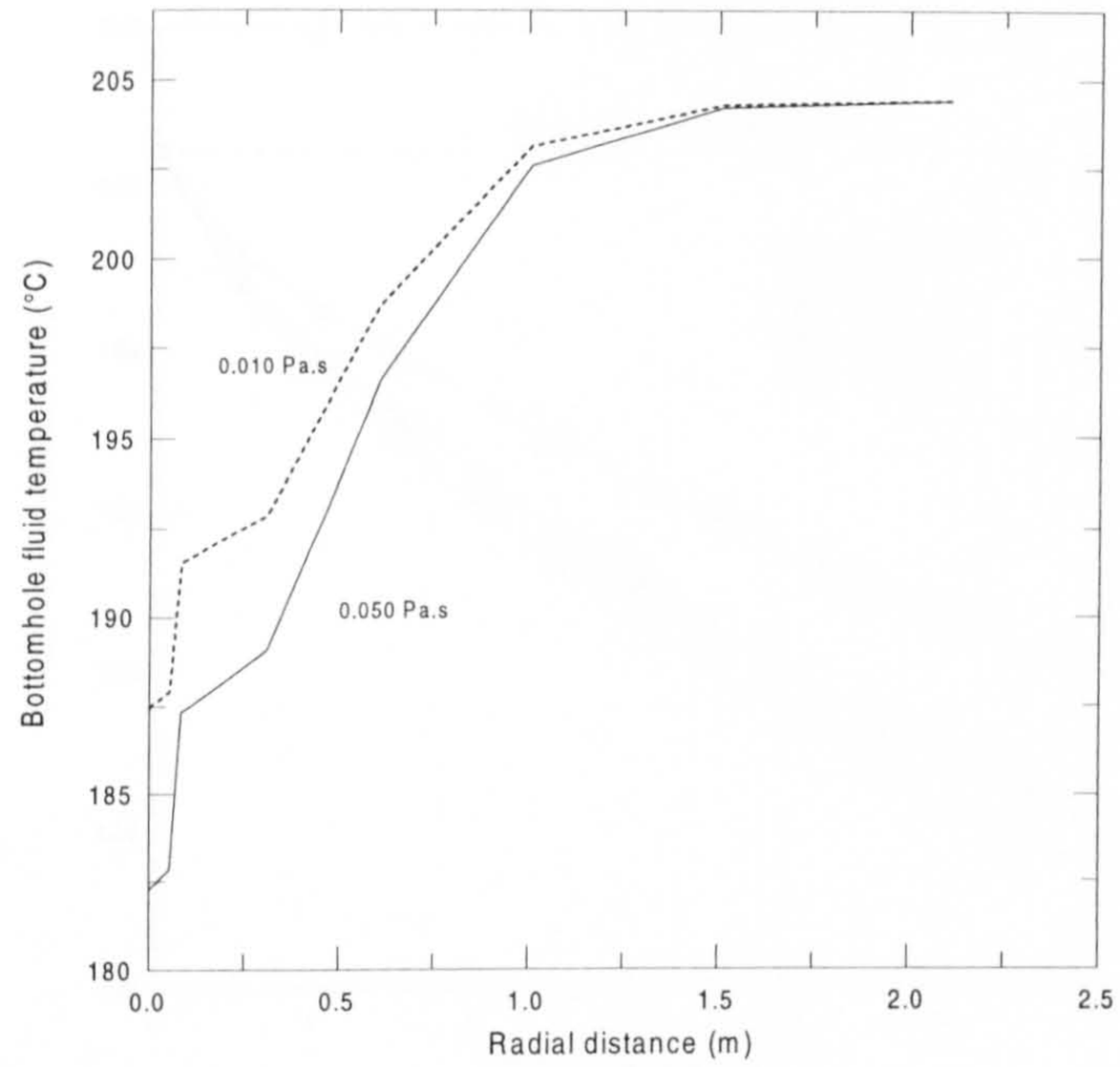

Fig. 9.24 Comparison of the radial temperature profiles for shut-in conditions with different fluid viscosities. The dashed line can be represent a drilling fluid with a similar water viscosity. The solid line represents a typical non-Newtonian drilling fluid.

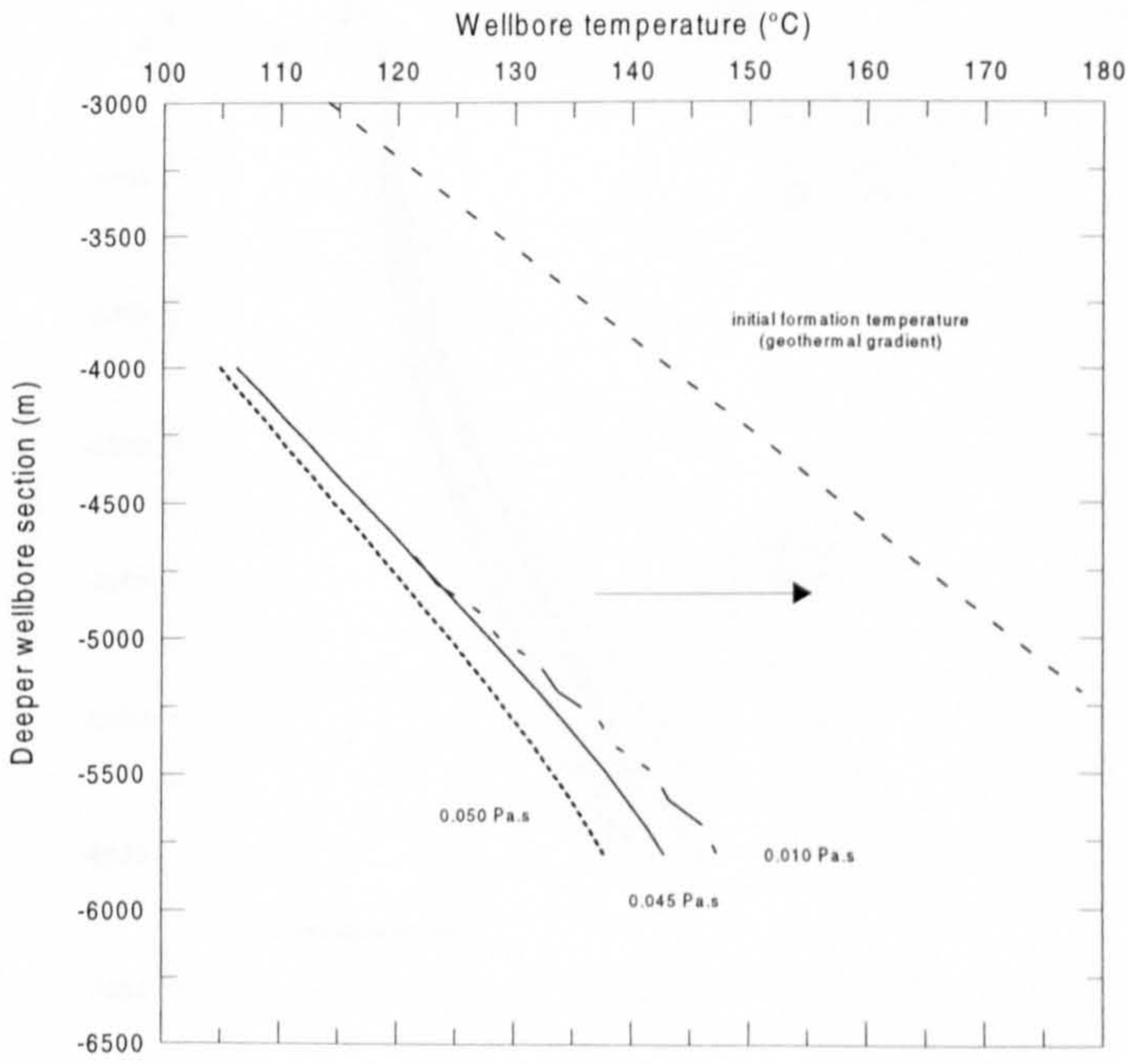

Fig. 9.25 Thermal recovery of the wellbore after 24 hours of shut-in time at different fluid viscosities.

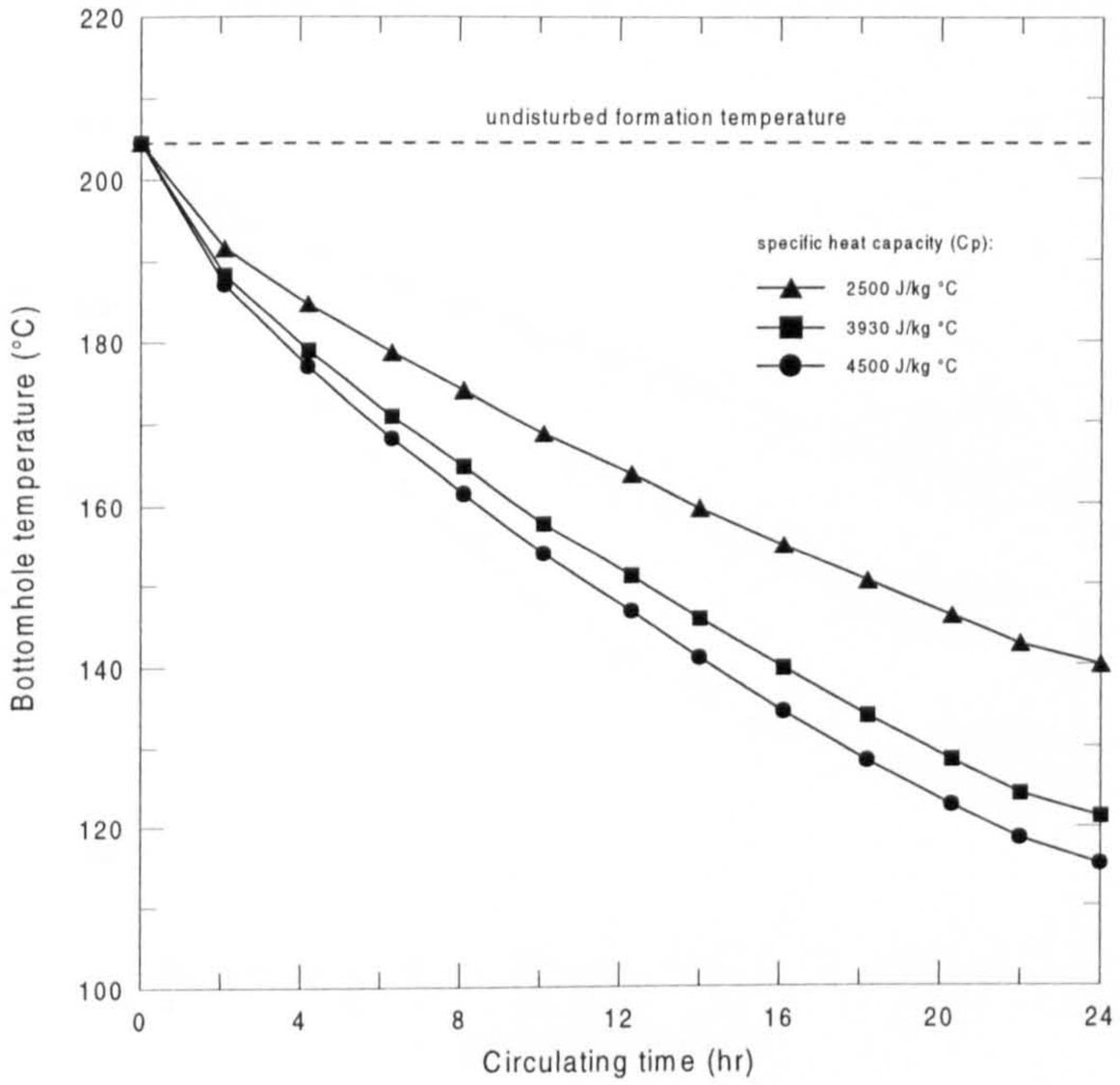

Fig. 9.26 Sensitivity of the bottomhole wellbore temperatures to the drilling fluid specific heat capacity.

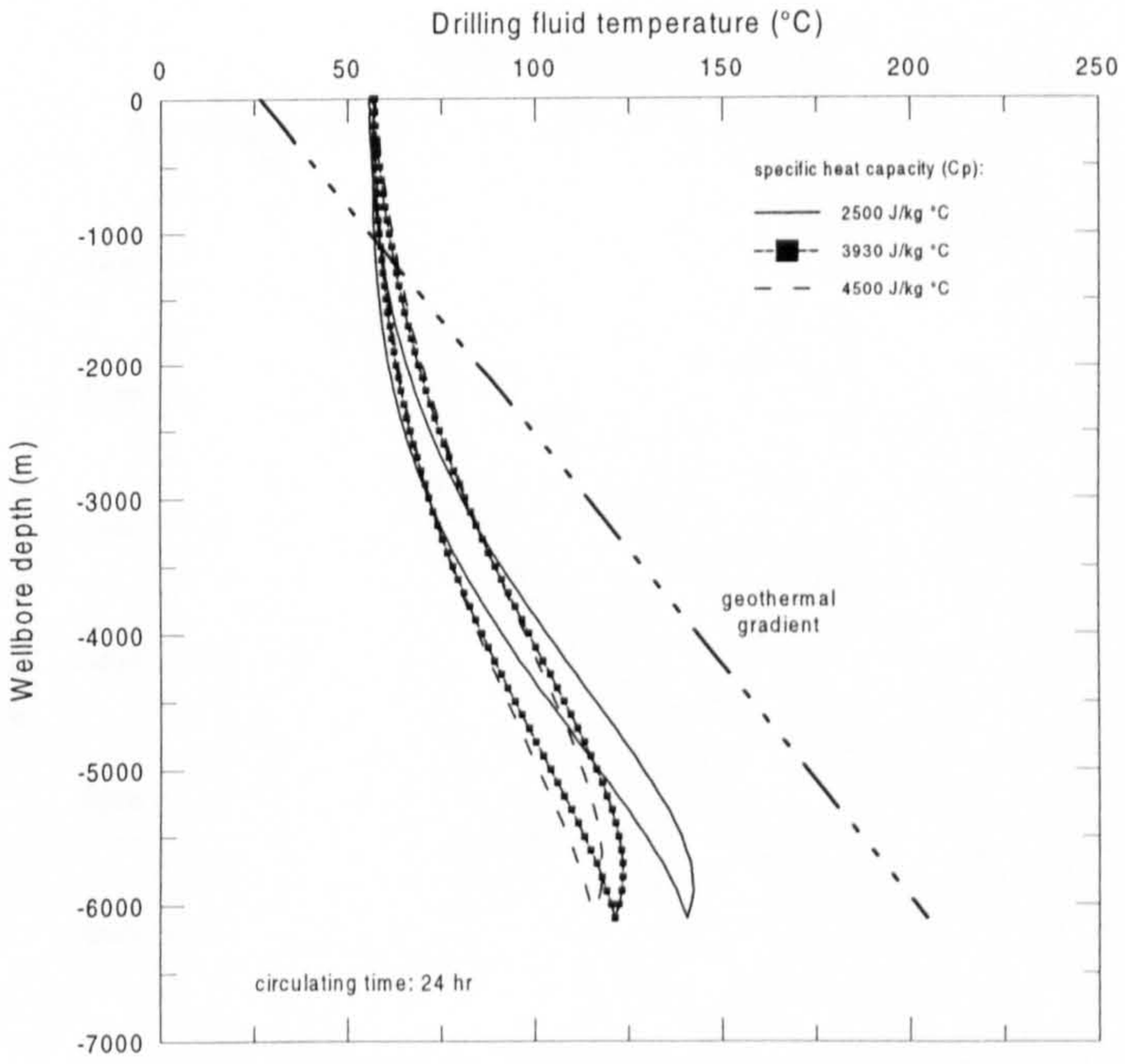

Fig. 9.27 Sensitivity of the circulating fluid temperature profile to the drilling fluid specific heat capacity..

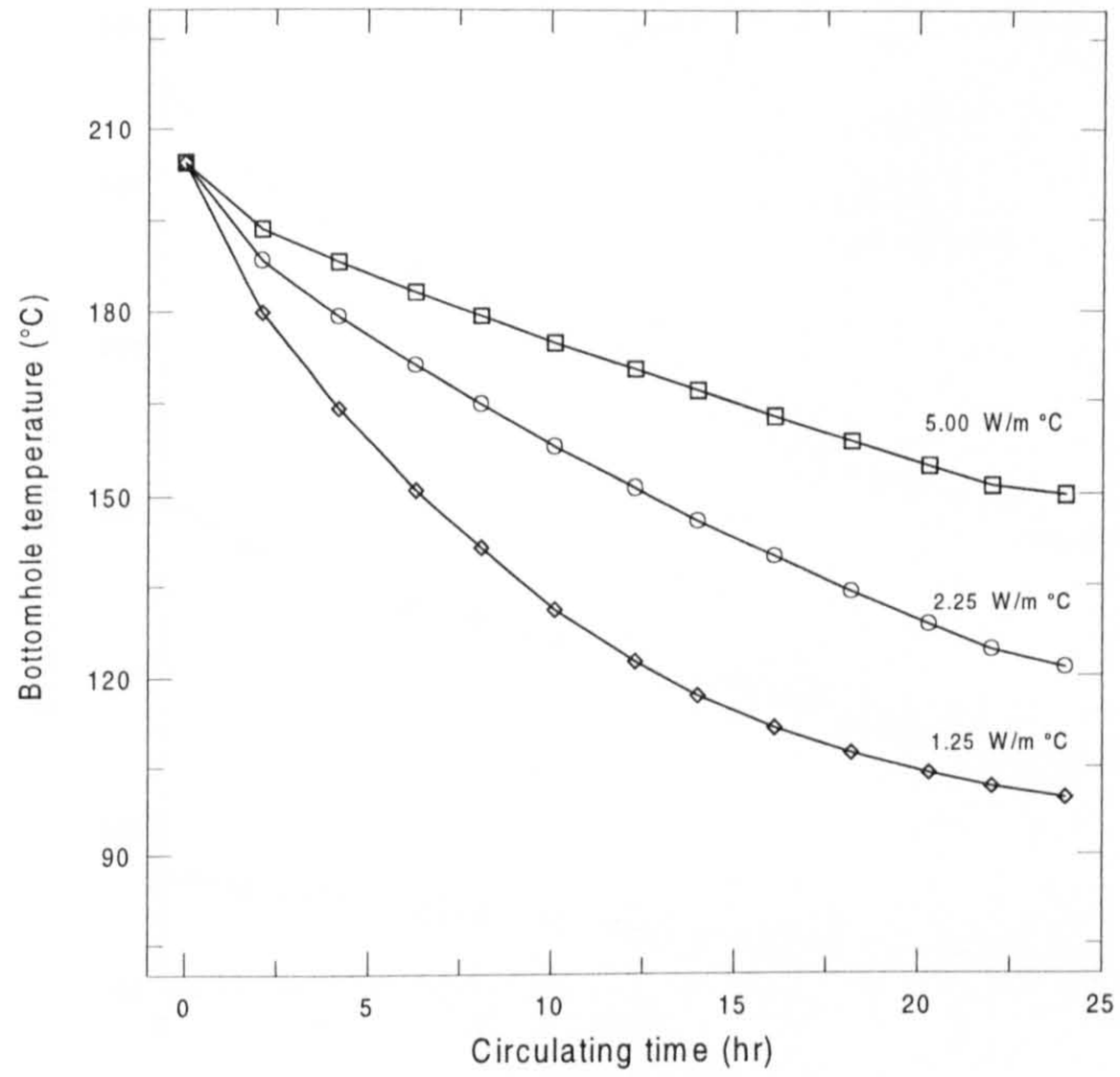

Fig. 9.28 Sensitivity of the bottomhole wellbore temperatures to the drilling fluid thermal conductivity.

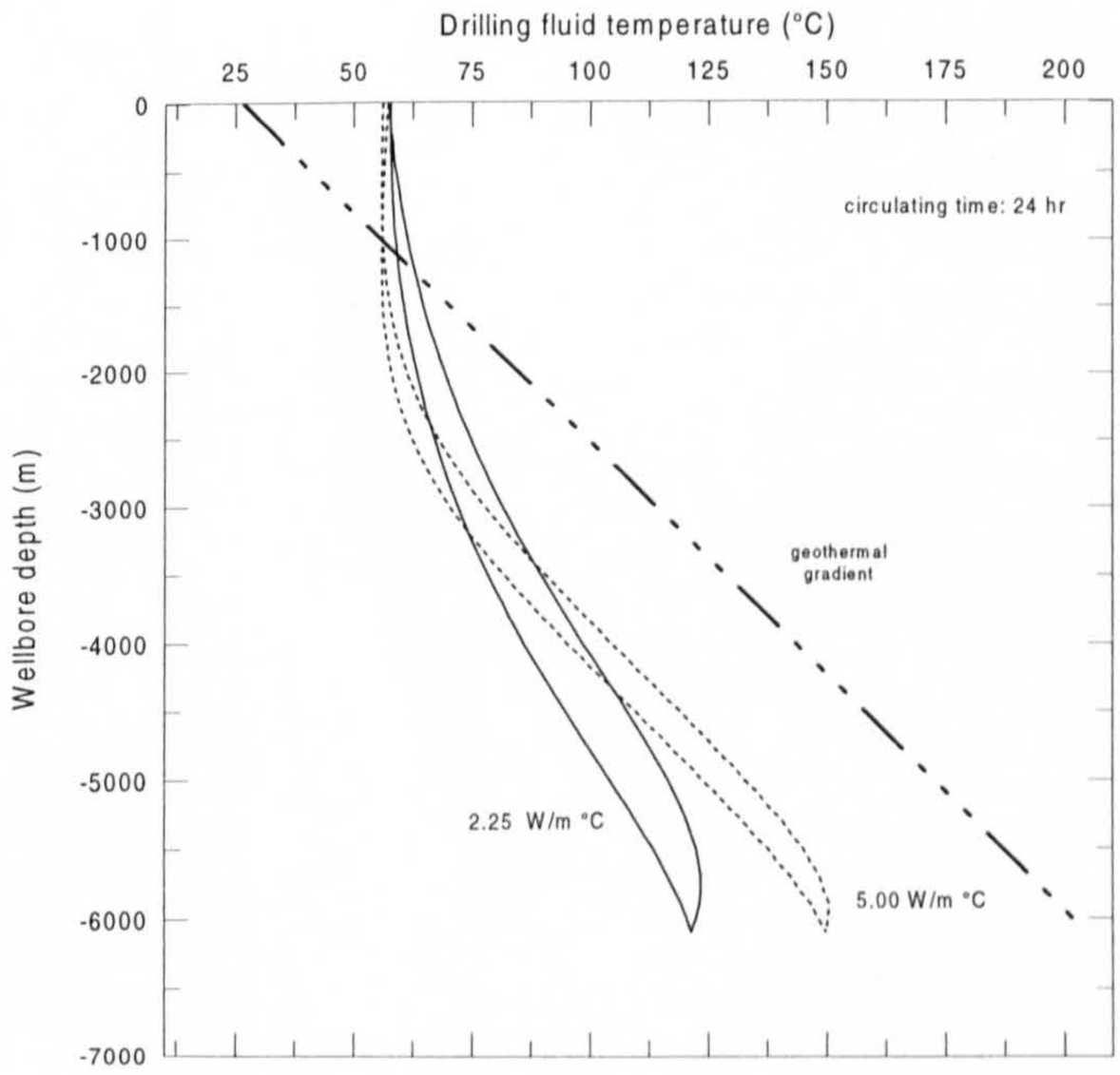

Fig. 9.29 Sensitivity of the circulating fluid temperature profile to the drilling fluid thermal conductivity.

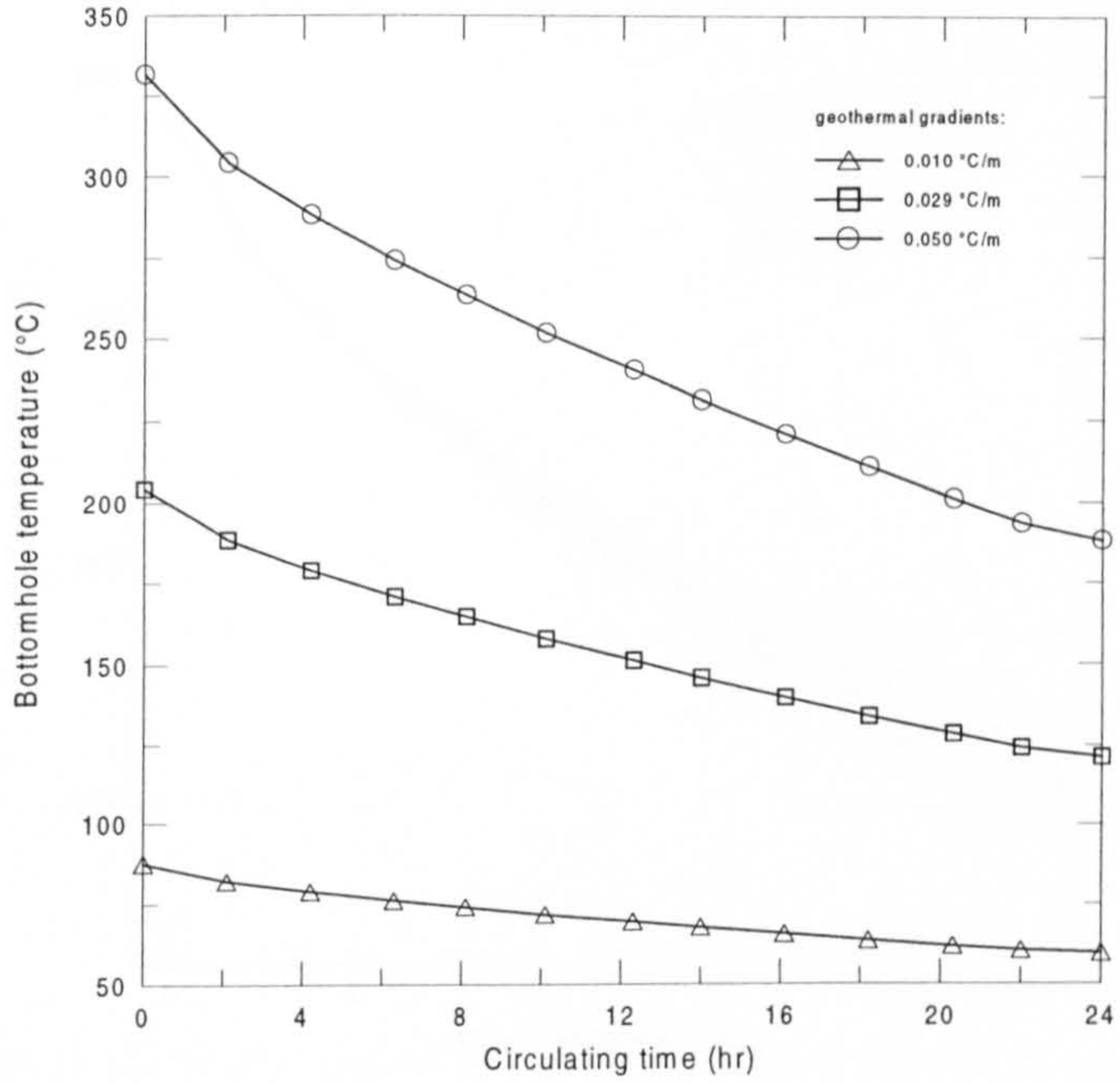

Fig. 9.30 Sensitivity of the bottomhole wellbore temperatures to the geothermal gradient.

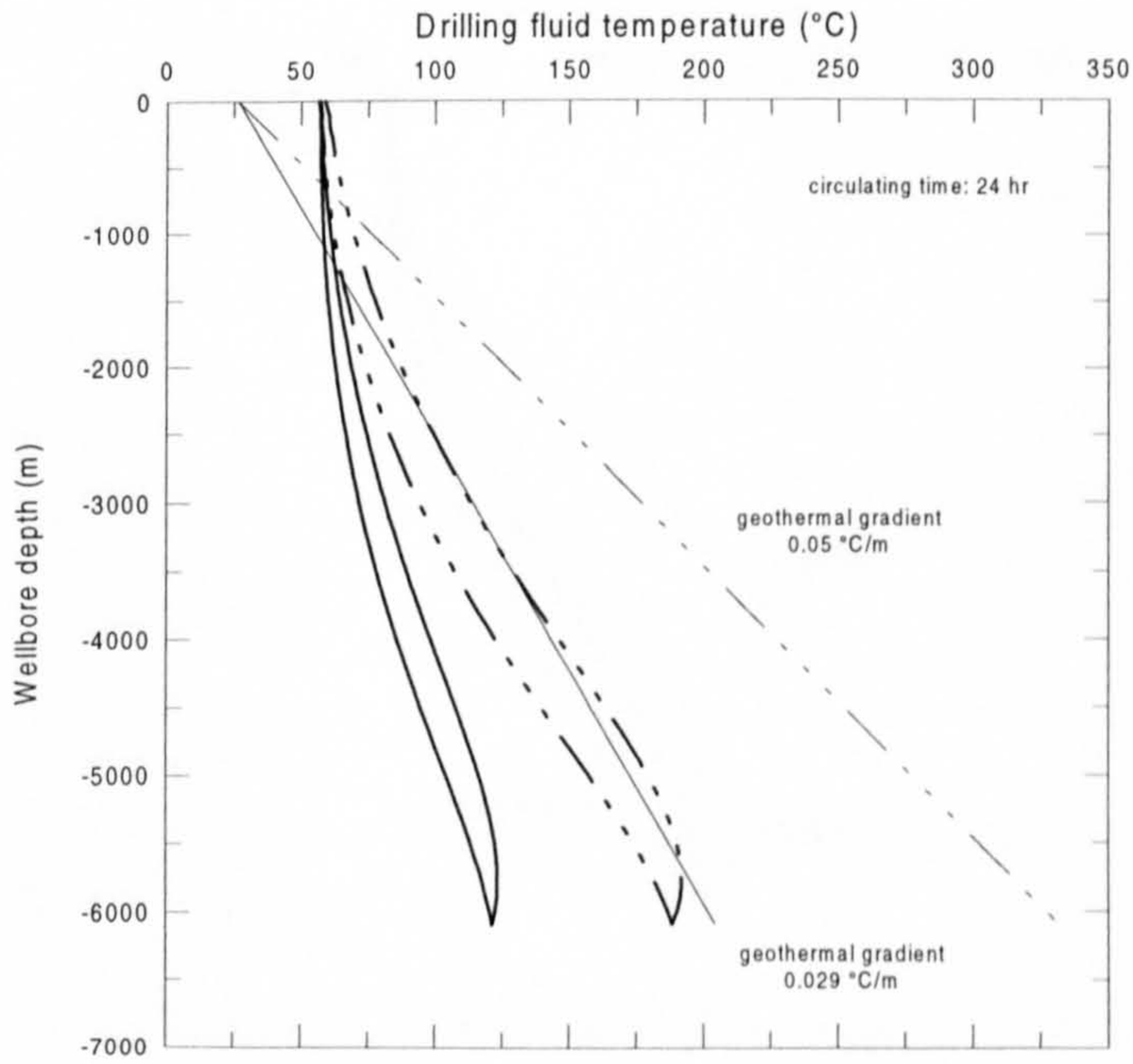

Fig. 9.31 Sensitivity of the circulating fluid temperature profile to the geothermal gradient.

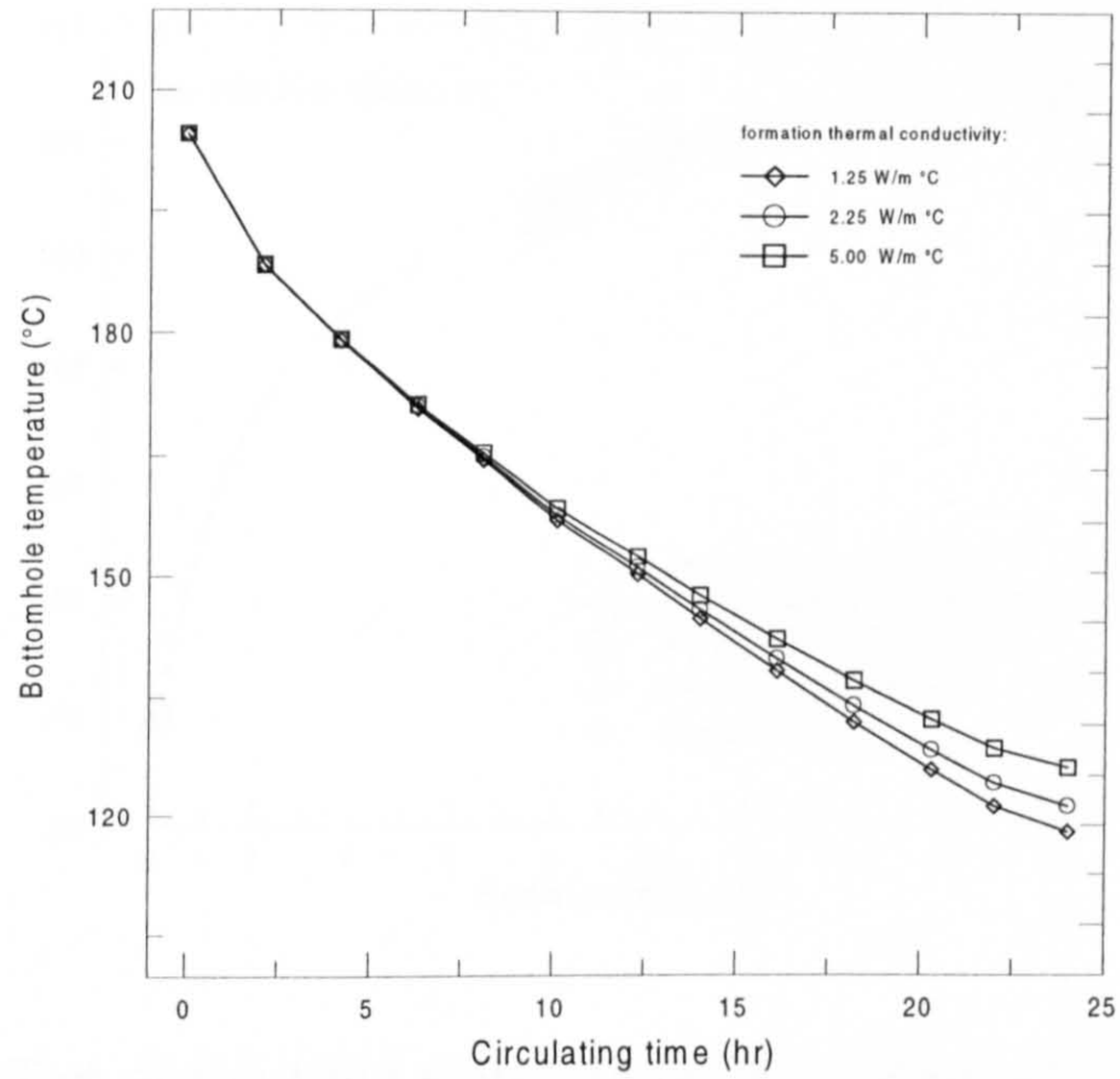

Fig. 9.32 Sensitivity of the bottomhole wellbore temperatures to the formation thermal conductivity.

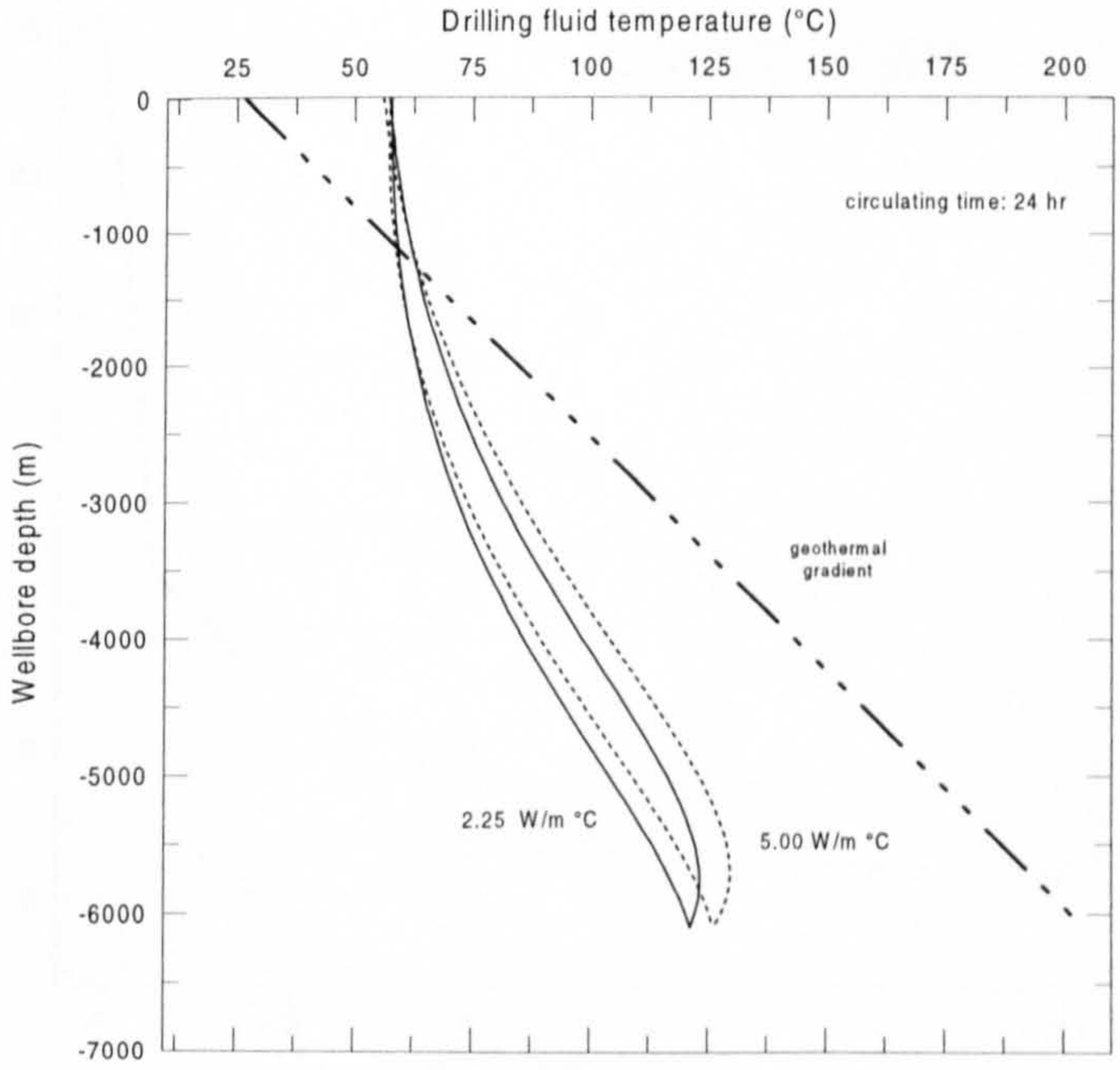

Fig. 9.33 Sensitivity of the circulating fluid temperature profile to the formation thermal conductivity.

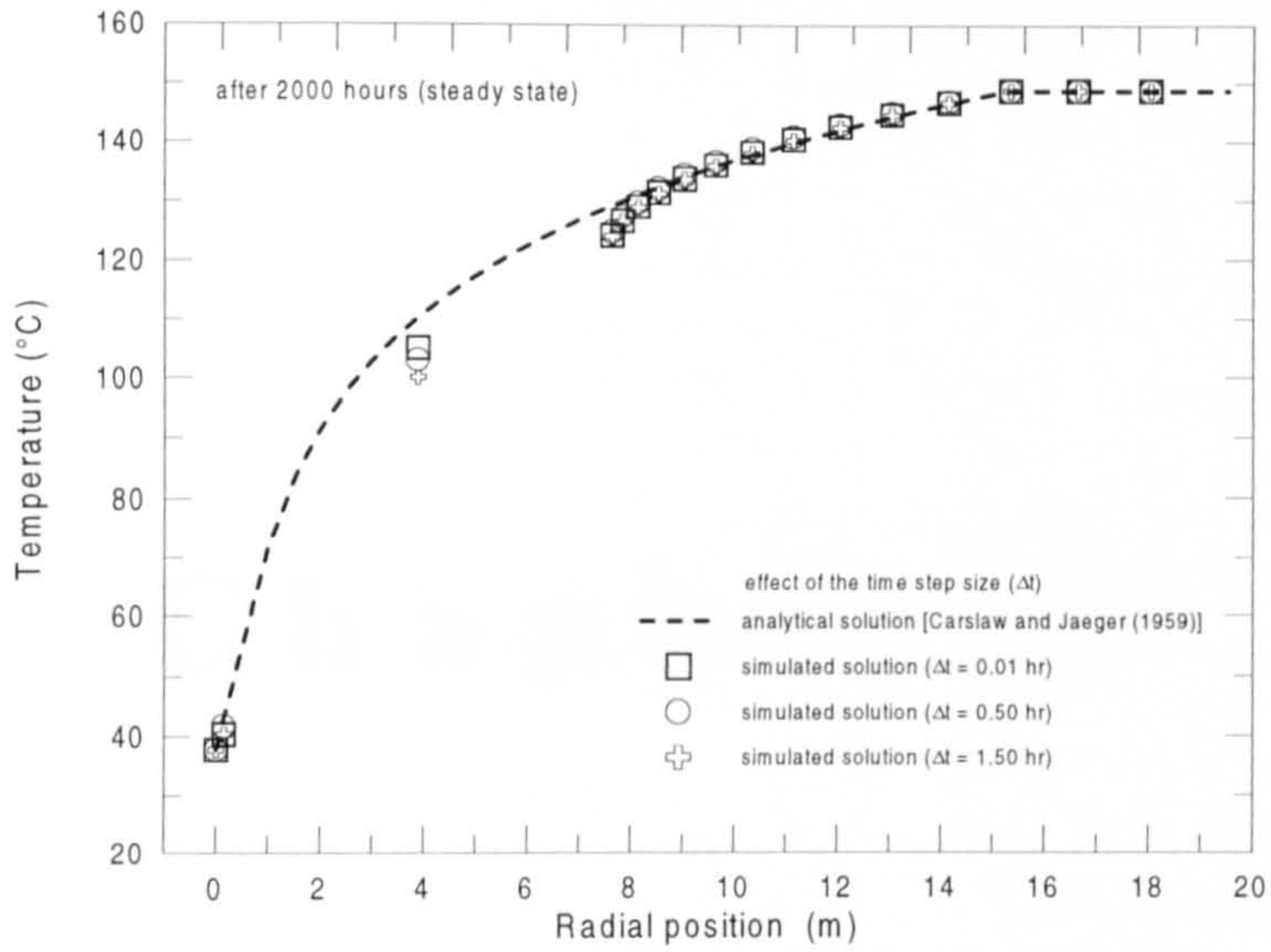

Fig. 9.34 Effect of the time step size on the temperature distribution of the heat transfer problem related to the analytical solution (numerical case 1).

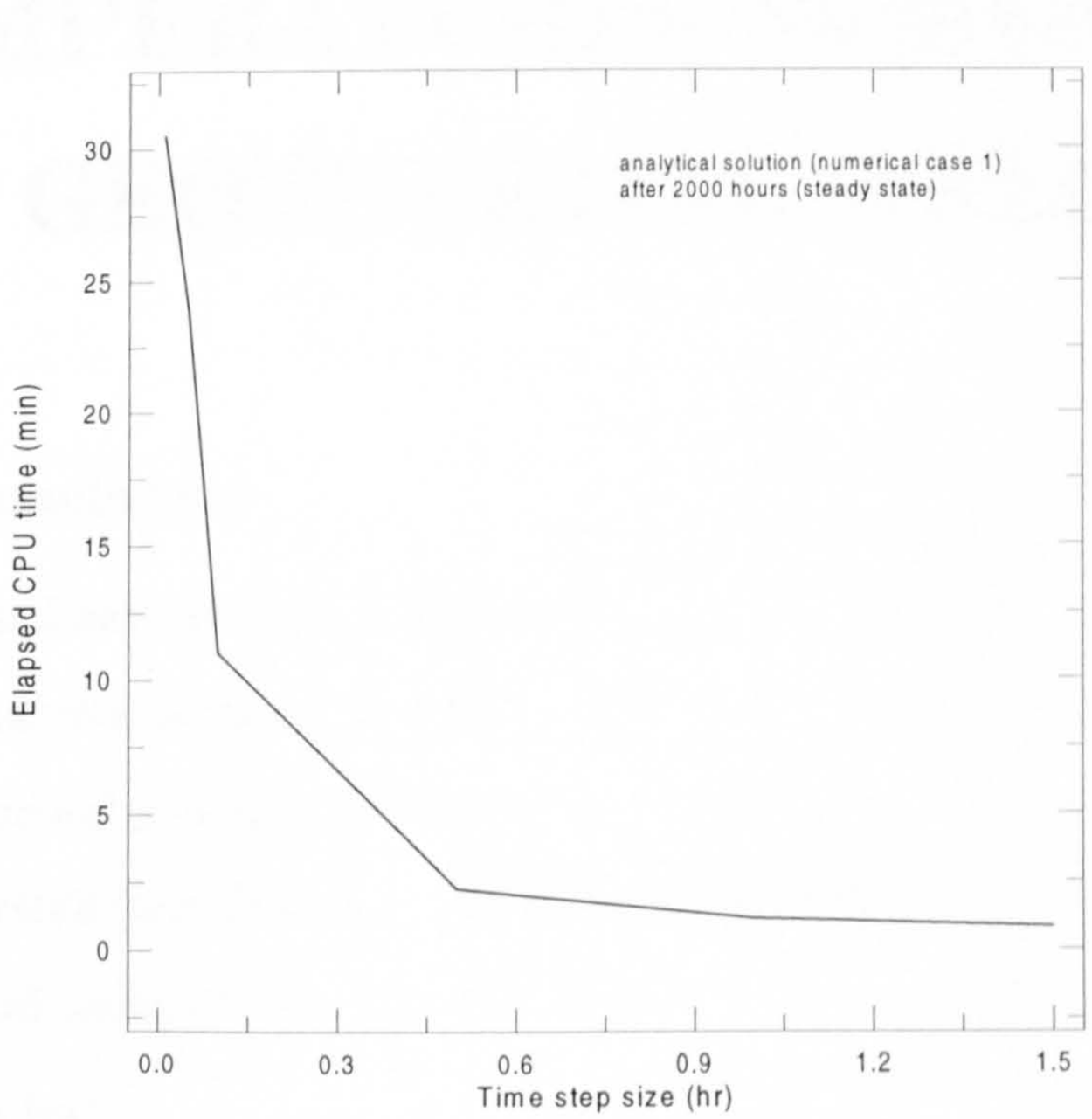

Fig. 9.35 Behaviour of the elapsed computing time against the time step size in the numerical simulation tests of the case 1.

Chapter 10

APPLICATION OF WELLTHER TO THE ESTIMATION OF TEMPERATURES IN MEXICAN GEOTHERMAL WELLS

10.1 Nomenclature

Cp	specific heat capacity [J kg^{-1} $°C^{-1}$]
D	internal diameter of pipe [m]
G	geothermal gradient [°C m^{-1}]
h	convective heat transfer coefficient [W m^{-2} $°C^{-1}$]
k	thermal conductivity [W m^{-1} $°C^{-1}$]
L	length [m]
r	radius [m]
Δr	radius step size [m]

T	temperature [°C]
T_{in}	inlet fluid temperature [°C]
t	time [hr]
t_c	circulating time [hr]
Δt	time step size [hr]
W	drilling fluid mass flowrate [kg hr^{-1}]
z	depth [m]
Δz	depth step size [m]

Greek symbols

φ	fluid losses factor (multiplier) [dimensionless]
μ	dynamic viscosity [Pa s]
ρ	density [kg m^{-3}]

10.2 Introduction

This chapter presents an application of the wellbore thermal simulator (WELLTHER) to the estimation of temperatures in and around a well during circulation and shut-in conditions in the presence of lost circulation. Estimated temperatures are compared with temperature logs measured during drilling stoppages. Temperatures were estimated using the computer simulator specifically developed to account for the transient convective heat transfer in the rock surrounding a well due to lost circulation. The code is capable of accounting for these losses at any point in the wellbore. This feature of the present code is important since normally wellbore simulators consider the heat transfer process in the rock as a merely conductive problem. The application was made to the study of two Mexican geothermal wells (well EAZ-2 from the Los Azufres field and well LV-3 from the Las Tres Virgenes field). Finally, a comparison between the numerical capabilities of the WELLTHER simulator and the wellbore thermal simulator (GEOTEMP) developed by Wooley (1980) is presented.

10.3 Lost Circulation Problem

As was previously mentioned in Chapters 1 and 2, most geothermal wells exhibit drilling fluid losses to the surrounding formation during their drilling stage. The physical model of drilling fluid circulation and circulation losses to the formation was illustrated in Fig. 8.1. From this figure, it can be seen that the drilling fluid enters the drill pipe at the top, flows down and exits the pipe at the bottom. There, it enters the annulus and flows upwards. If lost circulation exists, then some drilling fluid will flow into the formation and the amount of fluid exiting the well at the top depends on the amount of circulation losses. The well-formation interface is considered as a porous medium through which fluid may be lost (lost circulation) or gained by the well. The mathematical formulation developed in the heat transfer model of the WELLTHER simulator enables the fluid losses at any point in the wellbore to be simulated. Considering these characteristics, the simulator was applied to the interpretation of logged temperature data taken during the drilling and shut-in operations of two wells drilled in the Mexican geothermal fields of Los Azufres, Michoacan and Las Tres Virgenes, Baja California Sur. The location of these geothermal fields is shown in Fig. 2.4 (see Chapter 2).

10.4 Numerical Simulation

In the present study, the EAZ-2 well from the Los Azufres geothermal field and the LV-3 well from the Las Tres Virgenes geothermal field were considered. These numerical cases were analysed following the same numerical methodology presented in Chapter 9. The initial formation temperature profile of each wellbore was considered from actual temperature measurements carried out by personnel of the Comision Federal de Electricidad (CFE) [De Leon-Vivar (1996)]. On the basis of the drilling information provided by CFE, the LV-3 wellbore was the unique field case that reported the presence of fluid losses to the formation. Hence, the analysis of the circulating and shut-in temperatures under these conditions was performed. Even, the EAZ-2 wellbore did not report lost circulation problems, the analysis of this well was interesting to evaluate because a non-linear initial formation

temperature profile was considered. In addition, a comparison between logged temperature data and the simulated temperatures values obtained by the simulator was carried out. This fact constitutes an advantage because the capability of the simulator can be evaluated in a quantitative way, i.e that the deviation percentage between the calculated temperatures and the actual logged temperatures can be determined.

10.4.1 EAZ-2 geothermal well.

This well was drilled in the Los Azufres geothermal field, Mexico, as an exploratory well and is shown schematically in Fig. 10.1. It is 2200 m deep and was completed in February 1996 after 87 days since the start of drilling. Hole diameters are 17-1/2", 12-1/4", 8-1/2" and 5-7/8". Casing diameters are 13-3/8", 9-5/8" and 7". The liner has a diameter of 4-1/2" and runs from about 700 m to 2197 m. Several temperature logs were run during the construction of this well. The first series of temperature logs (T1-T4) was taken during the drilling of the 8-1/2" hole diameter stage to a depth of 808 m. Figure 10.2 shows the corresponding well geometry for this situation.

Figure 10.3 shows the temperature logs T1 and T4 which were taken at 6 and 24 hours of shut-in time. Logs T2 and T3 were taken off this graph for simplicity. It is seen that the surface logged temperature is about 25°C in both logs. Then they exhibit a normal behaviour and a crossover of the curves corresponding to these logs occurs at about 150 m and finally, they exhibit normal behaviour again, i.e., the temperatures increase with depth. The maximum bottomhole temperature is about 85°C at 24 hours shut-in. No circulation losses were reported for this well. Therefore, this case serves the purpose of studying a well without lost circulation which implies that heat transfer in the formation is purely conductive.

Employing field data taken from the drilling records of this well, simulation runs were performed for this case using the numerical code described in Chapter 8 and aiming at reproducing the temperature logs shown in Fig. 10.3. All the drilling input data used in the numerical simulation of this well are summarised in

Table 10.1. However, since no initial temperatures were available for this well, an assumed profile was used to start the simulation whose shape was constructed based on the last log taken, i.e., log T4. Simulation included a period of mud circulation followed by shut-in.

Figure 10.4 shows the results of the simulations performed for this case. Shown on this figure are simulated temperature profiles for 0,6 and 24 hours shut-in time. Also plotted on this figure are the initial temperature profile and temperature logs T1 and T4 for comparison purposes. It is seen that, except for the anomalous behaviour exhibited by the logged temperatures at shallow depths, the simulated profiles match well the logged profiles. The major differences occur for depths between 600 and 700 m for the temperatures at a shut-in time of 6 hours. A quantitative analysis indicates that the predicted temperatures have a good agreement with the logged temperatures. In all instances, the deviation error between the predicted and the actual measured temperatures ranges from 0.2°C to 2.5 °C and from 0.2°C to 2.7 °C for the shut-in profiles of 6 and 24 hours, respectively (Fig. 10.4).

It must be noted that the initial temperature profile shown in this figure represents the result obtained after assuming a profile to start the simulation and adjustment to match the logged temperatures. In this way, if such profile is considered as the static or equilibrium temperature, which the well and the surrounding formation will attain after a long time, then this procedure is in effect a means of obtaining the equilibrium temperature.

10.4.2 LV-3 geothermal well.

Well LV-3 was drilled in the Las Tres Virgenes geothermal field. The field location is shown in Fig. 10.5. It is 2150 m deep and was completed in November 1994. Hole diameters are 26", 17-1/2", 12-1/4" and 8-1/2". Casing diameters are 20", 13-3/8" and 9-5/8". The liner has a diameter of 7" and runs from about 1260 m to 2133 m. Several series of temperature logs were run during the drilling of well LV-3.

Figure 10.6 shows the well geometry during the measurement of the first series of temperature profiles (logs T1-T5). At this point, the well was 402 m deep and the 20" casing had been cemented to 48 m while the 17-1/2" hole runs down to the total depth. Logs T26-T30 (fifth series) were run when the well was 2000 m deep, near the end of its construction. If the liner in Fig. 10.5 is removed and the well depth is 2000 m, then the geometry of the well during the measurement of logs T26-T30 is obtained. These two series of temperature logs and their respective geometries were used for running simulation runs in order to reproduce the measured logs by computation.

Figures 10.7, 10.8a and 10.8b show the aforementioned series of temperature logs: series 1-logs T1-T5 and series 5-logs T26-T30. It is seen from Fig. 10.7 that temperature logs correspond to 0, 6, 12 and 18 hours shut-in time. It is observed that the first temperature logs indicate nearly isothermal conditions and that heating is fast between 0 and 6 hours but almost no heating occurs after this time for depths from about 25 to 150 m. From there onwards, heating is observed. At a depth of about 375 m, temperatures deviate from the general trend of the logs and are in fact lower than the temperatures above and below this point. This phenomenon is more pronounced at 6 hours shut-in time and it disappears at longer times. In the analysis of the drilling records for this case, it was found that very little lost circulation occurred at this depth.

Analysis of Fig. 10.8, logs T26-T30 is even more difficult. Logged temperatures were reported between 300 and nearly 2000 m. Shown on this figure are logs for 0, 6, 12, 18 and 24 hrs shut-in. Although there exists some peculiar behaviour at shallow depths, attention is centered on these logs at depths between 1300 and 1600 m where high circulation losses were reported (Fig. 10.8b). It may be observed that heating occurs as shut-in time proceeds but temperatures deviate from the heating pattern at about 1300 m where it may be thought that the hotter zone was contributing more heat at this depth. Immediately below this depth, an opposite trend is seen to occur, i.e., a slower heating rate. The heating effect noted

on Fig. 10.8 may be due to a drastic reduction in thermal resistance, i.e., increased heat transfer, due to the fact that the 9-5/8" casing is cemented up to 1281 m only, Fig. 10.5, and from there on the well is open. On the other hand, immediately below this depth, circulation losses were reported and this may explain the relatively smaller temperatures at about 1400-1450 m. From 1500 m onwards, it is observed that temperatures tend to a vertical shape and give rise to a nearly isothermal curve. In fact, from 1700 m downwards, no cooling seems to have occurred during drilling (circulation of water-air drilling fluid). It would appear as though the drilling fluid did not circulate to the bottom of the hole.

Data taken from the drilling records of this well were used to simulate a combined cycle of circulation and shut-in periods for the two cases described above. These runs helped in testing the methodology described in this work to simulate the heat transfer processes in geothermal wells in the presence of lost circulation. Again, an initial temperature profile was used if available or one was assumed and later adjusted or modified in order to reproduce the logged temperatures. The input data used in this numerical simulation are summarised in Table 10.2.

Figure 10.9 shows the simulated and logged temperature profiles for shut-in times of 0, 6, 12 and 18 hours. Also shown in this figure is the initial temperature profile which was generated by trial and error for this particular case. For simulation, a circulation loss of 40% (i.e., the multiplier $\varphi = 0.4$) of the total fluid was lost to the formation at a depth of 367 m (node length is 17.7 m). These losses amount to 6.3 kg/s (92 gpm) of mud. It is noticed from this figure that agreement between logged and simulated temperatures is satisfactory, except for the 6 hour shut-in case where the temperature differences are greater (about 4°C) and the inflection of the calculated curve is smaller than the logged curve. However, these differences disappear as time proceeds.

Figure 10.10 shows the logged and simulated temperature profiles for 0, 6, 12, 18 and 24 hours shut-in time. Again, the initial temperature is shown there which for this case, was actually obtained from the drilling records of this well. Lost

circulation was modelled by allowing fluid losses at depths of 1281, 1460, 1571 and 1685 m, in accordance with drilling reports on circulation losses. The total amount of fluid lost amounted to 30% of the total mud flowing into the well (7.4 kg/s). Of these losses, 50% were lost at the 1281 m depth.

From Figure 10.10, it may be observed that the lost circulation zone was modelled satisfactorily. The major differences of about 10°C were found at a depth of 900 m at the beginning of shut-in, and at 300 m, the computed profiles fall between the range of measured temperatures but with significant differences. However, the particular behaviour of the logged temperatures at 300 m is rather peculiar: the water table was located at this depth and measured temperatures could be influenced by a number of factors. It is also important to note that at depths greater than 1500 m, the computed results show that actually some cooling occurred there and subsequently the well heated up after the well was shut. However, this cooling is not observed in the logged temperatures, probably because the circulating fluid actually did flow into the formation without cooling the well significantly.

10.5 Comparison with the GEOTEMP wellbore thermal simulator

An evaluation of the numerical capabilities developed in the WELLTHER simulator in the context of other similar numerical simulators developed in the past was made. This evaluation was performed by means of a comparison between the WELLTHER and the GEOTEMP simulators. GEOTEMP is also a transient wellbore thermal simulator which was developed by Wooley (1980) for determining temperatures in and around the wellbore under circulating and shut-in conditions. GEOTEMP uses a different methodology to simulate the heat transfer processes associated with the drilling and shut-in operations of wellbores. One of the main limitations of this simulator is that it cannot simulate the convective processes involved which result from the fluid losses to the formation. Therefore, the main objective of this comparison is to demonstrate

that the actual logged temperatures of a wellbore with fluid losses can be reproduced more reliably by means of the WELLTHER simulator than by simulators which do not consider these convective problems.

In this context, the second simulated case of the LV-3 geothermal well was again considered. Hence, the input data recorded in Table 10.3 were used by the GEOTEMP simulator. The thermal recovery process of the wellbore was analysed. Five shut-in times were used to generate the temperature profiles during these numerical runs (0, 6, 12, 18 and 24 hours). For comparison purposes, the wellbore temperature profiles for the 6 and 24 hours of shut-in times were employed. Figures 10.11a and 10.11b show the results obtained to compare the GEOTEMP predicted temperature profiles with the WELLTHER predictions and the actual logged temperatures by CFE. As can be seen, the predicted temperature profiles by the WELLTHER simulator show a better agreement with the actual recorded temperatures. Very significant differences were observed when the temperature profiles predicted by GEOTEMP were compared. Clearly, it can be demonstrated that these differences are due to the fact that the GEOTEMP simulator does not consider the convective heat transfer process produced by the presence of the fluid losses to the formation. Consequently, the capabilities of the WELLTHER simulator can be used reliably to model these heat transfer processes in the wellbore drilling and completion operations including the presence of the lost circulation problem.

10.6 Discussion of Results

Numerical simulations for studying the transient heat transfer processes in geothermal wells during circulation and shut-in conditions and in the presence of lost circulation have been carried out. It was demonstrated that the heat transfer model incorporated in the WELLTHER simulator properly accounts for the energy balances in each region of the well and also the mass balances to represent the fluid losses problem to the formation. It was found that the lost circulation affects the value of the heat transfer coefficients in the annulus and the thermophysical

properties of the formation. In addition, appropiately properties must also be used if a mixture of drilling fluids is used. Simulation results obtained from the application of the present model to a well with lost circulation and another well without losses compared satisfactorily with the logged temperatures. The outcome of the present work is important in that it is one of first studies on the thermal effects of lost circulation on the shut-in (build-up) temperatures in a well.

10.7 References

J.S. De Leon-Vivar, Pressure and temperature logs taken in the well drilling and completion activities of the LV-3 and EAZ-2 wellbores. Internal Report, Comision Federal de Electricidad (CFE), J3A00-HGP-258/96 (1996).

G.R. Wooley, Computing downhole temperatures in circulation, injection, and production wells, Journal of Petroleum Technology, **September** 1509-1522 (1980).

Wellbore geometry				
Wellbore section	1	2	3	4
Wellbore diameter (m)	0.4445	0.3400	0.2450	0.1780
Wellbore depth, z (m)	20.0	189.0	599.0	
Depth step size, Δz (m)	20.0	38.0	40.0	
Drill pipe diameter (m) Thickness (m)	0.1143 0.0074			
Thermophysical and transport properties				
Component	k [W m^{-1} °C^{-1}]	Cp [J kg^{-1} °C^{-1}]	ρ [kg m^{-3}]	μ [Pa.s]
Formation	1.86	930.0	2620.0	------
Cement	0.70	2000.0	3140.0	------
Casing	43.30	440.0	7800.0	------
Drilling fluid	0.70	4100.0	1070.0	0.048
Flow and temperature data of the well drilling operations				
	Fluid flowrate [kg s^{-1}]	Geothermal gradient [°C m^{-1}]	Surface temperature [°C]	Inlet fluid temperature [°C]
	18.5	0.015*	20.0	25.0

* A non-linear initial formation temperature profile was assumed (Fig. 10.4)

Table 10.1 Input data used by the wellbore thermal simulator (WELLTHER) in the numerical simulation of the heat transfer processes of the EAZ-2 wellbore.

Wellbore geometry				
Wellbore section	1	2	3	4
Wellbore diameter (m)	0.660	0.508	0.340	0.244
Wellbore depth, z (m)	48.0	354.0		
Depth step size, Δz (m)	24.0	18.0		
Drill pipe diameter (m) Thickness (m)	0.1143 0.0074			
Thermophysical and transport properties				
Component	k [W m^{-1} $°C^{-1}$]	Cp [J kg^{-1} $°C^{-1}$]	ρ [kg m^{-3}]	μ [Pa.s]
Formation	1.86	930.0	2620.0	------
Cement	0.70	2000.0	3140.0	------
Casing	43.30	440.0	7800.0	------
Drilling fluid	0.70	4100.0	1080.0	0.040
Flow and temperature data of the well drilling operations				
	Fluid flowrate [kg s^{-1}]	Geothermal gradient [°C m^{-1}]	Surface temperature [°C]	Inlet fluid temperature [°C]
	15.76	0.015*	30.0	25.0

* A non-linear initial formation temperature profile was assumed (Fig. 10.9)

Table 10.2 Input data used by the wellbore thermal simulator (WELLTHER) in the numerical simulation of the heat transfer processes of the LV-3 wellbore in its first drilling stage (Fig. 10.6).

Wellbore geometry				
Wellbore section	1	2	3	4
Wellbore diameter (m)	0.660	0.508	0.340	0.244
Wellbore depth, z (m)	48.0	354.0	879.0	719.0
Depth step size, Δz (m)	24.0	70.0	88.0	45.0
Drill pipe diameter (m) Thickness (m)	0.1143 0.0074			

Thermophysical and transport properties				
Component	k [W m^{-1} $°C^{-1}$]	Cp [J kg^{-1} $°C^{-1}$]	ρ [kg m^{-3}]	μ [Pa.s]
Formation	1.86	930.0	2620.0	------
Cement	0.70	2000.0	3140.0	------
Casing	43.30	440.0	7800.0	------
Drilling fluid	0.70	4100.0	1080.0	0.040

Flow and temperature data of the well drilling operations				
	Fluid flowrate [kg s^{-1}]	Geothermal gradient [°C m^{-1}]	Surface temperature [°C]	Inlet fluid temperature [°C]
	24.72	0.012*	30.0	30.0

* A non-linear initial formation temperature profile was assumed (Fig. 10.10)

Table 10.3 Input data used by the wellbore thermal simulator (WELLTHER) in the numerical simulation of the heat transfer processes of the LV-3 wellbore in its second drilling stage (Fig. 10.5).

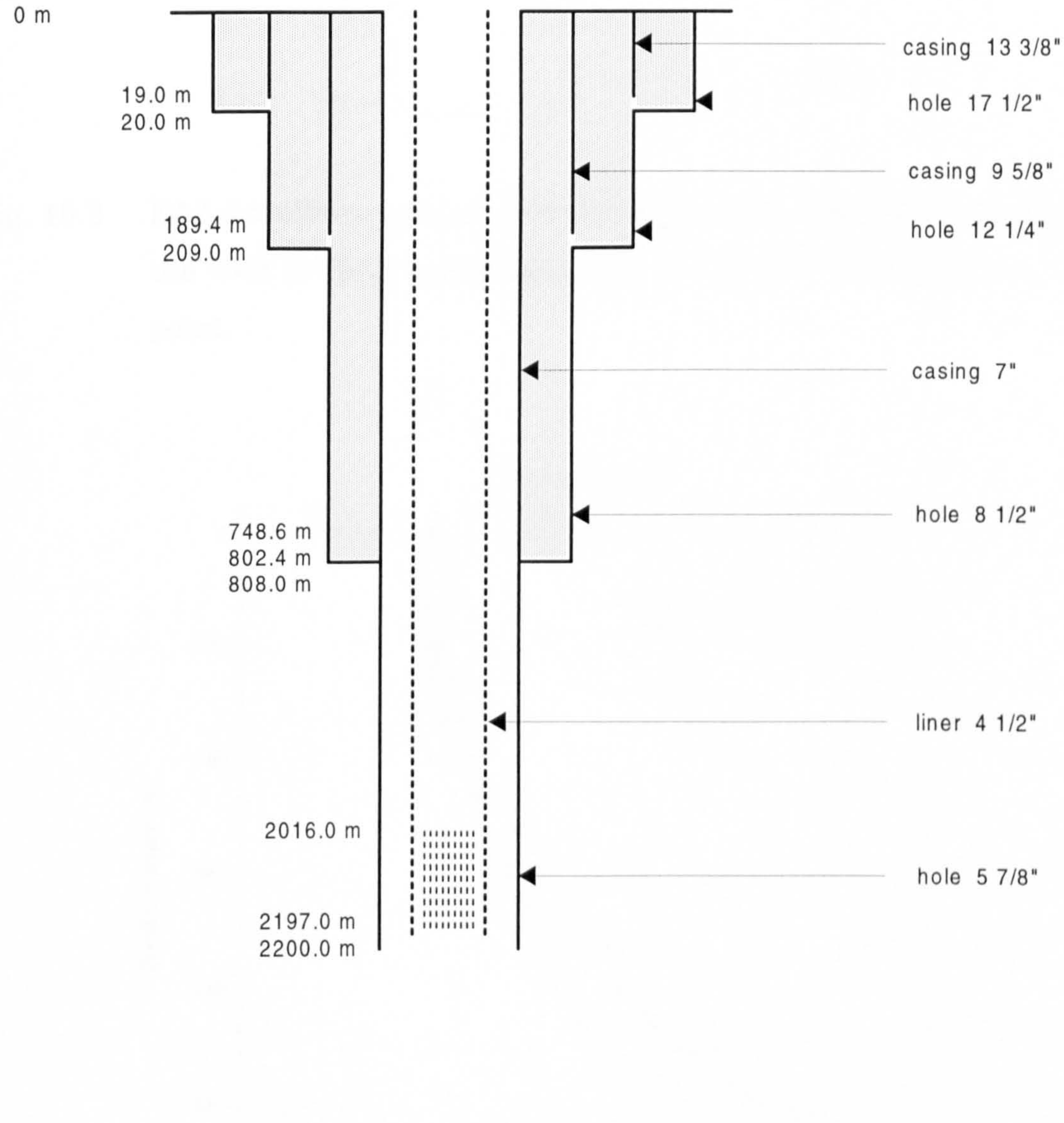

Fig. 10.1 Schematic diagram showing the completion of the EAZ-2 wellbore from Los Azufres geothermal field, Mexico.

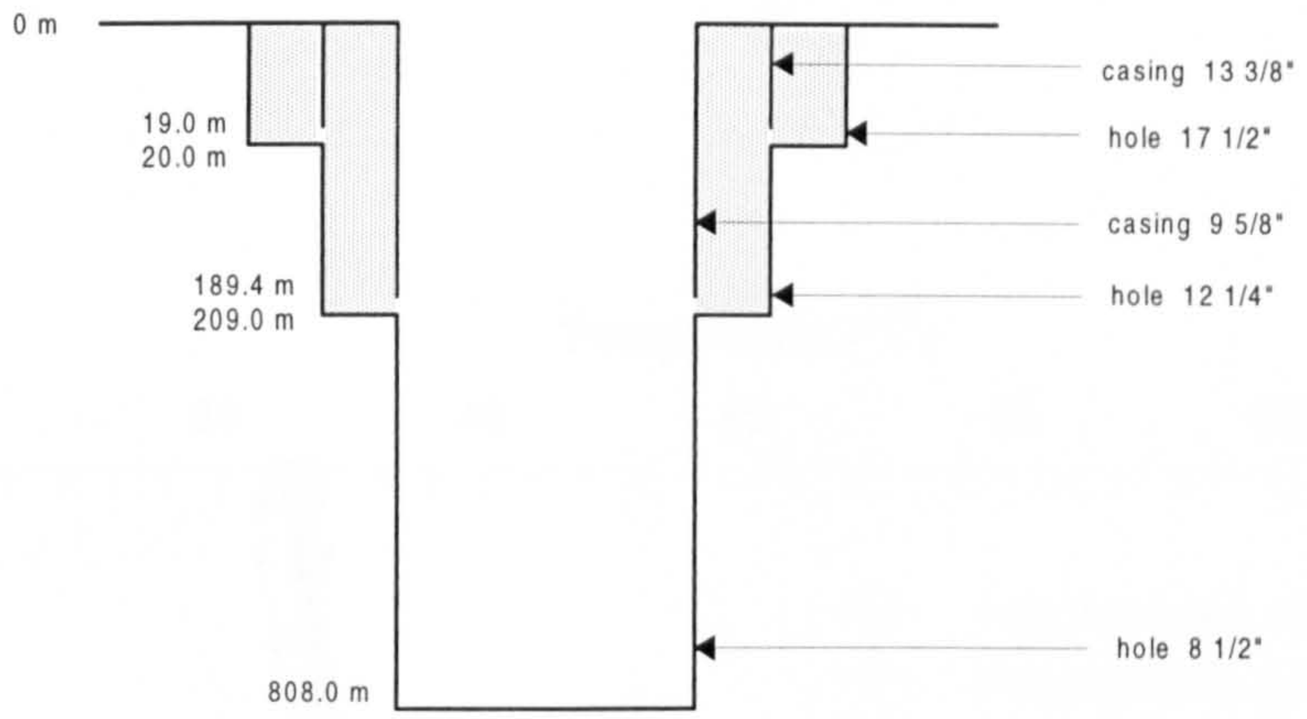

Fig. 10.2 EAZ-2 wellbore geometry which was studied in the first stage of the well drilling operations; logs T-1 to T-4 were taken at this point.

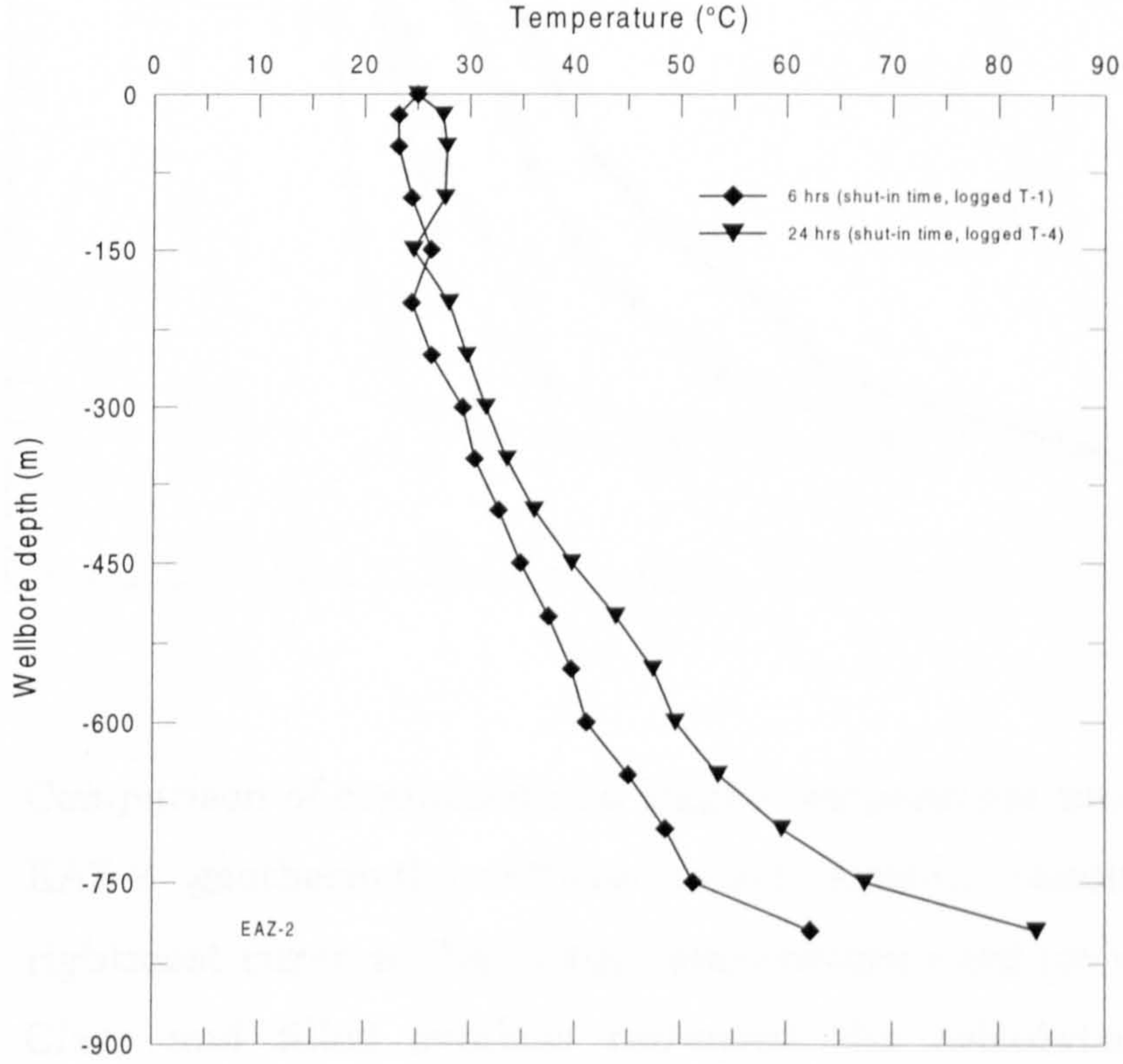

Fig. 10.3 Temperature logs T-1 and T-4 taken at 6 and 24 hours shut-in time in the EAZ-2 wellbore from the Los Azufres geothermal field, Mexico.

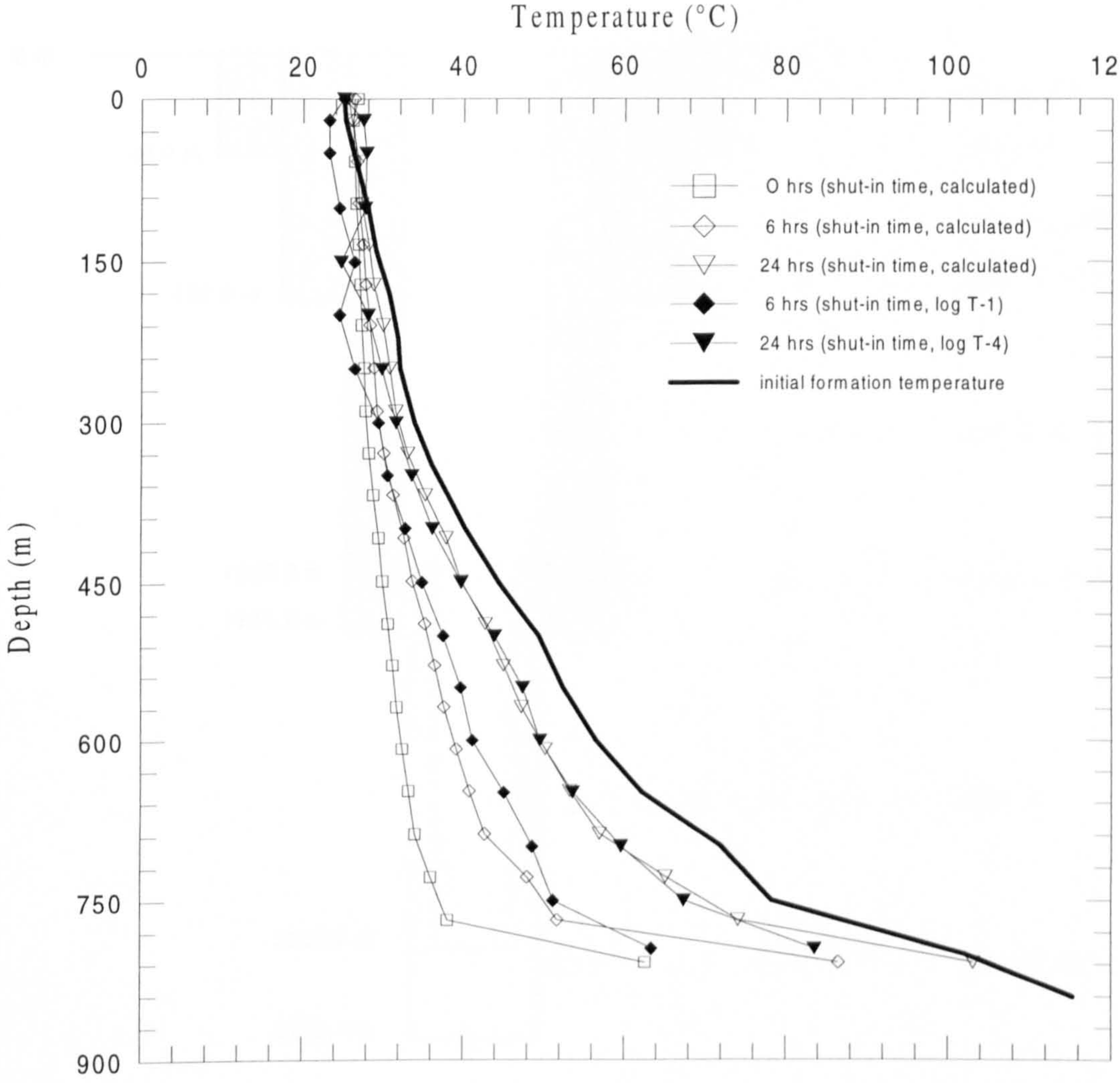

Fig. 10.4 Comparison of computed and logged temperature profiles in the EAZ-2 geothermal wellbore under shut-in conditions. The rightmost curve is the initial temperature used for simulation. Clear and filled symbols represent the calculated and the observed temperatures, respectively.

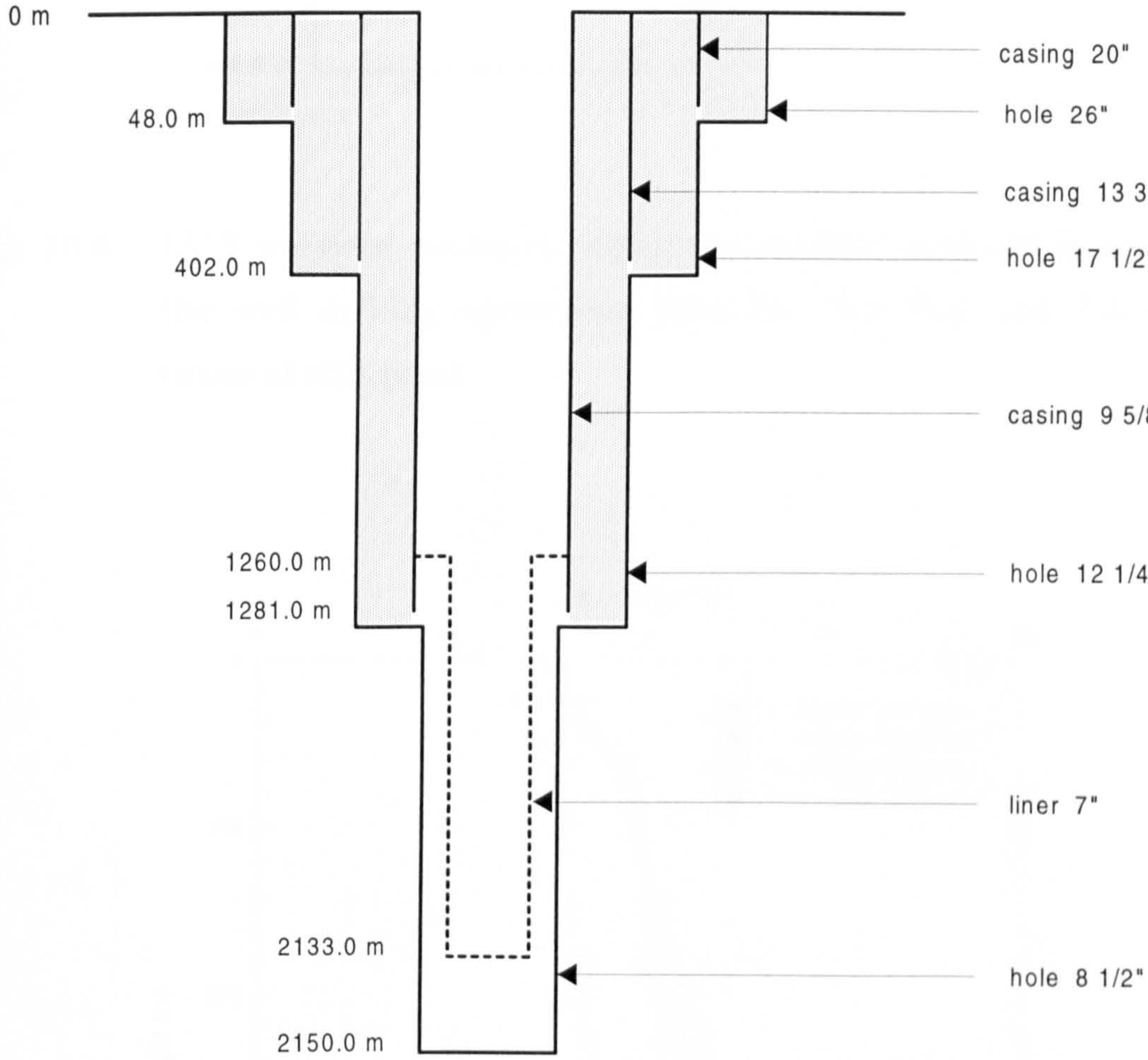

Fig. 10.5 Schematic diagram showing the completion of the LV-3 well from the Las Tres Virgenes geothermal field, Mexico. Temperature logs T-26 to T-30 were taken when the well was 2000 m deep and the liner had not been set in place. This case was used for simulation.

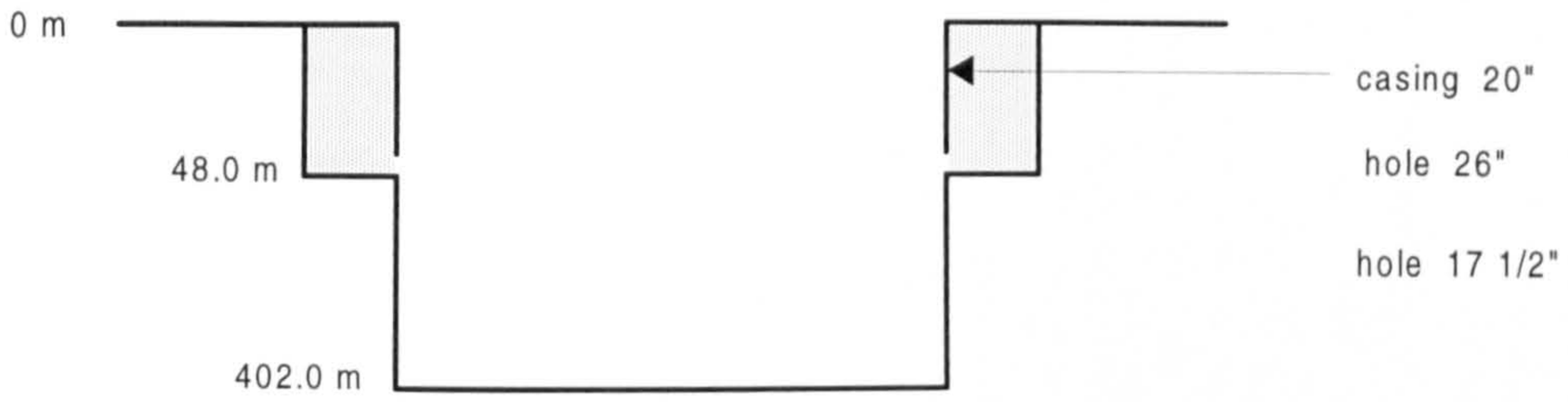

Fig. 10.6 LV-3 wellbore geometry which was studied in the first stage of the well drilling operations; logs T-1, T-3, T-4 and T-5 were taken at this point.

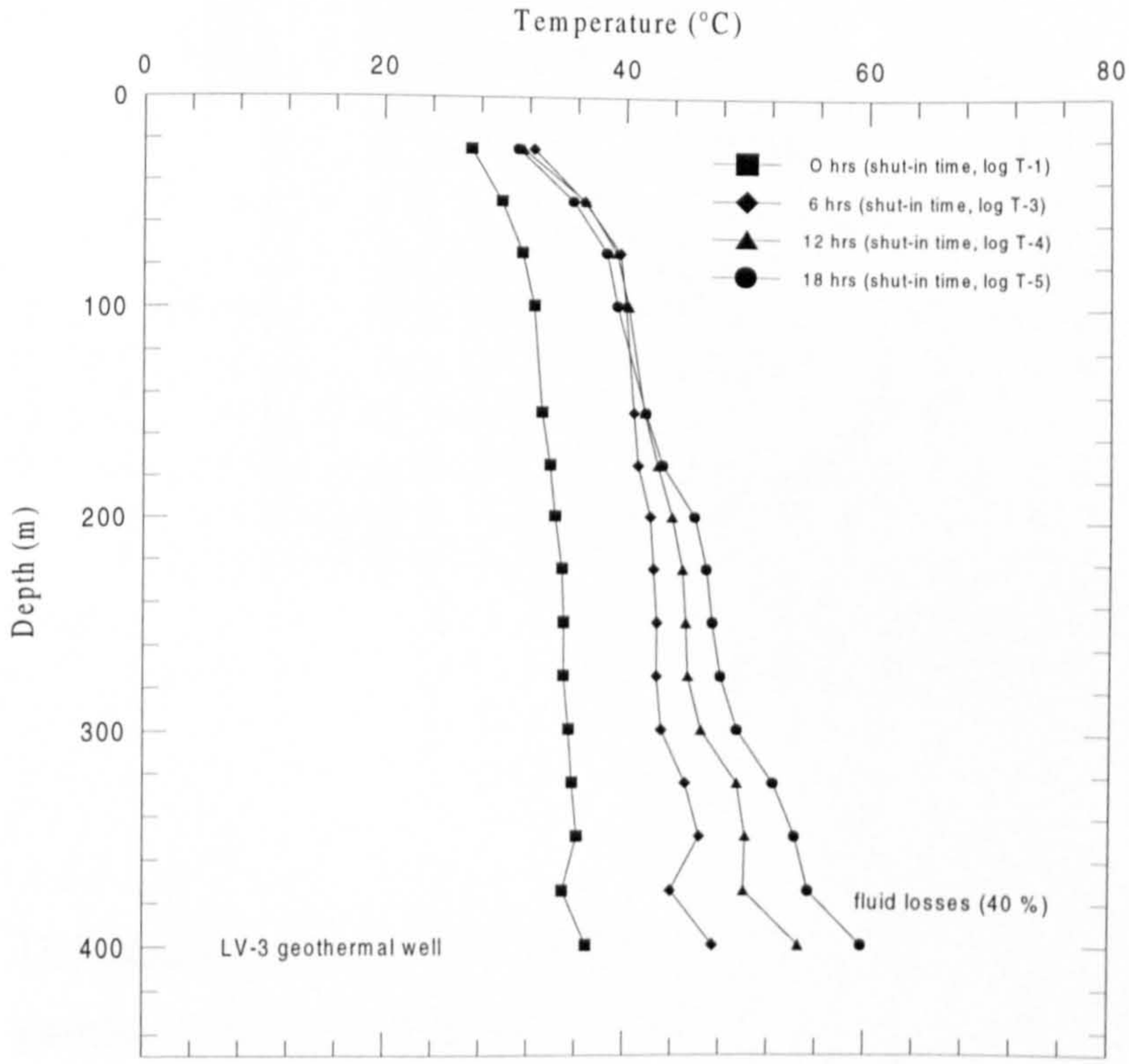

Fig. 10.7 Temperature logs T-1, T-3, T-4 and T-5 taken at 0, 6, 12 and 18 hours shut-in time in the LV-3 wellbore from the Las Tres Virgenes geothermal field, Mexico.

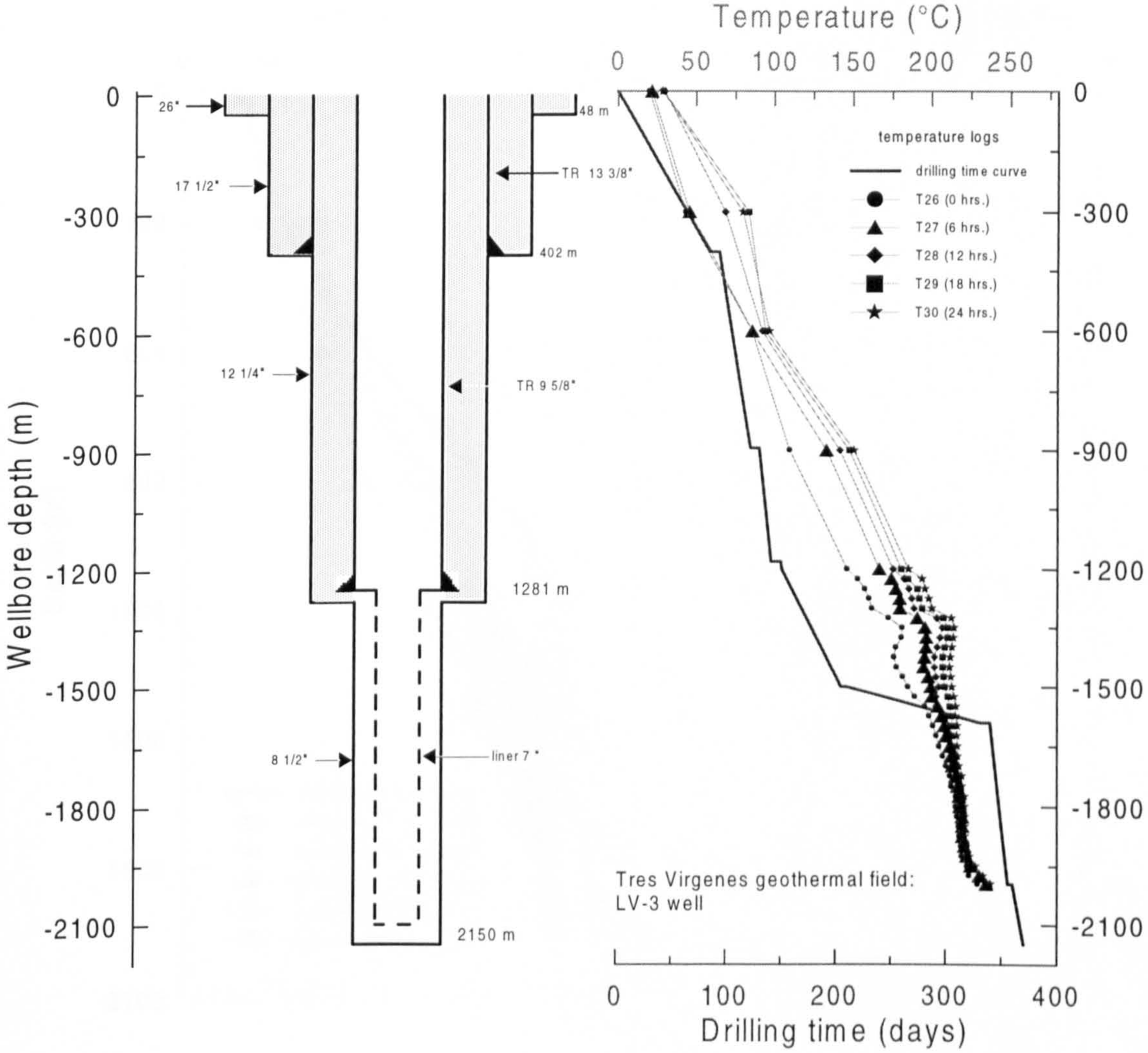

Fig. 10.8a Drilling history of the LV-3 well from the Las Tres Virgenes geothermal field, Mexico. Temperature logs T-26 to T-30 taken at 0, 6, 12, 18 and 24 hours shut-in time.

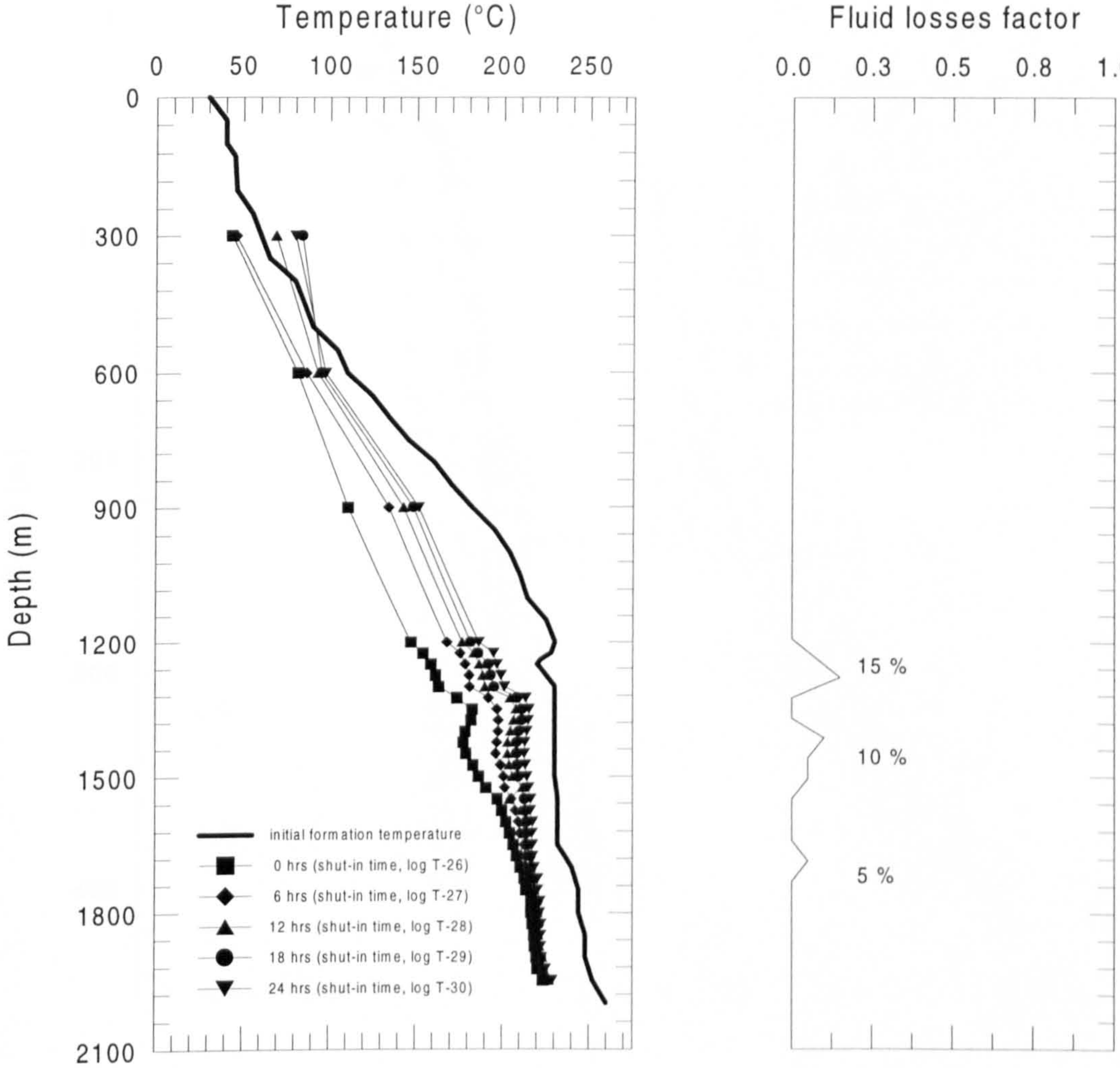

Fig. 10.8b Drilling history of the LV-3 well from the Las Tres Virgenes geothermal field, Mexico. Temperature logs T-26 to T-30 taken at 0, 6, 12, 18 and 24 hours shut-in time. The dimensionless fluid losses factor profile indicates the lost circulation zones.

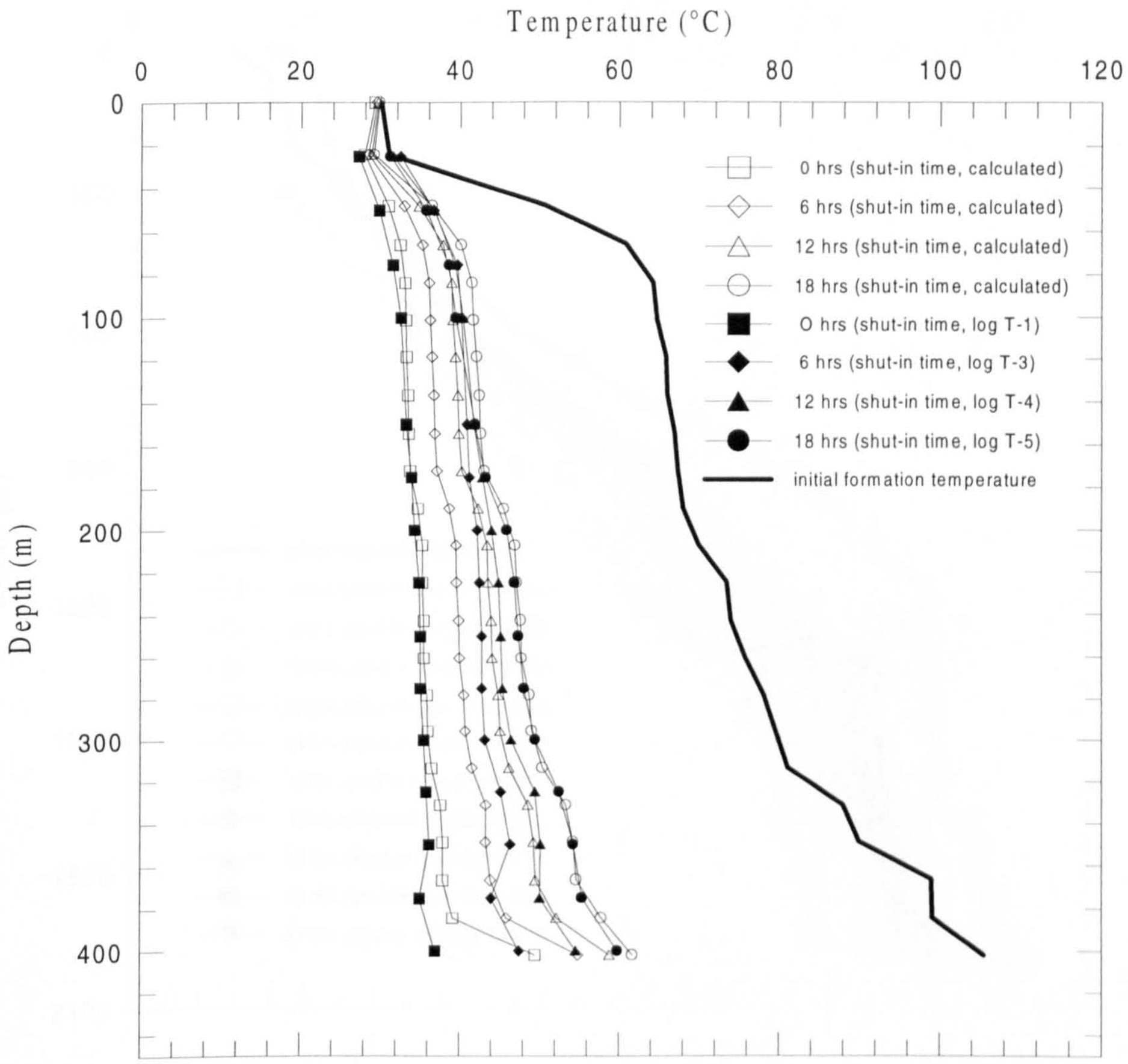

Fig. 10.9 Comparison of computed and logged temperature profiles in the LV-3 geothermal wellbore under shut-in conditions. The rightmost curve is the initial temperature used for simulation. Clear and filled symbols represent the calculated and the observed temperatures, respectively. The wellbore depth was 402 m.

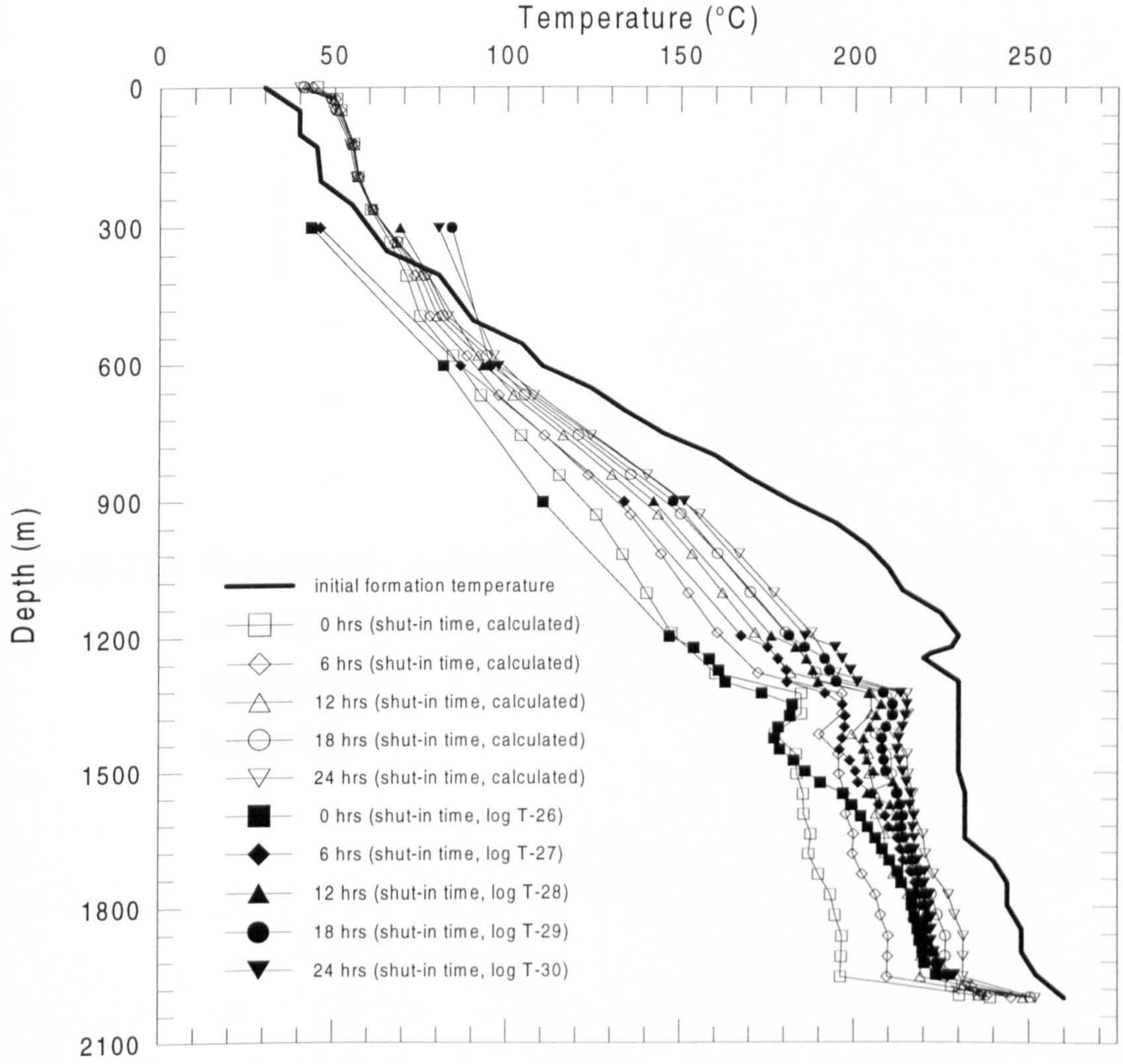

Fig. 10.10 Comparison of computed and logged temperature profiles in the LV-3 geothermal wellbore under shut-in conditions. The rightmost curve is the initial temperature used for simulation. Clear and filled symbols represent the calculated and the observed temperatures, respectively. The wellbore depth was 2000 m.

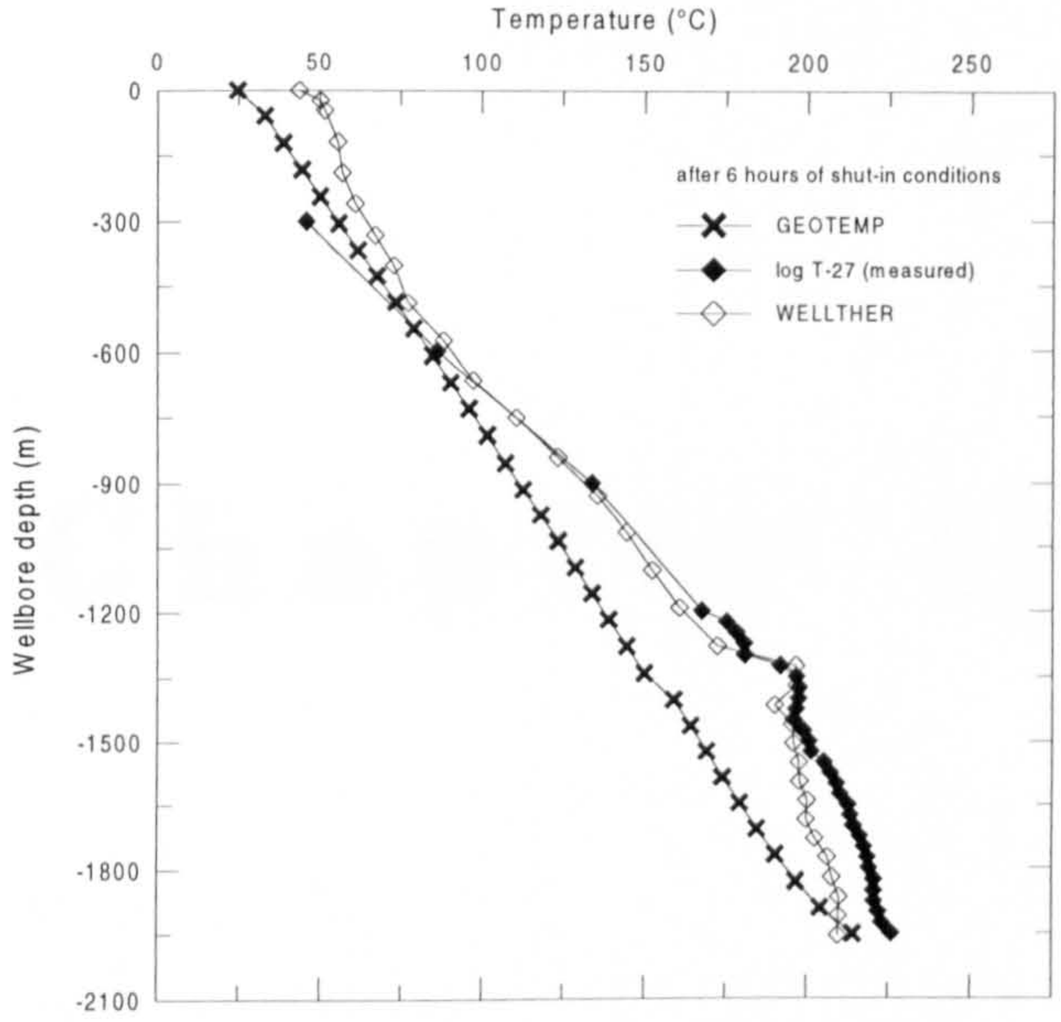

Fig. 10.11a Comparison against the temperature profiles predicted by use of GEOTEMP and WELLTHER simulators and the logged temperatures of the LV-3 wellbore under shut-in conditions (after 6 hours).

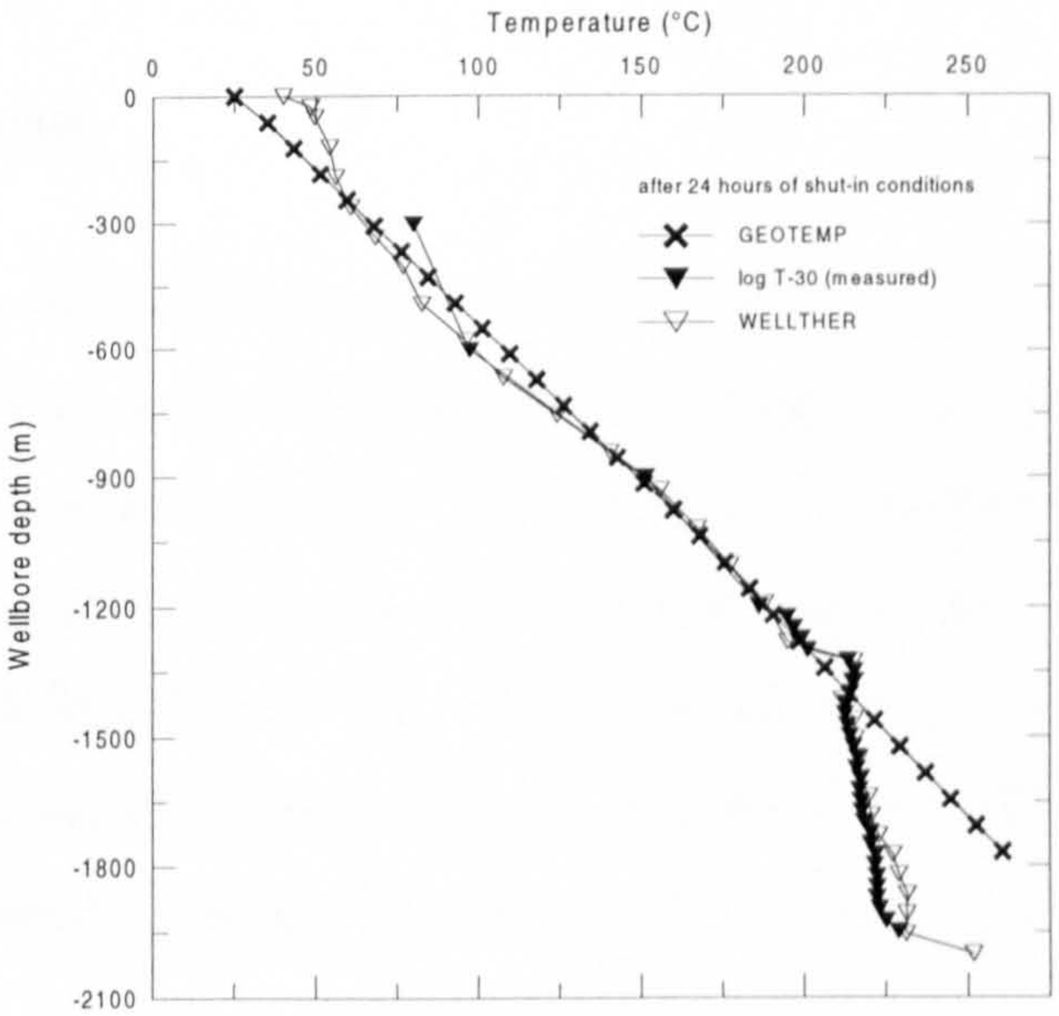

Fig. 10.9 Comparison against the temperature profiles predicted by use of the GEOTEMP and the WELLTHER simulators and the actual logged temperatures of the LV-3 wellbore under shut-in conditions (after 24 hours).

Chapter 11

SUMMARY AND CONCLUSIONS

11.1 Conclusions

The main objective of the thesis was to study the actual unsteady state of the heat transfer processes associated with geothermal well drilling and completion operations and their relationship to the temperature distributions of the wellbore and the surrounding formation. As a result of this primary objective, a computer simulator called WELLTHER has been developed to predict the transient temperature distributions in and around a geothermal wellbore under circulating and shut-in conditions in the presence of the fluid losses to the formation.

The WELLTHER simulator consists of a set of rigorous governing partial differential equations that describe the main heat transfer processes in the geothermal well drilling and shut-in operations. Transient (unsteady-state) heat flow conditions both in the wellbore and the formation were adopted. In the case of the formation, a two-dimensional (vertical and radial) transient conduction

model and a convection model were considered. WELLTHER uses a direct solution method to solve the finite-difference equations describing the transient heat transfer both in the wellbore and the surrounding formation.

The numerical unsteady solution coupled into the WELLTHER simulator was validated against the steady state analytical solution to radial temperature distribution in an infinitely long hollow cylinder with fluid flowing inside the cylinder at a constant known temperature. From this numerical validation, a good agreement between the predicted temperatures and the analytical solution was found (minimum differences less than 6.5 % were found). In addition, the capabilities of the WELLTHER simulator were tested against two numerical field cases reported in the technical literature. These cases have been used for a long time to verify the capabilities of newly developed simulators. Good agreement between the WELLTHER predictions and the temperature data reported previously were found. In all instances, the predicted and the actual measured temperatures agreed within 2 °C and 4 °C for the bottomhole and the surface (outlet) conditions, respectively.

From these validation tests, it was demonstrated that the WELLTHER simulator can accurately predict the transient temperature profiles in and around the wellbore during the circulation or the thermal recovery process. Under these conditions, the simulator predicts the temperature distribution in the drill pipe, the annulus and the surrounding formation. After analysing all the results derived from the validation tests, the following conclusions were reached.

- The assumption of steady state wellbore heat transfer which has been used by other simulators in the past is unwarranted because this state never is attained.

- During the early shut-in times, the wellbore fluid temperature is a function of the rate of heat conduction and convection in the fluid and the rate of heat loss which is a complex function of the formation thermophysical properties.

A parametric sensitivity analysis for evaluating the influence of wellbore and fluid variables on the temperature profiles in and around a wellbore under drilling (circulation) and shut-in (thermal recovery) conditions was also carried out. From these sensitivity studies, several variables which have stronger effects on the circulating and shut-in temperatures were identified. Regarding this sensitivity study the following conclusions can be drawn.

(a) The flow rate is an important variable for all flowing conditions. Low flowrates (less than 15.14 kg s^{-1}) can be ineffective at cooling the wellbore. Higher flowrates produce the greatest cooling effects within the wellbore.

(b) The inlet fluid temperature plays an important role for determining bottomhole temperatures for high rate wells, but for low rate wells fluid soon reaches the temperature of the formation, regardless of the inlet. The effect of inlet temperature is reduced in deeper wellbores.

(c) The drilling fluid density partially affects the bottomhole temperatures. Under circulation conditions, the bottomhole wellbore temperature decreases more rapidly with light weight fluids.

(d) The drilling fluid viscosity has an important impact on the bottomhole wellbore temperature. Under circulation conditions, drilling fluids with high viscosity values tend to insulate the drill pipe region (or wellbore) by decreasing the convective heat transfer coefficient. As a result of this, the cool drilling fluid is not heated as rapidly by the surrounding formation. Normally, the actual drilling fluids (non-Newtonian fluids) tend to be cooler than water (Newtonian fluid).

(e) The drilling fluid specific heat capacity has some little effect on the bottomhole wellbore temperature. Under circulation conditions, drilling fluids with higher values of specific heat capacity produce an insulation in the drill pipe region of the wellbore drilling system. Consequently, the cool drilling fluid does not exchange energy as rapidly with the formation.

(f) The drilling fluid thermal conductivity has some effect on the bottomhole wellbore temperature. Higher fluid thermal conductivities have a tendency to increase the heat exchange between the drill pipe and the surrounding formation. As a result of this, the cooler fluid temperature profile will correspond to fluid with low thermal conductivity values.

(g) The shape of the geothermal gradient or static formation temperature profile has a significant effect upon the bottomhole temperatures; high initial gradients tend to warm the fluid on the way down thus reducing the amount of cooling further down the wellbore. Regarding this, it is convenient to note that the static temperature profile of the wellbore must be considered as an important variable within the simulation. True static temperatures are the formation temperatures before the wellbore was drilled. Normally, log temperatures are lower than the true static formation temperatures. If log temperatures are used as input in the simulator, the circulating temperatures predicted would be unrealistically low. Hence, an effort to obtain the true static temperatures for the area studied need to be carried out. Several log temperatures taken at increasingly longer periods of time can be extrapolated to a pseudostatic temperature using the computer code called STATIC_TEMP which was developed with these purposes in mind. From this computation, a good approach to the static formation temperature profile can be assumed. In this way, an iterative method to obtain the actual static formation temperature can be performed if the predicted temperatures provided by the simulator are used again to extrapolate the initial temperature profile. Thus, when the initial temperature profile assumed is equal to the predicted initial temperature profile by the simulator, then the numerical method converges and a reliable estimation of the static formation temperature can be obtained.

(h) The formation thermal conductivity exhibited behaviour similar to the effect produced by the fluid thermal conductivity.

Finally, numerical simulations for studying the transient heat transfer processes in geothermal wells during circulation and shut-in conditions and in the presence of lost circulation were also carried out. It was demonstrated that the heat transfer model coupled in the WELLTHER simulator properly accounts for the energy balances in each region of the well and also the mass balances to represent the fluid losses problem to the formation. It was found that the lost circulation problem affects the value of the heat transfer coefficients in the annulus and the thermophysical properties of the formation. In addition, effective properties must also be used if a mixture of drilling fluids is used. Simulation results obtained from the application of the present model to a well with lost circulation and another well without losses, compared satisfactorily with logged temperatures. The outcome of the present work is important, in that it is one of first studies on the thermal effects of lost circulation on the shut-in (build-up) temperatures in a well. Research is underway to improve the present methodology.

11.2 Wellsite Operation of the WELLTHER Simulator

The computer code implemented in the WELLTHER simulator is a very versatile software tool that can be implemented in a personal computer system 386 or higher processor with at least 4 MB of RAM memory. This code can be used as a dynamic wellbore temperature simulator during the well design studies to predict temperature profiles within and surrounding the wellbore and their response to variations in the drilling parameters. The operation of the simulator would be most suited to periods of constant drilling through thick uniform formations, but it is designed to be used during the entire life of a wellbore from the beginning of the drilling operations to the completion stage.

Once the computer code has started producing temperature data, it may be left to run all the time, obtaining the necessary data from electronic sensors or logs after prefixed time intervals have elapsed. Hence, the salient drilling parameters, such as the flowrate, the drilling fluid density, drilling fluid viscosity, the inlet and outlet fluid temperature can be continuously updated. The

computer code is sufficiently versatile to allow for the intricate flow history involved in the well drilling activities.

The use of the simulator can improve the wellbore design with a better understanding of the bottomhole temperatures in a wellbore and its surroundings. This improvement could be used for designing the cement slurries which are greatly dependent upon the bottomhole temperatures at the time of the cementing operation as well as in the drilling fluid formulation and the logging activities.

11.3 Suggestions for Further Research

Based on the results presented in this research project and on the experience gained through the applications of the WELTHER simulator, the following recommendations are made for further study:

(i) An effort towards the development of reliable correlations for the specific heat capacity, the thermal conductivity and the convective heat transfer coefficients (CHTC) for typical drilling fluids needs to be made. Once developed, the improved correlations should further increase the level of confidence of the predictions of the wellbore temperatures obtained with the simulator. This work could complete the experimental programme that was initiated in this investigation which was related to the evaluation of the rheological behaviour of drilling fluids (non-Newtonian) and its effect on the estimation of the CHTC. At present, fifty-three numerical correlations of viscosity-temperature were derived. These correlations correspond to different drilling fluid systems which are commonly used in the geothermal well drilling industry. Hence, it would be highly suitable to measure the remaining thermophysical properties to these drilling fluid systems for predicting more accurately the transient behaviour of these wellbore drilling systems.

- The capabilities of the WELLTHER simulator should be extended to provide more flexibility. These should include the consideration of: the energy generation terms (such as the rotational energy due to the work of the drill string, the work done by the drill bit and the viscous energy due to the friction losses inside the drill pipe, the drill bit and the annulus); the variable flow area; the different type of drilling fluids (oil-based or air muds) and the possibility to analyse deviated wellbores.

- A graphical interface should be developed to represent easily the WELLTHER results. So, under certain conditions the simulator calculations may be replaced with readings from a graph or table.

Appendix I

Listing of STATIC_TEMP Computer Code

```
*     ********************************************************************** **********************************************************************
*     PROGRAM STATIC_TEMP

*     THIS COMPUTER PROGRAM ALLOWS TO CALCULATE STATIC FORMATION TEMPERATURES BY
*      MEANS OF FIVE DIFFERENTS ANALYTICAL METHODS:

*     [1] HORNER (LINE-SOURCE) METHOD [Dowdle and Cobb (1975)]
*     [2] IMPROVED HORNER METHOD [Roux et al (1980)]
*     [3] TWO-POINT METHOD [Kritikos and Kutasov (1988)]
*     [4] SPHERICAL-RADIAL METHOD [Ascencio et al (1994)]
*     [5] CYLINDRICAL-SOURCE METHOD [Hasan and Kabir (1994)]

*     ****************** COMPUTER PROGRAM WRITTEN BY: ***************

*     ********************************************************************** **********************************************************************

*     EDGAR SANTOYO GUTIERREZ

*     Ph.D. RESEARCH PROJECT:

*     ESTIMATION OF STATIC FORMATION TEMPERATURES IN THE PRESENCE OF FLUID LOSSES
*     DURING GEOTHERMAL WELL DRILLING

*     IN-HOUSE Ph.D. DEGREE PROGRAMME AT THE INSTITUTO DE INVESTIGACIONES ELECTRICAS (IIE)
*     CUERNAVACA, MEXICO WITH THE UNIVERSITY OF SALFORD, U.K.

*     ********************************************************************** **********************************************************************

      INTEGER M_SELECTION
      LOGICAL CONDITION
      DATA CONDITION/.TRUE./

      WRITE(*,10)
      WRITE(*,20)
      WRITE(*,30)
      WRITE(*,40)
      READ(*,50)M_SELECTION
      DO WHILE(CONDITION)
        IF(M_SELECTION.EQ.1)THEN
          WRITE(*,60)
          CALL HORNER
          WRITE(*,65)
          READ(*,*)ANSW
          IF(ANSW.EQ.1)THEN
                WRITE(*,40)
                READ(*,50)M_SELECTION
          ELSE
                CONDITION=.FALSE.
          ENDIF
        ELSE
          IF(M_SELECTION.EQ.2)THEN
                WRITE(*,70)
                CALL ROUX
                WRITE(*,65)
                READ(*,*)ANSW
                IF(ANSW.EQ.1)THEN
                  WRITE(*,40)
                  READ(*,50)M_SELECTION
                ELSE
                  CONDITION=.FALSE.
                ENDIF
      ELSE
                IF(M_SELECTION.EQ.3)THEN
                  WRITE(*,80)
                  CALL KRITIKOS
                  WRITE(*,65)
                  READ(*,*)ANSW
                  IF(ANSW.EQ.1)THEN
                        WRITE(*,40)
                        READ(*,50)M_SELECTION
                  ELSE
                        CONDITION=.FALSE.
                  ENDIF
                 ELSE
```

```
      IF(M_SELECTION.EQ.4)THEN
            WRITE(*,90)
            CALL ASCENCIO
            WRITE(*,65)
            READ(*,*)ANSW
            IF(ANSW.EQ.1)THEN
              WRITE(*,40)
              READ(*,50)M_SELECTION
            ELSE
              CONDITION=.FALSE.
            ENDIF
      ELSE
            IF(M_SELECTION.EQ.5)THEN
              WRITE(*,100)
              CALL HASAN
              WRITE(*,65)
              READ(*,*)ANSW
              IF(ANSW.EQ.1)THEN
                WRITE(*,40)
                READ(*,50)M_SELECTION
              ELSE
                CONDITION=.FALSE.
              ENDIF
            ELSE
              IF(M_SELECTION.LT.1 .OR. M_SELECTION.GT.5)THEN
                CONDITION=.FALSE.
              ENDIF
            ENDIF
          ENDIF
        ENDIF
      ENDIF
    ENDDO

*     *** OUTPUT FORMATS ***

10    FORMAT(5X,'*****************************************************'
     *  ,/,5X,'********* COMPUTER PROGRAM: STATIC_TEMP.FOR *********'
     *  ,/,5X,'*****************************************************')
20      FORMAT(//,5X,'** ANALYTICAL METHODS TO CALCULATE STATIC '
     *  'FORMATION',/,5X,'TEMPERATURES IN GEOTHERMAL WELLS (SFT):'
     *  ' **',//)
30    FORMAT(18X,'* AVAILABLE METHODS *',/)
40    FORMAT(/,13X,'*[1] HORNER (LINE-SOURCE) METHOD ',/
     *     ,17X,' [Dowdle and Cobb (1975)]*',/
     *     ,13X,'*[2] IMPROVED HORNER METHOD ',/
     *     ,17X,' [Roux et al (1980)]*',/
     *     ,13X,'*[3] TWO-POINT METHOD ',/
     *     ,17X,' [Kritikos and Kutasov (1988)]*',/
     *     ,13X,'*[4] SPHERICAL-RADIAL METHOD ',/
     *     ,17X,' [Ascencio et al (1994)]*',/
     *     ,13X,'*[5] CYLINDRICAL-SOURCE METHOD ',/
     *     ,17X,' [Hasan and Kabir (1994)]*',/
     *     ,13X,'*[6] NONE METHOD IS SELECTED - STOP *'
     *          ,//,30X,'SELECTION: ',$)
50    FORMAT(I2)
60      FORMAT(//,13X,'INPUT_ DATA FILE: WELL_DRILL.DAT',/
     *  13X,'OUTPUT_DATA FILE: HORNER.OUT',/)
65      FORMAT(/,13X,'DO YOU WANT TO CALCULATE SFT BY OTHER METHOD',/
     *       ,13X,'[YES(1)/NOT(2)] ?: ',$)
70    FORMAT(/,13X,'INPUT_ DATA FILE: WELL_DRILL.DAT',/
     *  13X,'OUTPUT_DATA FILE: ROUX.OUT',/)
80    FORMAT(/,13X,'INPUT_ DATA FILE: KRITIKOS.DAT',/
     *  13X,'OUTPUT_DATA FILE: KRITIKOS.OUT',/)
90    FORMAT(/,13X,'INPUT_ DATA FILE: WELL_DRILL.DAT',/
     *  13X,'OUTPUT_DATA FILE: ASCENCIO.OUT',/)
100   FORMAT(/,13X,'INPUT_ DATA FILE: WELL_DRILL.DAT',/
     *  13X,'OUTPUT_DATA FILE: HASAN.OUT',/)

      STOP
      END

*     ********************************************************************** **********************************************************************
```

```
*     ********************************************************************** ***************************************************************
*          SUBROUTINE HORNER: IS BASED ON THE LINE SOURCE SOLUTION OF THE
*          DIFFUSIVITY EQUATION [DOWDLE AND COBB (1975)].
*     ********************************************************************** ***************************************************************

          SUBROUTINE HORNER

          IMPLICIT REAL*4 (A-H,O-Z)
          REAL*4 SHUT_TIME(100),SUMXT,SHUT_TEMP(100),SUMYT,SUMXC,SUMYC,SUMXY
          REAL*4 DHT(100),LOGDHT(100),A,B,C,D,E,F,G,H,CTEA,CTEB
          CHARACTER LOGG*5,WELL*20
          LOGICAL FLAG
          INTEGER N,NDAT

               OPEN(UNIT=5,FILE='WELL_DRILL.DAT',STATUS='OLD')
               OPEN(UNIT=6,FILE='HORNER.OUT',STATUS='UNKNOWN')

*         NUMBER OF TEMPERATURE MEASUREMENTS TO BE CALCULATED

               WRITE(*,10)
               READ(*,*)NMEAS
               FLAG=.TRUE.
               COUNTER=0.

*         WELL DRILLING - DATA LOGGING

               WRITE(6,15)
               DO WHILE (FLAG)

*           CALCULATE OF DIMENSIONLESS HORNER TIME

                 WRITE(*,40)
                 READ(*,*)TC
                 WRITE(*,50)
                 READ(*,60)WELL
                 WRITE(*,70)
                 READ(*,*)DEPTH
                 WRITE(6,80)WELL,DEPTH
                 WRITE(6,20)
                 WRITE(6,30)
                 READ(5,*)NDAT
                 DO I=1,NDAT
                   READ(5,90)LOGG,SHUT_TIME(I),SHUT_TEMP(I)
                   DHT(I)=(TC+SHUT_TIME(I))/SHUT_TIME(I)
                   LOGDHT(I)=ALOG10(DHT(I))
                 ENDDO

*          DATA NUMBER

                 N=NDAT
                 SUMXT=0.0
                 DO I=1,N
                   SUMXT=SUMXT+LOGDHT(I)
                 ENDDO
                 SUMYT=0.0
                 DO I=1,N
                   SUMYT=SUMYT+SHUT_TEMP(I)
                 ENDDO
                SUMXC=0.0
                DO I=1,N
                  SUMXC=SUMXC+LOGDHT(I)**2
                ENDDO
                SUMYC=0.0
                DO I=1,N
                  SUMYC=SUMYC+SHUT_TEMP(I)**2
                ENDDO
                SUMXY=0.0
                DO I=1,N
                  SUMXY=SUMXY+LOGDHT(I)*SHUT_TEMP(I)
                ENDDO

                A=SUMYT*SUMXC
                B=SUMXT*SUMXY
                C=N*SUMXC
```

```
      D=SUMXT**2
      CTEA=(A-B)/(C-D)
      E=N*SUMXY
      F=SUMXT*SUMYT
      G=N*SUMXC
      H=SUMXT**2
      CTEB=(E-F)/(G-H)
      VAR=(SUMXC-(SUMXT**2)/N)*(CTEB**2)
      DIV=(SUMYC-(SUMYT**2)/N)
      COEF=SQRT(VAR/DIV)
      COUNTER=COUNTER+1
      DO I=1,NDAT
        TPREDICT=CTEA+CTEB*LOGDHT(I)
        WRITE(6,100)LOGG,SHUT_TIME(I),DHT(I),LOGDHT(I)
     *                          ,SHUT_TEMP(I),TPREDICT
        ENDDO
        WRITE(6,110)CTEA
        WRITE(6,120)CTEB,COEF
        WRITE(6,130)
        IF(COUNTER.EQ.NMEAS)THEN
          FLAG=.FALSE.
        ELSE
          FLAG=.TRUE.
        ENDIF
      ENDDO
      WRITE(6,130)

*     ********** OUTPUT FILE FORMATS - HORNER.OUT **********

10      FORMAT(/,13X,'No. TEMP-MEASUREMENTS TO BE CALCULATED: ',$)
15      FORMAT(/,'***************** HORNER METHOD ***************** ',/)
20      FORMAT(/,1X,'TEMP',6X,'SHUT-IN',6X,'DHT',5X,'Log DHT'
     *      ,5X,'SHUT-IN',5X,'PREDICTED')
30      FORMAT(1X,'LOGG',7X,'TIME',28X,'TEMP (øC)',3X,'TEMP (øC)',/)
40      FORMAT(/,13X,'MUD CIRCULATING TIME [Hours]= ',$)
50      FORMAT(13X,'NAME OF THE DRILLED WELL: ',$)
60      FORMAT(A20)
70      FORMAT(13X,'WELL DEPTH: ',$)
80      FORMAT(/,2X,A20,7X,'DEPTH = ',F7.1,1X,'[m]')
90      FORMAT(1X,A5,1X,F7.2,2X,F7.2,1X,I1)
100     FORMAT(1X,A5,4X,F7.2,2X,2X,F7.4,4X,F7.4,4X,F7.2,6X,F7.2)
110     FORMAT(/,4X,'STATIC FORMATION TEMPERATURE=',F7.2,1X,'(øC)')
120     FORMAT(/,4X,'SLOPE =',F7.2,3X,'CORRELATION FACTOR=',F7.4,/)
130     FORMAT(/,'************************************************** ')

        REWIND 5
        RETURN
        END


*     ********** **********

*       SUBROUTINE ROUX * USES AN IMPROVED METHOD BASED ON THE HORNER PLOT USING
*       EARLY SHUT-IN TEMPERATURE DATA TAKEN DURING WELL DRILLING OPERATIONS. THIS
*       METHOD  DETERMINES STATIC TEMPERATURES WHICH ARE CLOSER TO THE TRUE
*       RESERVOIR TEMPERATURE THAN THOSE OBTAINED FROM THE CONVENTIONAL HORNER
*       PLOT [ROUX ET AL (1980)].

*     ********** **********

        SUBROUTINE ROUX

        IMPLICIT REAL*4 (A-H,O-Z)
        REAL*4 SHUT_TIME(100),SUMXT,SHUT_TEMP(100),SUMYT,SUMXC,SUMYC,SUMXY
        REAL*4 DHT(100),LOGDHT(100),TPD,TDB
        CHARACTER ANAME*6,WELL*20,ANSWER*3,ANS2*3
        LOGICAL FLAG
        INTEGER N,NDAT,NMEAS
        DATA FLAG/.TRUE./

        OPEN(UNIT=5,FILE='WELL_DRILL.DAT',STATUS='OLD')
        OPEN(UNIT=6,FILE='ROUX.OUT',STATUS='UNKNOWN')

*     NUMBER OF TEMPERATURE MEASUREMENTS TO BE CALCULATED
```

```
      WRITE(*,10)
      READ(*,*)NMEAS
      COUNTER=0.

*     WELL DRILLING - DATA LOGGING

      WRITE(6,15)
      DO WHILE (FLAG)

*       CALCULATE OF DIMENSIONLESS HORNER TIME

        WRITE(*,40)
        READ(*,*)TC
        WRITE(*,50)
        READ(*,60)WELL
        WRITE(*,70)
        READ(*,*)DEPTH
        WRITE(6,80)WELL,DEPTH
        WRITE(6,20)
        WRITE(6,30)
        READ(5,*)NDAT
        DO I=1,NDAT
          READ(5,90)ANAME,SHUT_TIME(I),SHUT_TEMP(I)
          DHT(I)=(TC+SHUT_TIME(I))/SHUT_TIME(I)
          LOGDHT(I)=ALOG10(DHT(I))
        ENDDO

*       DATA NUMBER

        N=NDAT

*       CONVENTIONAL HORNER APPROXIMATION - DOWDLE AND COBB (1975)

        SUMXT=0.0
        DO I=1,N
          SUMXT=SUMXT+LOGDHT(I)
        ENDDO
        SUMYT=0.0
        DO I=1,N
          SUMYT=SUMYT+SHUT_TEMP(I)
        ENDDO
      SUMXC=0.0
      DO I=1,N
        SUMXC=SUMXC+LOGDHT(I)**2
      ENDDO
      SUMYC=0.0
      DO I=1,N
        SUMYC=SUMYC+SHUT_TEMP(I)**2
      ENDDO
      SUMXY=0.0
      DO I=1,N
        SUMXY=SUMXY+LOGDHT(I)*SHUT_TEMP(I)
      ENDDO
      A=SUMYT*SUMXC
      B=SUMXT*SUMXY
      C=N*SUMXC
      D=SUMXT**2
      CTEA=(A-B)/(C-D)
      HORNER_TEMP=CTEA
      E=N*SUMXY
      F=SUMXT*SUMYT
      G=N*SUMXC
      H=SUMXT**2
      CTEB=(E-F)/(G-H)
      SLOPE=CTEB
      VAR=(SUMXC-(SUMXT**2)/N)*(CTEB**2)
      DIV=(SUMYC-(SUMYT**2)/N)
      COEF=SQRT(VAR/DIV)
      COUNTER=COUNTER+1

*     CORRECTION OF THE STATIC FORMATION TEMPERATURE BY MEANS OF
*     ROUX ET AL (1980) METHOD

      WRITE(*,130)
      WRITE(*,135)
```

```
      READ(*,140)ANSWER
      IF(ANSWER.EQ.'YES')THEN
        WRITE(*,145)
        WRITE(*,150)
        READ(*,*)THERCOND
        WRITE(*,160)
        READ(*,*)HEATC
        WRITE(*,170)
        READ(*,*)DENS

*     CALCULATE OF THERMAL DIFFUSIVITY [m3/hr]

        ALFA=(THERCOND/(HEATC*DENS))*3600
        WRITE(*,180)
        READ(*,*)RADIUS
        FACTOR=ALFA/(RADIUS**2)
      ELSE
        WRITE(*,190)
        WRITE(*,195)
        READ(*,140)ANS2
        IF(ANS2.EQ.'YES')THEN
              WRITE(*,200)
              READ(*,*)FACTOR
        ELSE

*     FOR MOST COMMON LITHOLOGIES FACTOR=0.4 [ROUX ET AL (1980)]
              FACTOR=0.4
        ENDIF
      ENDIF

      TPD=FACTOR*TC
      CALL ROUX_CORRECTION(NDAT,DHT,TPD,TDB)
      SFT=HORNER_TEMP+(-SLOPE*TDB)
      DO I=1,NDAT
         TNEW=HORNER_TEMP+SLOPE*LOGDHT(I)
         TPREDICT=TNEW+(-SLOPE*TDB)
         WRITE(6,100)ANAME,SHUT_TIME(I),DHT(I),LOGDHT(I)
     *                    ,SHUT_TEMP(I),TPREDICT
      ENDDO

      WRITE(6,110)HORNER_TEMP
      WRITE(6,120)SLOPE,COEF
      WRITE(6,210)TPD,TDB
      WRITE(6,220)SFT
      WRITE(6,230)
      IF(COUNTER.EQ.NMEAS)THEN
        FLAG=.FALSE.
      ELSE
        FLAG=.TRUE.
      ENDIF
      ENDDO
      WRITE(6,230)

*     ********** OUTPUT FILE FORMATS - ROUX.OUT **********

10    FORMAT(/,13X,'No. TEMP-MEASUREMENTS TO BE CALCULATED: ',$)
15    FORMAT(/,'********** ROUX ET AL (1980) METHOD ********** ',/)
20    FORMAT(/,1X,'TEMP',6X,'SHUT-IN',6X,'DHT',5X,'Log DHT'
     *    ,5X,'SHUT-IN',5X,'PREDICTED')
30    FORMAT(1X,'LOGG',7X,'TIME',28X,'TEMP (øC)',3X,'TEMP (øC)',/)
40    FORMAT(/,13X,'MUD CIRCULATING TIME [Hours]= ',$)
50    FORMAT(13X,'NAME OF THE DRILLED WELL: ',$)
60    FORMAT(A20)
70    FORMAT(13X,'WELL DEPTH: ',$)
80    FORMAT(/,2X,A20,2X,'DEPTH = ',F7.1,1X,'[m]')
90    FORMAT(1X,A5,1X,F7.2,2X,F7.2)
100   FORMAT(1X,A5,4X,F7.2,2X,2X,F7.4,4X,F7.4,4X,F7.2,6X,F7.2)
110   FORMAT(/,4X,'STATIC FORMATION TEMPERATURE ',/,4X,
     *    '[HORNER APPROX.] =',F7.2,1X,'[øC]')
120   FORMAT(4X,'SLOPE =',F7.2,3X,'CORR. FACTOR =',F7.4,/)
130   FORMAT(/,13X,'DO YOU WANT TO CALCULATE THERMAL DIFFUSIVITY '
     *  '[YES/NOT]?: ')
135   FORMAT(/,13X,'[YES]: GIVE PETROPHYSICAL DATA OF THE FORMATION '
     *    ,/,13X,'[NOT]: THEN AVERAGE VALUES WILL BE ASSUMED?: ',$)
140   FORMAT(A3)
```

```
145     FORMAT(13X,'******** PETROPHYSICAL PROPERTIES OF THE FORMATION '
     *  ' ******** ',/)
150     FORMAT(13X,'THERMAL CONDUCTIVITY [W/m K]: ',$)
160     FORMAT(13X,'HEAT CAPACITY [J/kg K]: ',$)
170     FORMAT(13X,'DENSITY [kg/m3]: ',$)
180     FORMAT(13X,'WELL RADIUS [m]: ',$)
190     FORMAT(/,13X,'DO YOU KNOW THE VALUE OF FACTOR, ALFA/r**2 ? '
     *  '[YES/NOT]?: ')
195     FORMAT(/,13X,'[YES]: GIVE AN ESTIMATED VALUE OF IT, '
     *      ,/,13X,'[NOT]: THEN AVERAGE VALUES WILL BE ASSUMED?: ',$)
200     FORMAT(13X,'FACTOR ALFA/r**2 [1/hr]= ',$)
210     FORMAT(4X,'TPD =',F9.4,2X,'TDB =',F7.4)
220     FORMAT(4X,'FINAL STATIC FORMATION TEMPERATURE ',/,4X,
     *  '[ROUX APPROX.] =',F7.2,1X,'[øC]')
230     FORMAT(/,'********************************************************** ')


        REWIND 5
        RETURN
        END

*   ********************************************************************** **********************************************************

        SUBROUTINE ROUX_CORRECTION(NDAT,DHT,TPD,TDB)

        REAL*4 TDB
        REAL*4 DHT(100)
        INTEGER NDAT

        X=TPD
        X12=X**(1./2.)
        X13=X**(1./3.)
        X14=X**(1./4.)
        X15=X**(1./5.)
        IF(DHT(NDAT).GE.5.0 .AND. DHT(NDAT).LE.10.0)THEN
          TDB=(2.350177639+(0.0023974698*X)-(0.0608532075*X12)
     *      +(4.783275534*X13)-(5.905788104*X14)+(0.0365102305*X15))
        ELSE
          IF(DHT(NDAT).GT.10.0 .OR. DHT(NDAT).LT.1.25)THEN
            WRITE(*,899)
899         FORMAT(2X,'INVALID EQUATIONS FOR THE DHT RANGE ',/)
          ELSE
            IF(DHT(NDAT).GE.2.0 .AND. DHT(NDAT).LE.5.0)THEN
                TDB=(0.2516444578-0.0072067819*X+(0.3649971731*X12)
     *            -(0.0000793512*X13)-(3.498862147*X14)
     *            +(3.153440674*X15))
            ELSE
                TDB=(0.4873964248+(0.0027206158*X)-(0.286230844*X12)
     *            +(1.407670121*X13)-(0.7836277025*X14)
     *            -(0.7731555855*X15))
            ENDIF
          ENDIF
        ENDIF
        RETURN
        END

*   ********************************************************************** **********************************************************

*       SUBROUTINE KRITIKOS IS BASED ON THE TWO-POINT METHOD FOR DETERMINATION OF
*       UNDISTURBED RESERVOIR TEMPERATURE. THE METHOD IS BASED ON TEMPERATURE
*       MEASUREMENTS TAKEN A SHORT TIME AFTER CESSATION OF WELL DRILLING. THEN
*       TEMPERATURE LOGS ARE EXTRAPOLATED TO OBTAIN STATIC FORMATION TEMPERATURE
*       [KRITIKOS & KUTASOV (1988)].

*   ********************************************************************** **********************************************************

        SUBROUTINE KRITIKOS
        DIMENSION DT(100),TS(100,100),DEPTH(100),UFT(100)
        CHARACTER NAME*30
        INTEGER NU,NDATA,NUT
        LOGICAL VAR

*   INPUT FILE - DATA

        OPEN (UNIT=2,FILE='KRITIKOS.DAT',STATUS='UNKNOWN')
```

```
*     OUTPUT FILE - RESULTS

      OPEN (UNIT=6,FILE='KRITIKOS.OUT',STATUS='UNKNOWN')
      WRITE(6,*)'                '
      WRITE(6,7)
7     FORMAT(5X,'****** METHOD PROPOSED BY KRITICOS AND KUTASOV '
     *  ' (1988) *******')
      WRITE(6,*)'                '
      WRITE(6,9)
9     FORMAT(/,5X,'* CALCULATION OF STATIC FORMATION '
     *           'TEMPERATURES (SFT) *',/)

*     SCREEN INPUT DATA

      WRITE(*,10)
10    FORMAT(5X,'WELL TO SIMULATE : ',$)
      READ(*,15)NAME
15    FORMAT(A30)
      WRITE(6,20)NAME
20    FORMAT(5X,A30)
      WRITE(*,30)
30    FORMAT(/,5X,'NUMBER OF TEMPERATURE LOGS TAKEN: ',$)
      READ(*,*)NU
      WRITE(6,40)NU
40    FORMAT(/,5X,'No. TEMPERATURE LOGS (TAKEN) :',I3)
      NUT=1
      DO WHILE(NUT.LE.NU)
        WRITE(*,50)NUT
50       FORMAT(/,5X,'DELTA-TIME (',I2,') [days]: ',$)
        READ(*,*)DT(NUT)
        WRITE(6,60)NUT,DT(NUT)
60       FORMAT(/,5X,'DELTA-TIME (',I2,') [days]: ',F6.1)
        NUT=NUT+1
      ENDDO
      WRITE(*,70)
70    FORMAT(/,5X,'TIME OF DRILLING FLUID CIRCULATION (days): ',$)
      READ(*,*)TC
      WRITE(6,80)TC
80    FORMAT(/,5X,'TIME OF DRILLING FLUID CIRCULATION: ',F6.1,' days')
      WRITE(*,90)
90    FORMAT(/,5X,'NUMBER OF TEMPERATURE DATA: ',$)
      READ(*,*)NDATA
      WRITE(6,100)NDATA
100   FORMAT(/,5X,'NUMBER OF TEMPERATURE DATA: ',I3,/)

*     INPUT DATA BY READING FILE

      DO K=1,NDATA
        READ(2,*)DEPTH(K),(TS(K,N),N=1,NU)
      ENDDO
      VAR=.TRUE.
      ID=1
      IT=1
      WRITE(6,105)
105   FORMAT(5X,'DEPTH (m)',9X,'TEMPERATURE (øC)',5X,'SFT (øC)',/)
      DO WHILE(VAR)
      DT1=DT(ID)
      DT2=DT(ID+1)
      DO K=1,NDATA
        TS1=TS(K,ID)
        TS2=TS(K,ID+1)
        CALL KRIT(TC,DT1,DT2,TS1,TS2,TR)
        UFT(K)=TR
        WRITE(6,110)DEPTH(K),TS1,TS2,UFT(K)
110     FORMAT(5X,F7.1,12X,2F6.1,8X,F6.1)
      ENDDO
      IF(K.GE.NDATA)THEN
        WRITE(6,120)IT
120     FORMAT(/,5X,'Iteration No. ',I3,' for Static Formation'
     *    ' Temperature',///)
      ENDIF
      ID=ID+1
      IT=IT+1
      IF(ID.LT.NU)THEN
        VAR=.TRUE.
```

```
            ELSE
              VAR=.FALSE.
              WRITE(6,130)
130           FORMAT(5X,'** FINAL ITERATION **',/)
            ENDIF
          ENDDO

          RETURN
          END

*     ********************************************************************** **********************************************************************

          SUBROUTINE KRIT(TC,DT1,DT2,TS1,TS2,TR)
          DIMENSION X(2),EI(10)
          DATA D0 /2.184/

          D1=(D0**2)/4.
          D2=0.5772+ALOG(D1)
          FT1=DT1/TC
          FT2=DT2/TC
          X(1)=D1/FT2
          X(2)=D1/FT1

*     *** CALCULO DE LOS "EI" ***

          CALL INTGEXP(X,EI)
          F=(EI(1)+ALOG(FT2)-D2)/(EI(1)-EI(2)+ALOG(FT2/FT1))
          TR=TS2+F*(TS1-TS2)
          RETURN
          END

*     ********************************************************************** **********************************************************************

          SUBROUTINE INTGEXP(X,EI)
          DIMENSION X(2),EI(2)
          DO I=1,2
          IF(X(I).GT.1.0)THEN
           Z3=X(I)*EXP(X(I))
           Z4=X(I)**2+2.334733*X(I)+0.250621
           Z5=X(I)**2+3.330657*X(I)+1.681534
           EI(I)=Z4/Z5/Z3
          ELSE
           IF(X(I).LE.0.0)THEN
             WRITE(*,111)
111          FORMAT(2X,'ERROR-ARGUMENT OF THE EXPONENTIAL INTEGRAL')
           ELSE
             Z1=-ALOG(X(I))-0.57721566+0.99999193*X(I)-0.24991055*X(I)**2
             Z2=0.05519968*X(I)**3-0.00976004*X(I)**4+0.00107857*X(I)**5
             EI(I)=Z1+Z2
           ENDIF
          ENDIF
          ENDDO

          RETURN
          END

*     ********************************************************************** **********************************************************************

*     * SUBROUTINE ASCENCIO * IS BASED ON THE NEW METHOD TO ESTIMATE UNDISTURBED
*      FORMATION TEMPERATURES UNDER SPHERICAL AND RADIAL HEAT FLOW CONDITIONS. THE
*      METHOD USES WELL DRLLING TEMPERATURE DATA TAKEN DURING THE RETURN TO
*      EQUILIBRIUM [ASCENCIO ET AL (1994)].

*     ********************************************************************** **********************************************************************

          SUBROUTINE ASCENCIO

          REAL*4 SHUT_TIME(100),SUMXT,SHUT_TEMP(100),SUMYT,SUMXC,SUMYC,SUMXY
          REAL*4 ASCIO_TIME(100)
          CHARACTER LOGG*5,WELL*20
          LOGICAL FLAG
          INTEGER N,NDAT

          OPEN(UNIT=5,FILE='WELL_DRILL.DAT',STATUS='OLD')
          OPEN(UNIT=6,FILE='ASCENCIO.OUT',STATUS='UNKNOWN')
```

```
*     NUMBER OF TEMPERATURE MEASUREMENTS TO BE CALCULATED

          WRITE(*,10)
          READ(*,*)NMEAS
          FLAG=.TRUE.
          COUNTER=0.

*     WELL DRILLING - DATA LOGGING

          WRITE(6,15)
          DO WHILE (FLAG)

*       CALCULATE OF ASCENCIO TIME PARAMETER

          WRITE(*,50)
          READ(*,60)WELL
          WRITE(*,70)
          READ(*,*)DEPTH
          WRITE(6,80)WELL,DEPTH
          WRITE(6,20)
          WRITE(6,30)
          READ(5,*)NDAT
          DO I=1,NDAT
            READ(5,90)LOGG,SHUT_TIME(I),SHUT_TEMP(I)
            ASCIO_TIME(I)=(1./SQRT(SHUT_TIME(I)))
          ENDDO

*       DATA NUMBER

          N=NDAT
          SUMXT=0.0
          DO I=1,N
            SUMXT=SUMXT+ASCIO_TIME(I)
          ENDDO
          SUMYT=0.0
          DO I=1,N
            SUMYT=SUMYT+SHUT_TEMP(I)
         ENDDO
        SUMXC=0.0
        DO I=1,N
          SUMXC=SUMXC+ASCIO_TIME(I)**2
        ENDDO
        SUMYC=0.0
        DO I=1,N
          SUMYC=SUMYC+SHUT_TEMP(I)**2
        ENDDO
        SUMXY=0.0
        DO I=1,N
          SUMXY=SUMXY+ASCIO_TIME(I)*SHUT_TEMP(I)
        ENDDO
        A=SUMYT*SUMXC
        B=SUMXT*SUMXY
        C=N*SUMXC
        D=SUMXT**2
        CTEA=(A-B)/(C-D)
        E=N*SUMXY
        F=SUMXT*SUMYT
        G=N*SUMXC
        H=SUMXT**2
        CTEB=(E-F)/(G-H)
        VAR=(SUMXC-(SUMXT**2)/N)*(CTEB**2)
        DIV=(SUMYC-(SUMYT**2)/N)
        COEF=SQRT(VAR/DIV)
        COUNTER=COUNTER+1
        DO I=1,NDAT
          TPREDICT=CTEA+CTEB*ASCIO_TIME(I)
          WRITE(6,100)LOGG,SHUT_TIME(I),ASCIO_TIME(I)
*                              ,SHUT_TEMP(I),TPREDICT
        ENDDO
        WRITE(6,110)CTEA
        WRITE(6,120)CTEB,COEF
        WRITE(6,130)
        IF(COUNTER.EQ.NMEAS)THEN
          FLAG=.FALSE.
        ELSE
```

```
            FLAG=.TRUE.
          ENDIF
        ENDDO
        WRITE(6,130)


*     ********** OUTPUT FILE FORMATS - ASCENCIO.OUT **********

10      FORMAT(/13X,'NUMBER OF TEMP. MEASUREMENTS TO BE CALCULATED: ',$)
15      FORMAT(/,'********** ASCENCIO ET AL (1994) **********',/)
20      FORMAT(/,4X,'TEMP',6X,'SHUT-IN',3X,'1/SQRT(t)',3X,'SHUT-IN',
   *         5X,'PREDICTED')
30      FORMAT(4X,'LOGG',7X,'TIME',17X,'TEMP (øC)',3X,'TEMP (øC)',/)
50      FORMAT(/,13X,'NAME OF THE DRILLED WELL: ',$)
60      FORMAT(A20)
70      FORMAT(13X,'WELL DEPTH: ',$)
80      FORMAT(/,4X,A20,7X,'DEPTH = ',F7.1,1X,'[m]',/)
90      FORMAT(1X,A5,1X,F7.2,2X,F7.2,1X,I1)
100     FORMAT(4X,A5,4X,F7.2,2X,2X,F7.4,4X,F7.2,6X,F7.2)
110     FORMAT(/,3X,'STATIC FORMATION TEMPERATURE=',F7.2,1X,'[øC]')
120     FORMAT(/,3X,'SLOPE =',F7.2,3X,'CORRELATION FACTOR=',F7.4,/)
130     FORMAT(/,'********************************************************* ')

        REWIND 5
        RETURN
        END

*     ********************************************************************** **********

*     * SUBROUTINE HASAN * IS BASED ON THE GENERAL SOLUTION OF THE THERMAL DIFFUSIVITY
*      EQUATION UNDER TRANSIENT CONDITIONS. THREE ANALYTICAL EQUATIONS CAN BE USED TO
*      CALCULATE STATIC  FORMATION TEMPERATURES. THESE EQUATIONS OFFER THE ADVANTAGE
*      OF USING BOTTOMHOLE TEMPERATURE DATA TAKEN DURING WELL DRILLING OPERATIONS AT
*      EARLY TIMES [HASAN & KABIR (1994)].

*     ********************************************************************** **********

        SUBROUTINE HASAN
        COMMON/SHUTIN1/NDAT,TP,TIME
        COMMON/SHUTIN2/VARX

        REAL*4 TIME(100),SUMXT,TEMPWS(100),SUMYT,SUMXC,SUMYC,SUMXY
        REAL*4 VARX(100),TEMPPI(100)
        CHARACTER ANAME*5,WELL*20
        LOGICAL FLAG
        INTEGER N,NDAT

        OPEN(UNIT=5,FILE='WELL_DRILL.DAT',STATUS='OLD')
        OPEN(UNIT=6,FILE='HASAN.OUT',STATUS='UNKNOWN')

*     NUMBER OF TEMPERATURE MEASUREMENTS TO BE CALCULATED

        WRITE(*,10)
        READ(*,*)NMEAS
        FLAG=.TRUE.
        COUNTER=0.

*     WELL DRILLING - DATA LOGGING

          WRITE(6,15)
          DO WHILE (FLAG)
            WRITE(*,40)
            READ(*,*)TP
            WRITE(*,50)
            READ(*,60)WELL
            WRITE(*,70)
            READ(*,*)DEPTH
            WRITE(6,80)WELL,DEPTH
            WRITE(6,20)
            WRITE(6,30)
            READ(5,*)NDAT
            DO I=1,NDAT
              READ(5,90)ANAME,TIME(I),TEMPWS(I)
            ENDDO
*       SELECT AN APPROXIMATION METHOD
```

```
            CALL METHODS
*       DATA NUMBER
            N=NDAT
            SUMXT=0.0
            DO I=1,N
              SUMXT=SUMXT+VARX(I)
            ENDDO
            SUMYT=0.0
            DO I=1,N
              SUMYT=SUMYT+TEMPWS(I)
            ENDDO
           SUMXC=0.0
           DO I=1,N
             SUMXC=SUMXC+VARX(I)**2
           ENDDO
           SUMYC=0.0
           DO I=1,N
             SUMYC=SUMYC+TEMPWS(I)**2
           ENDDO
           SUMXY=0.0
           DO I=1,N
             SUMXY=SUMXY+VARX(I)*TEMPWS(I)
           ENDDO
           A=SUMYT*SUMXC
           B=SUMXT*SUMXY
           C=N*SUMXC
           D=SUMXT**2
           CTEA=(A-B)/(C-D)
           E=N*SUMXY
           F=SUMXT*SUMYT
           G=N*SUMXC
           H=SUMXT**2
           CTEB=(E-F)/(G-H)
            VAR=(SUMXC-(SUMXT**2)/N)*(CTEB**2)
            DIV=(SUMYC-(SUMYT**2)/N)
            COEF=SQRT(VAR/DIV)
            COUNTER=COUNTER+1
            DO I=1,NDAT
              TEMPPI(I)=CTEA+(CTEB*VARX(I))
              WRITE(6,100)ANAME,TIME(I),VARX(I),TEMPWS(I),TEMPPI(I)
            ENDDO
            WRITE(6,110)CTEA
            WRITE(6,120)CTEB,COEF
            WRITE(6,130)
            IF(COUNTER.EQ.NMEAS)THEN
              FLAG=.FALSE.
            ELSE
              FLAG=.TRUE.
            ENDIF
          ENDDO
          WRITE(6,130)
*     ********** OUTPUT FILE FORMATS - HASAN.OUT **********
10        FORMAT(/,13X,'No. TEMP-MEASUREMENTS TO BE CALCULATED: ',$)
15        FORMAT(/,'********** HASAN METHOD **********',/)
20        FORMAT(/,6X,'TEMP',6X,'SHUT-IN',5X,'FUNCTION',3X,'SHUT-IN',
     *        4X,'PREDICTED')
30        FORMAT(6X,'LOGG',7X,'TIME',9X,'(X)',5X,'TEMP (øC)',3X,
     *        'TEMP (øC)',/)
40        FORMAT(/,13X,'MUD CIRCULATING TIME [Hours]= ',$)
50        FORMAT(13X,'NAME OF THE DRILLED WELL: ',$)
60        FORMAT(A20)
70        FORMAT(13X,'WELL DEPTH: ',$)
80        FORMAT(/,2X,A20,7X,'DEPTH = ',F7.1,1X,'[m]')
90        FORMAT(1X,A5,1X,F7.2,2X,F7.2,1X,I1)
100       FORMAT(5X,A5,4X,F7.2,4X,F9.4,4X,F7.2,5X,F7.2)
110       FORMAT(/,4X,'STATIC FORMATION TEMPERATURE=',F7.2,1X,'[øC]')
120       FORMAT(/,4X,'SLOPE =',F7.2,3X,'CORRELATION FACTOR=',F7.4,/)
130       FORMAT(/,'********** ')

          REWIND 5
          RETURN
          END
```

```
*     ************************************************************** ******************************************************************
          SUBROUTINE METHODS
          COMMON/SHUTIN1/NDAT,TP,TIME
          COMMON/SHUTIN2/VARX
          COMMON/THERMALP/THKM,THKF,CPM,CPF,DENSM,DENSF,ALFA,RW,FLOWM,R
*         REAL*4 TIME(100),SUMXT,TEMPWS(100),SUMYT,SUMXC,SUMYC,SUMXY
          REAL*4 VARX(100),HORNER(100),FUNC1(100),FUNC2(100),TIME(100)
*         CHARACTER LOGG*5,WELL*20
*         LOGICAL FLAG
          INTEGER NDAT

          DATA PI/3.141593/

          WRITE(*,11)
11        FORMAT(/,13X,'********** APPROXIMATION METHODS **********',/)
          WRITE(*,200)
200       FORMAT(13X,'[1] EXPONENTIAL APPROXIMATION '/
     *         ,13X,'[2] LOG-LINEAR APPROXIMATION  '/
     *         ,13X,'[3] TIME-ROOT APPROXIMATION '
     *         '(FOR VERY EARLY-TIME DATA)'/
     *         ,13X,'[4] RIGOUROUS SOLUTION       ',4X,'SELECTION: ',$)
          READ(*,*)ISEL
          WRITE(*,201)
201       FORMAT(/,13X,'THERMOPHYSICAL PROPERTIES (FORMATION AND MUD)',
     *         /,13X,'[1 (AVERAGE VALUES) / 2 (AVAILABLE DATA): ',$)
          READ(*,*)IK1

          IF(IK1.EQ.1)THEN
            ALFA=1.20095E-6
            THKM=0.61
            RW=0.108
            THKF=2.51
            CPM=1200.00
            R=0.108
            FLOWM=140.0
          ELSE
            CALL THERMAL_PROP
          ENDIF
          TDIM=(ALFA*3600*TP)/(RW**2)
          IF(ISEL.EQ.1)THEN
*       CALCULATION OF THE OVERALL HEAT TRANSFER COEFFICIENT
            U=THKM/RW
            IF(TDIM.LE.1.5)THEN
              TD=(1.1282*SQRT(TDIM))*(1-0.3*SQRT(TDIM))
            ELSE
              TD=(0.4063+(0.5*ALOG(TDIM)))*(1.+(0.6/TDIM))
            ENDIF
            COEF1=R*U*TD
            COEF2=R*U*THKF
            VAR1A=(FLOWM*CPM)
            VAR2A=(2*PI)
            VAR3A=((THKF+COEF1)/COEF2)
            A=(VAR1A/VAR2A)*VAR3A
            A=A/3600.
            DO I=1,NDAT
              COEF4=-TIME(I)/A
              VARX(I)=EXP(COEF4)
            ENDDO
          ELSE
            IF(ISEL.EQ.2)THEN
              DO I=1,NDAT
                HORNER(I)=(TP+TIME(I))/TIME(I)
                VARX(I)=ALOG(HORNER(I))
              ENDDO
            ELSE
              IF(ISEL.EQ.3)THEN
                DO I=1,NDAT
                  DELTATD=(ALFA*3600*TIME(I))/(RW**2.)
                  FCF1=SQRT(TDIM+DELTATD)
                  FCF2=(1.-(0.3*FCF1))
                  FCF3=SQRT(TDIM)*(1.-(0.3*SQRT(TDIM)))
                  VARX(I)=FCF1*FCF2-FCF3
                ENDDO
              ELSE
                IF(ISEL.EQ.4)THEN
```

```
*           CALCULATION OF THE OVERALL HEAT TRANSFER COEFFICIENT
                  NDATA=NDAT
                  U=THKM/RW
                  DO JJ=1,NDATA
                    C1=((2*PI)/(FLOWM*CPM))*(R*U)*(R**2./ALFA)
                    C2=(1.1282*R*U)/THKF
                    C3=0.3*C2
                    ACH=SQRT(2.777+(3.3333/C2))
                    DELTD=(ALFA*3600*TIME(JJ))/(RW**2)
                    TIDIM=TDIM+DELTD
                    F1=ACH+SQRT(TIDIM)-1.667
                    F2=ACH-SQRT(TIDIM)+1.667
                    F3=1.+(C2*SQRT(TIDIM))-(0.3*C2*TIDIM)
                    TER1=F1/F2
                    TER2=(5.555/(ACH*C2))
                    TER3=F3**(3.333/C2)
                    FUNC1(JJ)=((TER1**TER2)/(TER3))**(-C1)
                    F4=ACH+SQRT(DELTD)-1.667
                    F5=ACH-SQRT(DELTD)+1.667
                    F6=1.+(C2*SQRT(DELTD))-(0.3*C2*DELTD)
                    TER4=F4/F5
                    TER5=(5.555/(ACH*C2))
                    TER6=F6**(3.333/C2)
                    FUNC2(JJ)=((TER4**TER5)/(TER6))**(-C1)
                    VARX(JJ)=-(FUNC1(JJ)-FUNC2(JJ))
                  ENDDO
                ENDIF
              ENDIF
            ENDIF
          ENDIF
          RETURN
          END
*     ********************************************************************** **********************************************************
          SUBROUTINE THERMAL_PROP
          COMMON/THERMALP/THKM,THKF,CPM,CPF,DENSM,DENSF,ALFA,RW,FLOWM,R
          WRITE(*,250)
250       FORMAT(/,2X,'DRILLING FLUID AND FORMATION THERMAL PROPERTIES',/)
          WRITE(*,300)
300       FORMAT(10X,'* THERMAL PROPERTIES OF THE FORMATION *',/)
          WRITE(*,350)
350       FORMAT(6X,'THERMAL CONDUCTIVITY [W/m K] = ',$)
          READ(*,*)THKF
          WRITE(*,400)
400       FORMAT(6X,'HEAT CAPACITY [J/kg K]      = ',$)
          READ(*,*)CPF
          WRITE(*,450)
450       FORMAT(6X,'DENSITY [kg/m3]             = ',$)
          READ(*,*)DENSF
          WRITE(*,475)
475       FORMAT(6X,'WELLBORE RADIUS [m]         = ',$)
          READ(*,*)RW
          WRITE(*,495)
495       FORMAT(6X,'RADIAL-DIST. FROM THE WELL [m]= ',$)
          READ(*,*)R
          WRITE(*,500)
500       FORMAT(/,10X,'* THERMAL PROPERTIES OF THE MUD *',/)
          WRITE(*,550)
550       FORMAT(6X,'THERMAL CONDUCTIVITY [W/m K] = ',$)
          READ(*,*)THKM
          WRITE(*,600)
600       FORMAT(6X,'HEAT CAPACITY [J/kg K]      = ',$)
          READ(*,*)CPM
          WRITE(*,650)
650       FORMAT(6X,'DENSITY [kg/m3]             = ',$)
          READ(*,*)DENSM
          WRITE(*,700)
700       FORMAT(6X,'MUD MASS [kg]  =',$)
          READ(*,*)FLOWM

*         THERMAL DIFFUSIVITY OF THE FORMATION
          ALFA=THKF/(CPF*DENSF)
          RETURN
          END
```

Appendix II

Listing of MODEL and POLYREG Computer Codes

```
*     ************************************************************ ************************************************************
*     NUMERICAL ALGORITHM - VISCOSITY
*     ************************************************************ ************************************************************

*     COMPUTER PROGRAM WRITTEN BY:      EDGAR SANTOYO GUTIERREZ
*     Ph.D. RESEARCH PROJECT:

*     ESTIMATION OF STATIC FORMATION TEMPERATURES IN THE PRESENCE OF FLUID LOSSES
*     DURING GEOTHERMAL WELL DRILLING

*     IN-HOUSE Ph.D. DEGREE PROGRAMME AT THE INSTITUTO DE INVESTIGACIONES ELECTRICAS (IIE)
*     CUERNAVACA, MEXICO WITH THE UNIVERSITY OF SALFORD, U.K.
*     ************************************************************ ************************************************************
      PROGRAM MODEL
      REAL SHEAR_RATE(10),SHEAR_STRESS(10),VARX(10),VARY(10)
      REAL MU_BINGHAM,MU_POWERL,MU_IMPOWERL
      LOGICAL BOND
      COMMON/DATA1/VARX,VARY,NDAT,INDICATOR
      OPEN(UNIT=5,FILE='POWER.DAT',STATUS='UNKNOWN')

      WRITE(*,9)
9     FORMAT(17X,'SHEAR RATE [1/s] - SHEAR STRESS [N/m2] DATA No.',$)
      READ(5,*)NDAT
      DO I=1,NDAT
        READ(5,*)SHEAR_RATE(I),SHEAR_STRESS(I)
        VARX(I)=SHEAR_RATE(I)
        VARY(I)=SHEAR_STRESS(I)
      ENDDO
      WRITE(*,10)
10    FORMAT(15X,'********** RHEOLOGICAL MODEL SELECTION **********',/)
      WRITE(*,20)
20    FORMAT(15X,'[1] BINGHAM MODEL',/)
      WRITE(*,30)
30    FORMAT(15X,'[2] POWER LAW MODEL',/)
      WRITE(*,40)
40    FORMAT(15X,'[3] IMPROVED POWER LAW MODEL (PIPE AND ANNULAR',/
     *     19x,'FLOW PARAMETERS ARE REQUIRED)',/)
      BOND=.TRUE.
      DO WHILE(BOND)
        WRITE(*,50)
50      FORMAT(15X,'SELECTION: ',$)
        READ (*,*) ISEL
        IF(ISEL.GT.3)THEN
          BOND=.TRUE.
        ELSE
          IF(ISEL.LT.1)THEN
            BOND=.TRUE.
          ELSE
            BOND=.FALSE.
          ENDIF
        ENDIF
      ENDDO
      IF(ISEL.EQ.1)THEN
        INDICATOR=ISEL
        CALL BINGHAM(MU_BINGHAM,ERROR)
        WRITE(*,111)MU_BINGHAM,ERROR
111     FORMAT(5X,'MU,ERROR=',2F10.3)
      ELSE
        IF(ISEL.EQ.2)THEN
          INDICATOR=ISEL
          CALL POWER_LAW(MU_POWERL,ERROR1)
          WRITE(*,112)MU_POWERL,ERROR1
112       FORMAT(5X,'MU,ERROR=',2F10.3)
        ELSE
          INDICATOR=3
          WRITE(*,95)
95        FORMAT(15X,'DRILLING SECTION [1(ANNULUS)/2(DRILLING PIPE)]:',$)
          READ(*,*)STATUS
          CALL IMPOWER_LAW(STATUS,MU_IMPOWERL,ERROR2)
          WRITE(*,113)MU_IMPOWERL,ERROR2
113       FORMAT(5X,'MU,ERROR=',2F10.3)
        ENDIF
      ENDIF
      STOP
      END
```

```
      SUBROUTINE IMPOWER_LAW(STATUS,MU,ERR)
      COMMON/DATA1/VARX,VARY,NDAT,INDICATOR
      COMMON/LOGDAT1/ADLOGA,BDLOGA,NDATOS,INDY
      COMMON /RHELOGI1/XTEMP,YTEMP,NDATA
      REAL VARX(10),VARY(10),CTEA,CTEB,R
      REAL DIFY(10),YCALC(10),MU,ADLOGA(10),BDLOGA(10),EFFMU
      REAL GAMAR
      REAL*8 XTEMP(10),YTEMP(10),C
      INTEGER NDATOS,NDAT,INDICATOR,INDY

      INDY=INDICATOR
      DO I=1,NDAT
        XTEMP(I)=VARY(I)
        YTEMP(I)=VARX(I)
      ENDDO
      NDATA=NDAT
      CALL CPARAM(C)
      C_PARA=C
      DO I=1,NDAT
        ADLOGA(I)=LOG10(VARX(I)+C_PARA)
        BDLOGA(I)=LOG10(VARY(I))
      ENDDO
      CALL LINEFIT(CTEA,CTEB,R)
      CTEK1=CTEA
      CTEA1=10**CTEA
      CTEK2=CTEB
      SUME1=0.0
      DO I=1,NDAT
        YCALC(I)=CTEK1+CTEK2*ADLOGA(I)
        YCALC(I)=10**(YCALC(I))
        DIFY(I)=((YCALC(I)-VARY(I))/VARY(I))*100
        SUME1=SUME1+ABS(DIFY(I))
      ENDDO
      AVERAGE_DI=SUME1/NDAT
      ERR=AVERAGE_DI
      IF(STATUS.EQ.1)THEN
        WRITE(*,100)
100     FORMAT(15X,'BULK VELOCITY-ANNULAR SECTION [m/s] =',$)
        READ(*,*)BULV_AN
        WRITE(*,104)
104     FORMAT(15X,'OUTER DIAMETER OF ANNULUS [m] =',$)
        READ(*,*)D1
        WRITE(*,105)
105     FORMAT(15X,'INNER DIAMETER OF ANNULUS [m] =',$)
        READ(*,*)D2
        DIA=D1-D2
        VAR3=(C_PARA/(2.*CTEB))
        GAMAR=((2*CTEB+1)/(3*CTEB))*((12*BULV_AN)/DIA)+VAR3
        EFFMU=(CTEA1*((GAMAR+C_PARA)**CTEB))/GAMAR
        MU=EFFMU
      ELSE
        WRITE(*,110)
110     FORMAT(15X,'BULK VELOCITY-PIPE SECTION [m/s] =',$)
        READ(*,*)BULV_PI
        WRITE(*,115)
115     FORMAT(15X,'PIPE DIAMETER [m] =',$)
        READ(*,*)DD1
        GAMAR=((3*CTEB+1)/(4*CTEB))*((8*BULV_PI)/DD1)+
     *  (C_PARA/(3.*CTEB))
        EFFMU=(CTEA1*((GAMAR+C_PARA)**CTEB))/GAMAR
        MU=EFFMU
      ENDIF
      RETURN
      END

      SUBROUTINE POWER_LAW(MU,ERR)
      REAL VARX(10),VARY(10),CTEA,CTEB,R,MU_EFFECTIVE(10)
      REAL DIFY(10),YCALC(10),MU,AD(10),BD(10),SUMAMU
      INTEGER NDATOS,NDAT,INDICATOR,IND
      COMMON/DATA1/VARX,VARY,NDAT,INDICATOR
      COMMON/LOGDATAR/AD,BD,NDATOS,IND

      IND=INDICATOR
      DO I=1,NDAT
        AD(I)=LOG10(VARX(I))
        BD(I)=LOG10(VARY(I))
```

```
ENDDO
NDATOS=NDAT
CALL LINEFIT(CTEA,CTEB,R)
CTEK=CTEA
CTEN=CTEB
SUMERROR1=0.0
SUMAMU=0.0
DO I=1,NDAT
  YCALC(I)=CTEA+CTEB*AD(I)
  YCALC(I)=10**(YCALC(I))
  DIFY(I)=((YCALC(I)-VARY(I))/VARY(I))*100
  SUMERROR1=SUMERROR1+ABS(DIFY(I))
  MU_EFFECTIVE(I)=(10**(CTEK))*(VARX(I)**(CTEN-1))
  SUMAMU=SUMAMU+MU_EFFECTIVE(I)
ENDDO
AVERAGE_DI=SUMERROR1/NDAT
AVERAGE_MU=SUMAMU/NDAT
STDEV1=0.0
STDEV2=0.0
DO I=1,NDAT
  STDEV1=STDEV1+(ABS(DIFY(I))-AVERAGE_DI)**2
  STDEV2=STDEV2+(MU_EFFECTIVE(I)-AVERAGE_MU)**2
ENDDO
STDEV1=SQRT(STDEV1/NDAT)
STDEV2=SQRT(STDEV2/NDAT)
ERROR2=(STDEV2/AVERAGE_MU)*100
ERR=AVERAGE_DI
ERR1=ERROR2
MU=AVERAGE_MU
RETURN
END

SUBROUTINE BINGHAM(MU,ERR)
IMPLICIT REAL (A-H,O-Z)
REAL VARX(10),VARY(10),CTEA,CTEB,R,MU_EFFECTIVE(10),MU_PLASTIC
REAL DIFY(10),YCALC(10),MU
COMMON/DATA1/VARX,VARY,NDAT,INDICATOR
INTEGER NDAT,INDICATOR

CALL LINEFIT(CTEA,CTEB,R)
MU_PLASTIC=CTEB
YIELD_POINT=CTEA
SUMAMU=0.0
SUMERROR1=0.0
DO I=1,NDAT
  YCALC(I)=CTEA+CTEB*VARX(I)
  DIFY(I)=((YCALC(I)-VARY(I))/VARY(I))*100
  SUMERROR1=SUMERROR1+ABS(DIFY(I))
  MU_EFFECTIVE(I)=(YIELD_POINT/VARX(I))+MU_PLASTIC
  SUMAMU=SUMAMU+MU_EFFECTIVE(I)
ENDDO
AVERAGE_DI=SUMERROR1/NDAT
AVERAGE_MU=SUMAMU/NDAT
STDEV=0.0
DO I=1,NDAT
  STDEV=STDEV+(MU_EFFECTIVE(I)-AVERAGE_MU)**2
ENDDO
STDEV=SQRT(STDEV/NDAT)
ERROR2=(STDEV/AVERAGE_MU)*100
ERR=AVERAGE_DI
MU=AVERAGE_MU
RETURN
END

SUBROUTINE LINEFIT(CTEA,CTEB,R)
REAL X(10),SUMX,Y(10),SUMY,SUMXC,SUMYC,SUMXY
REAL A,B,C,D,E,F,G,H,CTEA,CTEB,VAR,DIV
REAL VARX(10),VARY(10),AD(10),BD(10),AA(10),BB(10)
INTEGER NDATOS,NDAT,INDICATOR,IND,N
COMMON/DATA1/VARX,VARY,NDAT,INDICATOR
COMMON/LOGDATAR/AD,BD,NDATOS,IND
COMMON/LOGDAT1/AA,BB,NDATA,INDY

IF(INDICATOR.EQ.1)THEN
  DO I=1,NDAT
    X(I)=VARX(I)
    Y(I)=VARY(I)
```

```
  ENDDO
 ELSE
  IF(INDICATOR.EQ.2)THEN
    DO I=1,NDAT
      X(I)=AD(I)
      Y(I)=BD(I)
    ENDDO
  ELSE
    DO I=1,NDAT
      X(I)=AA(I)
      Y(I)=BB(I)
    ENDDO
  ENDIF
 ENDIF
 N=NDAT
 SUMX=0.0
 DO I=1,N
   SUMX=SUMX+X(I)
 ENDDO
 SUMY=0.0
 DO I=1,N
   SUMY=SUMY+Y(I)
 ENDDO
 SUMXC=0.0
 DO I=1,N
   SUMXC=SUMXC+X(I)**2
 ENDDO
 SUMYC=0.0
 DO I=1,N
   SUMYC=SUMYC+Y(I)**2
 ENDDO
 SUMXY=0.0
 DO I=1,N
   SUMXY=SUMXY+X(I)*Y(I)
 ENDDO
 A=SUMY*SUMXC
 B=SUMX*SUMXY
 C=N*SUMXC
 D=SUMX**2
 CTEA=(A-B)/(C-D)
 E=N*SUMXY
 F=SUMX*SUMY
 G=N*SUMXC
 H=SUMX**2
 CTEB=(E-F)/(G-H)
 VAR=(SUMXC-(SUMX**2)/N)*(CTEB**2)
 DIV=(SUMYC-(SUMY**2)/N)
 R=SQRT(VAR/DIV)
 RETURN
 END

 SUBROUTINE CPARAM(C)
 IMPLICIT REAL*8 (A-H,O-Z)
 COMMON /RHELOGI1/X,Y,NDAT
 COMMON /DATYY/YY

 REAL*8 LARGE,SMALL,X(10),Y(10),XX(10),YY(10),YYY(10)
 REAL*8 TAU1,GREATER,GREATER1,YVAR(10),SMALL1,LARGE1
 LOGICAL BANDER
 SMALL=1.0E+20
 SMALL1=1.0E+20
 LARGE1=-1.0E+2
 DO I=1,NDAT
      SMALL = MIN (SMALL,X(I))
      LARGE = MAX (LARGE,X(I))
      SMALL1 = MIN (SMALL1,Y(I))
      LARGE1 = MAX (LARGE1,Y(I))
 ENDDO
 DO I=1,NDAT
   YVAR(I)=Y(I)
 ENDDO
 VAR1=SMALL*LARGE
 TAU1=SQRT(VAR1)
 TRAMPA=TAU1
 X(NDAT+1)=TRAMPA
```

```
C       SORTING OF X(I) VECTOR
        DO M=1,NDAT+1
          GREATER=X(1)
          N=1
          DO MM=2,NDAT+1
            IF(GREATER.LT.X(MM))THEN
                  GREATER=X(MM)
              N=MM
            ENDIF
          ENDDO
          X(N)=0
          XX(M)=GREATER
        ENDDO
C       SORTING OF Y(I) VECTOR
        DO L=1,NDAT
          GREATER1=YVAR(1)
          NN=1
          DO LL=2,NDAT
            IF(GREATER1.LT.YVAR(LL))THEN
                  GREATER1=YVAR(LL)
              NN=LL
            ENDIF
          ENDDO
          YVAR(NN)=0
          YY(L)=GREATER1
        ENDDO
        BANDER=.TRUE.
        I=1
        DO WHILE(BANDER)
          IF(XX(I).EQ.TAU1)THEN
            DELTA1=XX(I-1)-XX(I)
            DELTA2=XX(I-1)-XX(I+1)
            RATIO=DELTA1/DELTA2
            YY(NDAT+1)=YY(I)+0.5
            CALL SORT(NDAT,YYY)
            DELTAG2=YYY(I-1)-YYY(I+1)
            DELTAG1=DELTAG2*RATIO
            GAMAR=YYY(I-1)-DELTAG1
            BANDER=.FALSE.
          ENDIF
          I=I+1
          IF(I.LE.NDAT)THEN
            BANDER=.TRUE.
          ELSE
            BANDER=.FALSE.
          ENDIF
        ENDDO
C       EVALUATION OF THE C-PARAMETER
        GAMA1=(SMALL1*LARGE1)-(GAMAR**2)
        GAMA2=(2*GAMAR)-SMALL1-LARGE1
        C=GAMA1/GAMA2
        RETURN
        END

        SUBROUTINE SORT(NDAT,YYY)
        COMMON /DATYY/YY
        REAL *8 YY(10),YYY(10)
        DO L=1,NDAT+1
          GREATER1=YY(1)
          NN=1
          DO LL=2,NDAT+1
            IF(GREATER1.LT.YY(LL))THEN
                  GREATER1=YY(LL)
              NN=LL
            ENDIF
          ENDDO
          YY(NN)=0
          YYY(L)=GREATER1
        ENDDO
        RETURN
        END
```

```
*     ************************************************************** ******************************************************
      PROGRAM POLYREG

*     POLYREG CONSIDERS A DATA REGRESSION PROCESS OF A POLYNOMIAL
*     FUNCTION OF M-DEGREE. POLYREG USES A NUMERICAL ALGORITHM PROPOSED
*     BY CONSTANTINIDES (1987).
*     ************************************************************** ******************************************************

      REAL X(100,20),Y(100),A(20,20),B(20,10),XAUX(100)
      OPEN(UNIT=5,NAME='VISTEMP.DAT',TYPE='OLD')

      READ(5,*)N,M
      IF(N.GT.M)THEN
        M1=M+1
        DO I=1,N
        X(I,1)=1.
        READ(5,*)XX,Y(I)
        DO K=1,M
          J=K+1
          X(I,J)=XX**K
        ENDDO
      ENDDO
      WRITE(6,*)
      DO I=1,M1
        DO J=1,N
          XAUX(J)=X(J,I)
        ENDDO
        DO J=1,M1
          PROD=0.
          DO K=1,N
            PROD=PROD+XAUX(K)*X(K,J)
          ENDDO
          A(I,J)=PROD
        ENDDO
        PROD=0.
        DO K=1,N
          PROD=PROD+XAUX(K)*Y(K)
        ENDDO
        B(I,1)=PROD
      ENDDO
      TYPE *,'AUGMENTED MATRIX OF THE EQUATIONS SYSTEM'
      DO I=1,M1
        TYPE *,'Row No.=',I,(A(I,J),J=1,M1),B(I,1)
      ENDDO
      CALL GAUSS(M1,1,A,B,DET)
      TYPE *,' '
      TYPE *,'RESULTS OF THE DATA REGRESSION   TERMS   COEFFICIENTS'
      DO I=1,M1
        J=I-1
        TYPE 100,J,B(I,1)
100     FORMAT(36X,I2,5X,E13.5,/)
      ENDDO
      ELSE
        TYPE *,'INSUFFICIENT DATA TO GENERATE A POLYNOMIAL EQUATION'
      ENDIF
      STOP
      END

      SUBROUTINE GAUSS(N,M,A,B,DET)
      REAL A(20,21),B(20,10)
      DIMENSION IND(20,2),IPIVOT(20)
      INTEGER REN,COL
      EQUIVALENCE (AMAX,CAMB,CERO)

      DET=1.
      DO J=1,N
        IPIVOT(J)=0
      ENDDO
      DO IREN=1,N
        AMAX=0.
        DO I=1,N
          IF(IPIVOT(I).NE.1)THEN
            DO J=1,N
              IF(IPIVOT(J).NE.1)THEN
```

```
            IF(ABS(AMAX).LE.ABS(A(I,J)))THEN
              REN=I
              COL=J
              AMAX=A(I,J)
            ENDIF
               ENDIF
        ENDDO
      ENDIF
    ENDDO
    PIVOTE=A(REN,COL)
    IF(ABS(PIVOTE).LT.0.00000001)GO TO 15
    DET=DET*PIVOTE
    IND(IREN,1)=REN
    IND(IREN,2)=COL
    IPIVOT(COL)=1
    IF(REN.NE.COL)THEN
      DET=-DET
      DO J=1,N
        CAMB=A(REN,J)
        A(REN,J)=A(COL,J)
        A(COL,J)=CAMB
      ENDDO
      IF(M.NE.0)THEN
        DO J=1,M
          CAMB=B(REN,J)
          B(REN,J)=B(COL,J)
          B(COL,J)=CAMB
        ENDDO
      ENDIF
    ENDIF
    A(COL,COL)=1.
    DO J=1,N
      A(COL,J)=A(COL,J)/PIVOTE
    ENDDO
    IF(M.NE.0)THEN
      DO J=1,M
        B(COL,J)=B(COL,J)/PIVOTE
      ENDDO
    ENDIF
    DO I=1,N
      IF(I.NE.COL)THEN
        CERO=A(I,COL)
        A(I,COL)=0.
        DO J=1,N
          A(I,J)=A(I,J)-CERO*A(COL,J)
        ENDDO
        IF(M.NE.0)THEN
          DO J=1,M
            B(I,J)=B(I,J)-CERO*B(COL,J)
          ENDDO
             ENDIF
      ENDIF
    ENDDO
  ENDDO
  DO IREN=1,N
    I=N-IREN+1
    IF(IND(I,1).NE.IND(I,2))THEN
      REN=IND(I,1)
      COL=IND(I,2)
      DO I=1,N
        CAMB=A(I,REN)
        A(I,REN)=A(I,COL)
        A(I,COL)=CAMB
      ENDDO
    ENDIF
  ENDDO
  RETURN
15  TYPE *,'A PROBLEM OF SINGULAR MATRIX WAS DETECTED'
  CALL EXIT
  END

*  ********************************************************************** **********************************************************************
```

Appendix III

Derivation of the Partial Differential Equations Describing the Transient Heat Flow in a Geothermal Wellbore System

The first law of thermodynamics postulates that the energy equation for an open, unsteady-state system given by a stationary volume element ($\Delta x \Delta y \Delta z$) through which a fluid is flowing at any given time [see Fig. 3.2.1 in the book by Bird et al (1960)], is represented by:

$$\left\{\begin{array}{c}\text{rate of accumulation}\\ \text{of internal and}\\ \text{kinetic energy}\end{array}\right\} = \left\{\begin{array}{c}\text{rate of internal}\\ \text{and kinetic energy}\\ \text{by convection (in)}\end{array}\right\} - \left\{\begin{array}{c}\text{rate of internal}\\ \text{and kinetic energy}\\ \text{by convection (out)}\end{array}\right\} \qquad \text{(III-1)}$$

$$+ \left\{\begin{array}{c}\text{net rate of}\\ \text{heat addition}\\ \text{by conduction}\end{array}\right\} - \left\{\begin{array}{c}\text{net rate of work}\\ \text{done by system on}\\ \text{surroundings}\end{array}\right\}$$

This energy equation can be written in vector-tensor notation as:

$$\frac{\partial}{\partial t}\rho\left(\hat{U}+\frac{1}{2}v^2\right) = -\left(\nabla \bullet \rho\upsilon\left(\hat{U}+\frac{1}{2}v^2\right)\right) - (\nabla \bullet q) - (\nabla \bullet [\tau \bullet \upsilon]) \qquad \text{(III-2)}$$

$$-(\nabla \bullet p\upsilon) + \rho\,(\upsilon \bullet g)$$

The terms on the right-hand represent: (i) the rate of energy input per unit volume by convection; (ii) the rate of energy input per unit volume by conduction; (iii) the rate of work done on the fluid per unit volume by viscous forces; (iv) the rate of work done on the fluid per unit volume by pressure forces and (v) the rate of work done on the fluid per unit volume by gravitational forces, respectively.

The left-hand term corresponds to the rate of gain of energy per unit volume (accumulation). The internal energy terms for a given constant control volume (at constant pressure) can be expressed as:

$$dU = Cp\ dT \qquad \text{(III-3)}$$

Applying this concept to the energy equation (III-2), it becomes:

$$\frac{\partial}{\partial t}\left(\rho\ Cp\ T\right) = -\left(\nabla \bullet \left(\rho\ Cp\ T\ v\right)\right) - \left(\nabla \bullet q\right) - \left(\tau : \nabla \upsilon\right) \qquad \text{(III-4)}$$

$$+\left(\frac{\partial \ln V}{\partial \ln T}\right)_p \frac{Dp}{Dt} + \rho\ T\ \frac{DCp}{Dt}$$

Neglecting the viscous dissipation and the thermal expansion effects as well as the pressure variation in the wellbore, the equation (III-4) can be reduced to:

$$\frac{\partial}{\partial t}\left(\rho\ Cp\ T\right) = -\left(\nabla \bullet \left(\rho\ Cp\ T\ v\right)\right) - \left(\nabla \bullet q\right) \qquad \text{(III-5)}$$

Expanding all the partial derivates of the energy equation under cylindrical coordinates, and assuming that the heat transfer in the wellbore system will be considered in the axial and radial directions with a temperature distribution axisysimmetric, i.e. that:

$$\frac{\partial T(z,r,t)}{\partial \theta} = 0 \qquad \text{(III-6)}$$

Some terms of the energy equation (III-5) can be neglected, and therefore this equation can be reduced to:

$$\frac{\partial}{\partial t}\left(\rho\ Cp\ T\right) = -\left[v_r \frac{\partial}{\partial r}\left(\rho\ Cp\ T\right) + v_z \frac{\partial}{\partial z}\left(\rho\ Cp\ T\right)\right] - \left[\frac{1}{r}\frac{\partial}{\partial r}\left(r q_r\right) + \frac{\partial q_z}{\partial z}\right] \qquad \text{(III-7)}$$

Considering that the components of the energy flux (q) in the radial and vertical directions are given by:

$$q_r = -\ k\frac{\partial T}{\partial r} \qquad \text{(III-8a)}$$

$$q_z = -\ k\frac{\partial T}{\partial z} \qquad \text{(III-8b)}$$

and applying the chain rule to derive a generalised energy equation that enables the variation of the thermophysical properties with temperature to be analysed, equation (III-7) becomes:

$$\left(\rho Cp+\rho T\frac{\partial Cp}{\partial T}+CpT\frac{\partial \rho}{\partial T}\right)\left(\frac{\partial T}{\partial t}+v_r\frac{\partial T}{\partial r}+v_z\frac{\partial T}{\partial z}\right)=$$

(III-9)

$$\left(k\frac{\partial^2 T}{\partial r^2}\right)+\left\{\left[\left(\frac{\partial k}{\partial T}\cdot\frac{\partial T}{\partial r}\right)+\frac{k}{r}\right]\frac{\partial T}{\partial r}\right\}+\left(k\frac{\partial^2 T}{\partial z^2}\right)+\left[\left(\frac{\partial k}{\partial T}\cdot\frac{\partial T}{\partial z}\right)\frac{\partial T}{\partial z}\right]$$

Finally, assuming that the thermophysical properties (ρ, Cp and k) are constants, a simplified energy equation is derived as follows:

$$(\rho Cp)\left(\frac{\partial T}{\partial t}+v_r\frac{\partial T}{\partial r}+v_z\frac{\partial T}{\partial z}\right)=\left(k\frac{\partial^2 T}{\partial r^2}\right)+\left(\frac{k}{r}\frac{\partial T}{\partial r}\right)+\left(k\frac{\partial^2 T}{\partial z^2}\right) \qquad \text{(III-10)}$$

Appendix IV

Listing of WELLTHER computer Code

```
$LARGE
      PROGRAM WELLTHER
*     WELLTHER (WELLBORE THERMAL SIMULATOR)

      REAL*4 KMET,VZ,VFA,XI,FU
      REAL*4 K, RO, CP
      REAL*4 KF, DENF, CPF, VISCF
      REAL*4 RADIO, DZ, DR
      INTEGER*2 CC,PARO,FOTO,CARGA
      DIMENSION K(21,70), RO(21,70), CP(21,70)
      DIMENSION T(21,70),RADIO(21)
      DIMENSION TG(70),DR(21)
      DIMENSION VZ(70),VFA(70),XI(70),DZ(70),FU(70)

      OPEN (UNIT=1, FILE='INPUT.DAT',STATUS='UNKNOWN')
      OPEN (UNIT=2, FILE='TPOZO.RES',STATUS='UNKNOWN')
      OPEN (UNIT=3, FILE='TIME.OUT',STATUS='UNKNOWN')
      OPEN (UNIT=4, FILE='ROCK.RES',STATUS='UNKNOWN')
      OPEN (UNIT=7, FILE='PHOTO.OUT',STATUS='UNKNOWN')
      OPEN (UNIT=12, FILE='REPORT.OUT',STATUS='UNKNOWN')
      OPEN (UNIT=24, FILE='T_DOWN.DAT',STATUS='UNKNOWN')
      OPEN (UNIT=34, FILE='PHI.DAT',STATUS='UNKNOWN')
      OPEN (UNIT=46, FILE='DISTEMP.DAT',STATUS='UNKNOWN')
      OPEN (UNIT=99, FILE='TEMPCIR2.DAT',STATUS='UNKNOWN')

      M=21
      N=70

      CALL DATA(RI,RE,NZMAX,NRMAX,TE,TS,GR,AT,AA,FM,
     *                  DENF,CPF,KF,VISCF,KMET,CPMET,DENMET,
     *                  CP,RO,K,DZ,DR,RADIO,VT,VA)

      WRITE(*,*)'( 0 ) LINEAR GEOTHERMAL GRADIENT'
      WRITE(*,*)'( 1 ) INITIAL CONDITION-T_DOWN PROFILE'
      WRITE(*,*)'( 2 ) NON-LINEAR GEOTHERMAL GRADIENT'
      READ(*,*)CARGA
      IF(CARGA.EQ.1)THEN
            DO J = 1, NZMAX + 1
              READ(24,28)Z, (T(I,J),I=1,NRMAX)
28            FORMAT(2X,21F6.1)
            ENDDO
      ENDIF
      IF(CARGA.EQ.2)THEN
       NZMAS = NZMAX+1
       DO J = 1,NZMAS
             KK = J
            READ(46,*)KK,Z,TG(J)
            DO I=1,NRMAX
             T(I,J)=TG(J)
            END DO
*1002       FORMAT(1X,F8.1,1X,F8.2)
       ENDDO
      ENDIF
      IF(CARGA.EQ.0)THEN
       CALL INITIAL(M,N,TS,GR,NRMAX,NZMAX,DZ,TG,T)
      ENDIF
      Z = 0
      DO J = 1, NZMAX + 1
            WRITE(2,1001)J,Z,T(1,J)
            WRITE(*,*)J,Z,T(1,J)
            Z = Z + DZ(J)
1001        FORMAT(1X,I2,1X,F8.1,1X,F8.2)
      ENDDO

*     POROSITY DISTRIBUTION

DO J =1,NZMAX + 1
            KK = J
            READ(34,*)KK,XI(J),FU(J)
```

```
      ENDDO
      RA = RADIO(4)
      WRITE(*,*)'( 0 ) CIRCULATION '
      WRITE(*,*)'( 1 ) SHUT-IN'
      READ (*,*)PARO
      IF(PARO.EQ.1)THEN
            FM = 0.
      ENDIF
    2 WRITE(*,1008)
      READ(*,*)TMONI
      WRITE(*,1006)
      READ(*,*)TIEMAX
      WRITE(*,1003)
      READ(*,*)DELT
      NT = TIEMAX/DELT
      DELT = DELT*3600.
      TIEMPO=0.
      TPRINT = TMONI
      WRITE(3,1031)
 1031 FORMAT(/,4X,'TIME',4X,'SURFACE',2X,'MIDDLE ZONE OF THE WELLBORE',
     *       2X,'BOTTOMHOLE ZONE OF THE WELLBORE',2X,//)
*
*    THERMOPHYSICAL PROPERTIES OF THE FORMATION

      DO II=1,NT
            TIEMPO=TIEMPO+DELT

**********************************************************************
            CALL TDPIPE(PARO,M,N,RI,TE,AT,FM,DENF,CPF,KF,VISCF,
     *                  DELT,NZMAX,DZ,T)
            CALL TMET(M,N,RI,RE,AT,AA,FM,DENF,CPF,KF,VISCF,DENMET,
     *                CPMET,KMET,DELT,NZMAX,DZ,RA,T,VZ,VFA,XI,FU)
            CALL TANU(PARO,M,N,RE,DELT,NZMAX,DZ,RA,T,VZ,XI,
     *                DENF,CPF,KF,VISCF)
            CALL TINTER(M,N,RE,NZMAX,K,DR,DZ,RA,T,VZ,XI,DENF,CPF,KF,VISCF)
            CALL TROCK(M,N,NZMAX,NRMAX,TG,K,RO,CP,
     *                 DELT,DR,DZ,RADIO,T,VFA,XI,DENF,CPF,KF)
**********************************************************************

            TIE1 = TIEMPO/3600.
            IF (TIE1.GE.TPRINT)THEN
              TPRINT = TPRINT + TMONI
              WRITE(3,1030)TIE1,T(3,1),T(2,30),T(1,61),PARO
 1030         FORMAT(F8.1,6X,F8.2,6X,F8.2,7X,F8.2,4X,I3)
              Z = 0.
              WRITE(2,1014)TIE1
              WRITE(4,1014)TIE1
              WRITE(2,*)
              WRITE(4,*)

              IF(PARO.EQ.0)THEN
                WRITE(2,*)'***** CIRCULATION PROCESS ***** ',PARO
                WRITE(2,*)
                WRITE(4,*)'***** CIRCULATION PROCESS ***** ',PARO
                WRITE(4,*)
              ELSE
                WRITE(2,*)'***** THERMAL RECOVERY PROCESS ***** ',PARO
                WRITE(2,*)
                WRITE(4,*)'***** THERMAL RECOVERY PROCESS ***** ',PARO
                WRITE(4,*)
              ENDIF

              WRITE(4,1026)
 1026         FORMAT(/,4X,'RADIUS',4X,'SURFACE',2X,'MIDDLE ZONE OF WELL',2X,
     *               'BOTTOMHOLE',2X,//)
              Z = 0.0

              DO J = 1,NZMAX+1
                WRITE(2,1020)Z,T(1,J),T(2,J),T(3,J),T(4,J),T(5,J),T(6,J)
```

```
1020        FORMAT(1X,F8.1,1X,6F8.2)
            IF(J.EQ.NZMAX)THEN
                  IF(PARO.EQ.1)THEN
                   TIE2=TIE1+TIEMAX
                   WRITE(99,778)TIE2,T(1,NZMAX)
778                FORMAT(1X,F8.1,2X,F8.2)
                  ELSE
                   WRITE(99,777)TIE1,T(1,NZMAX),T(3,1),T(5,NZMAX)
777                FORMAT(1X,F8.1,1X,4F8.2)
                  ENDIF
              ENDIF
              Z = Z + DZ(J)
            END DO
            DO I=1,NRMAX
               WRITE(4,1025)RADIO(I),T(I,1),T(I,10),T(I,NZMAX)
1025           FORMAT(2X,F7.4,4X,F8.3,7X,F8.3,8X,F8.3,4X)
             END DO
           END IF
      END DO

      WRITE(*,*)'PHOTO: YES = 1 OR NOT = 0'
      READ(*,*)FOTO
      IF (FOTO.EQ.1)THEN
            Z = 0
            IF(PARO.EQ.0)THEN
               WRITE(7,*)
               WRITE(7,*)'***** CIRCULATION PROCESS ***** '
               WRITE(7,*)
            ELSE
               WRITE(7,*)
               WRITE(7,*)'***** THERMAL RECOVERY PROCESS ***** '
               WRITE(7,*)
            ENDIF

            DO J = 1, NZMAX + 1
               WRITE(7,23)Z, (T(I,J),I=1,NRMAX)
23             FORMAT(2X,21F6.1)
               Z = Z + DZ(J)
             ENDDO
      ENDIF
      WRITE(*,*)T(1,NZMAX),T(3,1)
      Z = 0

      WRITE(2,*)
      WRITE(2,*)'***** FLUID VELOCITY PROFILES *****'
      WRITE(2,*)

      DO J = 1,NZMAX+1
            WRITE(2,1709)J, Z, VZ(J), VFA(J), XI(J)
1709        FORMAT(2X,I4,2X,F8.1,2X,2X,E14.4,2X,E14.4,2X,E14.4)
            Z = Z + DZ(J)
      ENDDO
*
  12 WRITE(*,1010)
      READ(*,*)CC
      IF(CC.EQ.1)THEN
            FM=0.
            PARO = 1
            GO TO 2
      ELSE IF(CC.NE.0)THEN
            WRITE(*,1011)
            GO TO 12
      END IF
      CLOSE(UNIT=1)
      CLOSE(UNIT=2)

1003 FORMAT(5X,'TIME STEP SIZE (HRS)',2X)
1006 FORMAT(5X,'TOTAL SIMULATION TIME (HRS)',2X)
1008 FORMAT(5X,'MONITORING TIME',2X)
```

```
1010 FORMAT(2X,'DO YOU WANT TO EVALUATE ANOTHER TEST? YES=1  NOT=0',2X)
1011 FORMAT(2X,'SELECT 1 O 0')
1012 FORMAT(2X,'' CIRCULATION=1  THERMAL RECOVERY=0')
1014 FORMAT(/,2X,'SIMULATED TIME (DRILLING PROCESS)=',F8.3,' horas',/)
1016 FORMAT(/,2X,'SIMULATED TIME (THERMAL RECOVERY)=',F8.3,' horas',/)
   STOP
   END

$LARGE

   SUBROUTINE DATA(RI,RE,NZMAX,NRMAX,TE,TS,GR,AT,AA,FM,
  *                DENF,CPF,KF,VISCF,KMET,CPMET,DENMET,
  *                CP,RO,K,DZ,DR,RADIO,VT,VA)
   REAL*4 K,KROC,KMET,KCEM,RO,CP,DR,DZ,RADIO,LZ,ETR,DTR,DAS,KF
   INTEGER KGP,IDECIS
   DIMENSION RO(21,70),CP(21,70),DR(21),DZ(70),K(21,70),RADIO(21)
   DIMENSION NZ(5),DPP(5),DELZ(5),DTR(5),C(10),LZ(5)

   NRMAX = 20
   PI = 3.14159
   ETR = 0.0100
   WRITE(*,1)
1   FORMAT(/,5X,'INPUT DATA CAN BE FED BY:'
  *        ,//,8X,'(  1  ): SCREEN (INTERACTIVELY)'
  *        ,/,8X, '(  2  ): INPUT DATA FILE'
  *        ,/,5X,'OPTION SELECTED :',$)
   READ(*,*)IDECIS
   IF(IDECIS.EQ.2)THEN
         READ(1,*) DAS,(DTR(I),I=1,3)
         READ(1,*) NS
         READ(1,*) (LZ(I), I=1,NS)
         READ(1,*) (DPP(I),I=1,NS)
         READ(1,*) (NZ(I), I=1,NS)
         READ(1,*) KCEM,CPCEM,DENCEM
         READ(1,*) DTP,ETP
         READ(1,*) KMET,CPMET,DENMET
         READ(1,*) KROC,CPROC,DENROC
         READ(1,*) TS,GR
         READ(1,*) FM,TE
         READ(1,*) KF,CPF,DENF,VISCF
         NZMAX = 1
         DO I = 1, NS
           NZMAX = NZMAX + NZ(I)
           DELZ(I) = LZ(I)/NZ(I)
         ENDDO
   ELSE
   WRITE(*,5)
5   FORMAT(16X,'********** SIMULATOR DATA **********',/)
   WRITE(*,10)
10  FORMAT(/,20X,'****** RADIAL GRID ******',/)
   WRITE(*,15)
15  FORMAT(/,2X,'WELLBORE DIAMETER =',$)
   READ(*,*)DAS
   DO I=1,3
         WRITE(*,20)I
20       FORMAT(/,2X,'DIAM. TUB. DE REC (',I1,') [m], D=',$)
         READ(*,*)DTR(I)
   ENDDO
   WRITE(*,30)
30  FORMAT(/,10X,'********* WELLBORE GEOMETRY **********',/)
500 WRITE(*,35)
35  FORMAT(/,2X,'No. DE SECTIONS OF THE WELLBORE:',$)
   READ(*,*)NS
   IF(NS.EQ.1)THEN
         WRITE(*,40)
40       FORMAT(/,2X,'LENGHT OF THE SECTION, [m]:',$)
         READ(*,*)LZ(1)
         WRITE(*,45)
```

```
45        FORMAT(/,2X,'SEGMENTS-SECTION :',$)
          READ(*,*)NZ(1)
          DELZ(1)=LZ(1)/NZ(1)
          NZMAX = NZ(1)
          WRITE(*,50)
50        FORMAT(/,2X,'WELLBORE DIAMETER-SECTION Z(1) D=',$)
          READ(*,*)DPP(1)
    ELSE IF(((NS.EQ.2).OR.(NS.EQ.3)).OR.(NS.EQ.4))THEN
          NZMAX = 0
          DO I=1,NS
           WRITE(*,55)I
55         FORMAT(/,2X,'LENGHT OF THE SECTION [m], Z(',I1,')=',$)
           READ(*,*)LZ(I)
           WRITE(*,60)I
60         FORMAT(/,2X,'WELLBORE DIAMETER-SECTION Z(',I1,') =',$)
           READ(*,*)DPP(I)
           WRITE(*,65)I
65         FORMAT(/,2X,'DEPTH STEP SIZE, NZ(',I1,')=', $)
           READ(*,*)NZ(I)
           DELZ(I)=LZ(I)/NZ(I)
           NZMAX = NZMAX + NZ(I)
          ENDDO
           WRITE(*,70)
70         FORMAT(/,2X,'CEMENT THERMAL CONDUCTIVITY [W/m oC]',$)
           READ(*,*)KCEM
           WRITE(*,75)
75         FORMAT(/,2X,'SPECIFIC HEAT CAPACITY-CEMENT [J/kg oC]=',$)
           READ(*,*)CPCEM
           WRITE(*,80)
80         FORMAT(/,2X,'CEMENT DENSITY [kg/m3]=',$)
           READ(*,*)DENCEM
    ELSE
           WRITE(*,85)
85         FORMAT(2X,'SELECT: 1, 2, 3 O 4')
           GO TO 500
    END IF
*
    WRITE(*,90)
90   FORMAT(/,10X,'********** DRILL PIPE CHARACTERISTICS **********',/)
    WRITE(*,95)
95   FORMAT(/,2X,'DRILL PIPE DIAMETER [m]=',$)
    READ(*,*)DTP
    WRITE(*,100)
100  FORMAT(/,2X,'THICKNESS OF THE DRILL PIPE [m]=',$)
    READ(*,*)ETP
    WRITE(*,105)
105  FORMAT(/,2X,'METAL THERMAL CONDUCTIVITY [W/m oC]=',$)
    READ(*,*)KMET
    WRITE(*,110)
110  FORMAT(/,2X,'METAL SPECIFIC HEAT CAPACITY [J/kg oC]=',$)
    READ(*,*)CPMET
    WRITE(*,120)
120  FORMAT(/,2X,'METAL DENSITY [kg/m3]=',$)
    READ(*,*)DENMET
    WRITE(*,125)
125  FORMAT(/,10X,'********* GEOTHERMAL RESERVOIR PROPERTIES *******',
   *           '***',/)
    WRITE(*,130)
130  FORMAT(/,2X,'FORMATION THERMAL CONDUCTIVITY [W/m oC]=',$)
    READ(*,*)KROC
    WRITE(*,135)
135  FORMAT(/,2X,'FORMATION SPECIFIC HEAT CAPACITY [J/kg oC]=',$)
    READ(*,*)CPROC
    WRITE(*,136)
136  FORMAT(/,2X,'FORMATION DENSITY [kg/m3]=',$)
    READ(*,*)DENROC
    WRITE(*,140)
140  FORMAT(/,2X,'SURFACE TEMPERATURE, TS =',$)
    READ(*,*)TS
```

```
      WRITE(*,145)
145   FORMAT(/,2X,'GEOTHERMAL GRADIENT, GR =',$)
      READ(*,*)GR
      WRITE(*,150)
150         FORMAT(/,10X,'*** INITIAL TEMPERATURE DISTRIBUTION',
     *           ' ***',/)
      WRITE(*,155)
155   FORMAT(3X,'DEGREE OF THE FUNCTION-INITIAL TEMPERATURE = ',$)
      READ(*,*)KGP
      DO I = 1, KGP+1
            WRITE(*,160)I
160         FORMAT(3X,'COEFFICIENTS OF THE FUNCTION C(',I1,') :',$)
            READ(*,*)C(I)
      ENDDO
*
      WRITE(*,165)
165   FORMAT(/,10X,'****** DRILLING FLUID PROPERTIES'
     *           ' ******',/)
      WRITE(*,170)
170   FORMAT(/,2X,'INLET MASS FLOWRATE OF FLUID [Kg/seg.]=',$)
      READ(*,*)FM
      WRITE(*,175)
175   FORMAT(/,2X,'INLET FLUID TEMPERATURE (oC)=',$)
      READ(*,*)TE
      WRITE(*,180)
180   FORMAT(/,2X,'FLUID THERMAL CONDUCTIVITY (W/m oC)=',$)
      READ(*,*)KF
      WRITE(*,185)
185   FORMAT(/,2X,'FLUID SPECIFIC HEAT CAPACITY (J/kg oC)=',$)
      READ(*,*)CPF
      WRITE(*,190)
190   FORMAT(/,2X,'FLUID DENSITY (kg/m3) =',$)
      READ(*,*)DENF
      WRITE(*,195)
195   FORMAT(/,2X,'FLUID VISCOSITY (N-s/m2) =',$)
      READ(*,*)VISCF
      ENDIF
*
      IF(IDECIS.EQ.1)THEN
            WRITE(1,200) DAS,(DTR(I),I=1,3)
200           FORMAT(2X,4F7.3)
            WRITE(1,205) NS
205           FORMAT(2X,I2)
            WRITE(1,210) (LZ(I),I=1,NS)
210           FORMAT(2X,4F7.2)
            WRITE(1,215) (DPP(I),I=1,NS)
215           FORMAT(2X,4F7.3)
            WRITE(1,220) (NZ(I),I=1,NS)
220           FORMAT(2X,4I5)
            WRITE(1,225) KCEM,CPCEM,DENCEM
225           FORMAT(2X,3F8.2)
            WRITE(1,230) DTP,ETP
230           FORMAT(2X,2F7.4)
            WRITE(1,235) KMET,CPMET,DENMET
235           FORMAT(2X,3F8.2)
            WRITE(1,240) KROC,CPROC,DENROC
240           FORMAT(2X,3F8.2)
            WRITE(1,245) TS,GR
245           FORMAT(2X,F5.2,2X,F5.3)
            WRITE(1,250) KGP
250           FORMAT(2X,I2)
            DO I = 1, KGP + 1
             WRITE(1,255) C(I)
255            FORMAT(2X,E16.10)
            ENDDO
            WRITE(1,260) FM,TE
260           FORMAT(2X,F6.2,3X,F5.2)
            WRITE(1,265) KF,CPF,DENF,VISCF
265           FORMAT(2X,3F8.2,2X,F7.2)
```

```
            ENDIF

        WRITE(12,300)
300   FORMAT(16X,'********** SIMULATOR DATA **********',/)
        WRITE(12,305)
305    FORMAT(20X,'****** RADIAL GRID ******',/)
        WRITE(12,310)DAS
310    FORMAT(2X,'WELLBORE DIAMETER =',F5.3,'m')
     DO I=1,3
            WRITE(12,315)I,DTR(I)
315         FORMAT(5X,'DRILL PIPE DIAMETER (',I1,')',F10.4,' m ')
     ENDDO
*
     WRITE(12,325)
325       FORMAT(/,10X,'********* CARACTERISTICAS DEL POZO **********',/)
    WRITE(12,330)NS
330       FORMAT(5X,'No. SECTIONS-WELLBORE:',I2,/)
    DO I=1,NS
             WRITE(12,335)I,LZ(I)
335          FORMAT(5X,'LENGHT OF THE SECTION:(',I1,')',F10.2,' m')
             WRITE(12,340)I,DPP(I)
340          FORMAT(5X,'WELLBORE DIAMETER-SECTION:(',I1,')',F10.5,' m')
             WRITE(12,345)NZ(I)
345          FORMAT(5X,'SEGMENTS OF THE SECTION :',I4)
             WRITE(12,350)DELZ(I)
350          FORMAT(5X,'DEPTH STEP SIZE-SECTION:',F10.2,' m',/)
           ENDDO
             WRITE(12,355)KCEM
355          FORMAT(5X,'K-CEMENT:',F10.4,
    *        '[W/m oC]')
             WRITE(12,360)CPCEM
360          FORMAT(5X,'CP-CEMENT :',F9.4,' J/kg oC')
             WRITE(12,365)DENCEM
365          FORMAT(5X,'RHO-CEMENT :',F10.2,' kg/m3')
    WRITE(12,370)
370   FORMAT(/,10X,'********** DRILL PIPE GEOMETRY',
    *        '**********',/)
     WRITE(12,375)DTP
375   FORMAT(5X,'DRILL PIPE DIAMETER :',F7.3,' m')
     WRITE(12,380)ETP
380   FORMAT(5X,'THICKNESS OF THE DRILL PIPE :',F7.4,' m',/)
     WRITE(12,385)KMET
385   FORMAT(5X,'K-METAL:',F7.4,' W/m oC')
     WRITE(12,390)CPMET
390   FORMAT(5X,'CP-METAL :',F9.4,' J/kg oC')
     WRITE(12,395)DENMET
395   FORMAT(5X,'RHO-METAL :',F10.2,' kg/m3',/)
     WRITE(12,400)
400   FORMAT(10X,'********* GEOTHERMAL RESERVOIR PROPERTIES *******',
    *          '***',/)
     WRITE(12,405)KROC
405   FORMAT(5X,'K-ROCK:',F7.4,'W/m oC')
    WRITE(12,410)CPROC
410   FORMAT(5X,'CP-ROCK :',F9.4,' J/kg oC')
    WRITE(12,415)DENROC
415   FORMAT(5X,'RHO-ROCK :',F10.2,' kg/m3',/)
     WRITE(12,420)TS
420   FORMAT(5X,'SURFACE TEMPERATURE :',F7.2,'oC')
     WRITE(12,425)GR
425   FORMAT(5X,'GEOTHERMAL GRADIENT :',F8.5,'oC/m',/)
*
     WRITE(12,445)
445   FORMAT(/,10X,'****** DRILLING FLUID PROPERTIES'
    *          '******',/)
     WRITE(12,450)FM
450   FORMAT(5X,'DRILLING FLUID-MASS FLOWRATE  :',F10.2,' Kg/hr')
     WRITE(12,455)TE
455   FORMAT(5X,'INLET FLUID TEMPERATURE :',F7.2,' oC',/)
     WRITE(12,460)KF
```

```
460   FORMAT(5X,'K-FLUID:',F7.4,'W/m oC')
      WRITE(12,465)CPF
465   FORMAT(5X,'CP-FLUID :',F9.4,' J/kg oC')
      WRITE(12,470)DENF
470   FORMAT(5X,'RHO-FLUID :',F10.2,' kg/m3')
      WRITE(12,475)VISCF
475   FORMAT(5X,'MU-FLUID :',F10.4,'(N-s/m2)',/)

      RE = DTP/2.0
      RI = RE - ETP

       CALL DATA1 (RI,RE,NRMAX,NZMAX,KROC,KCEM,DPP,DTR,DAS,
     *                    DENROC,CPROC,DENCEM,CPCEM,DZ,DELZ,ETR,
     *                    NZ,RO,CP,K,RADIO,DR,NS)

      AT = PI*RI**2
      AA = PI*(RADIO(4)**2 - RE**2)
      WRITE(12,600)AT,AA
600   FORMAT(2X,'FLUID FLOW AREA OF THE DRILL PIPE:'F10.4,2X,'m2'
     *,/,2X,'FLUID FLOW AREA OF THE ANNULUS:'F10.4,2X'm2',/)
      VT = FM/(DENF*AT)
      VA = FM/(DENF*AA)
      WRITE(12,605)VT,VA
605   FORMAT(2X,'FLUID VELOCITY IN THE DRILL PIPE:'
     *F10.4,2X,'m/s',/,2X,'FLUID VELOCITY IN THE ANNULUS:'
     *F10.4,2X'm/s',/)
*
      RETURN
      END
*

$LARGE
      SUBROUTINE DATA1(RI,RE,NRMAX,NZMAX,KROC,KCEM,DPP,DTR,DAS,
     *                    DENROC,CPROC,DENCEM,CPCEM,DZ,DELZ,ETR,
     *                    NZ,RO,CP,K,RADIO,DR,NS)

REAL*4 K,KROC,KCEM,RO,CP,DR,RADIO,DELZ,DZ,ETR,DTR,DAS
DIMENSION DPP(5),RO(21,70),CP(21,70),DTR(5)
DIMENSION K(21,70),RADIO(21),DR(21),NZ(5),DELZ(5),DZ(70)
NZ1P2 = NZ(1)
NZ2P2 = NZ(1) + NZ(2)
NZ3P2 = NZ(1) + NZ(2) + NZ(3)
DPP(1) = DAS
RADIO(1) = 0.0
RADIO(2) = (RI + RE)/2.0
RADIO(4) = DTR(1)/2.0 - ETR
RADIO(3) = (RE + RADIO(4))/2.0
RADIO(5) = RADIO(4) + ((DTR(2)/2.0 - ETR) - RADIO(4))/2.0
RADIO(6) = RADIO(5) + ((DTR(2)/2.0 - ETR) - RADIO(4))/2.0
RADIO(7) = RADIO(6) + ((DTR(3)/2.0 - ETR) - RADIO(6))/2.0
RADIO(8) = RADIO(7) + ((DTR(3)/2.0 - ETR) - RADIO(6))/2.0
RADIO(9) = RADIO(8) + (DPP(1)/2.0 - RADIO(8))/2.0
RADIO(10) = RADIO(9) + (DPP(1)/2.0 - RADIO(8))/2.0

      DO I = 11, NRMAX
        RADIO(I) = RADIO(I-1) + 0.1*(1 + (I-10))
      ENDDO
*
      DO I = 1,NRMAX-1
        DR(I) = RADIO(I+1) - RADIO(I)
      END DO

    IF(NS.EQ.3)THEN
      RADIO(4) = DTR(2)/2.0 - ETR
      RADIO(3) = (RE + RADIO(4))/2.0
      RADIO(5) = RADIO(4) + ((DTR(3)/2.0 - ETR) - RADIO(4))/2.0
      RADIO(6) = RADIO(5) + ((DTR(3)/2.0 - ETR) - RADIO(4))/2.0
      RADIO(7) = RADIO(6) + (DAS/2.0       - RADIO(6))/2.0
      RADIO(8) = RADIO(7) + (DAS/2.0       - RADIO(6))/2.0
```

```
          DO I = 9, NRMAX
            RADIO(I) = RADIO(I-1) + 0.1*(1 + (I-8))
          ENDDO
*
          DO I = 1,NRMAX-1
            DR(I) = RADIO(I+1) - RADIO(I)
          END DO
      ENDIF
      IF(NS.EQ.2)THEN
          RADIO(4) = DTR(3)/2.0 - ETR
          RADIO(3) = (RE + RADIO(4))/2.0
          RADIO(5) = RADIO(4) + (DAS/2.0 - RADIO(4))/2.0
          RADIO(6) = RADIO(5) + (DAS/2.0 - RADIO(4))/2.0

          DO I = 7, NRMAX
            RADIO(I) = RADIO(I-1) + 0.1*(1 + (I-6))
          ENDDO
          DO I = 1,NRMAX-1
            DR(I) = RADIO(I+1) - RADIO(I)
          END DO
      ENDIF
      IF(NS.EQ.1)THEN
          RADIO(4) = DAS/2.0
          RADIO(3) = (RE + RADIO(4))/2.0

          DO I = 5, NRMAX
            RADIO(I) = RADIO(I-1) + 0.1*(1 + (I-4))
          ENDDO
          DO I = 1,NRMAX-1
            DR(I) = RADIO(I+1) - RADIO(I)
          END DO
      ENDIF
*
      DO J =1, NZMAX
          DO I = 4,NRMAX
            K(I,J) = KROC
            RO(I,J) = DENROC
            CP(I,J) = CPROC
          END DO
          DZ(J) = DELZ(1)
      END DO
*
      IF(NS.EQ.2) THEN
          DO J = 1,NZ1P2
            DO I = 4,6
              K(I,J) = KCEM
              CP(I,J) = CPCEM
              RO(I,J) = DENCEM
            END DO
            DZ(J) = DELZ(1)
          END DO
          DO J = NZ1P2+1, NZMAX
            DZ(J) = DELZ(2)
          ENDDO

      ELSE IF(NS.EQ.3) THEN
      DO J = 1, NZ2P2
        DO I = 4,6
          K(I,J) = KCEM
          CP(I,J) = CPCEM
          RO(I,J) = DENCEM
        END DO
        DZ(J) = DELZ(1)
      END DO
      DO J = 1, NZ1P2
        DO I = 7,8
          K(I,J) = KCEM
          CP(I,J) = CPCEM
          RO(I,J) = DENCEM
```

```
          ENDDO
        END DO
        DO J = NZ1P2+1, NZ2P2
          DZ(J) = DELZ(2)
        ENDDO
        DO J = NZ2P2+1, NZMAX
          DZ(J) = DELZ(3)
        ENDDO

ELSE IF(NS.EQ.4) THEN
        DO J = 1, NZ3P2
          DO I = 4,6
            K(I,J) = KCEM
            CP(I,J) = CPCEM
            RO(I,J) = DENCEM
          END DO
          DZ(J) = DELZ(1)
        END DO
*
        DO J = 1, NZ2P2
          DO I = 7,8
            K(I,J) = KCEM
            CP(I,J) = CPCEM
            RO(I,J) = DENCEM
          END DO
        END DO
        DO J = 1, NZ1P2
          DO I = 9,10
            K(I,J) = KCEM
            CP(I,J) = CPCEM
            RO(I,J) = DENCEM
          END DO
        END DO
        DO J = NZ1P2+1, NZ2P2
          DZ(J) = DELZ(2)
        ENDDO
        DO J = NZ2P2+1, NZ3P2
          DZ(J) = DELZ(3)
        ENDDO
        DO J = NZ3P2+1, NZMAX
          DZ(J) = DELZ(4)
        ENDDO
    END IF
*
    RETURN
    END

$LARGE
    SUBROUTINE INITIAL(M,N,TS,GR,NRMAX,NZMAX,DZ,TG,T)
    REAL*4 TG,T,DZ
    DIMENSION TG(N),T(M,N),DZ(N)
*
    Z1 = 0.0
    NZMAS = NZMAX+1
    DO J = 1,NZMAS
        TG(J)=TS+GR*Z1
        DO I=1,NRMAX
          T(I,J)=TG(J)
        END DO
        Z1 = Z1 + DZ(J)
    ENDDO

    RETURN
    END

$LARGE
    SUBROUTINE TDPIPE(PARO,M,N,RI,TE,AT,FM,DENF,CPF,KF,VISCF,
   *                              DELT,NZMAX,DZ,T)
    REAL*4 KF,T,RI,DZ,TEMPE,A,B,C,D
```

```
INTEGER*2 PARO
DIMENSION T(M,N),TEMPE(70),A(70),B(70),C(70),D(70),DZ(70)

TA = T(1,NZMAX)
IF(PARO.EQ.1)THEN
      T(1,1) = T(2,1)
ELSE
      T(1,1) = TE
END IF
DO J = 2,NZMAX
      VT = FM/(DENF*AT)
      CALL COEFCON(RI,VT,DENF,VISCF,CPF,KF,HT)
      AUX1 = DENF*CPF
      AUX2 = 0.
      AUX3 = KF/RI
      AUX4 = (2.0*HT)/RI
      A(J) = (- VT + (AUX2/AUX1))*(DELT/(2.0*DZ(J))) -
*           (KF/AUX1)*(DELT/DZ(J)**2)
      B(J) = 1.0 + (AUX4 + (2.0*KF)/DZ(J)**2 + AUX3/RI + (2.0*KF)/
*           RI**2)*(DELT/AUX1)
      C(J) = (VT - (AUX2/AUX1))*(DELT/(2.0*DZ(J))) -
*           (KF/AUX1)*(DELT/DZ(J)**2)
      D(J) = T(1,J) + ((AUX4 + AUX3/RI + (2.0*KF)/DZ(J)**2 + (2.0*KF)/
*           RI**2)*(DELT/AUX1))*T(2,J)
 END DO

D(2) = D(2) - A(2)*T(1,1)
D(NZMAX) = D(NZMAX) - C(NZMAX)*T(1,NZMAX)
CALL TRIDAG(N,2,NZMAX,A,B,C,D,TEMPE)

DO J = 2,NZMAX
      T(1,J) = TEMPE(J)
END DO

RETURN
   END

$LARGE

   SUBROUTINE TMET(M,N,RI,RE,AT,AA,FM,DENF,CPF,KF,VISCF,DENMET,
  *                CPMET,KMET,DELT,NZMAX,DZ,RA,T,VZ,VFA,XI,FU)

   REAL*4 KMET,KF,DZ,RA,T,TEMPE,A,B,C,D,VZ,VFA,XI,PI,FU
   DIMENSION T(M,N),TEMPE(70),A(70),B(70),C(70),D(70),DZ(70)
   DIMENSION XI(70),VZ(70),VFA(70),FU(70)

   DATA PI /3.1416/

   NZM = NZMAX
    DO J = 1, NZM
         K = NZMAX+1 - J
         IF(XI(K).EQ.0.)THEN
           FMF = 0.
           VFA(K) = 0.
         ELSE
           FMF = FM*FU(K)
           VFA(K) = FMF/(DENF*2.*PI*DZ(J)*XI(K))
         ENDIF
         VA = FM/(DENF*AA)
         IF(K.EQ.NZM)THEN
          VZ(K+1) = VA
          VFA(K)= 0
         ENDIF
         VZ(K) = VZ(K+1) - (2.*RA*DZ(J)*VFA(K))/(RA**2 - RE**2)
         VZ(K+1) = VZ(K)
ENDDO      *
VZ(NZMAX+1) = VA

DO J = 1,NZMAX
```

```
      RM = (RI + RE)/2.0
      VT = FM/(DENF*AT)
      VA = VZ(J)
      IF (VA .LT. 0.)THEN
        VA = 0.
      ENDIF
      DELZ = DZ(J)
      CALL COEFCON(RI,VT,DENF,VISCF,CPF,KF,HT)
      CALL COEFCONA(RE,VA,DENF,VISCF,CPF,KF,RA,DELZ,HE,HA)
      DKMET = 0.0
      AUX1 = DENMET*CPMET
      AUX2 = DKMET*((T(2,J+1) - T(2,J-1))/(2.0*DZ(J)))
      AUX3 = KF/RM
      AUX4 = (2.0*HT*RI)/(RE**2 - RI**2)
      AUX5 = (2.0*HE*RE)/(RE**2 - RI**2)
      A(J) = (AUX2/(2.0*DZ(J)) - KMET/(DZ(J)**2))*(DELT/AUX1)
      B(J) = 1.0 + (2.0*(KMET/(DZ(J)**2)) + 2.0*(KF/((RI**2 +
     &       ((RA - RE)/2.0)**2)/2.0)) + AUX4 + AUX5)*(DELT/AUX1)
      C(J) = - (AUX2/(2.0*DZ(J)) + KMET/(DZ(J)**2))*(DELT/AUX1)
      D(J) = T(2,J) + (AUX4*T(1,J) + AUX5*T(3,J) + (KF/((RI**2 +
     &       ((RA-RE)/2.0)**2)/2.0))*(T(1,J) + T(3,J)) + (AUX3/(RI +
     &       (RA-RE)/2.0))*(T(3,J) - T(1,J)))*(DELT/AUX1)
      END DO

      D(1) = D(1) - A(1)*T(2,1)
      D(NZMAX) = D(NZMAX) - C(NZMAX)*T(2,NZMAX)
      CALL TRIDAG(N,1,NZMAX,A,B,C,D,TEMPE)

      DO J = 1,NZMAX
            T(2,J) = TEMPE(J)
      END DO

      RETURN
      END
*
$LARGE

      SUBROUTINE TANU(PARO,M,N,RE,DELT,NZMAX,DZ,RA,T,VZ,XI,
     *                DENF,CPF,KF,VISCF)

      REAL*4 KF,DZ,RA,T,TEMPE,A,B,C,D,XI,VZ
      INTEGER*2 PARO
      DIMENSION T(M,N),TEMPE(70),A(70),B(70),C(70),D(70),DZ(70)
      DIMENSION XI(70), VZ(70)

      NZM = NZMAX-1
      IF(PARO.EQ.1)THEN
            T(3,NZMAX) = T(4,NZMAX)
      ELSE
            T(3,NZMAX) = T(1,NZMAX)
      END IF

      DO J = 1,NZM
            V = VZ(J)
            IF(V.LT.0.)THEN
              V = 0.
            ENDIF
            DELZ = DZ(J)
            CALL COEFCONA(RE,V,DENF,VISCF,CPF,KF,RA,DELZ,HE,HA)
            HA = HA*(1. - XI(J))
            AUX1 = DENF*CPF
            AUX2 = 0.
            AUX3 = KF/(RE + (RA-RE)/2.0)
            AUX4 = (2.0*HE*RE)/(RA**2 - RE**2)
            AUX5 = (2.0*HA*RA)/(RA**2 - RE**2)
            A(J) = (V + AUX2/AUX1)*(DELT/(2.*DZ(J))) - (KF/AUX1)*
     *           (DELT/DZ(J)**2)
            B(J) = 1.0 + (AUX4 + AUX5 + (2.*KF)/DZ(J)**2 + (2.0*KF)/
```

```
*             ((RA-RE)/2.0)**2)*(DELT/AUX1)
      C(J) = - ( V + AUX2/AUX1)*(DELT/(2.0*DZ(J))) -
*                  (KF/AUX1)*(DELT/DZ(J)**2)
      D(J) = T(3,J) + ((AUX4 + KF/((RA-RE)/2.0)**2)*T(2,J) +
*             (AUX5 + KF/((RA-RE)/2.0)**2)*T(4,J))*(DELT/AUX1) +
*             (AUX3/AUX1)*(DELT/(RA - RE))*(T(4,J) - T(2,J))
 END DO
 D(1) = D(1) - A(1)*T(3,1)
 D(NZM) = D(NZM) - C(NZM)*T(3,NZMAX)
 CALL TRIDAG(N,1,NZM,A,B,C,D,TEMPE)
 DO J = 1,NZM
      T(3,J) = TEMPE(J)
 END DO
 RETURN
    END
*

$LARGE

    SUBROUTINE TINTER(M,N,RE,NZMAX,K,DR,DZ,RA,T,VZ,XI,
   *                          DENF,CPF,KF,VISCF)

    REAL*4 KF,KEF,DR,RA,T,DZ,VZ,XI,K
    DIMENSION DR(M),T(M,N),VZ(70),XI(70),DZ(70),K(M,N)

    DO J = 1,NZMAX
          VA = VZ(J)
          IF(VA. LT. 0.)THEN
            VA = 0.
          ENDIF
          DELZ = DZ(J)
          CALL COEFCONA(RE,VA,DENF,VISCF,CPF,KF,RA,DELZ,HE,HA)
          HA = HA*(1.-XI(J))
          KEF = KF**XI(J)*K(4,J)**(1. - XI(J))
          T(4,J) = ((HA + KF/DR(3))*T(3,J))/(HA + KEF/DR(4) + KF/DR(3))
    *             + ((KEF/DR(4))/(HA + KEF/DR(4) + KF/DR(3)))*T(5,J)
     END DO

     RETURN
     END
*

$LARGE

    SUBROUTINE TROCK(M,N,NZMAX,NRMAX,TG,K,RO,CP,
   *                      DELT,DR,DZ,RADIO,T,VFA,XI,DENF,CPF,KF)

    REAL*4 DR,DZ,T,TEMPE,TG,A,B,C,D,RADIO,TMO,TOLD,VFA
    REAL*4 KF,KEF,XI,VR
    REAL*4 K, RO, CP
    LOGICAL FLAGM
    DIMENSION RADIO(M),DR(M),T(M,N)
    DIMENSION K(M,N), RO(M,N), CP(M,N)
    DIMENSION TEMPE(70),TMO(70),TOLD(70)
    DIMENSION A(70),B(70),C(70),D(70),TG(N),DZ(70)
    DIMENSION VFA(70), XI(70), VR(21,70)

    NZMAS = NZMAX+1
    NRM = NRMAX-1

    DO I = 5,NRM
          T(I,NZMAS) = TG(NZMAS)
          NIT = 1
          BIG =0.
          FLAGM = .TRUE.
          DO J = 1,NZMAX
           TMO(J) = T(I,J)
          ENDDO
```

```
 DO WHILE(FLAGM)
        DO J = 1,NZMAX
         KEF = KF**XI(J)*K(I,J)**(1. - XI(J))
         DENCPEF= DENF*CPF*XI(J) + RO(I,J)*CP(I,J)*(1. - XI(J))
         AUX1 = KEF
         AUX2 = 0.
         AUX3 = KEF/RADIO(I)
         AUX4 = DENCPEF
         A(J) = (AUX2/(AUX4*2.0*(2.0*DZ(J))) -
&                    AUX1/(AUX4*(2.0*DZ(J)**2)))*DELT
         B(J) = 1.0 + 2.0*(AUX1/(AUX4*(2.0*DZ(J)**2)))*DELT
         C(J) = - (AUX2/(AUX4*2.0*(2.0*DZ(J))) +
&                     AUX1/(AUX4*(2.0*DZ(J)**2)))*DELT
         D(J) = TMO(J) + ((AUX1/(AUX4*(DR(I-1)**2 + DR(I)**2)))*
&                    (T(I+1,J) - 2.0*TMO(J) + T(I-1,J)) +
&                    (AUX3/(2.0*AUX4*(DR(I-1) + DR(I))))*
&                    (T(I+1,J) - T(I-1,J)))*DELT

        END DO

        D(1) = D(1) - A(1)*T(I,1)
        D(NZMAX) = D(NZMAX) - C(NZMAX)*T(I,NZMAS)

        CALL TRIDAG(N,1,NZMAX,A,B,C,D,TEMPE)

        DO J = 1,NZMAX
          TOLD(J) =T(I,J)
          DIFF=ABS(TOLD(J) - TEMPE(J))
          IF(DIFF.GT.BIG)THEN
                BIG=DIFF
          ELSE
                IF(NIT .GT. 1)THEN
                  BIG = DIFF
                ENDIF
          ENDIF
           T(I,J)=TEMPE(J)
         ENDDO

         IF(NIT.LT.5)THEN
          IF(BIG.GT.1.)THEN
            FLAGM=.TRUE.
            NIT=NIT+1
          ELSE
            FLAGM=.FALSE.
          ENDIF
         ELSE
          WRITE(*,*)'I = ', I ,' J =', J
          WRITE(*,75)NIT
75        FORMAT(/,15X,'TEMPERATURES NOT CONVERGED AT J: ',I4,/)
          FLAGM=.FALSE.
         ENDIF
    ENDDO
   END DO

   DO J = 1,NZMAX3
        DO I=5,NRM
         VR(I,J) = RADIO(I-1)*VFA(J)/RADIO1(I)
        ENDDO
ENDDO
DO J = 1,NZMAX
        T(NRMAX,J) = TG(J)
        NIT = 1
        BIG =0.
        FLAGM = .TRUE.
        DO I = 5,NRM
         TMO(I) = T(I,J)
        ENDDO
 DO WHILE(FLAGM)
        DO I = 5,NRM
```

```
      KEF = KF**XI(J)*K(I,J)**(1. - XI(J))
      DENCPEF= DENF*CPF*XI(J) + RO(I,J)*CP(I,J)*(1. - XI(J))
      AUX1 = KEF
      AUX2 = 0.
      AUX3 = KEF/RADIO(I) - VR(I,J)*DENF*CPF
      AUX4 = DENCPEF
      A(I) = (AUX2/(AUX4*2.0*(DR(I-1) + DR(I))) -
     &            AUX1/(AUX4*(DR(I-1)**2 + DR(I)**2)))*DELT
      B(I) = 1.0 + 2.0*(AUX1/(AUX4*(DR(I-1)**2 + DR(I)**2)))*DELT
      C(I) = - (AUX2/(AUX4*2.0*(DR(I-1) + DR(I))) +
     &            AUX1/(AUX4*(DR(I-1)**2 + DR(I)**2)))*DELT
      D(I) = TMO(I) + ((AUX1/(AUX4*(2.0*DZ(J)**2)))*
     &            (T(I,J+1) - 2.0*TMO(I) + T(I,J-1)) +
     &            (AUX3/(2.0*AUX4*(2.0*DZ(J))))*
     &            (T(I,J+1) - T(I,J-1)))*DELT
      END DO

      D(5) = D(5) - A(5)*T(4,J)
      D(NRM) = D(NRM) - C(NRM)*T(NRMAX,J)
      CALL TRIDAG(N,5,NRM,A,B,C,D,TEMPE)
       DO I = 5,NRM
         TOLD(I) =T(I,J)
         DIFF=ABS(TOLD(I) - TEMPE(I))
         IF(DIFF.GT.BIG)THEN
                BIG=DIFF
         ELSE
                IF(NIT .GT. 1)THEN
                  BIG = DIFF
                ENDIF
         ENDIF
         T(I,J) = TEMPE(I)
       END DO

       IF(NIT.LT.3)THEN
        IF(BIG.GT.1.)THEN
          FLAGM=.TRUE.
          NIT=NIT+1
        ELSE
          FLAGM=.FALSE.
        ENDIF
       ELSE
        WRITE(*,*)'I = ', I, '   J =', J
        WRITE(*,*)'BIG =', BIG
        WRITE(*,81)NIT
81      FORMAT(/,15X,'TEMPERATURES NOT CONVERGED AT R: ',I4,/)
        FLAGM=.FALSE.
       ENDIF
     END DO
    END DO

    RETURN
    END
*

$LARGE
          SUBROUTINE COEFCON(RI,VT,DENF,VISCF,CPF,KF,HT)
    REAL*4 KF
    RET=(DENF*VT*(2.*RI))/VISCF
    PR=CPF*VISCF/KF
    TRAN=2300.
    IF(RET.GT.TRAN)THEN
     EPSI=(1.82*LOG10(RET)-1.64)**(-2)
     TN1=(EPSI/8.)*(RET-1000.)*PR
     TN2=1.+12.7*SQRT(EPSI/8.)*(PR**(2./3.)-1.)
     TNU=TN1/TN2
     HT=TNU*KF/(RI*2.)
    ELSE
     TNU=4.364
     HT=TNU*KF/(RI*2.)
```

```
      ENDIF
      RETURN
      END

$LARGE
      SUBROUTINE COEFCONA(RE,VA,DENF,VISCF,CPF,KF,RA,DEZ,HE,HA)
      REAL*4 KF,RA
      REA=(DENF*VA*(2.*RA - 2.*RE))/VISCF
      PR=CPF*VISCF/KF1
      TRAN=2300.
      IF(REA.GT.TRAN)THEN
       EPSI=(1.82*LOG10(REA)-1.64)**(-2)
       AN1=(EPSI/8.)*(REA-1000.)*PR
       AN2=1.+12.7*SQRT(EPSI/8.)*(PR**(2./3.)-1.)
       ANU=AN1/AN2
       HA=(ANU*KF)/(2.*RA - 2.*RE)
      ELSE
       DEA=RA*2.-RE*2.
       ANU=1.86*(REA*PR*(DEA/DEZ1))**(1./3.)
       HE=(ANU*KF)/(2.*RE*TETA)
       HA=(ANU*KF)/(2.*RA*TETA)
      ENDIF
      RETURN
      END

$LARGE
      SUBROUTINE TRIDAG(N,IF,L,A,B,C,D,V)
      IMPLICIT REAL*4 (A-H,O-Z)
      REAL*4 A,B,C,D,BETA,GAMMA,V
      DIMENSION A(N),B(N),C(N),D(N),BETA(70)
      DIMENSION GAMMA(70),V(N)
      BETA(IF)=B(IF)
      GAMMA(IF)=D(IF)/BETA(IF)
      IFP1=IF+1
      DO I=IFP1,L
       BETA(I)=B(I)-A(I)*C(I-1)/BETA(I-1)
       GAMMA(I)=(D(I)-A(I)*GAMMA(I-1))/BETA(I)
      ENDDO
      V(L)=GAMMA(L)
      LAST=L-IF
      DO K=1,LAST
       I=L-K
       V(I)=GAMMA(I)-C(I)*V(I+1)/BETA(I)
      ENDDO
      RETURN
      END
```

Appendix V

Listing of International Papers Published by the Author

(1) E. Santoyo, A. García, S. Santoyo-Gutiérrez y G. Espinoza, Evaluación de coeficientes de transferencia de calor (CTC) de fluidos no-Newtonianos para la perforación de pozos geotérmicos, *Memorias del Congreso Nacional de Ingeniería Mecánica (ANIIM-DGIT)*, 27-29 Noviembre, Puebla, México, 10 p. (1996).

(2) A. Garcia, I. Hernandez, G. Espinosa and E. Santoyo, TEMLOPI: A thermal simulator for estimation of drilling mud and formation temperatures during drilling geothermal wells. Submitted to Computers and Geosciences (1997).

(3) A. Garcia, E. Santoyo, G. Espinosa, I. Hernandez and H. Gutierrez, Estimation of temperatures in geothermal wells during circulation and shut-in in the presence of lost circulation, Submitted to Transport in Porous Media (1997).